Micro-scale Testing of Fiber Reinforced Polymer Resin and Additive to Evaluate Kinetic Parameters for Pyrolysis Modeling

A Major Qualifying Project
Submitted to the Faculty of
Worcester Polytechnic Institute
in partial fulfillment of the requirements for the
Degree of Bachelor of Science
By

_____
Krista Anderson

_____
Victoria Grimes

_____
Zachary Stewart

_____
Shuyang Wang

May 2015
Project Number: FM14

_____
Professor Nicholas Dembsey, Advisor

_____
Professor David DiBiasio, Advisor

Abstract

The testing of Fiber Reinforced Polymers (FRP) is an essential building block to understanding the chemical and physical properties involved in their decomposition. The goal of this project was to evaluate the kinetic parameters of a specific resin and additive via micro-scale testing and model their micro-scale decomposition using the fire pyrolysis program, Gpyro. Samples of different resin-additive ratios were evaluated using Thermogravimetric Analysis (TGA) and Differential Scanning Calorimetry (DSC). These data were used to determine kinetic parameters of the resin and additive based on optimization of standard 0D models. To check the validity of these 0D models, thermal lag analysis was conducted and the model Gpyro was used to conduct 1D simulations of TGA specimens. The resultant kinetic parameters will be discussed in the context of the thermal lag analysis and the results of the 1D simulation. The applicability of using the kinetic parameters for general pyrolysis simulation of FRP using models like Gpyro will be discussed.

Acknowledgments

Authorship

Section	Author
Introduction and Background	Zachary Stewart
Experimental Methods	Krista Anderson
Thermal Lag	Shuyang Wang
Gpyro Modeling	Krista Anderson
Isoconversional Method	Victoria Grimes
Optimized Parameters	Victoria Grimes
Heat of Decomposition	Zachary Stewart
Conclusion	Krista Anderson

Table of Contents

Table of Figures

Table of Tables

Chapter 1: Introduction and Background

Fiber-Reinforced Polymers (FRPs) are integral building materials due to their durability and low cost [1]. However, the material must be able to meet certain fire safety standards. It is difficult to reach these standards due to the availability of the FRP and the costs required to conduct large-scale fire testing. Decomposition properties and kinetic parameters can be studied to help test these materials for fire safety requirements.

This project focused on micro-scale testing. It is a more cost effective way of gathering information to analyze materials. The testing equipment included the Differential Scanning Calorimeter (DSC) and Thermogravimetric Analysis (TGA). The data gathered from these two machines was mathematically analyzed for kinetic parameters including the activation energy and heat of decomposition. Simulations were done in Gpyro, a pyrolysis modeling software, in order to determine the program's applicability in modeling kinetic parameters.

As the study on FRPs continued, it became apparent that thermal lag was present in the devices used. Thermal lag is when the temperature the machine reports from the thermocouple does not match the actual sample temperature due to thermal resistance [2]. A thorough investigation on thermal lag is discussed in this report.

These different facets of research were chosen to be analyzed because these are the first steps in modeling materials for kinetic parameters in modeling software. After years of extensive research, the hope is that materials like a FRP would pass a fire test without extensive large scale testing. With more time and study, this advancement could revolutionize the way buildings adhere to fire safety standards.

Objectives

1. Determine kinetic parameters including the activation energy and heat of decomposition using proposed mathematical analyses, and determine the accuracy of these methods for the Epoxy and Additive mixture

2. Study more about how samples behave in the TGA by studying 0D, quasi-0D, and 1D analysis

3. Further study the thermal resistance limitations of the TGA and DSC by characterizing aspects of thermal lag.

4. Determine whether a computational pyrolysis program (Gpyro) can accurately model results obtained from the TGA.

Chapter 2: Experimental Methods

Thermogravimetric Analysis (TGA)

The TGA is an essential tool that is used to characterize materials. The amount of mass lost as the sample is heated is monitored throughout the test as a function of either time or temperature using a precise balance pan [3]. The test takes place in a furnace that encloses the sample. A thermocouple is placed inside the furnace to record temperature, which is assumed to be the temperature of the sample. The sample tested must be in the rage of 1-10 mg to obtain accurate results [4]. Well known samples like PMMA were first tested to establish correct testing procedures, and the ASTM D3850-12 was followed to help develop a consistent testing procedure. For the complete testing procedure, refer to Appendix C.

Differential Scanning Calorimetry (DSC)

The DSC measures the heat absorption of a material as a function of temperature and time [5]. There are two enclosed pans in the DSC; one is an empty reference pan, and the other pan holds the sample. The difference in heat absorption is measured between the two pans. The DSC works with samples that are 1-5 mg. The DSC was calibrated between tests by running baseline and cell constant calibrations. ASTM D7426-08 was consulted and a consistent testing procedure was developed. For the complete testing procedure, refer to Appendix D.

Samples

Samples were provided by Kreysler & Associates. The details of the samples can be seen in Table 1 below. The samples include an Epoxy resin with varying levels of ATH, and a sample of Fireblock. The samples were solidified drops that ranged from 1-10mg each, which is why different sizes are accounted for in the subsequent simulations.

Table 1: Materials for Testing

Material
Epoxy (Neat)
Epoxy + 5% ATH
Epoxy + 10% ATH
Epoxy + 20% ATH
Fireblock

Chapter 3: Thermal Lag

Limitations in the TGA and DSC are characterized by the presence of thermal lag. The furnace is designed to heat the gas flow at a constant rate, and a thermocouple is placed in the furnace to estimate and record the sample temperature. Thermal lag is the difference between the sample temperature and the gas temperature [6]. In order to better understand thermal lag, simulations were done using the data provided by the TGA to study the thermal lag time. There are three types of thermal lag discussed in this study: machine, diffusive and combined thermal lag.

Ideal Lumped Sample (Machine Thermal Lag)

It is assumed that the material is an ideal lumped sample [7]. For this case, there is convection resistance to heat transfer between the surrounding environment and the material. The heat transfer coefficient varies in this example. The rate of convection heat transfer between the body and its environment can be determined from Newton's law of cooling:

$$\rho V C \left(\frac{dT}{dt}\right) = h * A(T_{\bowtie} - Ti) \qquad (1)$$

$T_{\bowtie}$: The temperature of gas blowing (ambient temperature)

Ti: The initial temperature

Quasi-Lumped Sample (Diffusive Thermal Lag)

Diffusive thermal lag is when it is assumed that the heating through the sample is Quasi-lumped. The heating process requires transferring heat from the surface of the object to the center. In this example, there is conduction resistance in the sample. The conduction thermal resistance is expressed below.

$$R_{cond} = \frac{L_c}{A_c * k} \qquad (2)$$

The rate of conduction heat transfer existing in the body can be expressed as:

$$\rho V C \left(\frac{dT}{dt}\right) = \frac{A_c * k}{L_c}(T_{\bowtie} - Ti) \qquad (3)$$

Combined Resistance (Combined Thermal Lag)

Convection resistance (R_h) and conduction resistance(R_c) are added together for combined thermal lag [8].

$$\sum R = R_c + R_h = \frac{L}{Ak} + \frac{1}{Ah} \qquad (4)$$

The rate of the combined resistances to heat transfer can be expressed as:

$$\rho V C \left(\frac{dT}{dt}\right) = \left(\frac{L}{Ak} + \frac{1}{Ah}\right)^{-1} (T_\bowtie - Ti) \qquad (5)$$

Characteristic Time

Characteristic time (t_c) is the measurement of change. Equations 6, 7, and 8 below are for t_c and incorporate different resistances. The equations for t_c are replaced in equations 1, 3, and 5 for each type of thermal lag.

$$Machine\ thermal\ lag: \qquad t_c = \left(\frac{h}{2\rho Lc}\right)^{-1} s \qquad (6)$$

$$Diffusive\ thermal\ lag: \qquad t_c = \left(\frac{k}{2\rho L^2 c}\right)^{-1} s \qquad (7)$$

$$Combined\ thermal\ lag: \qquad t_c = \left(\left(\frac{L}{Ak} + \frac{1}{Ah}\right)^{-1} \frac{1}{\rho V c}\right)^{-1} s \qquad (8)$$

Parameters Chosen for Thermal Lag Simulation

The simulation below was done using data provided by the TGA for Epoxy + 5% ATH at a heating rate (β) of 10 C/min.

Table 2: Data for Thermal Lag Simulations

Parameter	Chosen Value	Source
Average Density [ρ]	1060.85(kg/m^3)	-
Thermal Conductivity [k]	0.23(W/m*K)	[9]
Specific Heat Capacity [C]	1400(J/kg* K)	[9]
Heat Transfer Coefficient [h]	5 to 20 (W/m^2*K)	10, 15, and 20 W/m^2*K [10] [11] [12] [13] [14] [15]
Radius [L]	0.5 to 2(mm)	0.75, 1 and 1.45 mm are chosen from drop measurement
The initial temperature [T_0]	31°C	-

To calculate an accurate density, the drop is assumed to be an ellipsoid. The equation of volume for one drop is shown below. L1 is the long radius, L2 is the short radius, and h is the height:

$$V = \left(\frac{1}{2} * \frac{4}{3} * \pi * (L1 * L2 * h)\right) * \frac{1}{2} \qquad (9)$$

The surface area of one drop is assumed to be the surface area of a half sphere:

$$A = 0.5 * (4 * 3.14 * R^2) + 3.14 * R^2 \qquad (10)$$

Exact Solution

The exact solution for actual sample temperature is calculated by using the first order linear ordinary differential equation method [16]. Equations 1, 3, and 5 are rewritten as equation 11 below in terms of t_c. β is the heating rate, and t_c is the characteristic time. T infinity is a function of time, which is expressed as $T_\infty = T_0 + \beta t$.

$$\frac{dT}{dt} = t_c(T_0 + \beta t - Ti) \qquad (11)$$

Equation 11 is solved using ODE to get the actual sample temperature. The exact solution is shown below. Equations regarding t_c (6, 7, and 8) are replaced for each type of thermal lag. The solution shown in equation 12 is then graphed to investigate the thermal lag time.

$$T(x) = \left(T_0 + \beta x - \frac{\beta}{t_c}\right) - e^{-t_c x}\left(-\frac{\beta}{t_c}\right) \qquad (12)$$

The case of diffusive thermal lag is shown below. Different radii are used in the analysis. From Table 3, it can be seen that as the radius gets larger, t_c and the lag time also get larger. The lag time can be expressed in terms of t_c to document the rate at which the lag time changes.

Table 3: Radius, tc and Lag time for Diffusive Thermal Lag (Conduction Resistance)

L [mm]	t_c [min]	Lag time	Lag time [min]
0.75	0.12	5.1*t_c	0.62
1	0.24	5.2*t_c	1.2
1.45	0.45	5.3*t_c	2.4
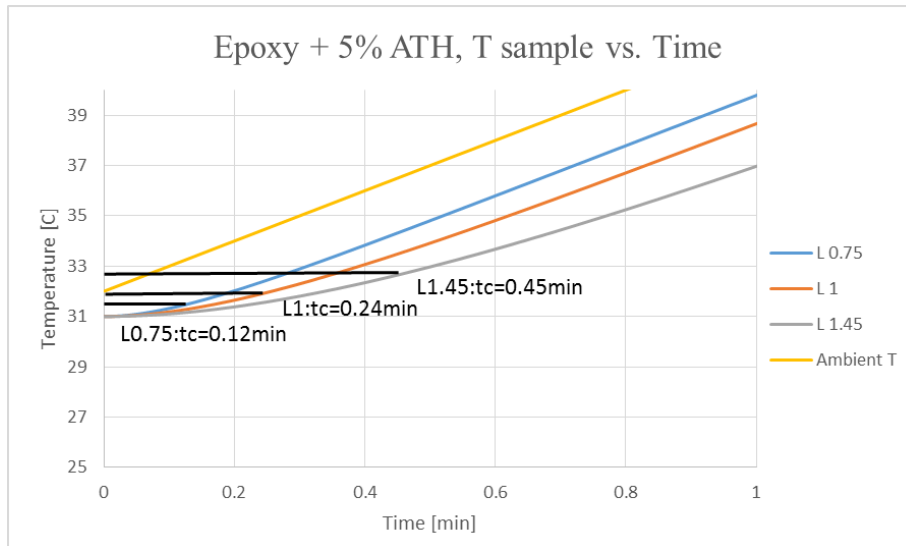
Figure 1: Characteristic time of Diffusive Thermal Lag using different radius
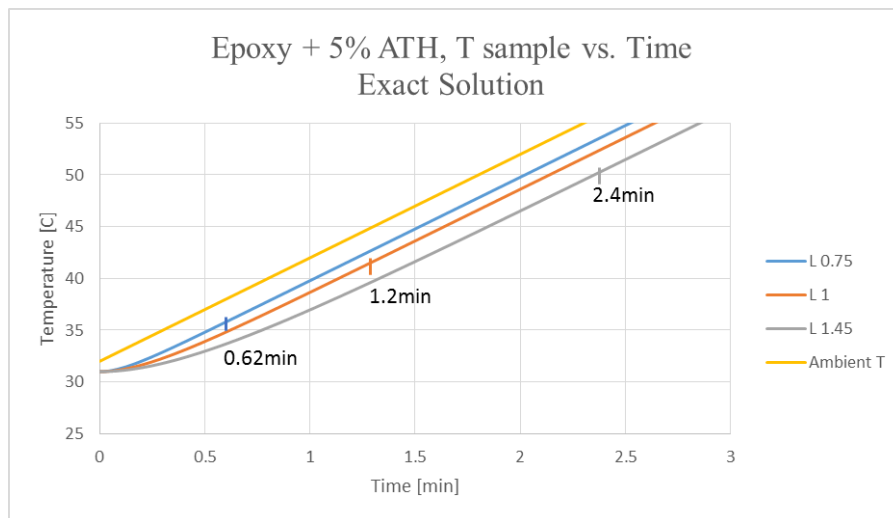
Figure 2: Lag time of Diffusive Thermal Lag using different radii

The relationship between ambient temperature and the sample temperature can be seen in Figure 1. As the radius gets smaller, the actual sample temperature gets closer to the ambient temperature. The temperature difference between the gas and the material is around 1C to 6C as time increases as radius increases. Both t_c and lag time are marked on the diagram. Lag time is the time at which the rate of change of the sample temperature becomes constant. It is 1min to 3min for diffusive thermal lag. The lag time is about five times t_c. Although the diffusive thermal lag was used as an example, the results for machine and combined thermal lag are shown in Tables 4 and 5.

Table 4: Heat Transfer Coefficient, tc, and Lag time for Machine Thermal Lag (Convection Resistance)

h[W/m^{2*}K]	t_c[min]	Lag time	Lag time [min]
10	0.84	6.1*t_c	5.2
15	0.56	6.1*t_c	3.4
20	0.42	6.2*t_c	2.6

From Table 4, as h gets larger, t_c and the lag time gets smaller. The lag time is six times t_c. The machine lag time is 3min to 5min. The temperature difference between gas and the material is around 5C, 7C and 9C for each h values.

Table 5: L+h, tc, and Lag time for Combined Thermal Lag (Both Resistance)

L[mm]+h[W/m^{2}*K]	t_c[min]	Lag time	Lag time [min]
0.75+20	0.83	6.8*t_c	5.4
1+20	0.84	6.9*t_c	5.8
1.45+20	0.85	6.9*t_c	5.9

For the combined thermal lag, the heat transfer coefficient is equal to 20 W/m^{2*}K and the radius of the sample is varied. Table 5 shows the characteristic time is around 0.8min. The lag time is about seven times t_c and is 5min to 6min. The difference between the ambient temperature and the sample temperature is 12C to 13C. Full solutions for machine and combined thermal lag can be seen in Appendix J.
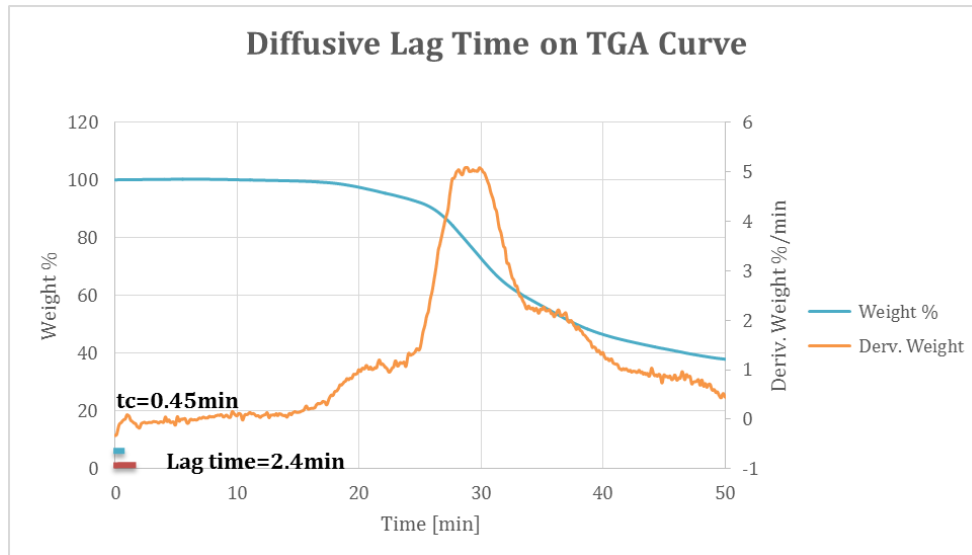
Figure 3: The longest diffusive thermal lag time and characteristic time marked on TGA Curve

The lag time is marked on the TGA results in Figure 3. The red bar shows the longest lag time that allows the sample temperature to go to quasi steady state. The next step would be determining how much thermal lag effects TGA results. There are similar results when looking at machine and combined thermal lag. Full results can be found in Appendix J.

Chapter 4: Gpyro Modeling

Gpyro is a pyrolysis program that was studied to model Mass Loss Rate (MLR) curves and better understand data from the TGA. Due to lack of Epoxy details, previous work using Hetron and ATH was used for the Gpyro modeling [17]. The simulations were completed based on the following assumptions:

- Behavior is one-dimensional
- Each species has its own set of material properties, including thermal conductivity, density, specific heat capacity, and emissivity
- Two reactions are occurring, each with its own activation energy, pre-exponential factor, change in enthalpy, and n-value
- No volume change occurs (charring material)
- No re-radiation occurs into the material and there is no contact conductance

Governing Equations

Below are some of the governing equations Gpyro uses for a 1D simulation for a constant volume.

Condensed-Phase Mass Conservation:
$$\frac{\partial \bar{\rho}}{\partial t} = -\dot{\omega}''' \quad (13)$$

    ρ: Density (kg/m^3)

    t: time (min)

    ω: Volumetric reaction rate (kg/m^3*s)

Condensed-Phase Species Conservation:
$$\frac{\partial (\bar{\rho} Y_i)}{\partial t} = \dot{\omega}'''_{fi} - \dot{\omega}'''_{di} \quad (14)$$

    ρ: Density (kg/m^3)

    Y: Mass Fraction

    t: time (min)

    ω: Volumetric reaction rate (kg/m^3*s)

Gpyro uses the following equation, assuming a single-step, nth order reaction, as a starting point:

$$\frac{d\alpha_o}{dt} = Z \exp\left(-\frac{E}{RT}\right)(1 - \alpha_o)^n \quad (15)$$

    α_o: Conversion (1-m/m_o)

t: time (min)

Z: Pre-exponential Factor (1/s)

E: Activation Energy (kJ/mol)

R = Ideal gas constant (0.008314 kJ/mol*K)

T: Initial Temperature (K)

n: Exponent

The above equation is manipulated to account for multiple reactions, and can be seen in the equation below, with the same variables as seen in equation 14 and 15:

$$\dot{\omega}''' = (1 - \alpha_o)^n \frac{(\overline{\rho} Y \Delta z)}{\Delta z} Z \exp\left(-\frac{E}{RT}\right) (16)$$

Input Parameters and Calculations

Tables 6-8 below show some of the properties inputted into Gpyro for the simulations. Hetron is used for the resin [9], and ATH is used for the additive [17].

Table 6: Material Properties for Gpyro

	k [W/m*K]	ρ [kg/m^3]	c [J/kg*K]	ε [-]
Hetron	0.23	1200	1400	0.84
Hetron Residue	0.19	253	1900	0.9
ATH	1.22	2300	1200	0.81
ATH Residue	0.24	1558	1200	0.89

Table 7: Reaction Properties for Gpyro

	Z [s^-1]	E [kJ/mol]	ΔH [J/kg]	n [-]
Hetron -> Hetron Residue	5*10^13	195	1.72*10^5	1.125
ATH -> ATH Residue	2.5*10^11	140.1	1*10^6	1.24

Table 8: Boundary Conditions for Gpyro

BC	q_e [W/m^2]	h_c [W/m^2*K]	T_{ab} [K]	Re-Radiation?
1	500 (Varies)	0	300	False

Heat flux values were calculated using conditions typically found in the TGA, and the values were subsequently used to determine the heating rate, using the equation for the exposed face boundary condition and temperature equation.

$$-k\frac{\partial T}{\partial z} = \varepsilon\dot{q}_e'' - h_c(T - T_\infty) - \varepsilon\sigma(T^4 - T_\infty^4) \qquad (17)$$

$$T = T_0 + \beta t \qquad (18)$$

With equation 17, the exposed face boundary condition, the cooling convection is set to zero and the re-radiation is turned off, which sets the middle and far right hand side of the equation to zero. When the re-radiation is turned on, re-radiation occurs at the exposed surface of the material, and heat is lost from the sample to the ambient surroundings. Having a contact conductance of zero at the unexposed face implies that the boundary condition is fully insulated. Also, with a charring material, there is no change in cell size (z). This means the only variable affecting the change in temperature is the heat flux, which is what allows it to be used to calculate the heating rate. Once heat flux values were determined, they were run in Gpyro to get histories for temperature (T) and time (t). These values were put into equation 18 to determine the heating rate (β). See Appendix E.9 and E.10 for full details regarding heat flux values used in Gpyro and heating rate calculations.

Simulations

Simulations were done in Gpyro for the Hetron with various levels of ATH, and can be seen in Table 9 below.

Table 9: Material Simulations for Gpyro

Material
Hetron +5% ATH
Hetron+ 25% ATH
Hetron + 40% ATH
Hetron + 50% ATH
Hetron + 57% ATH

The results discussed in this paper will be for Hetron + 25% ATH. Full results can be found in Appendix E. Figure 4 below shows MLR curves for TGA data and the Gpyro simulations for Hetron + 25% ATH. The TGA data is listed as heating rates and the Gpyro simulations are listed

as heat flux values, which provided a heating rate of +/- 5 degrees of the actual TGA heating rate.
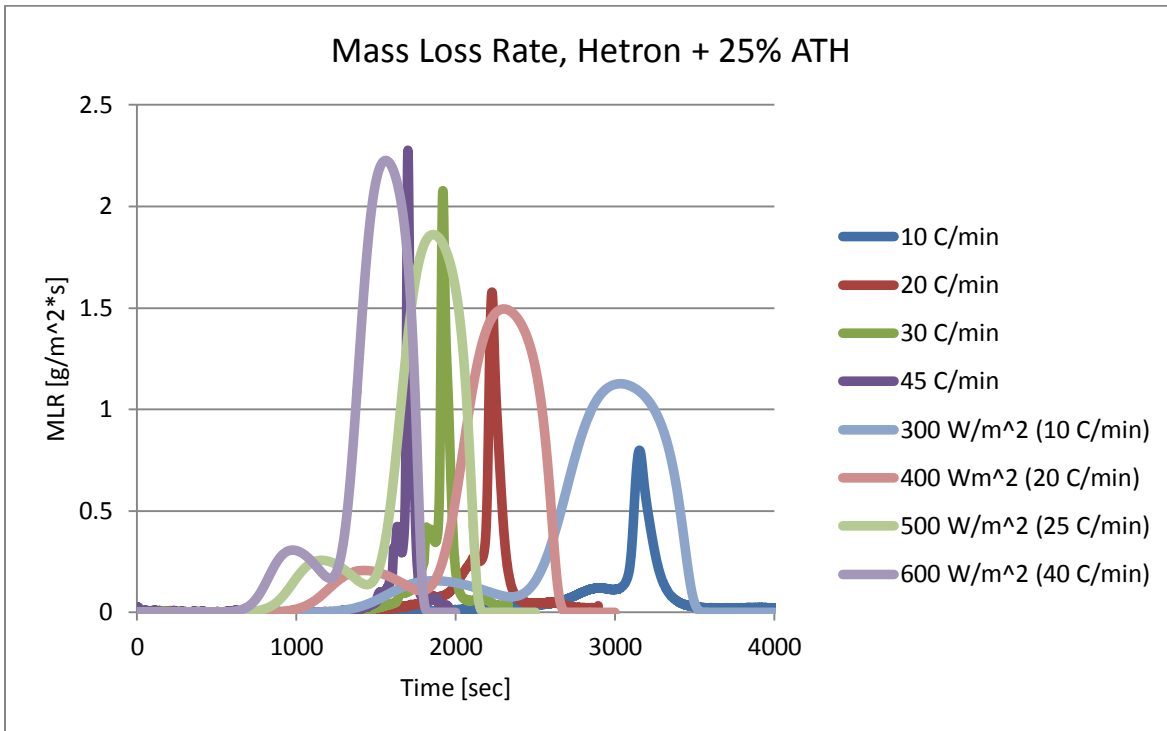
Figure 4: Mass Loss Rate, Hetron + 25% ATH Gpyro Simulation with TGA Data

It can be seen on Figure 4 that both peaks on the Gpyro simulation fall within a half order of magnitude of the TGA data, but that the timeframe is off, particularly for the first peak. The second peak matched the timeframe well. To better understand why the timeframe is off, Hetron + 25% ATH data was taken for two heating rates, 10 C/min and 30 C/min, and the MLR was graphed in terms of time and temperature. An ideal mixing model simulation was also completed and graphed along with the TGA data and the Gpyro simulation. With the ideal mixing model, the two peaks found on the MLR curve are each taken to be a single independent reaction, one for ATH and one for Hetron, using their optimized parameters. The peaks are modeled in an additive approach where they are proportioned in respect to the amount found in the mixture, using the equations below [17].

$$\alpha_{total}(t) = f_1 r_1 \alpha_{o,1} + f_2 r_2 \alpha_{o,2} \qquad (19)$$

$$f_n r_n = Z_n \qquad (20)$$

The weight-loss fractions (f1=0.13, f2=0.56) are taken for pure Hetron and pure ATH and multiplied by their mixture proportion (r1=0.25, r2=0.75). Alpha was calculated at each time step for equation 19. A scaling constant must be used, which for each particular mixture is the weight-loss fraction multiplied by the mixture proportion in equation 20. Full details on the ideal mixing model used can be found in Appendix E.12.

The same input parameters that were applied to the Gpyro model were applied to the ideal mixing model. The ideal mixing model simulated values for the actual material sample as opposed to the TGA furnace. This helps in the comparison between the actual sample temperature and the TGA furnace temperature. The results can be seen in the Figure 5 below.
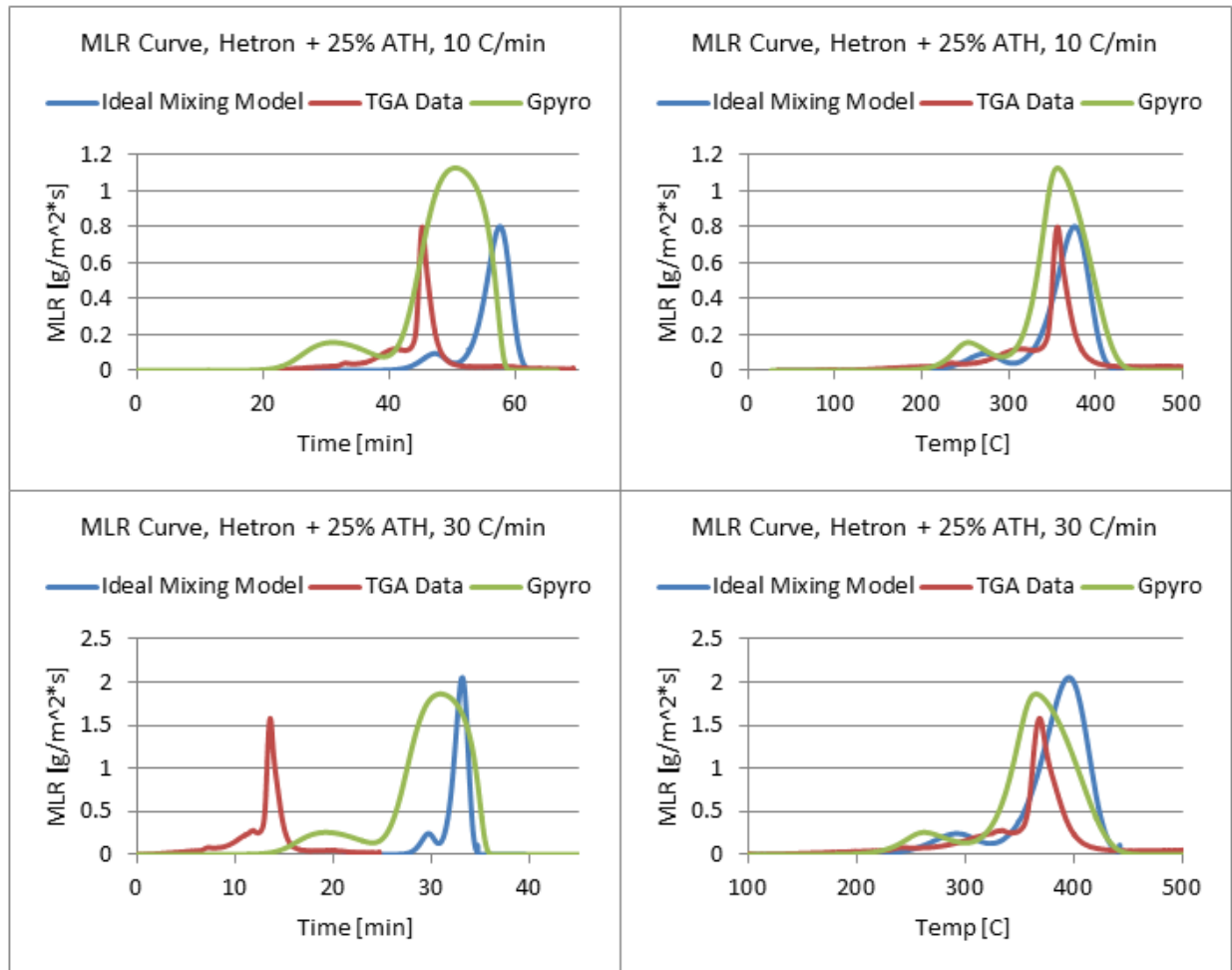
Figure 5: Gpyro vs Ideal Mixing Model vs TGA Data

From Figure 5 above, there are a few important aspects to note. First, there is a significant lag in the time graph when looking at the TGA data, but not as much lag in the temperature graph. This

can be seen for both heating rates. This could be suggesting that the sample temperature is deviating greatly from the TGA furnace temperature due to the energy required for decomposition of the sample. Second, at a lower heating rate, there is less of a lag, which is consistent with other research [18][19][20][21]. It should also be noted that when using Gpyro inputs in the ideal mixing model, the ideal mixing model and Gpyro model track each other well. There is only a small lag when looking at the two different peaks, and the peaks magnitudes match well.

It was also important to look at a chart of time vs temperature for the different samples to better model the lag that is shown in the previous figures. These can be seen in Figure 6 below.
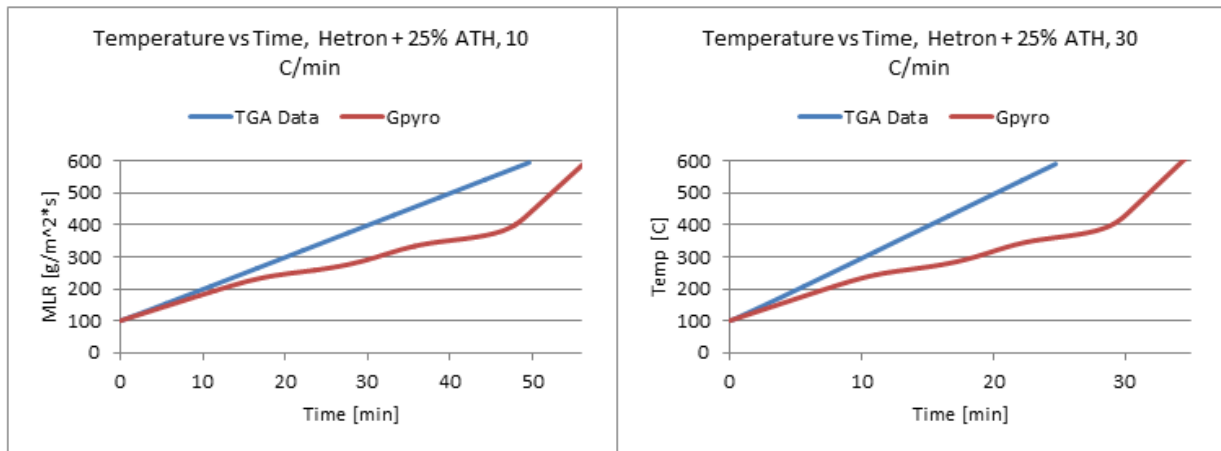
Figure 6: Temperature Lag in Gpyro

The two graphs further show the temperature lag that shows up in the MLR vs time curves in Figure 5. The heating rate of 10 C/min shows a lag of about 5 minutes, while the heating rate of 30 C/min shows a lag of about 10 minutes. Even though the Gpyro simulations show a smaller lag with a lower heating rate, it is still suggesting a fairly large time lag which potentially could be affecting TGA data significantly. This is consistent with other research [18][19][20][21].

Chapter 5: Kinetic Modeling

Kinetic modeling was done on the Epoxy resin and ATH mixtures outlined in Chapter 2. Samples with 0%, 5%, 10%, and 20% added ATH were tested. Any results referenced for pure ATH were done on previously tested data [17]. This section will provide data on the specific analysis methods used and discuss trends in our TGA results.

Below is a typical representation of our data for each material at the heating rates of 10 C/min and 30 C/min.
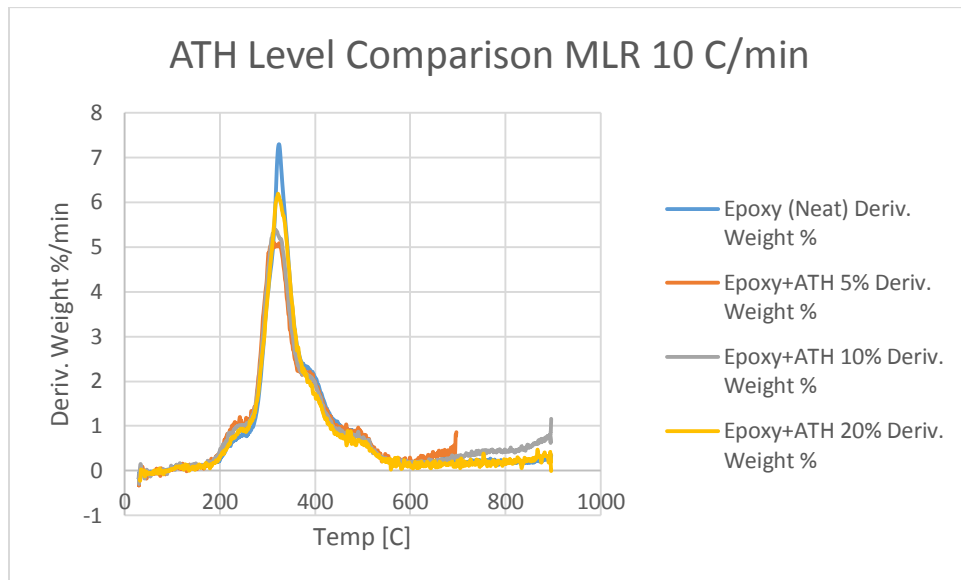
Figure 7: ATH Level Comparison MLR 10 C/min
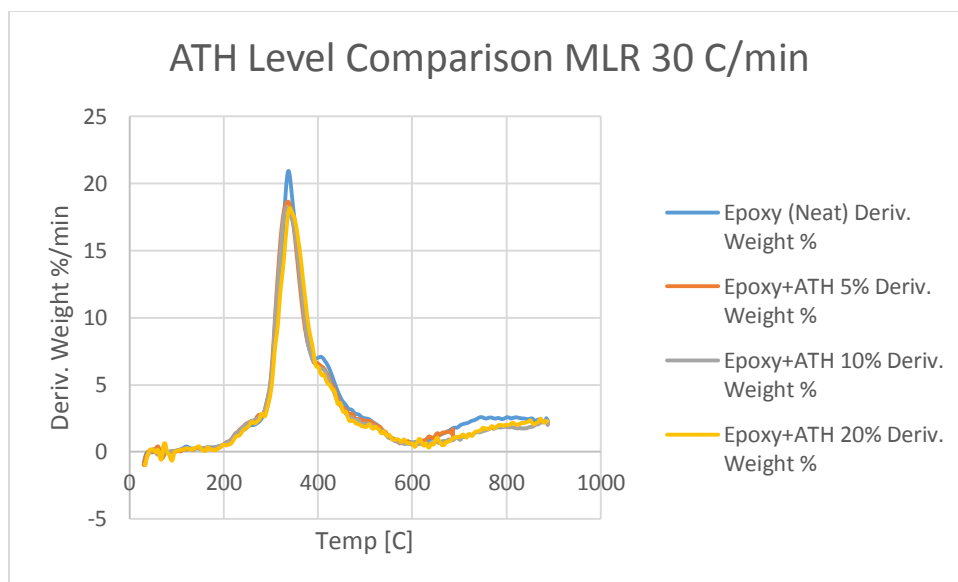
Figure 8: ATH Level Comparison MLR 30 C/min

These mass loss rate curves are shown for both 10 C/min and 30 C/min to cover a wide range of heating rates. Each graph shows one main peak around 350 C and several other smaller ridges on either side of the peak. When the ATH level increases, the height of the peak shows a small increase, but the temperature at which the material peaks remains the same. With the higher heating rate there is less of a difference in the peak heights. From this data, the activation energy for the sample, the pre-exponential factor, A, and exponent, n, from the kinetic model can be determined.

Isoconversional Method

The use of an isoconversional method is beneficial for determining the activation energy from TGA data. Because kinetic models are so complex in nature, it is beneficial to simplify them as much as possible and assume a one-step reaction [9], which is what the isoconversional method is based off. The isoconversional method associates the main peak on a MLR curve with constant activation energy over the entire range of conversion [22]. The isoconversional method chosen was the Ozawa, Flynn, and Wall method (OFW). This method uses data from four heating rates, which increases the accuracy of the results. It was chosen because it is a simple model to use and is a validated approach in literature [23]. The activation energies at each conversion value should be constant based off of the main peak in the MLR curve, and an average can be taken over the length of the entire reaction. For the complete isoconversional method including the mathematical approach, see Appendix F.1.

Activation Energy Results

The activation energy for each material was determined based off of an average of the activation energies over the Epoxy resin's range of decomposition, which is approximately from $\alpha_1 = 0.5$ to 0.9, where α_1 is defined in terms of the initial and final masses; $\alpha_1 = \frac{m_o - m}{m_o - m_f}$. Figure 9 below shows the range of activation energies for Epoxy plus 5% ATH.
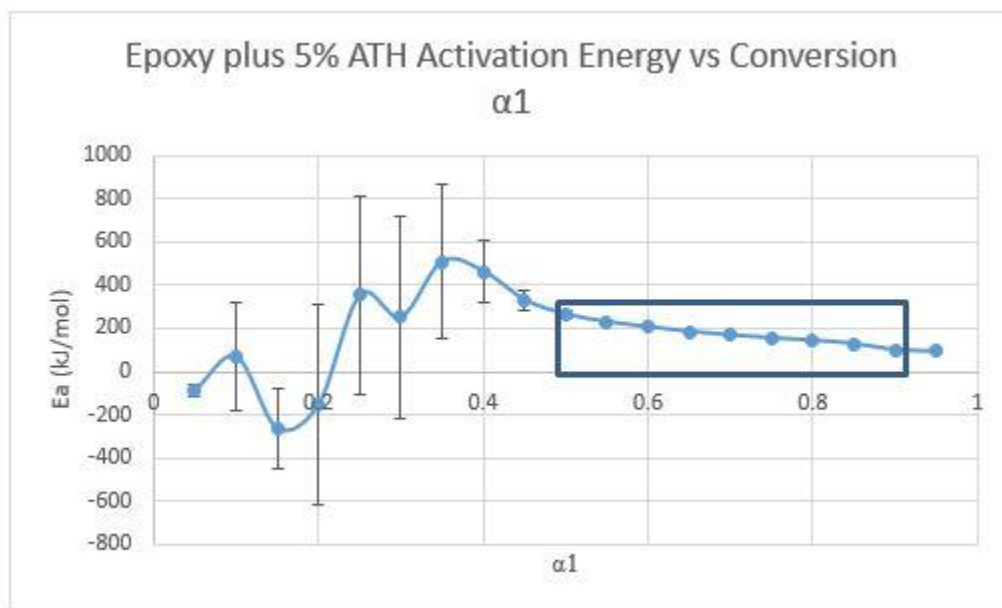
Figure 9: Activation Energy vs Conversion (Epoxy + 5% ATH)

The activation energies within the range of conversion (outlined in the blue box) are relatively constant, which is consistent with the isoconversional method. However, the activation energies at the lower conversion values fluctuate drastically, suggesting a multi-step reaction. After looking at literature data on this subject, it was found that variation in activation energies for solid-state kinetics is common [24]. When using isoconversional methods the variation in activation energy is the largest source of error. Solid-state decompositions mainly decomposes in two or more reaction steps, which would make the isoconversional method inconsistent for solid-state decomposition. Epoxy materials range anywhere from two or more reactions, which would explain why the isoconversional method is inaccurate [25] [26] [27]. Although Epoxy plus 5% ATH was used as an example, it is relevant to study all materials in this way to examine their consistency with this theory. Figures 10, 11, and 12 show activation energies over a range of conversion for Epoxy (Neat), Epoxy plus 10% ATH, and Epoxy plus 20% ATH.
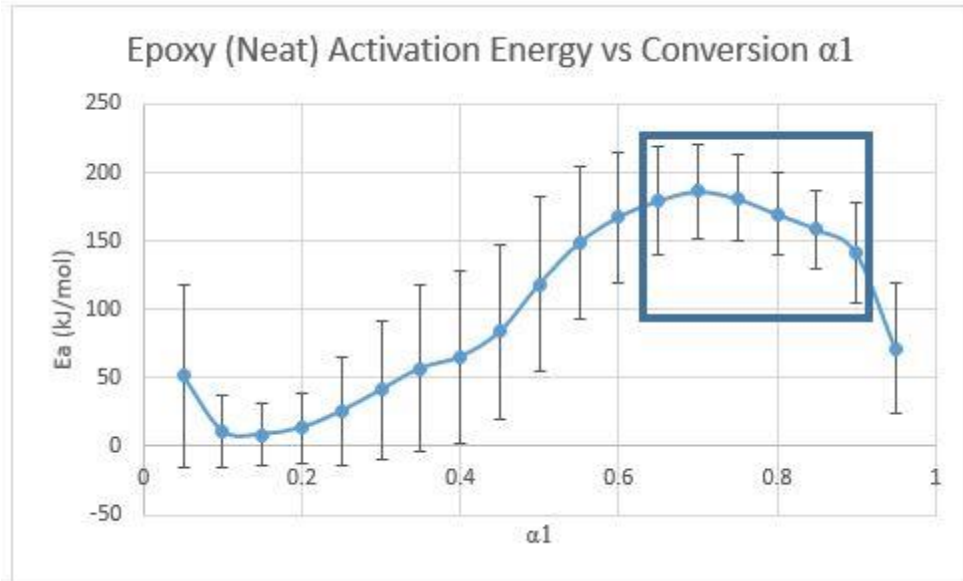
Figure 10: Epoxy (Neat) Activation Energy vs Conversion α1
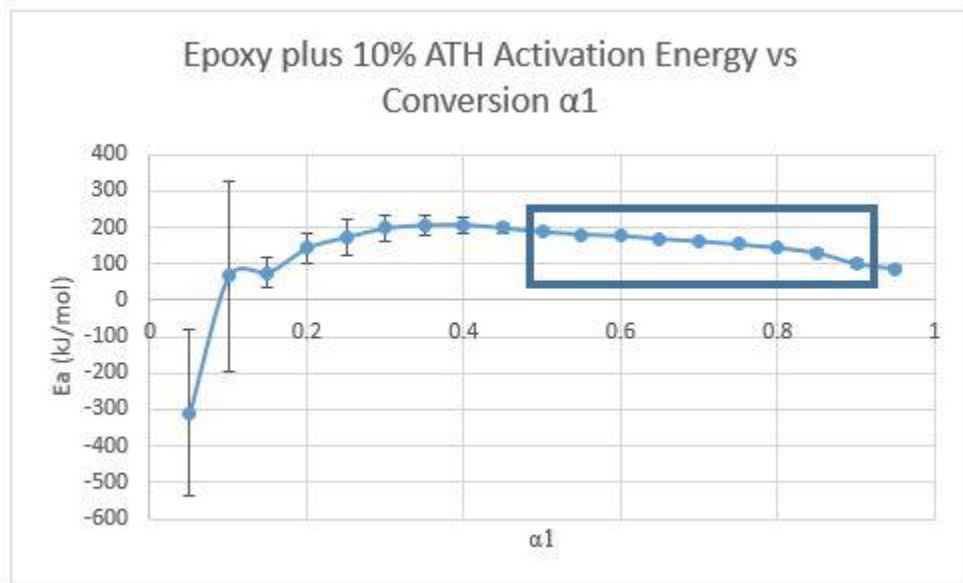
Figure 11: Epoxy plus 10% ATH Activation Energy vs Conversion α1
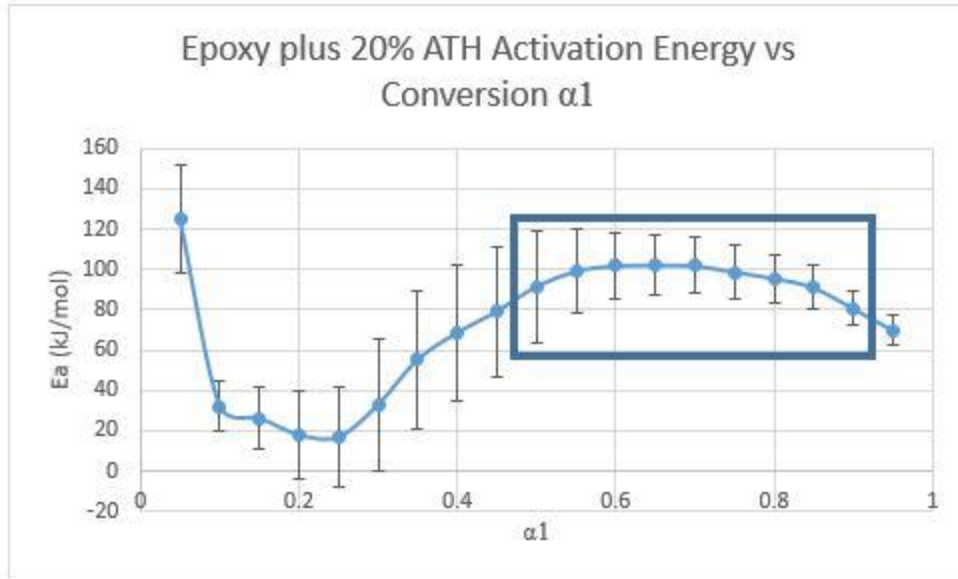
Figure 12: Epoxy plus 20% ATH Activation Energy vs Conversion α1

For each material, the conversion range from 0.5 to 0.9 is the most consistent section of the graph; however, the remaining sections vary drastically in activation energy. Epoxy plus 5% ATH and Epoxy plus 10% ATH have the most consistent results, seen by both the constant activation energy and the low error within the decomposition range. Epoxy (Neat) and Epoxy plus 20% ATH have higher errors, resulting in activation energies that start lower around 0.9 conversion, increase around 0.7, and decrease again around 0.5. There is no reason that is apparent as to why this error is occurring, thus the error could be explained by common testing errors and uncertainty. The total error for each material is displayed in Table 10 along with the results for the activation energies.

Table 10: Activation Energies for Epoxy Resin Mixture

Material	Activation Energy [kJ/mol]
Epoxy (Neat)	150 +/- 41
Epoxy plus 5% ATH	180 +/- 6
Epoxy plus 10% ATH	160 +/- 6
Epoxy plus 20% ATH	100 +/- 15
Pure ATH	150 +/- 12

Although we expect the activation energies to be consistent, there is a range of approximately 80 kJ/mol. Despite error values previously discussed, this is still a wide range. This would lead us to conclude that the Epoxy resin is not a one-step reaction, and a different method of evaluating the activation energy is needed for such a material.

Optimized Parameters

In order to model mixtures, the Runge-Kutta 4th Order Method (RK4) was used to simulate the kinetic model for our data (Appendix F.2). Two main equations were applied to each material, assuming a one-step reaction.

$$\frac{d(1-\alpha_1)(t)}{dt} = A exp\left(-\frac{E_a}{RT(t)}\right)(1 - \alpha_1(t))^n \qquad (21)$$

$$\frac{dT(t)}{dt} = \beta \qquad (22)$$

Equation 21 represents the kinetic model, and Equation 22 represents the heating rate. The kinetic model used is partially derived from the Arrhenius equation, representing the rate constant, and involves an nth order kinetic model. This model was chosen following Esther Kim's theory of simplicity [9]. These two equations can be combined to form the main equation used when modeling our materials.

$$\frac{d(1-\alpha_1)}{dt} = \left[A exp\left(-\frac{E_a}{R(T_o+\beta*t)}\right)\right](1 - \alpha_1)^n \qquad (23)$$

Where: $\alpha_1 = \frac{m_o - m}{m_o - m_f}$,

   T_o = Initial temperature (K)

   t = Time (min)

   β = Heating rate (C/min)

   E_a = Activation energy (kJ/mol)

   R = Ideal gas constant (0.008314 kJ/molK)

   A = Pre-exponential constant

   m = Mass of the sample (mg)

   m_o = Initial mass of the sample (mg)

   n = Exponent

The values of A and n were changed to fit the simulated model to the experimental data. In this model, the activation energy previously found via the isoconversional method was used as a constant throughout the data for all four heating rates to minimize the amount of error associated with the process. A weighted error scheme was used to minimize the error between the experimental and simulated curves for each of the heating rates, and values for A and n were found for each material. Figures 13 and 14 are examples of the results of this modeling process.
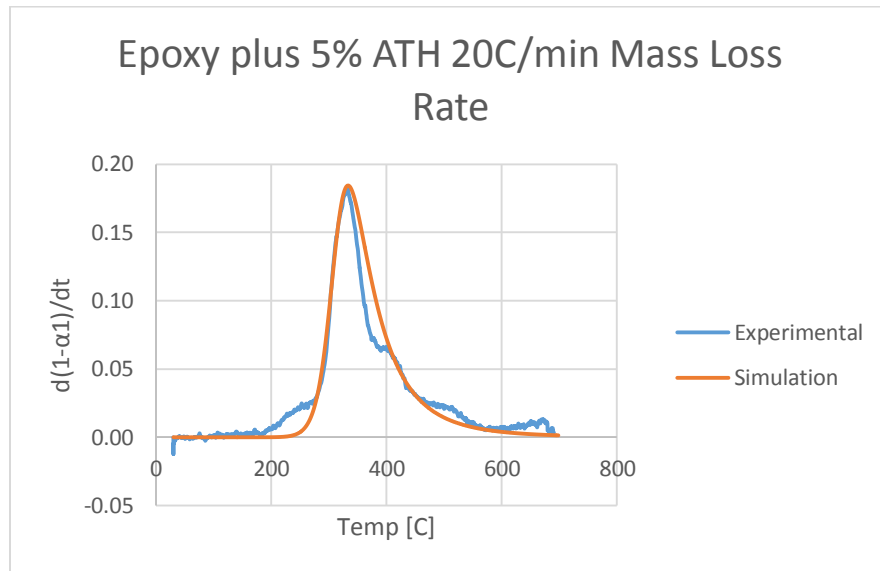
Figure 13: Epoxy plus 5% ATH Model MLR Curve
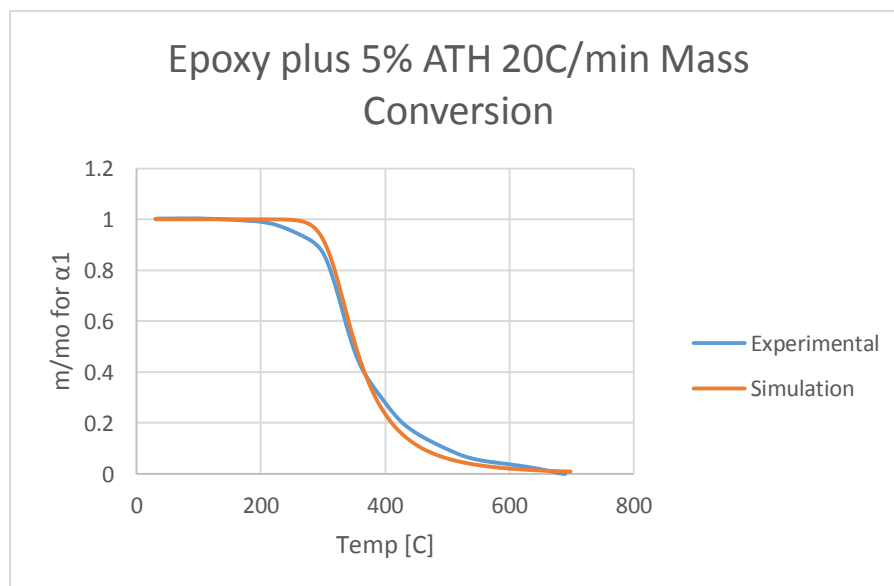
Figure 14: Epoxy plus 5% ATH Model Mass Conversion Curve

Figures 13 and 14 show the simulated model fitting well with the experimental results; however this method is not a perfect match. In the MLR curve for Epoxy plus 5% ATH the simulated curve does not accurately model the ridges to the right and left of the main peak. This is a result of the inconsistent activation energies because of the compensation effect between the activation energy and the values for A and n. If the value for the activation energy is not accurate, the values for A and n will also be inaccurate as they adjust themselves to fit the simulated curve to the experimental data. Table 11 is a summary of the optimized parameters determined for each material.

Table 11: Optimized Parameters for Epoxy Resin Mixture

Material	Activation Energy and Associated Error [kJ/mol]	Pre-exponential Factor A	Exponent n
Epoxy (Neat)	151.4 +/- 41	$5.5*10^{12}$	3.3
Epoxy plus 5% ATH	176.6 +/- 6	$1.6*10^{15}$	4.2
Epoxy plus 10% ATH	156 +/- 6	$8.3*10^{13}$	4.75
Epoxy plus 20% ATH	95.8 +/- 15	$7.2*10^{7}$	2.0
Pure ATH	153.5 +/- 12	$1.97*10^{14}$	1.42

Although we were able to determine the values for A and n through the validated method of RK4 [9], these values should not be used without obtaining more accurate values of the activation energy. The values are specific to each material and do not represent characteristics of the Epoxy resin in total.

Heat of Decomposition (HoD)

Heat of Decomposition (HoD) is a thermodynamic property that was determined in order to further discover the kinetic parameters of Epoxy with various levels ATH. Fireblock, along with Epoxy (Neat), Epoxy + 5% ATH, Epoxy + 10% ATH, and Epoxy + 20% ATH was studied. Both the derivative weight curve from the TGA and the heat flow curve from the DSC were used in order to produce this analysis.

In order to find the HoD, the average DSC data for each material for 10 C/min was overlaid with the average TGA data for each material. The reaction can be seen by the spike in the TGA data. The start and end of the reaction are used as limits on the DSC curve. A line was created connecting the two limits, and the area between the line and the DSC curve was integrated via Riemann's sum, seen in equation 24 below.

$$S = \sum_{i=1}^{n}(f_i - g_i) * \Delta x \qquad (24)$$

The figure below shows the overlaid curves and the shaded reaction area. The first figure shows Fireblock which behaves typically under these conditions. Fireblock is shown as an example because it is a simple material and its behavior is consistent.
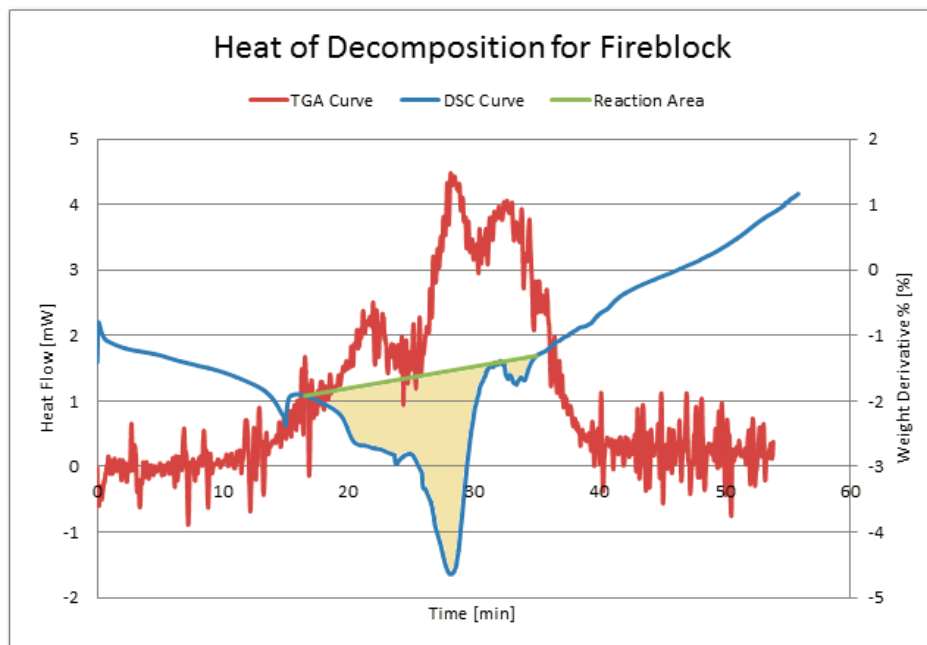
Figure 15: Heat of Decomposition for Fireblock

Figure 16 is the HoD for Epoxy + 5% ATH. This material is more complex than Fireblock, showing inconsistent curves when overlaid with the reaction. This proved to be difficult in analyzing results.
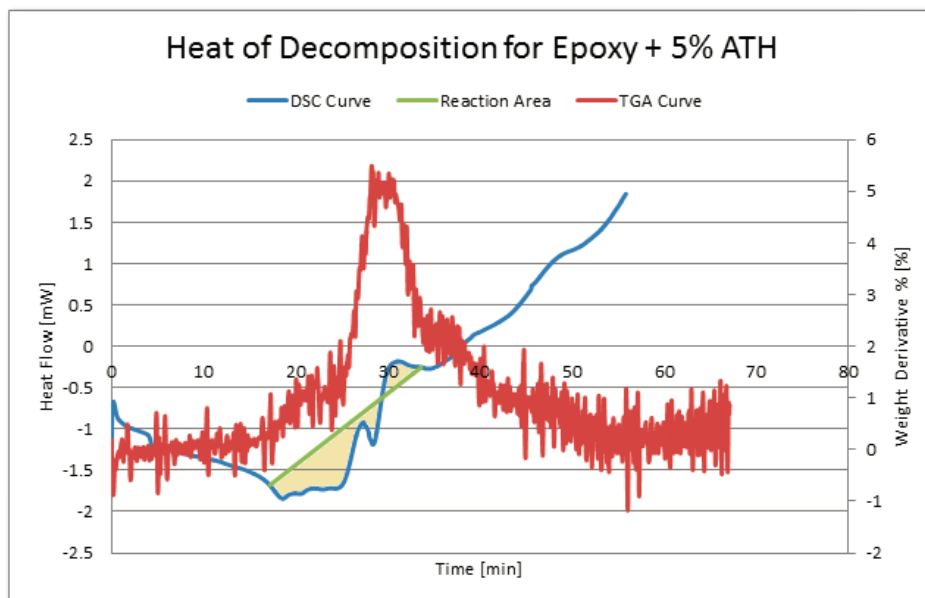
Figure 16: Heat of Decomposition for Epoxy + 5% ATH

The values of integration represent the HoD value. These results are seen in Table 12. Epoxy was a difficult substance to analyze, creating variation in the heat flow. This resulted in average TGA and DSC data that was much harder to fit into a practical and simple integration. Although the data was difficult to analyze, some conclusions can still be reached by these findings. As the amount of ATH increases so do the HoD values. This shows that as ATH is added to the Epoxy, the substance becomes more difficult to decompose.

Table 12: Heat of Decomposition

Material	Heat of Decomposition (kJ/g)
Fireblock	278.0
Epoxy (Neat)	973.4
Epoxy with 5% ATH	1061.4
Epoxy with 10% ATH	1173.9
Epoxy with 20% ATH	1218.1

Chapter 6: Conclusions

Conclusions were drawn regarding the Epoxy and ATH mixtures through testing, analyses, and simulations.

It was determined that the simplified kinetic model can be applied to the material studied, but there were limitations in regards to its accuracy. While the simplified model allowed a greater comprehension of the material, a more complex model might be better suited for this application, considering the possibility of multiple reactions. Through the study of Heat of Decomposition, it was seen that as the amount of ATH in a material is increased, more energy is required for it to decompose.

There were some important conclusions from the various simulations that were completed. The study on thermal lag proved its existence in instruments like the TGA and DSC. Gpyro showed that it can model TGA data fairly well in terms of magnitude and heating rate, but not as well in terms of timeframe, which could also be indicating a lag time. The ideal mixing model that was run using Gpyro data which matched well with the Gpyro curve. The simulation was done in terms of sample temperature as opposed to TGA furnace temperature.

It is recommended that there be further work regarding the use of a complex model for data simulations. A complex model would allow for more realistic results and provide more accurate data. A more accurate method should be developed for calculating HoD, as the current method includes large sources of user error. There needs to be continued work on the thermal lag model. Further study on the effects of thermal lag on experimental data will provide a greater understanding of how experimental results are affected, and in turn how kinetic properties are characterized. Gpyro should also continue to be analyzed in its ability to model experimental data.

References

[1] Bakis, C., Bank, L., Brown, V., Cosenza, E., Davalos, J., Lesko, J., Triantafillou, T. (n.d.). Fiber-Reinforced Polymer Composites for Construction—State-of-the-Art Review. Journal of Composites for Construction, 73-73.

[2] Comesaña, R., Gómez, M. A., Álvarez, M. A., & Eguía, P. (2012). Thermal lag analysis on a simulated TGA-DSC device. *Thermochimica Acta, 547*, 13-21. doi:10.1016/j.tca.2012.08.008

[3] PerkinElmer. (2010). Thermogravimetric Analysis (TGA). *A Beginner's Guide.* Product website. http://www.perkinelmer.com/CMSResources/Images/44-74556GDE_TGABeginnersGuide.pdf

[4] TA Instruments (2014). Thermogravimetric Analysis. Product website. http://www.tainstruments.com/product.aspx?siteid=11&id=11&n=1

[5] TA Instruments (2007). DSC Differential Scanning Calorimeter. Product website. http://nmtprg.weebly.com/uploads/3/1/1/0/31101989/ta_mdsc_manual.pdf

[6] Cassel, R. B, (2001) pp. 1-5."How TZero Technology Improves DSC Performance Part V: Reducing Thermal Lag," in TA Instruments Application Notes: Document. Reference TA283 Newcastel DE: TA Instruments

[7] Yunus & Afshin, (2015). Mcgraw-Hill Education. (n.d.). In (pp. 218-223). Chapter 4: Transient Heat Conduction

[8] Quattrochi, D & Spakovszky (2009), Z. (Eds.), *Thermodynamics and Propulsion*. Chapter16.4: Thermal Resistance Circuits. (n.d.). University of Leeds: Nikos Drakos.

[9] Kim, E., Dembsey, N. (2014). Parameter Estimation for Comprehensive Pyrolysis Modeling: Guidance and Critical Observations. *Fire Technology*, 5(2), 443-477.

[10] Lewis, R., Nithiarasu,P., & Seetharamu, K. (2004). Fundamentals of the Finite Element Method for Heat and Fluid Flow. John Wiley& Sons Ltd. Chichester, West Sussex, England.

[11] Oyedun, A.O., Gebreegziabher,T., & Hui, C.W., (2013). Co-Pyrolysis of Biomass and Plastics waste: A modeling Approach. *Chemical Engineering Transactions.* 35, 883-888.

[12] Kim, M., & Quintiere, J.G., (2007). Predicting Polymer Burning Using TGA/DSC. *Department of Fire Protection Engineering, University of Maryland, USA.*

[13] Lede, J., (2010). Biomass Pyrolysis: Comments on Some Sources of Confusion in the Definitions of Temperatures and Heating Rates. *Energies*, 3, 886-898.

[14] Lam, K.L., Oyedun, A.O., Hui, C.W., (2012). Experimental and Modeling Studies of Biomass Pyrolysis. *Chinese Journal of Chemical Engineering.* 20(3), 543-550.

[15] Comesana, R., Gomez, M.A., Alvarez, M.A., Eguia, P., (2012). Thermal Lag Analysis on a Simulated TGA-DSC Device. *Thermochimica Acta.* 547, 13-21.

[16] Arfken, G. (1985). Mathematical Methods for Physicists, 3rd ed. Orlando, FL: Academic Press, pp. 440-445

[17] Gillespie, B., Long, M., McMillan, N. & Walde, C. (2014). *Determining Limitations of Kinetic Models for Pyrolysis Simulation of Fiber Reinforced Polymer Composites.* (Undergraduate Major Qualifying Project).

[18] Cazes, J. (2004). *Analytical Instrumentation Handbook, Third Edition*. Boca Raton, FL: CRC Press.

[19] Kim, E., Dembsey, N. & Shivkumar, S., Evaluating effects of applying different kinetic models to pyrolysis modeling of fiberglass-reinforced polymer composites. *Fire and Materials,* 39(2), 153-173.

[20] Lautenberger, C. (2007). A Generalized Pyrolysis Model for Combustible Solids. (Doctoral dissertation).

[21] Narayan, R. & Antal, M.J. (1996). Thermal Lag, Fusion, and the Compensation Effect during Biomass Pyrolysis. *Industrial & Engineering Chemistry Research,* 35(5), 1711-1721.

[22] Khawam, A., & Flanagan, D. R., (2005), Role of isoconversional methods in varying activation energies of solid-state kinetics, I. isoconversional kinetic studies, *Thermochimica Acta, vol. 429 ,* 93–102.

[23] Sbirrazzuoli, N., Vincent, L., Mija, A., & Guigo, N., (2009), Integral, differential and advanced isoconversional methods; Complex mechanisms and isothermal predicted conversion-time curves, *Chemometrics and Intelligent Laboratory Systems, vol. 96,* 219-226.

[24] Vyazovkin, S., (2000), Kinetic concepts of thermally stimulated reactions in solids: A view from a historical perspective, International Reviews in Physical Chemistry, 19:1, 45-60.

[25] Dao, D. Q., Luche, J., Richard, F., Rogaume, T., Bourhy-Weber, C., Ruban, S., (2013), Determination of characteristic parameters for the thermal decomposition of epoxy resin/carbon fibre composites in cone calorimeter, *International Journal of Hydrogen Energy 38*, pg. 8167-8178.

[26] Liu, W., Varley, R. J., Simon, G. P., Understanding the decomposition and fire performance processes in phosphorus and nanomodified high performance epoxy resins and composites, (2007), *Polymer*, vol. 48, is. 8, pg. 2345-2354.

[27] Kandola, B. K., Biswas, B., Price, D., Horrocks, A. H., (February 2010), Studies on the effect of different levels of toughener and flame retardants on thermal stability of epoxy resin, *Polymer Degradation and Stability*, vol. 95, is. 2, pg. 144-152.

Appendix

Authorship

Appendix	Author
A	Zachary Stewart
B	Krista Anderson
C	Shuyang Wang
D	Shuyang Wang
E	Krista Anderson
F	Victoria Grimes and Zachary Stewart
G	Victoria Grimes
H	Victoria Grimes
I	Victoria Grimes and Zachary Stewart
J	Shuyang Wang

Appendix A: Background Literature Review

In addition to the material presented in the formal report, additional research was done to further understand other aspects of the project. The research was compiled in Appendix A in order to better understand the information presented in the report.

The first thing that was researched was standards of testing materials. Since the Differential Scanning Calorimeter and Thermogravimetric Analysis machines were used the ASTM standards were researched to assure the machines were being used correctly. ASTM International (American Society for Testing and Materials) produces a set of codes and standards on various topics in the testing of materials. The codes discuss general practices for certain testing methods, but specifically are not designed to instruct the user on proper techniques.

ASTM E2105 − 00: Standard Practice of General Techniques of Thermogravimetric Analysis (TGA) Coupled with Infrared Analysis (TGA/IR)

This can analyze samples from the TGA with IR spectroscopy. There are two methods: Evolved Gas Trapping Techniques: Vapor phase samples can be trapped in a heated-low volume gas cell where they are analyzed then disposed of. The temperature of the TGA is held constant while the sample is being analyzed in order to get more accurate results. A problem with this method is that the vapor concentration can lose its integrity by decomposition or decomposition of the cell walls, which makes the data more inaccurate. To prevent against this, reference spectrums of the same material tested are created before testing the sample to ensure that the sample does not lose integrity while analyzing it. The second technique is the Evolved Gas Analysis using a Flow cell. The flow cell is placed in the IR beam and the gas from the sample is trapped via a stopped flow routine and the spectrometers then scan the gas sample. This method allows the gas sample to be analyzed over a full IR spectrum without the interruption of evolved gas flow or sample heating.

ASTM D3850-12: Standard Test Method for Rapid Thermal Degradation of Solid Electrical Insulating Materials by Thermogravimetric Method (TGA)

These tests use the mass loss vs. temperature data using a controlled time rate of heating. A material's stability can be evaluated based on the rate at which it sublimates [1]. This is

especially useful for insulating and building materials. This data can also be used as a basis for what this data should look like for insulation materials in the same basic group as the one tested. The calibration of the TGA counts on a number of things. The flow rate of gas through the cell matters when calibrating and one should be picked and remain constant throughout the tests. The common values are from 0.7 to 1.6 mL/s. The surface area of the sample also matters. If a small surface area sample is compared to a large surface area sample (both of the same mass), the smaller surface area sample will lose mass slower than the larger surface area sample.

The other information that was researched was background knowledge on fiber reinforced polymers and why there are important building materials. Fiber reinforced polymers are known for being strong and stiff fibers that are cheap and light. This composite material is more durable and has better mechanical properties that the constituents that make it [2]. Fiber reinforced polymers became commercialized in the sixties when they began to be used for space and air travel. Currently, FRP materials are being used in infrastructure construction.

In addition to this material, there was also some analysis done about the company Kreysler. Kreysler and Associates is a construction company that innovates the use of composites in their building materials [3]. Kreysler makes the fire performance of their polymers a priority. With the right additives, they say that their fiber reinforced polymer can pass the ASTM E-84 Surface Burning Characteristic test easily. There are many benefits to working with fiber reinforced polymers which make them an appealing material to Kreysler. These include its low weight, flexibility, customizable properties, durability, and corrosion resistance.

Kreysler uses a variety of different fiber reinforced polymers. For the molding process of their surface coating of materials, they use a resin compatible with a matrix resin. They manufacture clear fiber reinforced polymers in order to have an appropriate matrix polymer. The most common composition of fiber and matrix is glass fiber and polyester resins. Kreysler understands the multifaceted material that is fiber reinforced polymers and finds it to make these materials reach fire protection standards in order to be able to use them.

Appendix B: Epoxy and ATH Manufacturing Information

The sample material tested for the data in this report was an Epoxy resin with various levels of ATH added to it, and was provided by Kreysler and Associates. Epoxy resins are a type of resin that commonly used when it is desirable for a material to be fire retardant [4]. Epoxy Resins are widely used in high-temperature and structural applications [5]. ATH, or Alumina Trihydrate, is a flame retardant that can be added to the resin to enhance the fire retardant abilities of the material. Various levels of ATH with the epoxy resin were tested in this research: Epoxy plus 5% ATH, 10% ATH, and 20% ATH. A Fireblock was also tested. The epoxy resin mixtures were formed into small solidified drops, which were used for testing in the TGA and DSC. The drops ranged from 1-10mg, had radii of 0.5-1.5mm, and an ellipsoid shape. It should be noted that such small drops are very difficult to make, and that the drops might not be completely homogeneous. This is an important consideration when acquiring test results of the material.

Appendix C. Thermogravimetric Analysis

Thermogravimetric Analysis (TGA) measurements can be used to select materials for certain applications. It can predict product performance and improve product quality. It measures

accurately the sample mass loss or gain by the changing of temperature with high accuracy. It can be used to characterize any material that exhibits a weight change and to detect phase changes due to decomposition, oxidation or dehydration. It can be performed simultaneously with DTA and DSC, sometimes separately. And all data and information can be used to graph a model to generate results. The rate of weight change can be drawn diagram either as a function of increasing temperature, or isothermally as a function of time.

Appendix C.1: Standard Operating Procedure

Standard Operating Procedure (TGA) [6]

Always when performing a TGA run, place the specified cardboard on top of the furnace to cover it and to avoid anything from falling inside the furnace. In the case that something does fall inside the furnace, PLEASE do NOT perform any tests and do NOT try to take it out. The inside of the furnace can get damaged by sharp objects. Notify immediately the responsible user.

1) Open the selected gas tank and set the pressure with the regulate at 20 psi (NO MORE OR LESS: 20 psi)

2) Select type of pan and material according to your set of samples and temperature requirements (Remember! Aluminum Melting Point: 660.37 °C; Platinum Melting Point 1,774 °C)

3) Open the icon Q Series Explorer and initiate the instrument

4) Prepare your procedure and data file in advance:

→ Starting from the Notes tab: change your name on user name, and make sure that you are using the correct pan type and the correct gas flow (#1 correspond to Nitrogen, and #2 correspond to Air >>> notice that because of a mistake on the software, both gases are denoted as Nitrogen, so make sure you chose the correct number!). Balance and sample flows MUST NOT be changed >>> Balance flow = 40 mL/min and Sample flow = 60 mL/min ALWAYS

→ Click Apply before moving to the Procedure tab

→ On the Procedure tab you will create and save (under your OWN folder, not anybody else's) your method and procedure (Note: they are the same thing but the instrument requires 2 different files)

→ Creating and saving your method: name your method on the method name, open Editor and modify it as you please, dragging the steps you consider of your convenience. Remember to add at the end of the run, a "stabilize to 25 oC" step at the end of each run *IMPORTANT: FURNACE MUST NOT BE OPENED AT HIGHER TEMPERATURES THAN ROOM TEMPERATURE)*

→ Once you are done and before closing this window: SAVE the method as a *.mth file under YOUR folder (Note: this is very important since if you fail doing this, you can overwrite somebody else's method). Once you are done saving your method, on the procedure line, go to the save icon and save the same method but as a PROCEDURE (*.prc file) once again, under your folder.

→ Click Apply and move to the Summary tab

→ In the summary tab you will first CALL your procedure from the procedure tab (open >>). Secondly you will name your sample, as it will show in the results sheet. And finally you will save your results with the corresponding name on YOUR folder (IMPORTANT: make sure you complete this step to avoid overwriting data of previous users).

5) Load and TARE the correct pan (make sure the last user, used the same pan material you will use, in the contrary case, make an appointment with the responsible user to change and CALIBRATE the instrument with the correct pan type. (NOTE: this is very important, tests performed otherwise are not reliable)

6) Previously weight your sample to make sure you are in between the range of the microbalance. Keep the amount of sample below 20 mg to assure quality of the results.

7) Load the sample on the pan, as homogeneously as possible, trying to cover all the surface of the pan

8) Click apply and start (green button from computer or START from the touch screen)

In the left bottom of the screen, it will show the amount of time that the run will take. Please, take it consideration that sometimes it takes longer for the furnace to cool down to room temperature. Remember not to open the furnace at different temperatures than room temperature.

Once the run is complete: open the furnace, unload the pan.

After your run is complete REMEMBER to *CLEAN* platinum pans using the flame burner until the pan is red. Repeat 2 or 3 times until you are sure the pan is clean. After the pan is clean, load it back and CLOSE the furnace

Appendix D: Differential Scanning Calorimetry

The Differential Scanning Calorimeter (DSC) is a machine used to study polymers and what happens to them when they are heated or cooled. Typically, the samples are heated, but can be cooled through the use of liquid nitrogen. The DSC machine consists of two pans. One pan has the polymer sample, and the other pan sits empty as a reference pan. The sample pan is located in front of the machine, and the reference pan sits in the back. The operator must measure out the sample before each experiment. For the DSC, the sample should be in the range of 5-10 mg. The sample should also be thin. This reduces thermal gradients across the material. Each pan sits on top of a heater with thermocouple sensors located below. Thermocouple sensors work by joining one end of two metals together that are dissimilar. When the meeting point of the two metals is heated or cooled, a voltage is produced. This voltage is correlated back to the temperature via the computer.

Appendix D.1: Standard Operating Procedure

<div align="center">Standard Operating Procedure (DSC) [7]</div>

All of your DSC experiments will have the following general outline. In some cases, not all of these steps will be performed. See the instrument control software online help for anything not covered in this manual.

- Attaching and setting up external accessories as required (e.g., purge gas, cooling accessory). If you are planning to run subambient experiments with the LNCS, use helium as the purge gas. If you are using the LNCS for rapid cooling above ambient (i.e., isothermal crystallization), then nitrogen may be used as a purge gas. If you are using the RCS 90 or RCS 40 for cooling, nitrogen may be used as a purge gas.

NOTE: Please make sure that you run your experiments with the same gas that you used to calibrate the system. For example, if you calibrate using nitrogen, make your runs with nitrogen.

- Selecting and preparing a sample. This involves preparing a sample of the appropriate size and weight, selecting the pan type and material, and encapsulating the sample in the pan. For details refer to the online documentation.
- Loading the sample pan (and a similarly prepared empty reference pan) into the cell or onto the Autosampler tray.

- Entering experiment and procedure information through the TA controller, this includes both sample and instrument information.
- Starting the experiment.

Load the sample pan into the cell as follows:

1. Remove the lids. If the DSC has an autolid assembly, touch the LID OPEN key on the DSC Control Menu touch screen to raise the lid from the cell. See the figure to the right.
2. Carefully place the sample pan on the front right raised platform and the reference pan on the rear left platform (shown in the figure below). Cen-tering the pans will give more accurate results.
3. Cover the cell. If the DSC has an autolid assembly, touch the LID CLOSED key on the DSC Control Menu touch screen to return the lid to the cell.

Before you start the experiment, ensure that the DSC is connected with the controller and you have entered all necessary information through the instrument control software.

Start the experiment by by selecting Start on the instrument control software, touching the START key on the instrument touch screen, or by pressing the Start key on the keypad (Auto Q20/Q20/Q10). When you start the instrument, the system automatically runs the experiment to completion.

If for some reason you need to discontinue the experiment, you can stop it at any point by selecting Stop through the instrument control software, touching the STOP key on the instrument touch screen, or by pressing the STOP key on the keypad (Auto Q20/Q20/Q10). Another function that stops the experiment is REJECT. However, the Reject function discards all of the data from the experiment; the Stop function saves any data collected up to the point at which the experiment was stopped.

Appendix D.2: Calibration

Calibration is important in the DSC to obtain accurate and reproducible data. It is important that the DSC be calibrated accurately over the desired temperature range [8]. It is also important to calibrate for the each specific material used, to ensure the data collected will be as accurate as possible. For the DSC, there are two calibration sets that must be completed before testing of a material should begin. First, the baseline calibration test is run. The baseline calibration is run to adjust the slope and curve that the DSC produces [9]. The onset calculations that the DSC reads for the start of any pyrolysis behavior are taken in part from the set values of the baseline calibration. For example, the start of the decomposition in a material will result in a change in the heat flow curve. The DSC will show this as a change in the curve because it was the heat flow was deviating from the baseline calibration. After the baseline calibration is run, a cell constant (Enthalpy) calibration must be run. In this calibration, indium, a standard metal, is used in the DSC in place of a testing material [10]. The indium is heated beyond the transition where it melts. It is then compared to the standard accepted melting point of indium, and the difference between the two values is taken for the cell constant calibration. Once these two calibrations have been run and the data entered into a calibration file, the testing of a selected material may proceed. Outlined below are the exact calibration instructions for both the Baseline and Cell Constant test for a Q Series DSC.

Baseline Calibration

- Start with a completely empty DSC (e.g. no pans)
- In the DSC program, on the top tool bar, click Calibrate → Calibration Wizard → And say no to saving (because you have not completed any calibrations yet)
- In the Calibration Wizard, click Baseline Calibration → Input your desired Heating Rate and Final Temperature (the same one you will use for your testing material) → Make sure "Use Current" is selected → Click Next → Click Next again
- Where there is a place to put in a sample mass, set equal to zero
- Date file button: Click on the button to the right of this file (the one with the three dots) → Right click and select "New text document" → delete the entire text (not including the .txt) and rename the file to the HR and material you are calibrating for (e.g. 10C Material 1a) → Open file
- Click Next, then under pan type put "None"

- Go back to main screen of DSC run the calibration using SOP for running and cooling down the machine

After the test is complete and the DSC has cooled, save the data and double check that the data file saved to the location and name that you specified. After the Baseline Calibration is completely done, the Cell Constant Calibration needs to be completed.

Cell Constant Calibration

- Load front pan with the Indium sample and put the reference pan on the back sample holder
- Click Calibrate → Calibration Wizard → Say no to save because the Baseline was previously saved
- Select the cell constant/temperature test
- Under standard put Indium
- Enter heating rate and final temperature (the same you used in the previous calibration) and make sure the "Use Current" is selected → Click next → Click next again
- Enter Indium weight (e.g. 10.6mg)
- Create NEW data file using the same method as before but title it with the HR, material and the word Indium (e.g. 10C Material 1a INDIUM) → Open file
- Pan type=Tzero Aluminum → Click Next
- Click finish and run the DSC as normal, make sure data saved to correct location

Once the calibrations are done, the calibration values need to be added to a new calibration file.

To add Baseline constants to the calibration:

- To get the baseline values:
  - Click Calibration (top tool bar)→ Analyze → Open Baseline data file
  - Click Analyze then click "Limits OK", Accept and record the slope and offset
- To create calibration set:
  - Click Experimental (top tool bar) → Wizard → Select DSC Ramp → Click next
  - Enter Heating rate and final temperature → Click next

- o Select Indium data file created → Click next
- o Under Calibration set click the button with the three dots
  - ▪ Rename Calibration Set to HR Material (e.g. 10C Material 1a)
- o Enter the offset and slope from the baseline calibration into the calibration set and leave the cell constant values alone for now
- Go back to the main page of the DSC test
- Click Calibration → Analyze → Open Cell Constant file (the one with the indium)
- Click Analyze → Limits OK → Click Accept and make sure the Calibration Set previously made is selected (e.g. 10C Material 1a) (This resets the Cell Constant values for the calibration)
- If you then go to Calibrate (top tab) → Cell/Temp Table it shows you what you have for the values

After these steps are taken, the baseline and cell constant calibration values should be inputted and saved to the new calibration set that was created. When running an actual test, the user can select the desired calibration from the "Notes" tab in the DSC program.

Appendix E: Gpyro

Appendix E.1: Gpyro Basics and Governing Equations

Gpyro is a pyrolysis model used to conduct simulations in 0D, 1D, 2D, or 3D. In its most simple form, it is a code for 1D transient heat conduction. A 1D simulation corresponds to gradients (temperature, density, etc.) that are perpendicular to the simulated surface and are much larger than the parallel gradients. Gpyro breaks down the sample into a set of cells, which can be seen in the figure below. In this Gpyro analysis, a charring material was simulated, so there is no change in the size of the cells (z). This further simplifies the governing equations into partial differential equations, which can be found in the Gpyro Technical Reference, Section 4.2 [11].
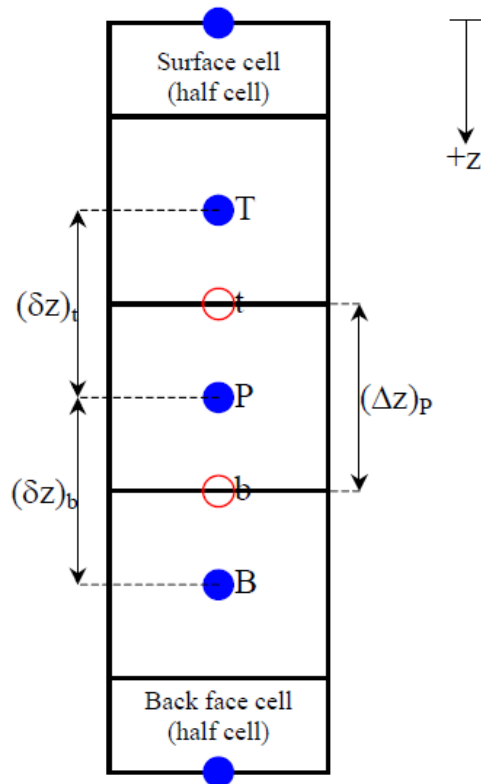
Figure 17: Schematic of simulated cells in Gpyro

Two main curves that Gpyro can produce are the DTG Curve and a Mass Loss Curve. While they can be created separately in Gpyro, it should be noted that by integrating the DTG data, the

percent mass lost can be calculated. The DTG Curve is the negative derivative of $(1-\alpha)$, where $\alpha=(1-m/mo)$. The current mass is m, and the initial mass is mo. The equation below confirms the integration of the DTG Curve will provide the mass fraction. Below are the simplified equations regarding the use of alpha and the mass fraction, which is important in the analysis of a 0D simulation [12].

$$(1 - \alpha) = \left[1 - \left(1 - {}^{m}/_{m_o}\right)\right] = {}^{m}/_{m_o} \qquad (1)$$

$$\frac{d\alpha}{dt} = Ae^{-\frac{E}{RT}}(1 - \alpha)^n \qquad (2)$$

To further confirm the integration of the Mass Loss Rate, the above equations were used to calculate the integration and the results are graphed below.
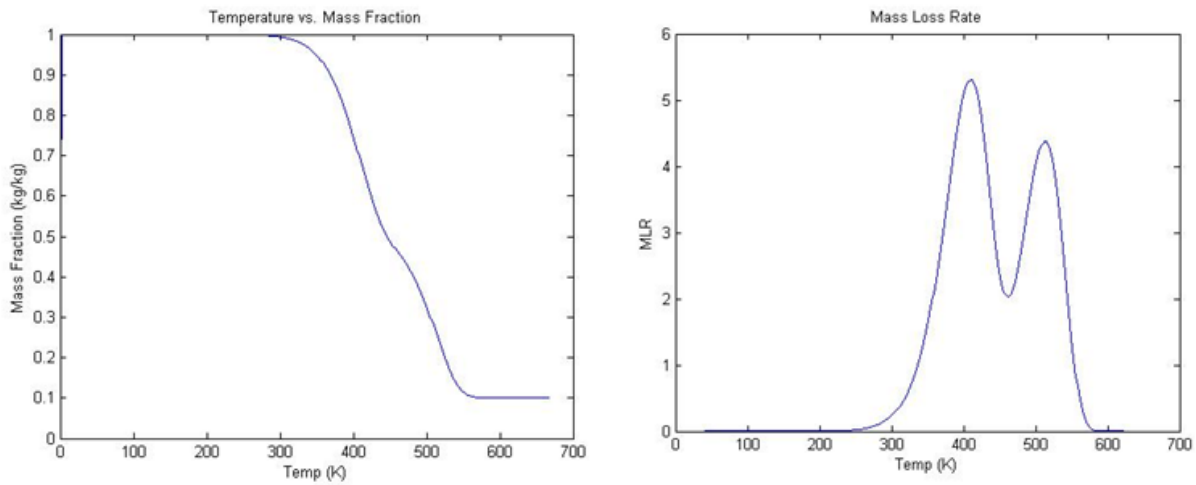
Figure 18: Confirmation of DTG Curve Integration

Gpyro uses one main equation to calculate the DTG Curve and the derivative of that curve, which can be seen below based on the input parameters.

$$\frac{d}{dt}\left(\frac{m}{m_0}\right) = -\frac{\dot{\omega}\Delta z}{m_0} = -\frac{\dot{\omega}\Delta z}{\rho\Delta z} \qquad (3)$$

This is the governing equation used in Gpyro for calculating the DTG Curve. It can be integrated to provide the TG curve, which is the mass fraction curve. The governing equation for that calculation can be seen below.

$$\frac{m}{m_0}(t) = 1 - \frac{1}{m_0}\int_0^t \dot{\omega}(\tau)\Delta z(\tau)d\tau \qquad (4)$$

In the above two equations, m and mo are the mass fractions, change in z is the cell size (height), t is time, ρ is density, and ω is the volumetric reaction rate.

Appendix E.2: Running Gpyro

Once Gpyro has been downloaded onto a computer, the program is executed through the command prompt by using: gpyro input_file.data where "input_file.data" is the data from the executed experiment [13]. A Microsoft Excel sheet is provided with the program that allows the user to input known values and material properties for the simulation. There are a few tabs that the user needs to pay particular attention to. The "output" tab is where the user lists what profile and point dumps Gpyro needs to provide. There is a list of what Gpyro can dump in the Gpyro User's Guide, Table 1 [13]. The "sprops" tab is where the user specifies the material properties, and the "rxns" tab is where the user specifies the reactions that take place. The geometry of the sample is put under the "geom" tab, the mass fractions go under the "IC" tab, and the applied boundary conditions go under the "BC" tab. The user must also specify how long to run the test, which can be found in the "cases" tab. The user should note, however, that the excel file does not always translate perfectly to the input file, so once the user is comfortable with the excel file and the units Gpyro uses; they should work from the input file. In older versions of excel, the User can press "Ctrl+g" to create a new input file, but should always check that the values transferred correctly. When running a test, the user needs to put the input file and the Gpyro file, "gpyro.exe" into the same folder. The user then drags the input file to the Gpyro file, and Gpyro should open the command prompt window and run the program. The user can reference the Gpyro User's Guide but it should be noted that for Gpyro version 0.8, the User Guide has not be updated, so not everything it in is applicable [13].

Appendix E.3: Gpyro 0D Example

Gpyro comes with several example simulations. The first simulation that was evaluated was sample 1, which is the 0D simulation. This was a 0D simulation for a solid that had two-step kinetics and had four different heating rates [13]. This 0D example is looking at a single particle that has such small temperature gradients it can essentially be ignored. It is important to note that in a 0D simulation, the MLR data is multiplied by 1,000, so to bring the values back to the true data, the MLR column provided by Gpyro must be divided by 1,000. The DTG Curve shown below is for all four heating rates.
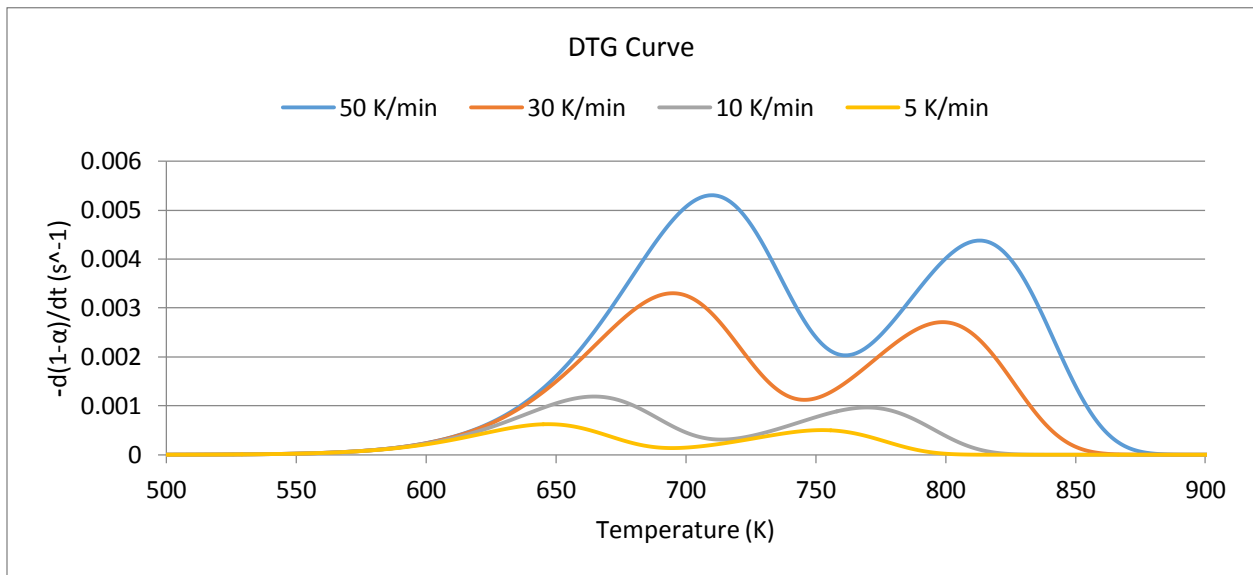
Figure 19: DTG Curve for 0D simulation

The curves each have two peaks. In this example, we start with a virgin material, then have an intermediate material, and then are left with a residue. As the heating rate is increased, the temperature at which the MLR peaks is slightly increased, as is the rate of mass lost. The Mass Fraction curve was also produced, and can be seen below.
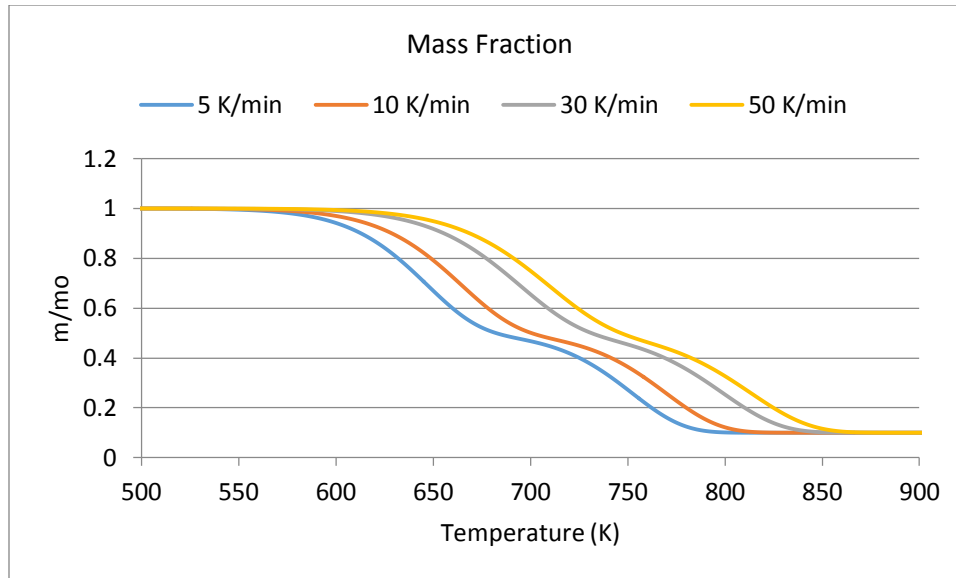
Figure 20: Mass Fraction Curve for Gpyro 0D

It can also be seen in this graph that as the heating rate is increased, the temperature at which mass is lost and the mass fraction is increased. However, it should also be noted that in the end, all four heating rates led to a final value of about 10% initial mass.

Gpyro 0D Conformation

In order to test out understanding of how Gpyro models reactions, the example 0D material used in Gpyro was tested using the RK4 method described in Appendix F.2: Runge Kutta Modeling. A heating rate of 50 C/min was used to develop a simulation graph of the weight loss derivative. Because Gpyro simulates two reactions, in order to simulate the reactions together, the individual weight loss derivatives for each reaction were modeled and added together. The area under the curve of the first reaction was determined to find the mass fraction of the second reaction. This represents the amount of mass left over after the first reaction. This number was determined to be 0.5. The magnitude was off by a factor of 10, but it was later discovered that the Gpyro was multiplied by a factor of 10 in the results.
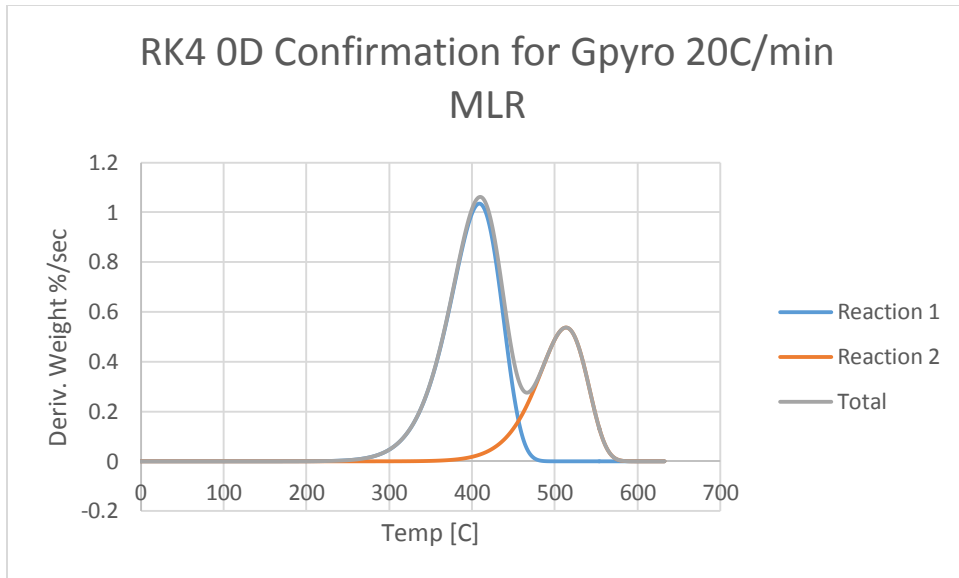
Figure 21: RK4 0D MLR for Gpyro
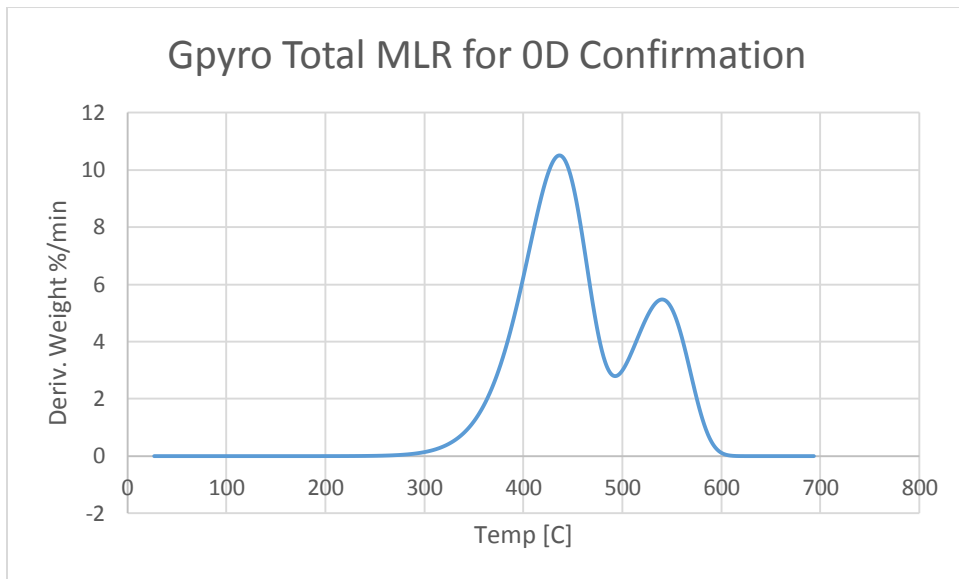
Figure 22: Gpyro 0D MLR Results

Appendix E.4: Gpyro 1D Example (Baseline Parameters)

The next Gpyro example that was analyzed was sample 3, which is a charring example from the Cone Calorimeter. This is a 1D simulation. In this simulation, the variation of the temperature laterally into the sample, along with variations in density and mass fraction, is very small when compared to the variations in the longitudinal direction [14]. For example, when a slab surface is exposed to a heat flux that is uniform, the temperature gradients that are perpendicular to the surface of the slab are larger than the temperature gradients that are parallel to the surface of the slab. The following three tables shown below are the baseline parameters provided for sample #3. The values highlighted in yellow were the chosen values to create profiles for at varying levels to better understand how they affect Gpyro.

Table 13: Material Properties (Gpyro Sample 3)

Name	k (W/m^2*K)	ρ (kg/m^3)	c (J/kg*K)	ε (-)
Virgin	0.200	500	1500	0.65
Intermediate	0.150	200	1500	0.95
Residue	0.100	50	1500	0.90

Table 14: Reactions (Gpyro Sample 3)

Species (A)	Species (B)	Z (s^-1)	E (kJ/mol)	ΔH (J/kg)	n (-)
Virgin	Intermediate	5*10^8	130	6*10^5	1
Intermediate	Residue	5*10^10	175	1*10^5	1

Table 15: Boundary Conditions (Gpyro Sample 3)

Index	qe (W/m^2)	Reradiation	hc (W/m^2*K)
1	25,000	True	10
2	25,000	True	10
3	0	False	0

Some of the results that are provided are the temperatures taken at three points along the slab of the material. Point 0 corresponds to the surface of the slab, and 0.004m and 0.008m correspond

to the points in the positive z-direction into the cell, with 0.008m being the back face of the slab. Two different heat flux values were simulated; 25 kW/m^2 and 50 kW/m^2. The graphs of the two different trials are shown in the figures below.
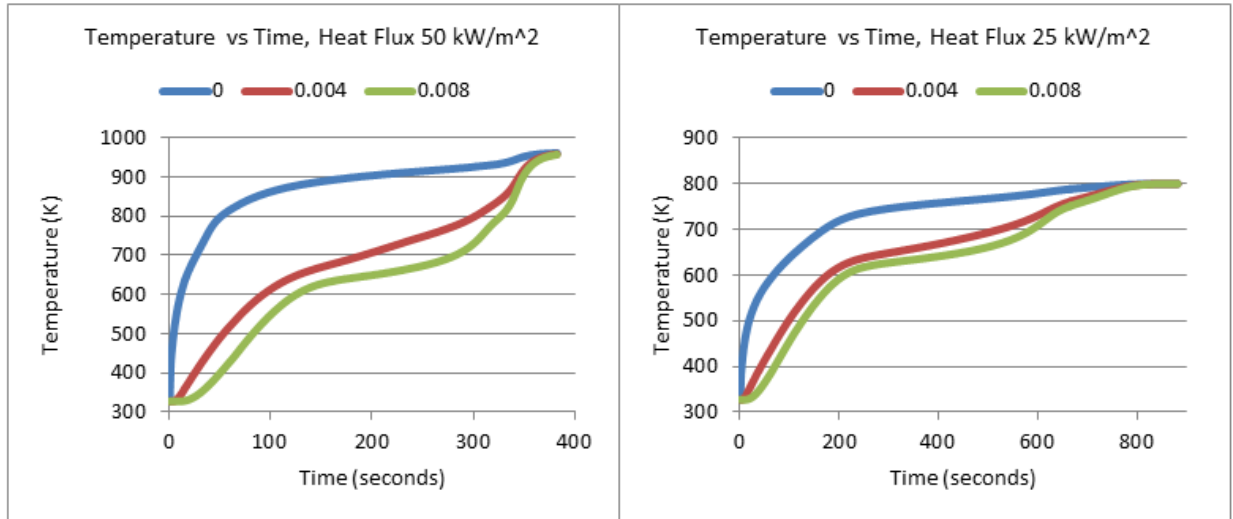
Figure 23: Gpyro Sample 3 Multiple Heat Flux Values

There are a few differences and similarities that can be noted between the two graphs. First, for both levels of heat flux, the surface of the slab (0m) records a temperature higher for most of the duration of the trial, and the point 0.008m records the lowest temperatures for most of the duration of the trial. It can also be seen in both trials that the temperature of the slab coordinates eventually converges. For the heat fluc of 25 kW/m^2, the slab converges to 800K at about 780 seconds. For the heat flux of 50 kW/m^2, the slab converges to 975K at about 400 seconds. So by increasing the heat flux by a factor of two, the time it takes for the slab coordinates to converge to the same temperature is approximately halved.

The MLR data is also provided in the output results for this example at each level of heat flux, shown in the figure below.
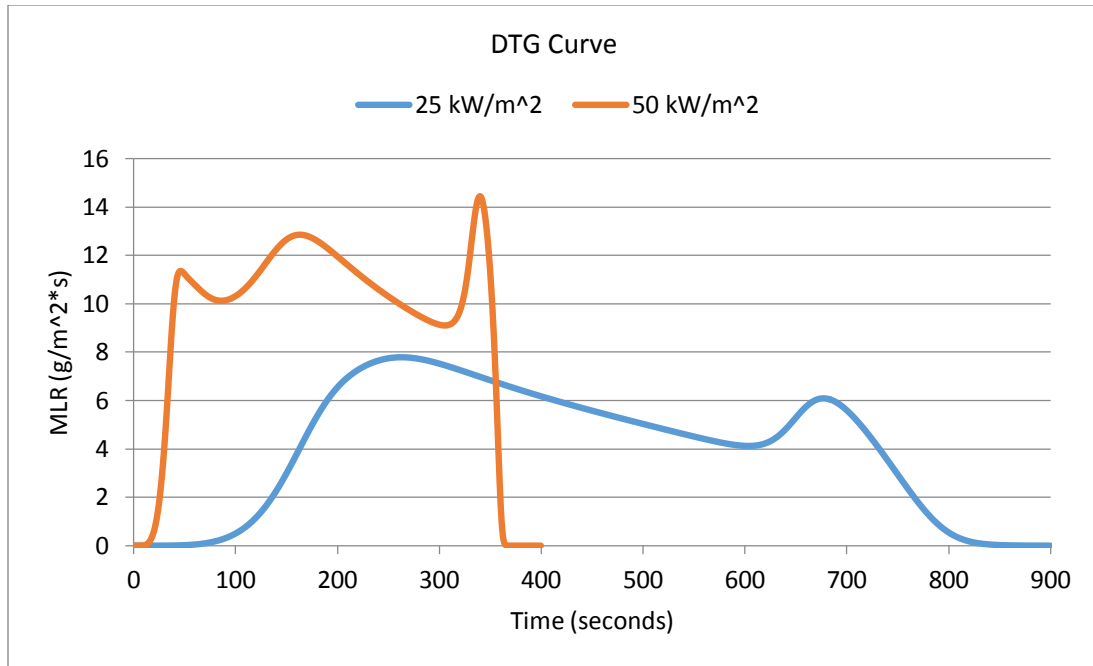
Figure 24: DTG Curve Gpyro Sample 3, Multiple Levels of Heat Flux

In this example, there are two distinct peaks for the lower level heat flux and three peaks for the higher heat flux. When a material is subjected to higher levels of heat flux, there is more of an insulating effect from the substrate below the reaction zone, causing the reaction peaks that cannot be seen at lower heat flux levels [15].

One of the governing equations used by Gpyro that can relate back to the above figures is the condensed phase mass conservation equation [13].

$$\frac{(\rho \Delta z)_1 - (\rho \Delta z)_2}{\Delta t} = -(\omega \Delta z) \qquad (5)$$

In this equation, ρ is the bulk density, change in z is the cell size, change in t is the change in time, and ω is the volumetric reaction rate. One of the assumptions Gpyro makes is that only the mass that is gaseous is allowed to cross into different cells (Lautenberger, 2014). What the above equation is saying is that the product of $(\rho \Delta z)$ will decrease proportionally to the cell size multiplied by the volumetric reaction rate from the condensed phase. Essentially, the density multiplied by the size of the cell will decrease because there is the formation of has in that specific cell. In a charring material, the creation of gas will result in a decrease in bulk density because there is an increase in porosity at the surface of the material. In contrast, in a thermoplastic material, gas formation will result in just a change in cell size (Δz), so the cell will

just shrink. For materials that are non-deal, there may be a simultaneous reduction in ρ and ω. This implied in a 1D simulation, each cell analyzed is treated as a simple sample [13].

Using the MLR and Temperature data, temperature profiles were created for each level of heat flux. The graphs can be seen below along with a table that describes each profile. It should be noted that as time goes on, the gradients become relatively flat.
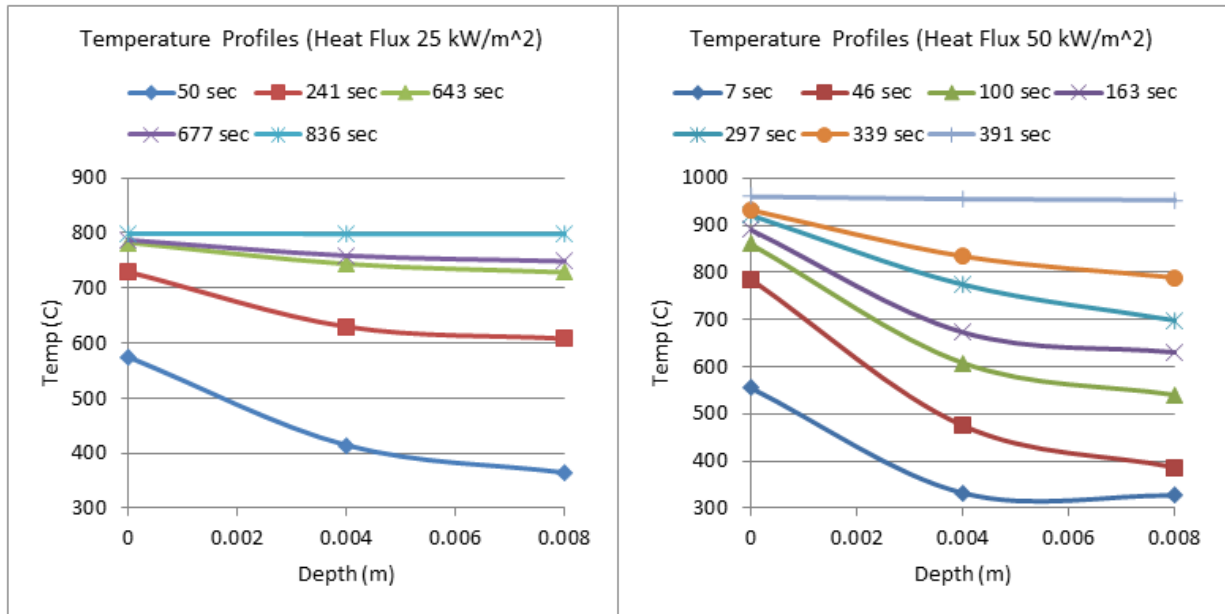
Figure 25: Gpyro Sample 3, Temperature Profiles

Table 16: Time (sec) for Temperature Profiles Compared to DTG Curve

Location	Time (q25) (sec)	Time (q50) (sec)

Before Any Mass Loss	50	7
Peak 1	214	46
Valley 1	643	100
Peak 2	677	163
Valley 2	-	297
Peak 3	-	339
End	836	391

Looking at the first graph (heat flux 25 kW/m^2), the smallest temperature profile was for before any mass loss occurred, compared to the end result, which had the highest temperature profile values. For the first temperature profile graph, at the end, there was no variation in the temperature profile. The higher heat flux level produced similar temperature profiles, with the start of the trial producing the smallest temperature profile with the largest variation and the end of the trial producing a profile with no variation but the highest temperatures. When looking at the slopes of the profiles, there is a greater slope between the top and middle of the cell than the middle and the bottom of the cell. This could be due to the heat flux that is at the surface, and the subsequent char layer that is forming.

Appendix E.5: Gpyro 1D-Understanding Baseline Parameters

The charring example (#3) was run in Gpyro using all the provided parameters. These parameters were taken as the baseline parameters. Different parameters where run at different levels, to see how the results were affected. Values were then chosen (or calculated) based on the provided results, for a TGA simulation. To start, below is the DTG curve for Gpyro sample 3, with the baseline parameters.
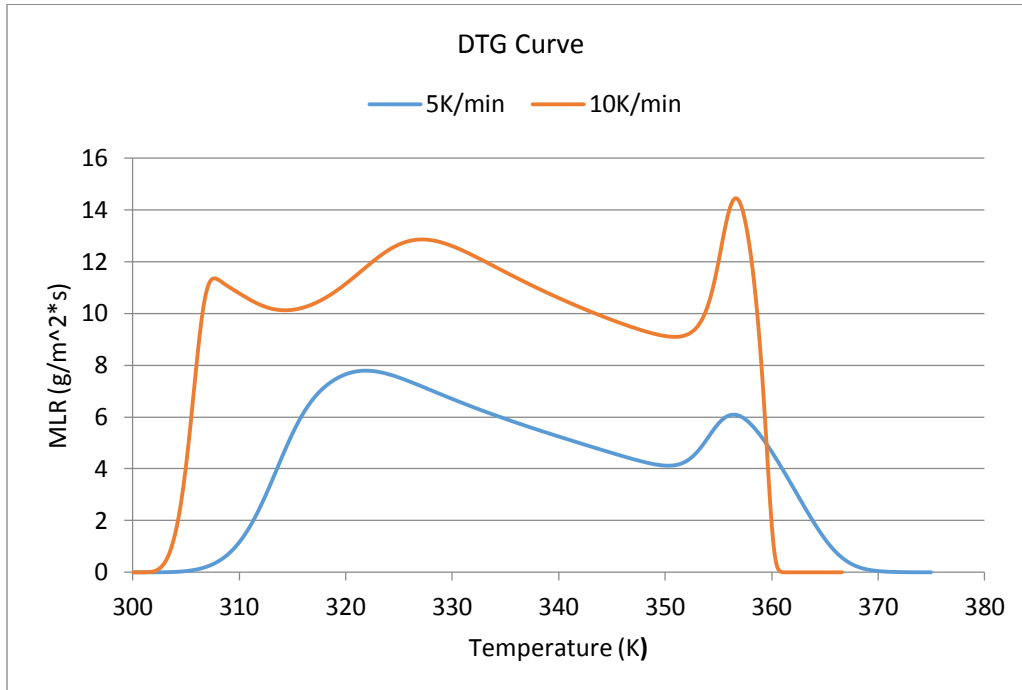
Figure 26: DTG Curve for Gpyro Sample 3 (Char)

Keeping all variables the same, the heat flux at the exposed surface was varied from 5 kW/m^2 to 75 kW/m^2. The results can be seen below.
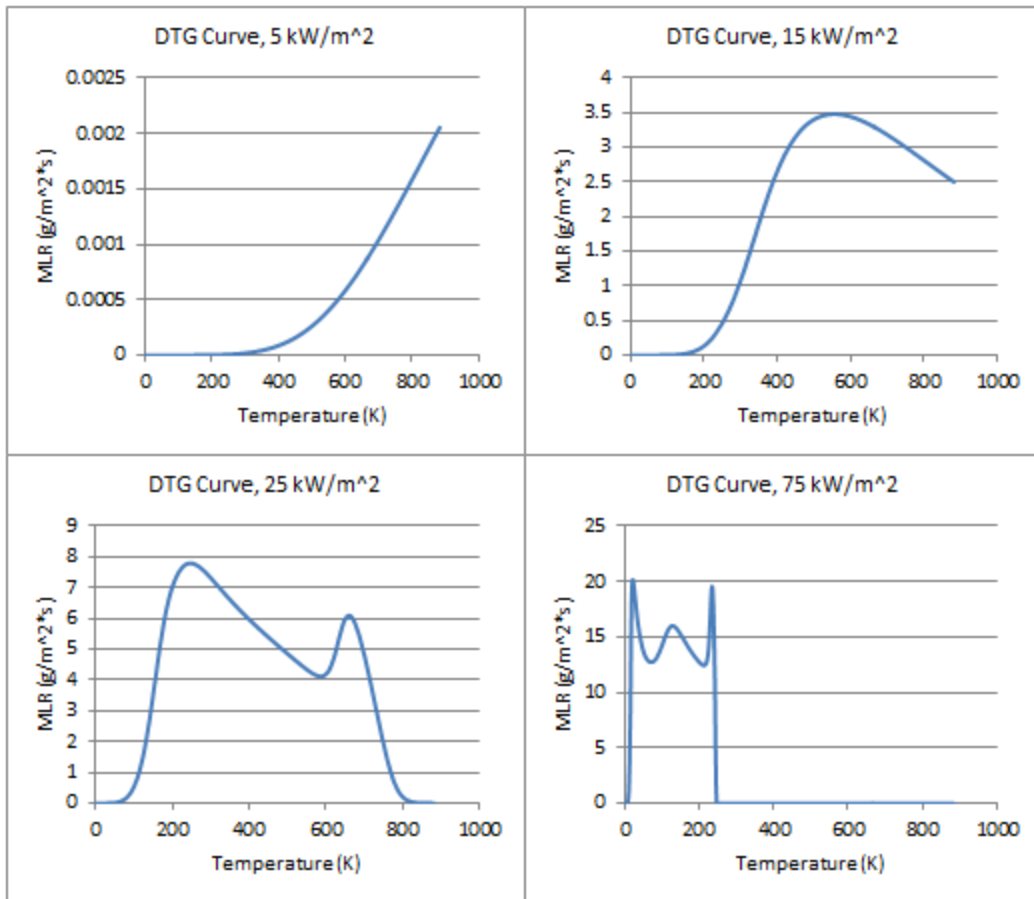
Figure 27: DTG Curve, Multiple levels of Heat Flux, Sample 3

The four graphs above where graphed using the same temperature limit (900K). It can be seen that as the level of heat flux is increased, the MLR becomes increasingly larger and the temperature range for a complete reaction to take place is significantly shortened. All of the values were graphed together to better understand how they vary from one another, which can be seen in the graph below.
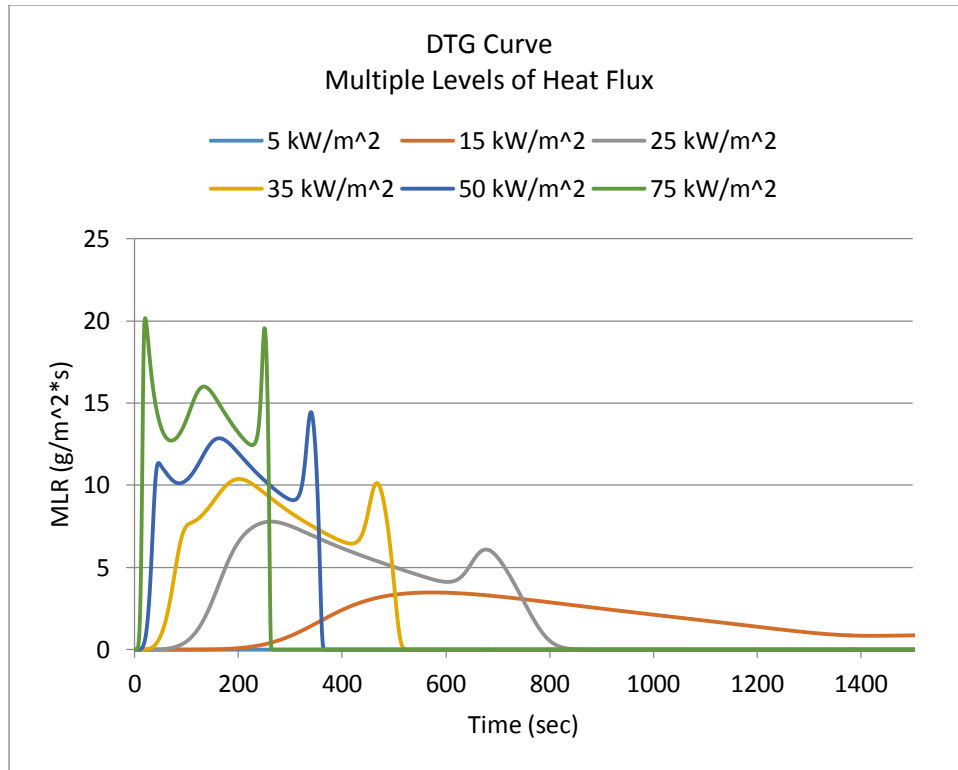
Figure 28: Varying levels of Heat Flux, DTG Curve

Next, the heat flux was set back to its baseline value of 25 kW/m^2, and the input parameters for a resin were imputed using FRP Parameter Estimation Results for a Resin (Kim, 2014). The DTG Curve was produced, and compared to the result provided in the Parameter Estimation Guide. The two curves showed similar results, and can be seen in the figure below.
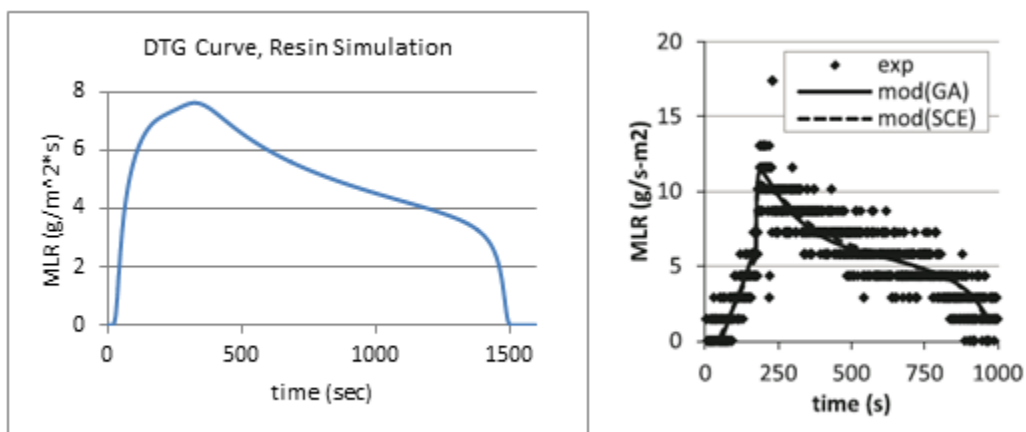
Figure 29: DTG Curve Resin Simulation Comparison

The differences between the two graphs are probably because in the second graph, the input parameters were not specified (just the resin and heat flux). But, overall, the shape of the two graphs is very similar. The best choice for a heat flux is the lowest value that shows a good agreement with the modeling and actual data [16]. For our current simulation, comparing it to the provided graph, this would fall in the range of 25 kW/m^2 to 50 kW/m^2 to get the best match.

The profiles at each level of heat flux were also created, and those can be seen below.

5 kW/m^2
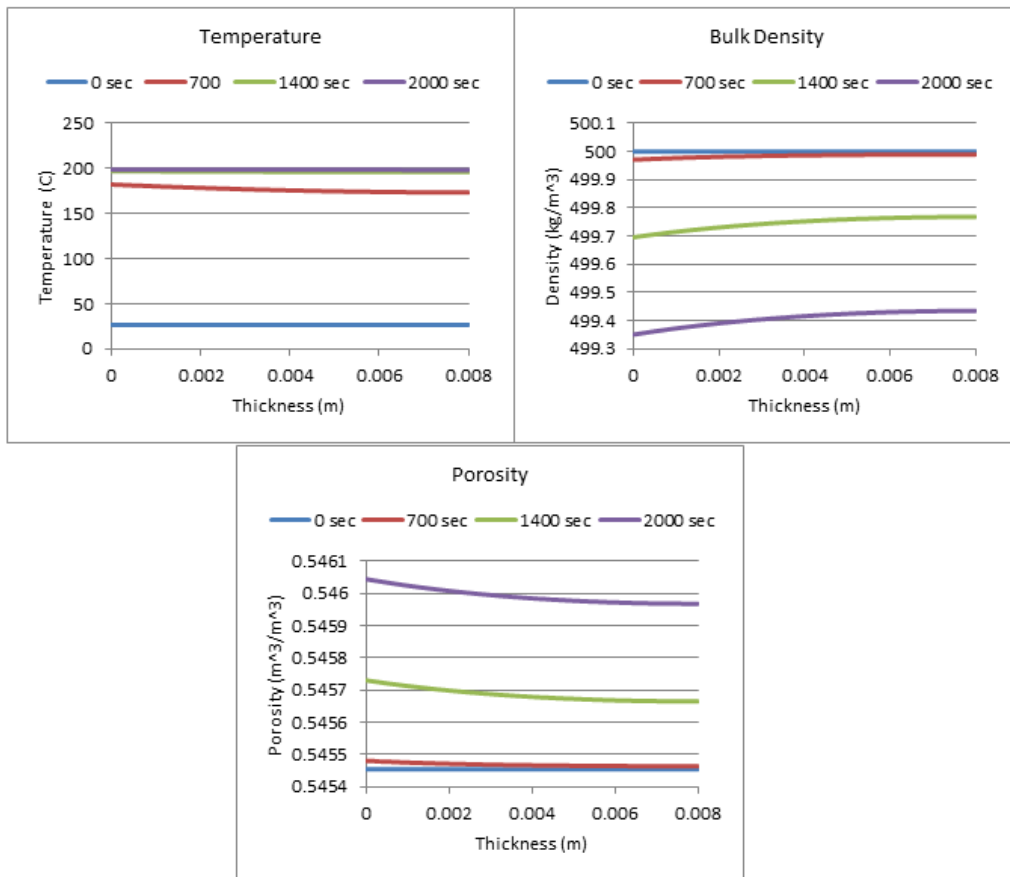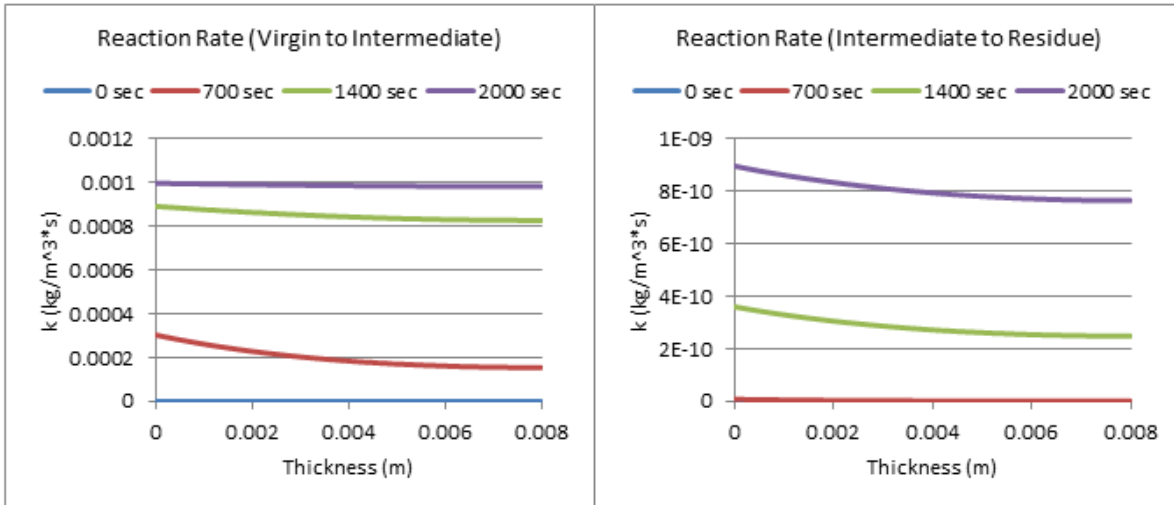
Figure 31: Profiles of Reaction Rate with a Heat Flux of 5 kW/m^2
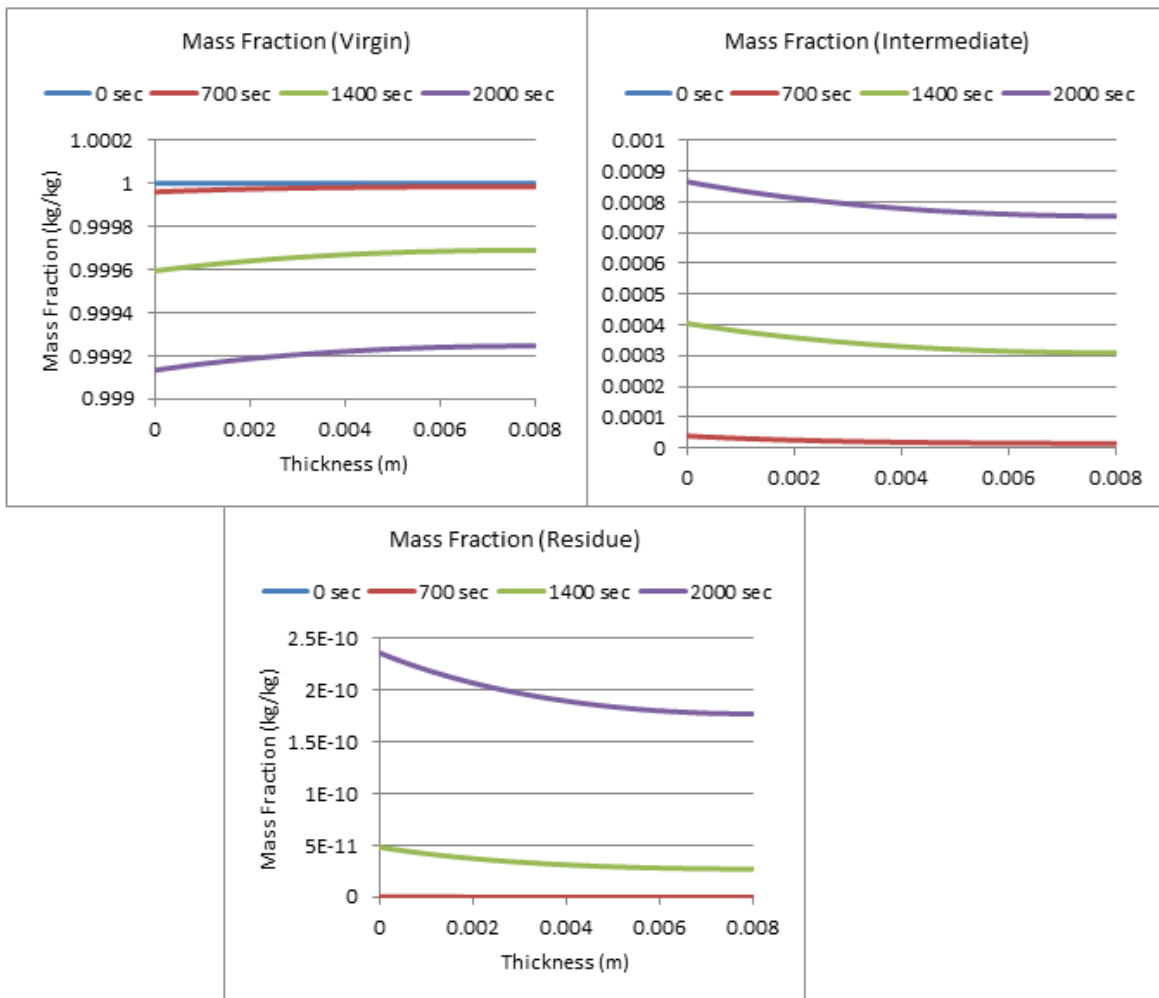
Figure 32: Profiles of Mass Fraction with a Heat Flux of 5 kW/m^2

15 kW/m^2
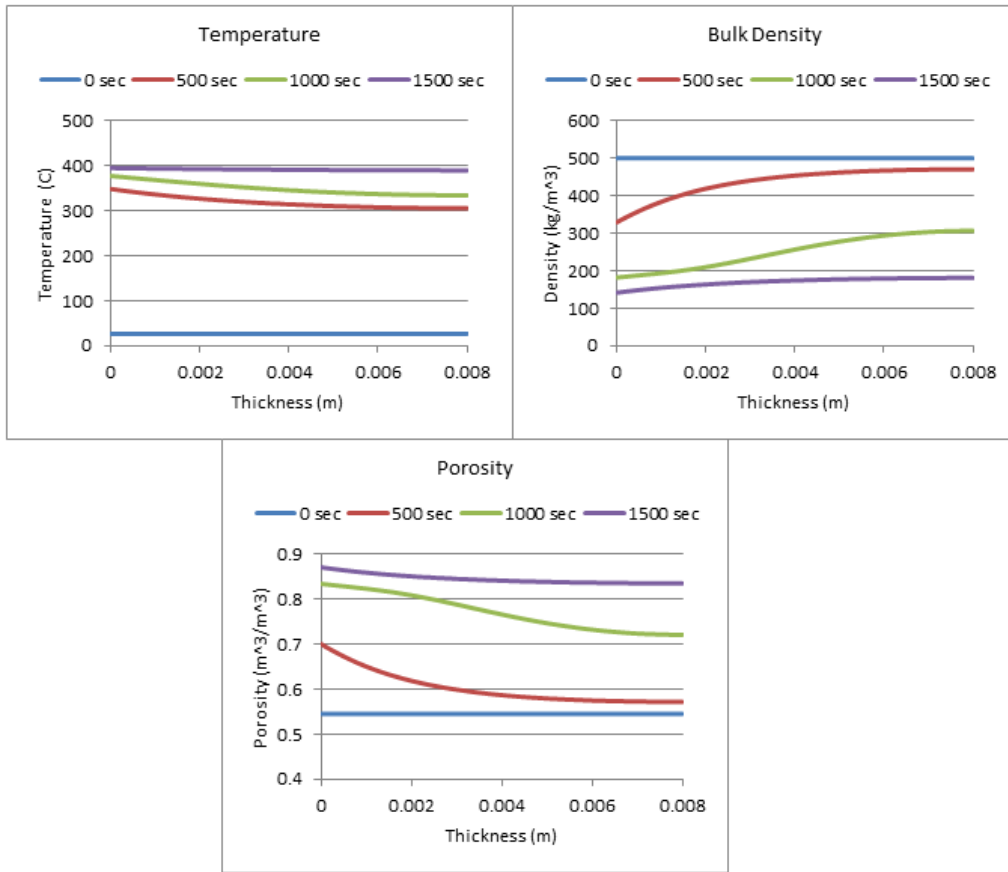
Figure 33: Profiles with a Heat Flux of 15 kW/m^2
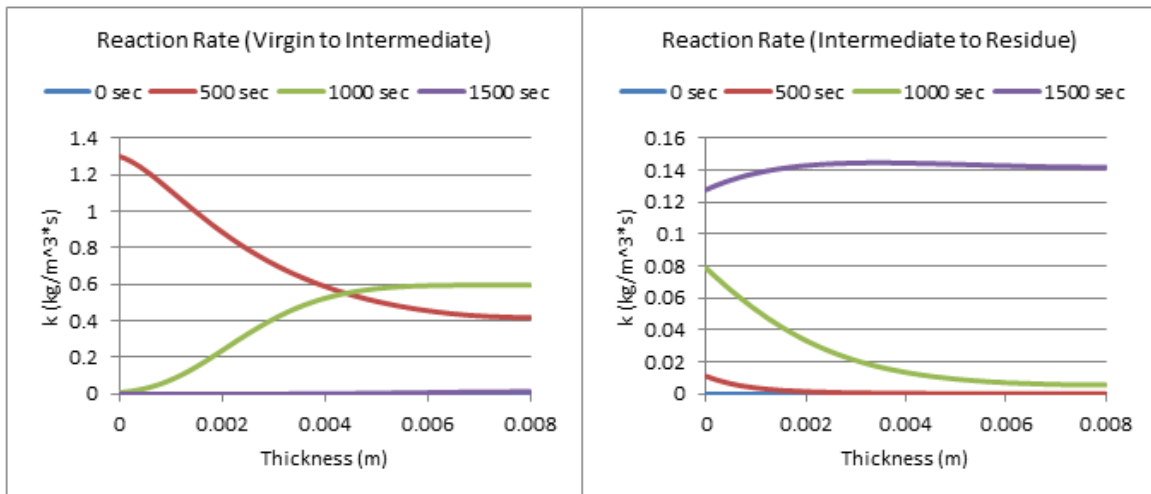
Figure 34: Profiles of Reaction Rate with a Heat Flux of 15 kW/m^2
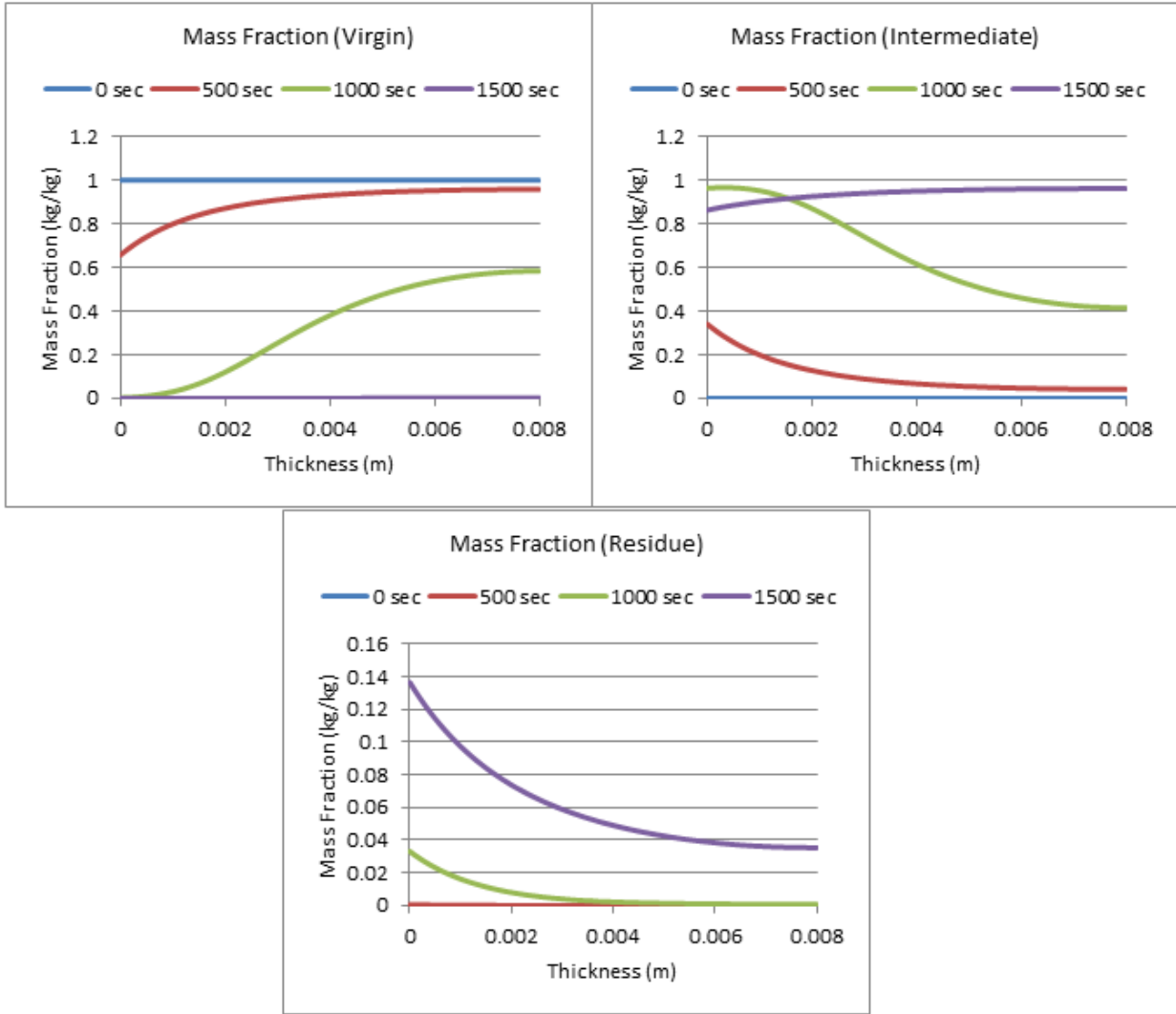
Figure 35: Profiles of Mass Fraction with a Heat Flux of 15 kW/m^2

25 kW/m^2
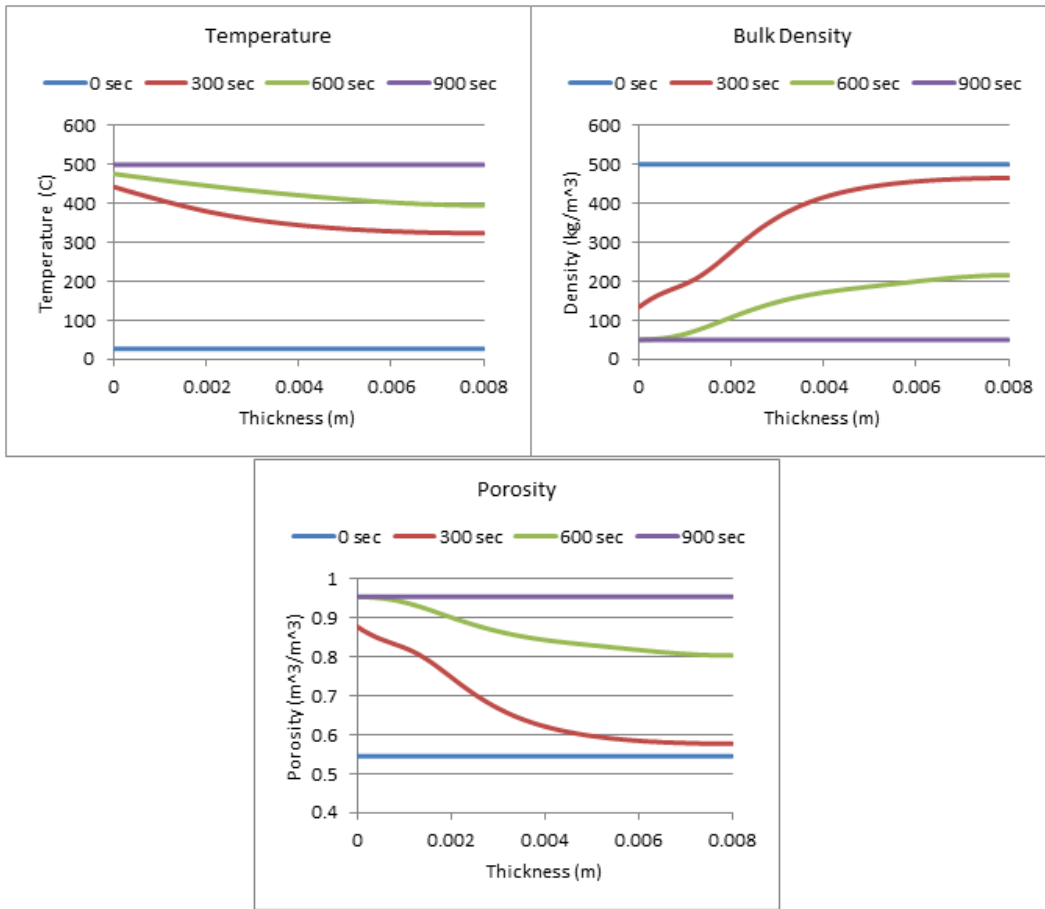
Figure 36: Profiles with a Heat Flux of 25 kW/m^2
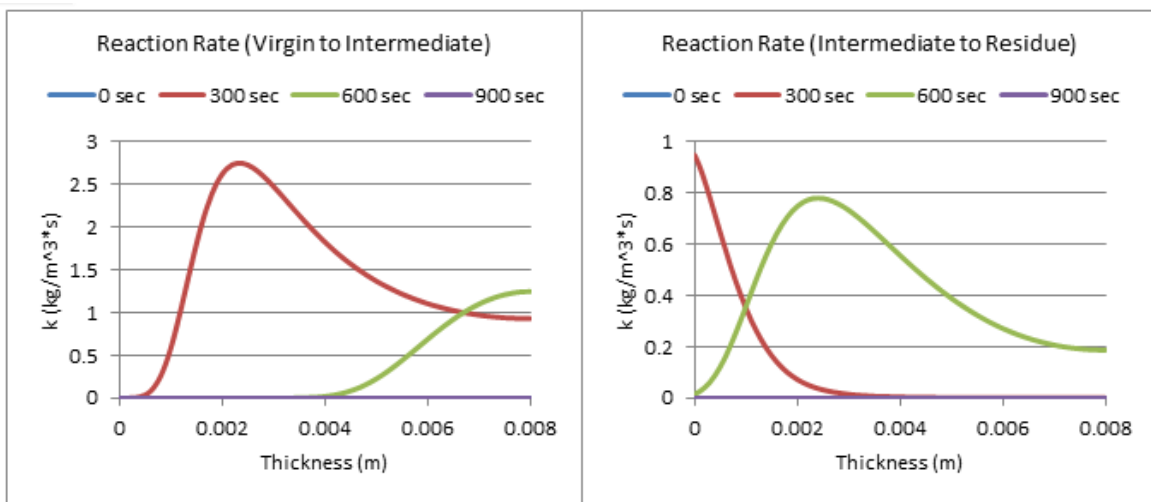
Figure 37: Profiles of Reaction Rate at a Heat Flux of 25 kW/m^2
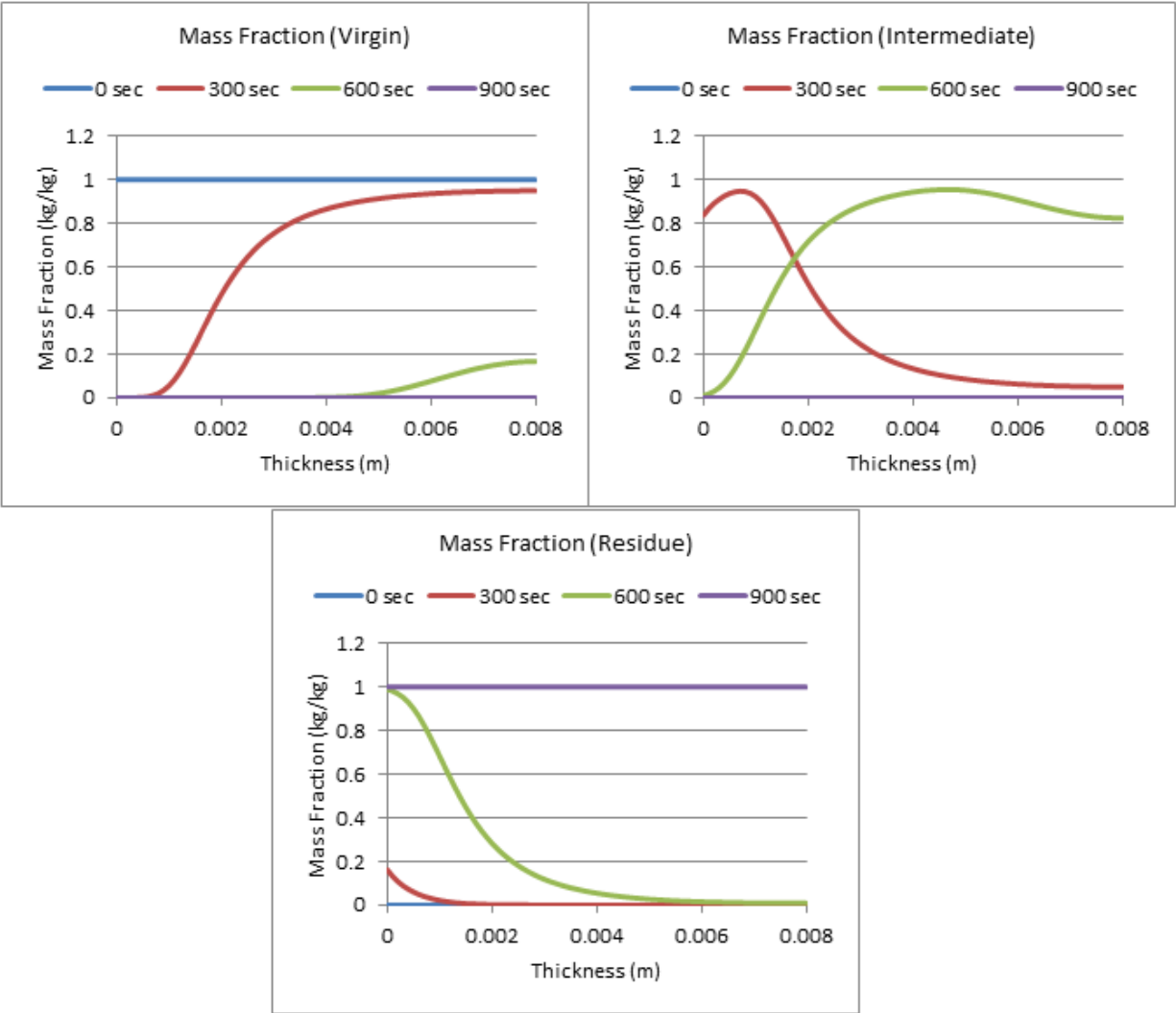
Figure 38: Profiles of Mass Fraction at a Heat Flux of 25 kW/m^2

35 kW/m^2
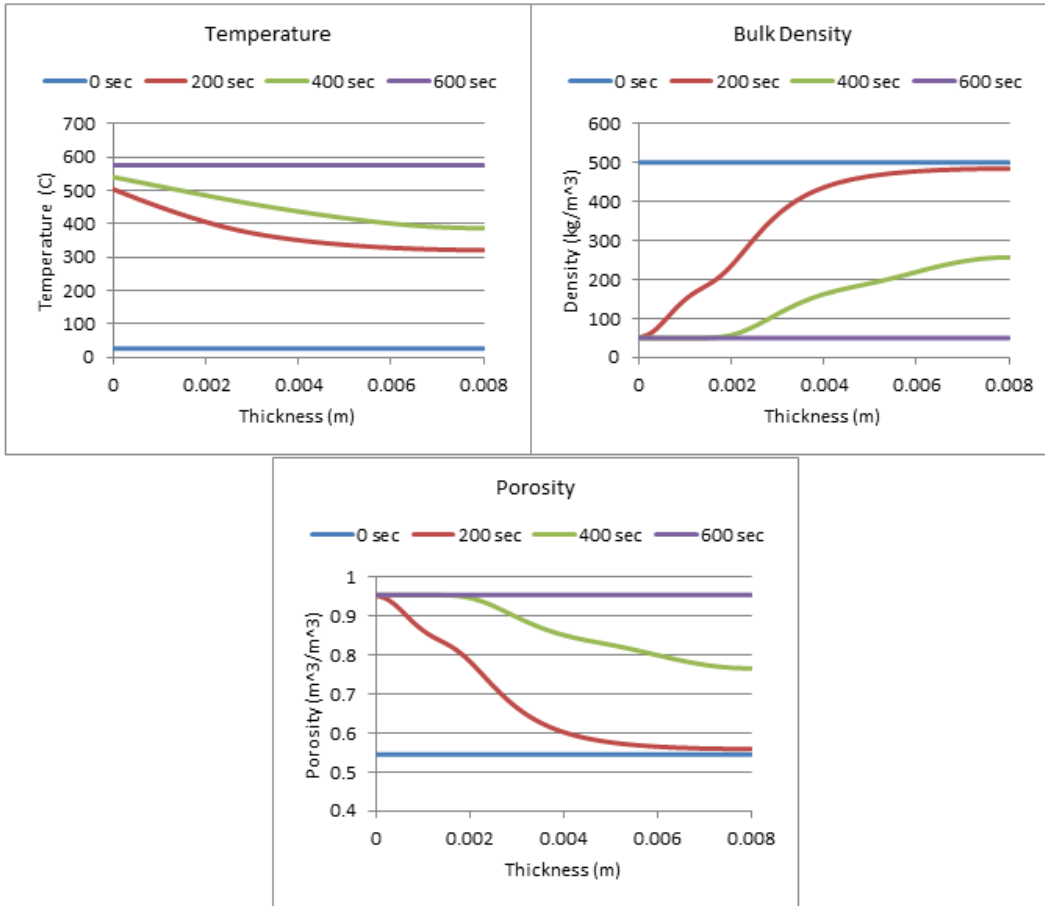
Figure 39: Profiles with a Heat Flux of 35 kW/m^2
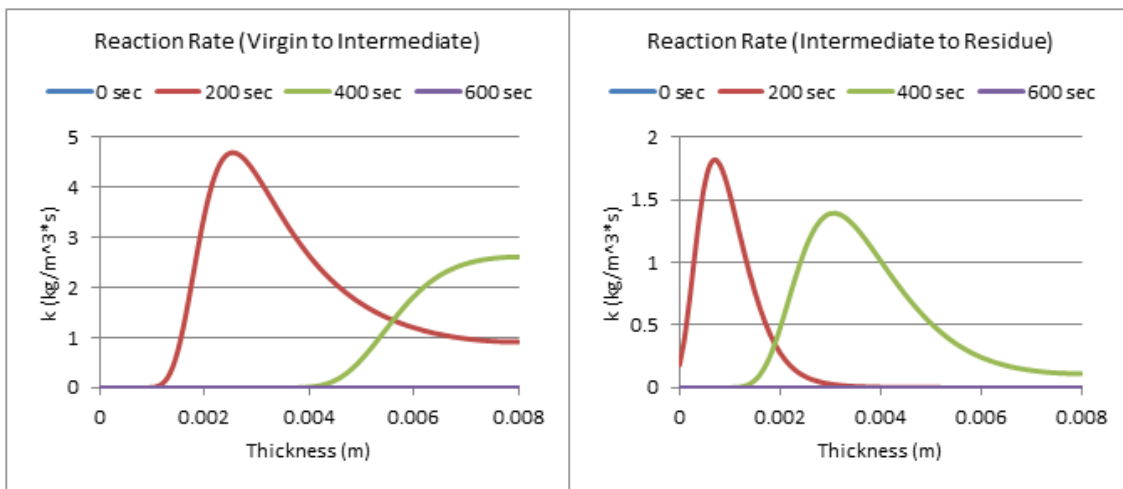
Figure 40: Profiles of Reaction Rate with a Heat Flux of 35 kW/m^2
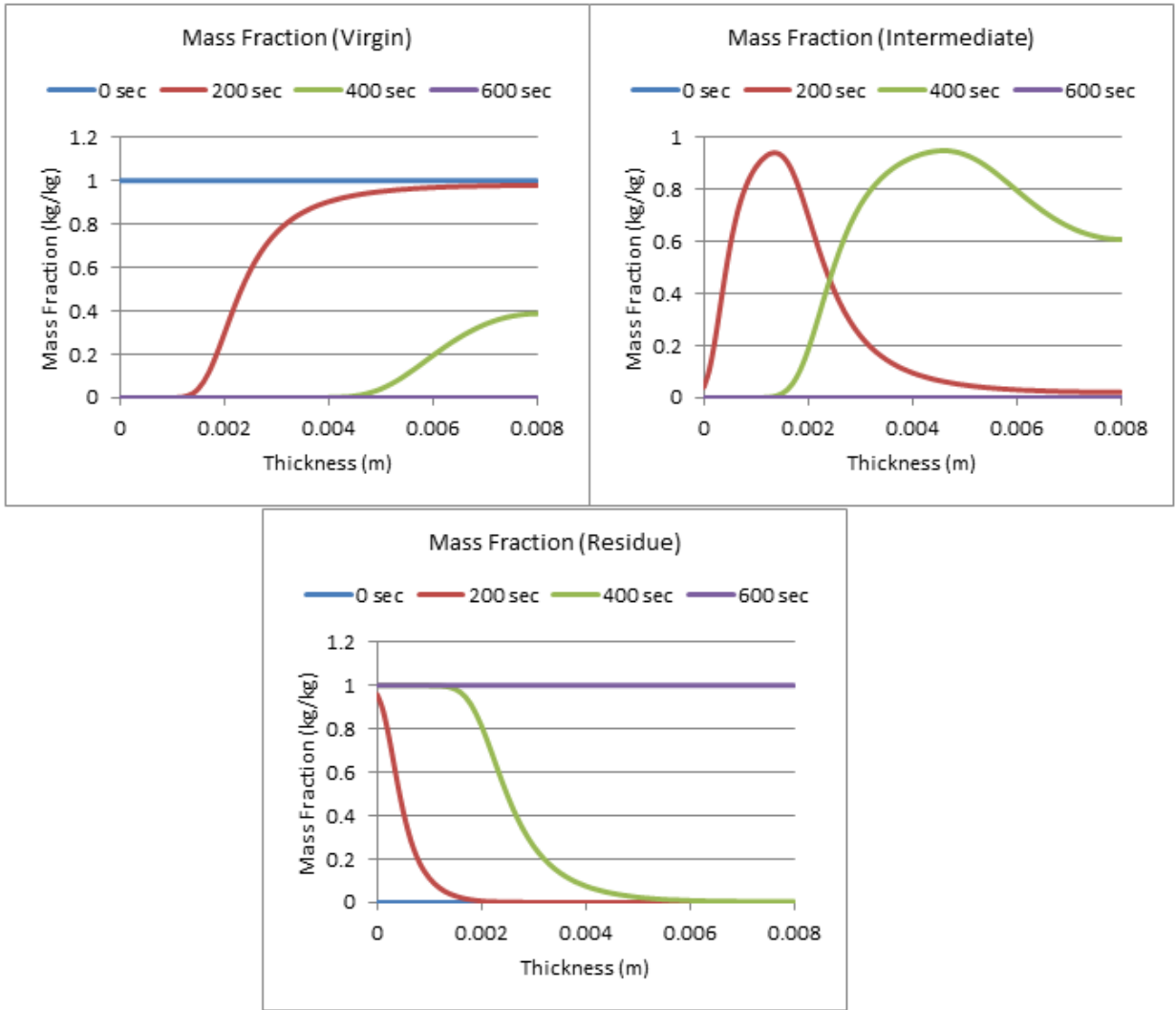
Figure 41: Profiles of Mass Fraction with a Heat Flux of 35 kW/m^2

50 kW/m^2
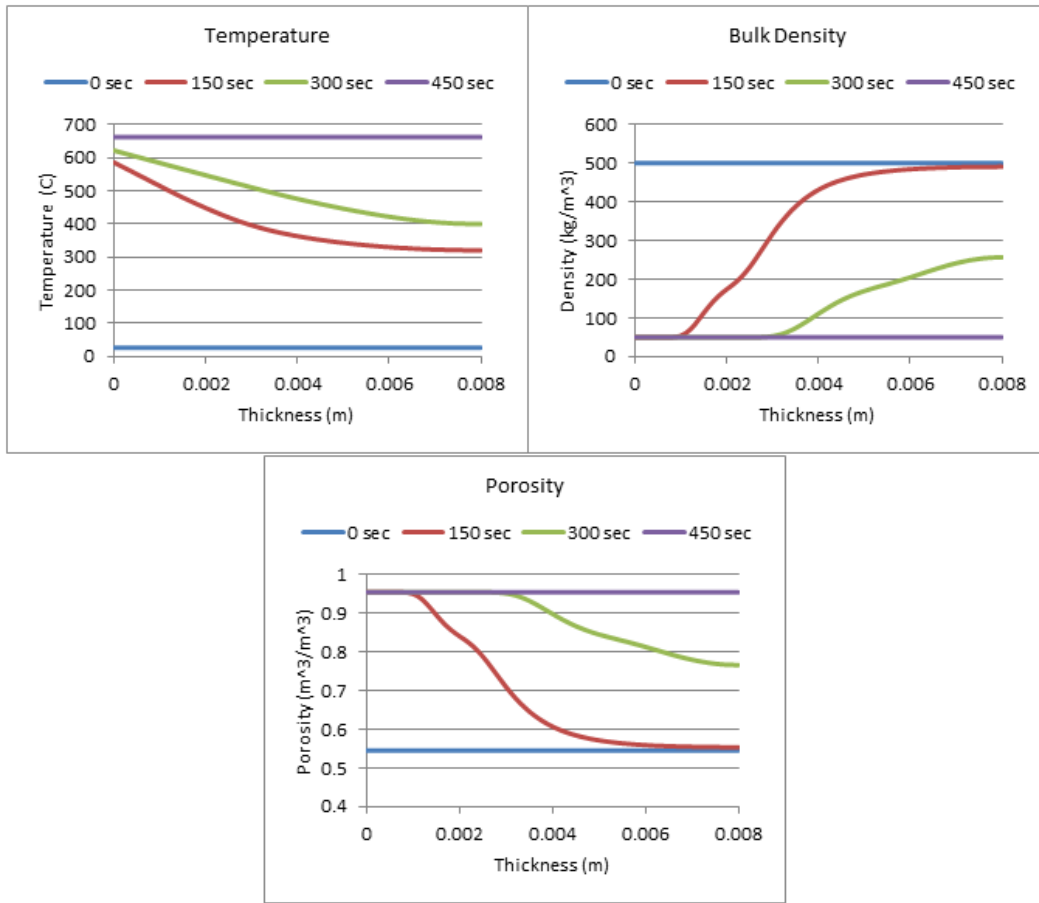
Figure 42: Profiles with a Heat Flux of 50 kW/m^2
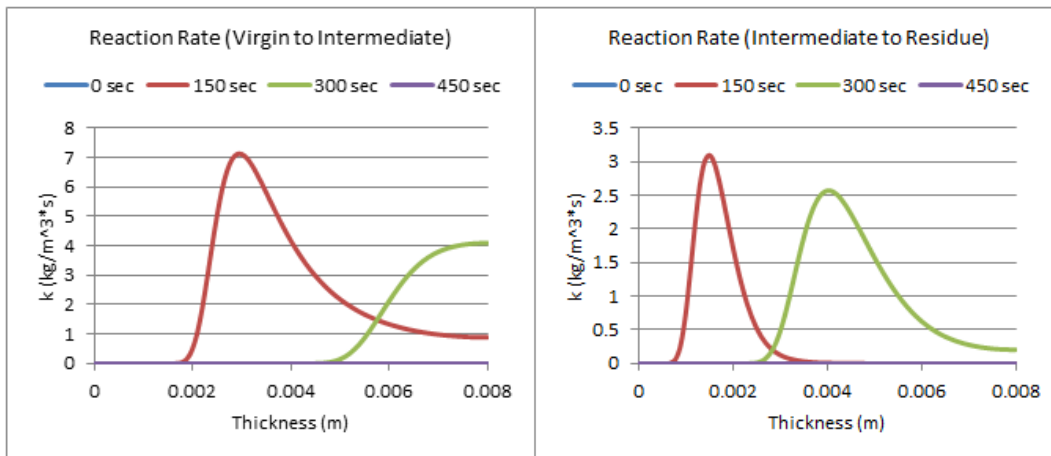
Figure 43: Profiles of Reaction Rate with a Heat Flux of 50 kW/m^2
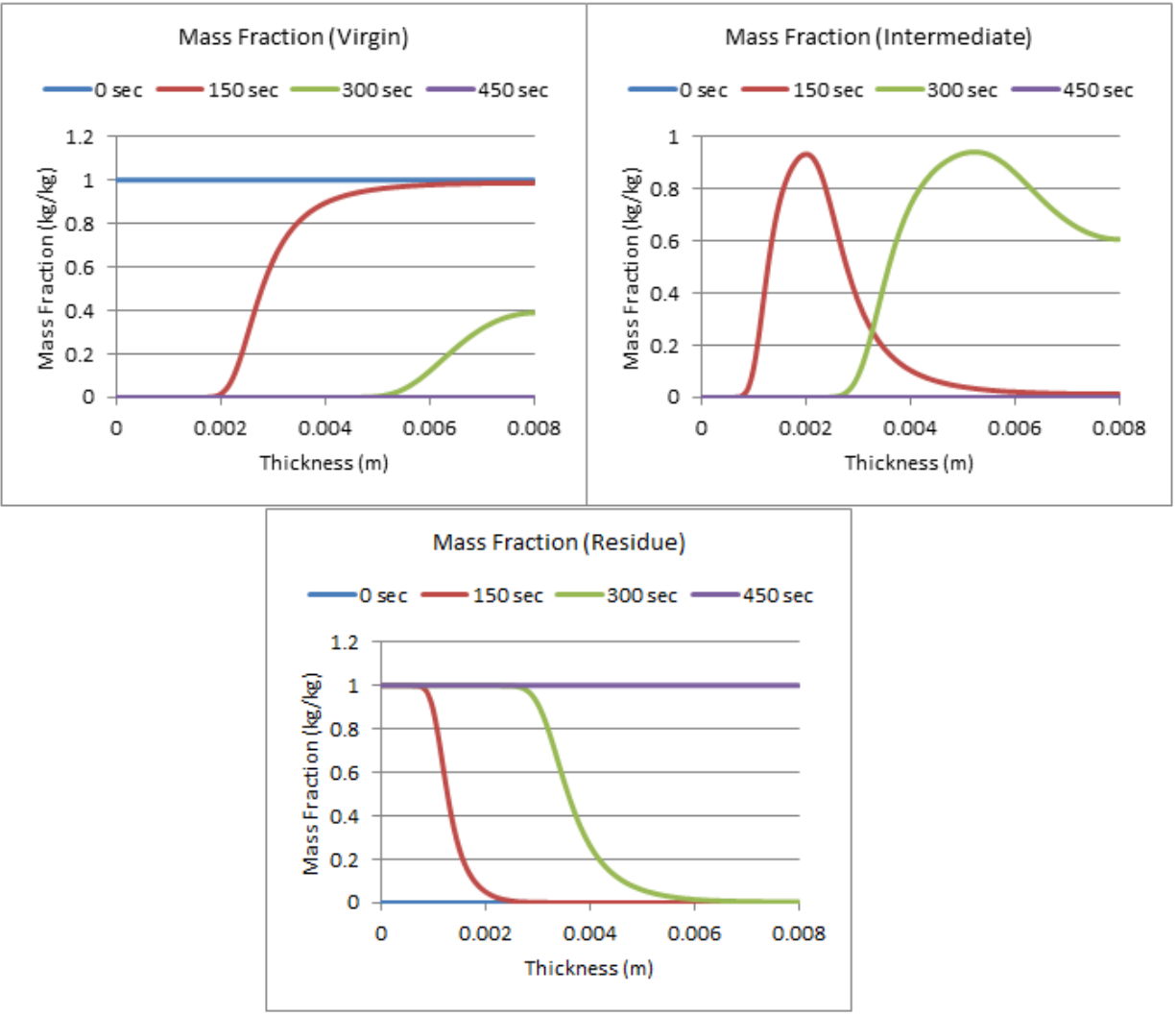
Figure 44: Profiles of Mass Fraction with a Heat Flux of 50 kW/m^2

75 kW/m^2
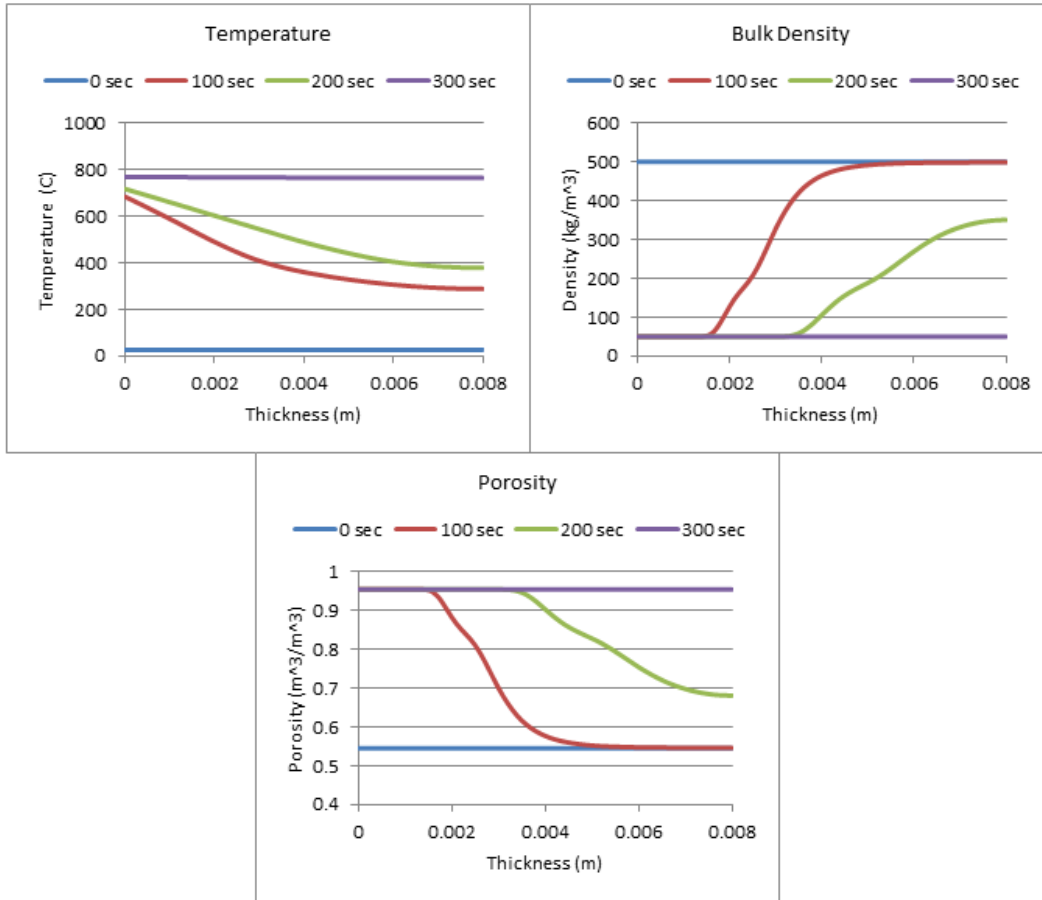
Figure 45: Profiles with a Heat Flux of 75 kW/m^2
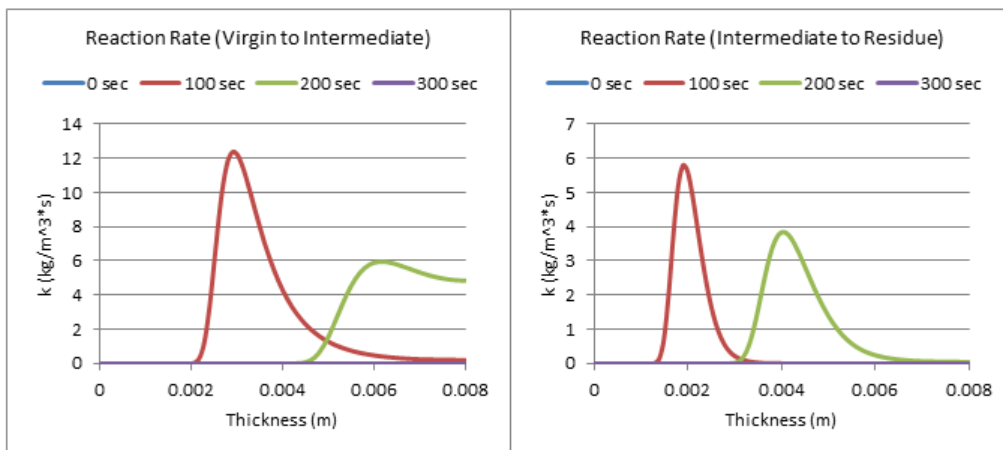
Figure 46: Profiles of Reaction Rate with a Heat Flux of 75 kW/m^2
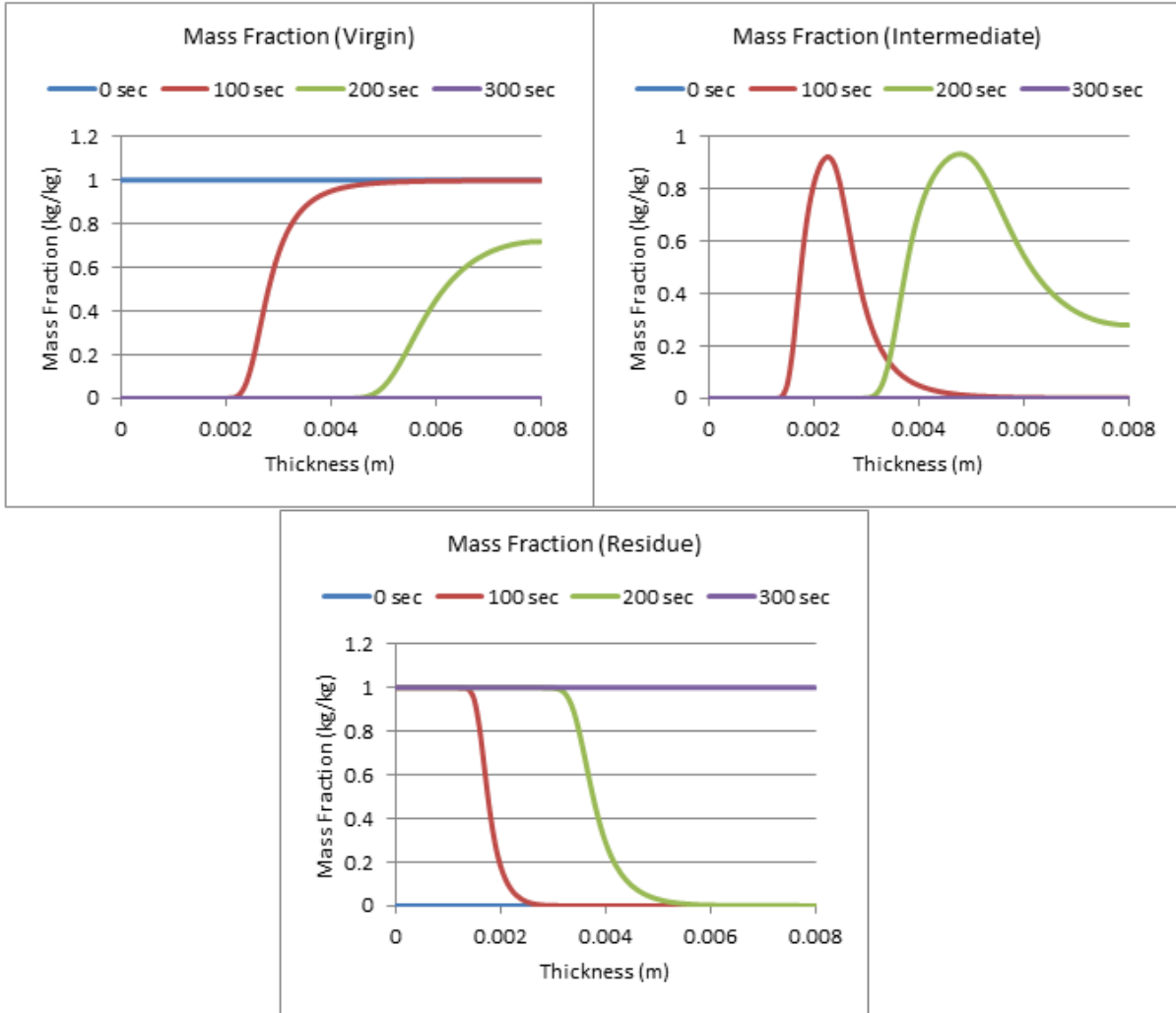
Figure 47: Profiles of Mass Fraction with a Heat Flux of 75 kW/m^2

Next, the same conditions were applied to pure ATH (the additive), and the following DTG Curve was produced. A heat flux of 50 kW/m^2 was used for the end result.
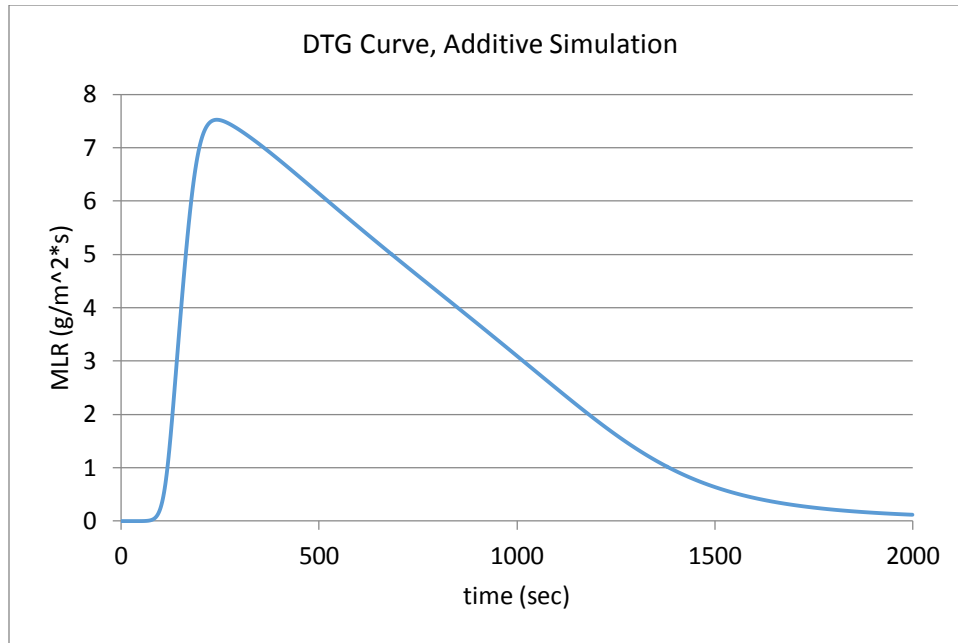
Figure 48: DTG Curve, Additive Simulation

Having the resin and additive graphed separately will help in a better understanding once a mixed model is produced.

The next parameter to be better understood is the contact conductance. Its baseline value in Gpyro is 10 W/m^2*K. Since a baseline simulation has already been completed, the contact conductance was varied to higher and lower values, and the graphs can be seen below, using the rest of the baseline parameters.
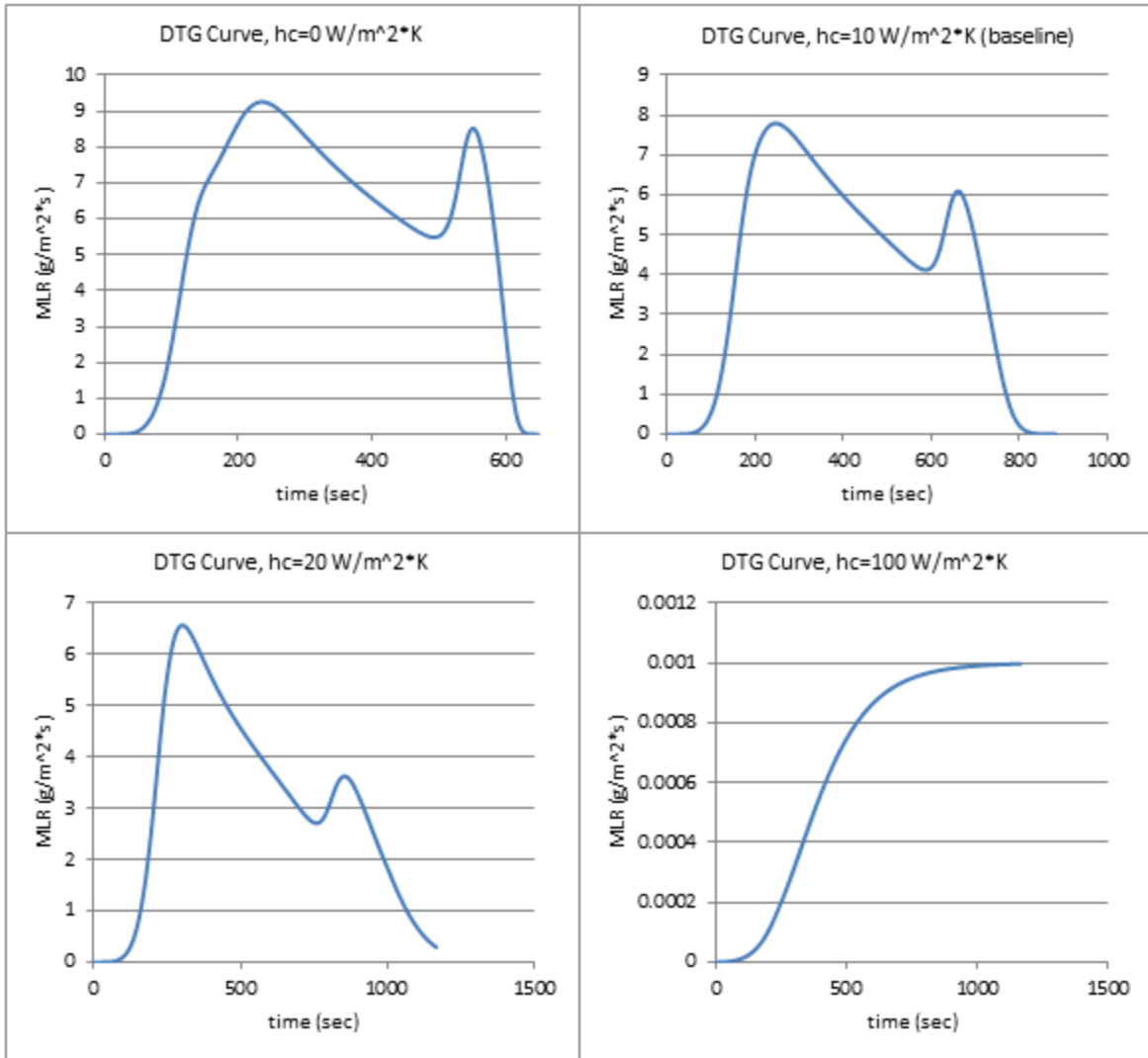
Figure 49: Gpyro Sample 3, Contact Conductance

As the contact conductance is increased, the amount of mass lost is decreased, and the time it takes for the mass loss to be complete is greatly lengthened. Considering the small sample size used in the TGA, once simulating an actual material, it would be best to assume perfect insulation at the back interface (hc= 0 W/m^2*K). The values were graphed all together to better see their differences, which can be seen in the graph below.
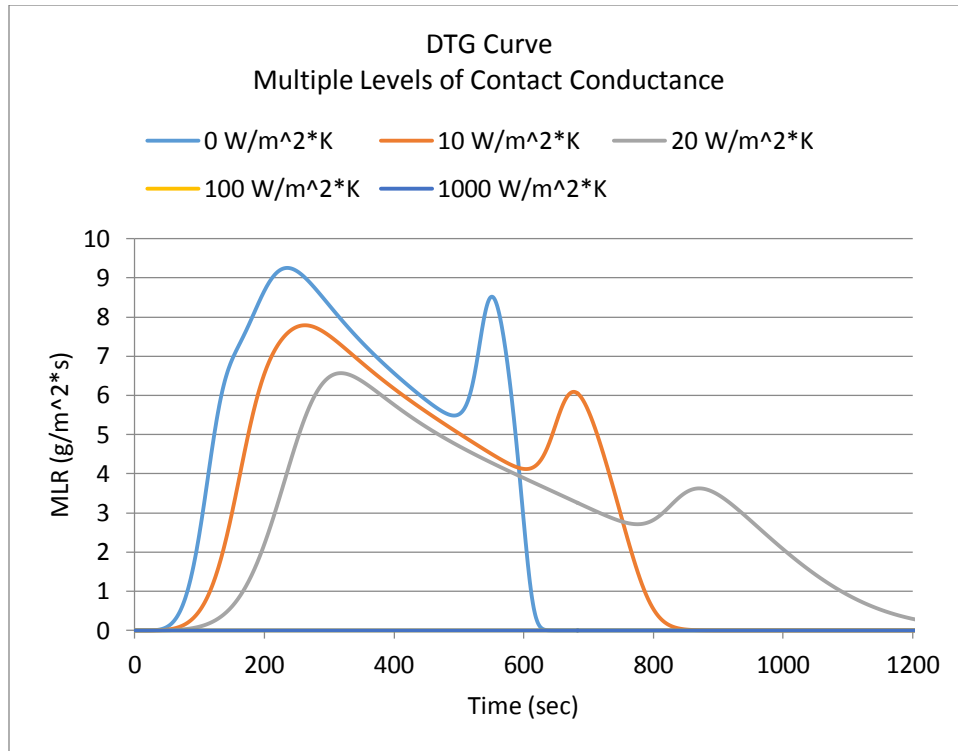
Figure 50: DTG Curve Multiple Levels of Contact Conductance

To ensure that setting the contact conductance to zero is Gpyro would work, it was compared against a very small contact conductance, against various levels of heat flux. The results can be seen in the graphs below.
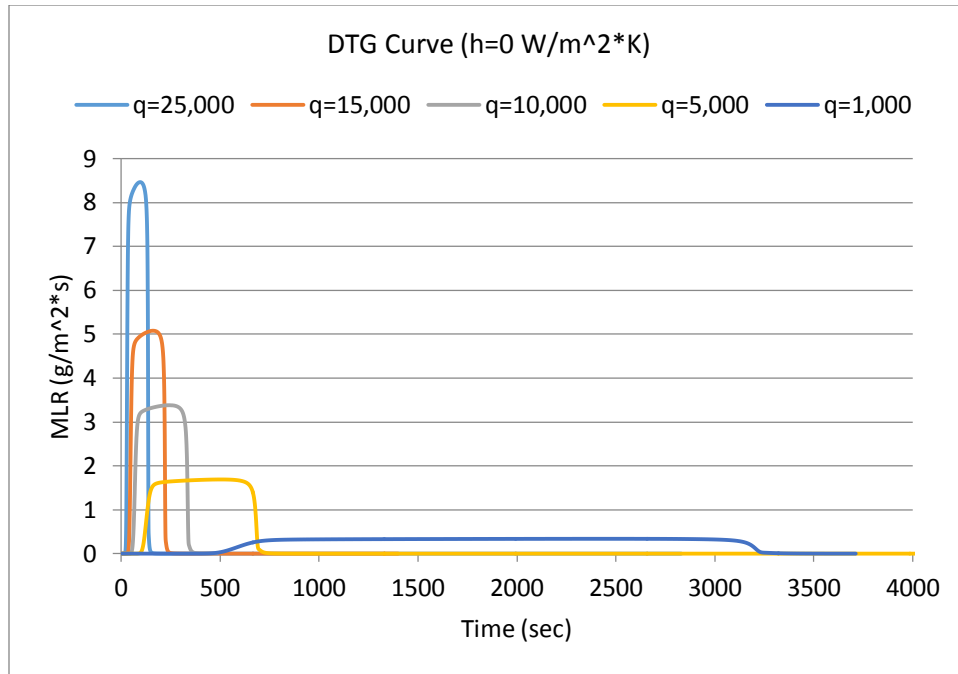
Figure 51: DTG Curve, h=0 W/m^2*K
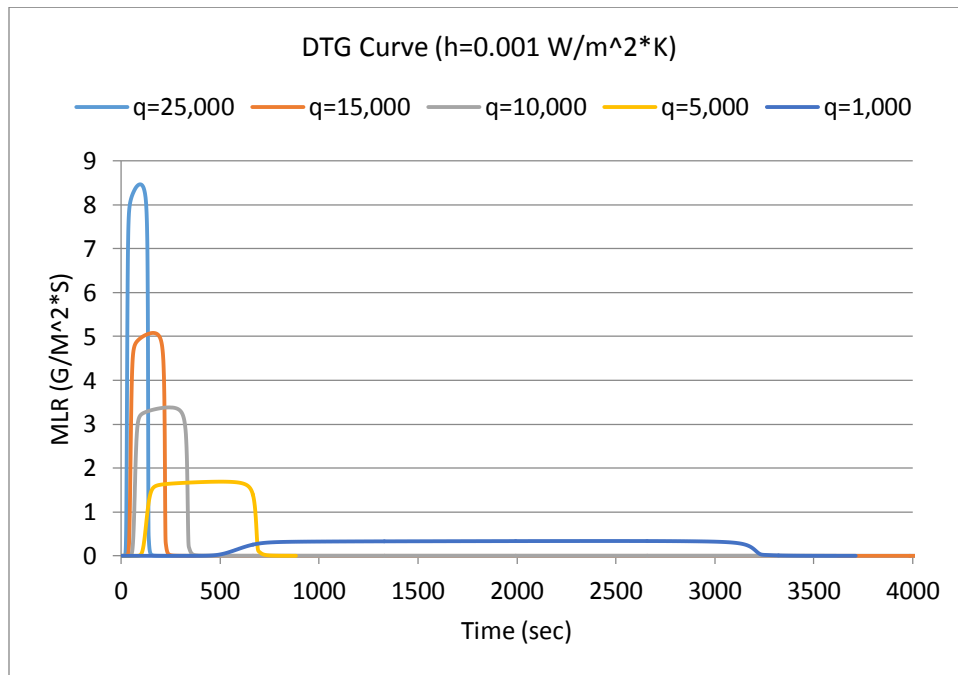
Figure 52: DTG Curve, h=0.001 W/m^2*K

The profiles for the different levels of contact conductance were also created, which can be seen below.

0 W/m^2*K
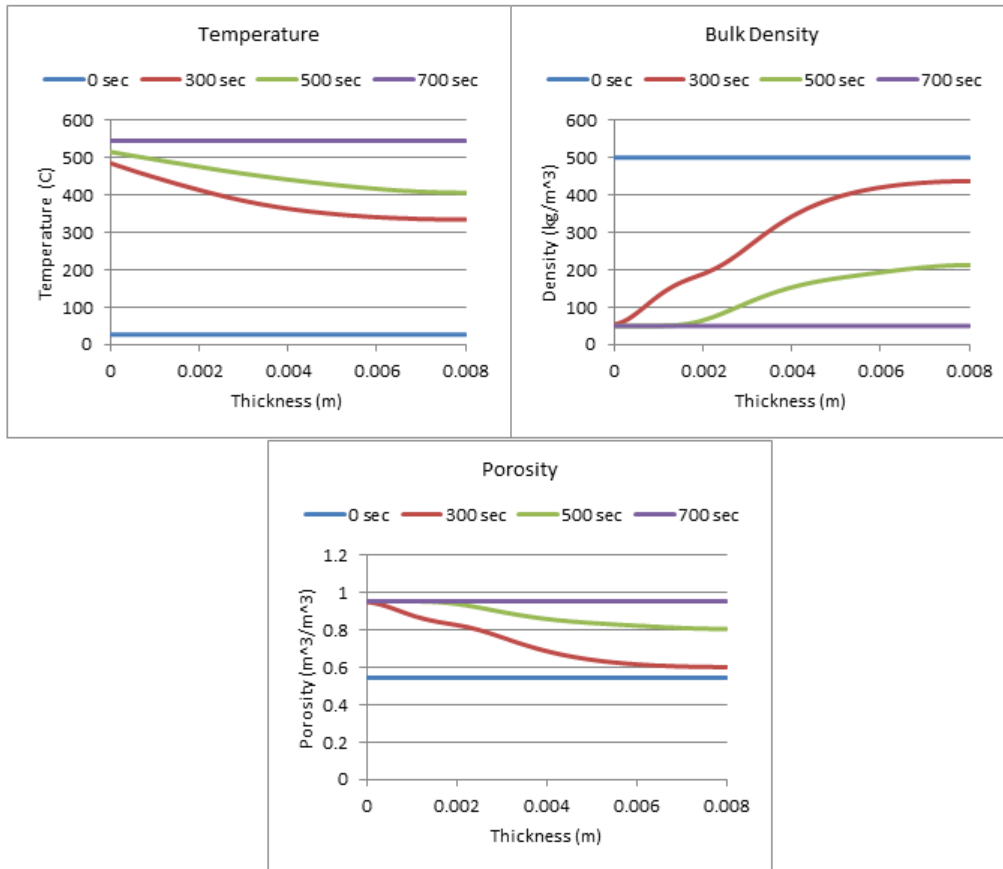
Figure 53: Profiles with a Contact Conductance of 0 W/m^2*K
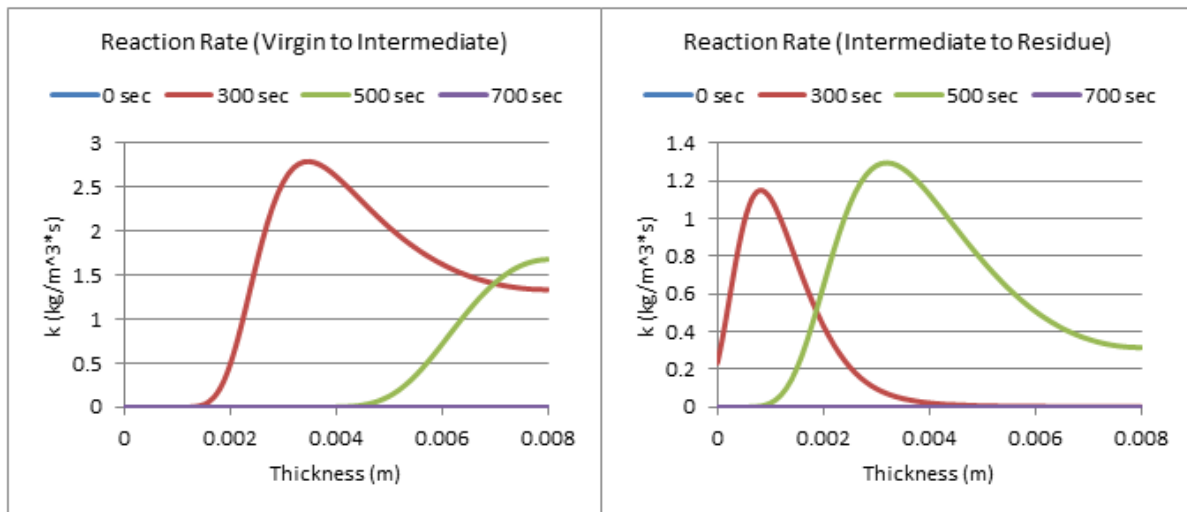
Figure 54: Profiles of Reaction Rate with a Contact Conductance of 0 W/m^2*K
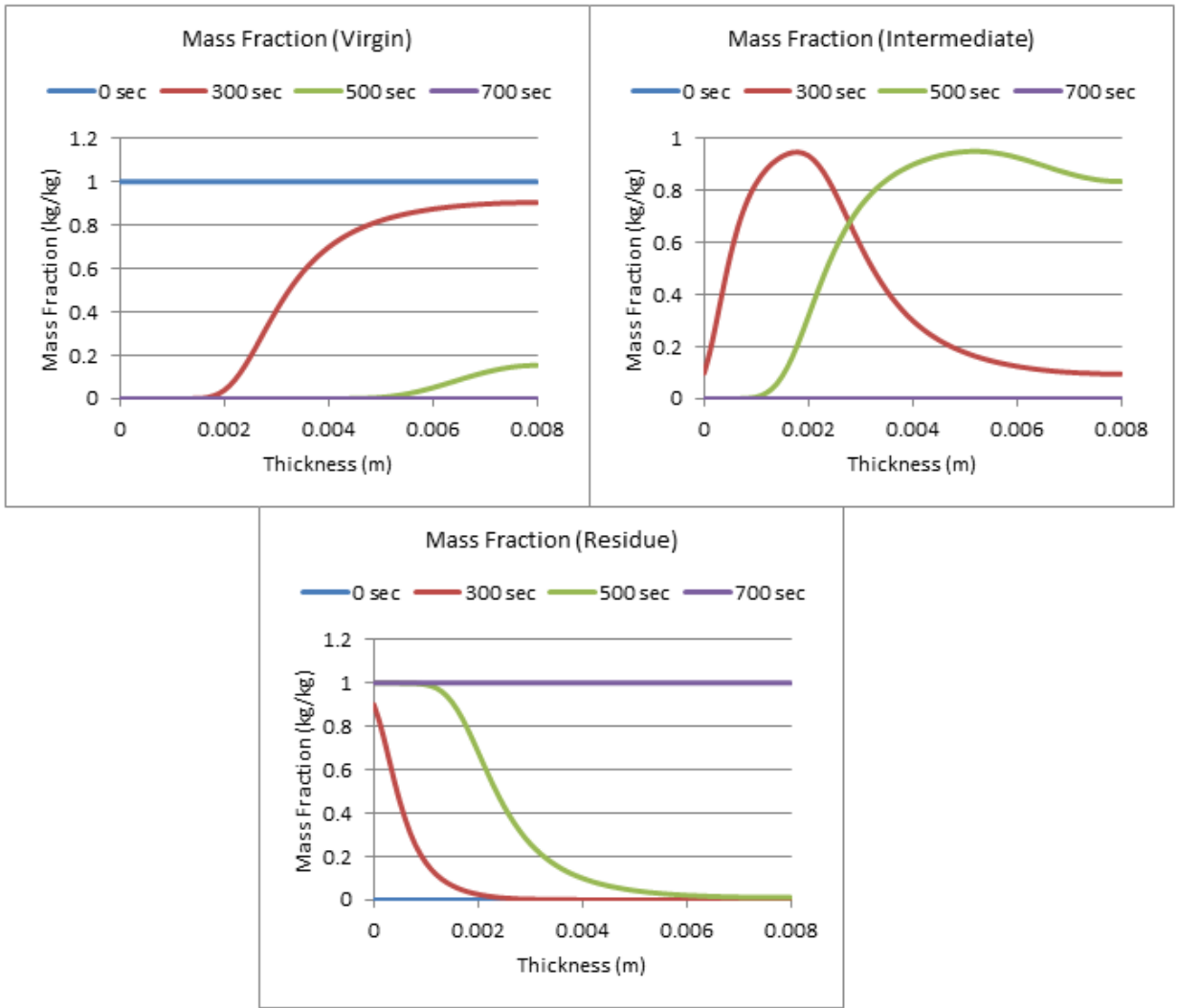
Figure 55: Profiles of Mass Fraction with a Contact Conductance of 0 W/m^2*K

10 W/m^2*K
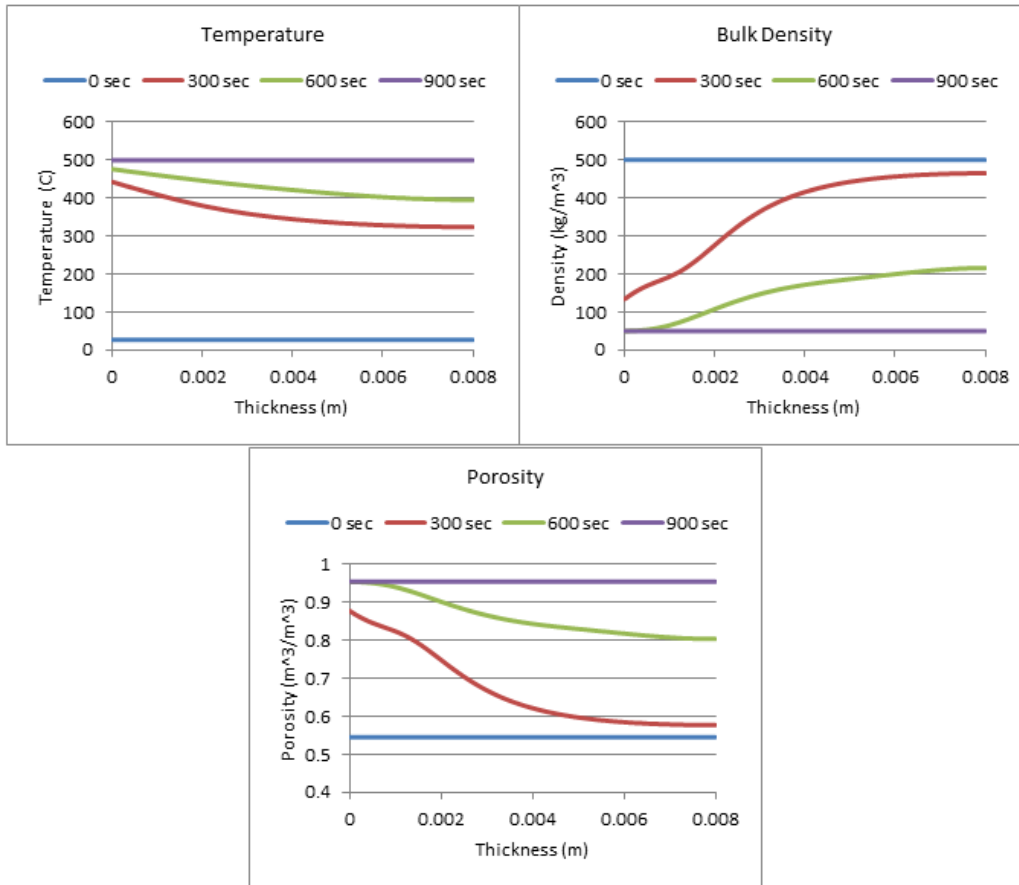
Figure 56: Profiles with a Contact Conductance of 10 W/m^2*K
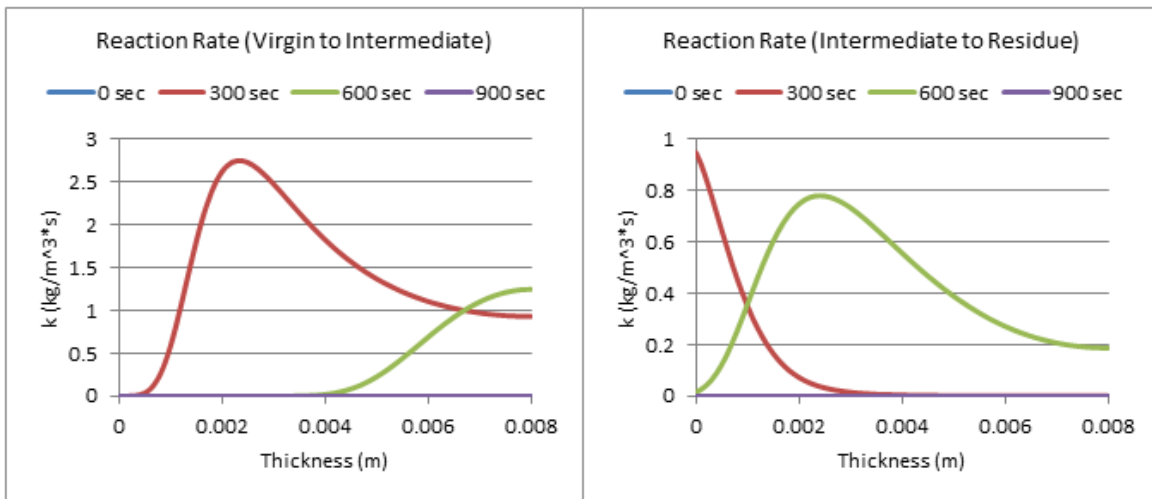
Figure 57: Profiles of Reaction Rate with a Contact Conductance of 10 W/m^2*K
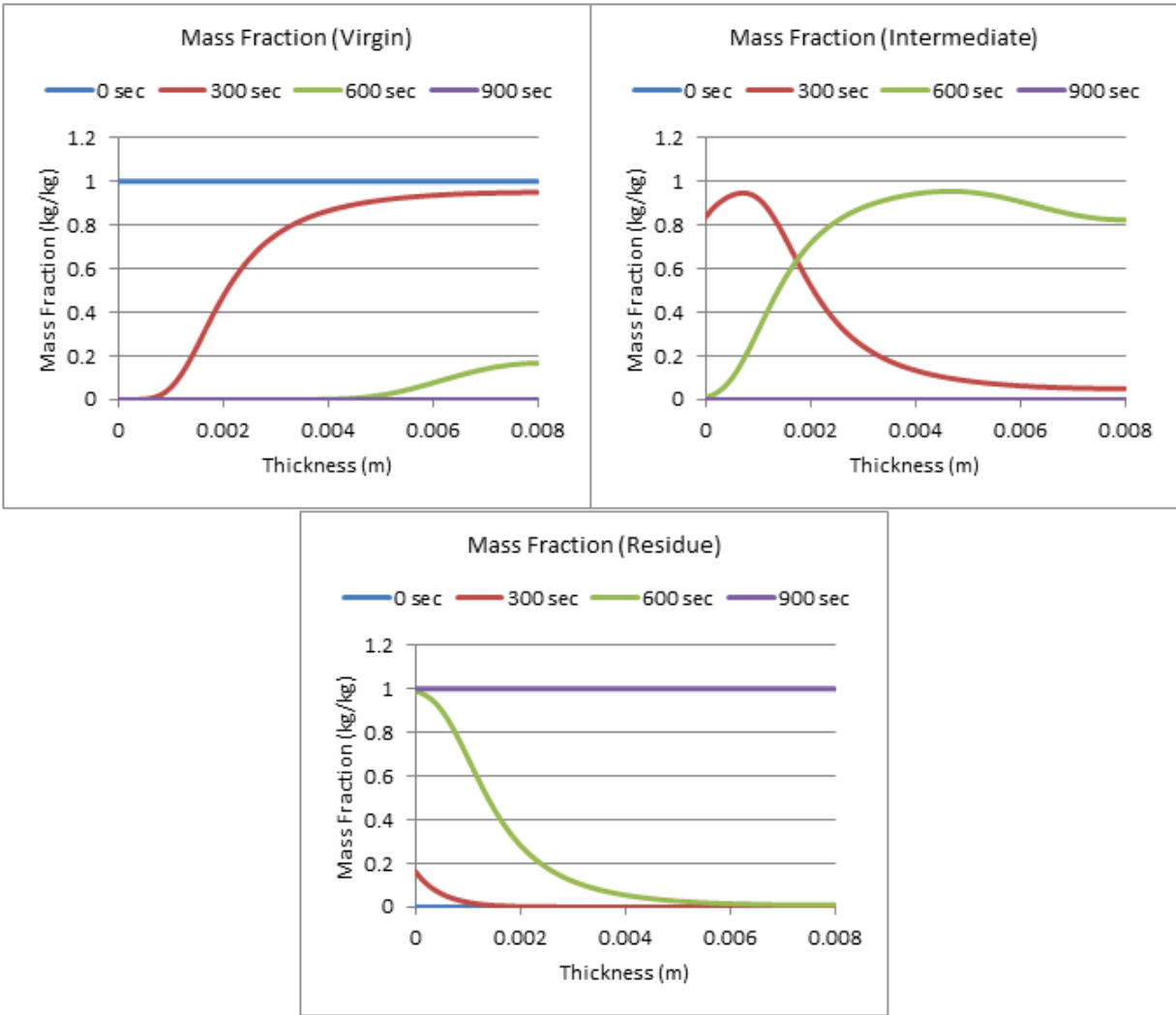
Figure 58: Profiles of Mass Fraction with a Contact Conductance of 10 W/m^2*K

20 W/m^2*K
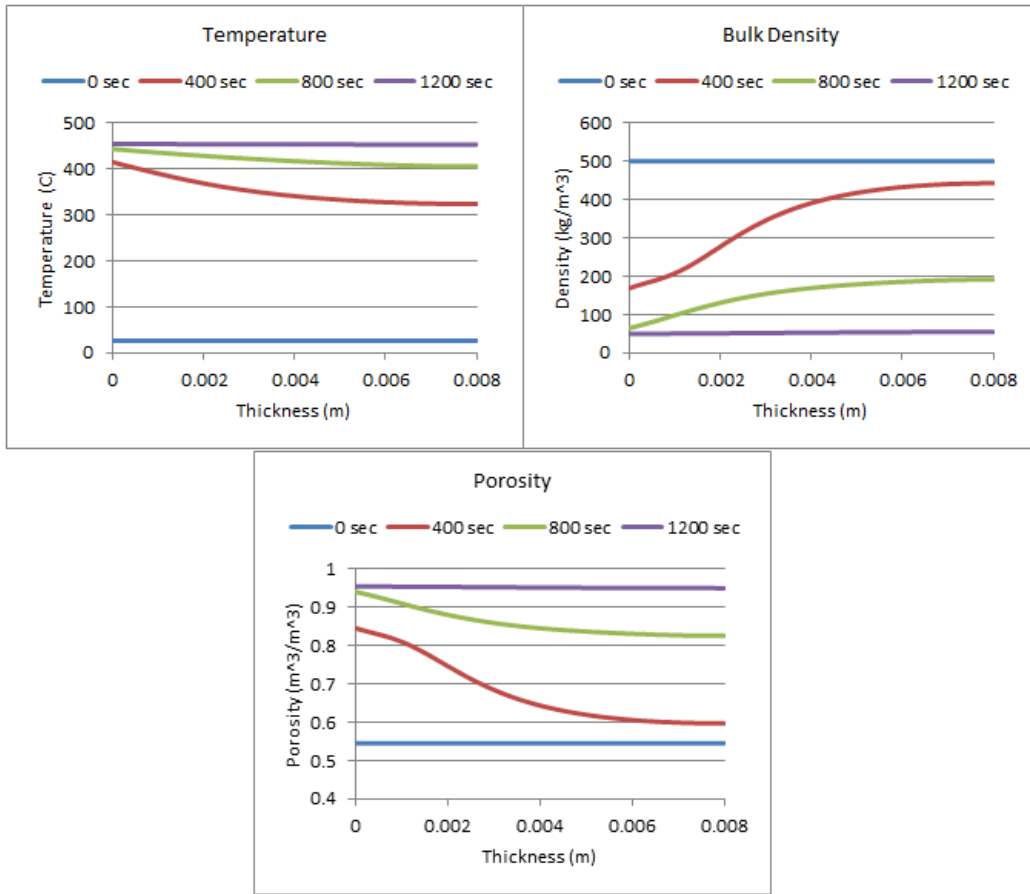
Figure 59: Profiles with a Contact Conductance of 20 W/m^2*K
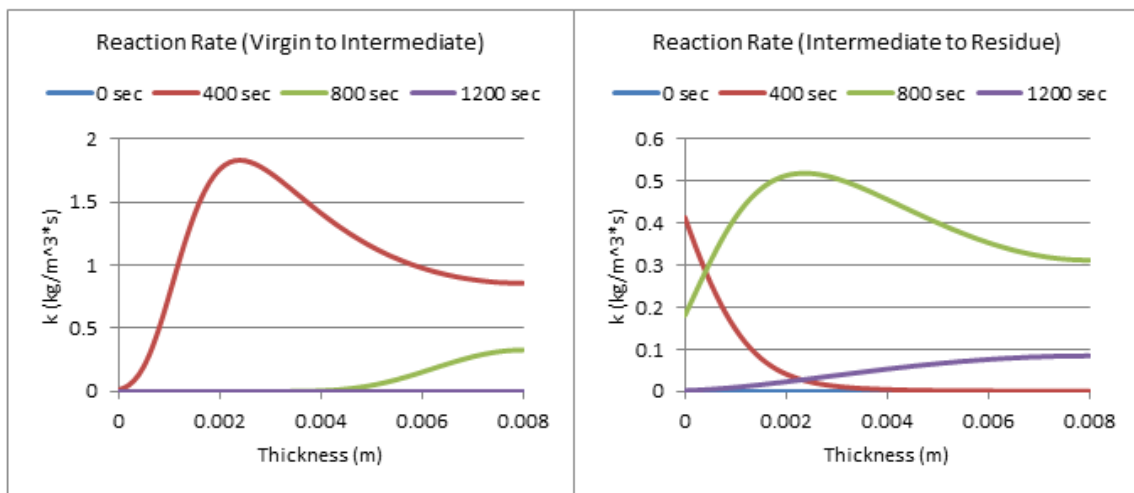
Figure 60: Profiles of Reaction Rate with a Contact Conductance of 20 W/m^2*K
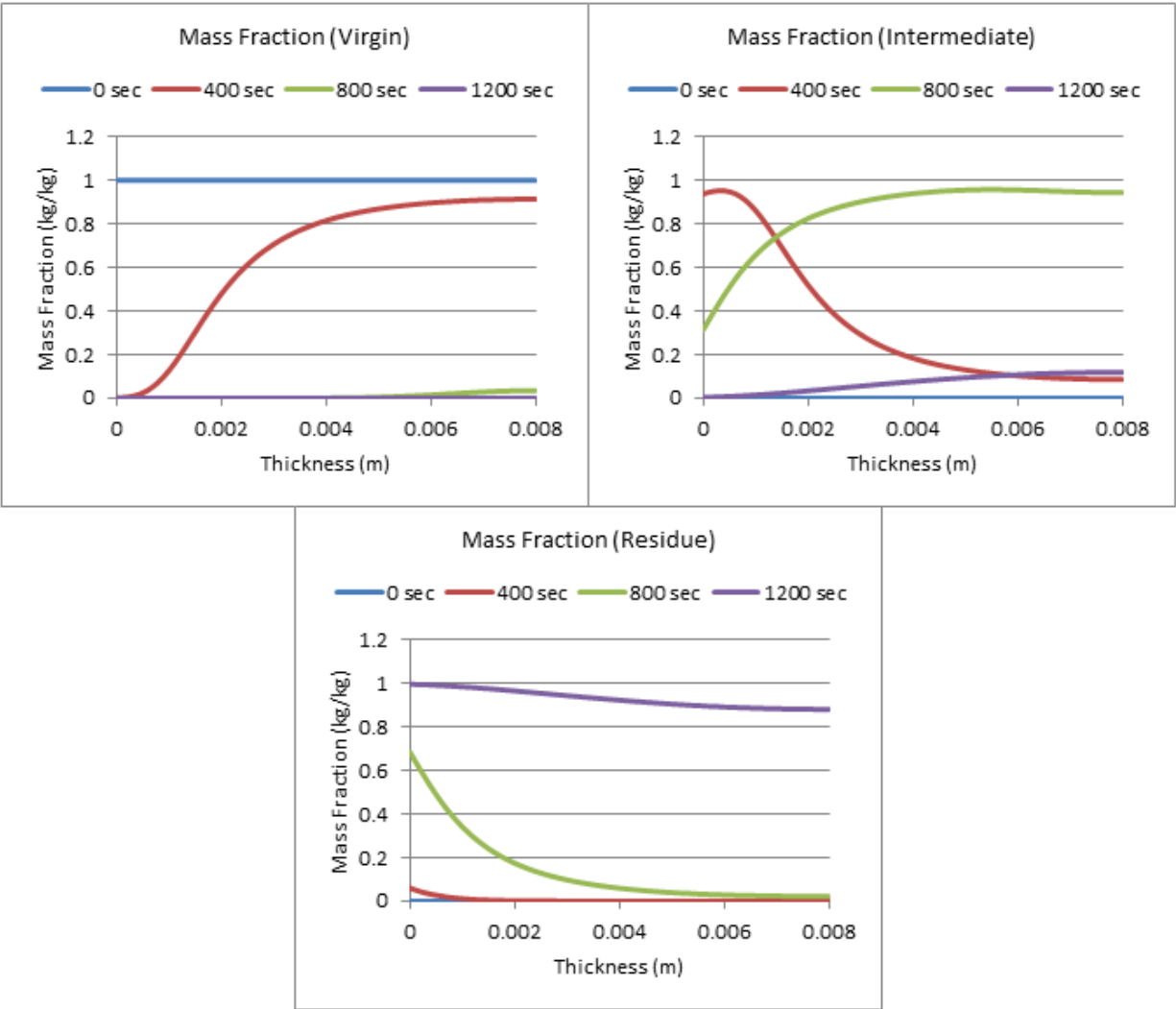
Figure 61: Profiles of Mass Fraction with a Contact Conductance of 20 W/m^2*K

100 W/m^2*K
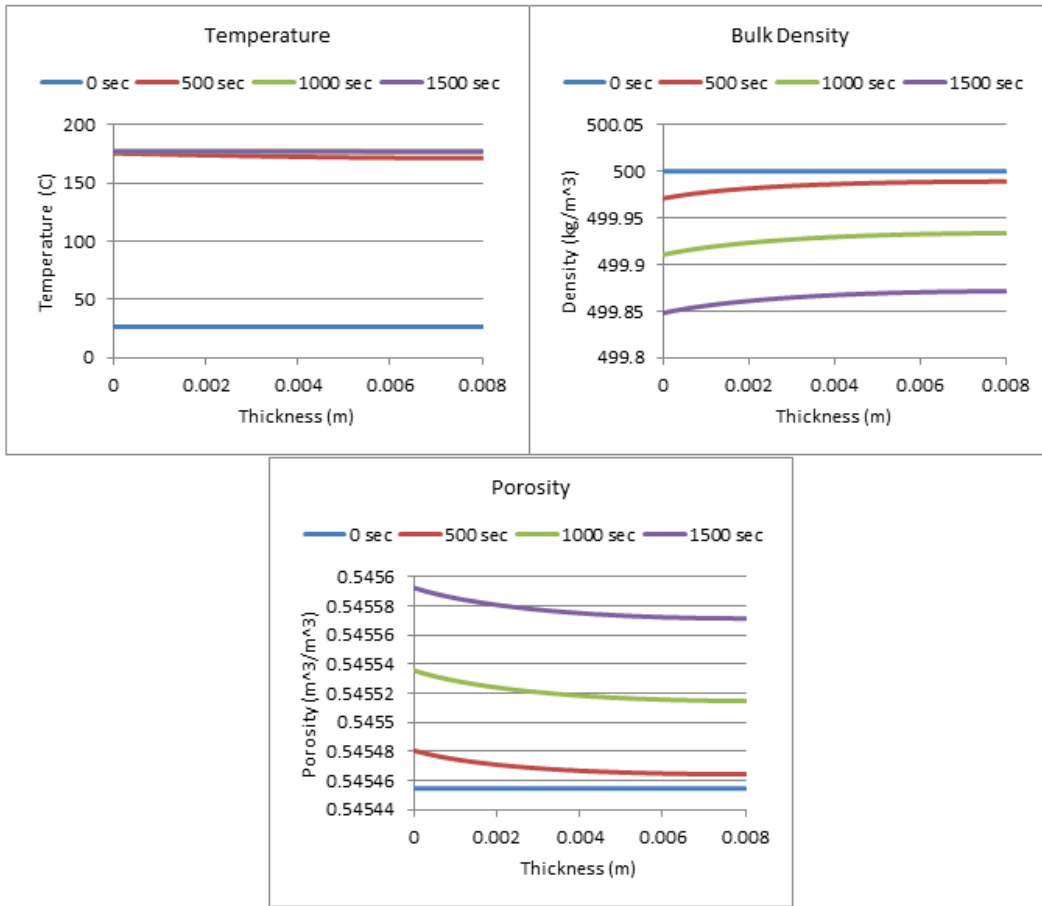
Figure 62: Profiles with a Contact Conductance of 100 W/m^2*K
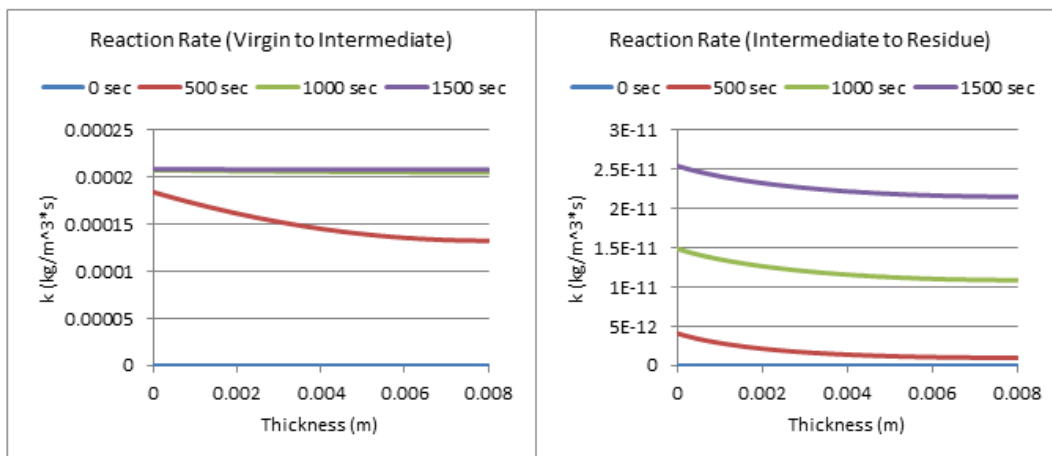
Figure 63: Profiles of Reaction Rate with a Contact Conductance of 100 W/m^2*K
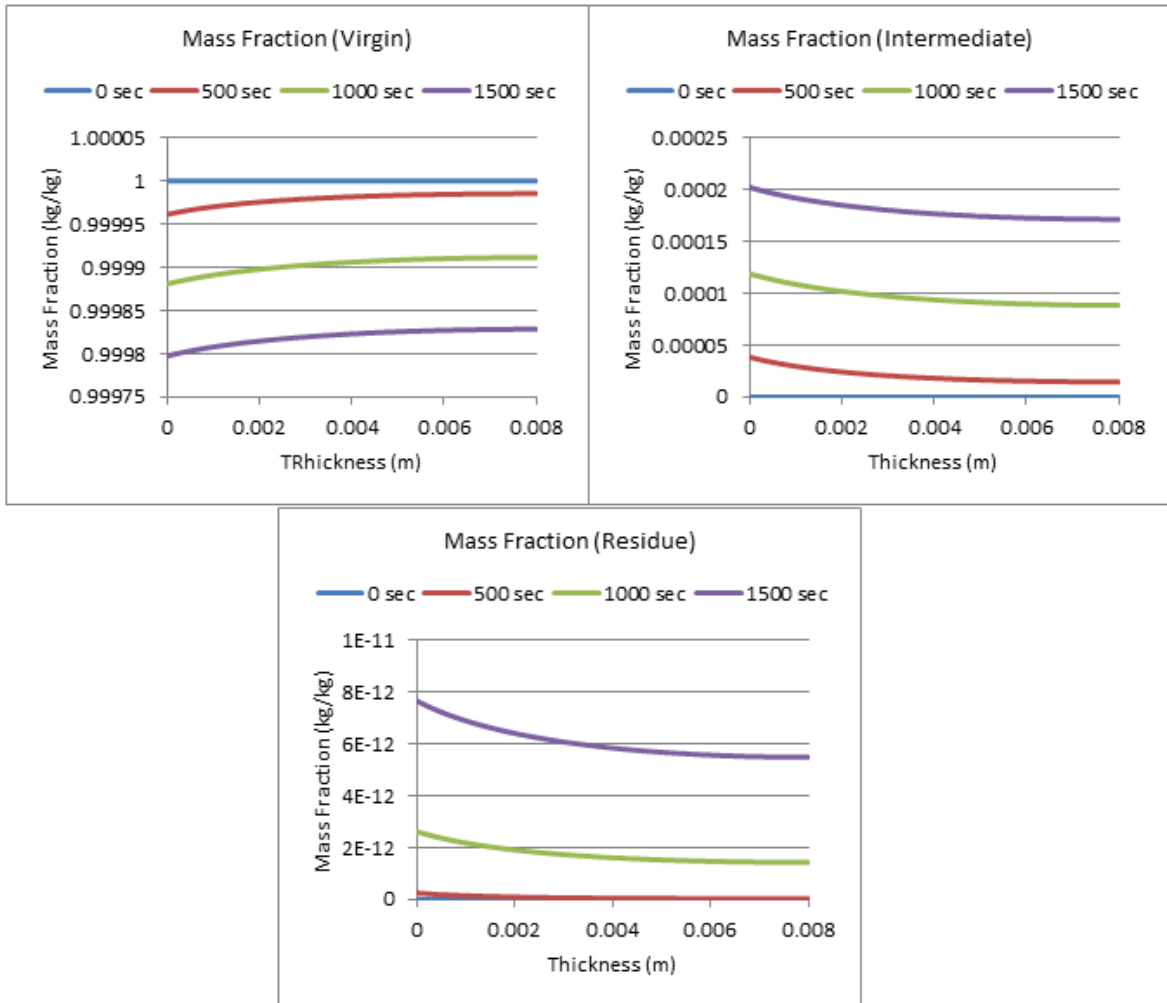
Figure 64: Profiles of Mass Fraction with a Contact Conductance of 100 W/m^2*K

1000 W/m^2*K
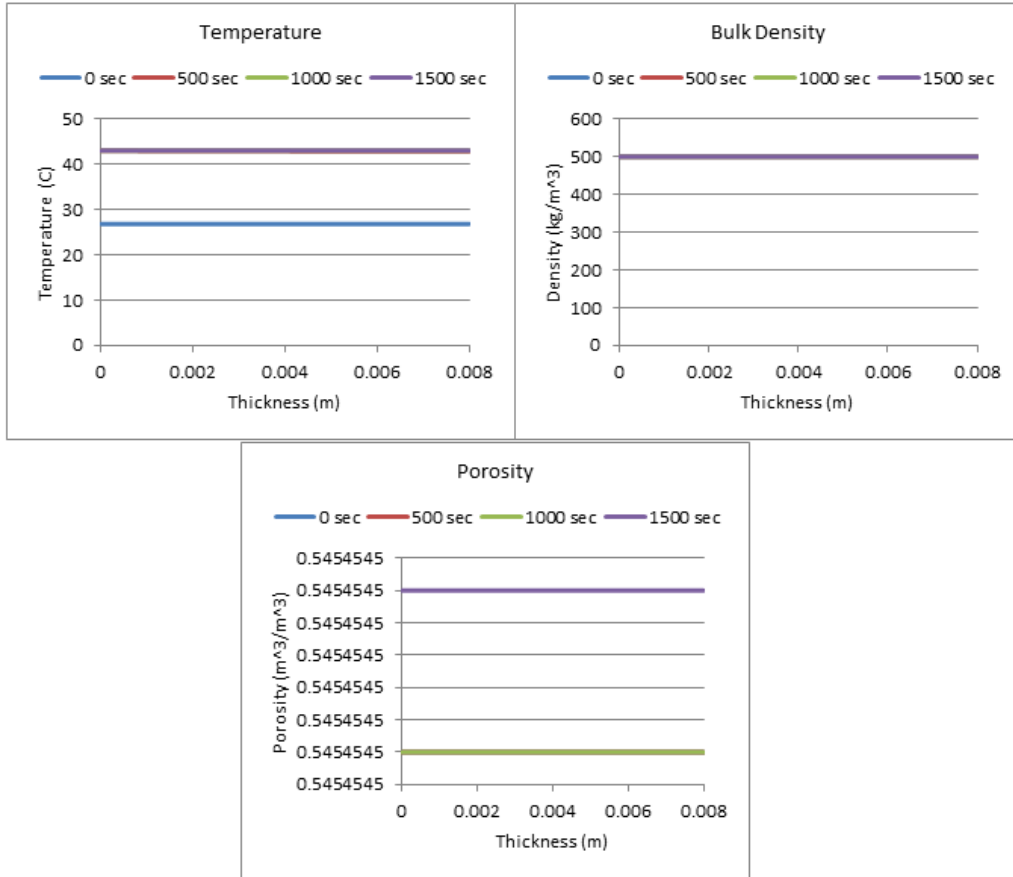
Figure 65: Profiles with a Contact Conductance of 1000 W/m^2*K
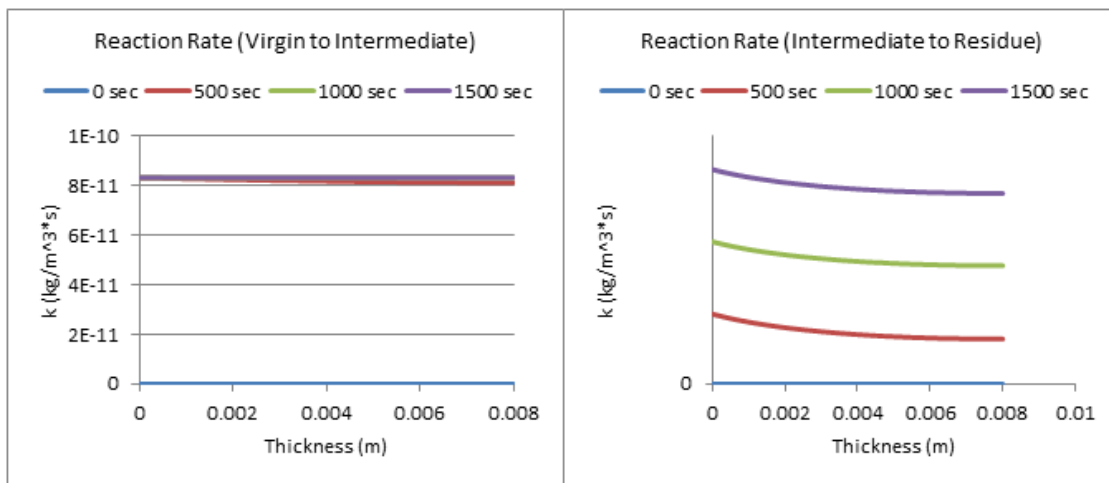
Figure 66: Profiles of Reaction Rate with a Contact Conductance of 1000 W/m*2*K
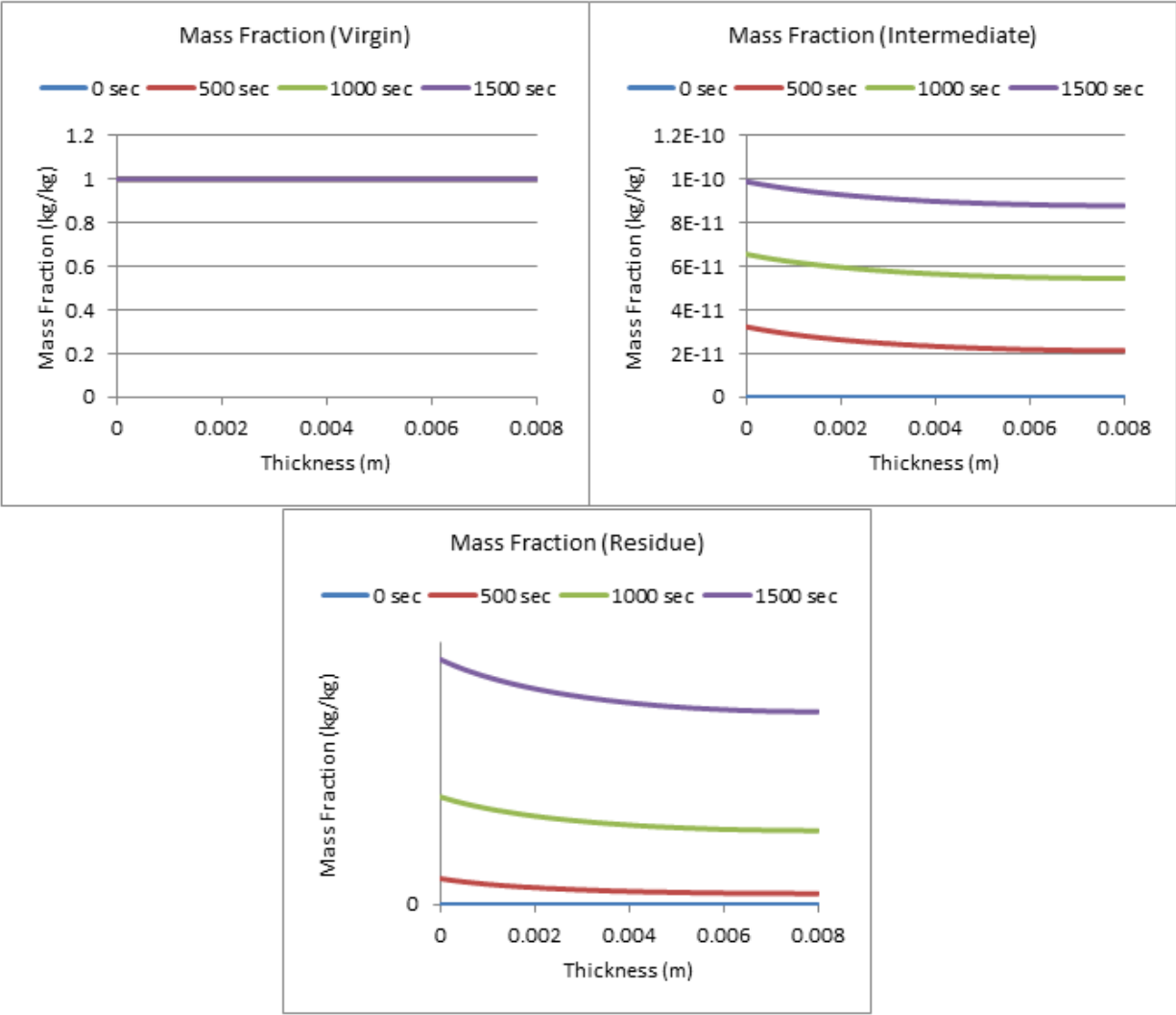
Figure 67: Profiles of Mass Fraction with a Contact Conductance of 1000 W/m^2*K

Appendix E.6: Gpyro 1D Resin/ATH Mixtures

Next, the boundary conditions were set to their chosen values, and the Resin/ATH mixtures were run at varying amounts of ATH. The results are shown the section below. The two tables below show the input parameters for Resin and ATH [16].

Table 17: Material Properties (Resin/ATH Mixture)

Name	k (W/m*K)	ρ (kg/m^3)	c (J/kg*K)	ε (-)	ϒ (m)
Resin	0.230	1200	1400	0.84	0
Resin Residue	0.190	253	1900	0.90	3.84*10^-3
ATH	1.220	2300	1200	0.81	0
ATH Residue	0.240	1558	1200	0.89	4.75*10^-3

Table 18: Reactions (Resin/ATH Mixture)

Species (A)	Species (B)	Z (s^-1)	E (kJ/mol)	ΔH (J/kg)	n (-)
Resin	Resin Residue	3.2*10^12	183	2.5*10^6	1.3
ATH	ATH Residue	1.6*10^12	160	3.7*10^6	5

These properties were first analyzed in a 0D simulation in Gpyro to check that the kinetic properties match up with typical DTG Curves for Pure Hetron (Resin) and Pure ATH. These results can be seen in the graphs below. Although there is not a perfect match between the two, they are fairly similar and generally follow the same trend.
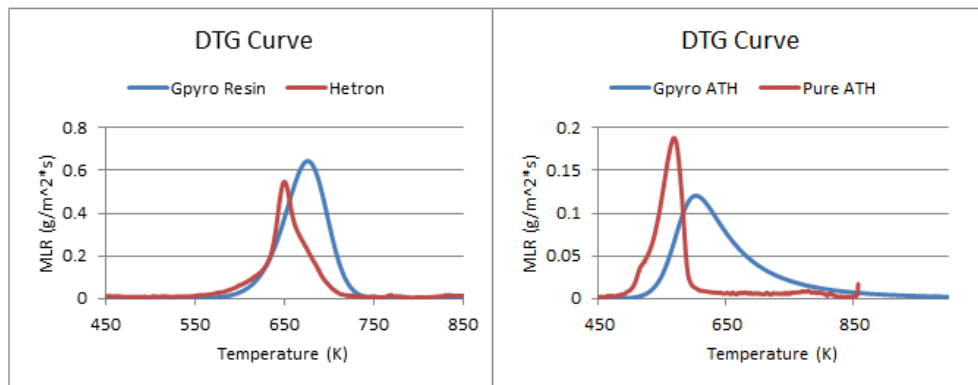
Figure 68: DTG Curves Simulating Pure Resin and Pure Additive

The resin DTG Curves were very similar, while the ATH DTG Curves were slightly different. This is probably due to the type of ATH used in the two different tests. But, when comparing the weight loss fraction, the Pure ATH had a weight-loss fraction of 0.34, while the Gpyro ATH showed a weight-loss fraction of 0.33, which is very similar. Profiles were created using the new kinetic parameters at varying levels of ATH, which can be seen below.

5% ATH

First, in the input of the Gpyro program, the percent ATH was changed from 0% to 5% ATH.

MLR Curve

The graph below shows the mass loss curve for the simulated sample. It peaks around 250 seconds at a MLR of about 7.8 g/m^2*s.
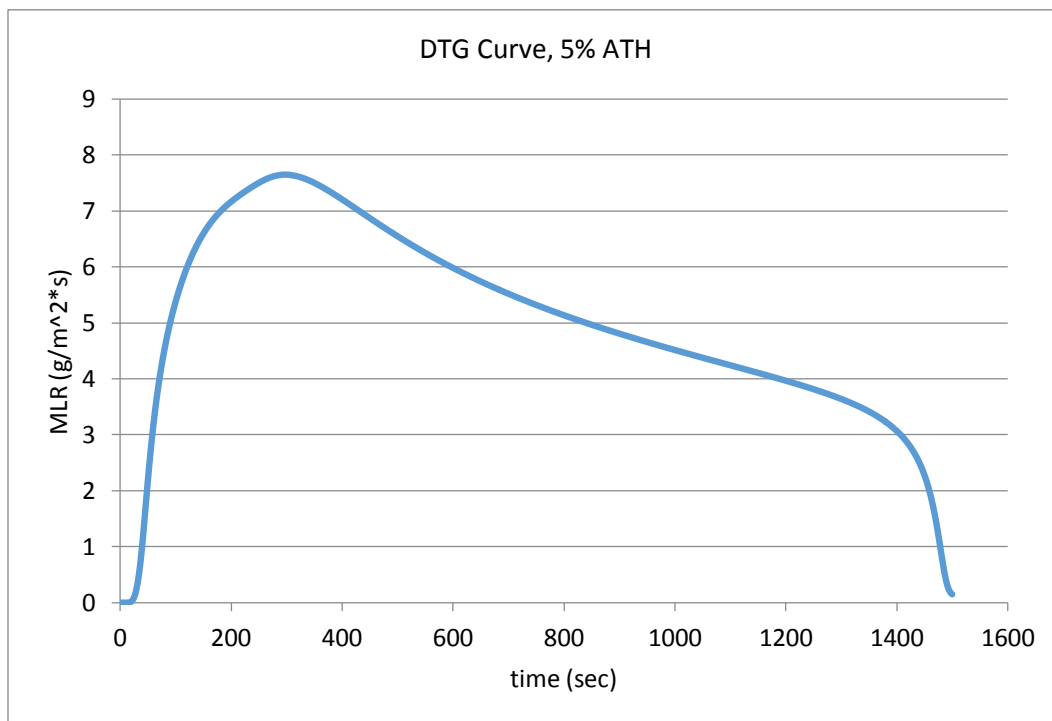
Figure 69: DTG Curve 5% ATH

Temperature Profiles

This is a temperature profile for a sample 8mm thick on 500 second intervals.
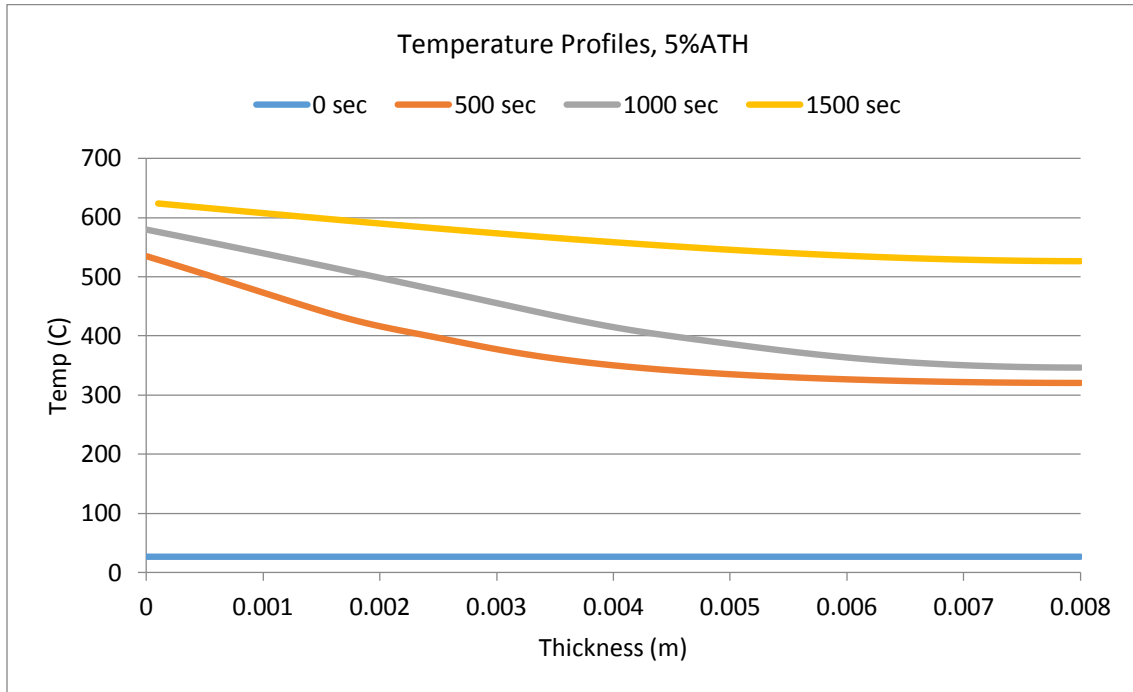
Figure 70: Temperature Profiles 5% ATH

Bulk Density

The graph below shows the bulk density of the sample at intervals of 500 seconds. The density starts at around 1200 kg/m^3 (which can be seen at t=0 sec) and ends around 250 kg/m^3, which can be seen at 1500 sec. The simulation ran for a total of 1500 sec.
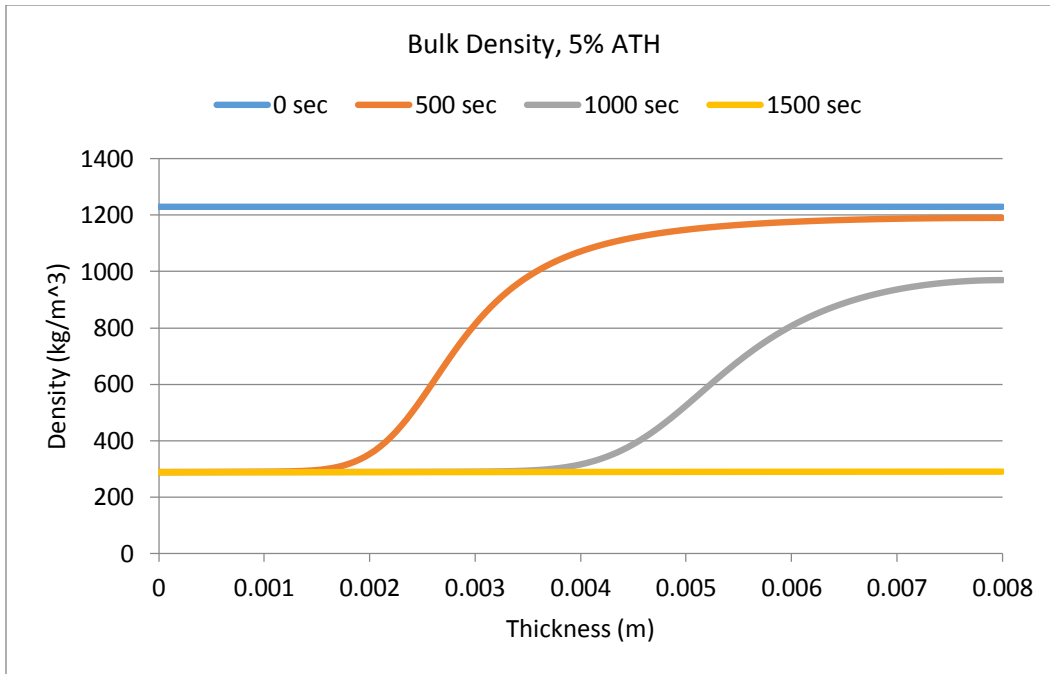
Figure 71: Bulk Density 5% ATH

Reaction Rates

Below are two reaction rate graphs. The first reaction is the resin to resin residue, and the second is the ATH to ATH residue.
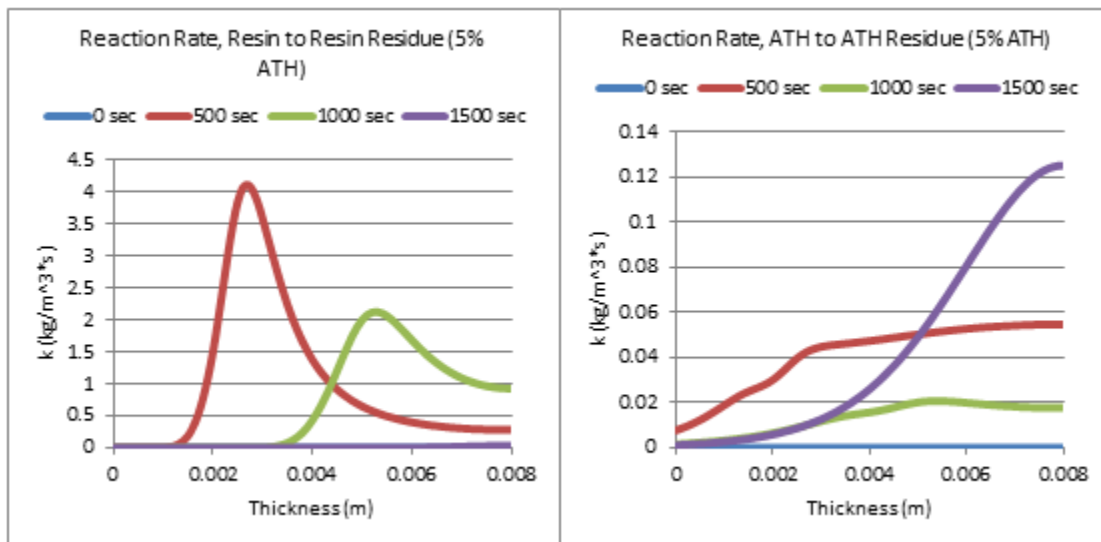
Figure 72: Reaction Rates 5% ATH

Mass Fractions

The Mass Fractions were taken across the sample at an interval of 500 seconds. It starts at about 1 since it is the pure resin. The two middle curves show that the reaction is happening deeper into the sample as the test continues. When graphing the mass fraction of the residue, it shows the inverse of the pure resin graph.
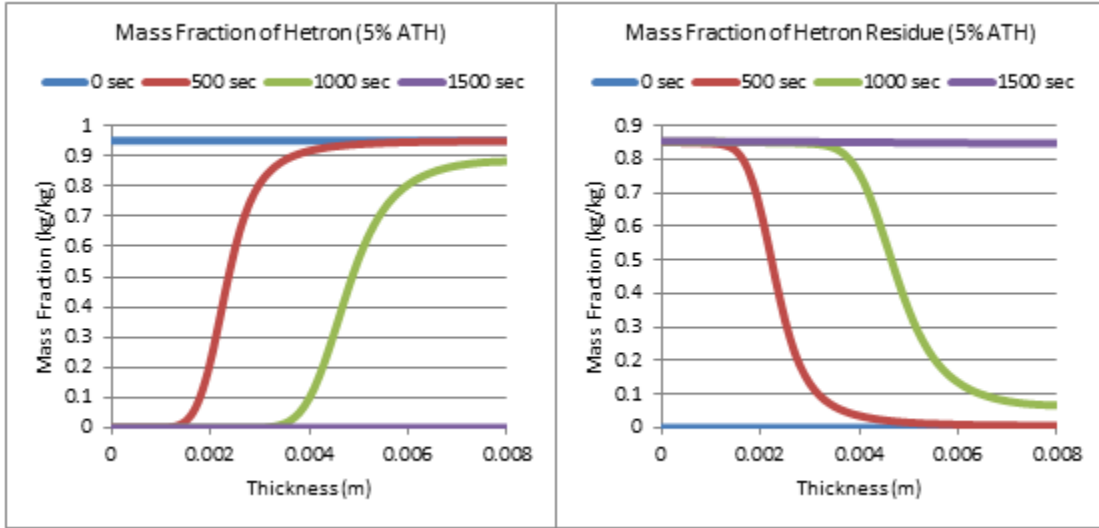
Figure 73: Mass Fractions 5% ATH

10% ATH

MLR Curve

When the percent of ATH is increased to 10% ATH, the curve peaks at around 8 g/m^2*s and the test runs for 1500 seconds. This is a very small change when 5% ATH.
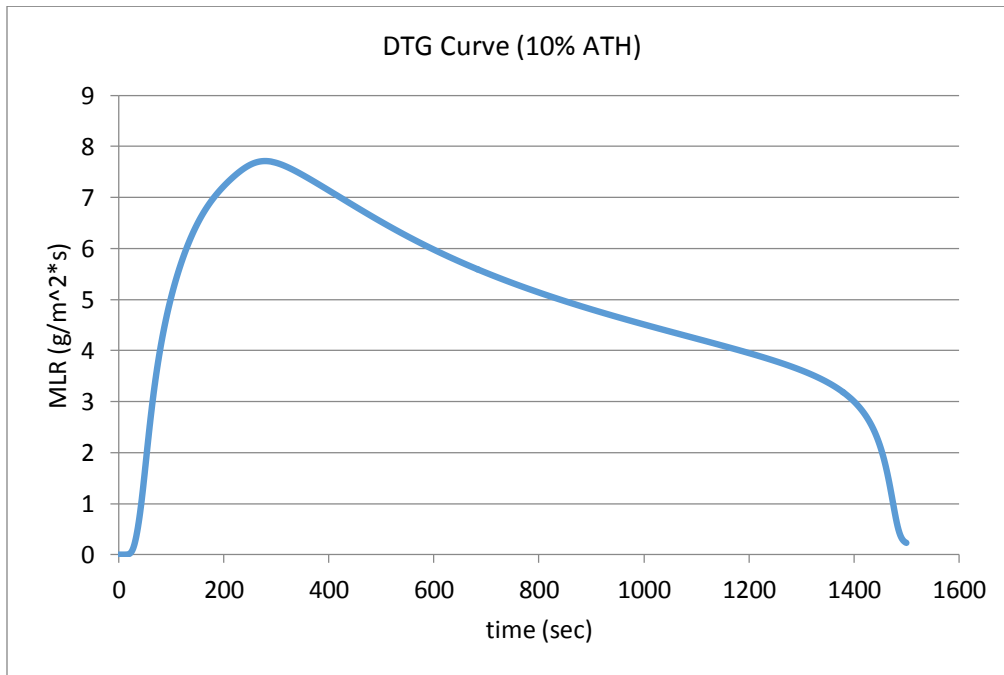
Figure 74: DTG Curve 10% ATH

Temperature Profiles

The graph below shows the temperature profiles at 500 second intervals. It should be noted that as time goes on, the slope of the gradients is decreased. The sample used was 8mm thick. Once again, when compared to the 5% ATH temperature profiles, there are only very small changes.
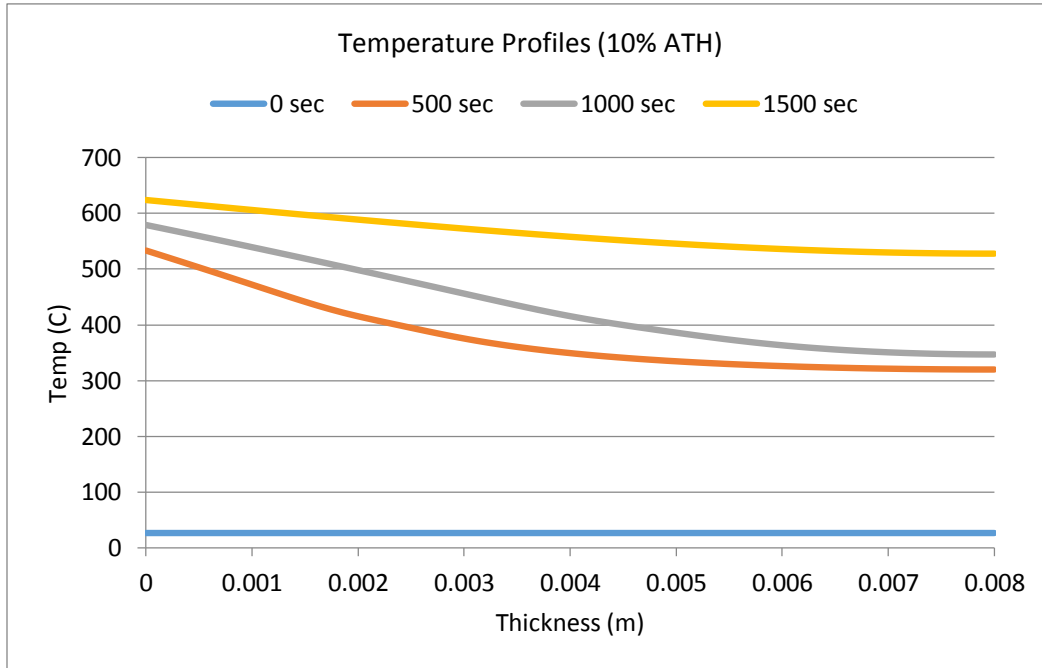
Bulk Density

The graph below shows how the bulk density of the simulated sample changes as time progresses in the trial. While the starting density is approximately the same as with the 5% ATH, the ending bulk density is slightly higher.
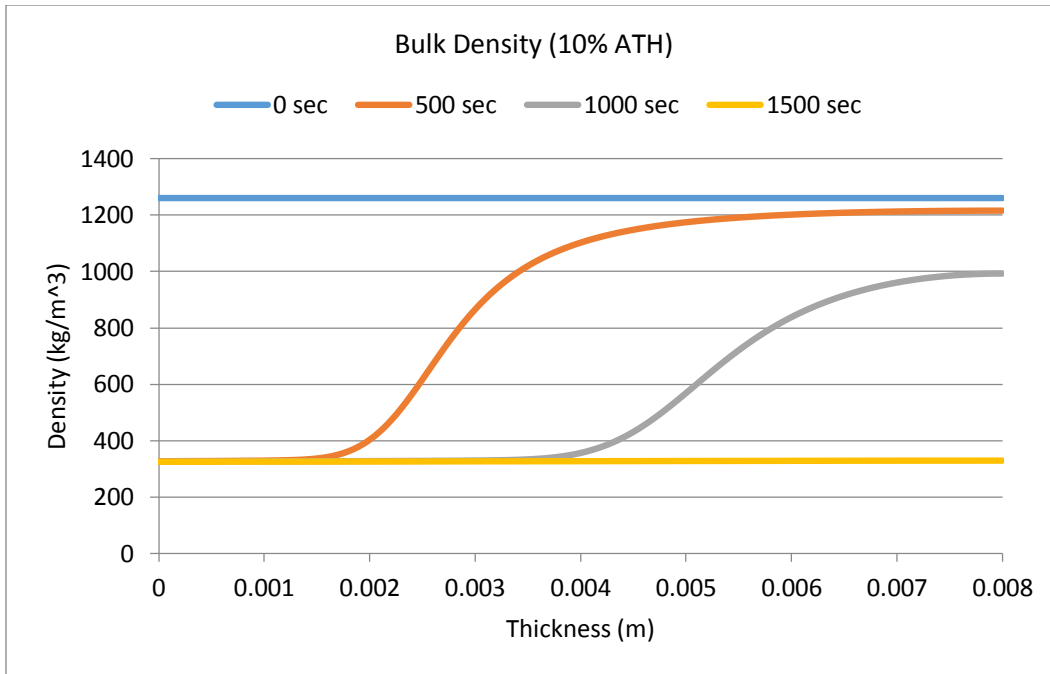
Figure 76: Bulk Density 10% ATH

Reaction Rates

Below are the two reaction rates for the provided sample in Gpyro.
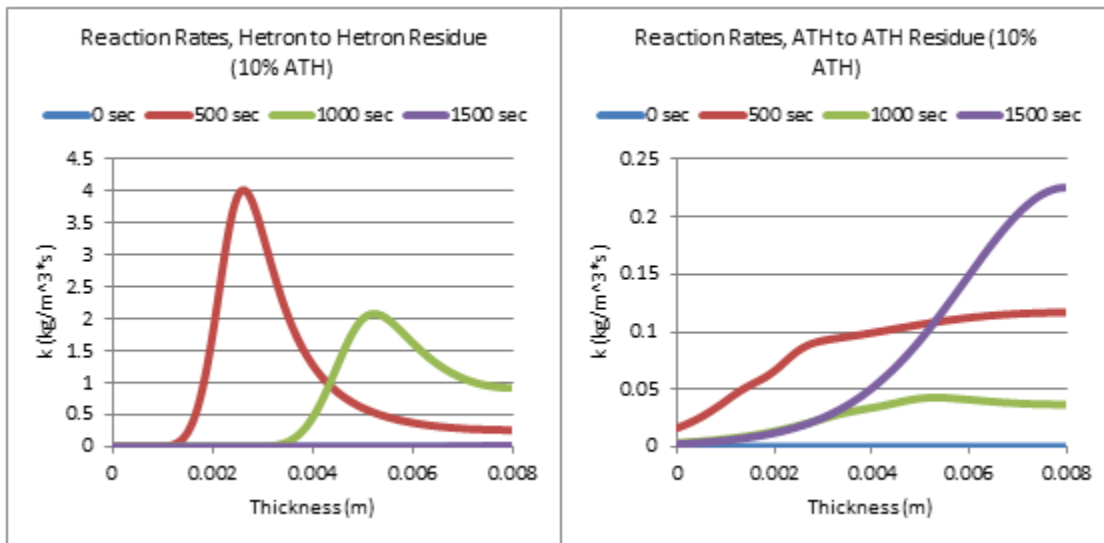
Figure 77: Reaction Rates 10% ATH

20% ATH

MLR Curve

Once again, the MLR does not deviate significantly when 20% ATH is added.
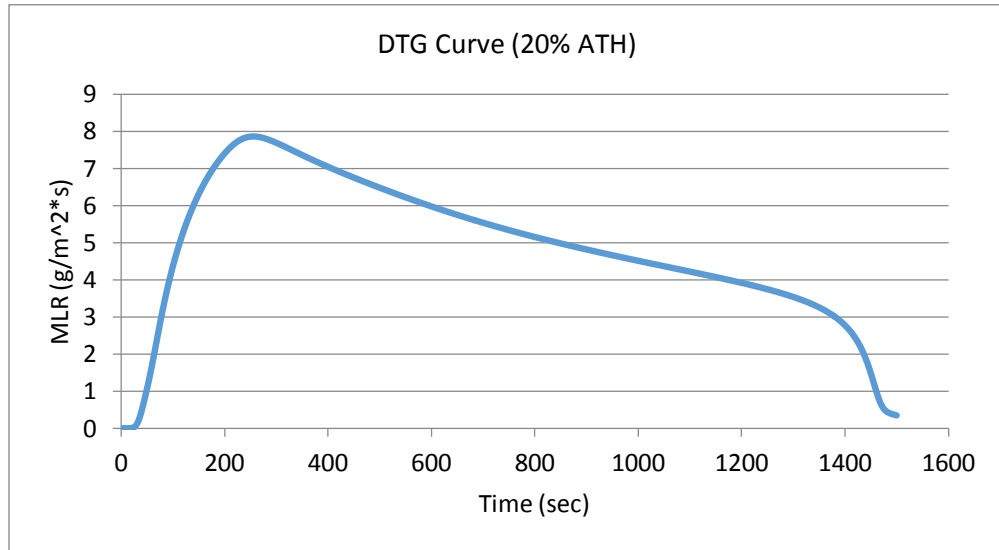
Figure 78: DTG Curve 20% ATH

Temperature Profiles
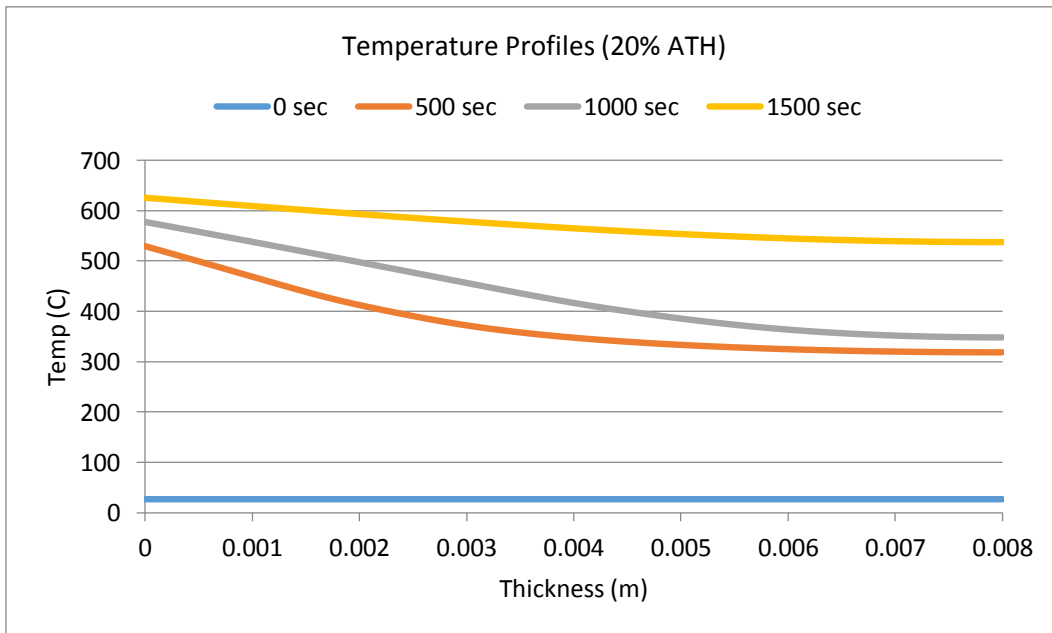
Figure 79: Temperature Profiles 20% ATH

Bulk Density
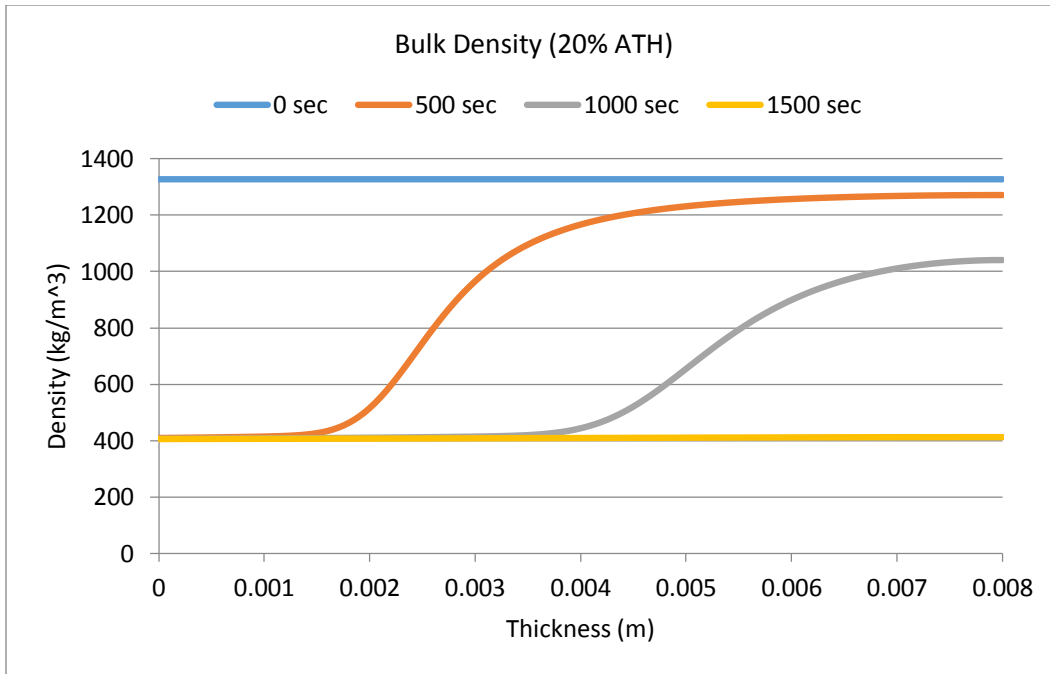
Figure 80: Bulk Density 20% ATH

Reaction Rates
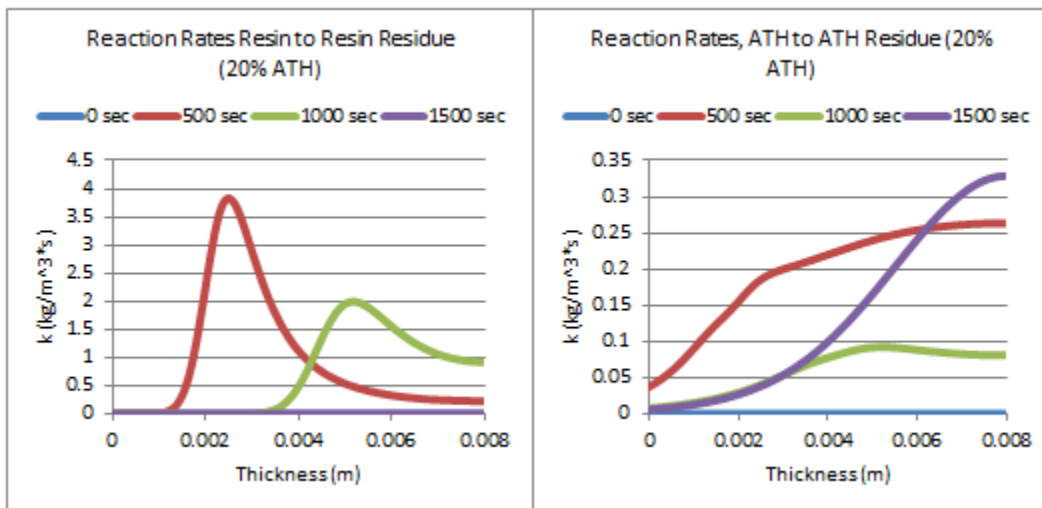
Figure 81: Reaction Rates 20% ATH

The DTG Curves were graphed together, along with a few higher levels of ATH, to see how much they deviate from each other. The results can be seen in the graph below.
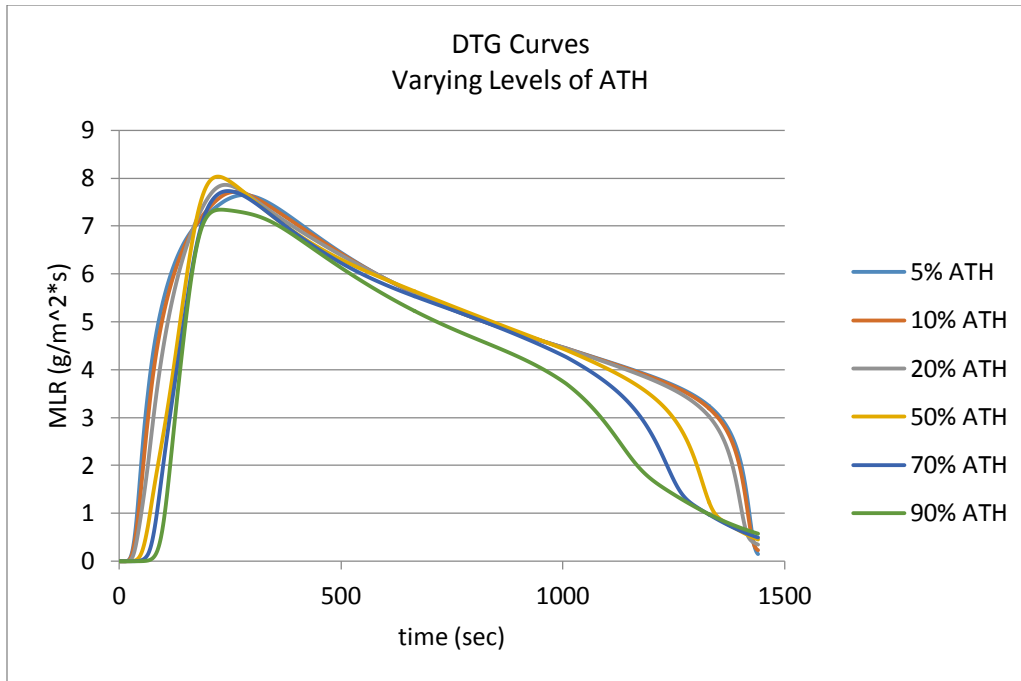
Figure 82: DTG Curve, Varying levels of ATH

It can be seen on the graph above that as the level of ATH is increased, the Gpyro simulations do not show any significant changes. Once the initial profiles were created, the thickness was varied to achieve a thickness closer to that which found be used in the TGA. 8mm is the baseline Gpyro thickness, so 5mm and 2mm were also studied. The profiles can be seen below.

MLR (5% ATH)

The graph below shows the history for 5% ATH mixture at three different thicknesses. The curve for 8mm thick is the baseline value provided in Gpyro. As the thickness of the sample decreases,

the reaction occurs over a shorter time span and at a much faster rate. This is an expected result, so it can be concluded that the results Gpyro is showing are correct.
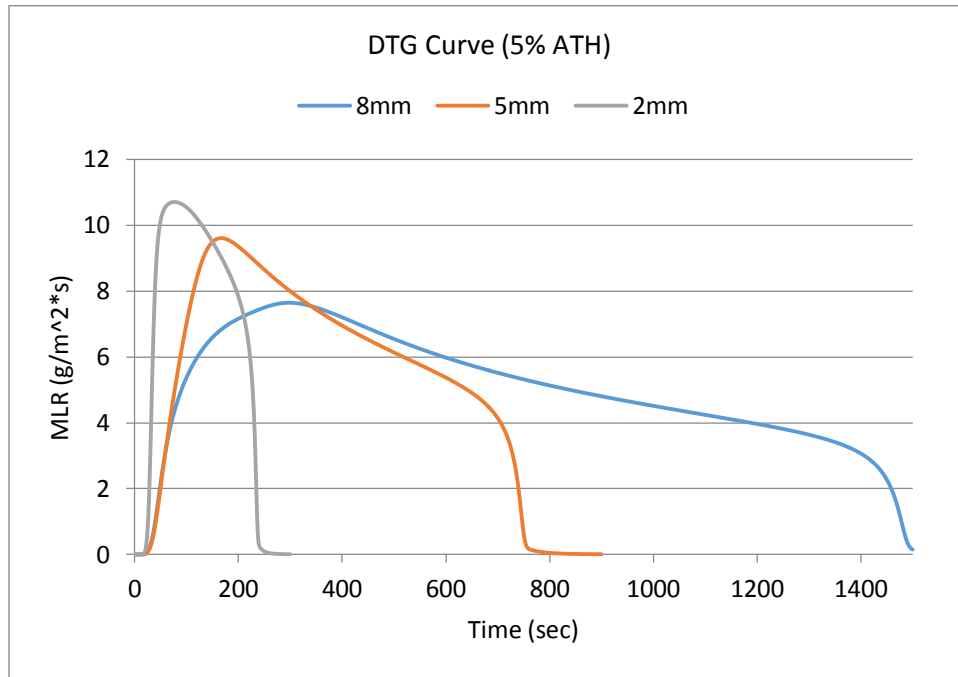
Figure 83: DTG Curve (5% ATH)

Temperature Profiles (5% ATH)
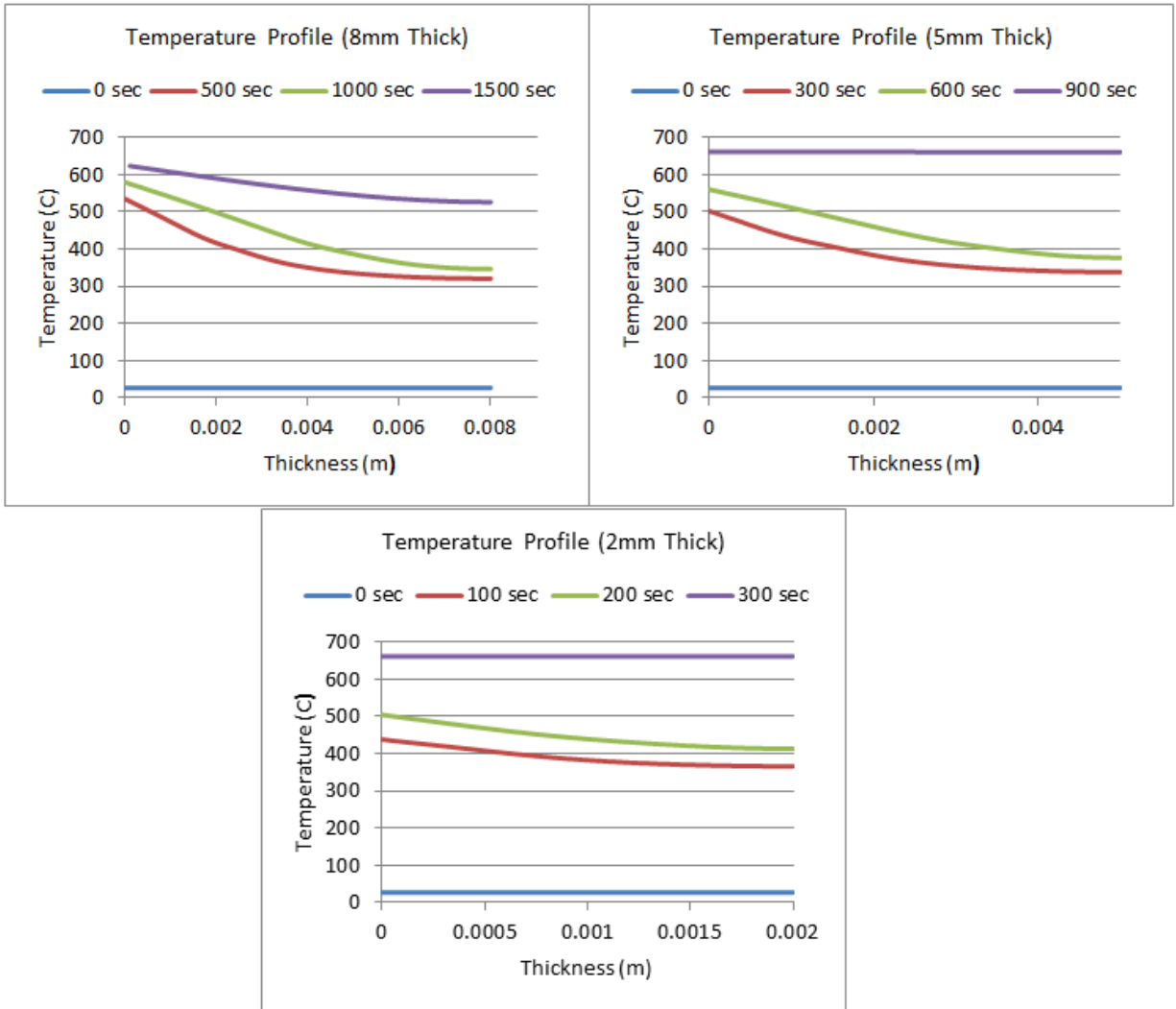
Figure 84: Temperature Profiles for 5% ATH (Varying Thickness)

Porosity (5% ATH)
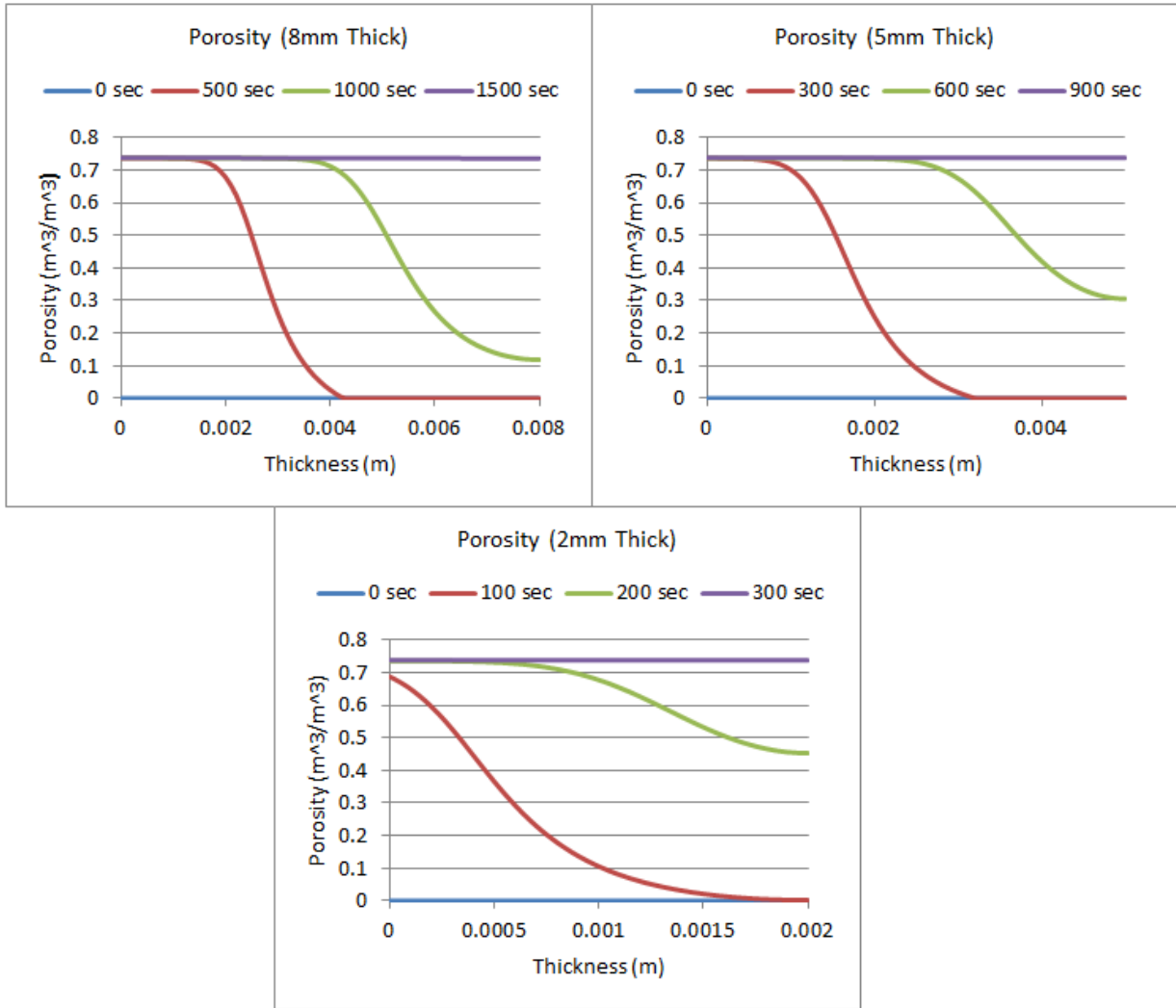
Figure 85: Porosity Profiles for 5% ATH (Varying Thickness)

Bulk Density (5% ATH)
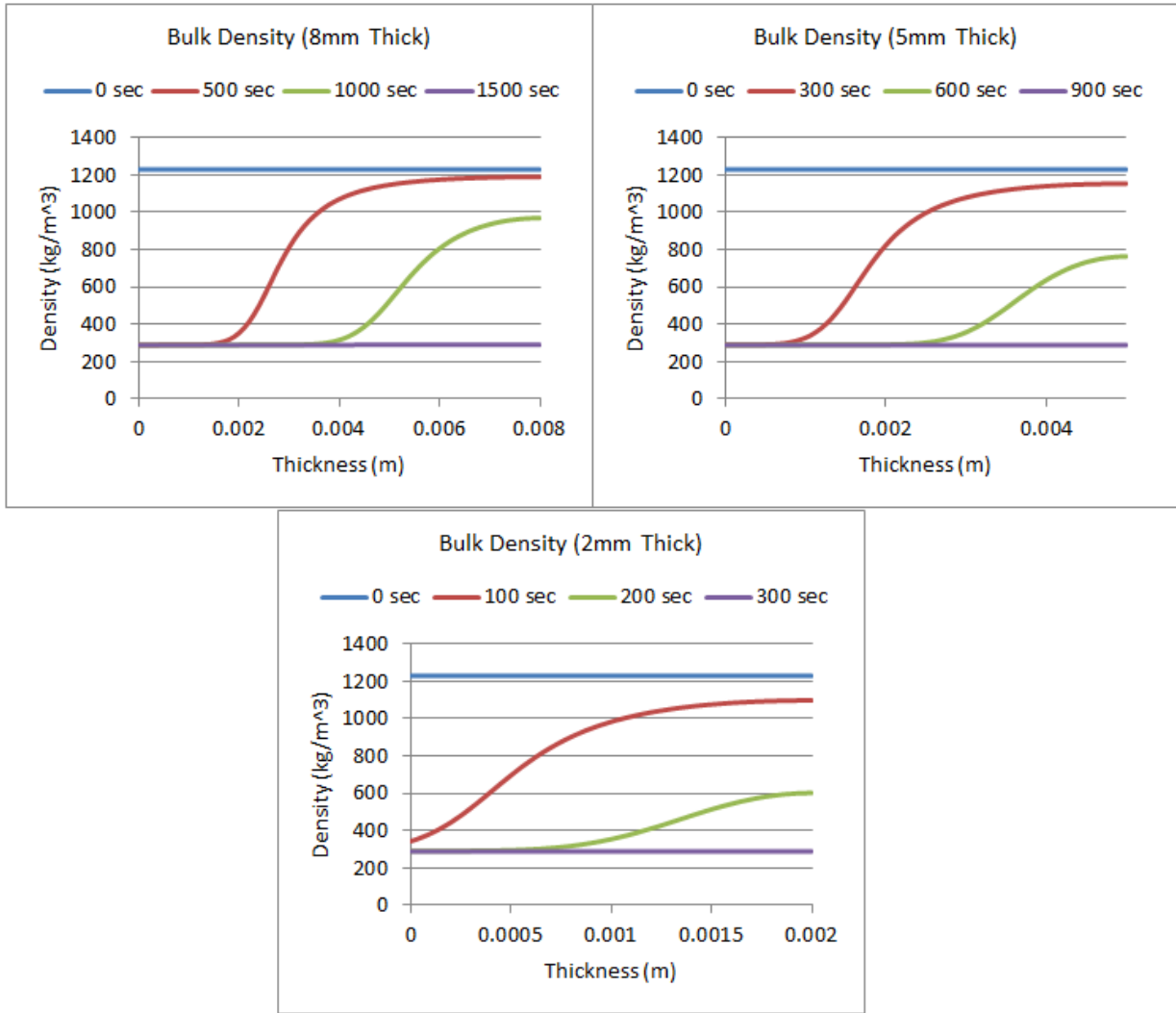
Figure 86: Bulk Density for 5% ATH (Varying Thickness)

Reaction Rate (Resin to Resin Residue) 5% ATH
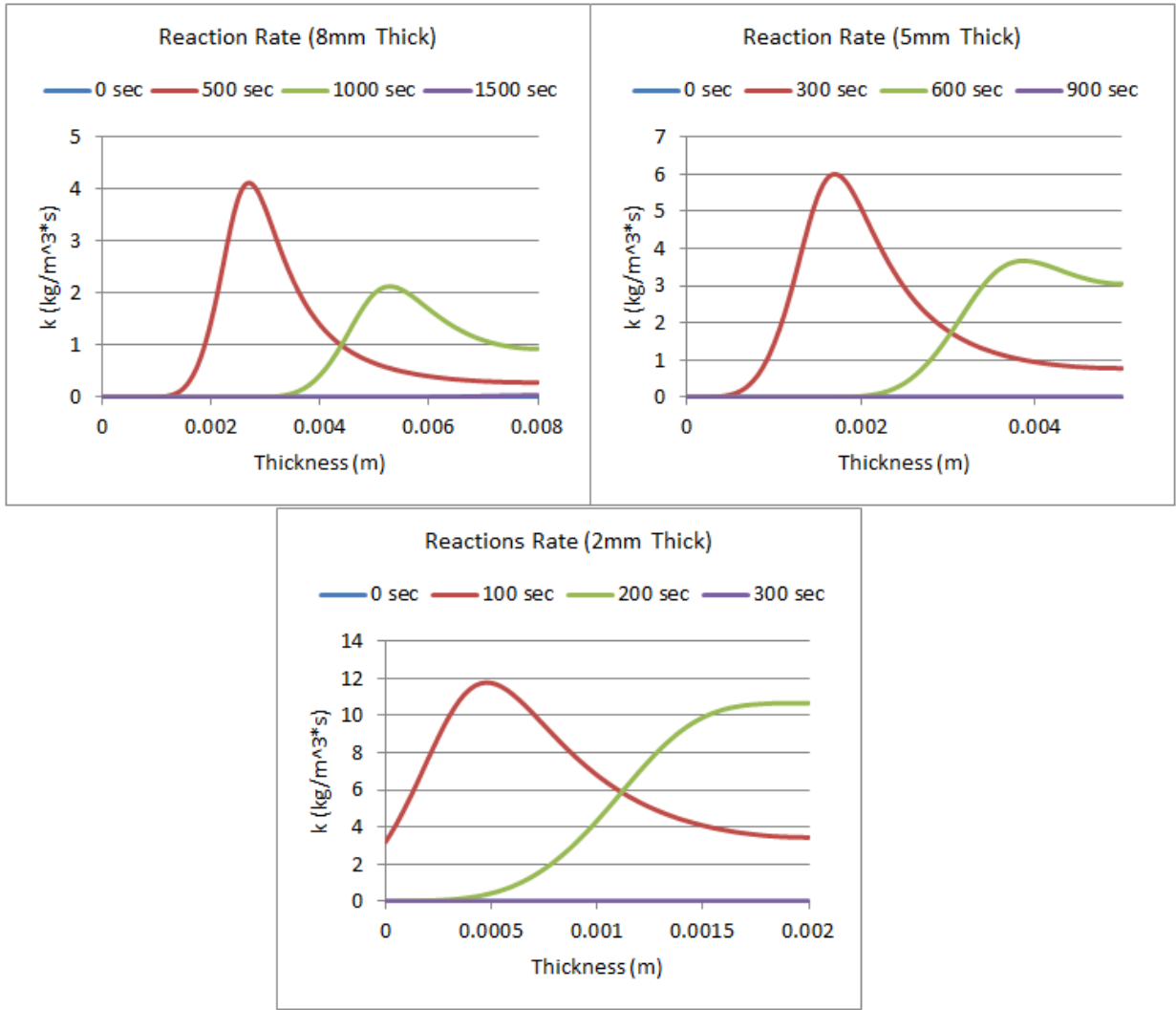
Figure 87: Reaction Rate (Resin) for 5% ATH (Varying Thickness)

Reaction Rate (ATH to ATH Residue) 5% ATH
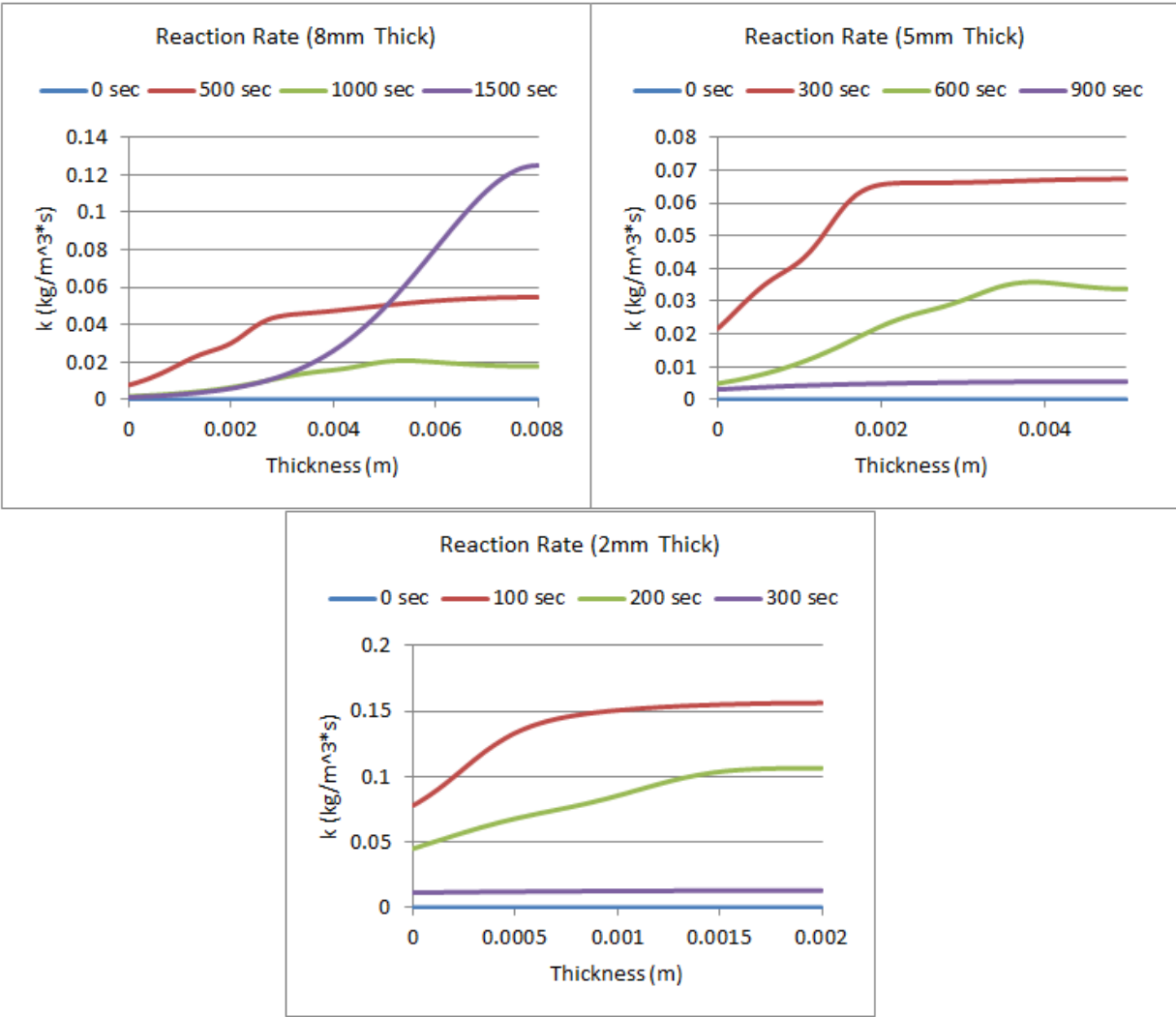
Figure 88: Reaction Rate (ATH) for 5% ATH (Varying Thickness)

Mass Fraction of Resin (5% ATH)
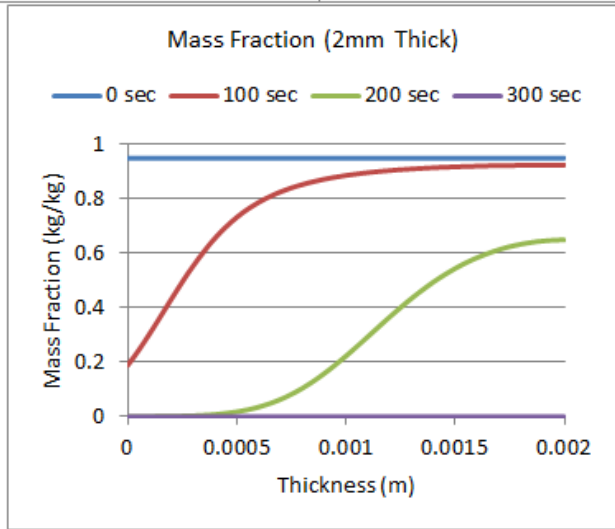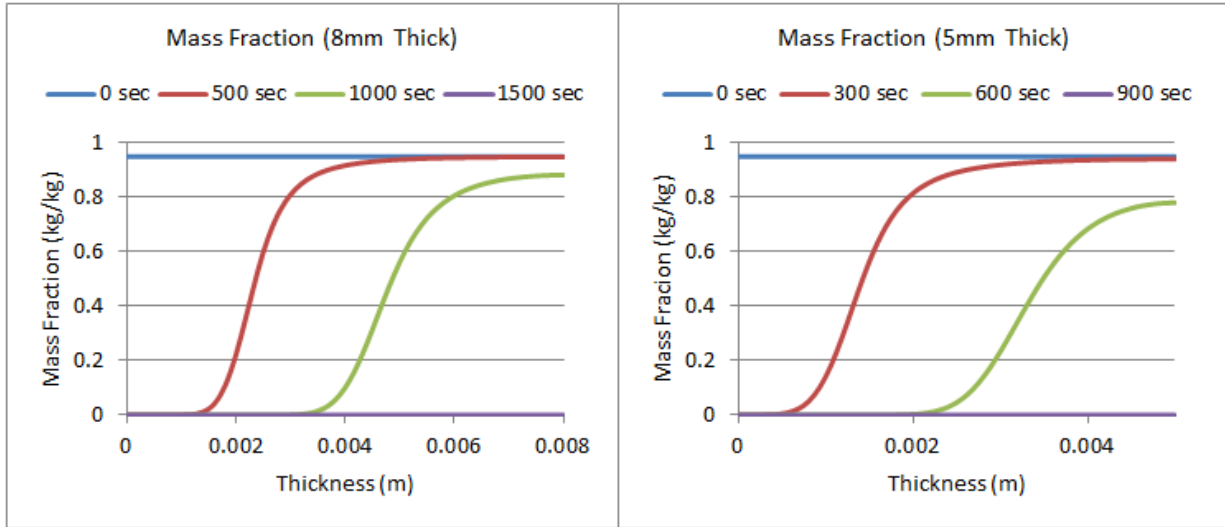
Figure 89: Mass Fraction (Resin) for 5% ATH (Varying Thickness)

Mass Fraction of Resin Residue (5% ATH)
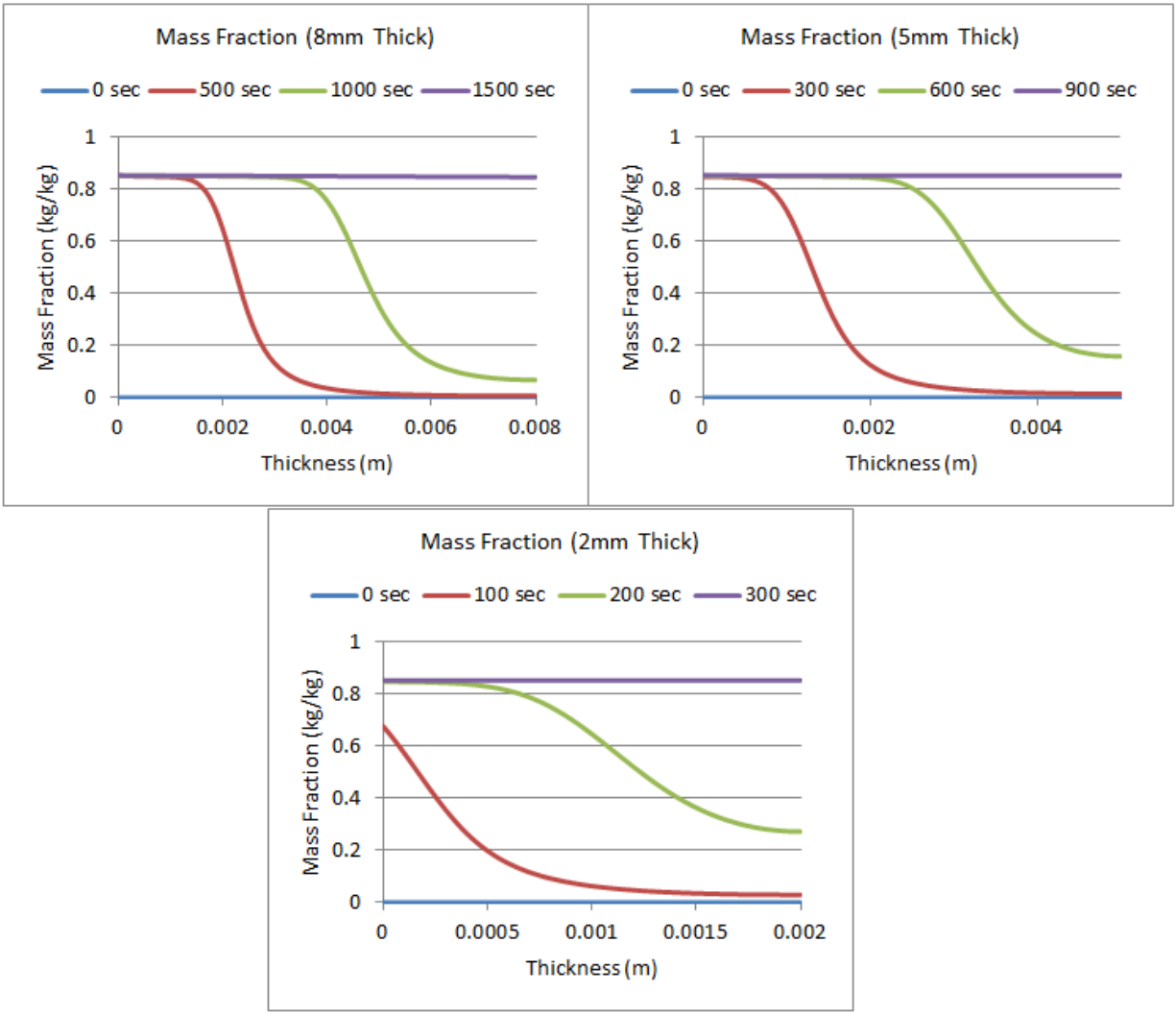
Figure 90: Mass Fraction (Resin Residue) for 5% ATH (Varying Thickness)

Mass Fraction of ATH (5% ATH)
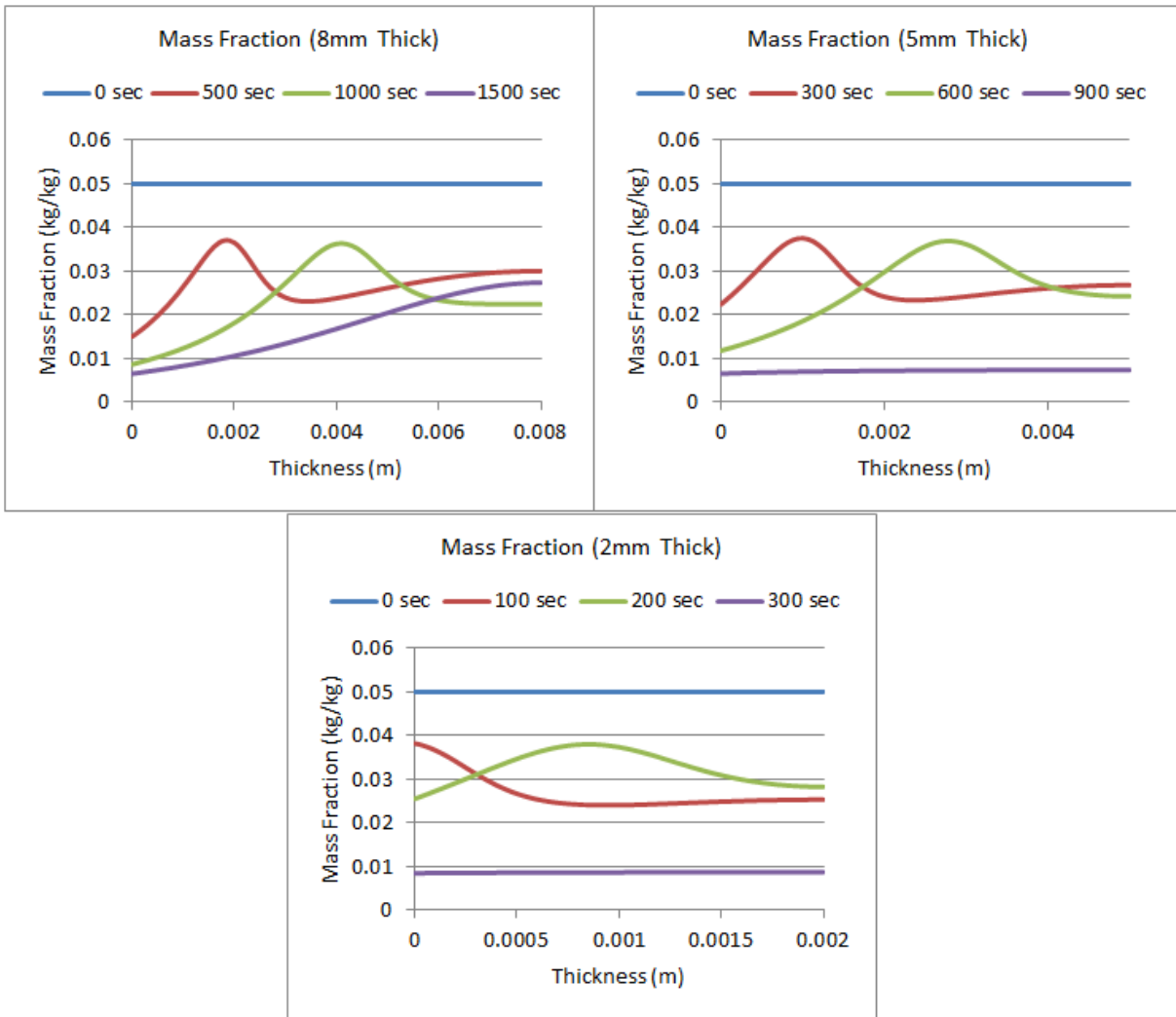
Figure 91: Mass Fraction (ATH) for 5% ATH (Varying Thickness)

Mass Fraction of ATH Residue (5% ATH)
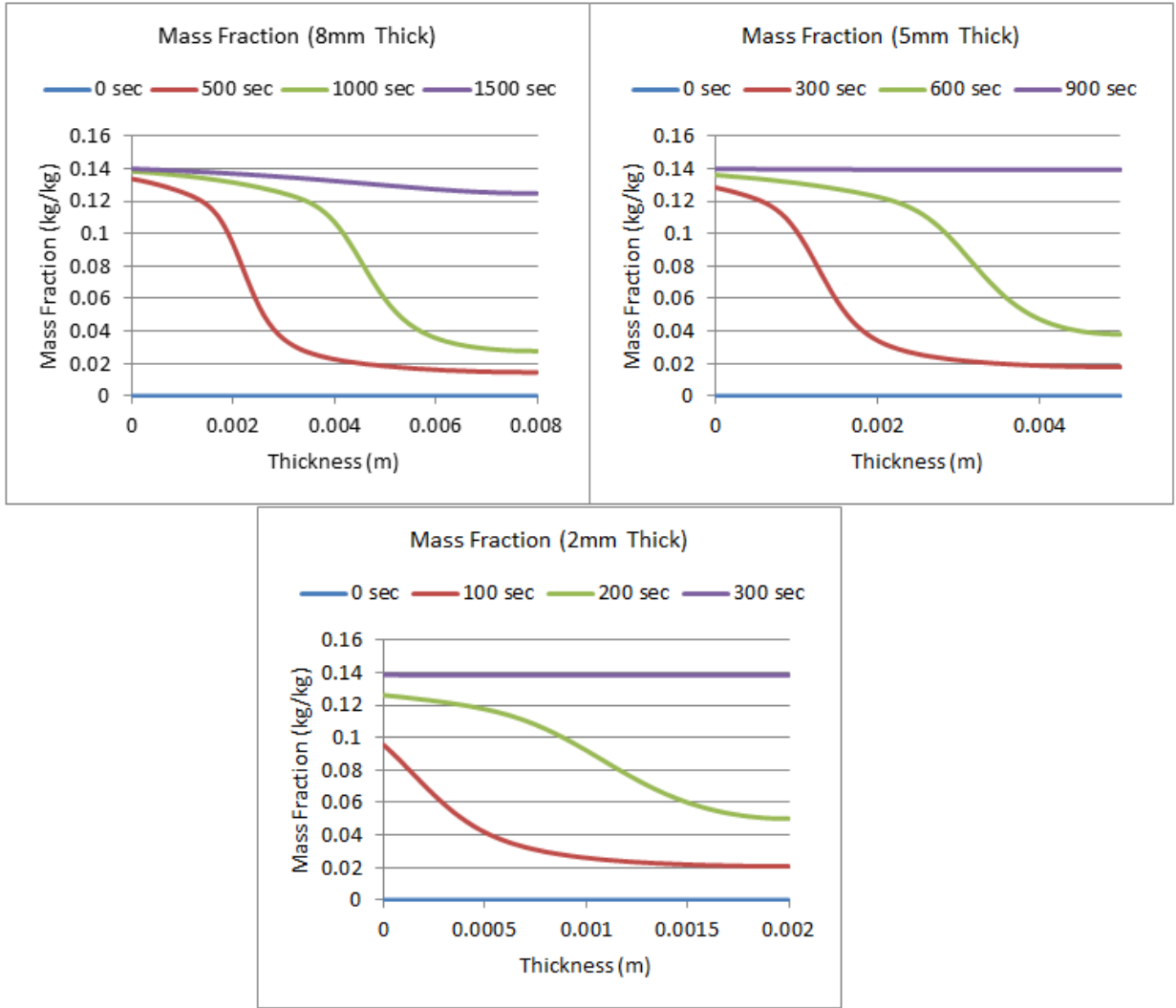
Figure 92: Mass Fraction (ATH Residue) for 5% ATH (Varying Thickness)

MLR (10% ATH)

The graph below shows three MLR curves for varying thickness in a sample. This graph shows the MLR for a resin with 10% ATH. When compared to the MLR curve for 5% ATH, there are only very small changes that occur. This can be seen in the profiles as well. So by increasing the amount of ATH from 5% to 10%, the properties of the material do not significantly change.
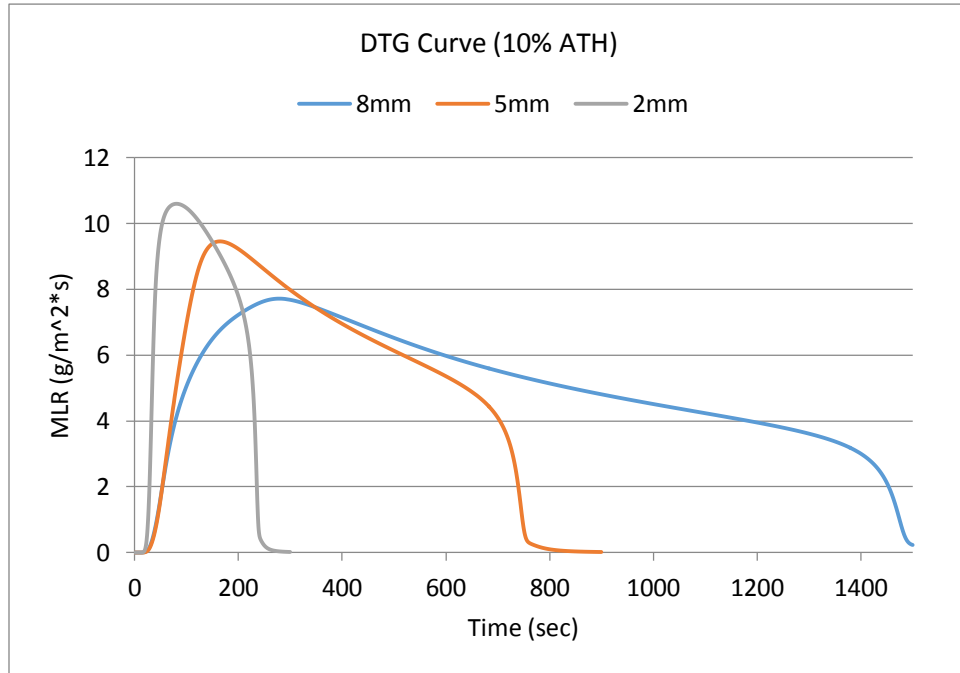
Figure 93: DTG Curve (10% ATH)

Temperature Profiles (10% ATH)
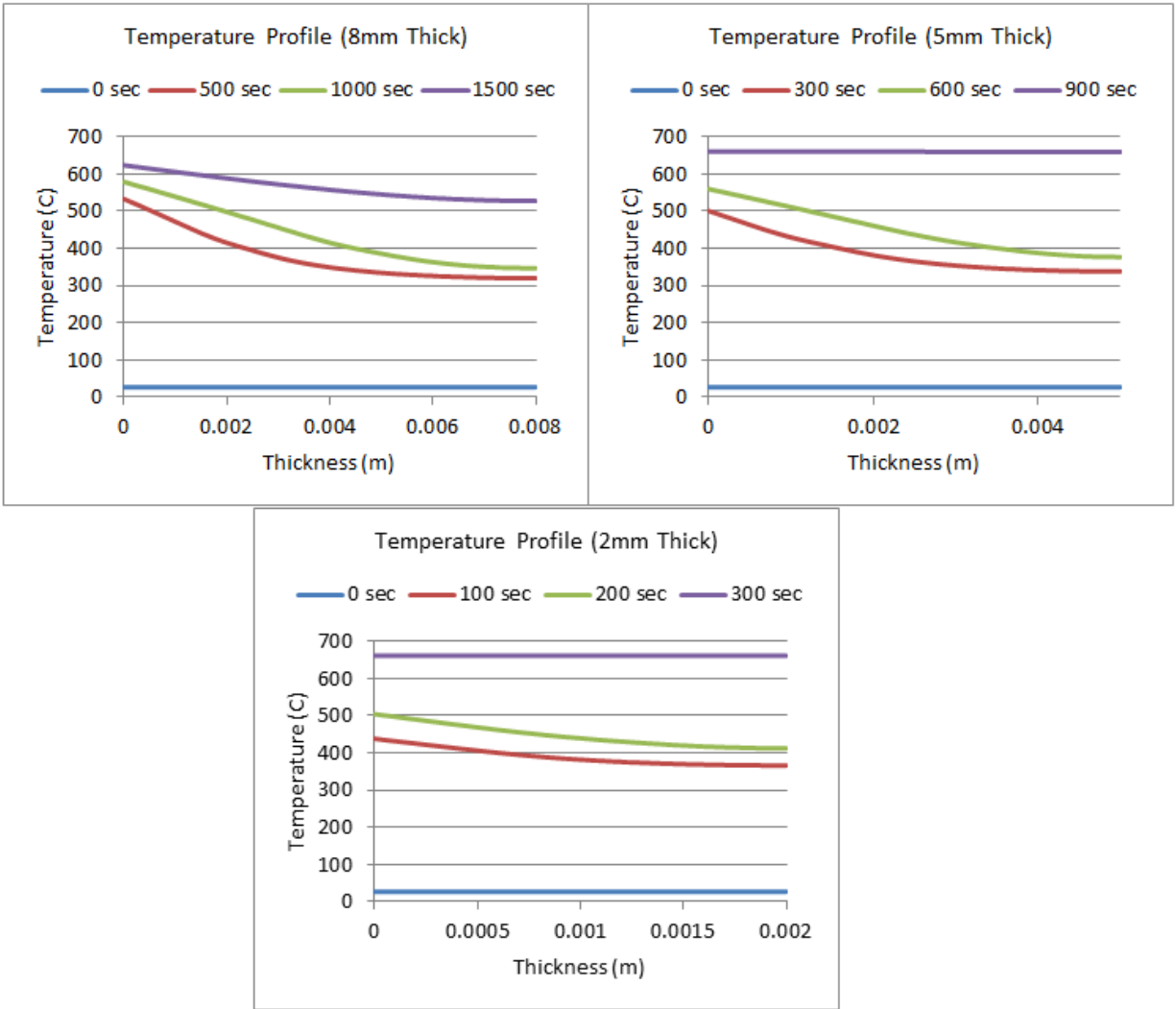
Figure 94: Temperature Profile for 10% ATH (Varying Thickness)

Porosity (10% ATH)
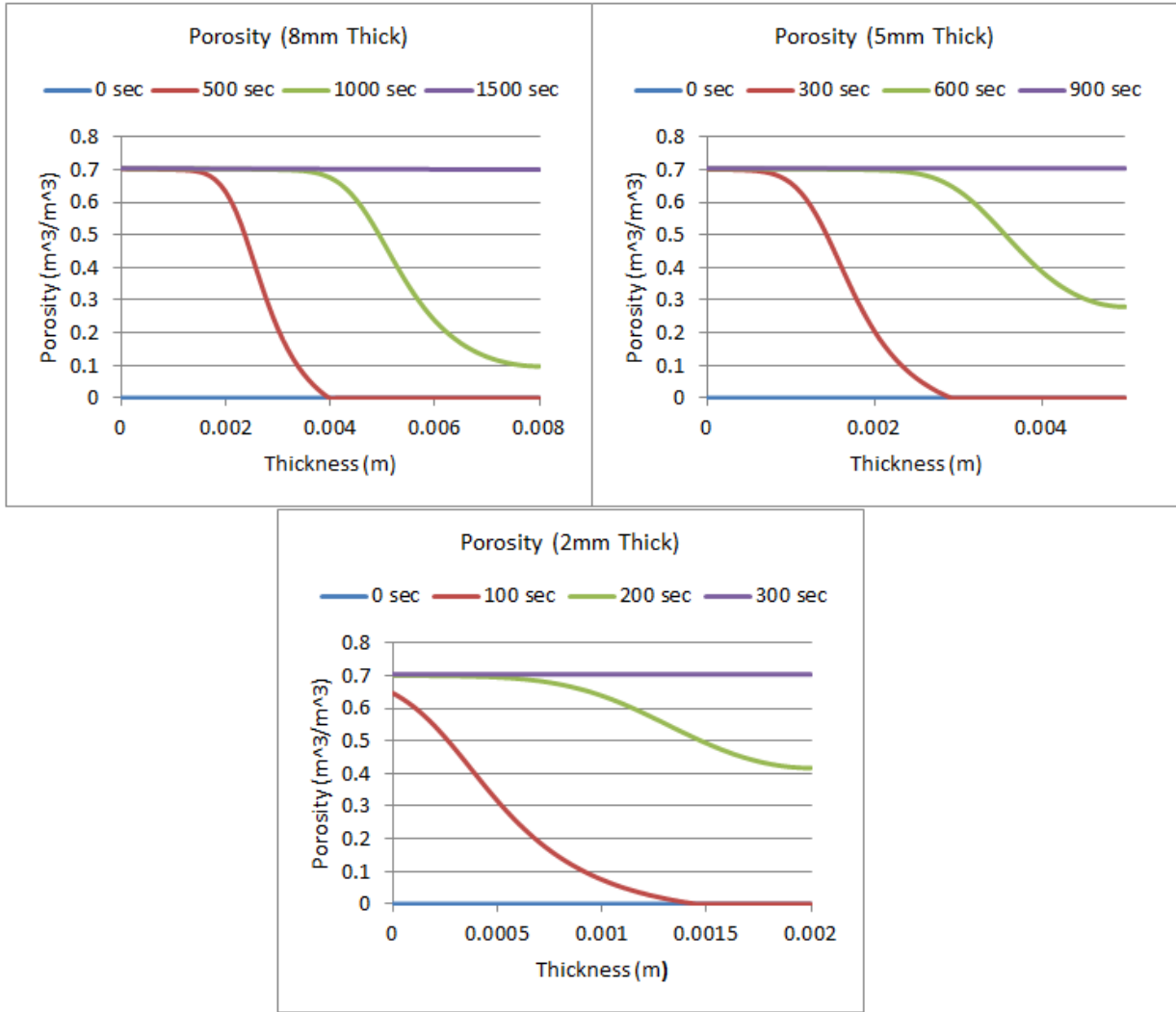
Figure 95: Porosity for 10% ATH (Varying Thickness)

Bulk Density (10% ATH)
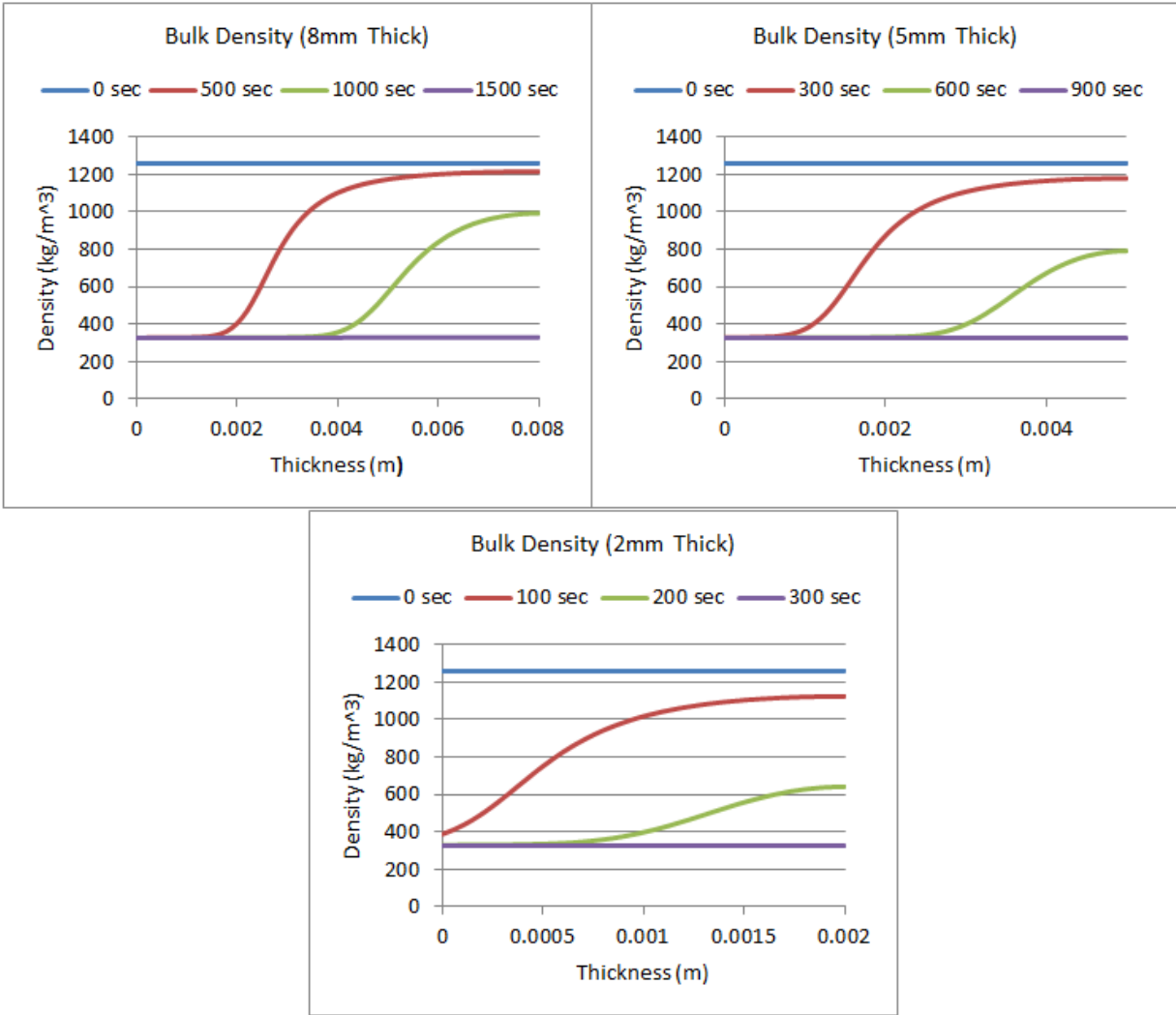
Figure 96: Bulk Density for 10% ATH (Varying Thickness)

Reaction Rate (Resin to Resin Residue) 10% ATH
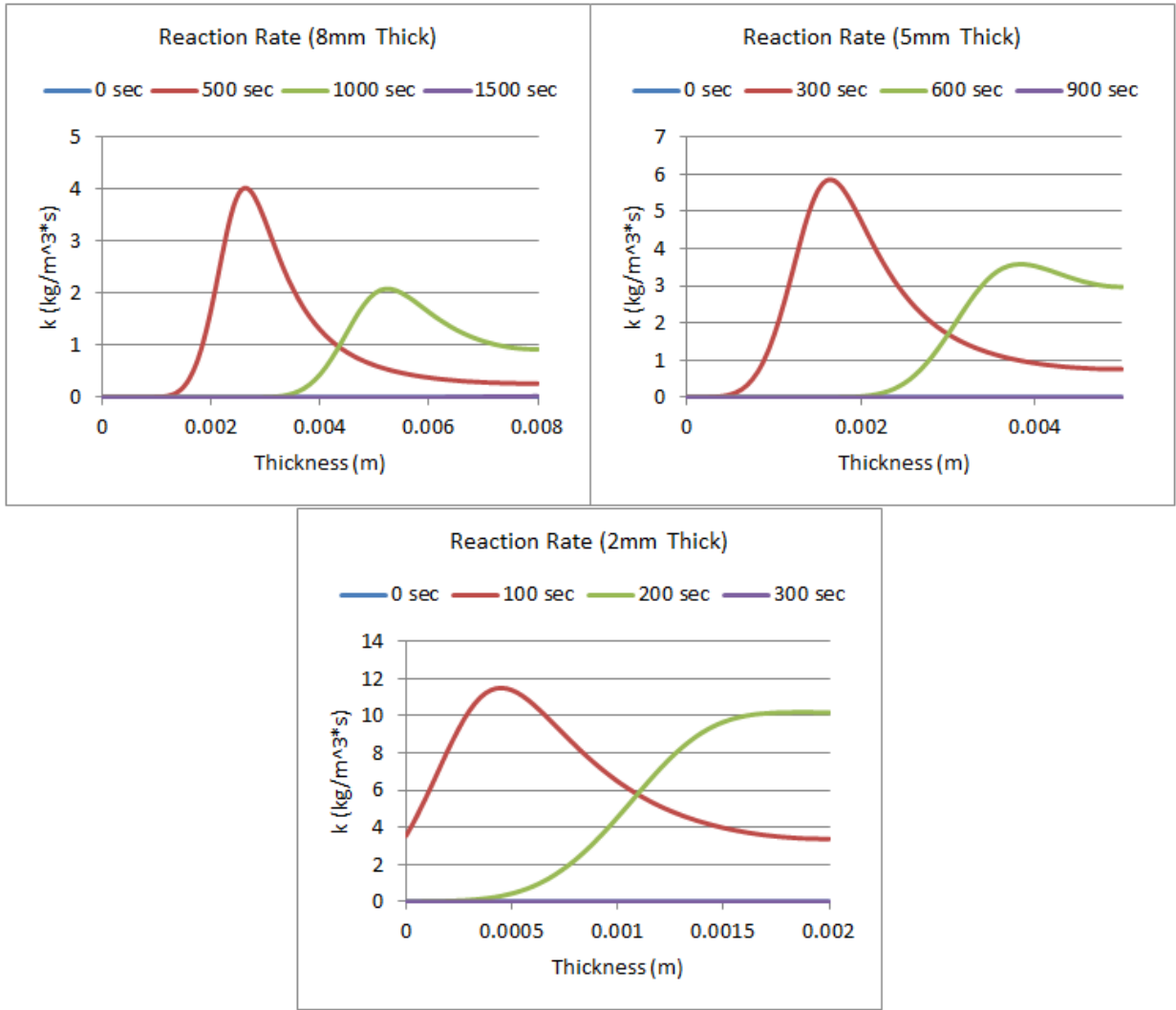
Figure 97: Reaction Rate (Resin) for 10% ATH (Varying Thickness)

Reaction Rate (ATH to ATH Residue) 10% ATH
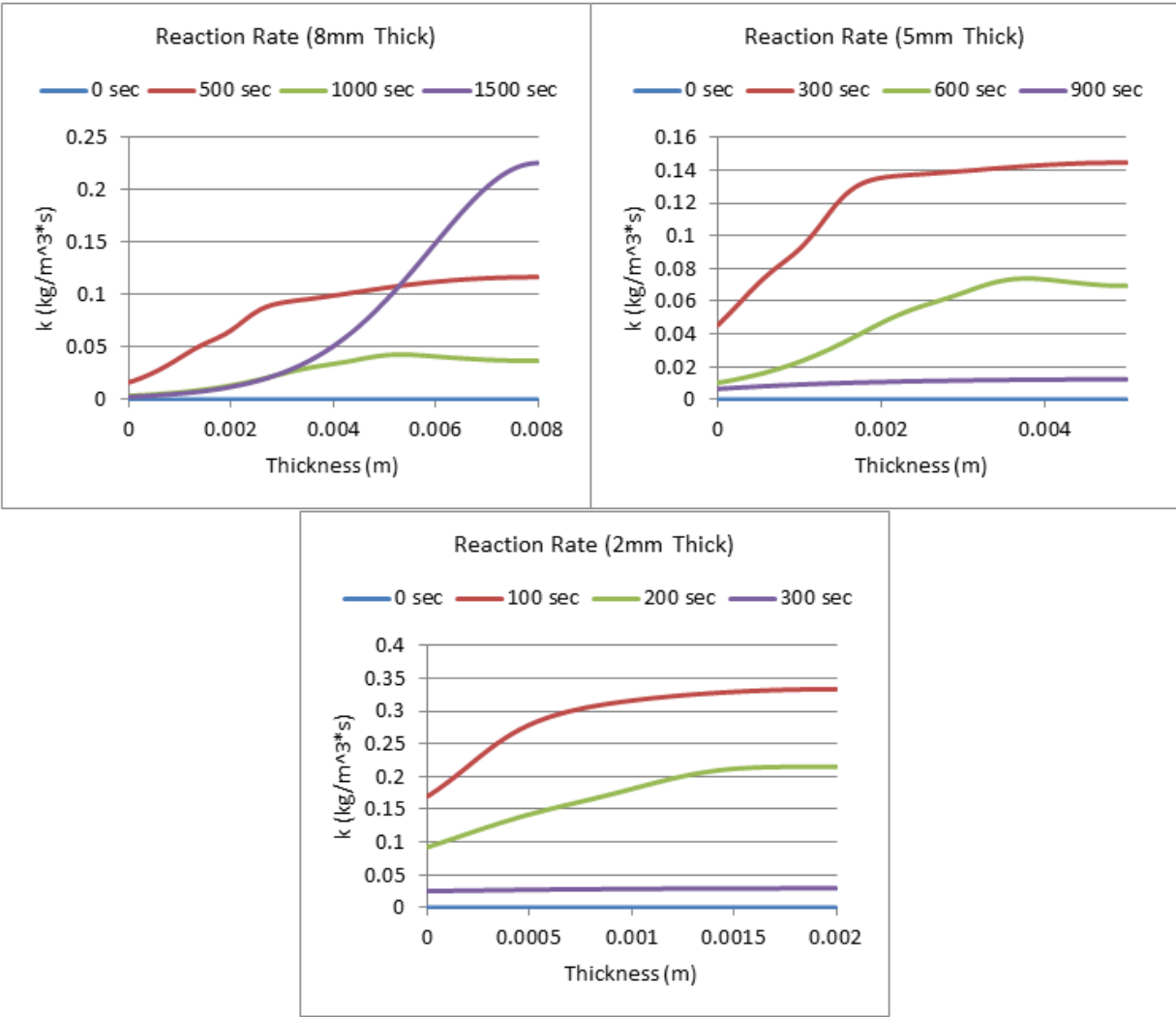
Figure 98: Reaction Rate (ATH to ATH Residue) 10% ATH, Varying Thickness

Mass Fraction (resin) 10% ATH
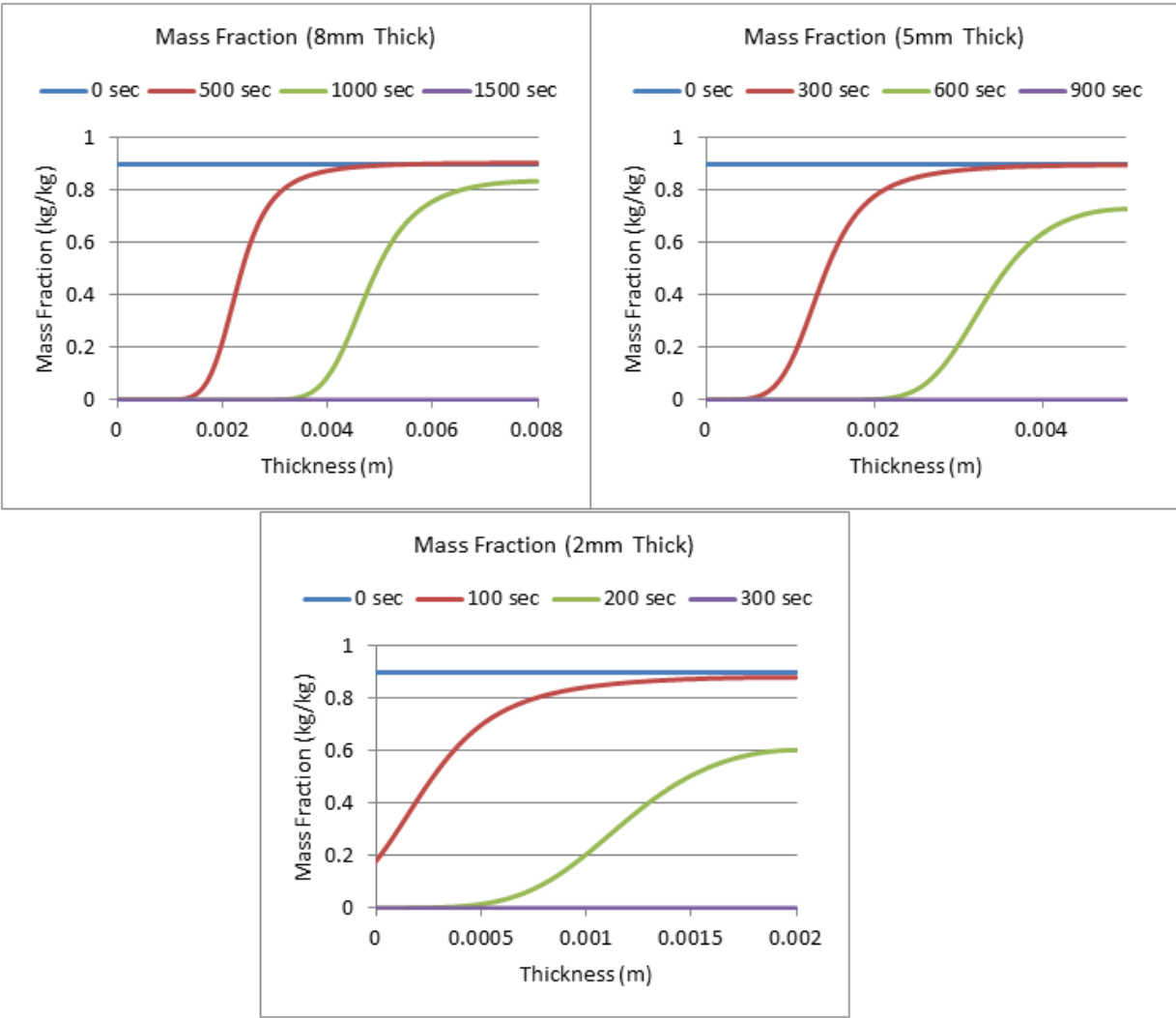
Figure 99: Mass Fraction (Resin) for 10% ATH (Varying Thickness)

Mass Fraction (Resin Residue) 10% ATH
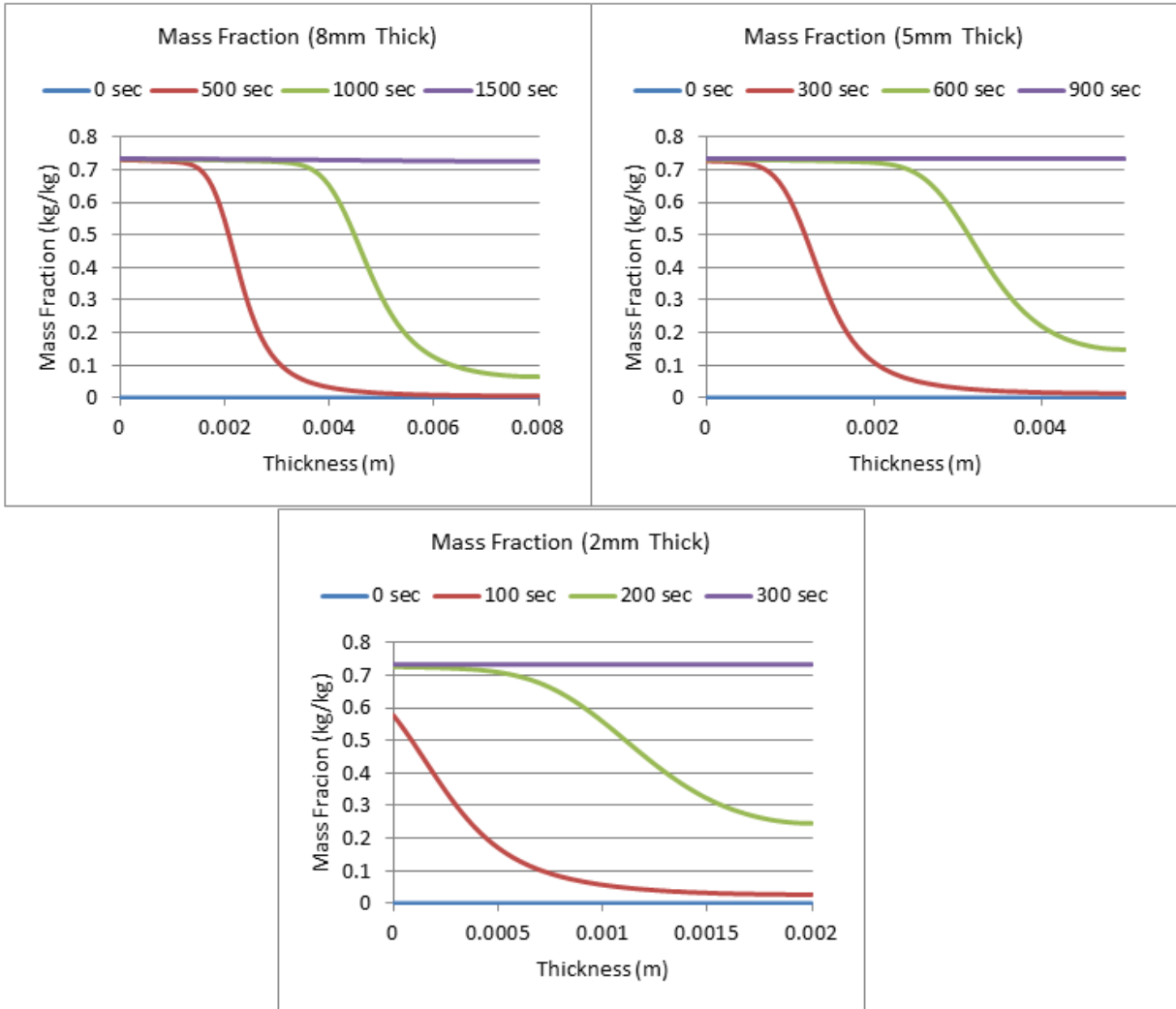
Figure 100: Mass Fraction (Resin Residue) for 10% ATH

Mass Fraction (ATH) for 10% ATH
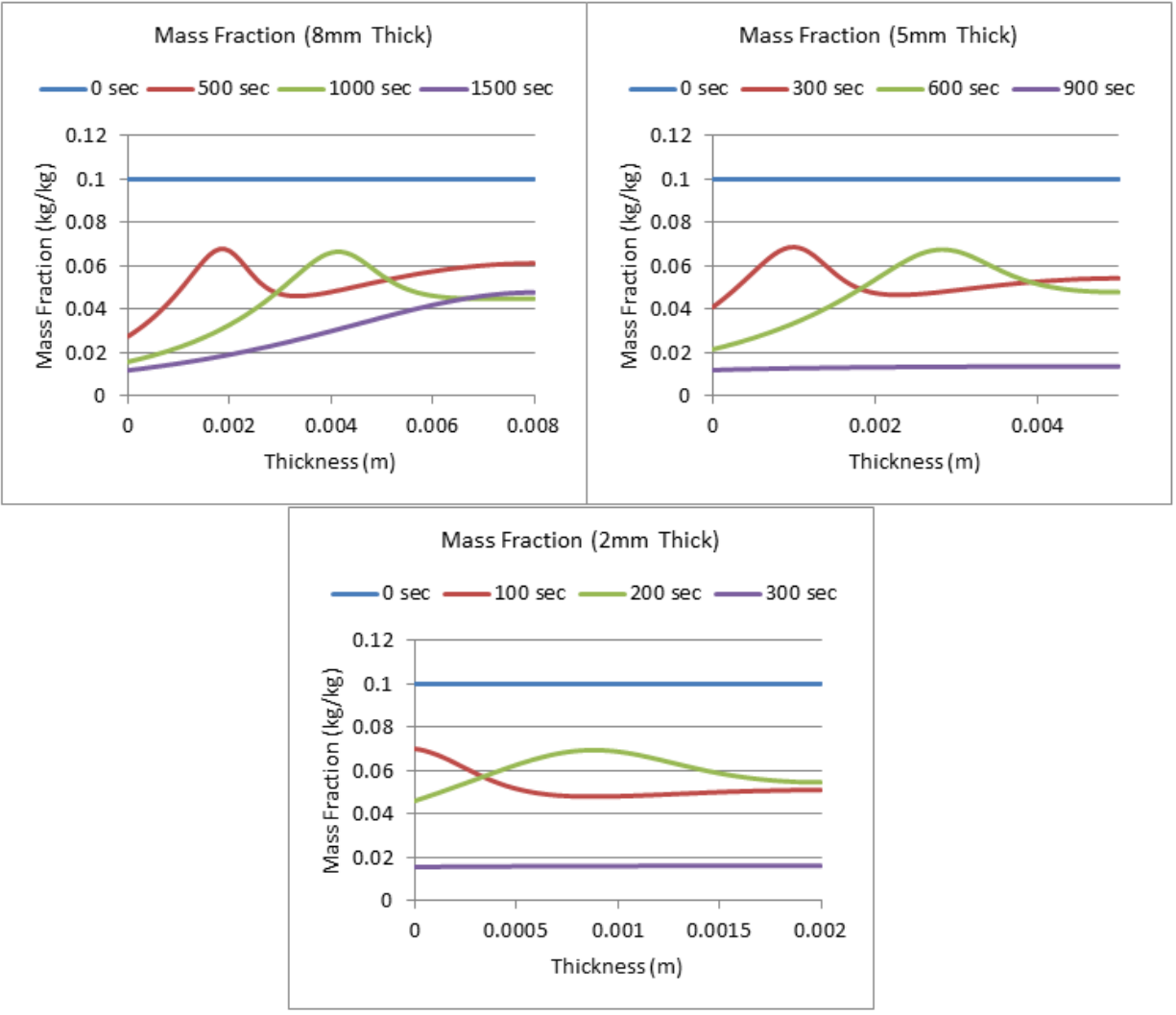
Figure 101: Mass Fraction (ATH) for 10% ATH (Varying Thickness)

Mass Fraction of ATH Residue (10% ATH)
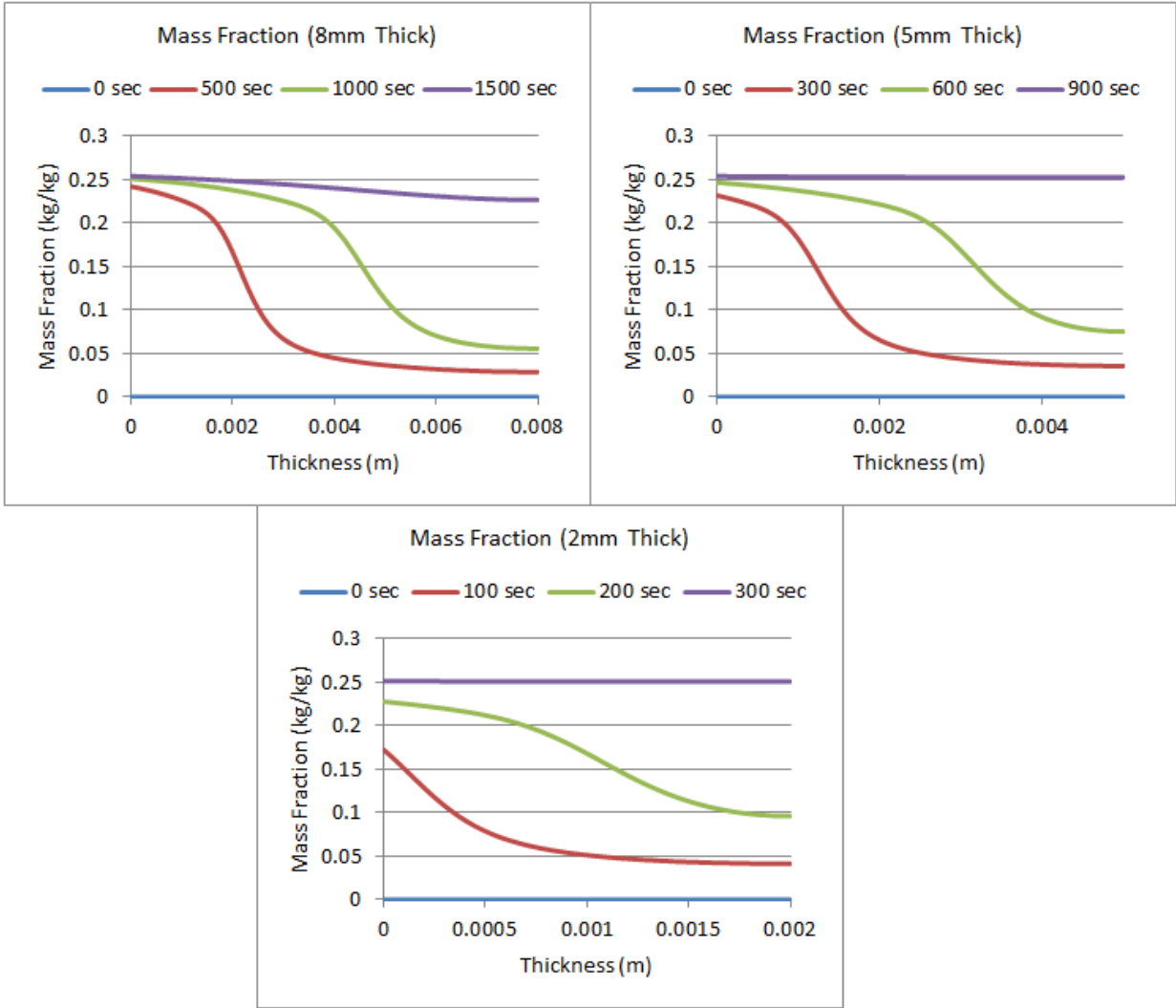
Figure 102: Mass Fraction (ATH Residue) for 10% ATH (Varying Thickness)

MLR (20% ATH)

The graph below shows three MLR curves for varying thickness in a resin sample with 20% ATH. From comparison to the other MLR graphs, it varies very little. This would suggest that the addition of 20% ATH does not cause significant changes when compared to the MLR graphs of lower levels of ATH. The profiles at 20% ATH can be seen below.
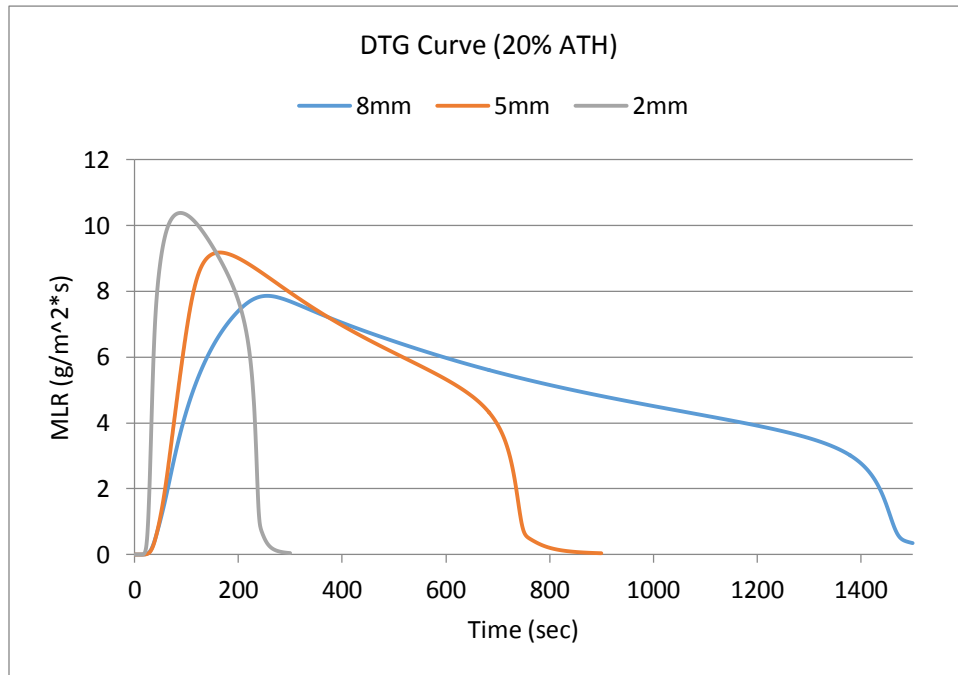
Figure 103: DTG Curves (20% ATH)

Temperature Profiles (20% ATH)
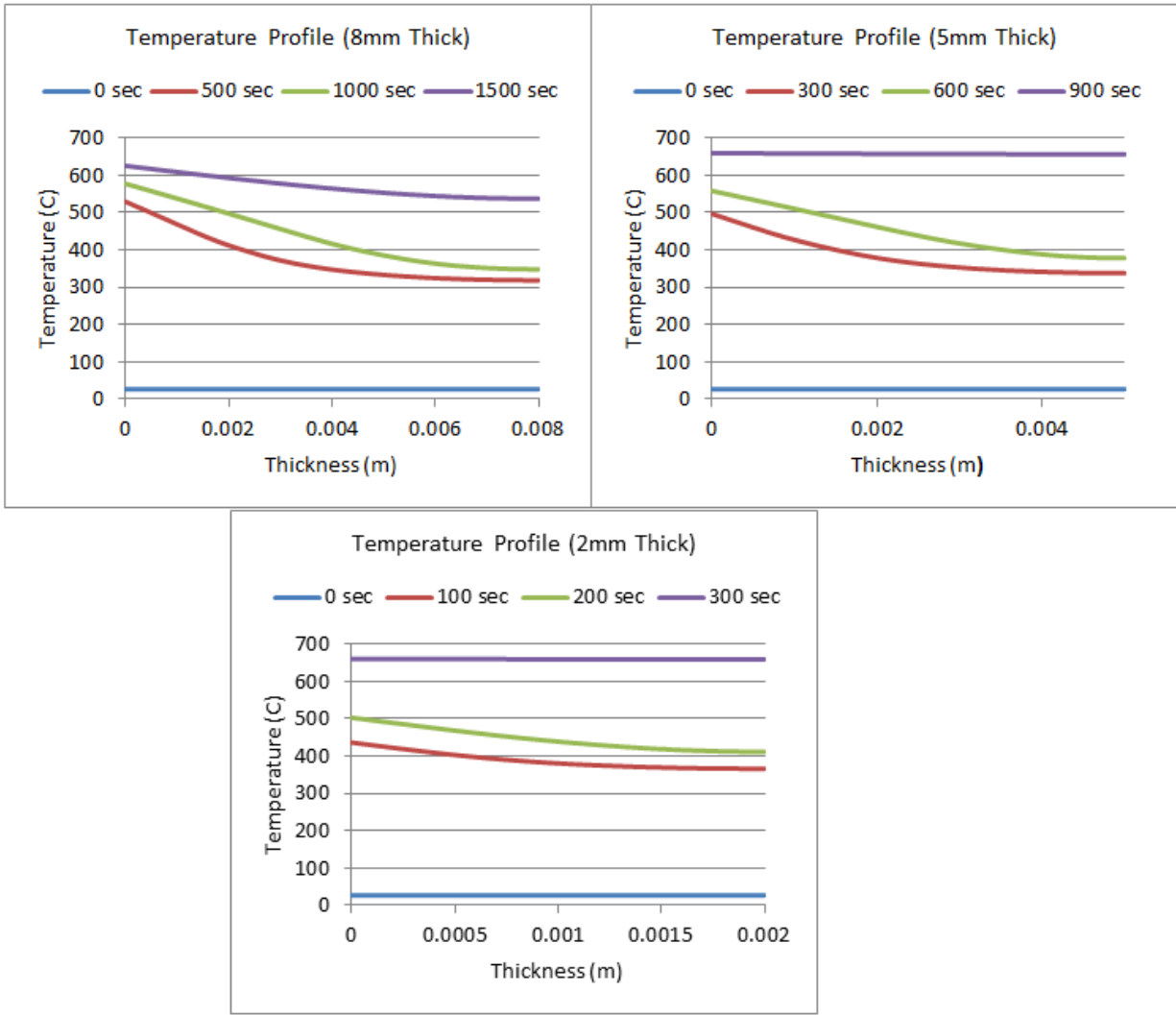
Figure 104: Temperature Profiles for 20% ATH (Varying Thickness)

Porosity (20% ATH)
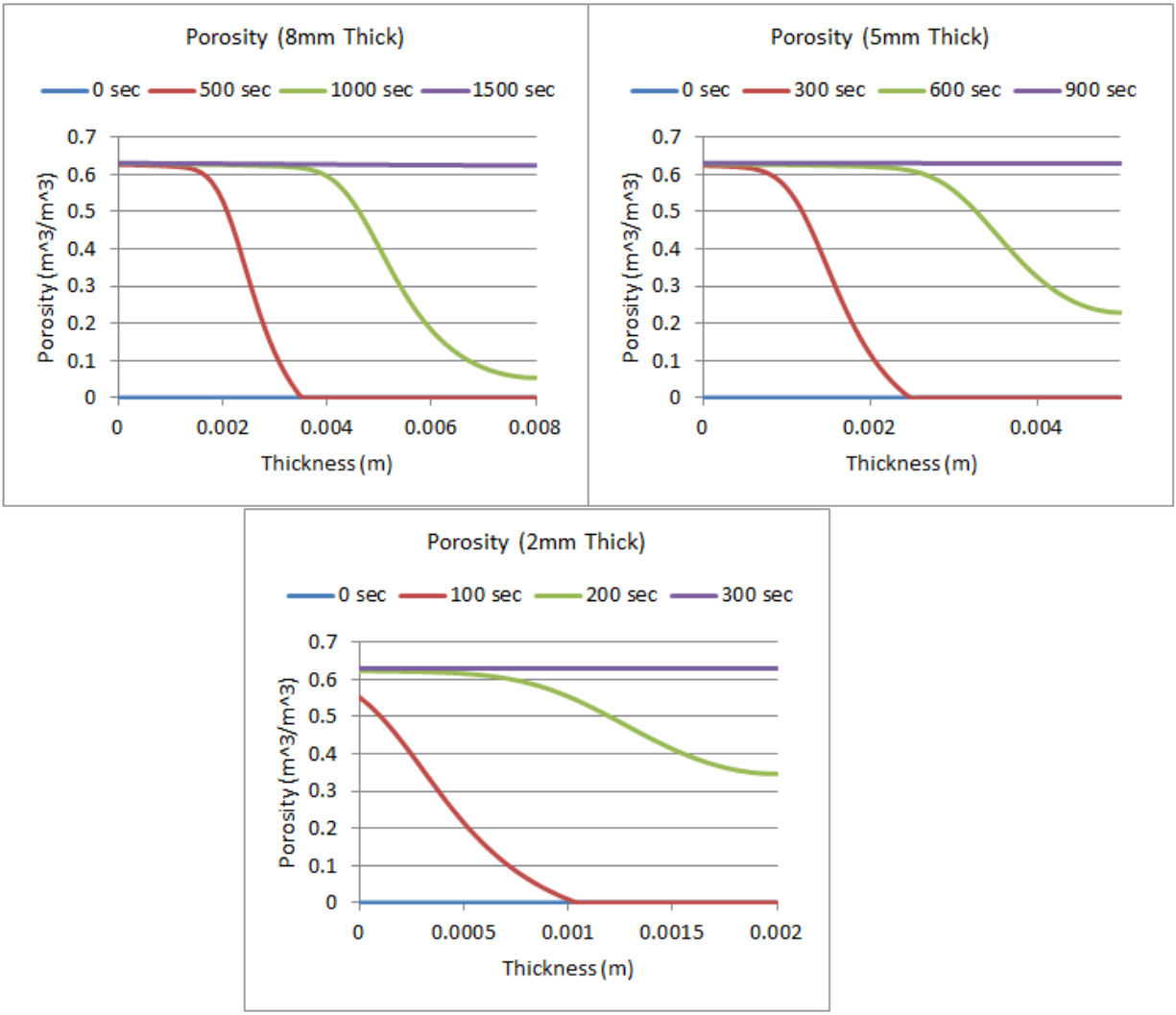
Figure 105: Porosity for 20% ATH (Varying Thickness)

Bulk Density (20% ATH)
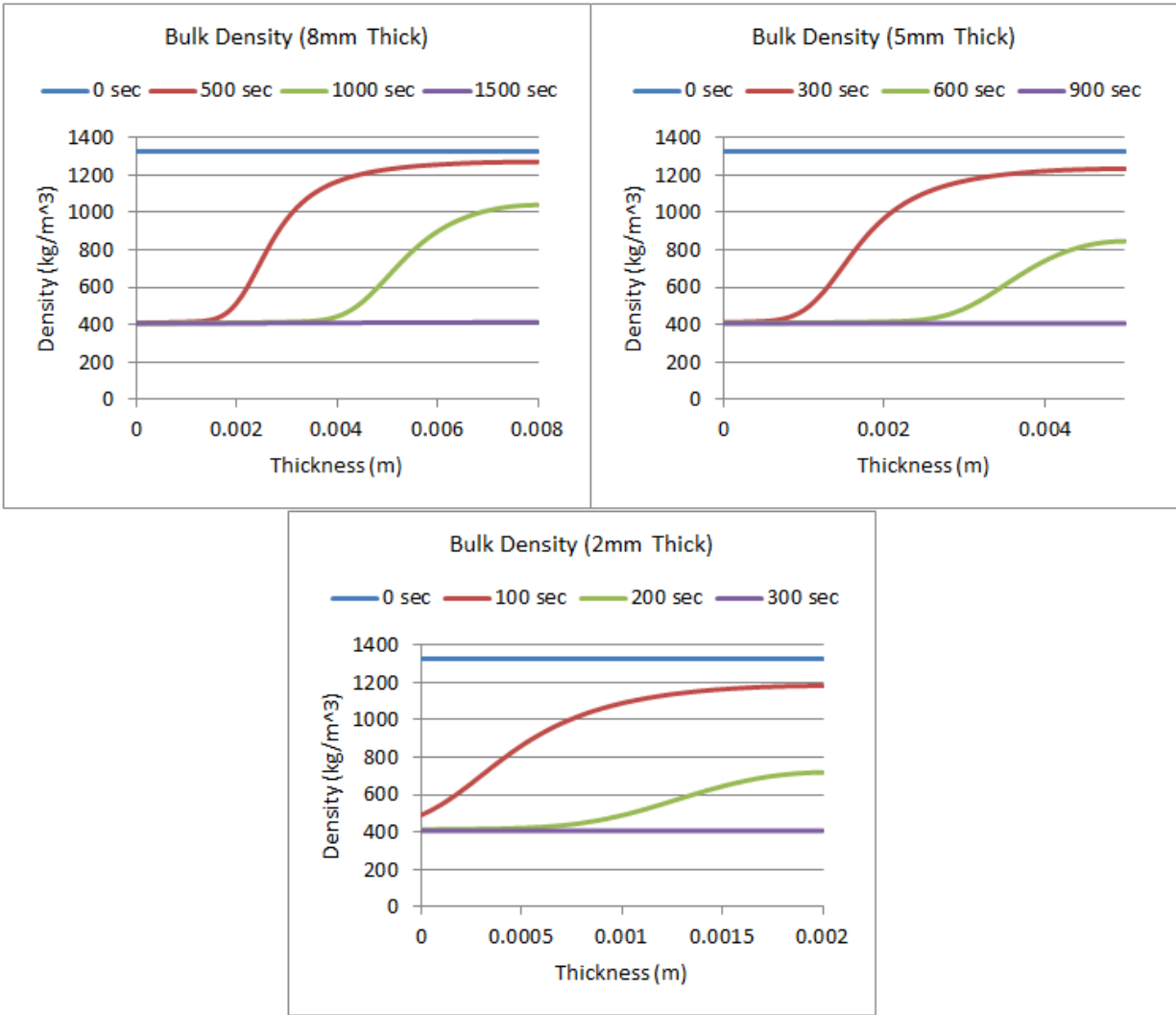
Figure 106: Bulk Density for 20% ATH (Varying Thickness)

Reaction Rate (Resin to Resin Residue) 20% ATH
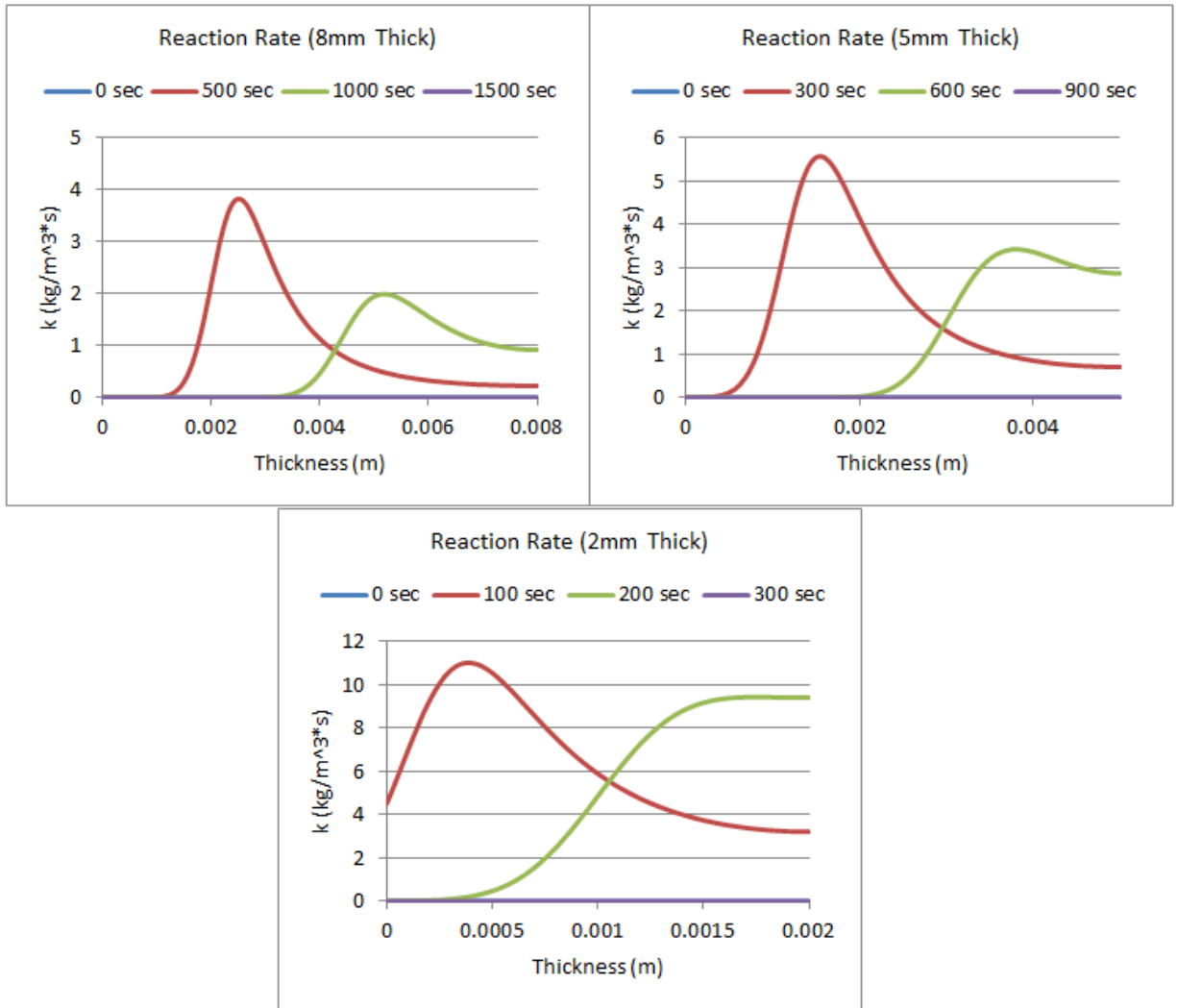
Figure 107: Reaction Rate (Resin) for 20% ATH (Varying Thickness)

Reaction Rate (ATH to ATH Residue) 20% ATH
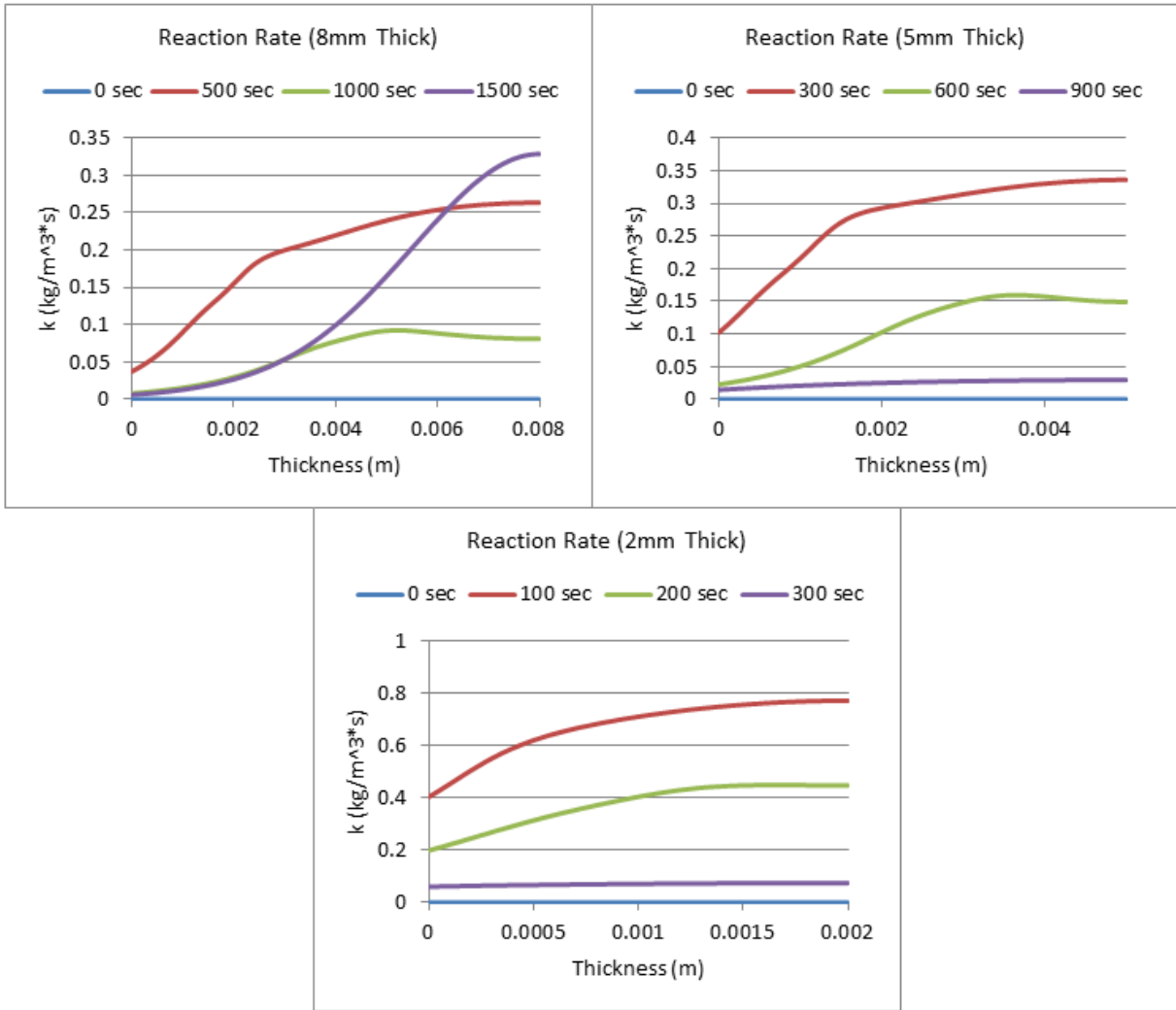
Figure 108: Reaction Rate (ATH) for 20% ATH (Varying Thickness)

Mass Fraction of Resin (20% ATH)
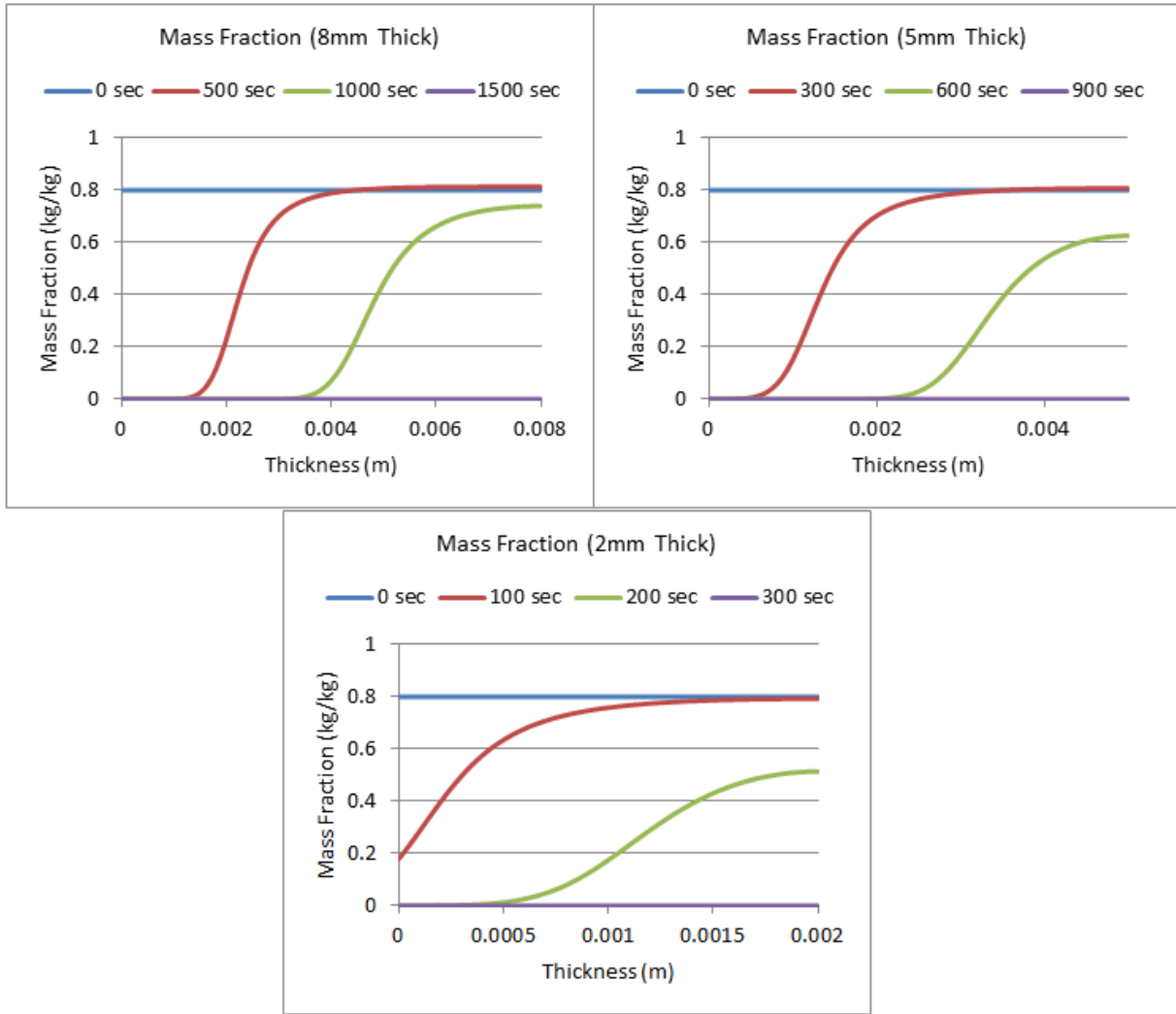
Figure 109: Mass Fraction (Resin) for 20% ATH (Varying Thickness)

Mass Fraction for Resin Residue (20% ATH)
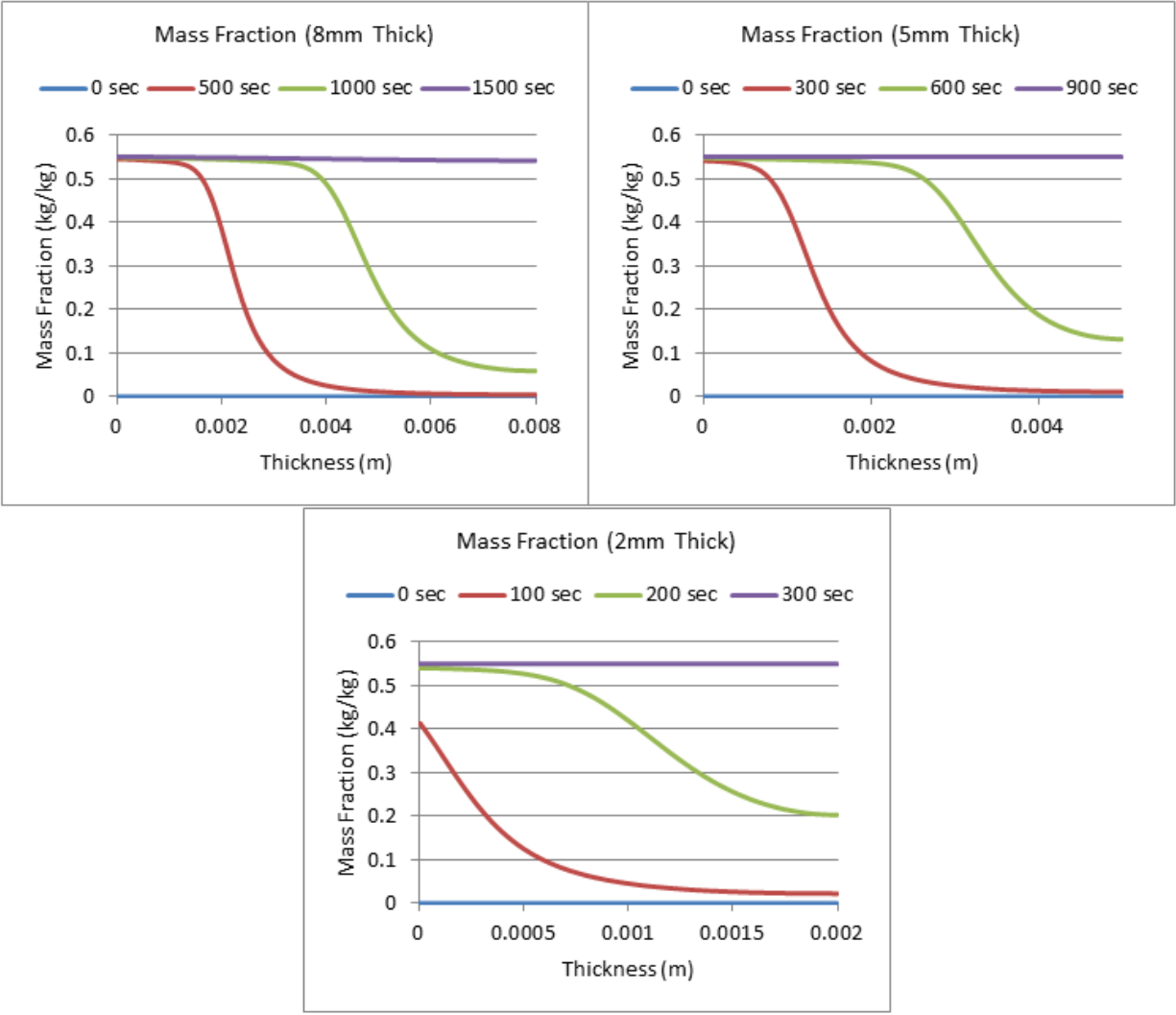
Figure 110: Mass Fraction (Resin Residue) for 20% ATH (Varying Thickness)

Mass Fraction of ATH (20% ATH)
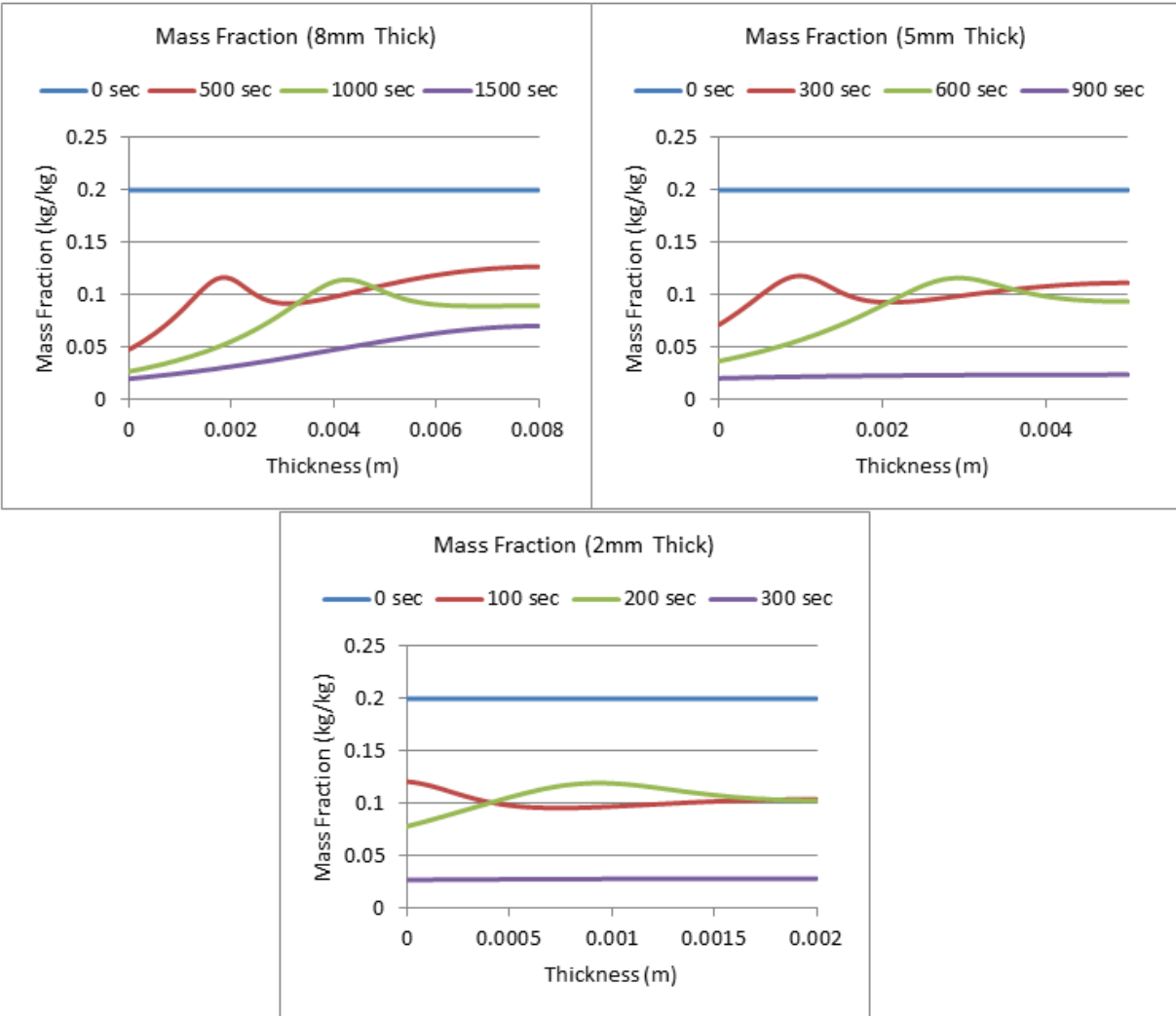
Figure 111: Mass Fraction (ATH) for 20% ATH (Varying Thickness)

Mass Fraction (ATH Residue) 20% ATH
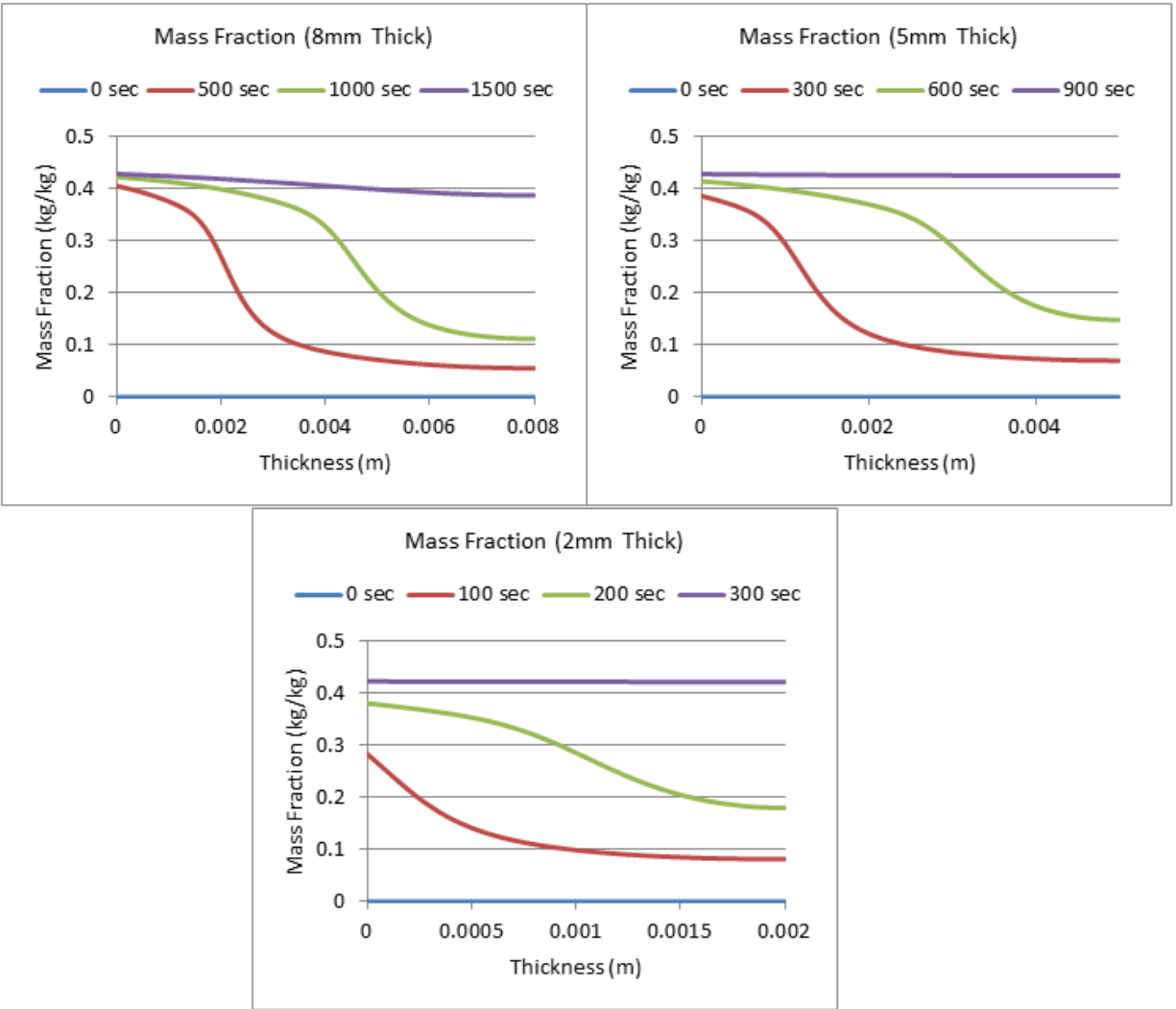
Figure 112: Mass Fraction (ATH Residue) for 20% ATH (Varying Thickness)

Appendix E.7: Gpyro 1D-Boundary Conditions

The next step was better understanding the boundary conditions, particularly the contact conductance and re-radiation, and how the results are affected when Gpyro is run at the actual sample size (1mm). The profiles can be seen below. A normalization of the DTG curve was attempted, although this proved to not be best method of converting data.

5%ATH, 1mm, qe=25,000W/m^2, re-radiation on, hc=10W/m^2*K, hcc=0W/m^2*K
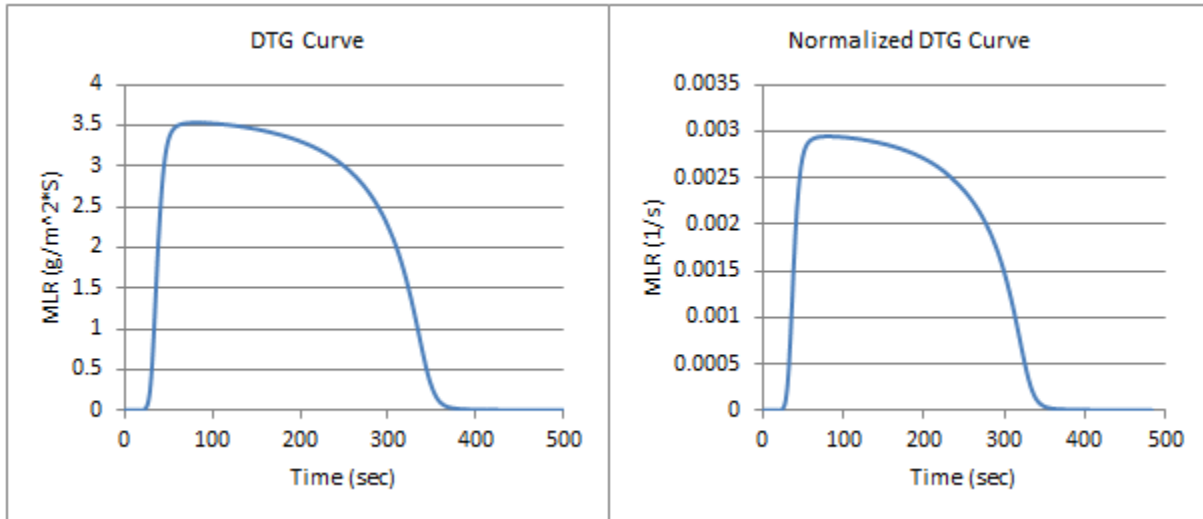
Figure 113: DTG and Normalized DTG Curve, 5%ATH, 1mm, qe=25,000W/m^2, re-radiation on, hc=10W/m^2*K, hcc=0W/m^2*K
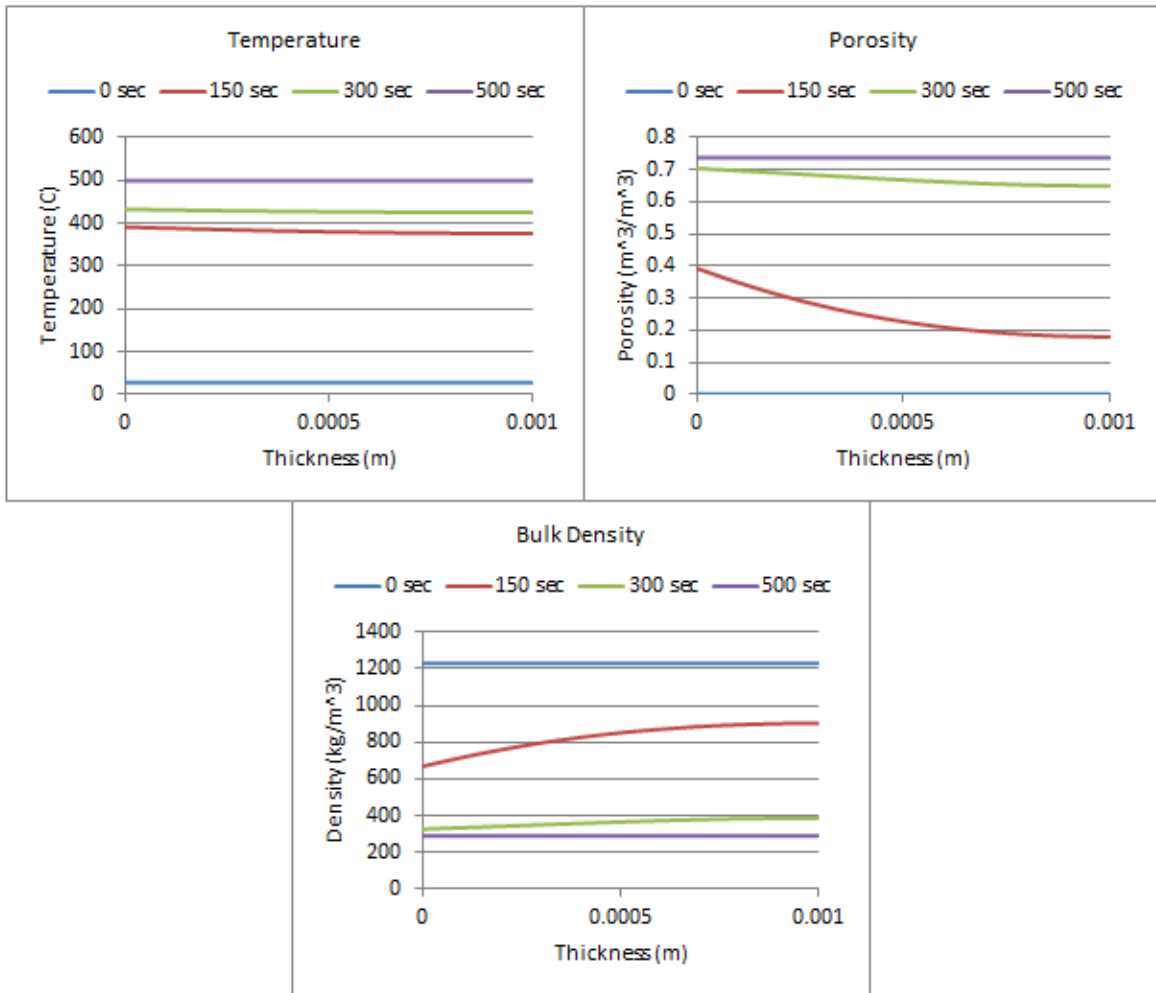
Figure 114: Temperature, Porosity, and Bulk Density Profiles, 5%ATH, 1mm, qe=25,000W/m^2, re-radiation on, hc=10W/m^2*K, hcc=0W/m^2*K
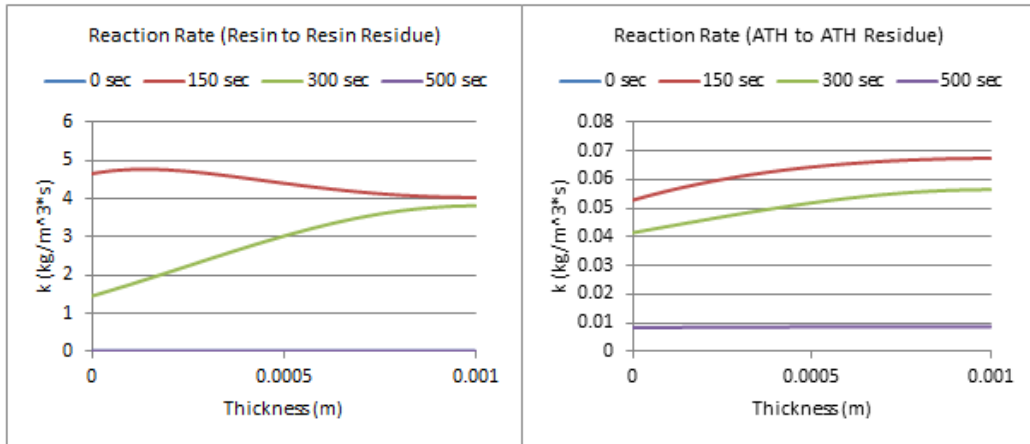
Figure 115: Reaction Rates (Resin and ATH), 5%ATH, 1mm, qe=25,000W/m^2, re-radiation on, hc=10W/m^2*K, hcc=0W/m^2*K
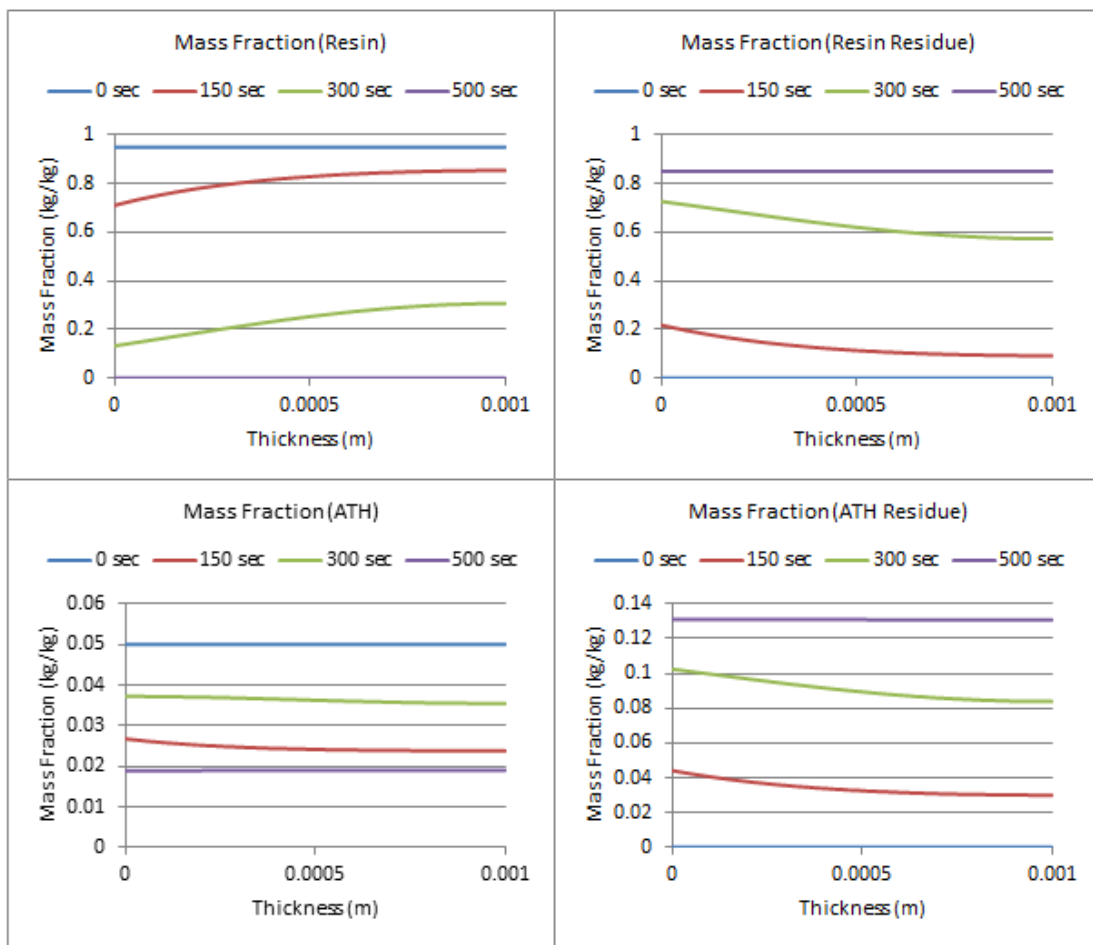
Figure 116: Mass Fractions, 5%ATH, 1mm, qe=25,000W/m^2, re-radiation on, hc=10W/m^2*K, hcc=0W/m^2*K

5% ATH, 1mm, qe=25,000W/m^2*K, re-radiation off, hc=0W/m^2*K, hcc=0 W/m^2*K
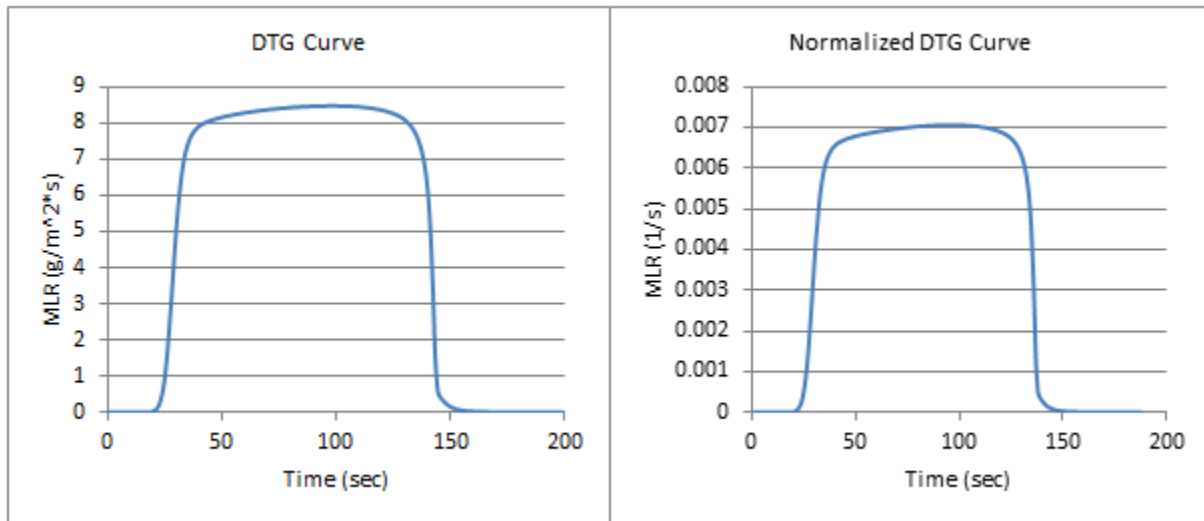
Figure 117: DTG and Normalized DTG, 5% ATH, 1mm, qe=25,000W/m^2*K, re-radiation off, hc=0W/m^2*K, hcc=0 W/m^2*K
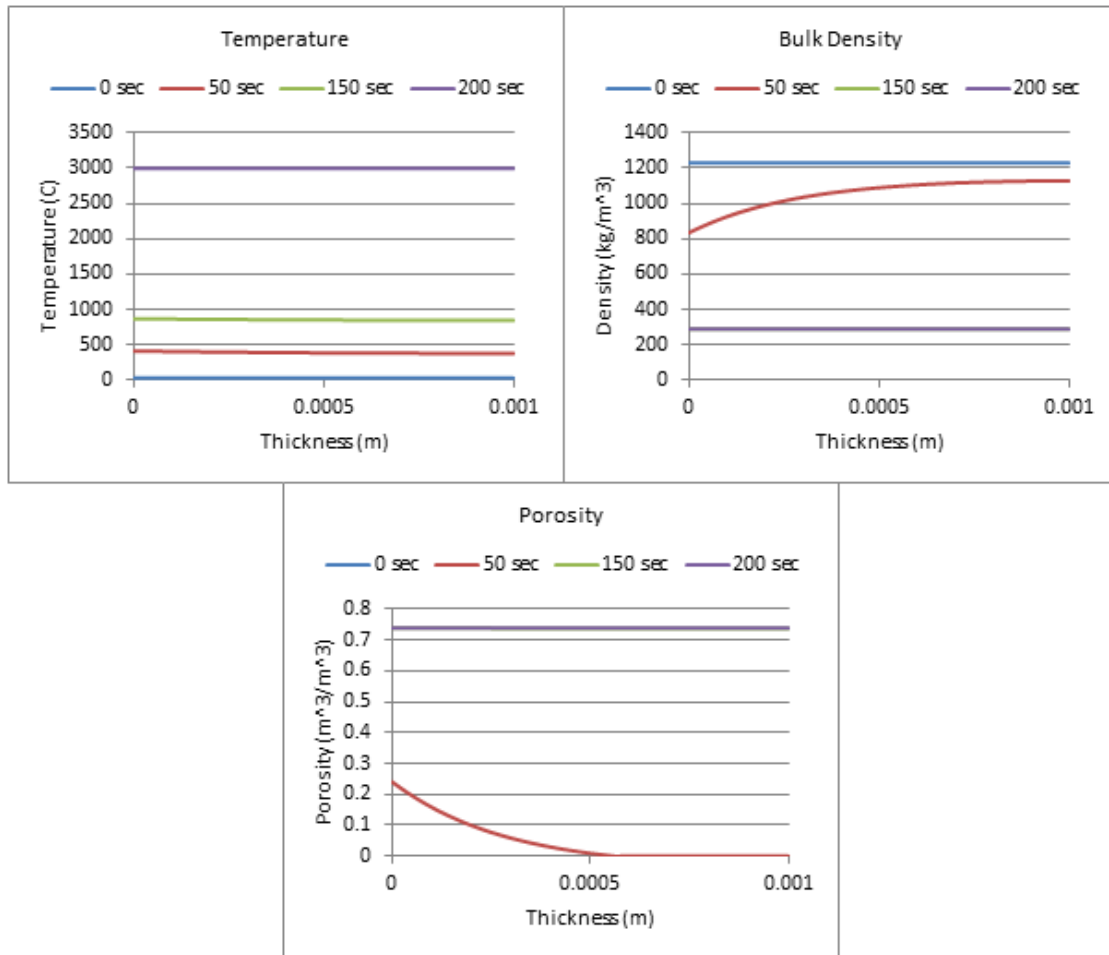
Figure 118: Temperature, Bulk Density, and Porosity Profiles, 5% ATH, 1mm, qe=25,000W/m^2*K, re-radiation off, hc=0W/m^2*K, hcc=0 W/m^2*K
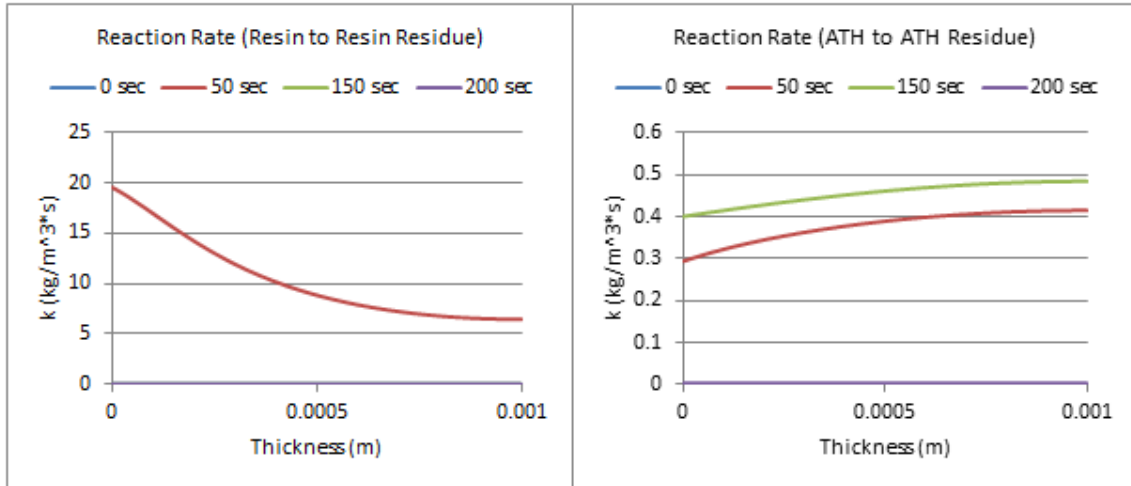
Figure 119: Reaction Rates, 5% ATH, 1mm, qe=25,000W/m^2*K, re-radiation off, hc=0W/m^2*K, hcc=0 W/m^2*K
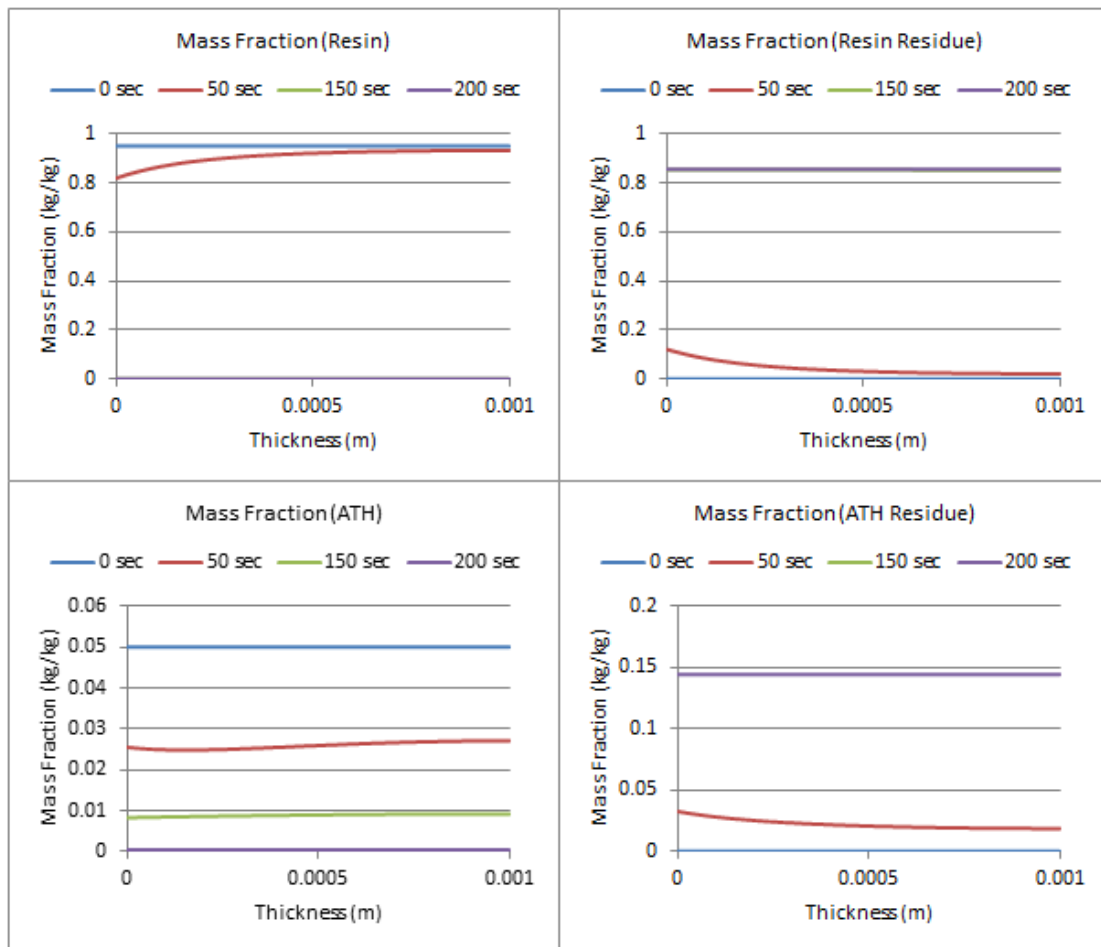
Figure 120: Mass Fractions, 5% ATH, 1mm, qe=25,000W/m^2*K, re-radiation off, hc=0W/m^2*K, hcc=0 W/m^2*K

5% ATH, 1mm, qe=15,000W/m^2, re-radiation off, hc=0W/m^2*K, hcc=0W/m^2*K
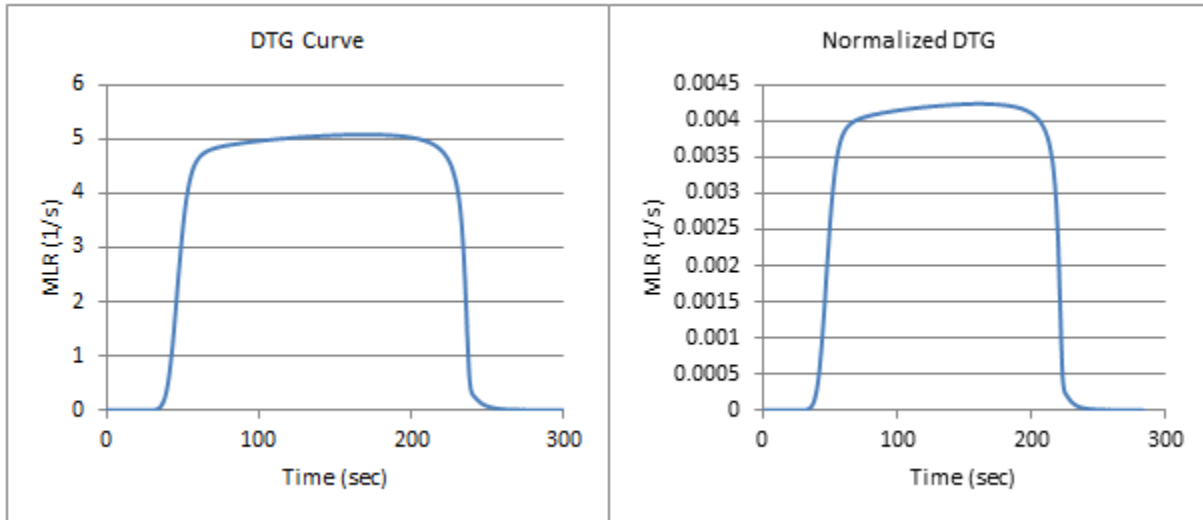
Figure 121: DTG and Normalized DTG Curves, 5% ATH, 1mm, qe=15,000W/m^2, re-radiation off, hc=0W/m^2*K, hcc=0W/m^2*K
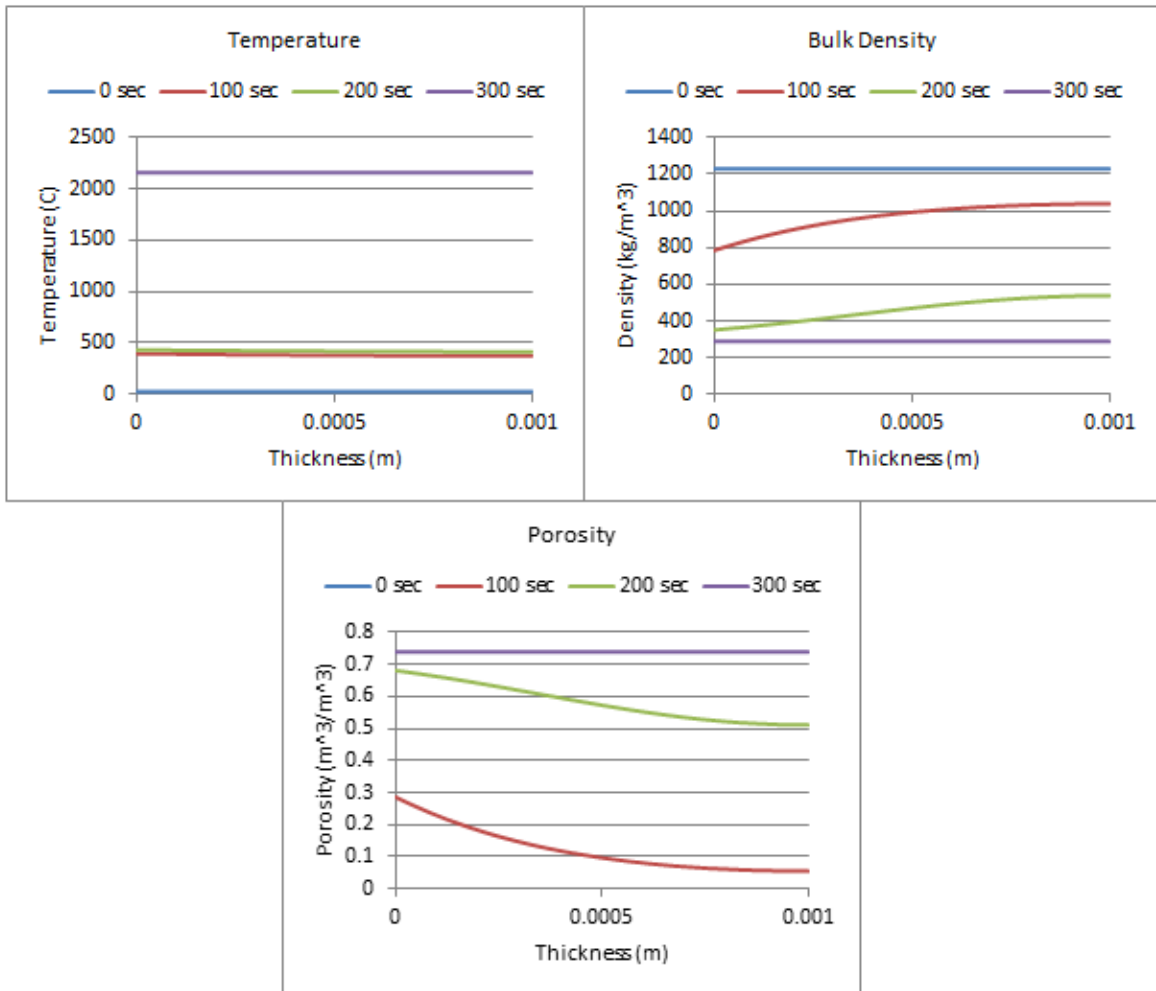
Figure 122: Temperature, Bulk Density, and Porosity Profiles, 5% ATH, 1mm, qe=15,000W/m^2, re-radiation off, hc=0W/m^2*K, hcc=0W/m^2*K
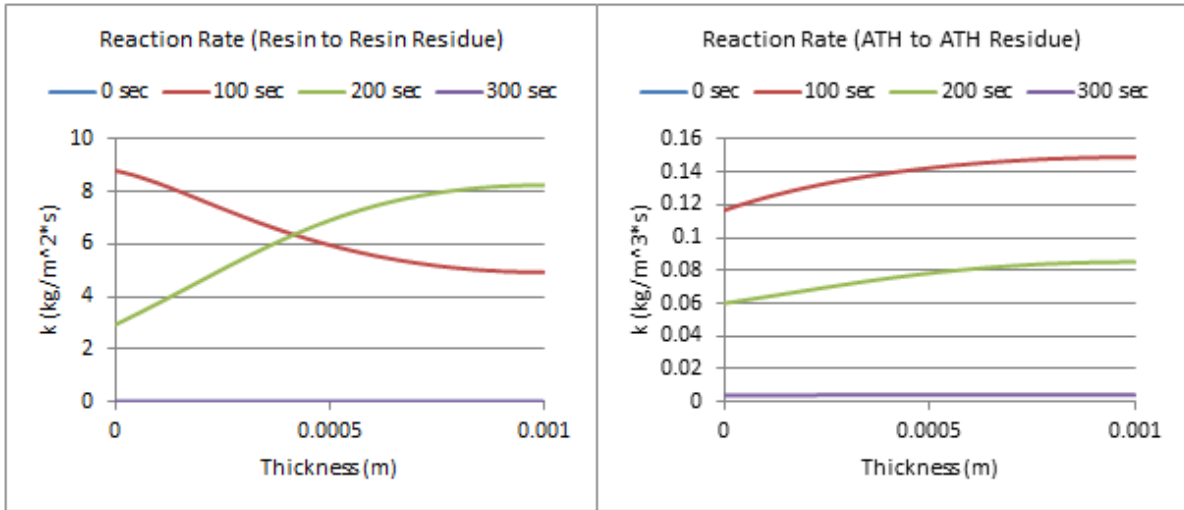
Figure 123: Reaction Rates, 5% ATH, 1mm, qe=15,000W/m^2, re-radiation off, hc=0W/m^2*K, hcc=0W/m^2*K
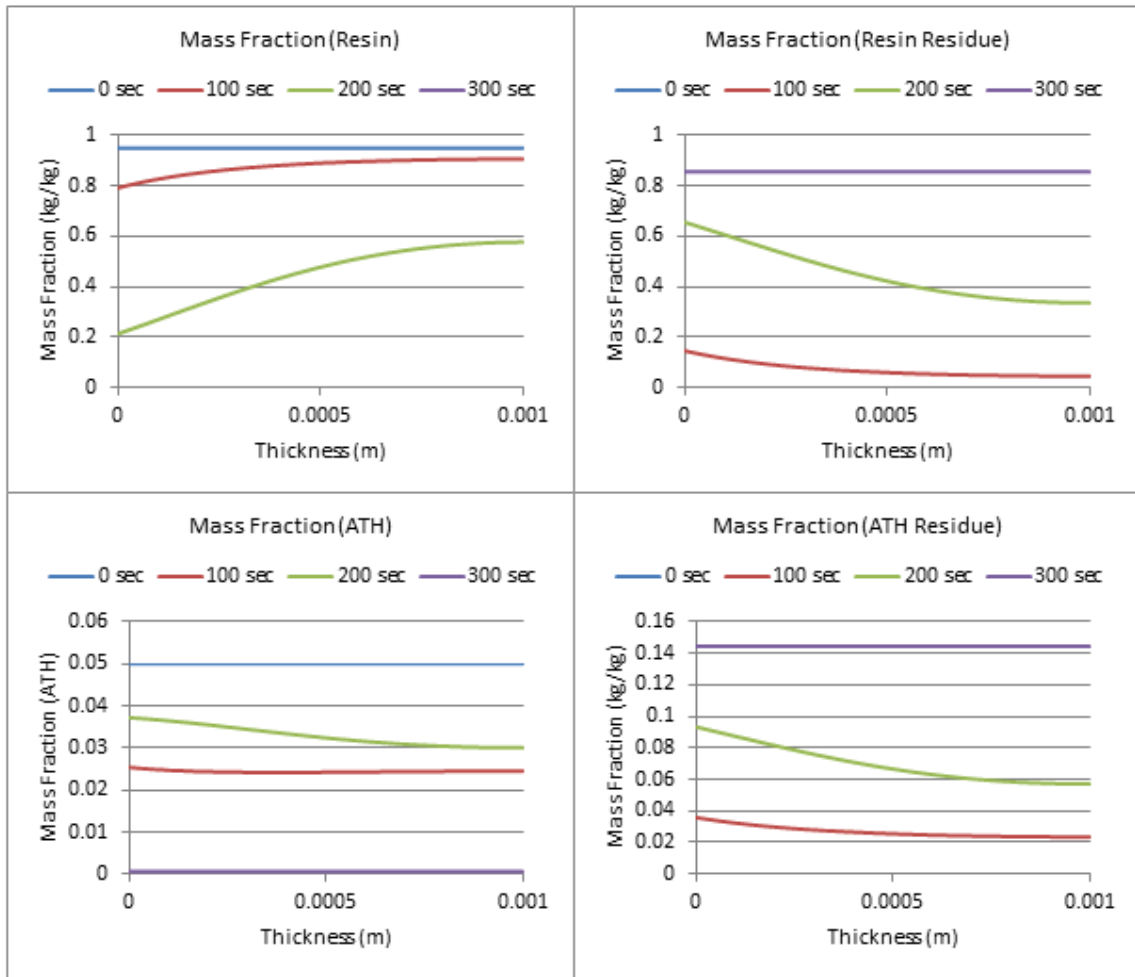
Figure 124: Mass Fractions, 5% ATH, 1mm, qe=15,000W/m^2, re-radiation off, hc=0W/m^2*K, hcc=0W/m^2*K

5% ATH, 1mm, qe=5,000W/m^2, re-radiation off, hc=0W/m^2*K, hcc=0W/m^2*K
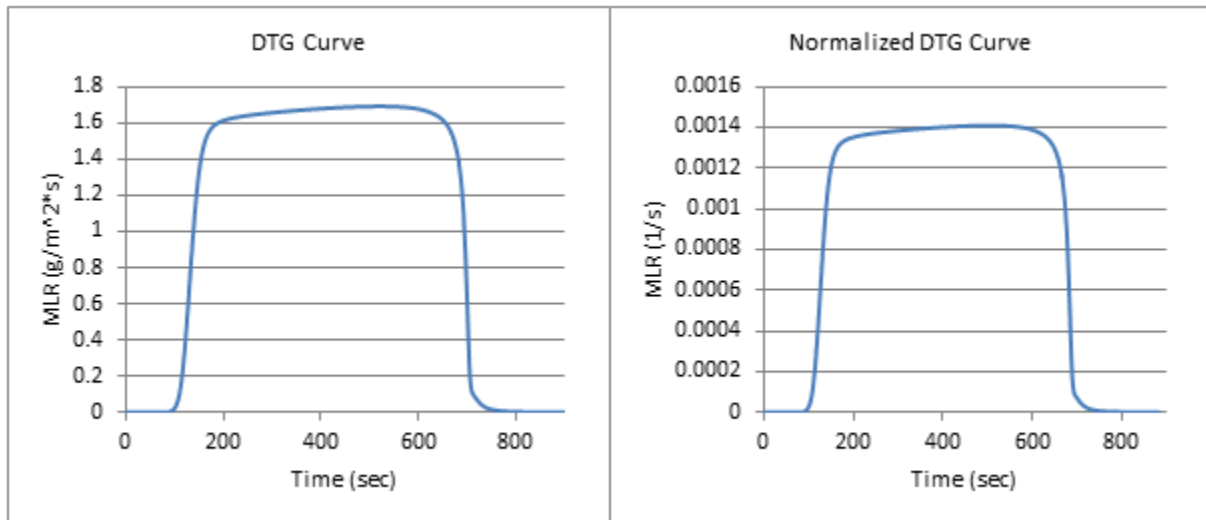
Figure 125: DTG and Normalized DTG Curve, 5% ATH, 1mm, qe=5,000W/m^2, re-radiation off, hc=0W/m^2*K, hcc=0W/m^2*K
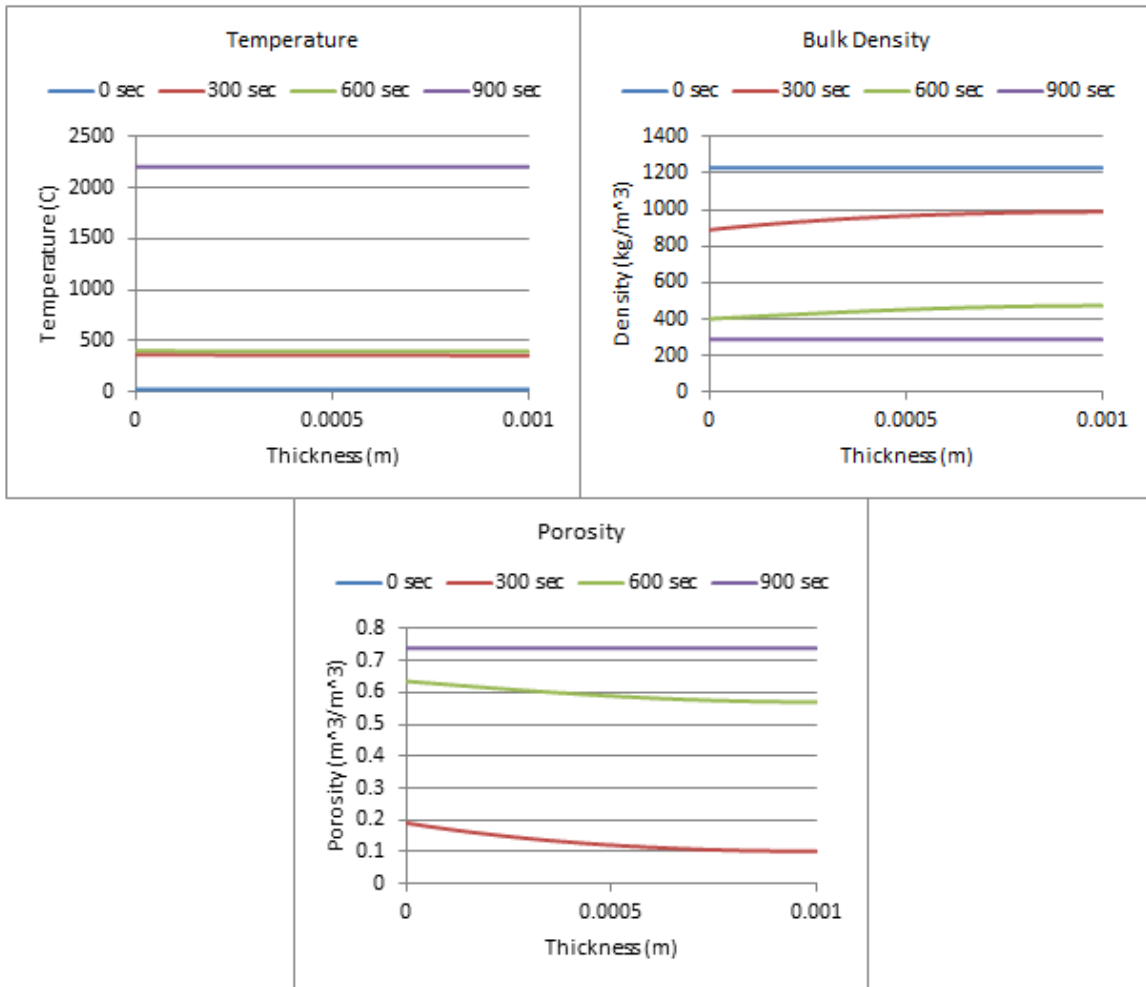
Figure 126: Temperature, Bulk Density, and Porosity Profiles, 5% ATH, 1mm, qe=5,000W/m^2, re-radiation off, hc=0W/m^2*K, hcc=0W/m^2*K
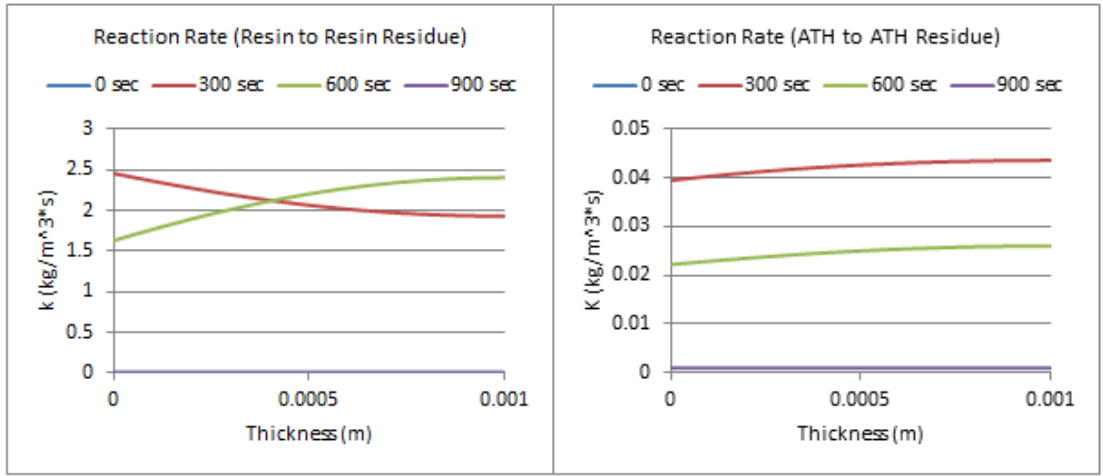
Figure 127: Reaction Rate Profiles, 5% ATH, 1mm, qe=5,000W/m^2, re-radiation off, hc=0W/m^2*K, hcc=0W/m^2*K
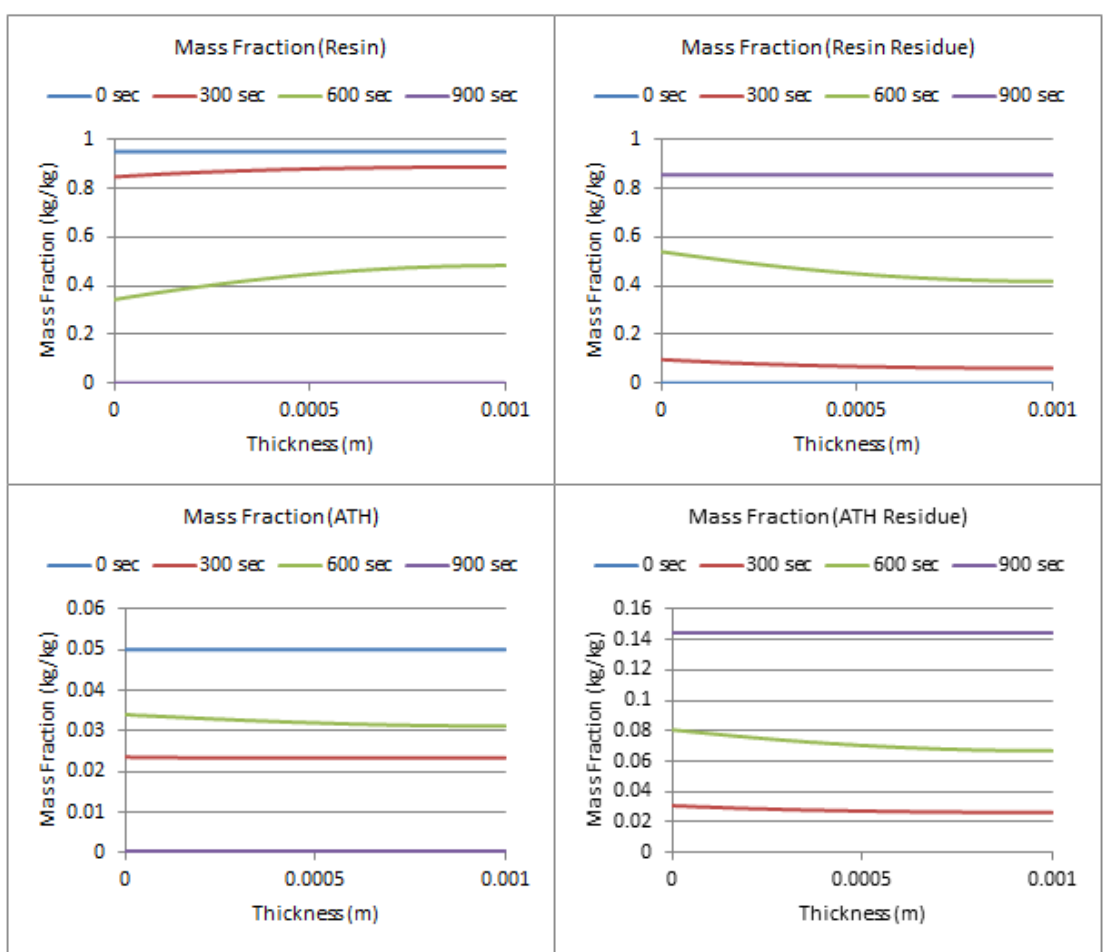
Figure 128: Mass Fraction Profiles, 5% ATH, 1mm, qe=5,000W/m^2, re-radiation off, hc=0W/m^2*K, hcc=0W/m^2*K

5% ATH, 1mm, qe=1,000W/m^2, re-radiation off, hc=0W/m^2*K, hcc=0W/m^2*K
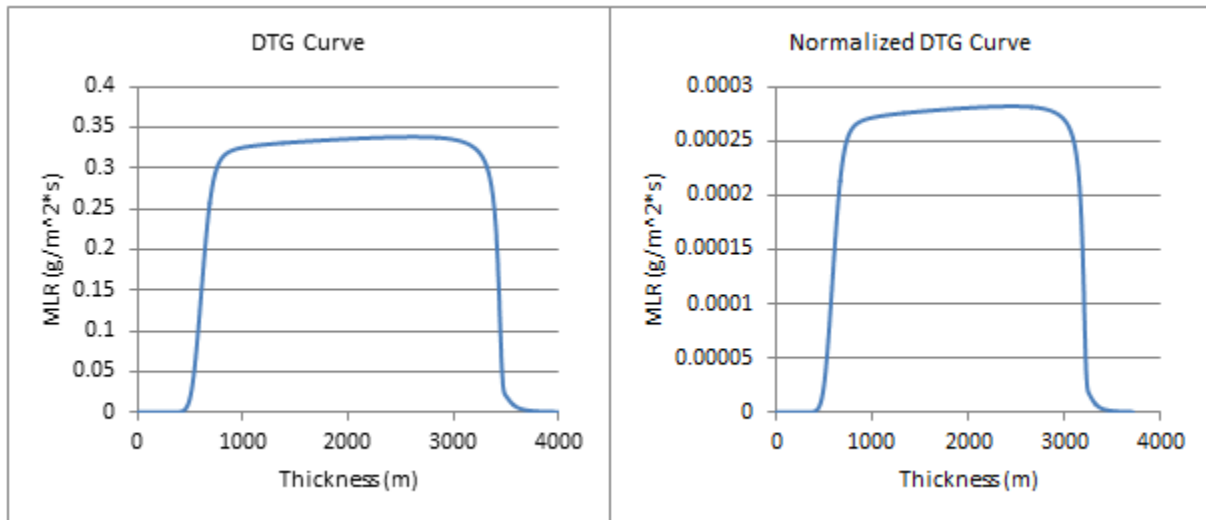
Figure 129: DTG and Normalized DTG Curve, 5% ATH, 1mm, qe=1,000W/m^2, re-radiation off, hc=0W/m^2*K, hcc=0W/m^2*K
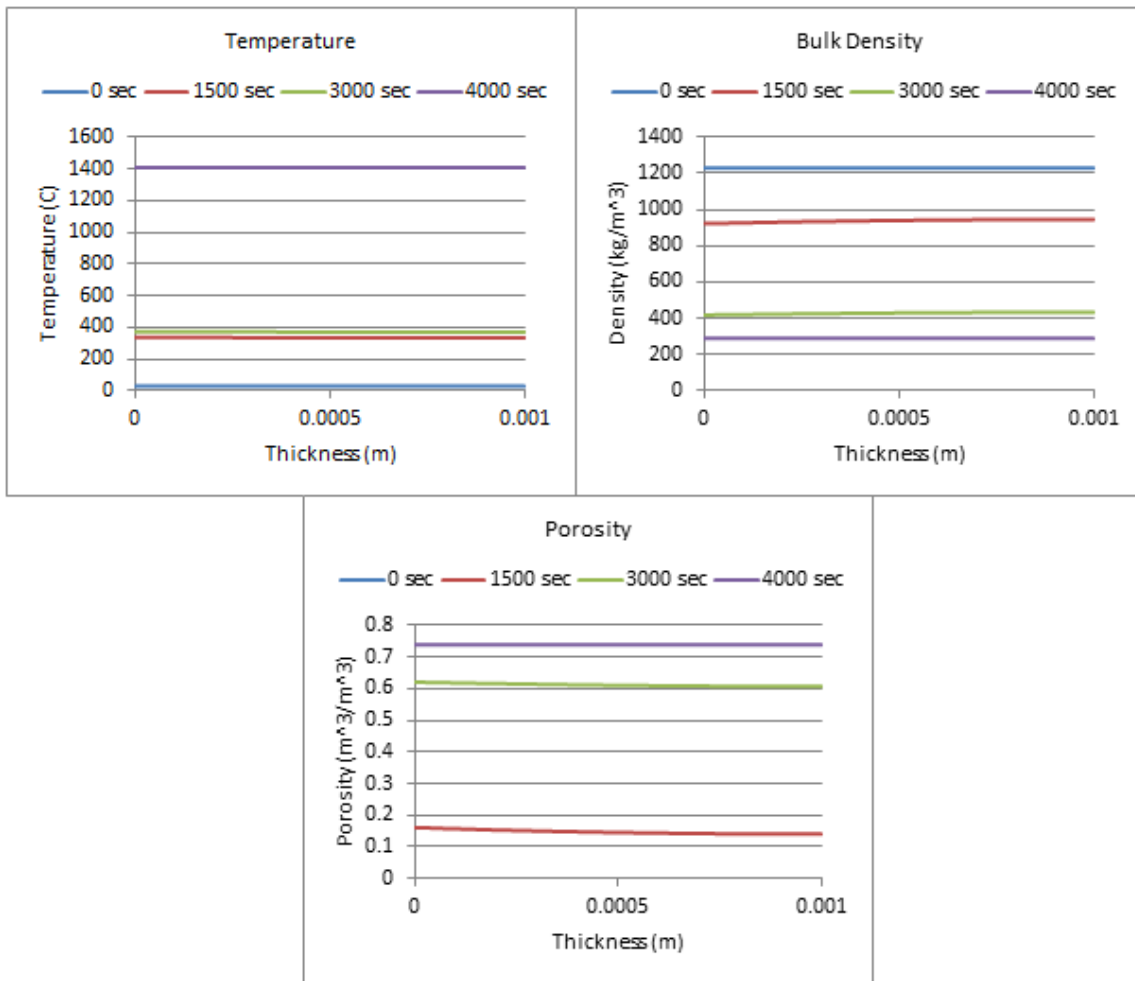
Figure 130: Temperature, Bulk Density, and Porosity Profiles, 5% ATH, 1mm, qe=1,000W/m^2, re-radiation off, hc=0W/m^2*K, hcc=0W/m^2*K
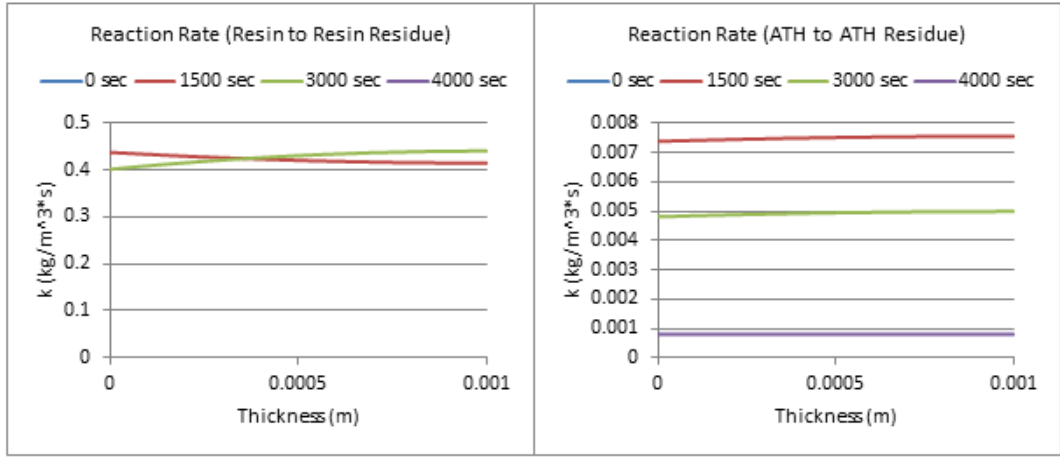
Figure 131: Reaction Rate Profiles, 5% ATH, 1mm, qe=1,000W/m^2, re-radiation off, hc=0W/m^2*K, hcc=0W/m^2*K
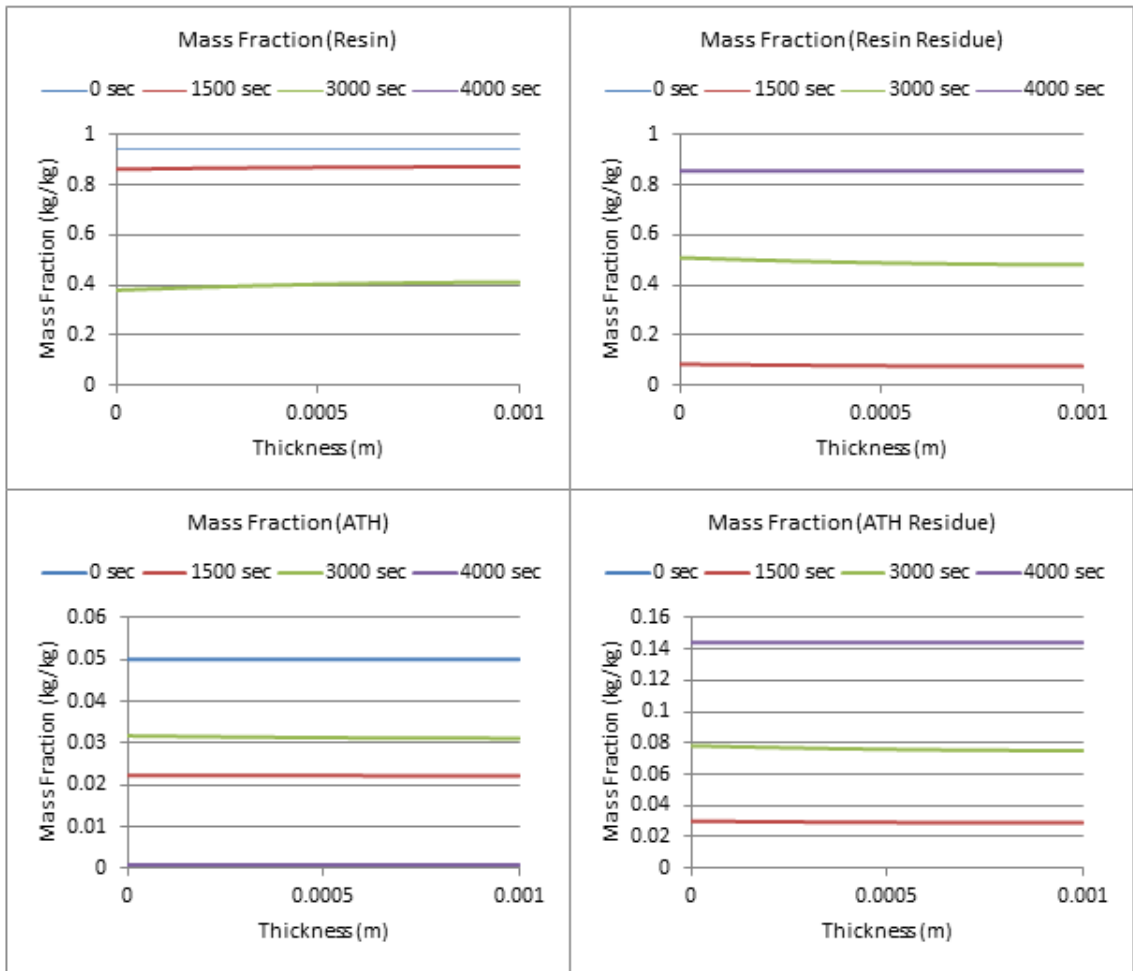
Figure 132: Mass Fraction Profiles, 5% ATH, 1mm, qe=1,000W/m^2, re-radiation off, hc=0W/m^2*K, hcc=0W/m^2*K

Appendix E.8: Gpyro 1D-Hetron/ATH Optimized Parameter Simulations

After the initial simulations were done, tuned up optimized parameters we inputted as the final parameters. Also, pure ATH values were used [17]. The tuned up values were used to give more accurate results in Gpyro. The new values, along with the old for comparison, can be seen in the tables below.

Table 19: Resin/Hetron Values for Gpyro

	E (J/mol)	Z (s^-1)	n (-)	Weight-Loss Fraction
Ester Kim	185	3.2*10^12	1.3	0.78
MQP	195.37	5*10^13	1.125	0.94

Table 20: ATH Values for Gpyro

	E (J/mol)	Z (s^-1)	n (-)	Weight-Loss Fraction
Ester Kim	160	1.6*10^12	5	0.33
MQP	140.1	2.5*10^11	1.24	0.34

Table 21: Heat of Decomposition Values for Gpyro

	Heat of Decomposition (ATH) (J/kg)	Heat of Decomposition (Hetron) (J/kg)
Ester Kim	3.8*10^6	2.5*10^6
MQP	1*10^6	1.72*10^5

Once the new values were put into Gpyro, the same type of simulation was completed. This time, the decided on input values were inputted along with the new optimized parameters. Since there is now an understanding of how the change in thickness affects the results, the measured average sample size (1mm) was used. This time, the simulation is run at various levels of ATH. There was also an attempt to normalize the DTG Curve, which later proved to be an inaccurate way of representing the data. It is known that we need a low value for the heat flux. Starting with 1,000 W/m^2*K, profiles are made for varying levels of ATH, shown below.

5% ATH, 1mm, Ester Kim/MQP Mixed Model, qe=1000W/m^2, re-radiation off, hc/hcc=0W/m^2*K
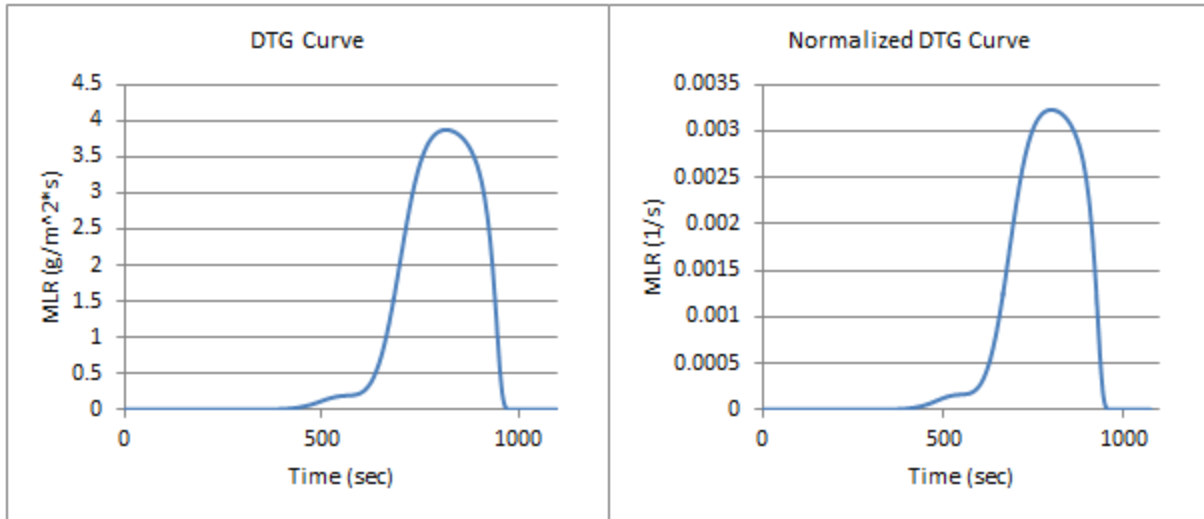
Figure 133: DTG and Normalized DTG Profiles (Mixed Model), 5% ATH, 1mm, Ester Kim/MQP Mixed Model, qe=1000W/m^2, re-radiation off, hc/hcc=0W/m^2*K
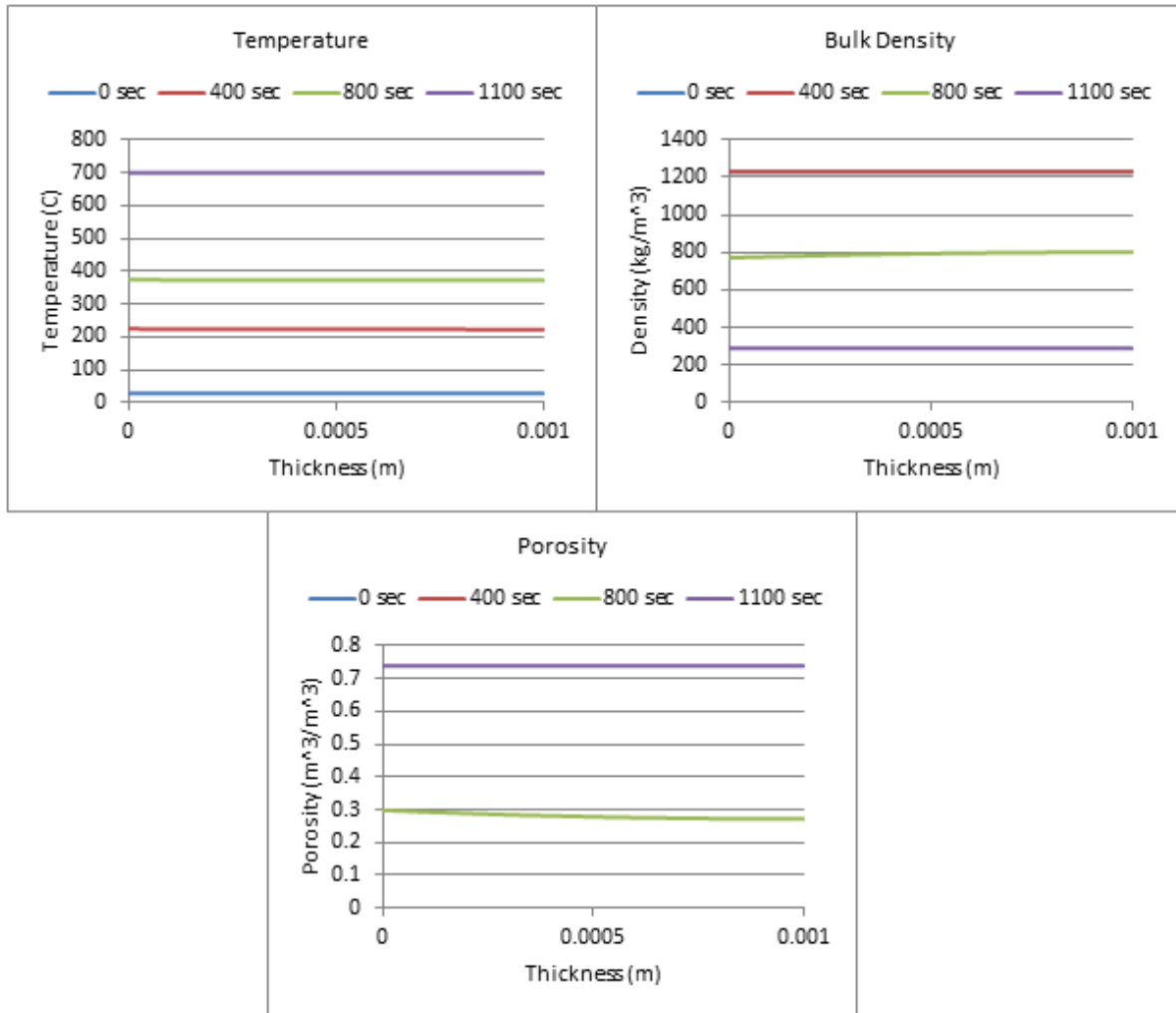
Figure 134: Temperature, Bulk Density, and Porosity Profiles (Mixed Model), 5% ATH, 1mm, Ester Kim/MQP Mixed Model, qe=1000W/m^2, re-radiation off, hc/hcc=0W/m^2*K
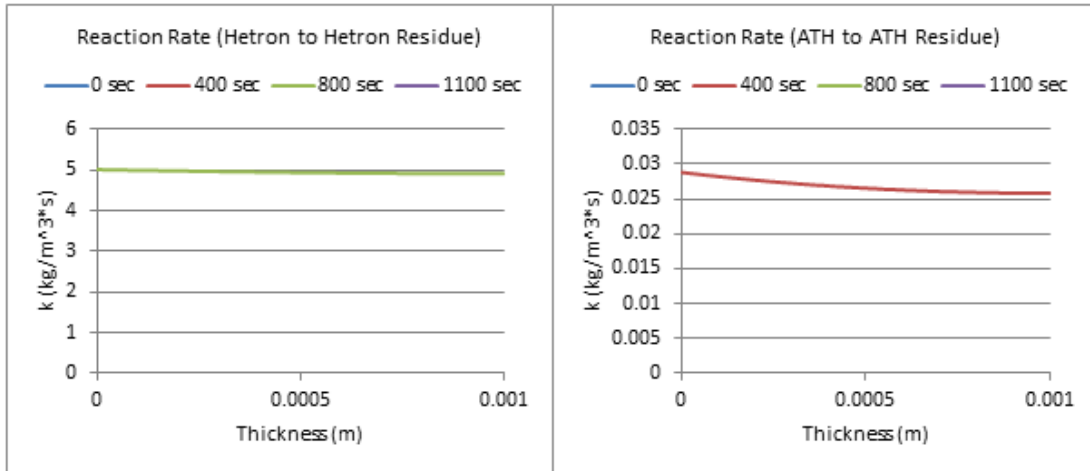
Figure 135: Reaction Rate Profiles (Mixed Model), 5% ATH, 1mm, Ester Kim/MQP Mixed Model, qe=1000W/m^2, re-radiation off, hc/hcc=0W/m^2*K
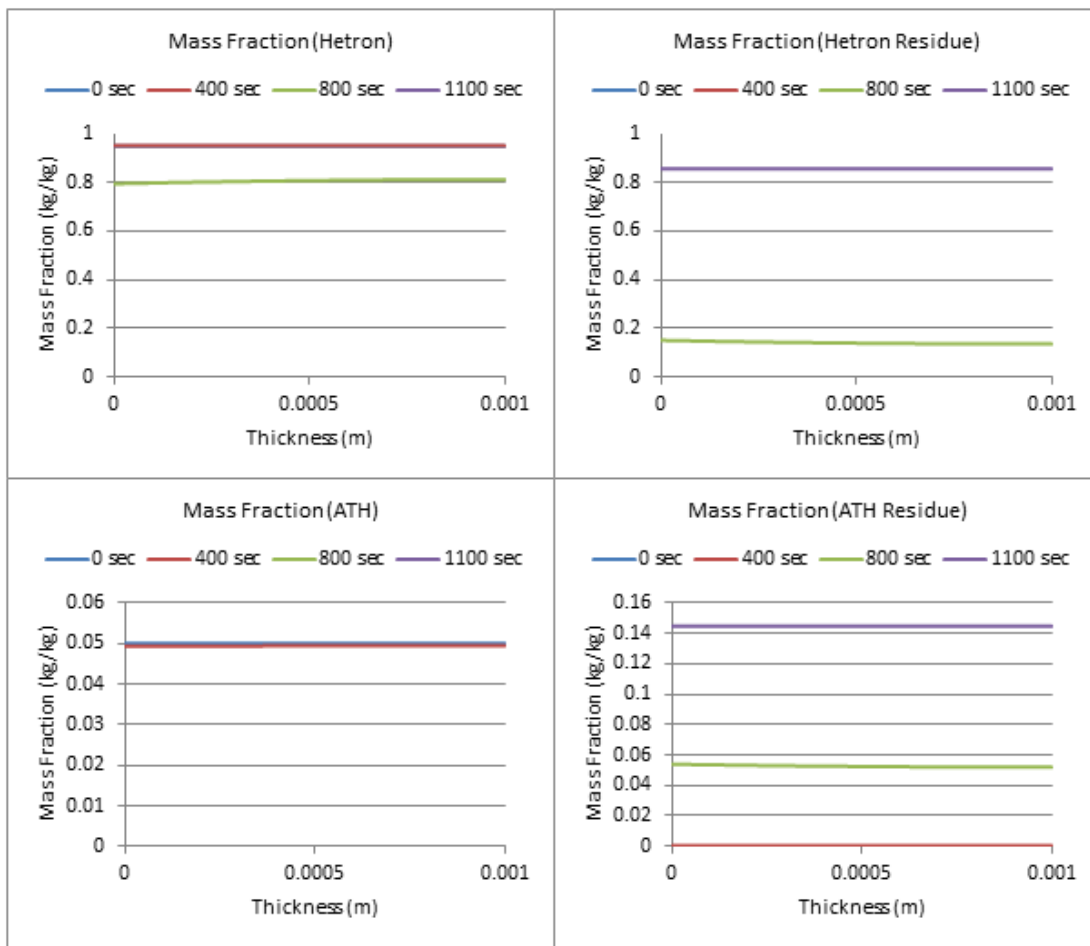
Figure 136: Mass Fraction Profiles (Mixed Model), 5% ATH, 1mm, Ester Kim/MQP Mixed Model, qe=1000W/m^2, re-radiation off, hc/hcc=0W/m^2*K

25% ATH, 1mm, Ester Kim/MQP Mixed Model, qe=1000W/m^2, re-radiation off, hc/hcc=0W/m^2*K
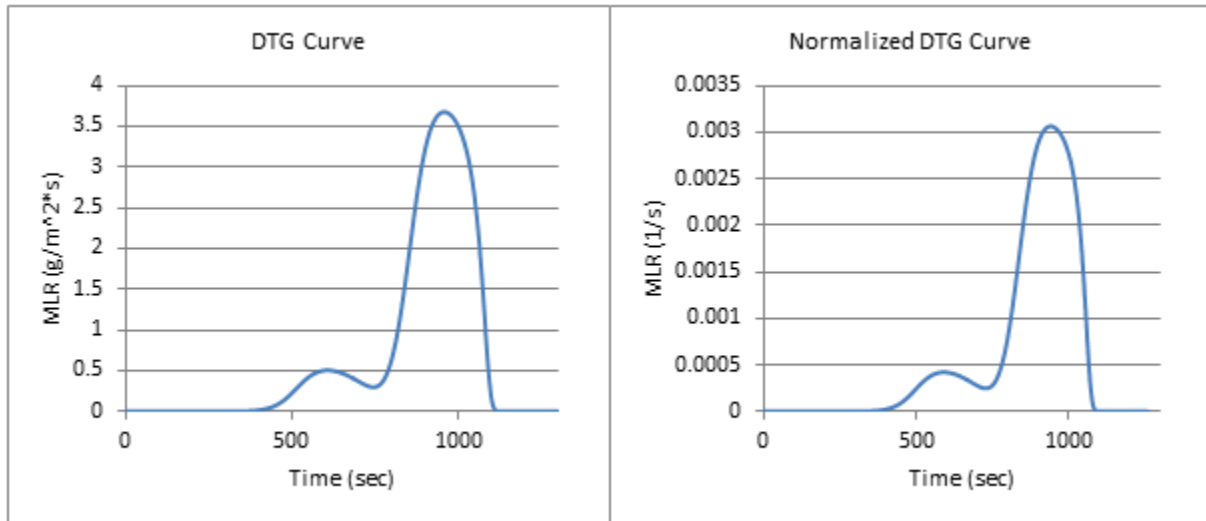
Figure 137: DTG and Normalized DTG Curve (Mixed Model), 25% ATH, 1mm, Ester Kim/MQP Mixed Model, qe=1000W/m^2, re-radiation off, hc/hcc=0W/m^2*K
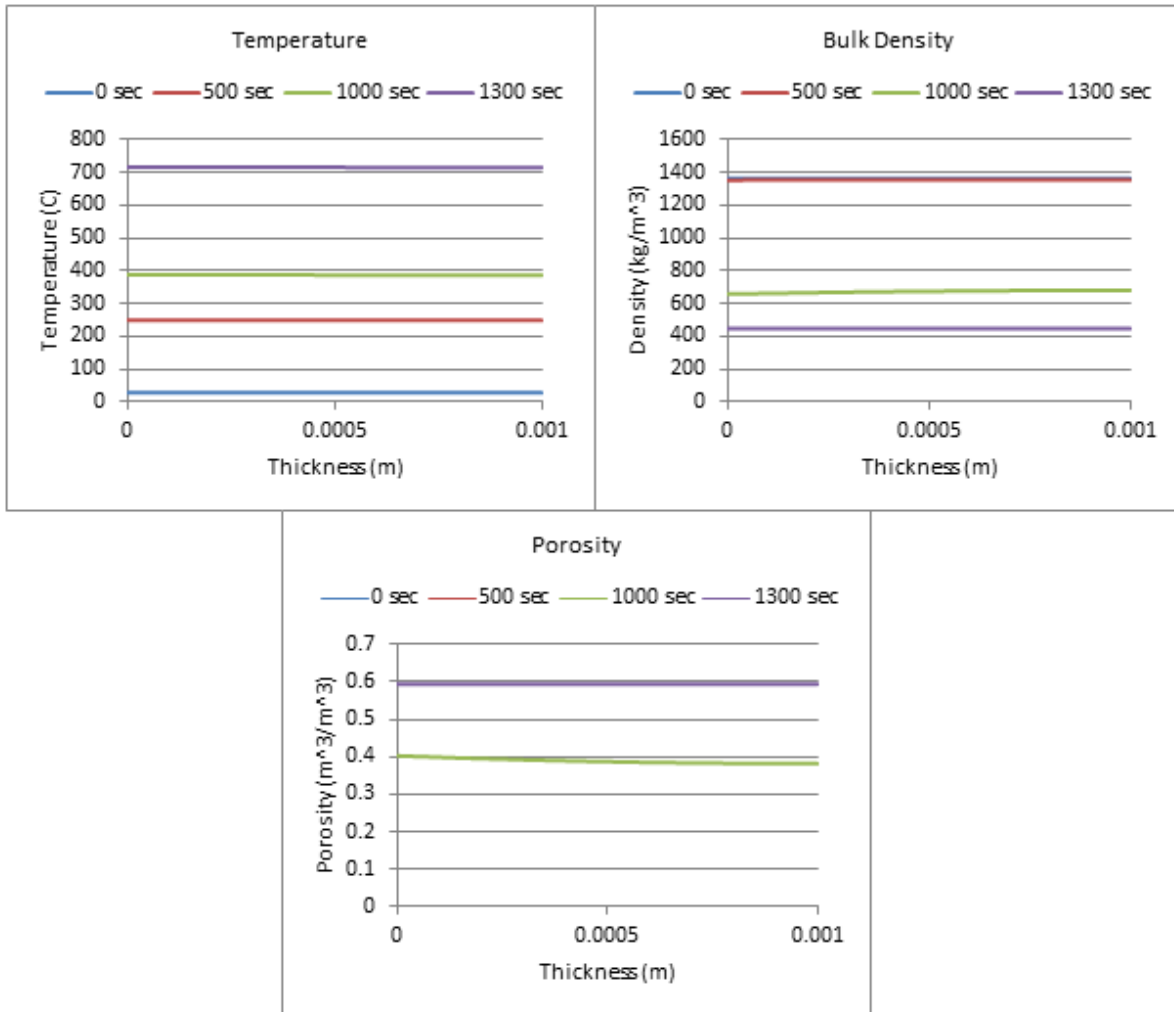
Figure 138: Temperature, Bulk Density, and Porosity Profiles (Mixed Model), 25% ATH, 1mm, Ester Kim/MQP Mixed Model, qe=1000W/m^2, re-radiation off, hc/hcc=0W/m^2*K
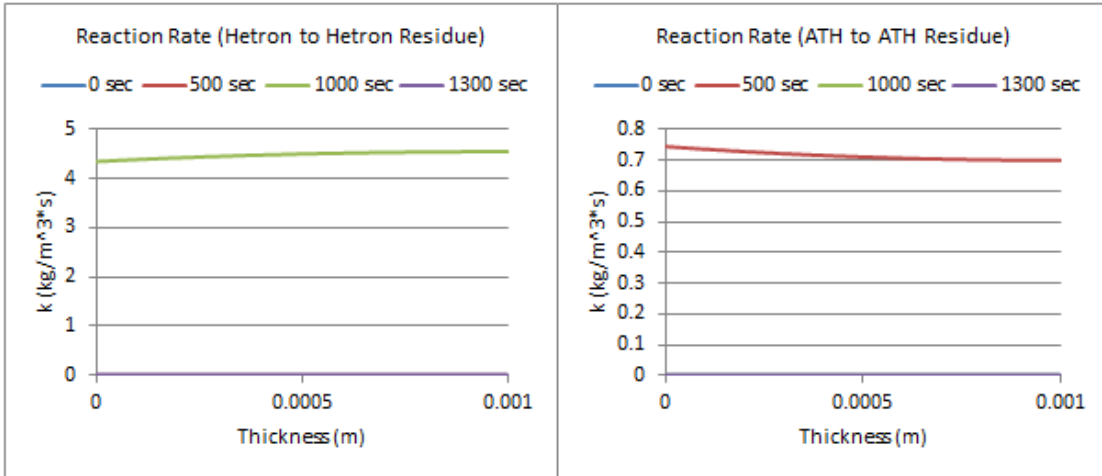
Figure 139: Reaction Rate Profiles (Mixed Model), 25% ATH, 1mm, Ester Kim/MQP Mixed Model, qe=1000W/m^2, re-radiation off, hc/hcc=0W/m^2*K
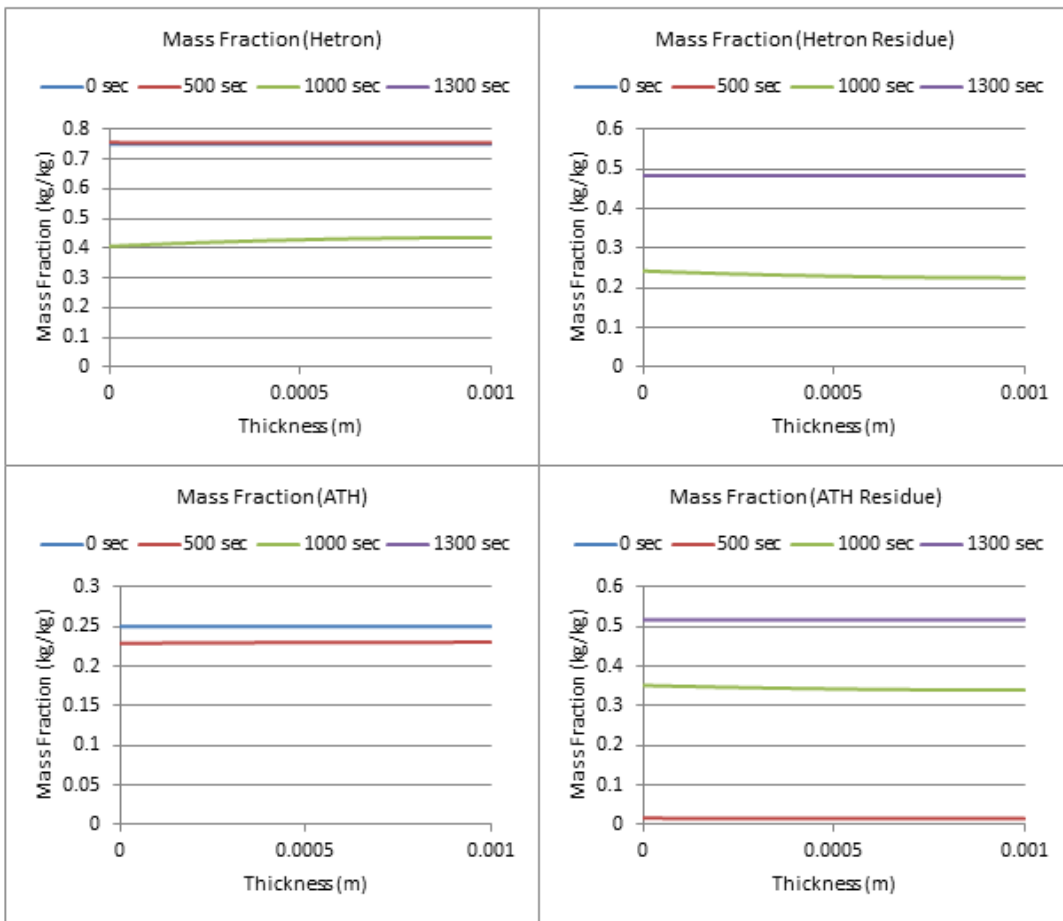
Figure 140: Mass Fraction Profiles (Mixed Model), 25% ATH, 1mm, Ester Kim/MQP Mixed Model, qe=1000W/m^2, re-radiation off, hc/hcc=0W/m^2*K

40% ATH, 1mm, Ester Kim/MQP Mixed Model, qe=1000W/m^2, re-radiation off, hc/hcc=0W/m^2*K
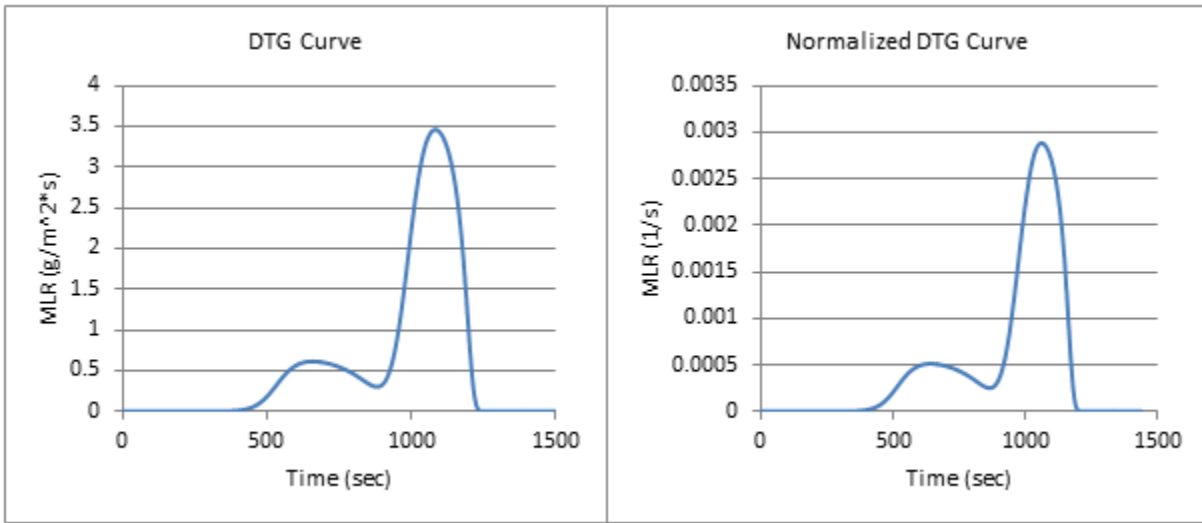
Figure 141: DTG and Normalized DTG Curve (Mixed Model), 40% ATH, 1mm, Ester Kim/MQP Mixed Model, qe=1000W/m^2, re-radiation off, hc/hcc=0W/m^2*K
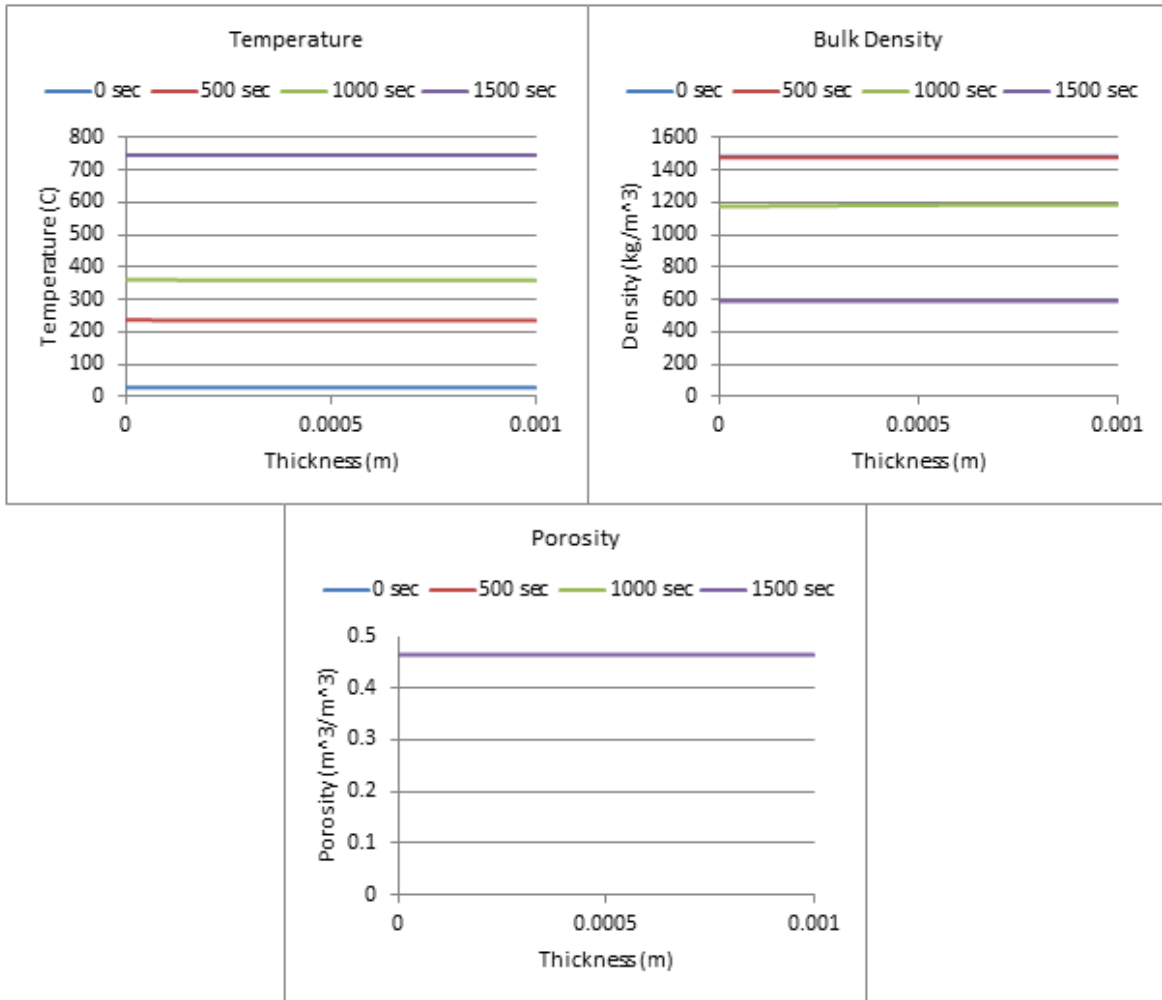
Figure 142: Temperature, Bulk Density, and Porosity Profiles (Mixed Model), 40% ATH, 1mm, Ester Kim/MQP Mixed Model, qe=1000W/m^2, re-radiation off, hc/hcc=0W/m^2*K
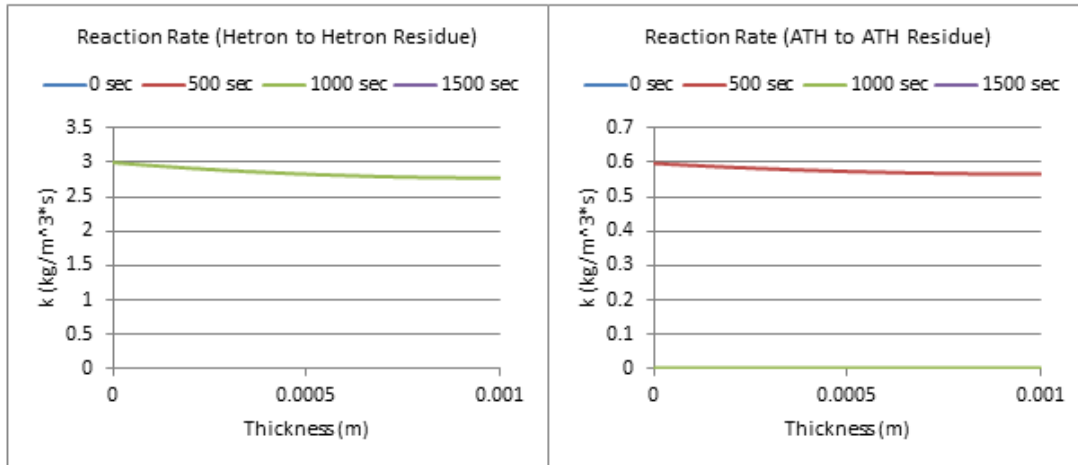
Figure 143: Reaction Rate Profiles (Mixed Model), 40% ATH, 1mm, Ester Kim/MQP Mixed Model, qe=1000W/m^2, re-radiation off, hc/hcc=0W/m^2*K
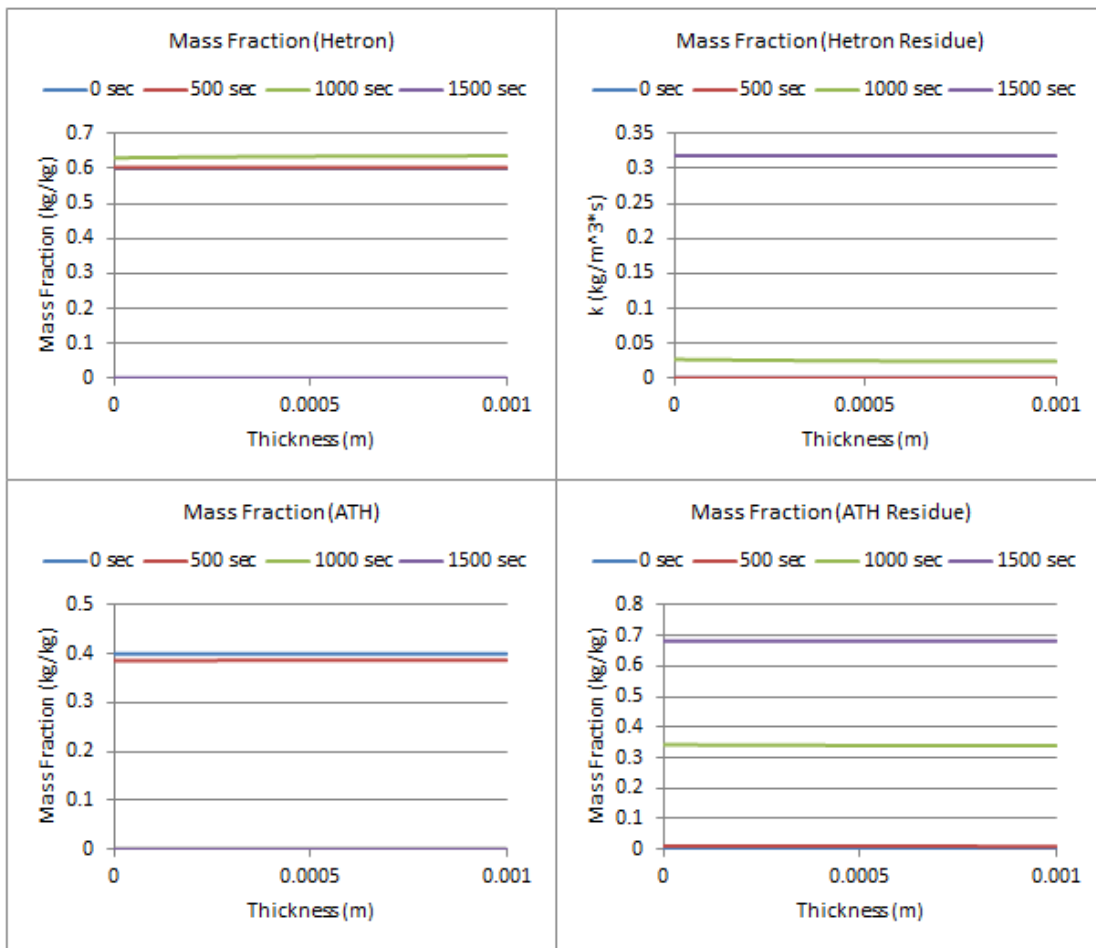
Figure 144: Mass Fraction Profiles (Mixed Model), 40% ATH, 1mm, Ester Kim/MQP Mixed Model, qe=1000W/m^2, re-radiation off, hc/hcc=0W/m^2*K

50% ATH, 1mm, Ester Kim/MQP Mixed Model, qe=1000W/m^2, re-radiation off, hc/hcc=0W/m^2*K
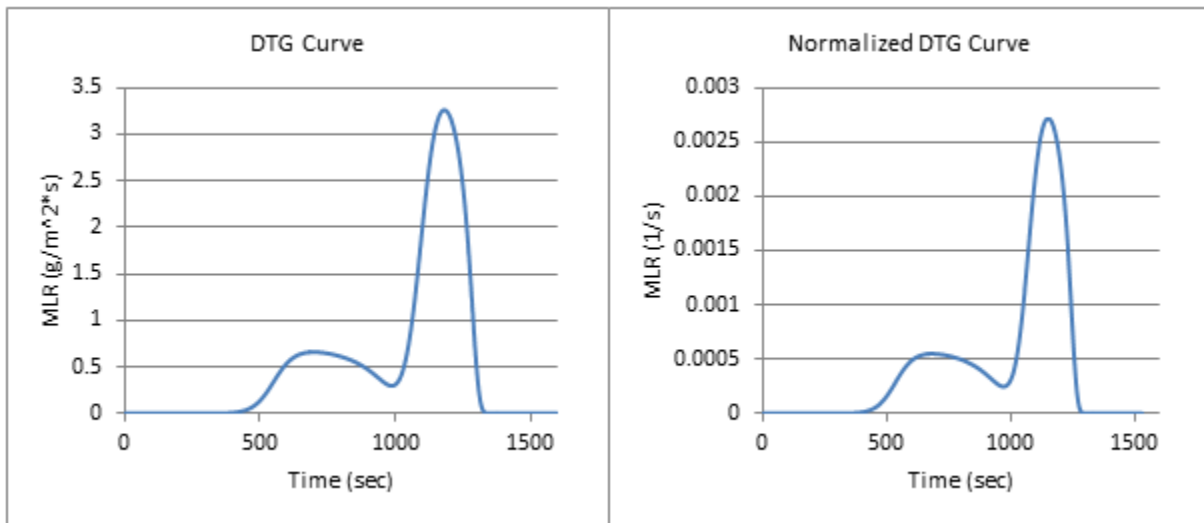
Figure 145: DTG and Normalized DTG Curves (Mixed Model), 50% ATH, 1mm, Ester Kim/MQP Mixed Model, qe=1000W/m^2, re-radiation off, hc/hcc=0W/m^2*K
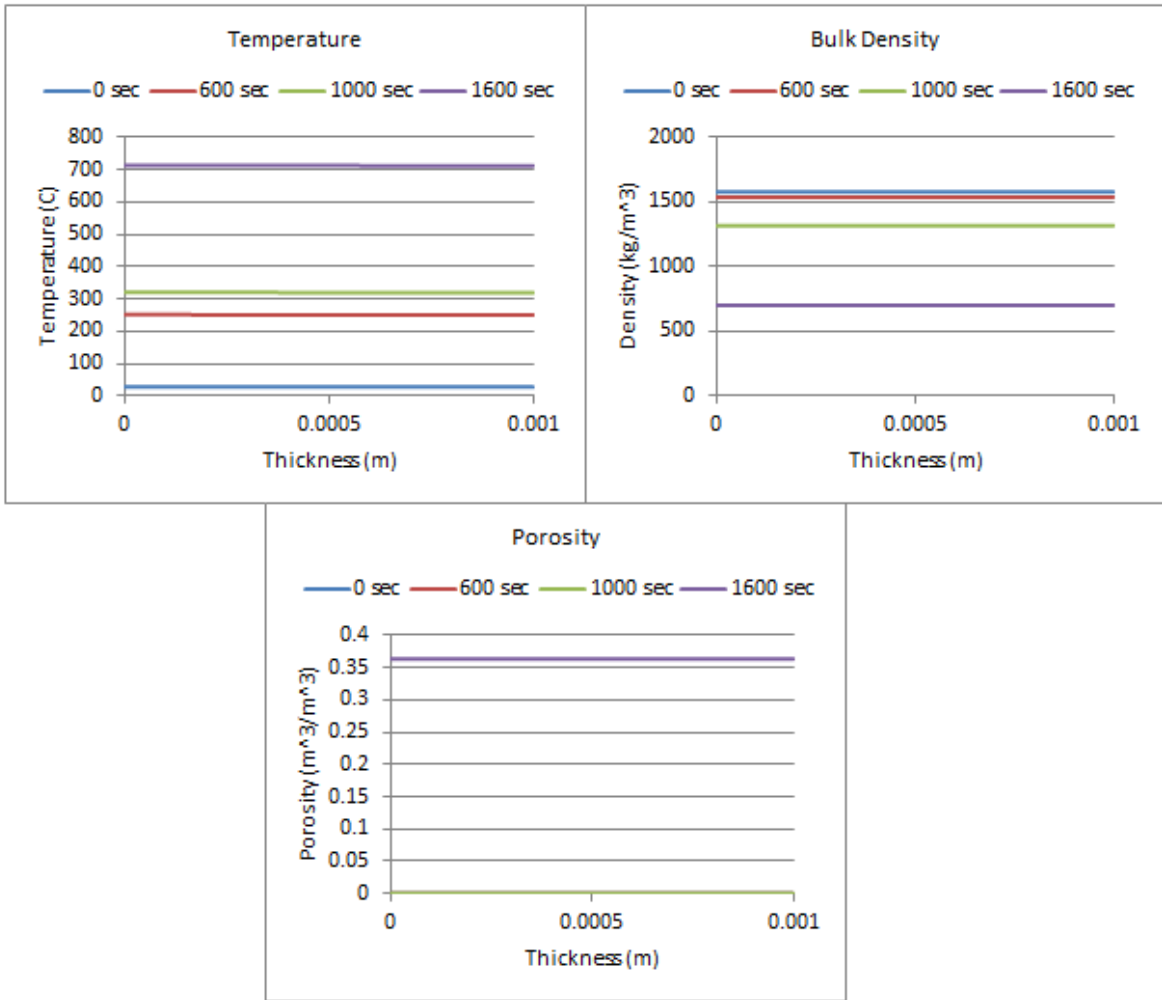
Figure 146: Temperature, Bulk Density, and Porosity Profiles (Mixed Model), 50% ATH, 1mm, Ester Kim/MQP Mixed Model, qe=1000W/m^2, re-radiation off, hc/hcc=0W/m^2*K
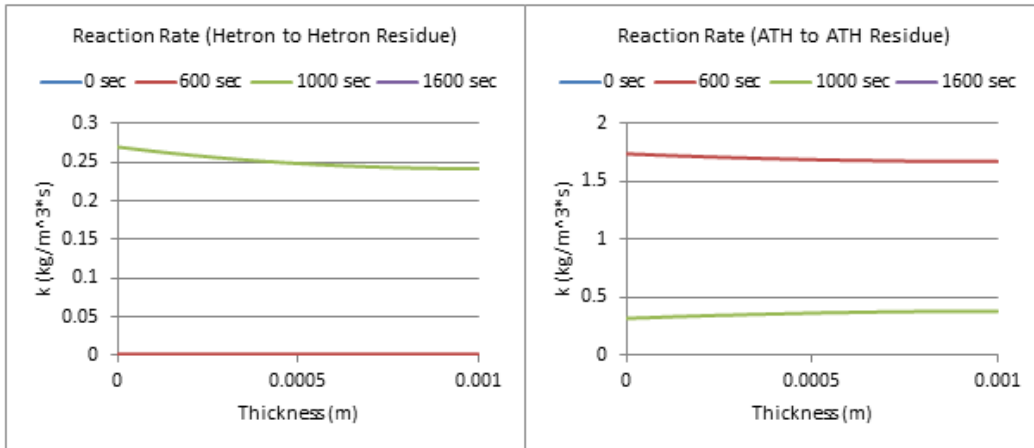
Figure 147: Reaction Rate Profiles (Mixed Model), 50% ATH, 1mm, Ester Kim/MQP Mixed Model, qe=1000W/m^2, re-radiation off, hc/hcc=0W/m^2*K
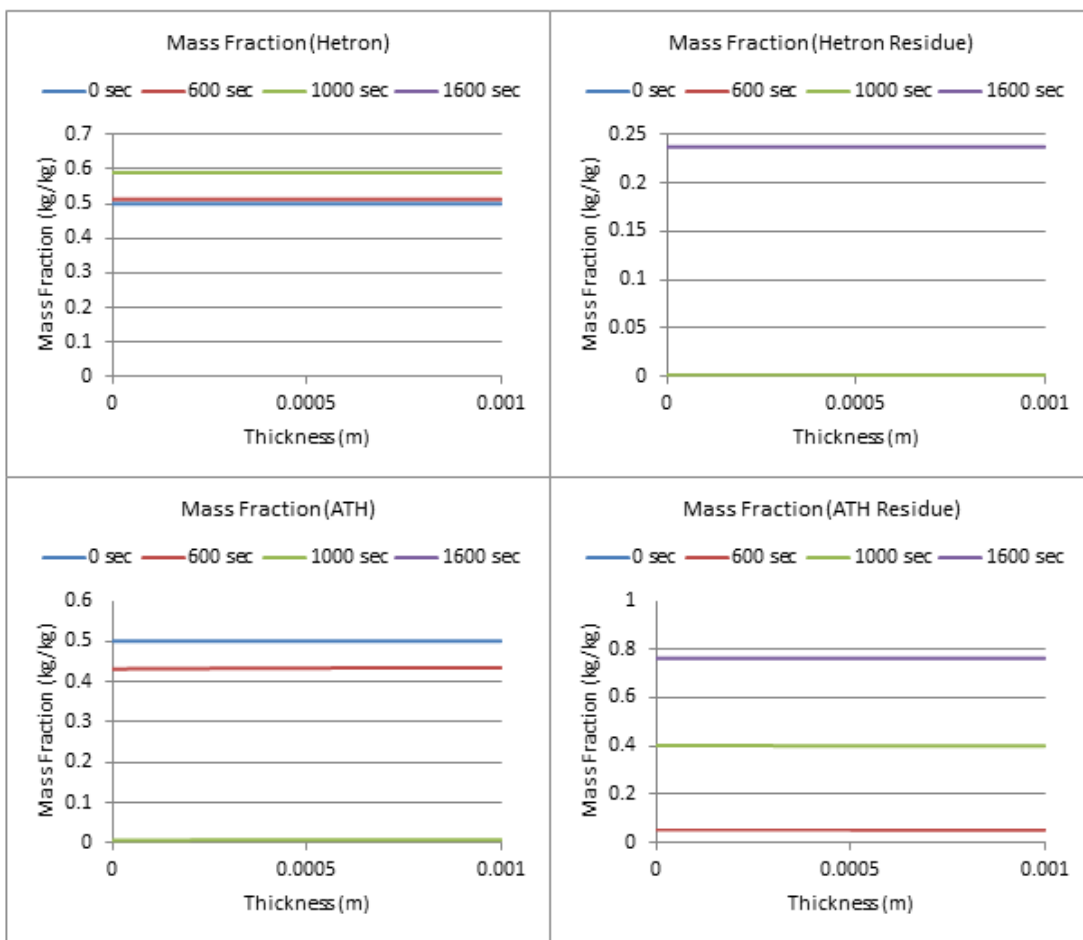
Figure 148: Mass Fraction Profiles (Mixed Model), 50% ATH, 1mm, Ester Kim/MQP Mixed Model, qe=1000W/m^2, re-radiation off, hc/hcc=0W/m^2*K

57% ATH, 1mm, Ester Kim/MQP Mixed Model, qe=1000W/m^2, re-radiation off, hc/hcc=0W/m^2*K
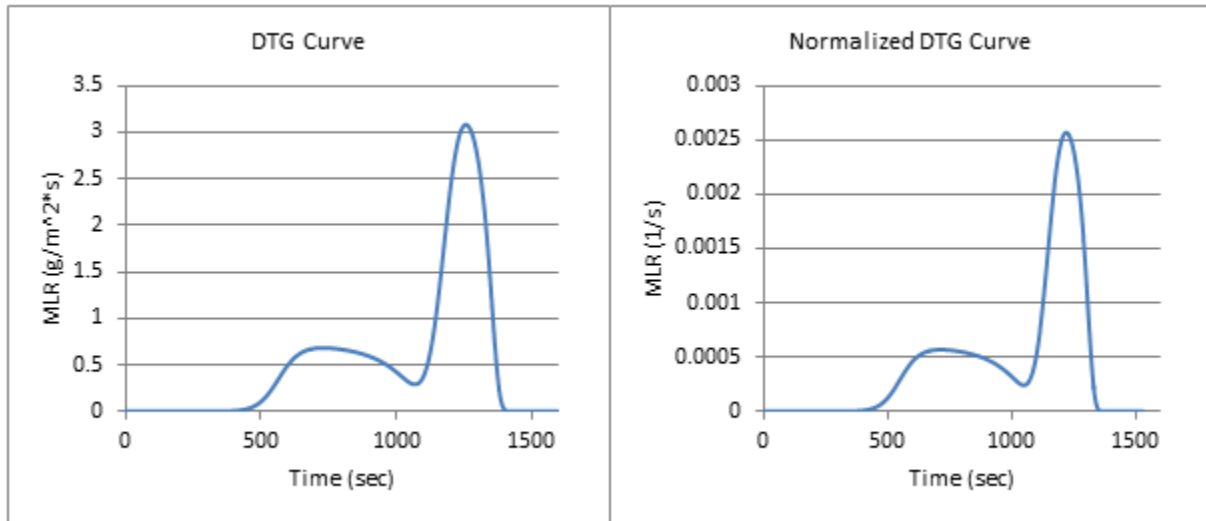
Figure 149: DTG and Normalized DTG Curves (Mixed Model), 57% ATH, 1mm, Ester Kim/MQP Mixed Model, qe=1000W/m^2, re-radiation off, hc/hcc=0W/m^2*K
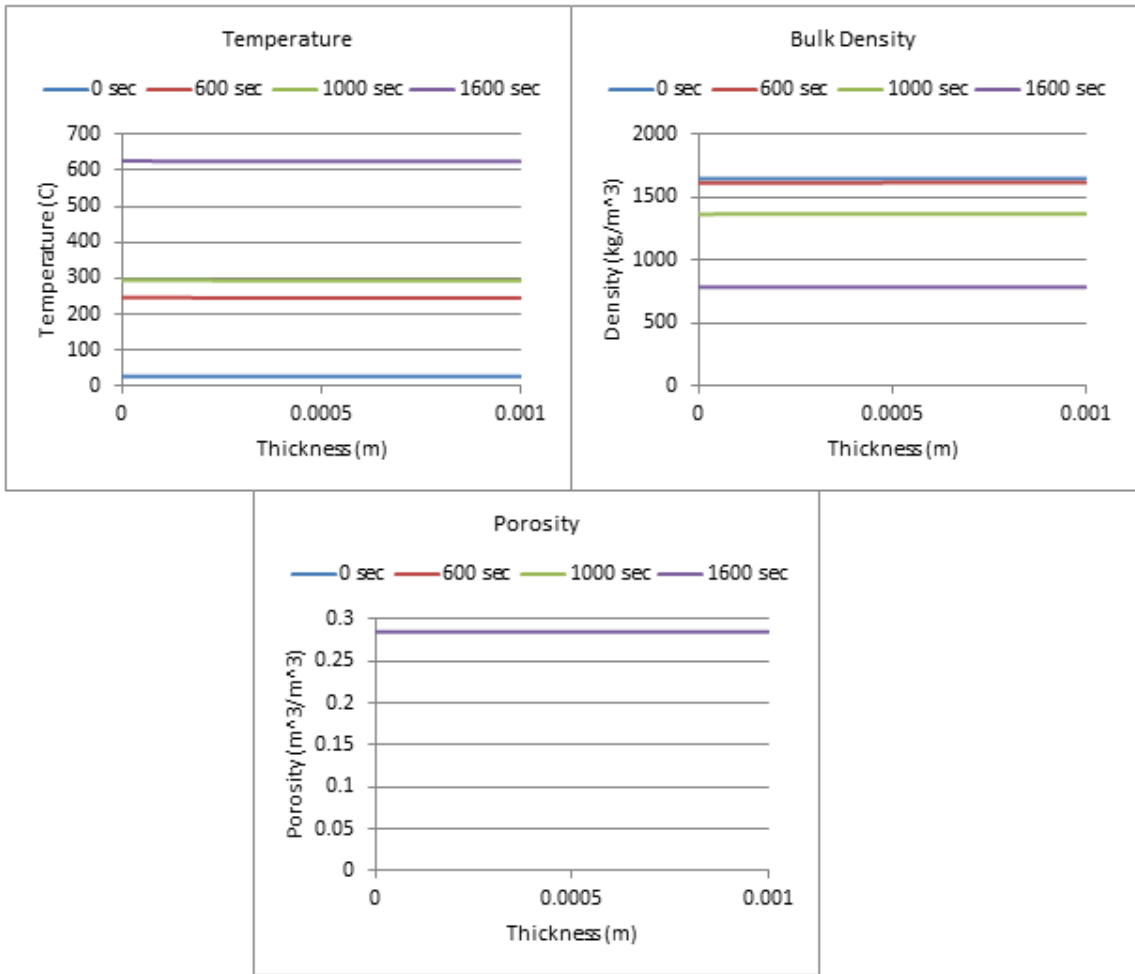
Figure 150: Temperature, Bulk Density, and Porosity Profiles (Mixed Model), 57% ATH, 1mm, Ester Kim/MQP Mixed Model, qe=1000W/m^2, re-radiation off, hc/hcc=0W/m^2*K
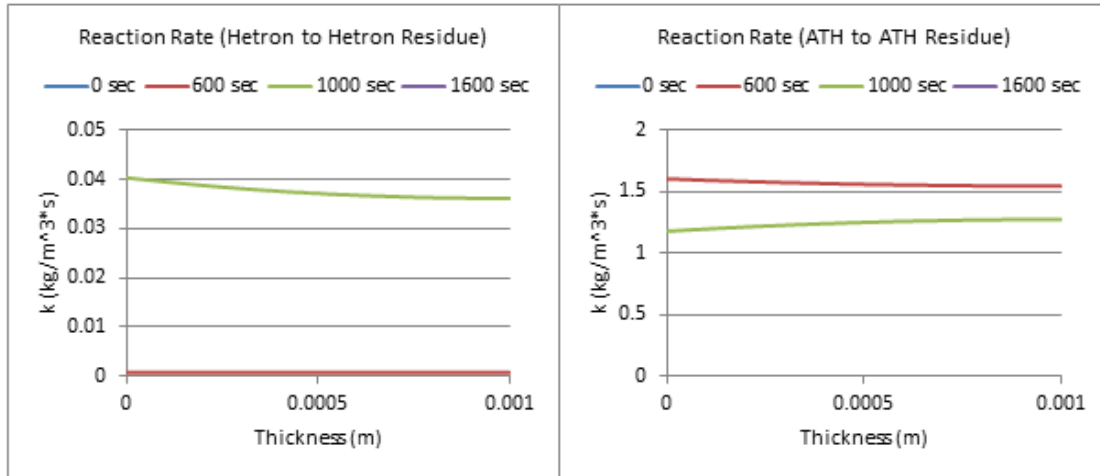
Figure 151: Reaction Rate Profiles (Mixed Model), 57% ATH, 1mm, Ester Kim/MQP Mixed Model, qe=1000W/m^2, re-radiation off, hc/hcc=0W/m^2*K
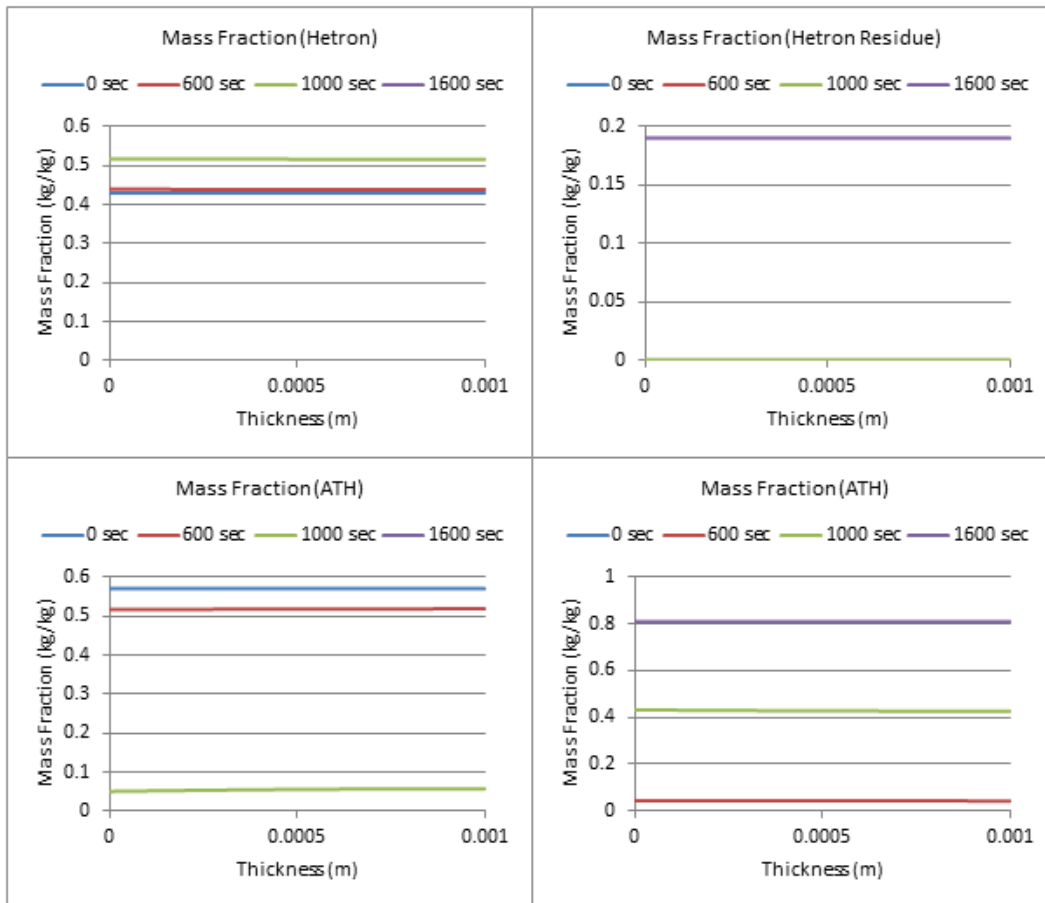
Figure 152: Mass Fraction Profiles (Mixed Model), 57% ATH, 1mm, Ester Kim/MQP Mixed Model, qe=1000W/m^2, re-radiation off, hc/hcc=0W/m^2*K

Appendix E.9: Heat Flux Calculations and Profiles

Heat Flux values were calculated using typical conditions found in the TGA, and a range of 100-800 W/m^2 was calculated. A sample calculation shown below is how these values were determined. Values were taken from previous work and from current data.

HoD= 1,000 J/g (ATH) -> 40%, HoD= 172 J/g (Hetron) -> 60%

HoD= 1,000 J/g (0.4) + 172 J/g (0.6) = 500 J/g (Used as average HoD)

Average MLR=0.2 1/s (Taken from TGA data)

1mg (average sample size) * 0.2 1/s = 2*10^-4 g/s

Area=2*pi*r^2= 1.6*10^-6 m^2 (Using measured drop size for 1mg sample)

(500 J/g)*(0.001 g)*(1/400 s) = 0.00125 W (400 s was length of Gpyro simulation for decomposition)

0.00125 W/(1.6*10^-6 m^2) = 800 W/m^2

The same process as seen above was used for different mixtures, different time frames, and different sizes to best approximate the range of data used. Profiles were created at each level of heat flux to help better narrow down the range of viable options. These profiles can be seen below.

5% ATH, qe=100 W/m^2
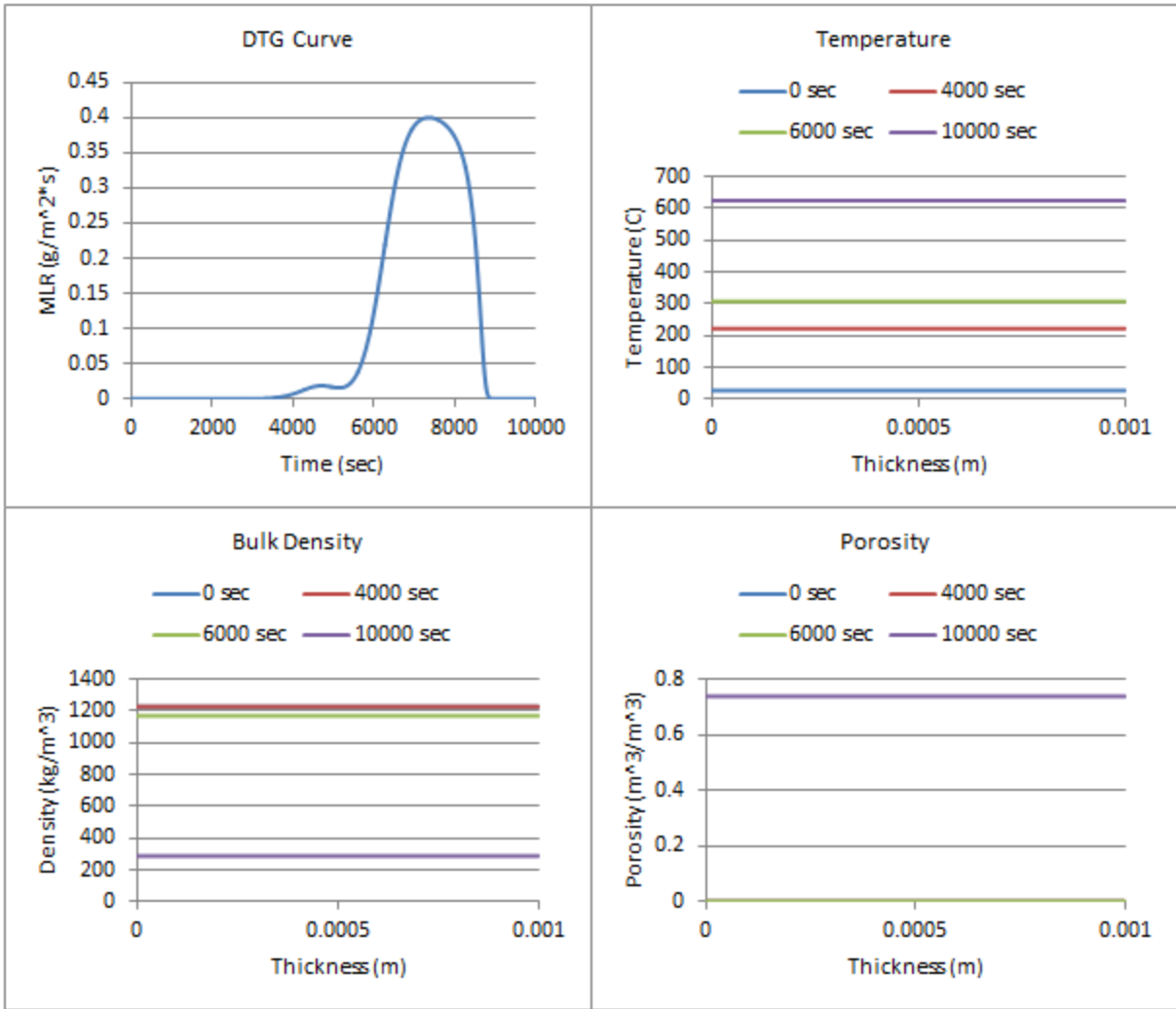
Figure 153: Profiles (100 W/m^2, 5% ATH)
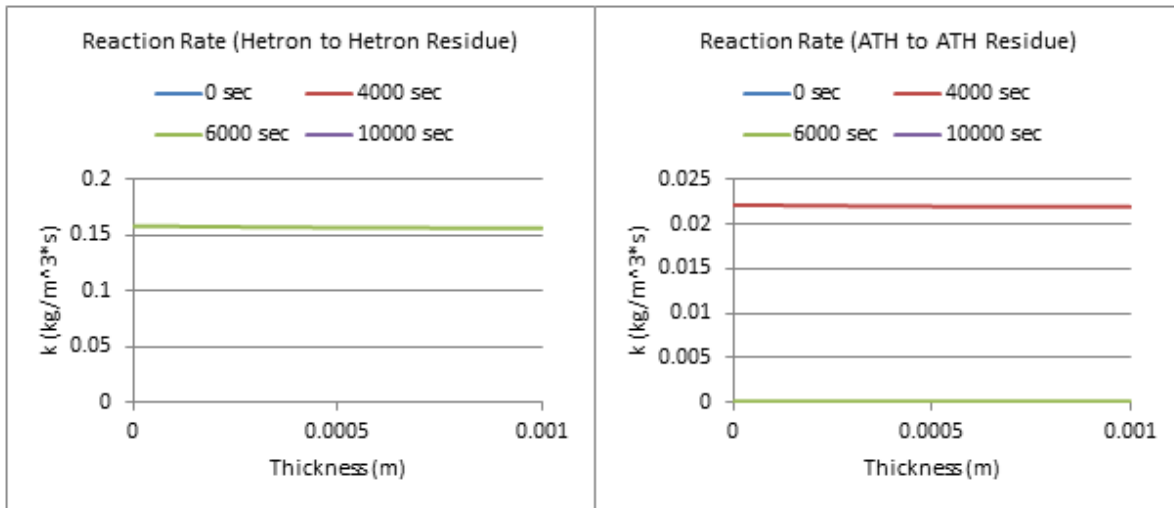
Figure 154: Reaction Rates (100 W/m^2, 5% ATH)
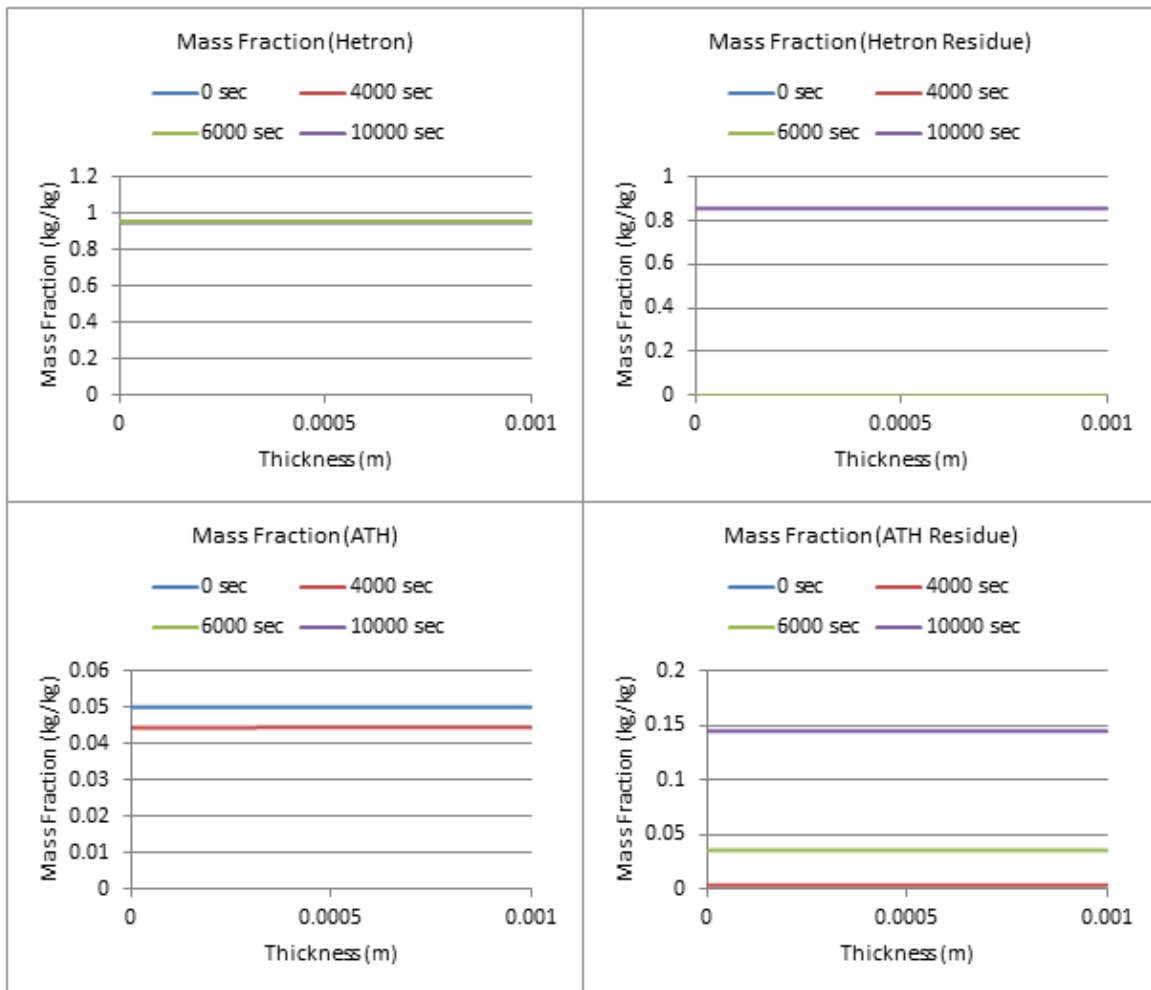
Figure 155: Mass Fractions (100 W/m^2, 5% ATH)

5% ATH, qe=200 W/m^2
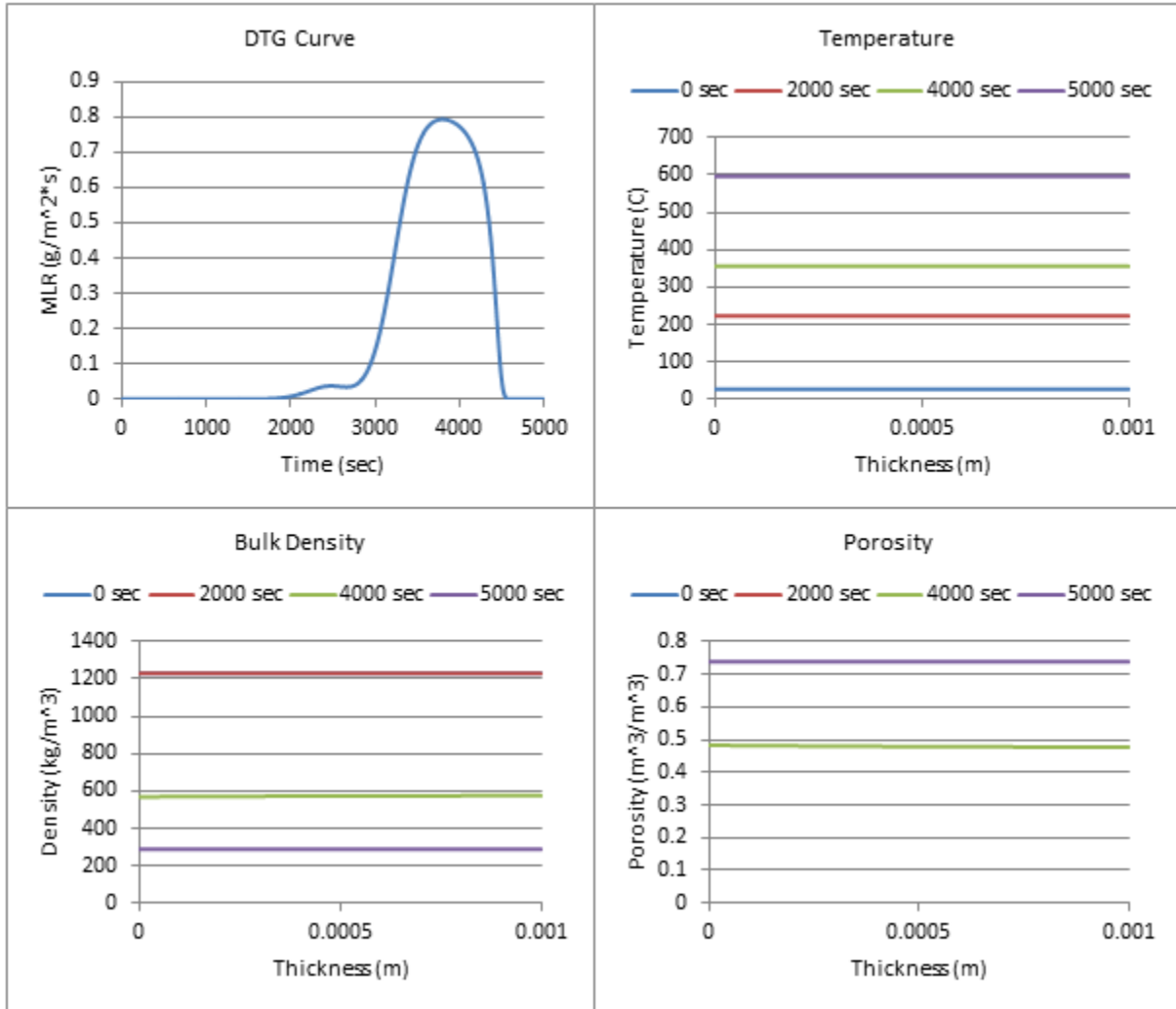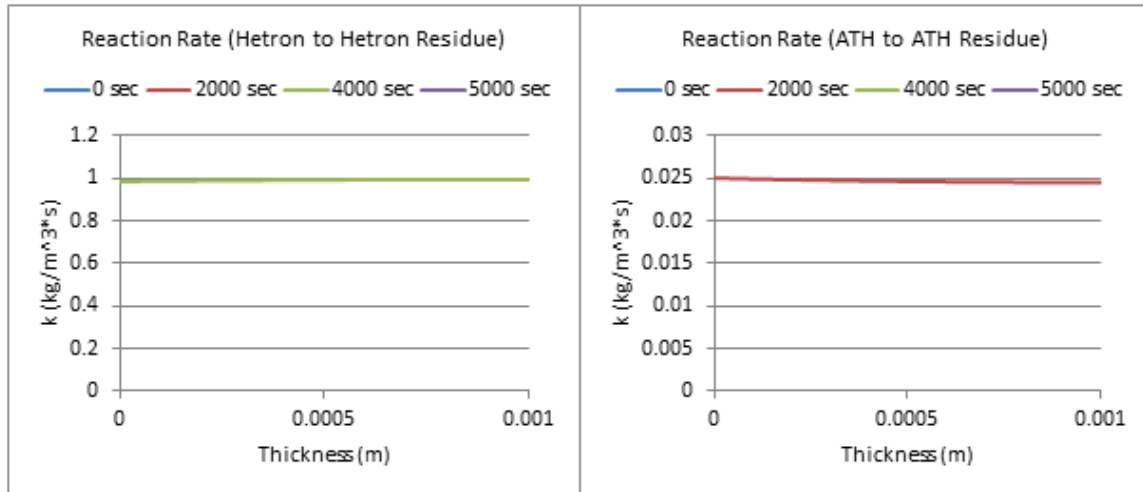
Figure 157: Reaction Rate Profiles (200 W/m^2, 5% ATH)
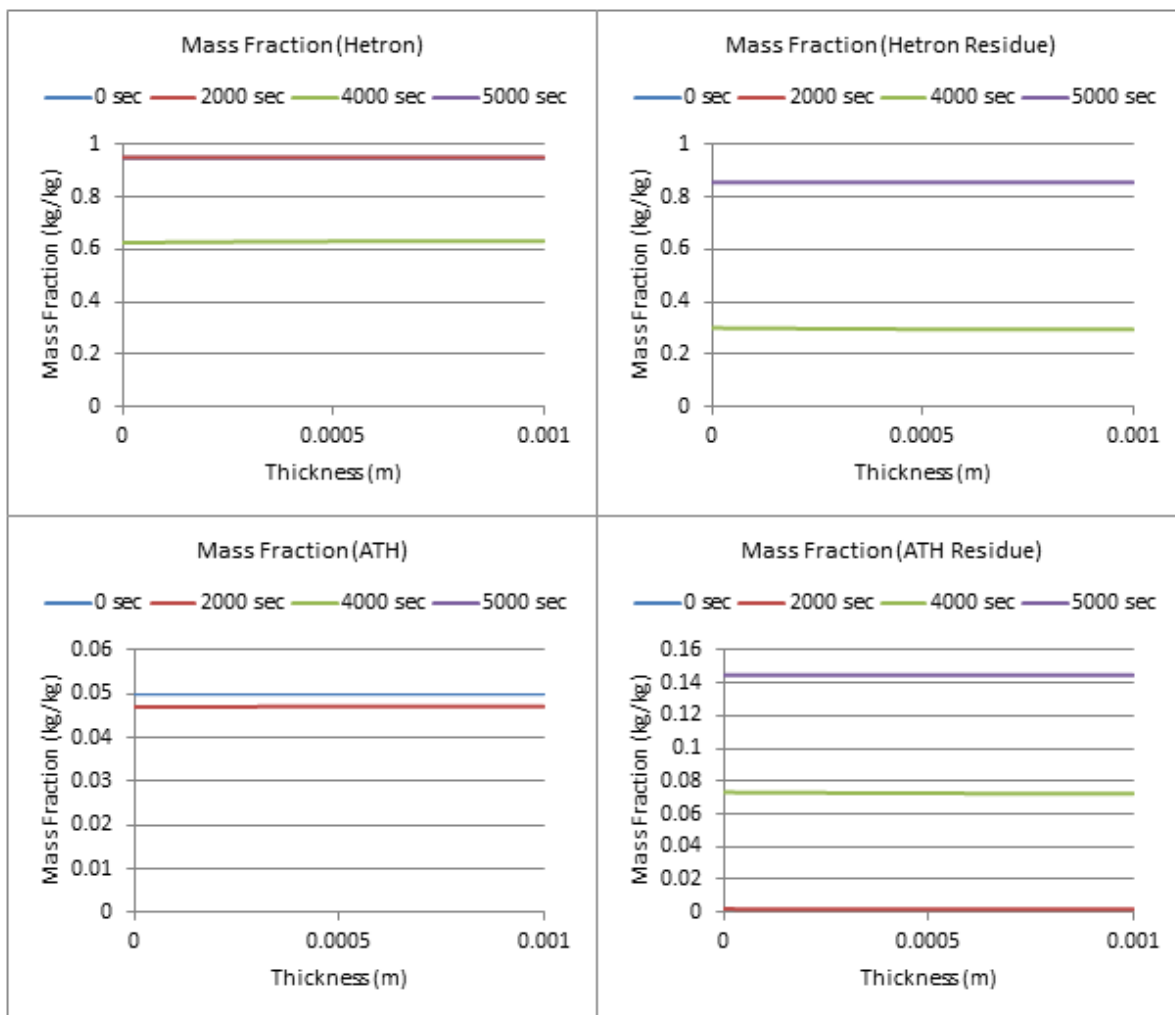
Figure 158: Mass Fraction Profiles (200 W/m^2, 5% ATH)

5% ATH, qe= 300 W/m^2
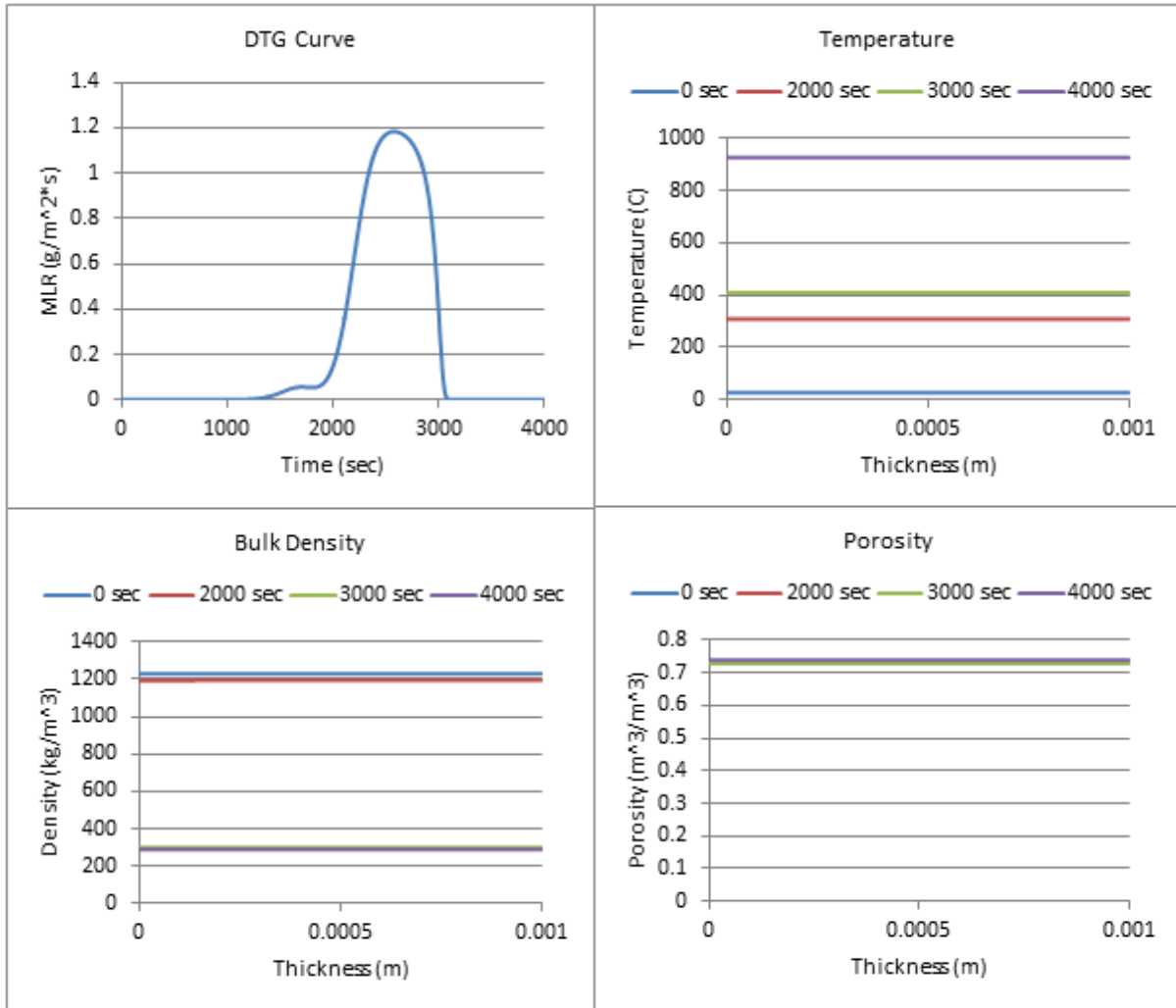
Figure 159: Profiles (300 W/m^2, 5% ATH)
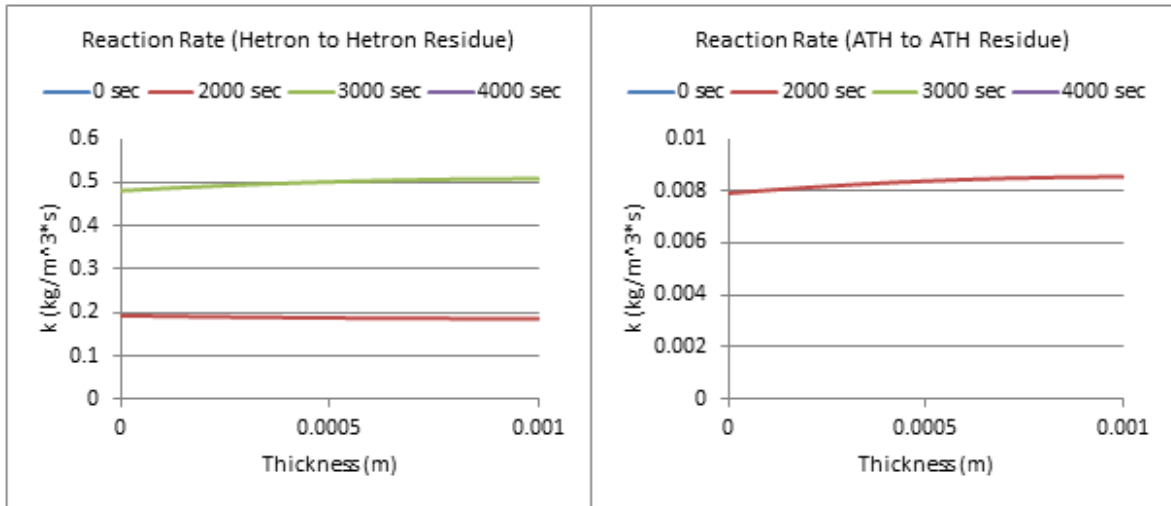
Figure 160: Reaction Rate (300 W/m^2, 5% ATH)
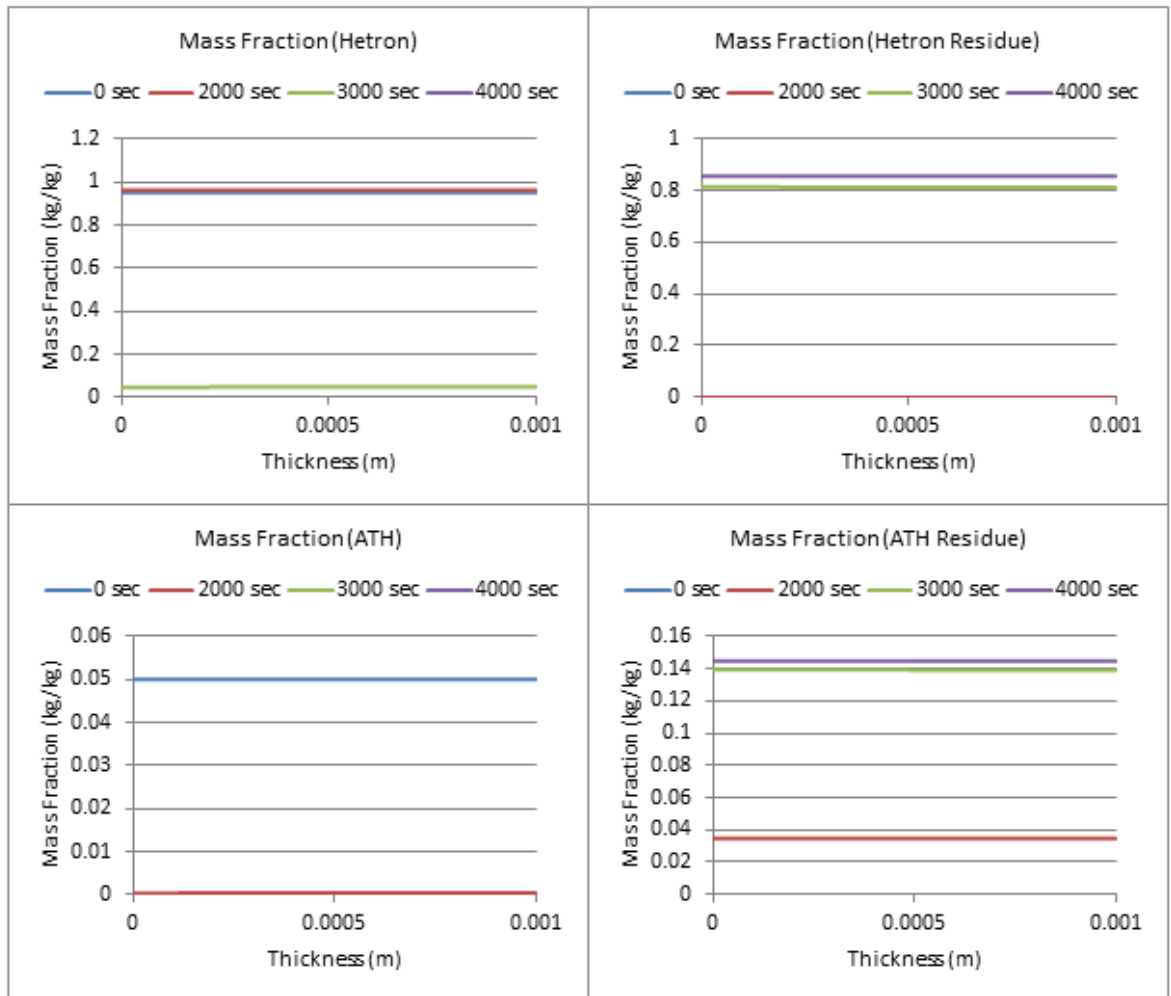
Figure 161: Mass Fraction Profiles (300 W/m^2, 5% ATH)

5% ATH, qe=400 W/m^2
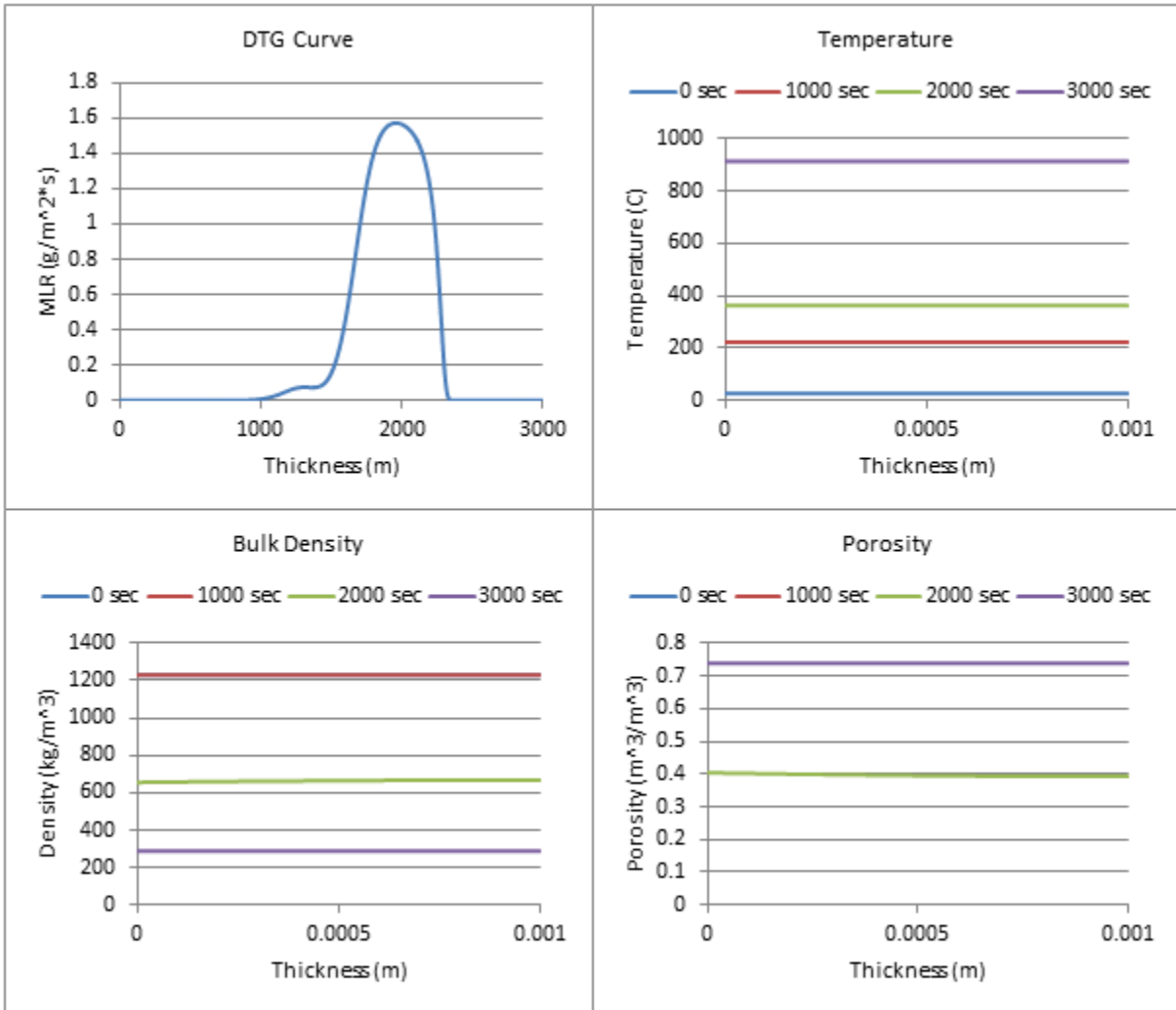
Figure 162: Profiles (400 W/m^2, 5% ATH)
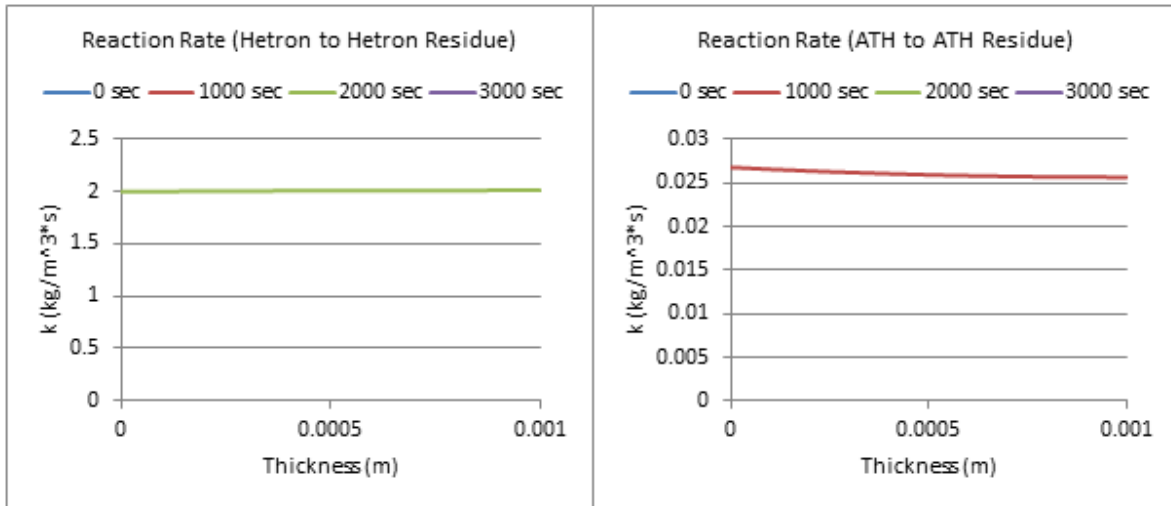
Figure 163: Reaction Rate Profiles (400 W/m^2, 5% ATH)
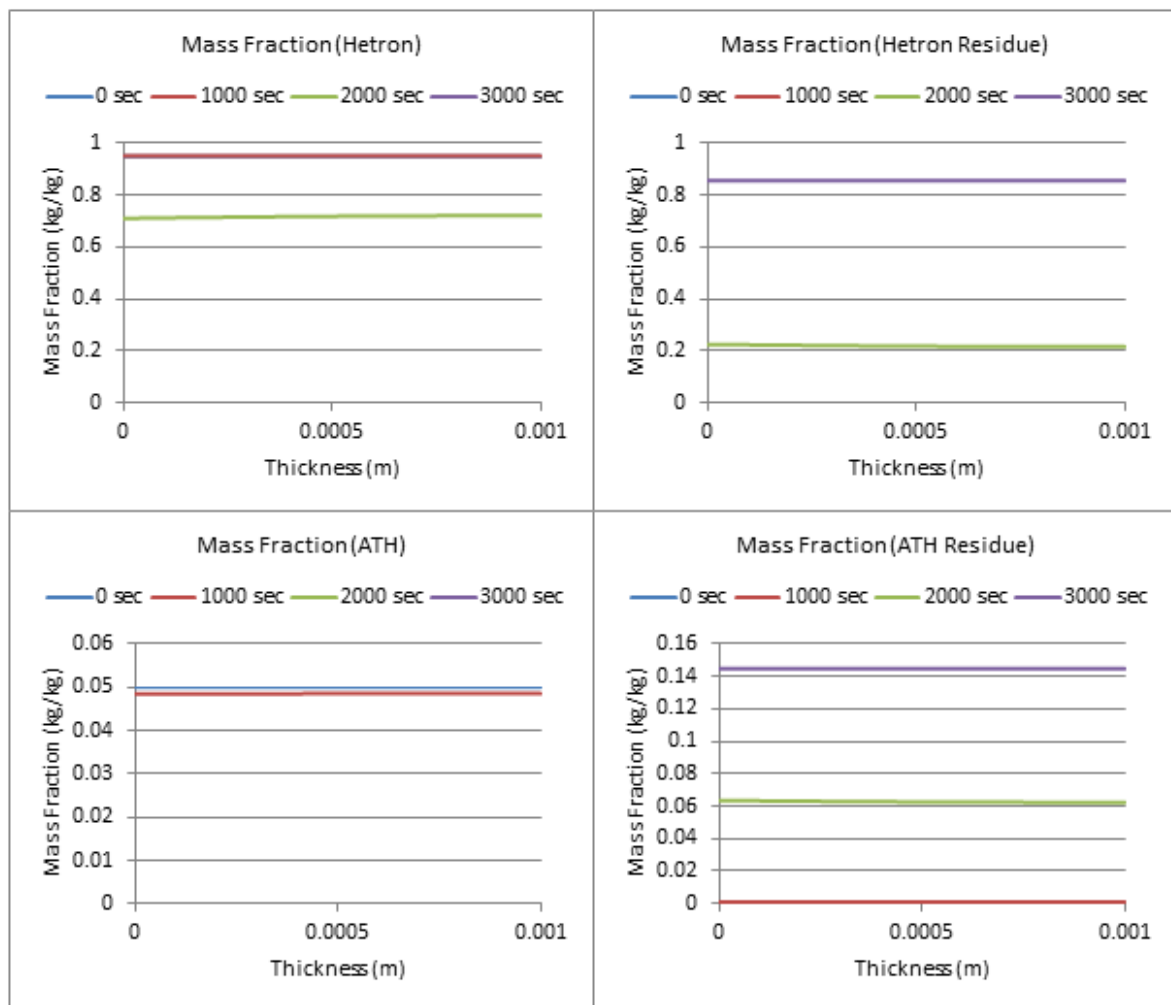
Figure 164: Mass Fraction Profiles (400 W/m^2, 5% ATH)

5% ATH, qe=500 W/m^2
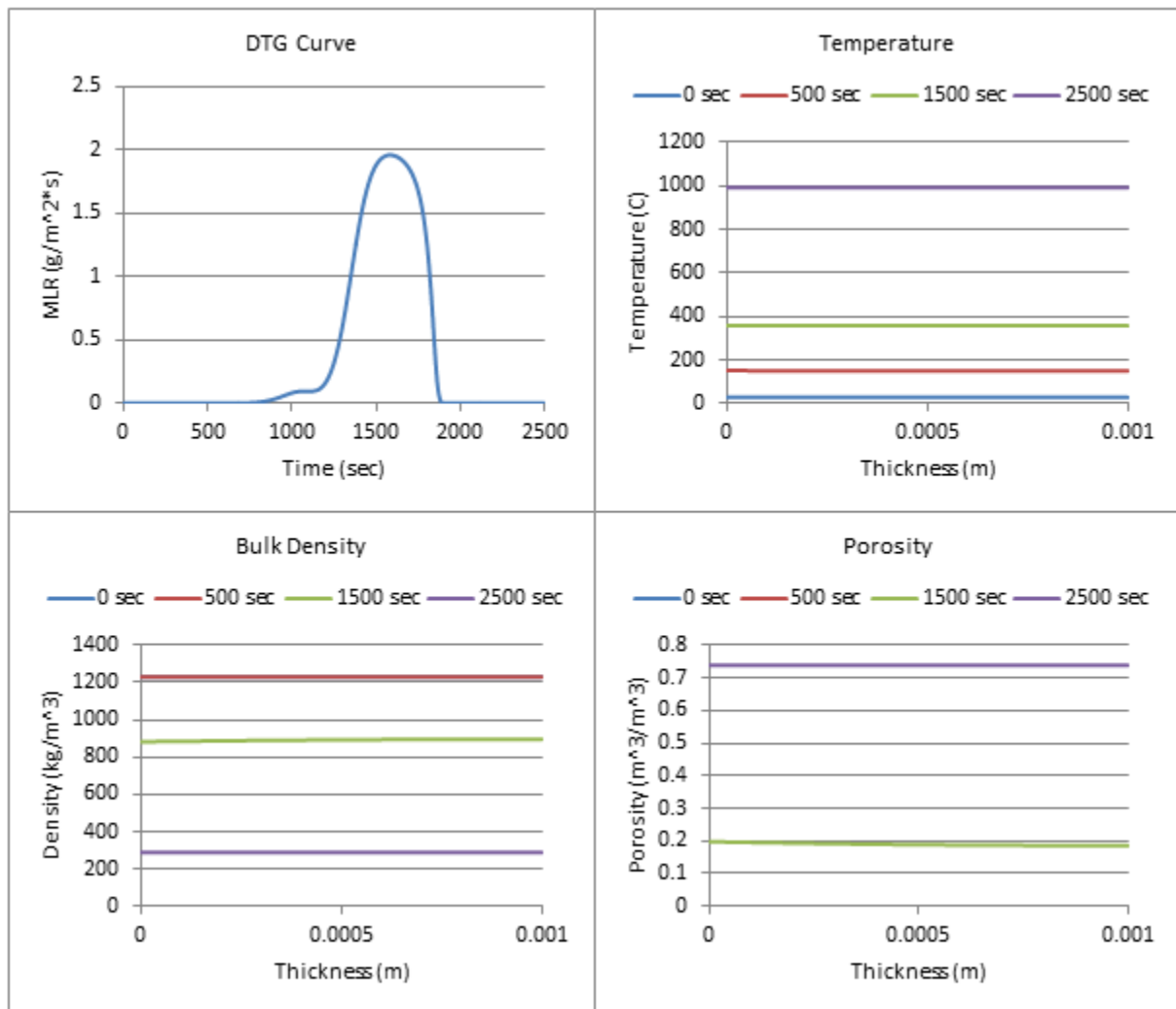
Figure 165: Profiles (500 W/m^2, 5% ATH)
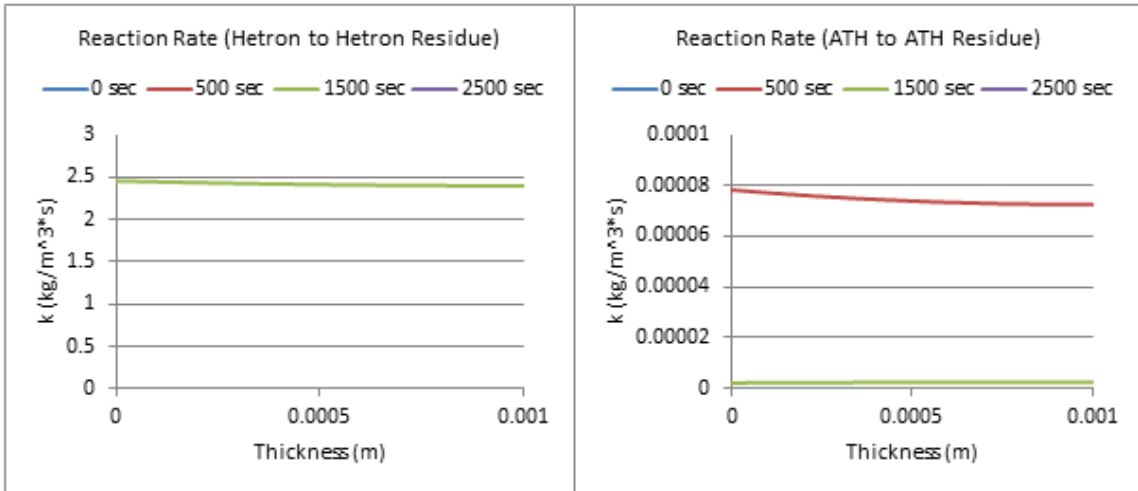
Figure 166: Reaction Rate Profiles (500 W/m^2, 5% ATH)
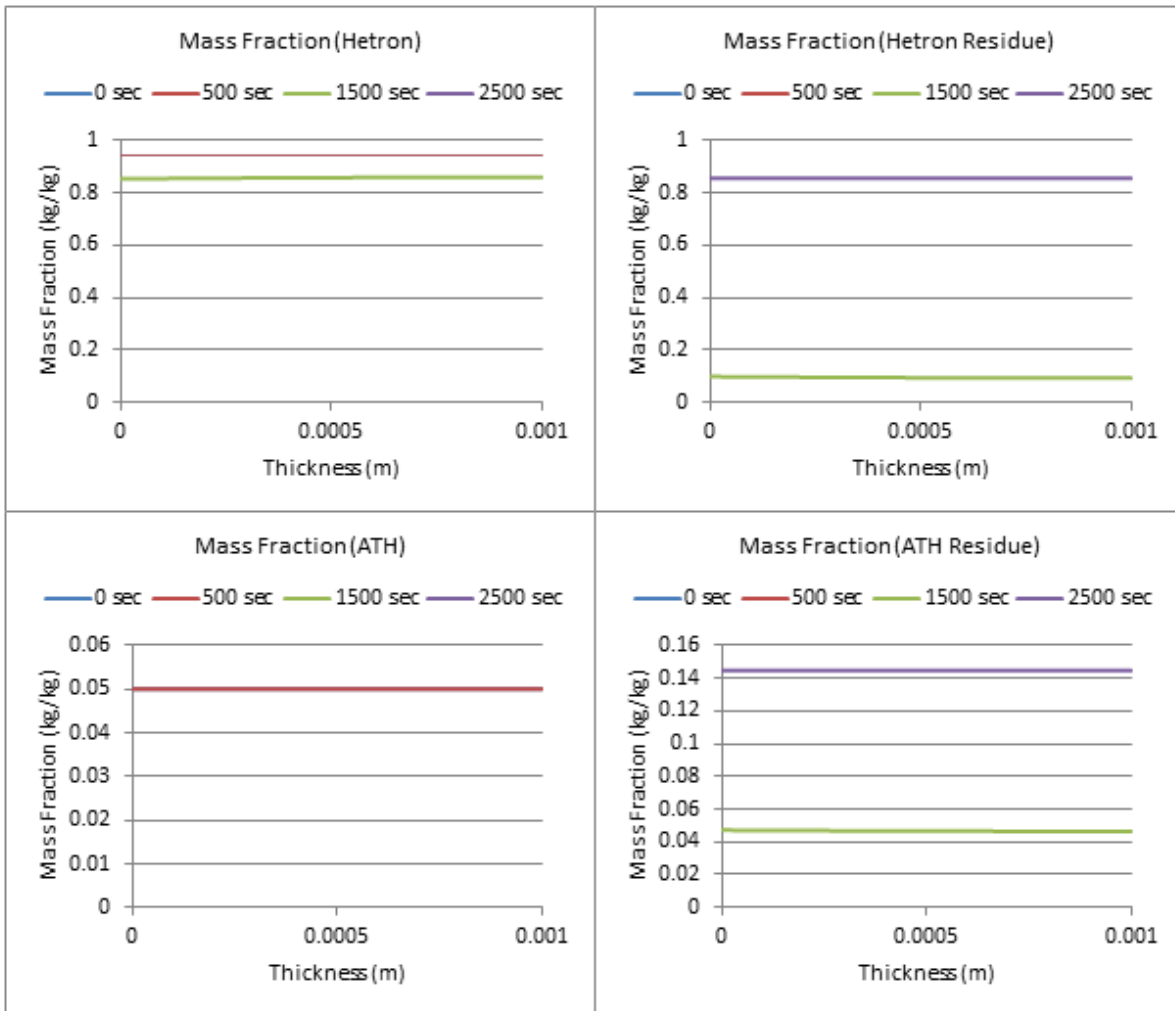
Figure 167: Mass Fraction Profiles (500 W/m^2, 5% ATH)

5% ATH, qe=600 W/m^2
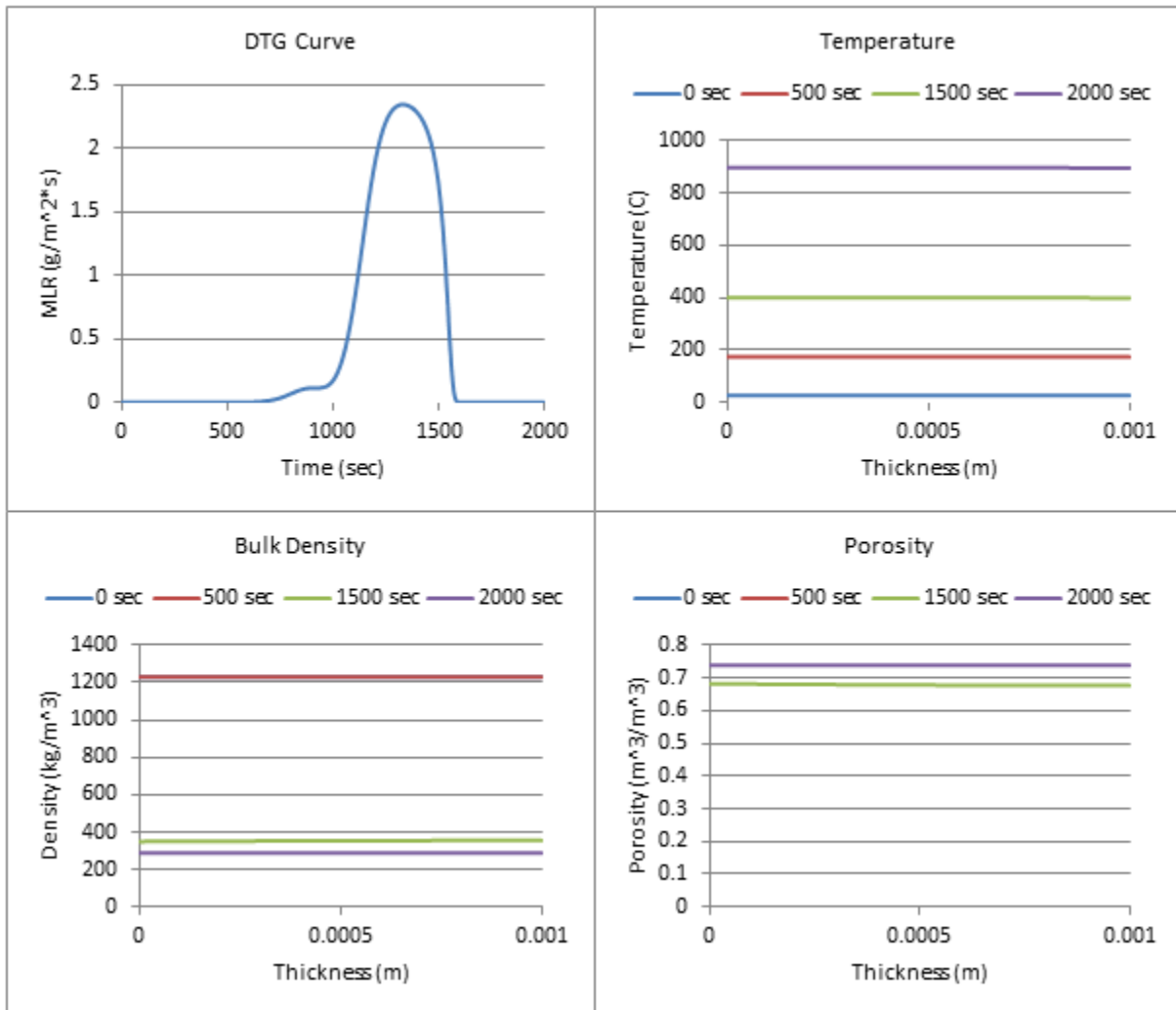
Figure 168: Profiles (600 W/m^2, 5% ATH)
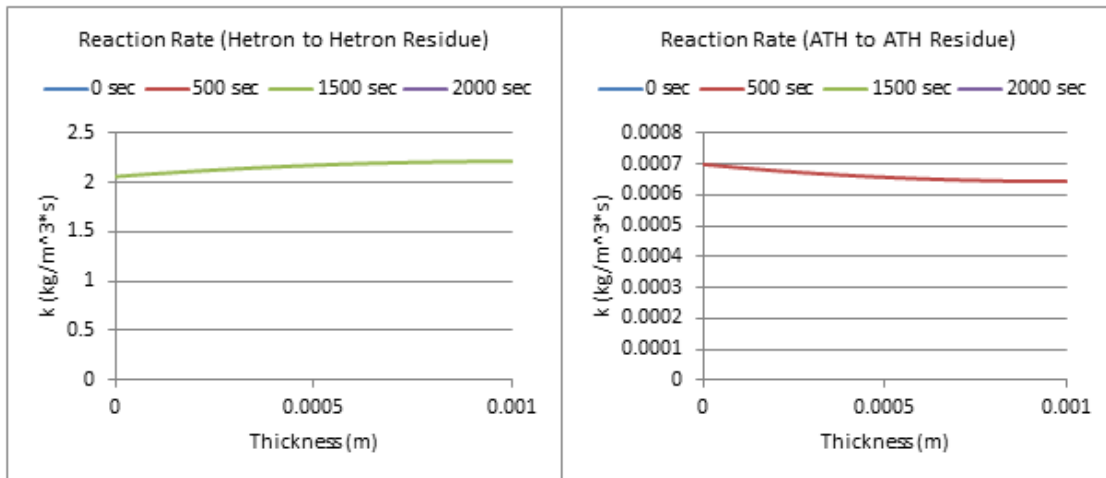
Figure 169: Reaction Rate Profiles (600 W/m^2, 5% ATH)
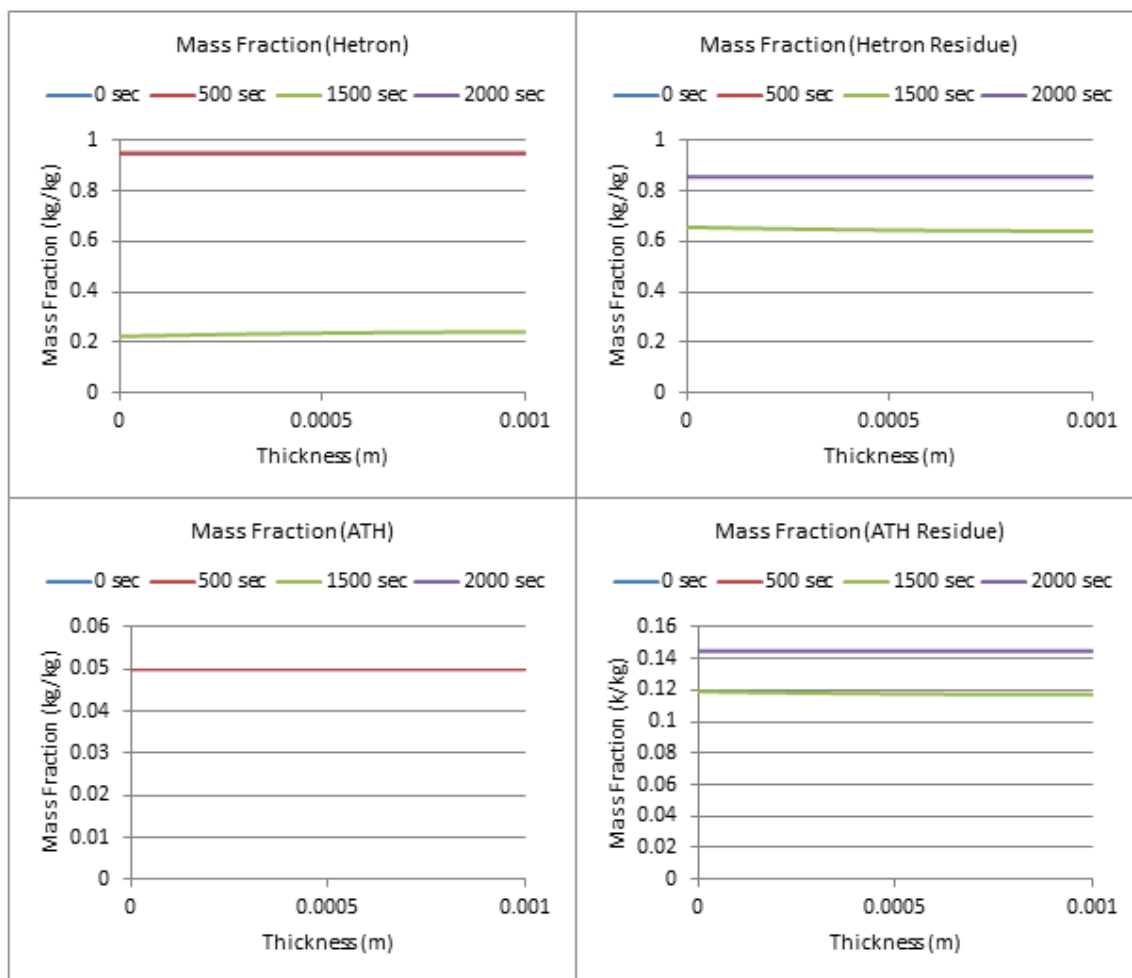
Figure 170: Mass Fraction Profiles (600 W/m^2, 5% ATH)

5% ATH, qe= 700 W/m^2
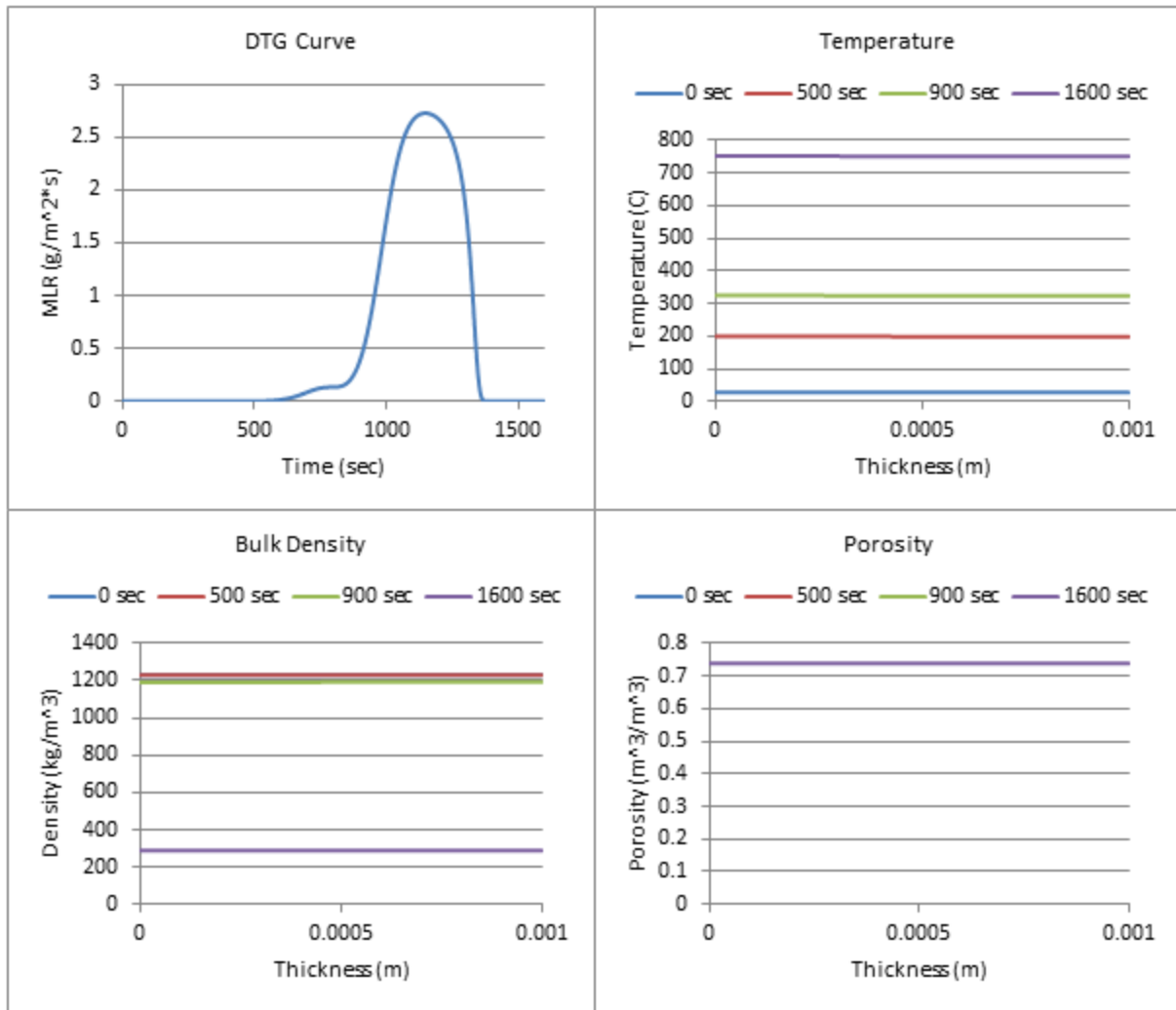
Figure 171: Profiles (700 W/m^2, 5% ATH)
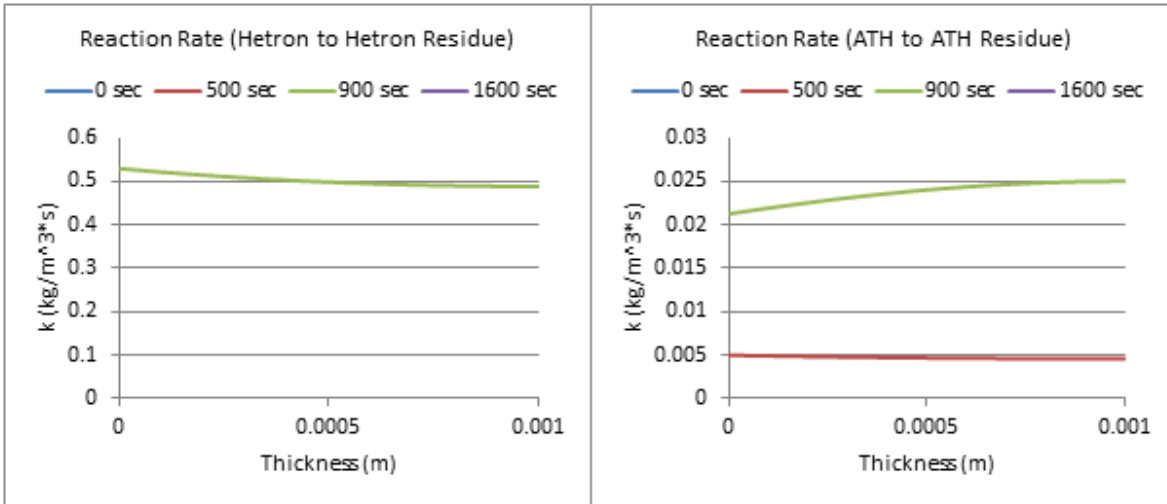
Figure 172: Reaction Rate Profiles (700 W/m^2, 5% ATH)
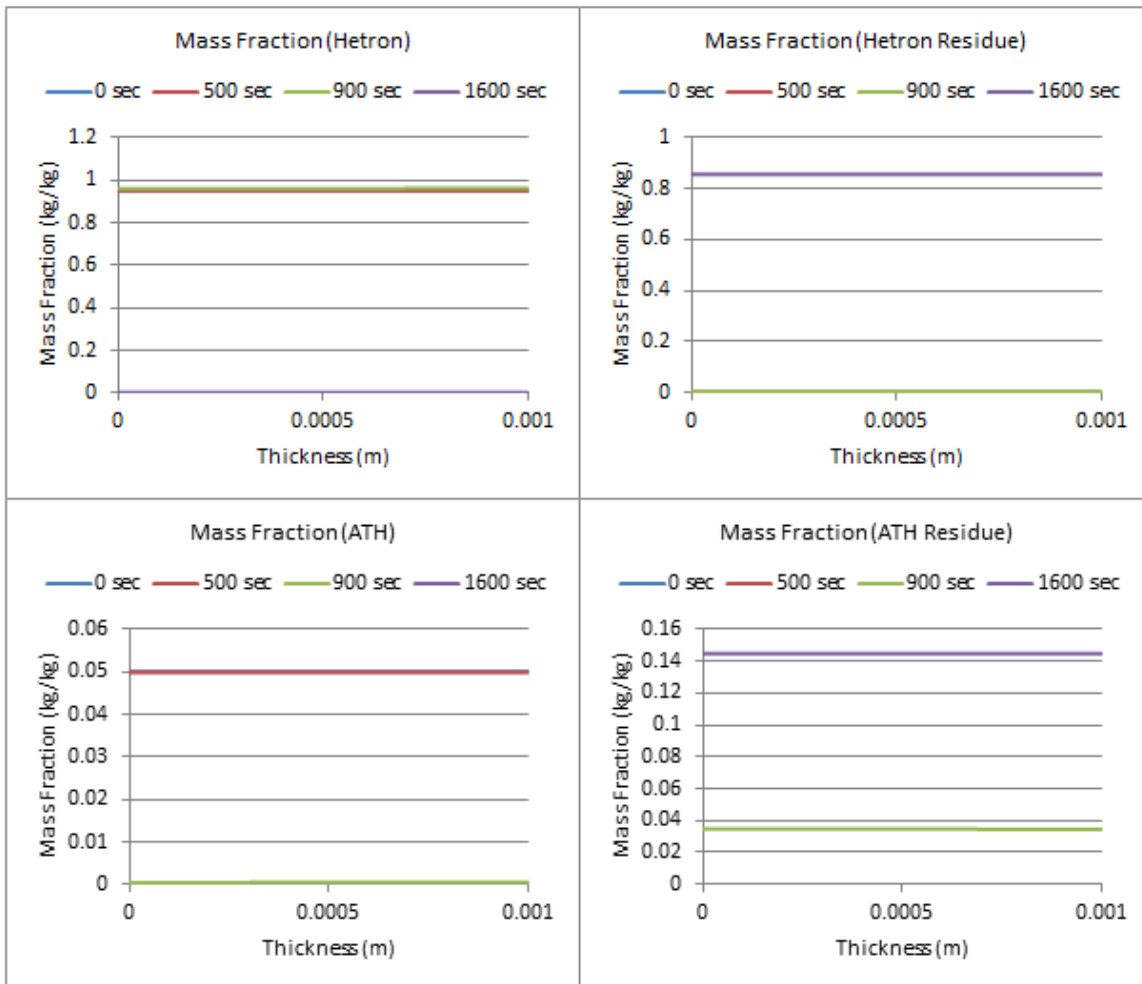
Figure 173: Mass Fraction Profiles (700 W/m^2, 5% ATH)

5% ATH, qe= 800 W/m^2
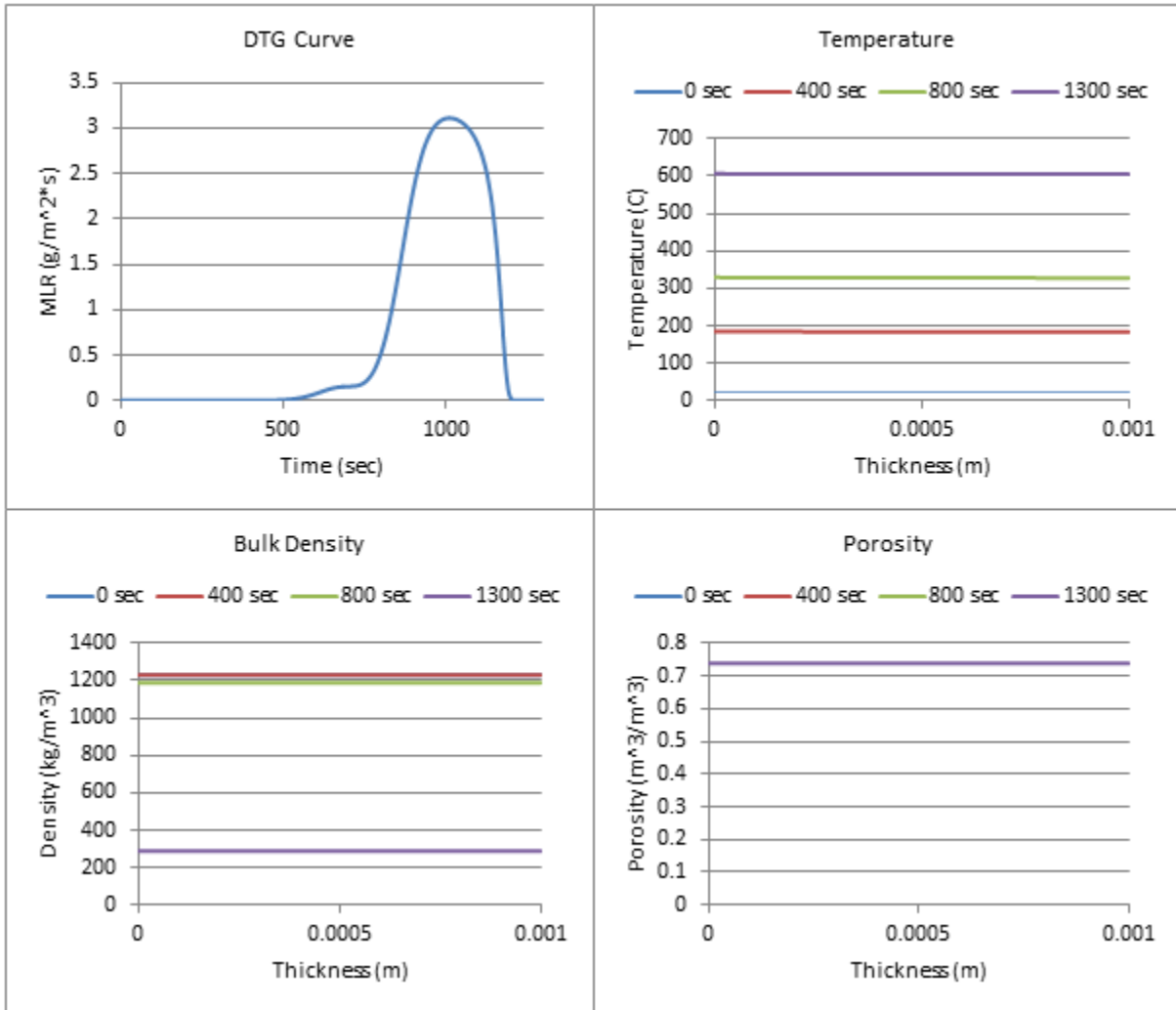
Figure 174: Profiles (800 W/m^2, 5% ATH)
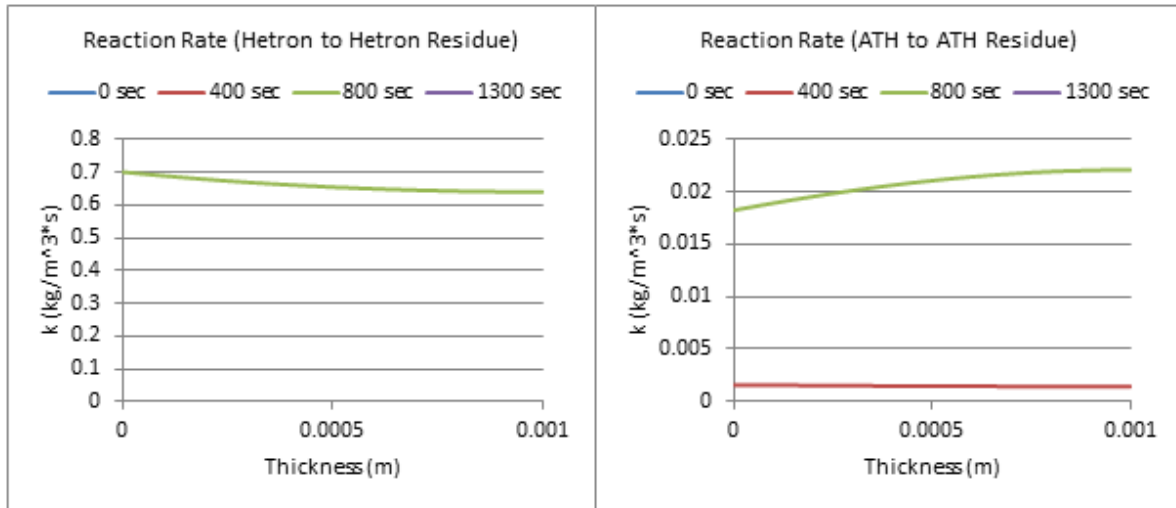
Figure 175: Reaction Rate Profiles (800 W/m^2, 5% ATH)
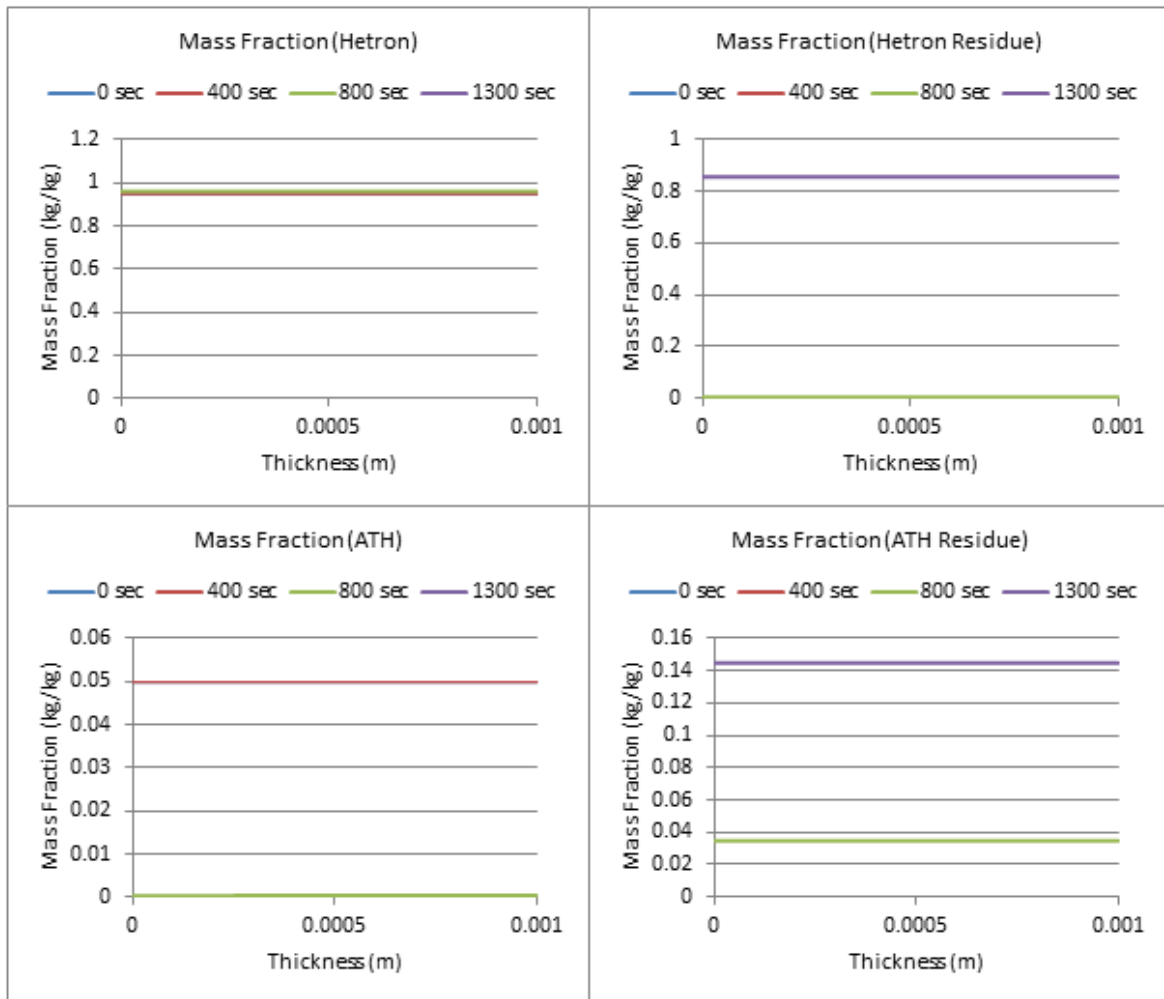
Figure 176: Mass Fraction Profiles (800 W/m^2, 5% ATH)

25% ATH, qe= 100 W/m^2
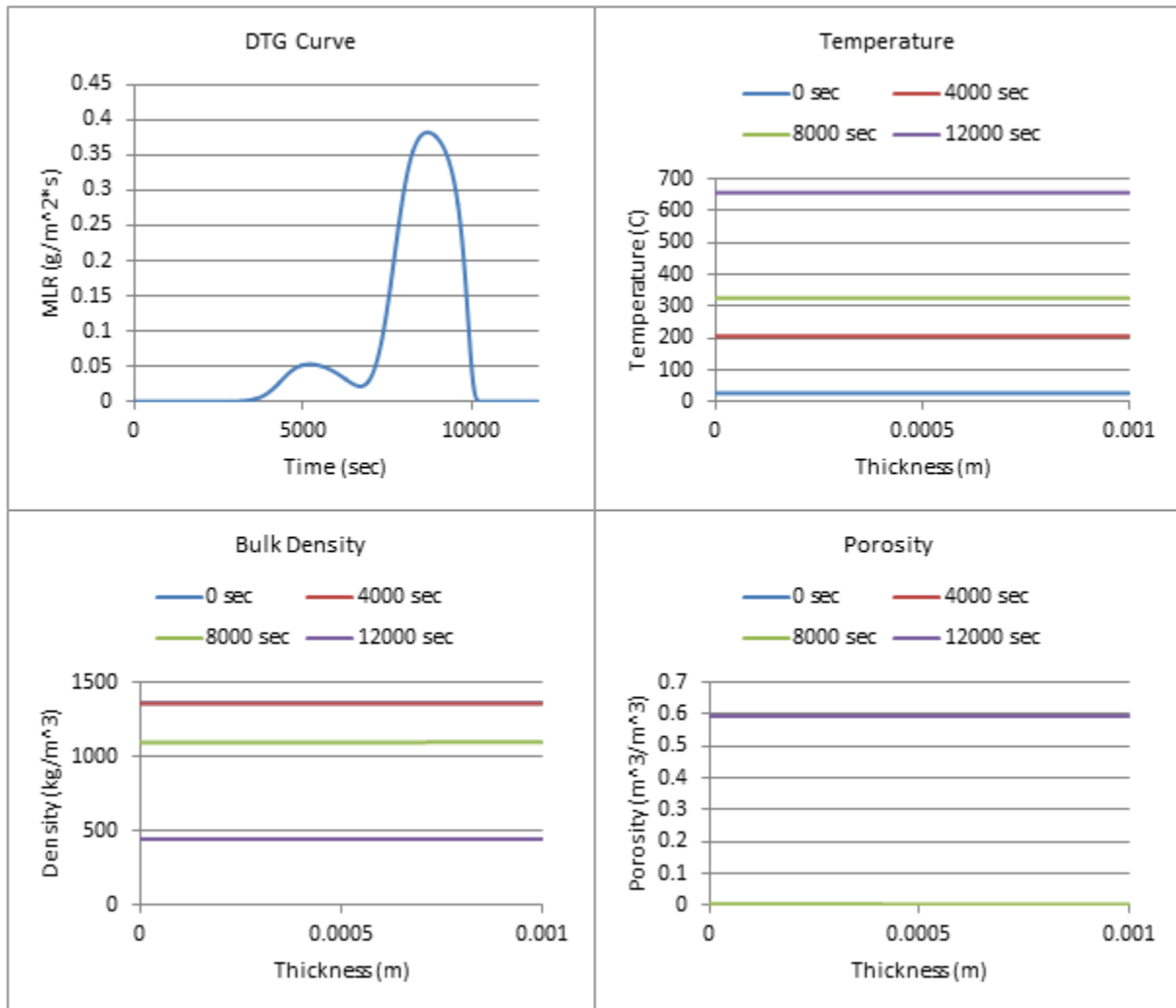
Figure 177: Profiles (100 W/m^2, 25% ATH)
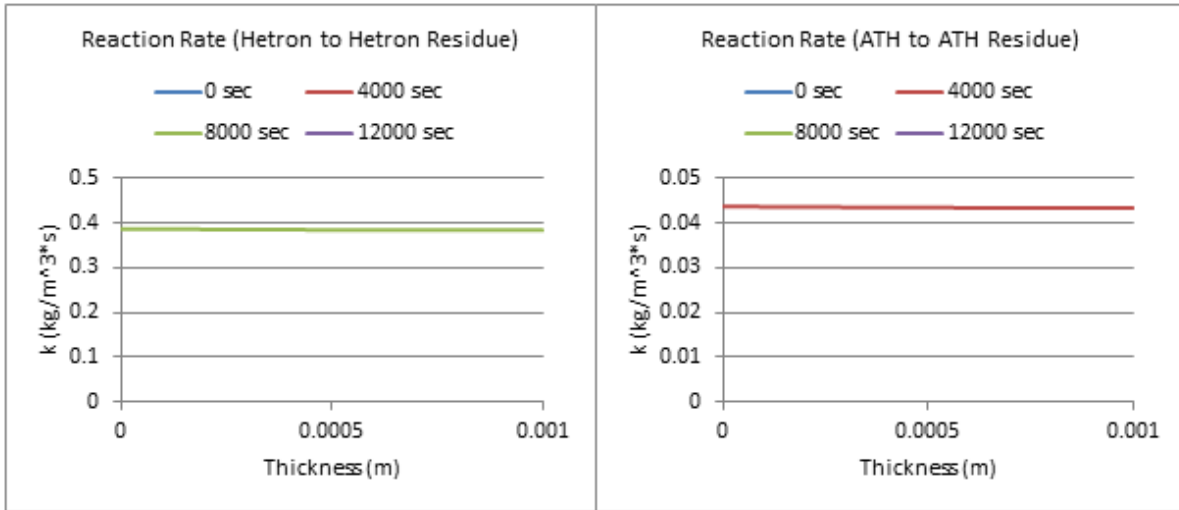
Figure 178: Reaction Rate Profiles (100 W/m^2, 25% ATH)
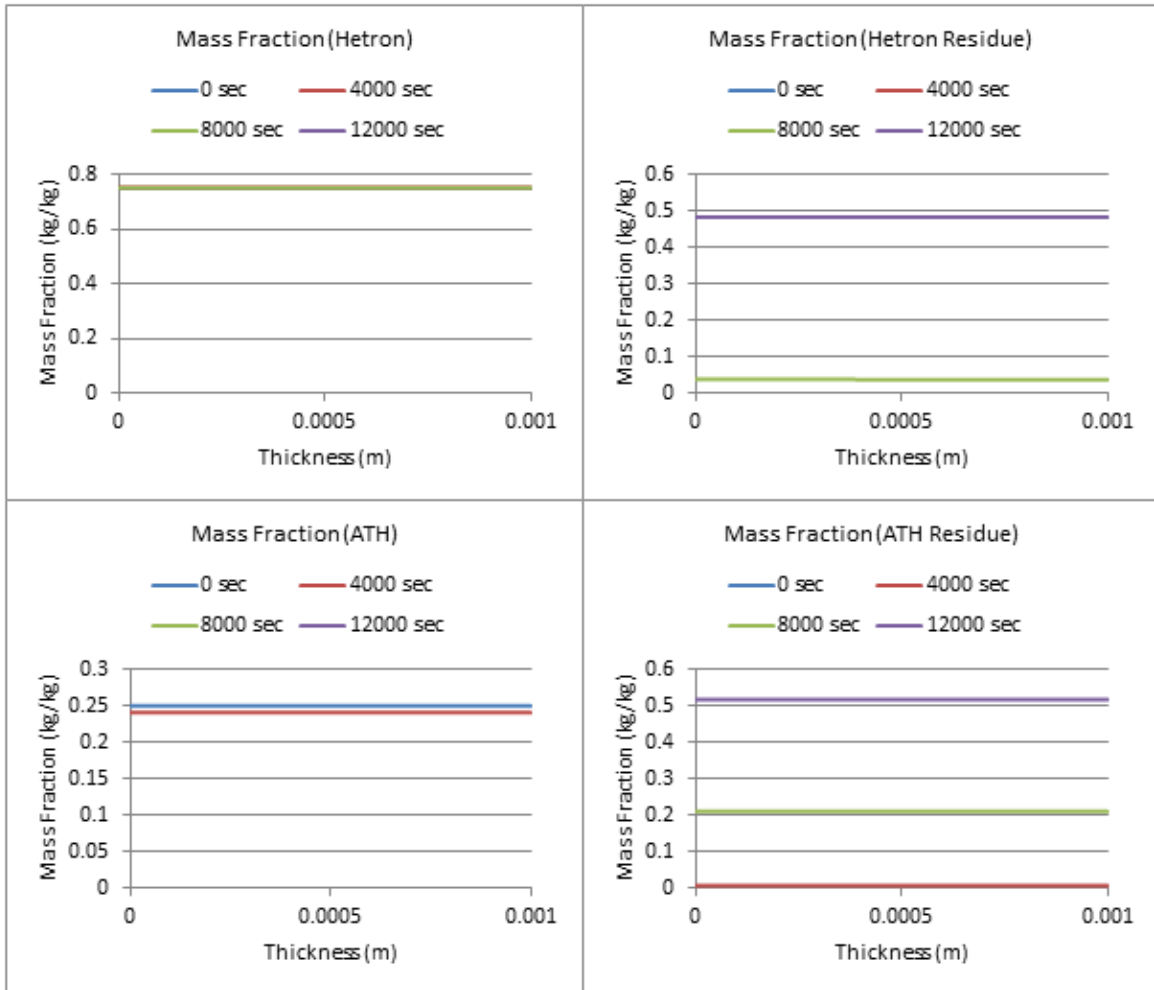
Figure 179: Mass Fraction Profiles (100 W/m^2, 25% ATH)

25% ATH, qe= 200 W/m^2
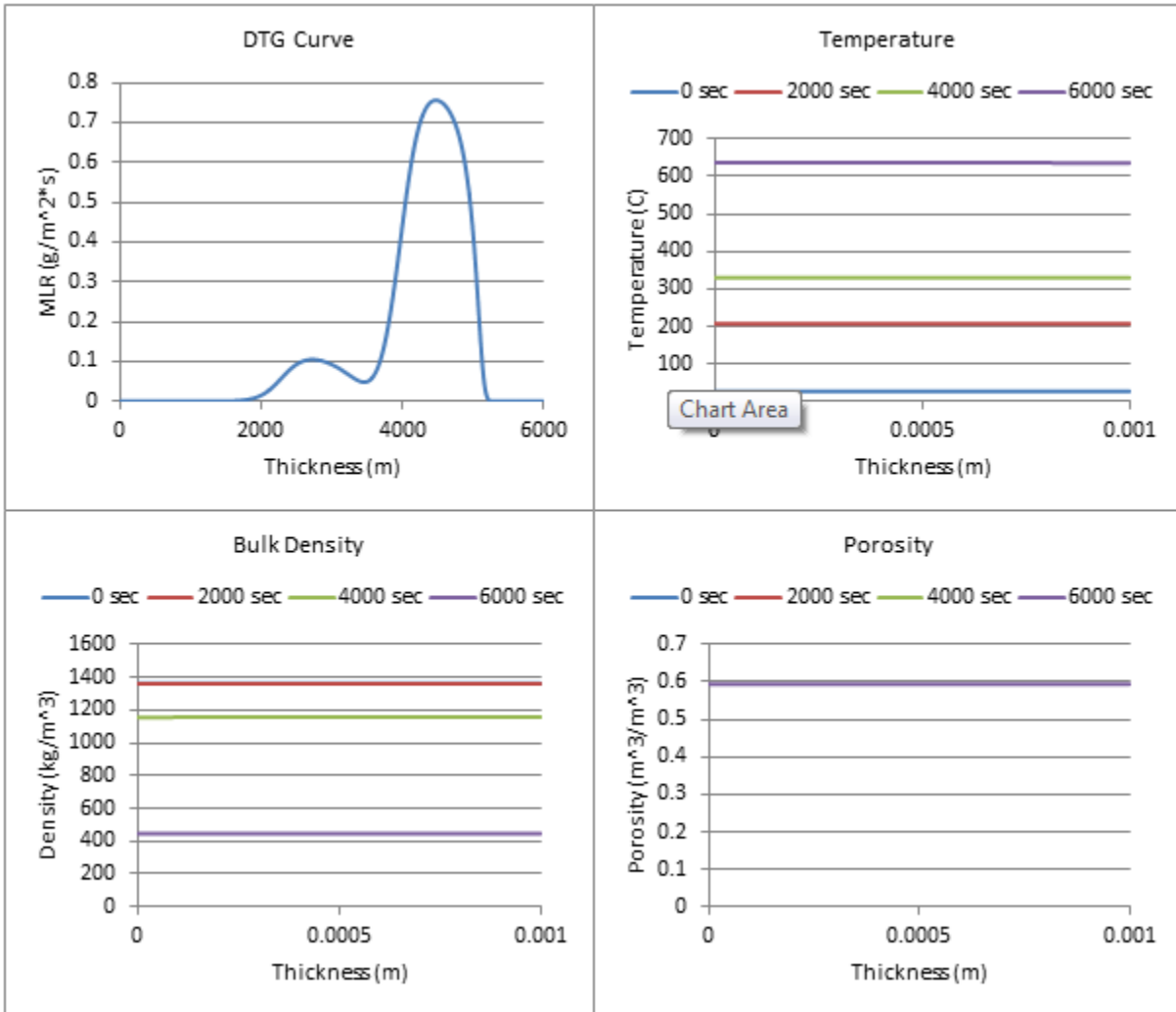
Figure 180: Profiles (200 W/m^2, 25% ATH)
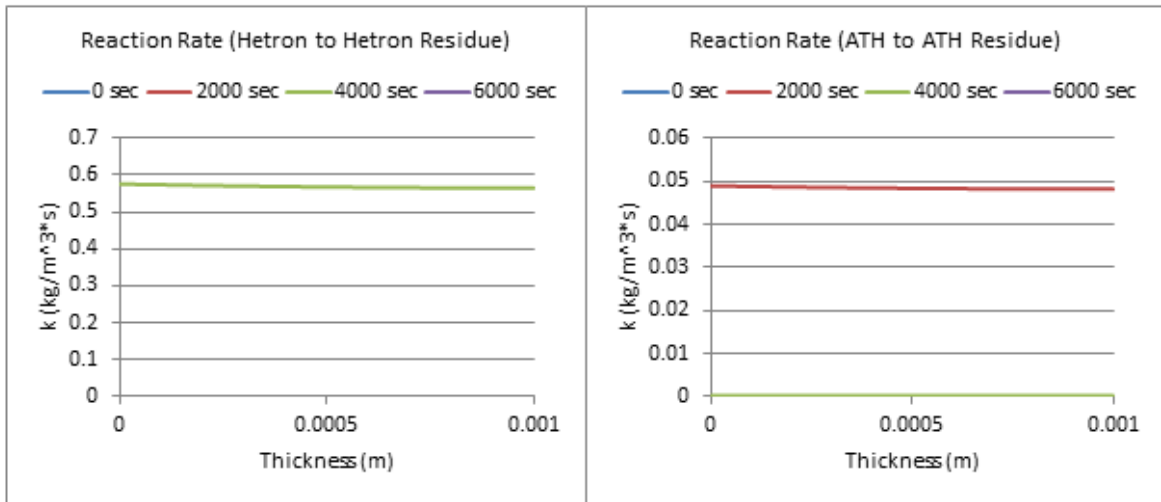
Figure 181: Reaction Rate Profiles (200 W/m^2, 25% ATH)
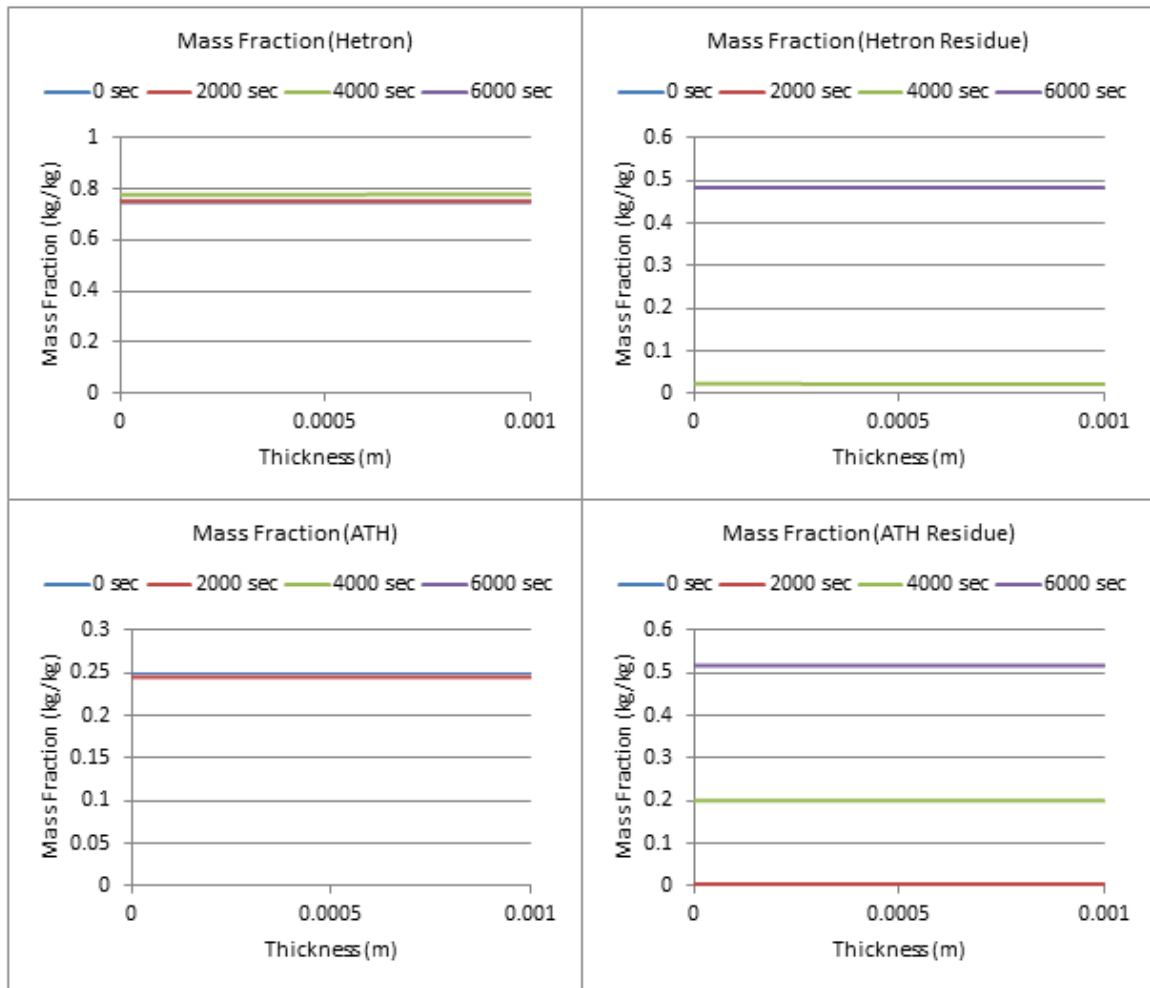
Figure 182: Mass Fraction Profiles (200 W/m^2, 25% ATH)

25% ATH, qe= 300 W/m^2
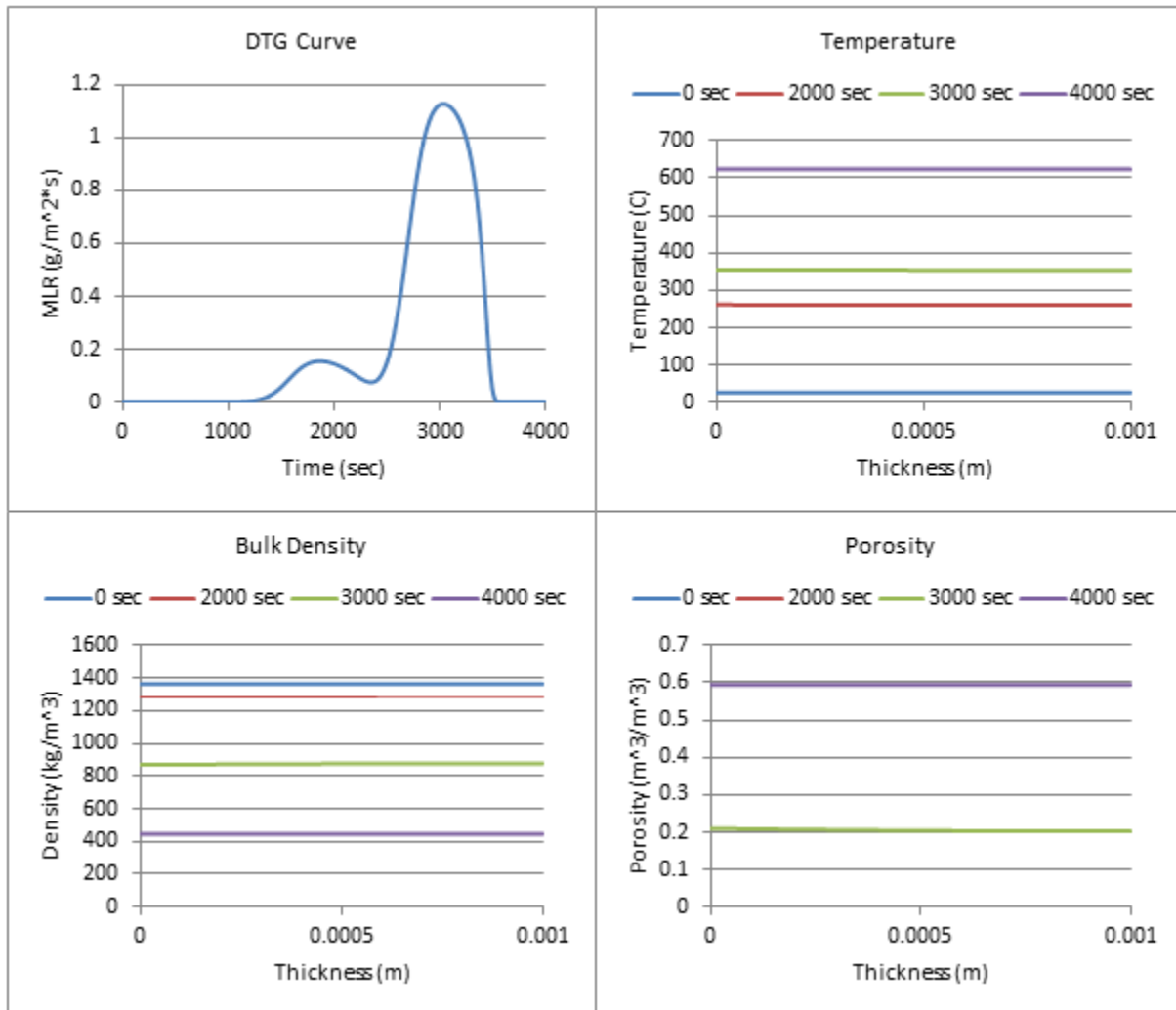
Figure 183: Profiles (300 W/m^2, 25% ATH)
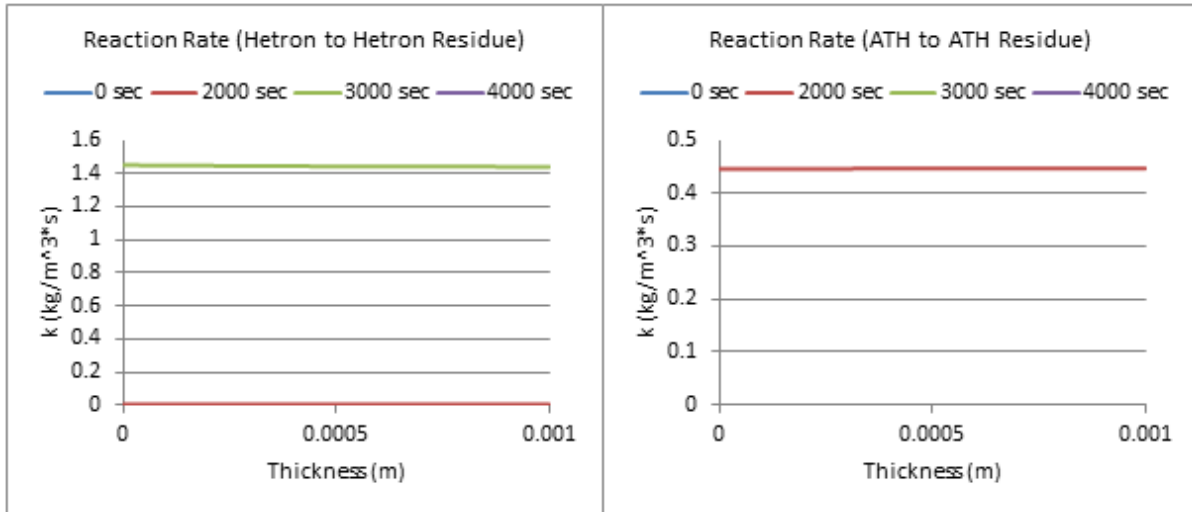
Figure 184: Reaction Rate Profiles (300 W/m^2, 25% ATH)
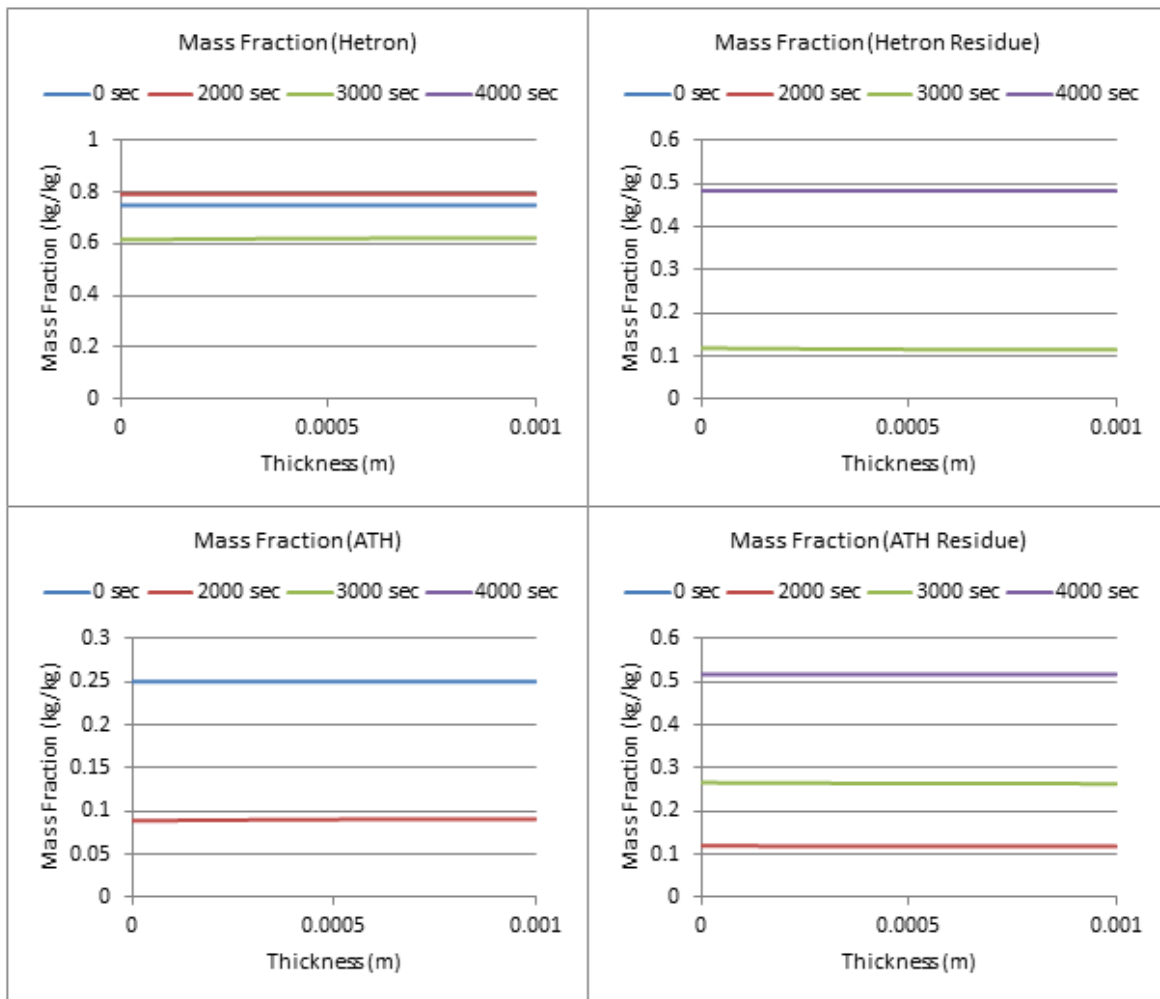
Figure 185: Mass Fraction Profiles (300 W/m^2, 25% ATH)

25% ATH, qe= 400 W/m^2
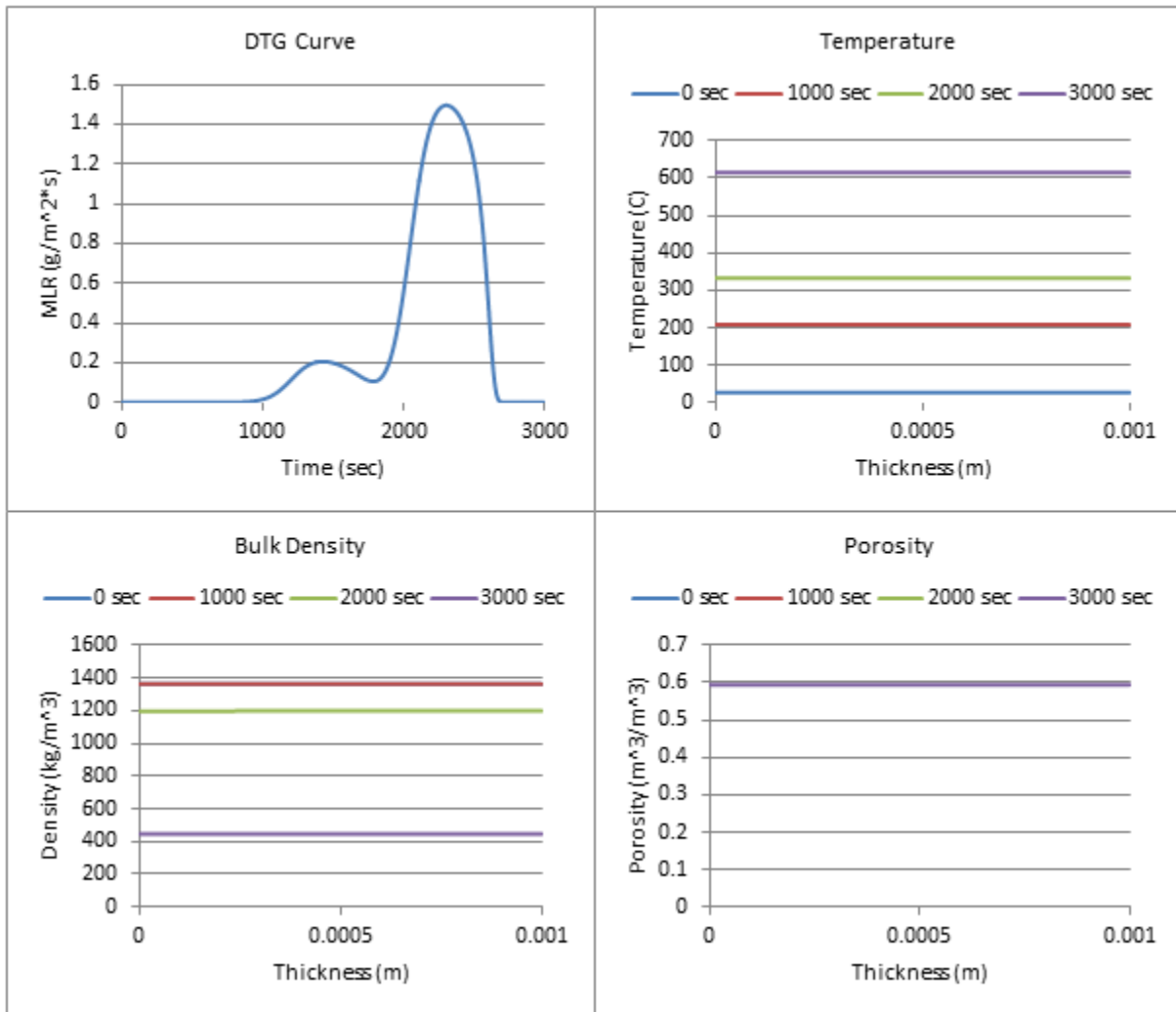
Figure 186: Profiles (400 W/m^2, 25% ATH)
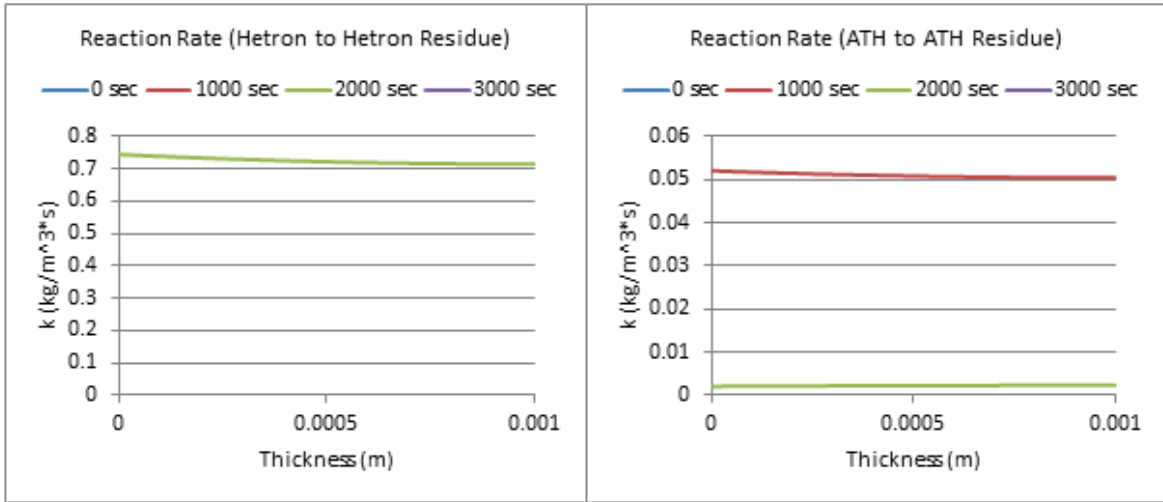
Figure 187: Reaction Rate Profiles (400 W/m^2, 25% ATH)
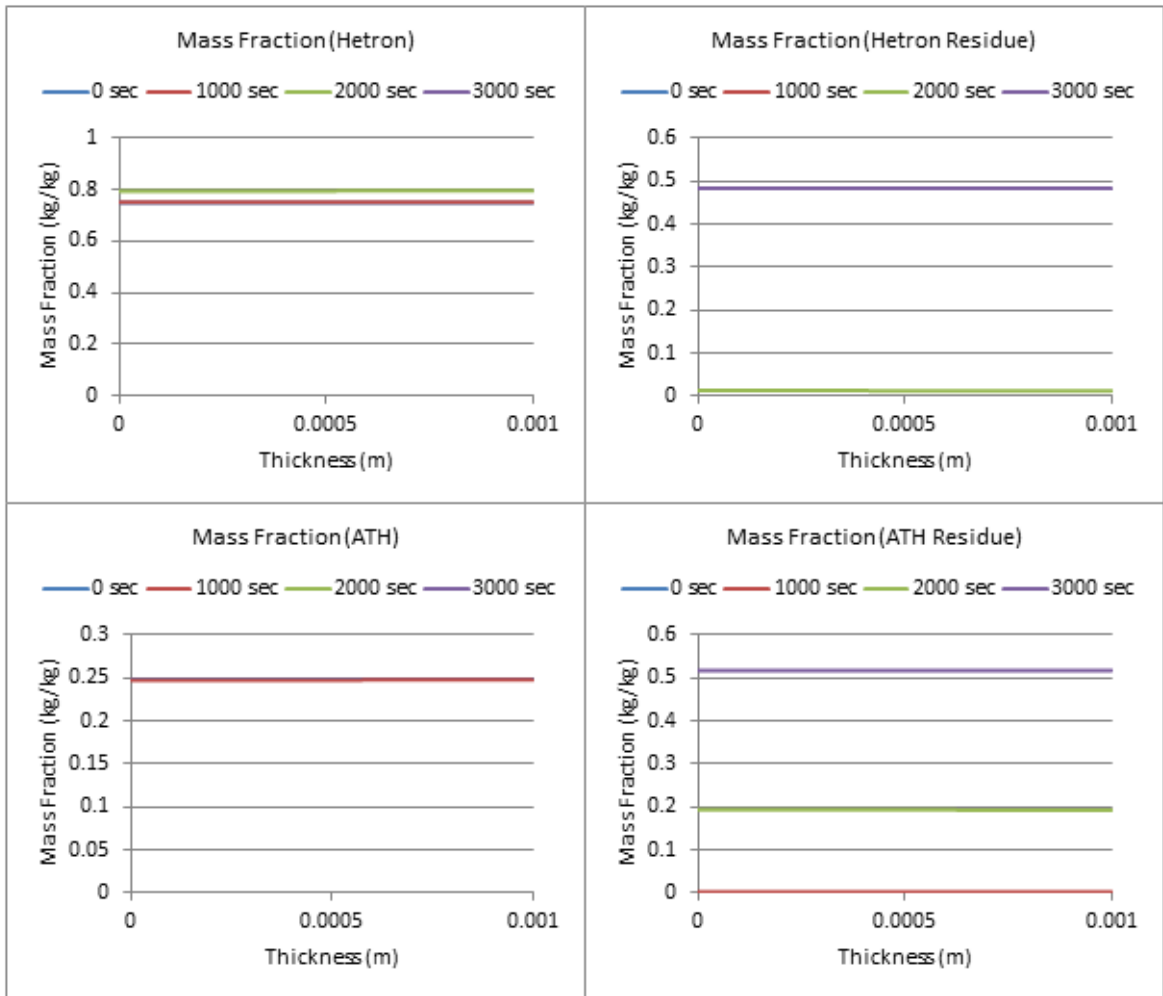
Figure 188: Mass Fraction Profiles (400 W/m^2, 25% ATH)

25% ATH, qe= 500 W/m^2
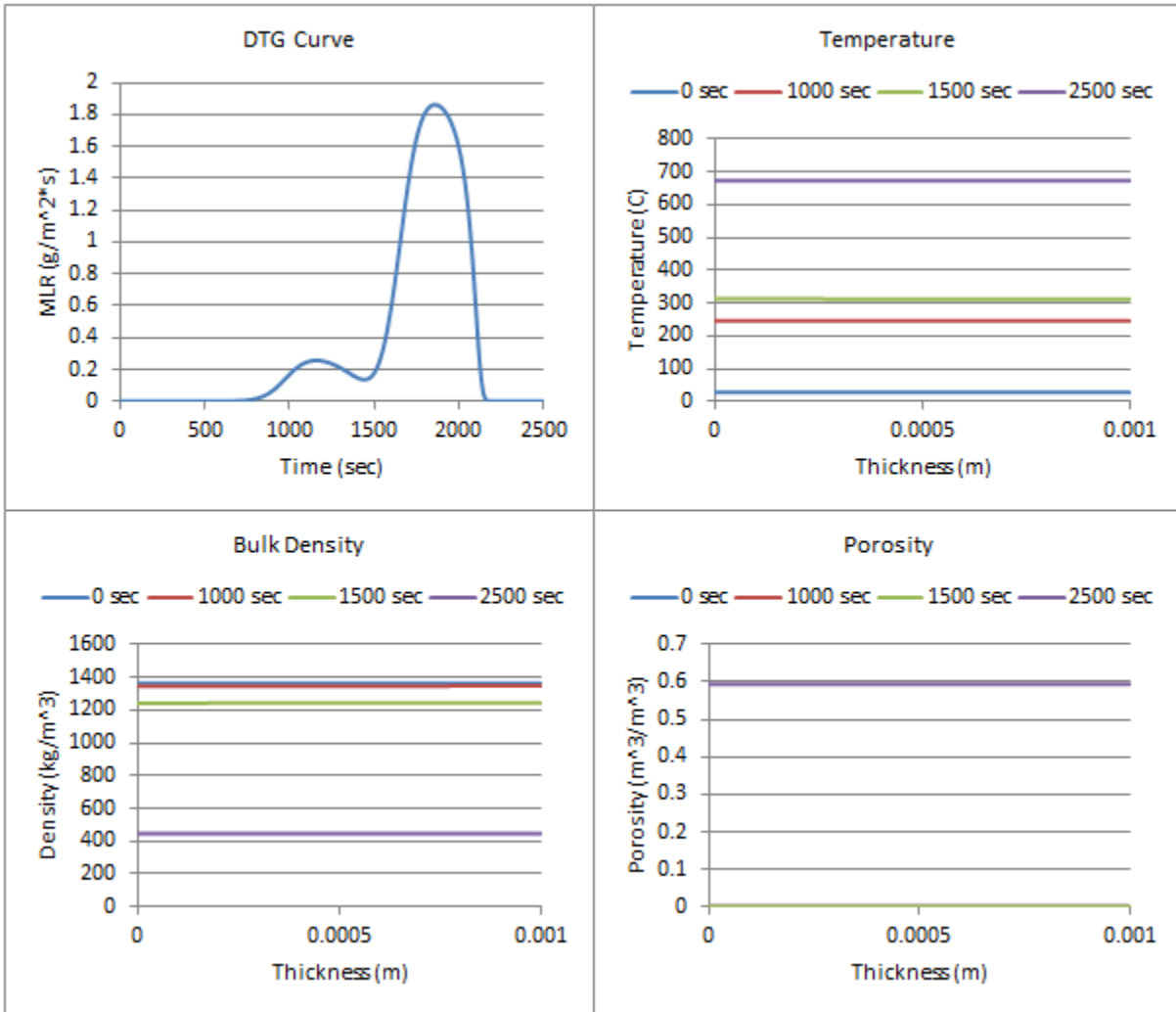
Figure 189: Profiles (500 W/m^2, 25% ATH)
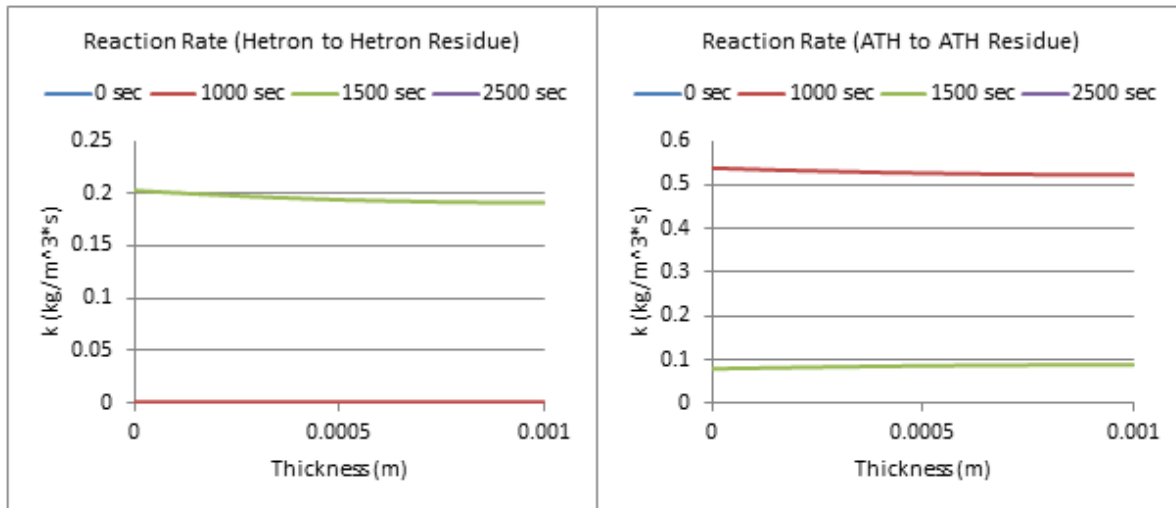
Figure 190: Reaction Rate Profiles (500 W/m^2, 25% ATH)
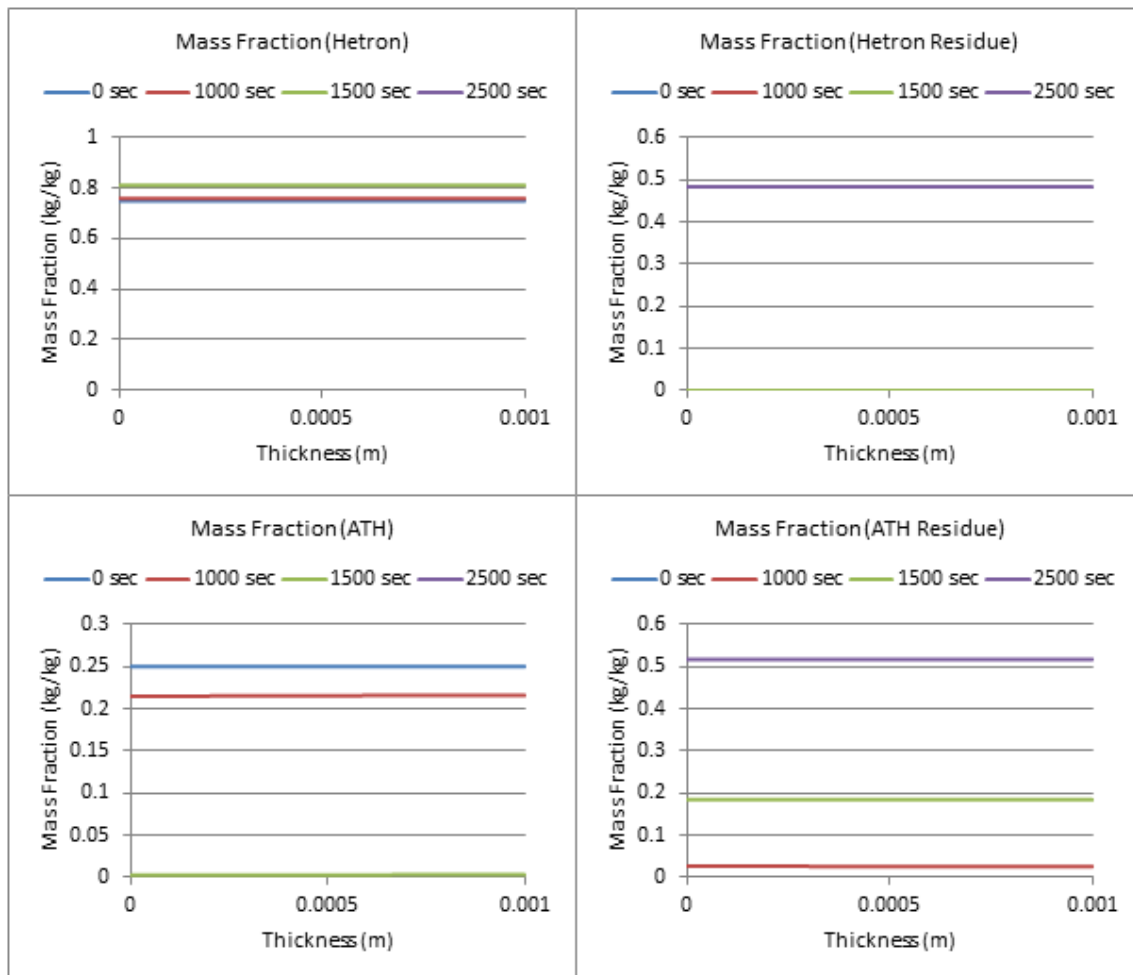
Figure 191: Mass Fraction Profiles (500 W/m^2, 25% ATH)

25% ATH, qe= 600 W/m^2
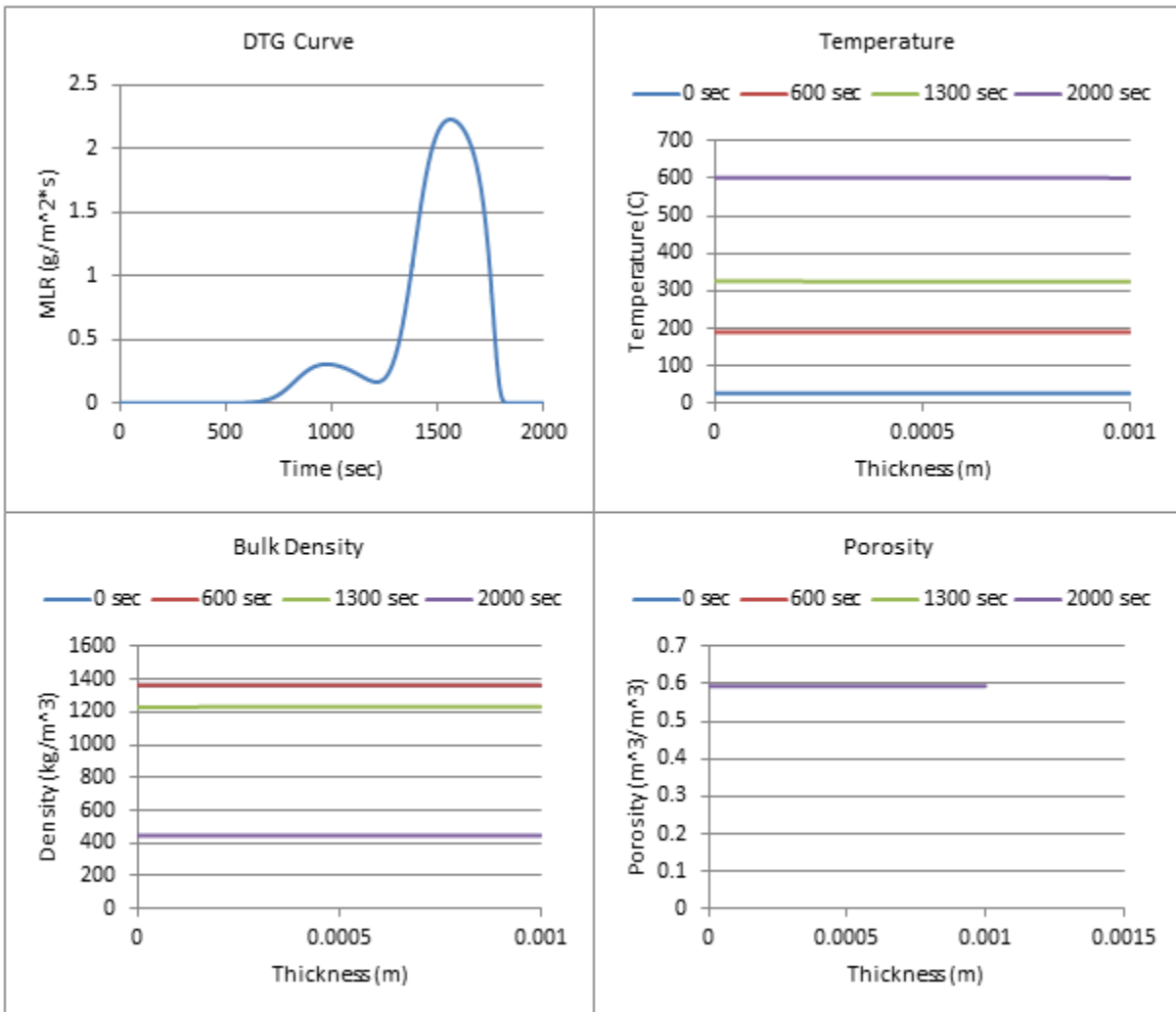
Figure 192: Profiles (600 W/m^2, 25% ATH)
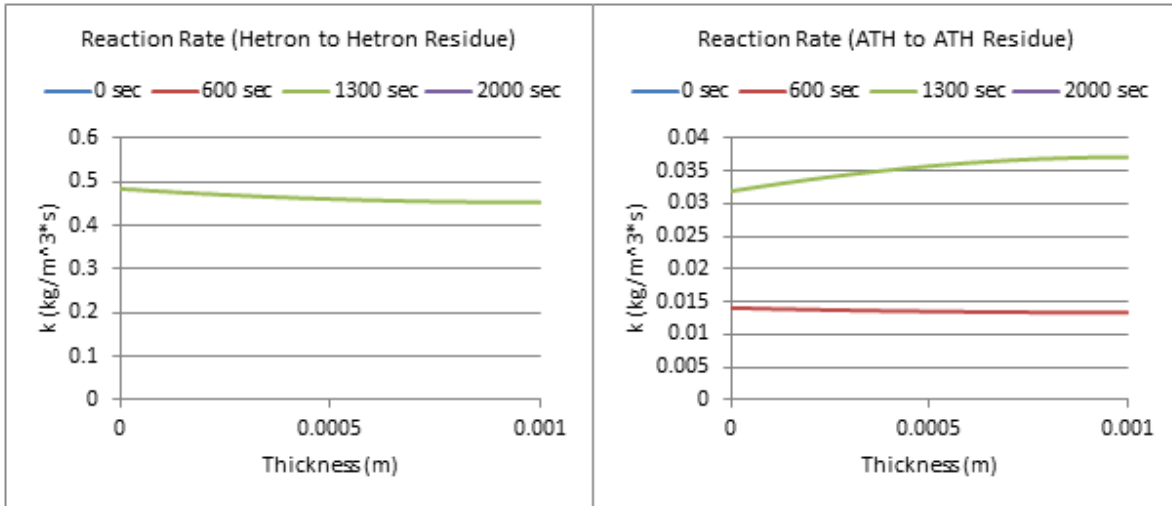
Figure 193: Reaction Rate Profiles (600 W/m^2, 25% ATH)
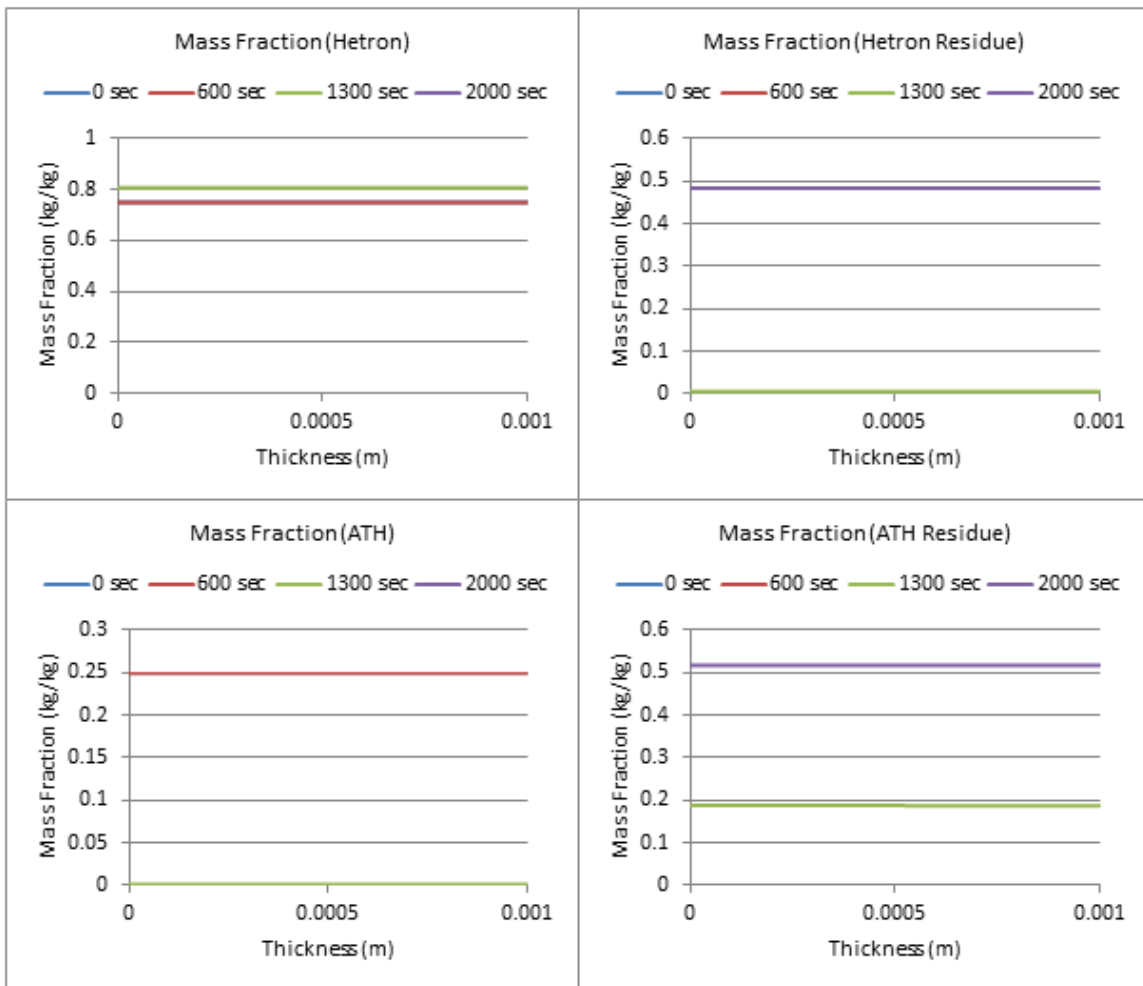
Figure 194: Mass Fraction Profiles (600 W/m^2, 25% ATH)

25% ATH, qe= 700 W/m^2
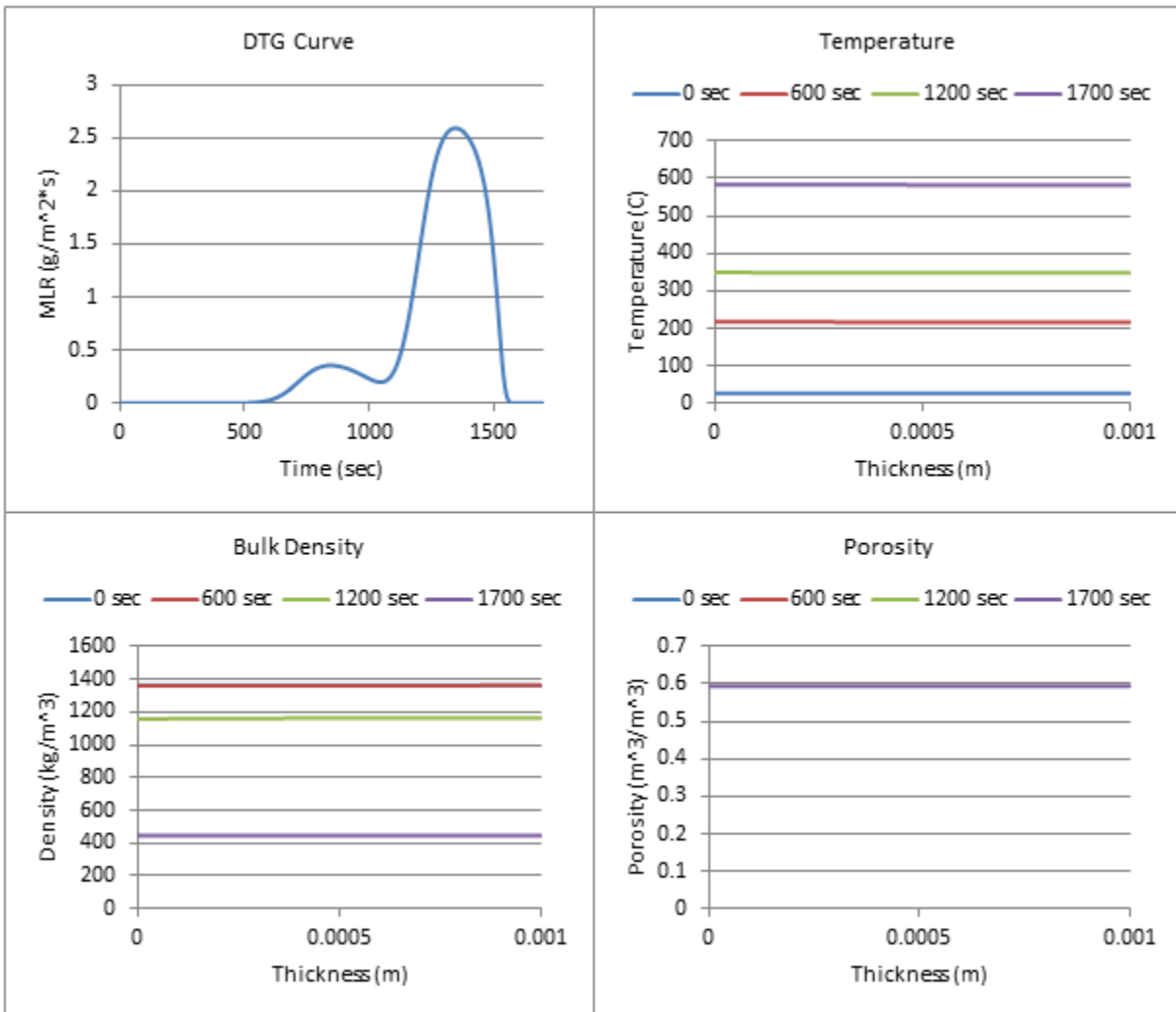
Figure 195: Profiles (700 W/m^2, 25% ATH)
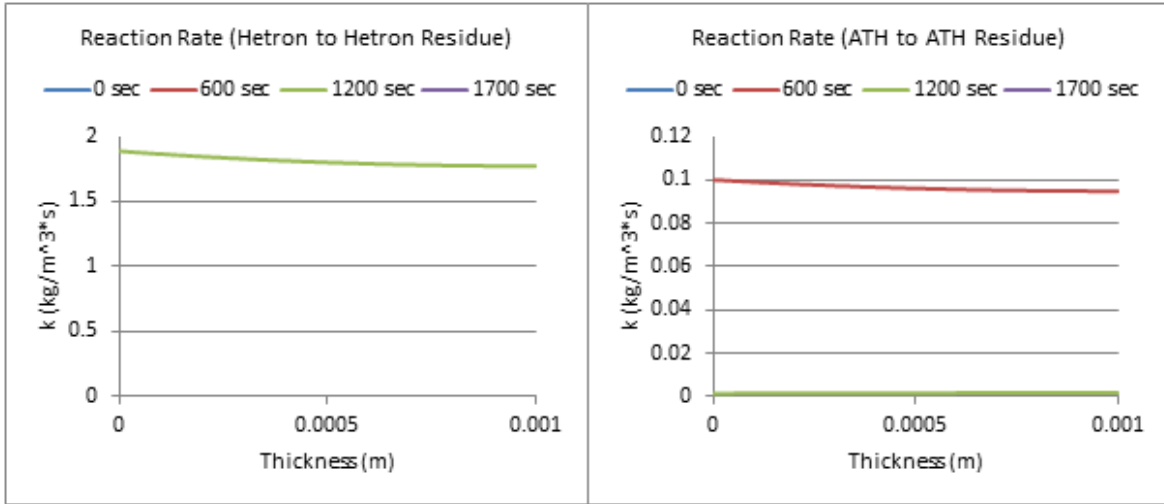
Figure 196: Reaction Rate Profiles (700 W/m^2, 25% ATH)
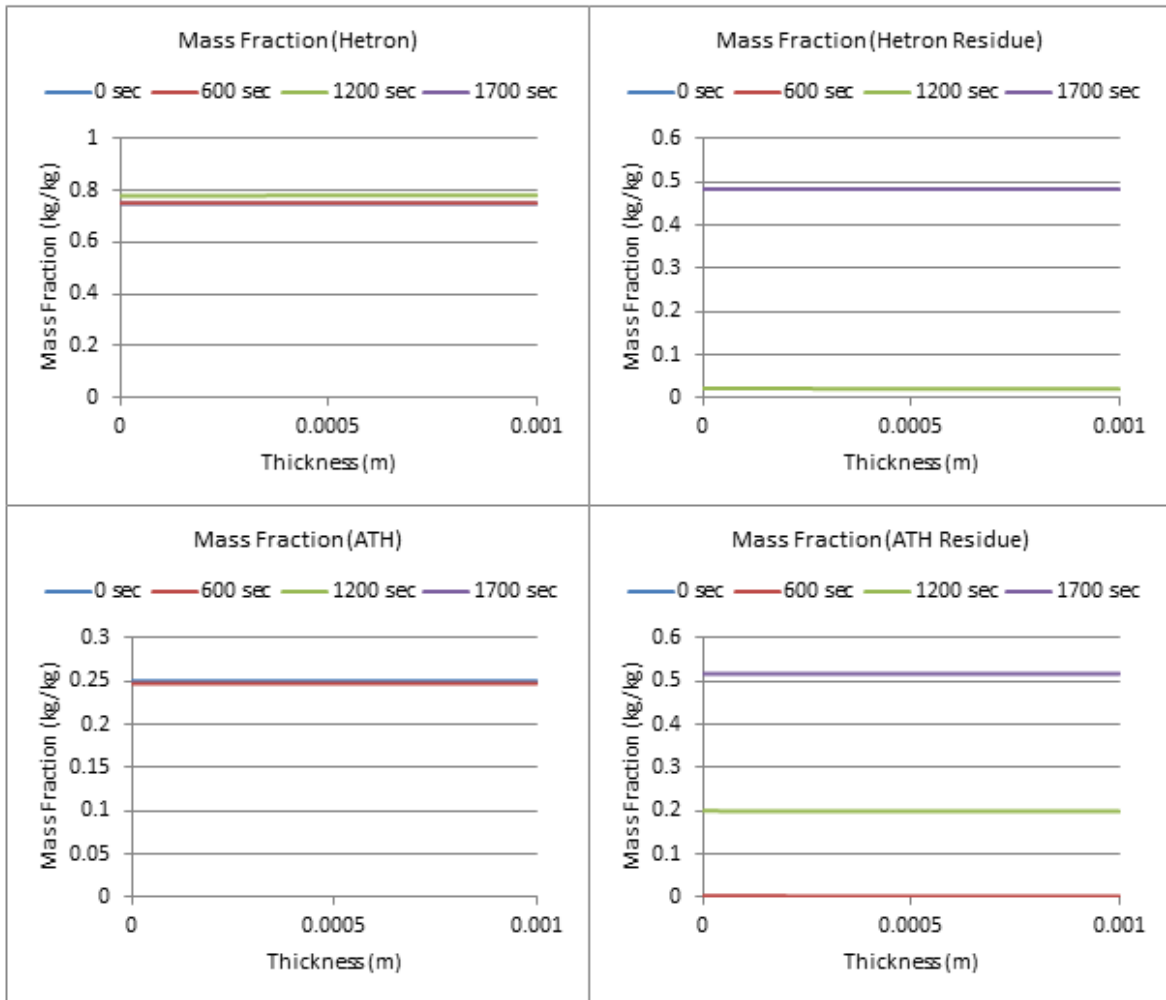
Figure 197: Mass Fraction Profiles (700 W/m^2, 25% ATH)

25% ATH, qe= 800 W/m^2
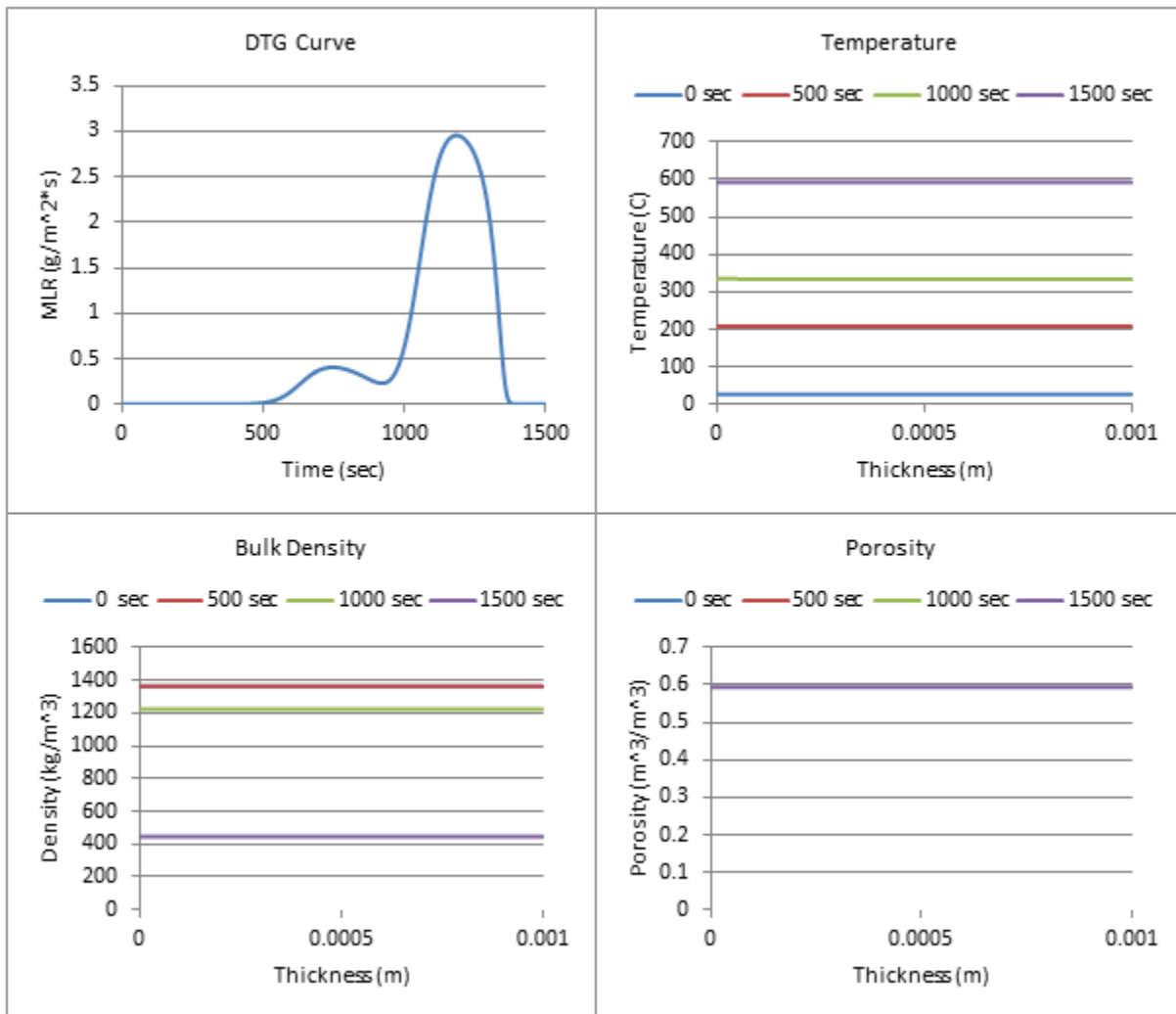
Figure 198: Profiles (800 W/m^2, 25% ATH)
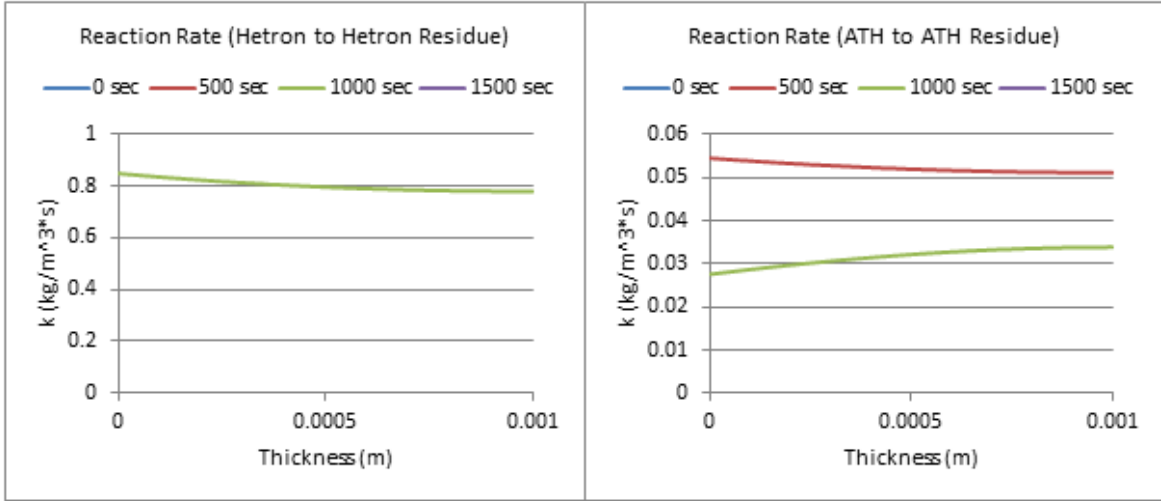
Figure 199: Reaction Rate Profiles (800 W/m^2, 25% ATH)
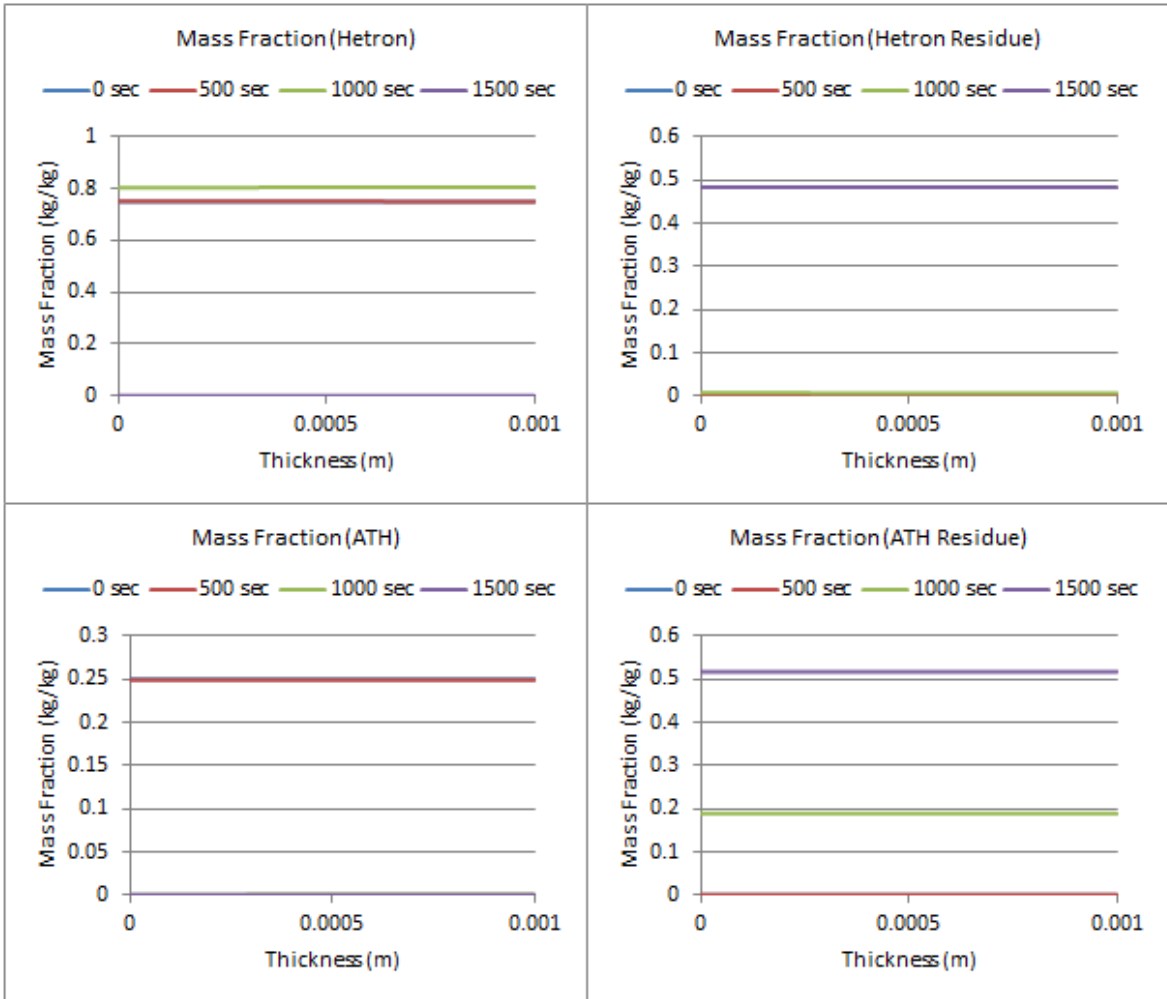
Figure 200: Mass Fraction Profiles (800 W/m^2, 25% ATH)

40% ATH, qe= 100 W/m^2
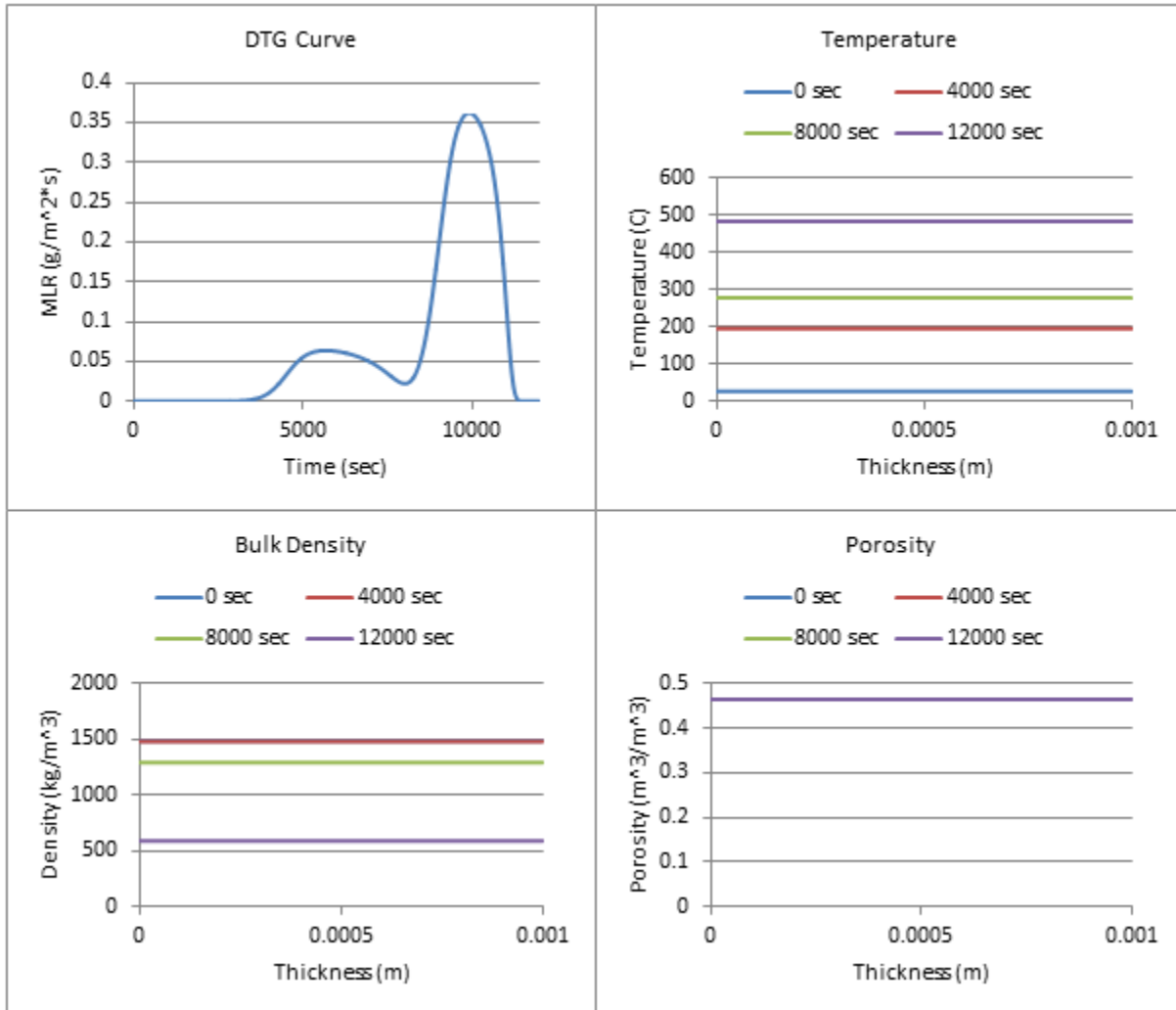
Figure 201: Profiles (100 W/m^2, 40% ATH)
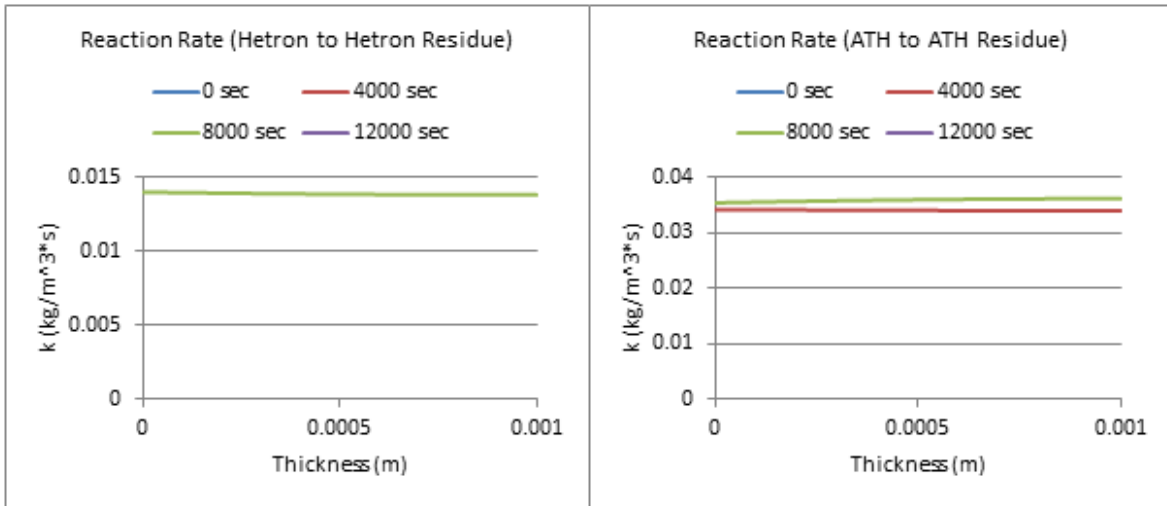
Figure 202: Reaction Rate Profiles (100 W/m^2, 40% ATH)
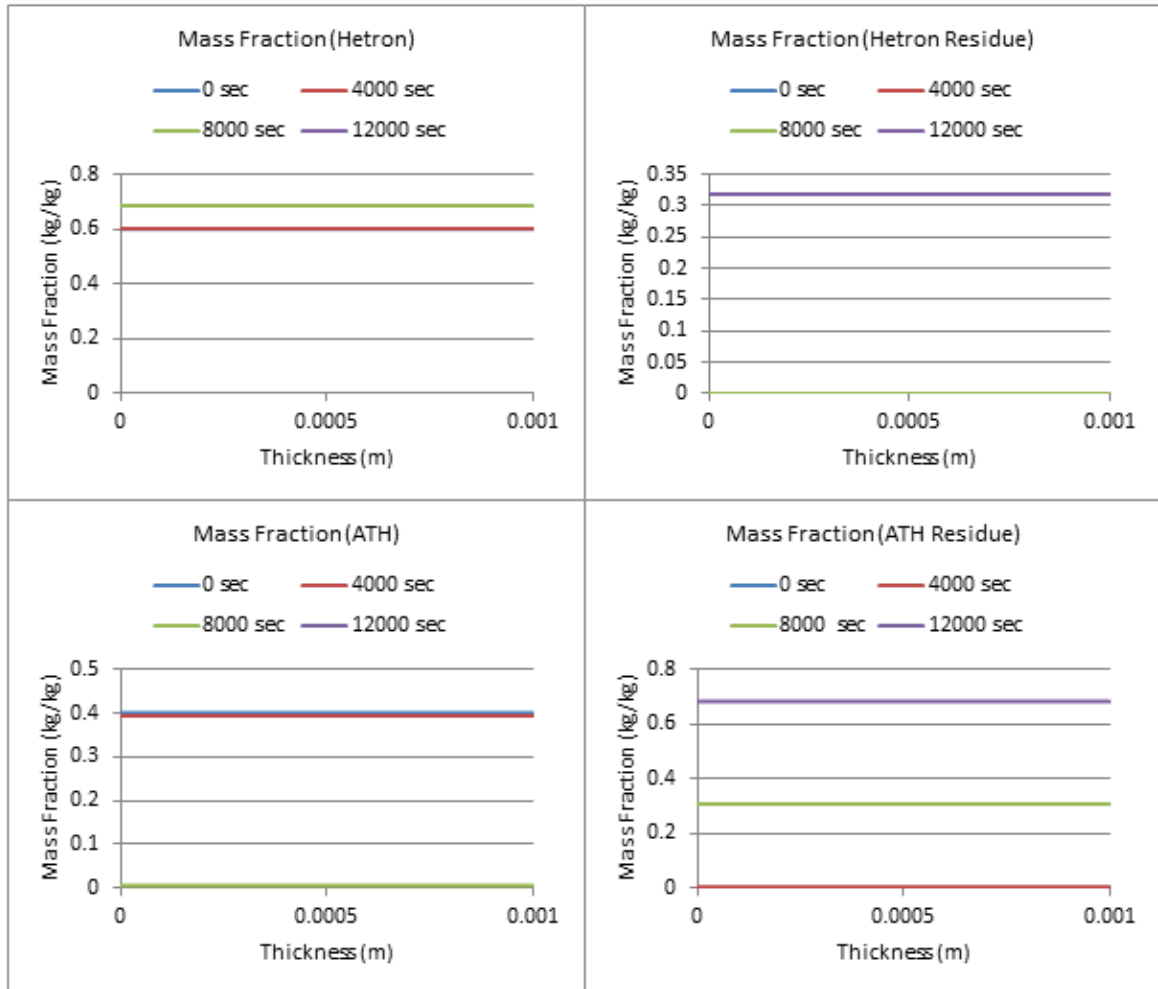
Figure 203: Mass Fraction Profiles (100 W/m^2, 40% ATH)

Page **194** of **324**
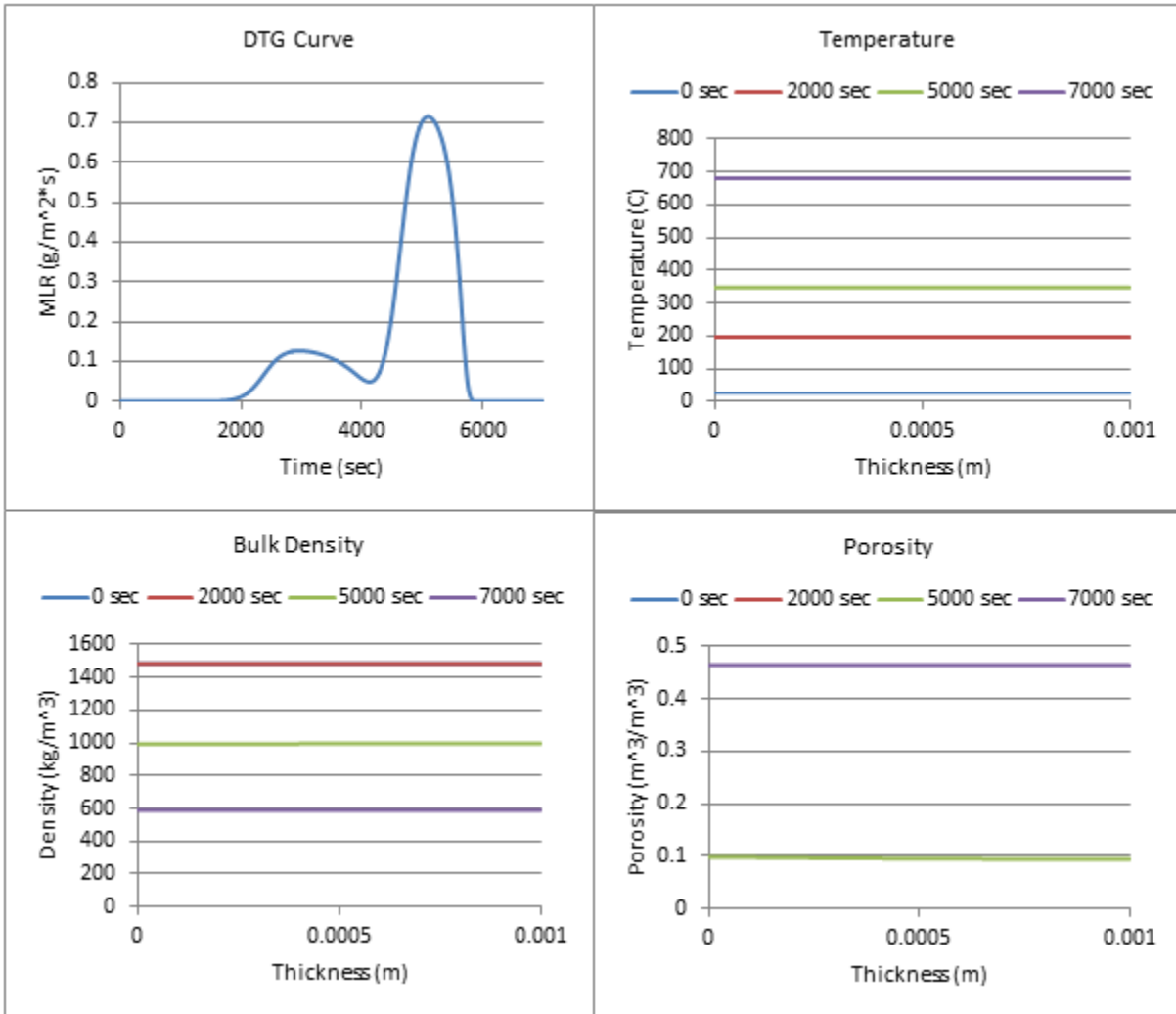
40% ATH, qe= 200 W/m^2

Figure 204: Profiles (200 W/m^2, 40% ATH)
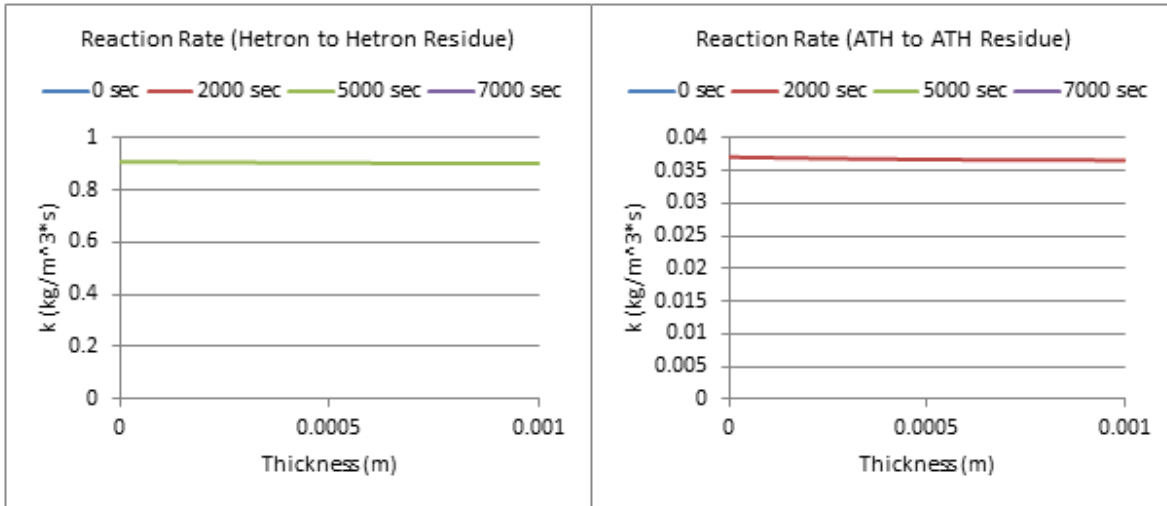
Figure 205: Reaction Rate Profiles (200 W/m^2, 40% ATH)
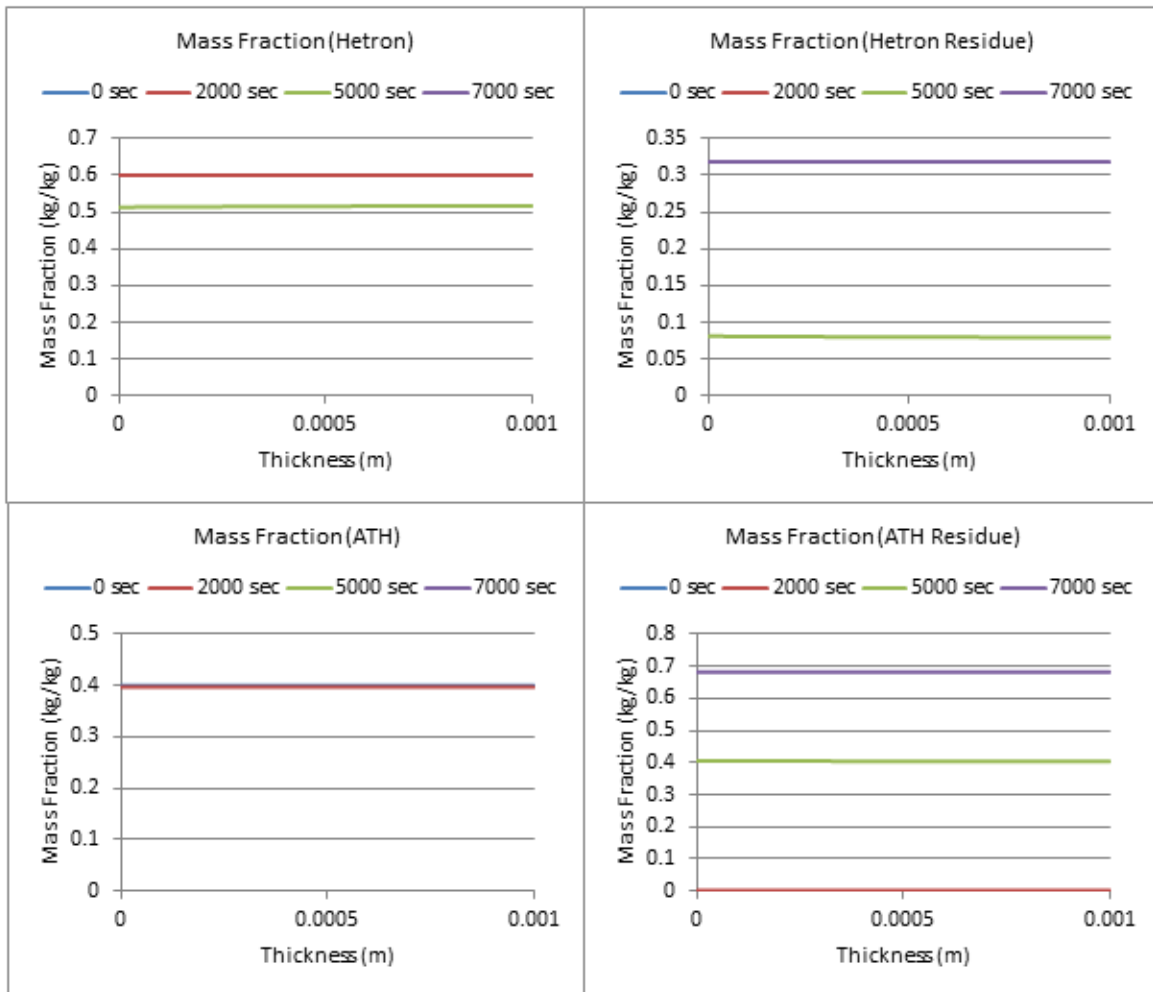
Figure 206: Mass Fraction Profiles (200 W/m^2, 40% ATH)

40% ATH, qe= 300 W/m^2
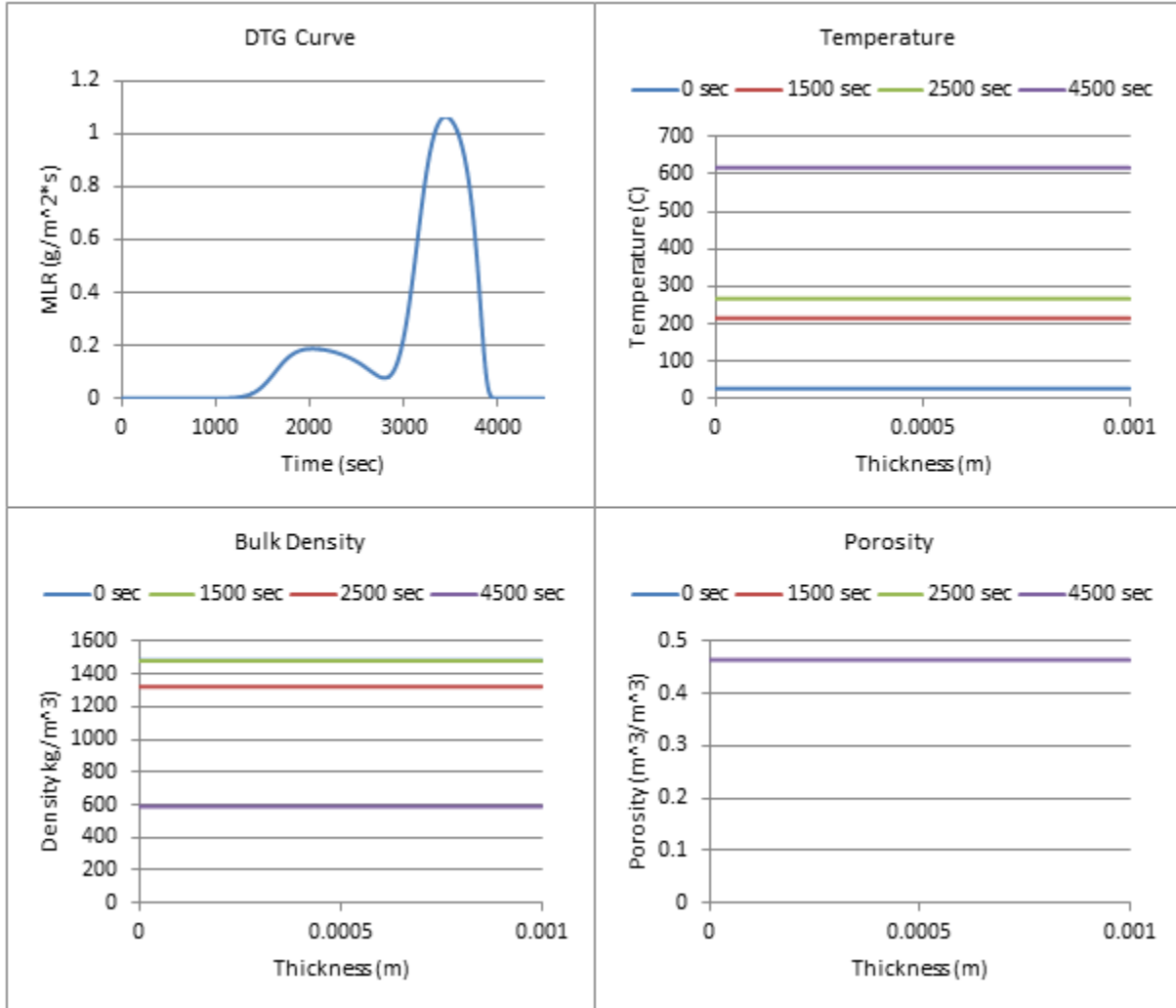
Figure 207: Profiles (300 W/m^2, 40% ATH)
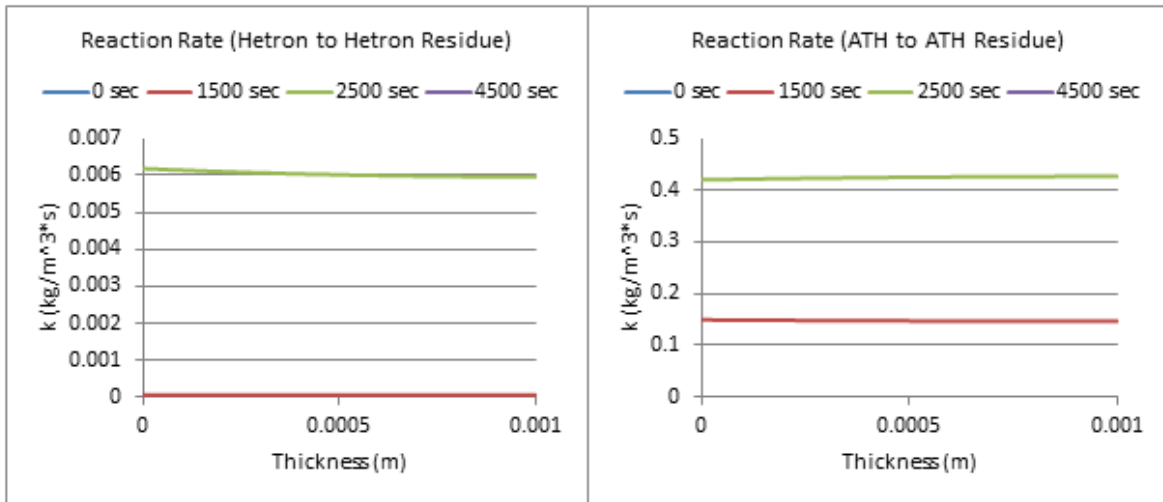
Figure 208: Reaction Rate Profiles (300 W/m^2, 40% ATH)
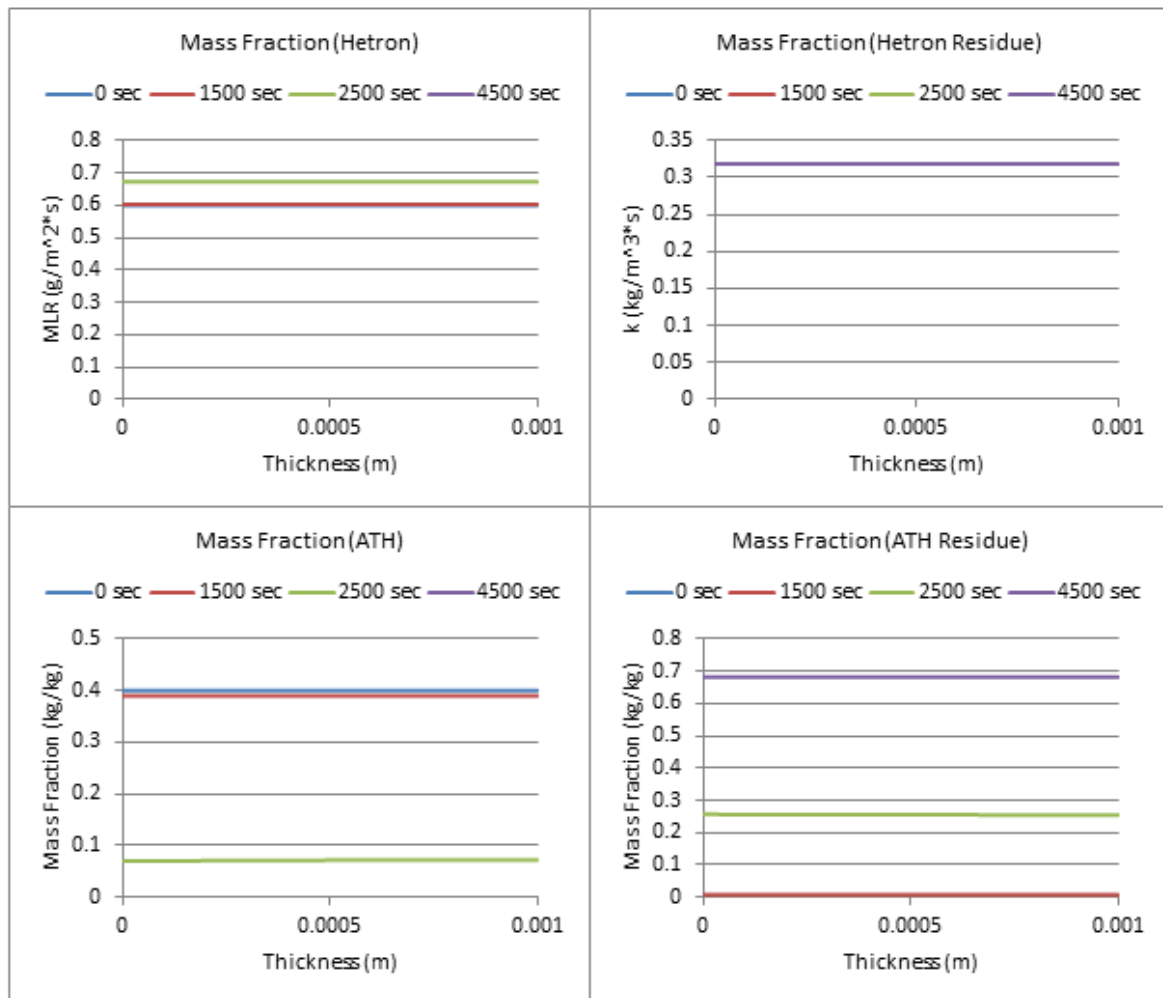
Figure 209: Mass Fraction Profiles (300 W/m^2, 40% ATH)

40% ATH, qe= 400 W/m^2
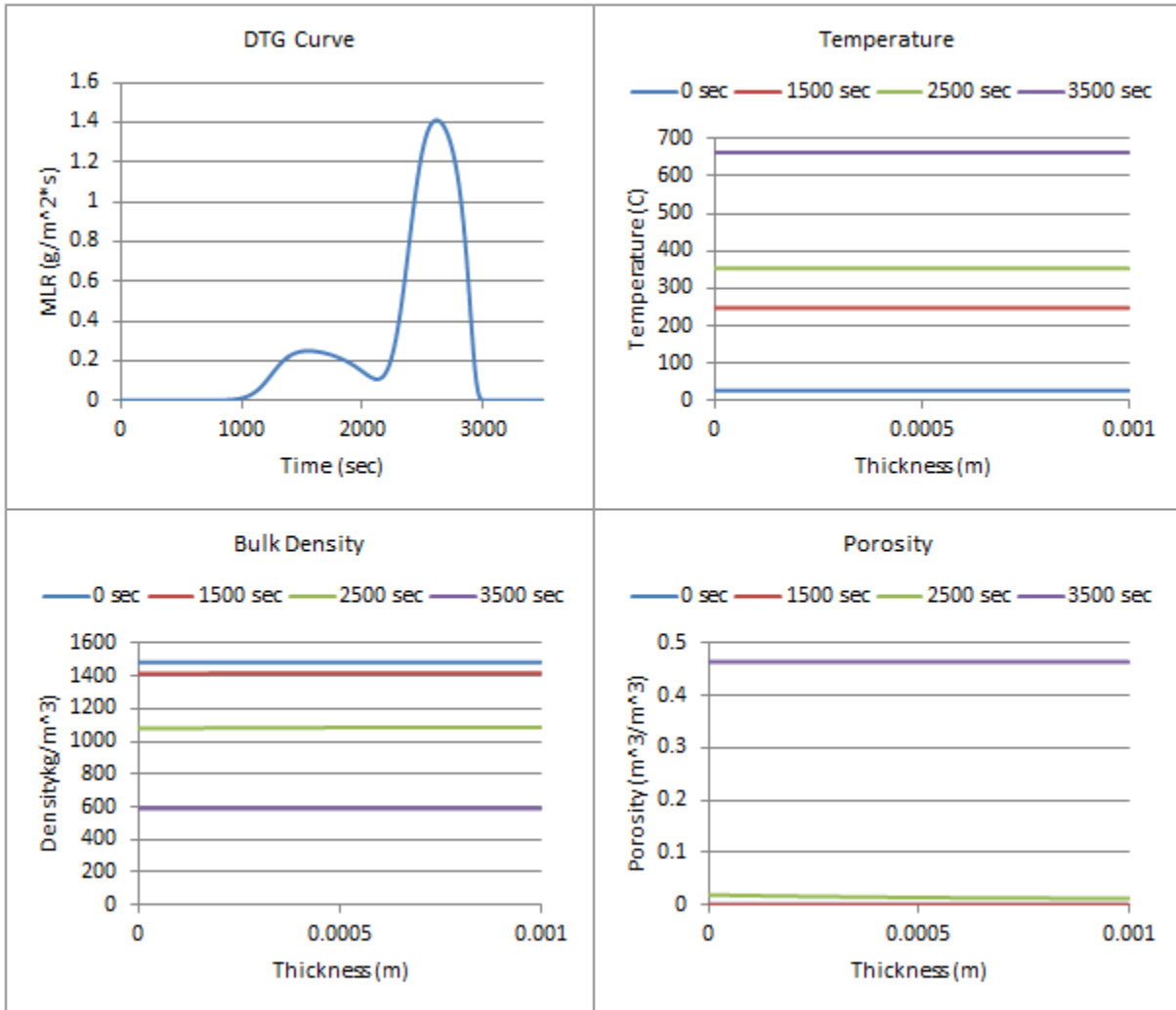
Figure 210: Profiles (400 W/m^2, 40% ATH)
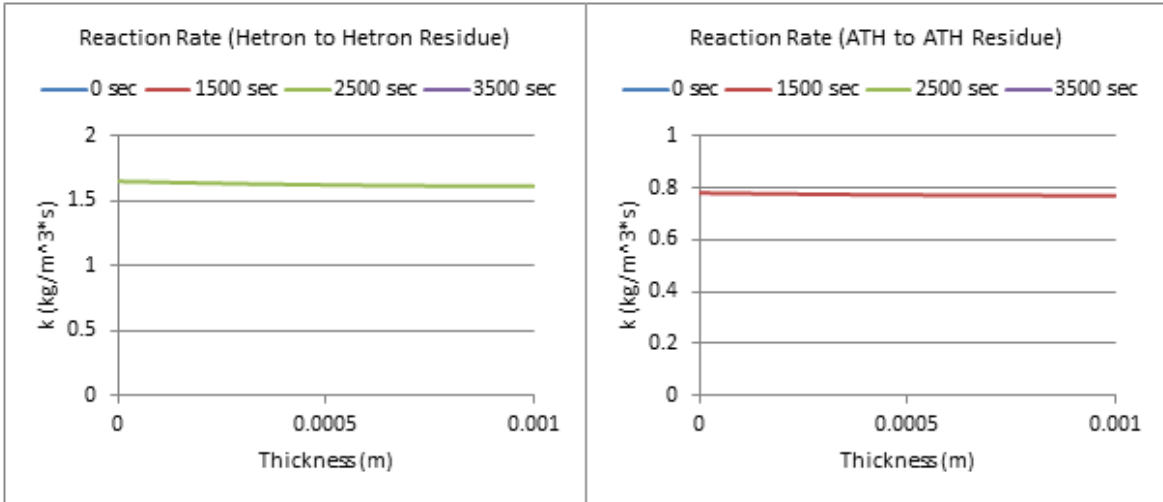
Figure 211: Reaction Rate Profiles (400 W/m^2, 40% ATH)
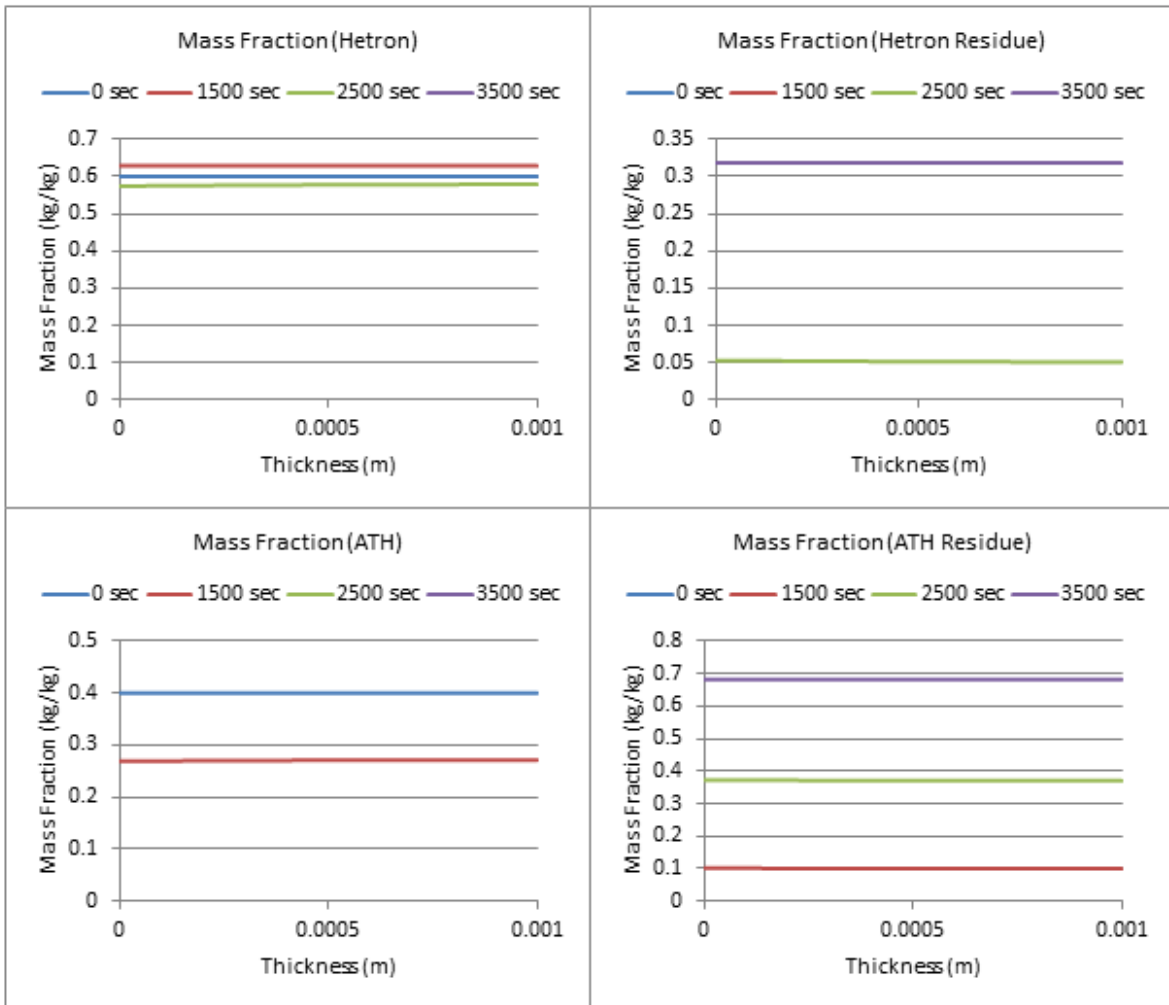
Figure 212: Mass Fraction Profiles (400 W/m^2, 40% ATH)

40% ATH, qe= 500 W/m^2
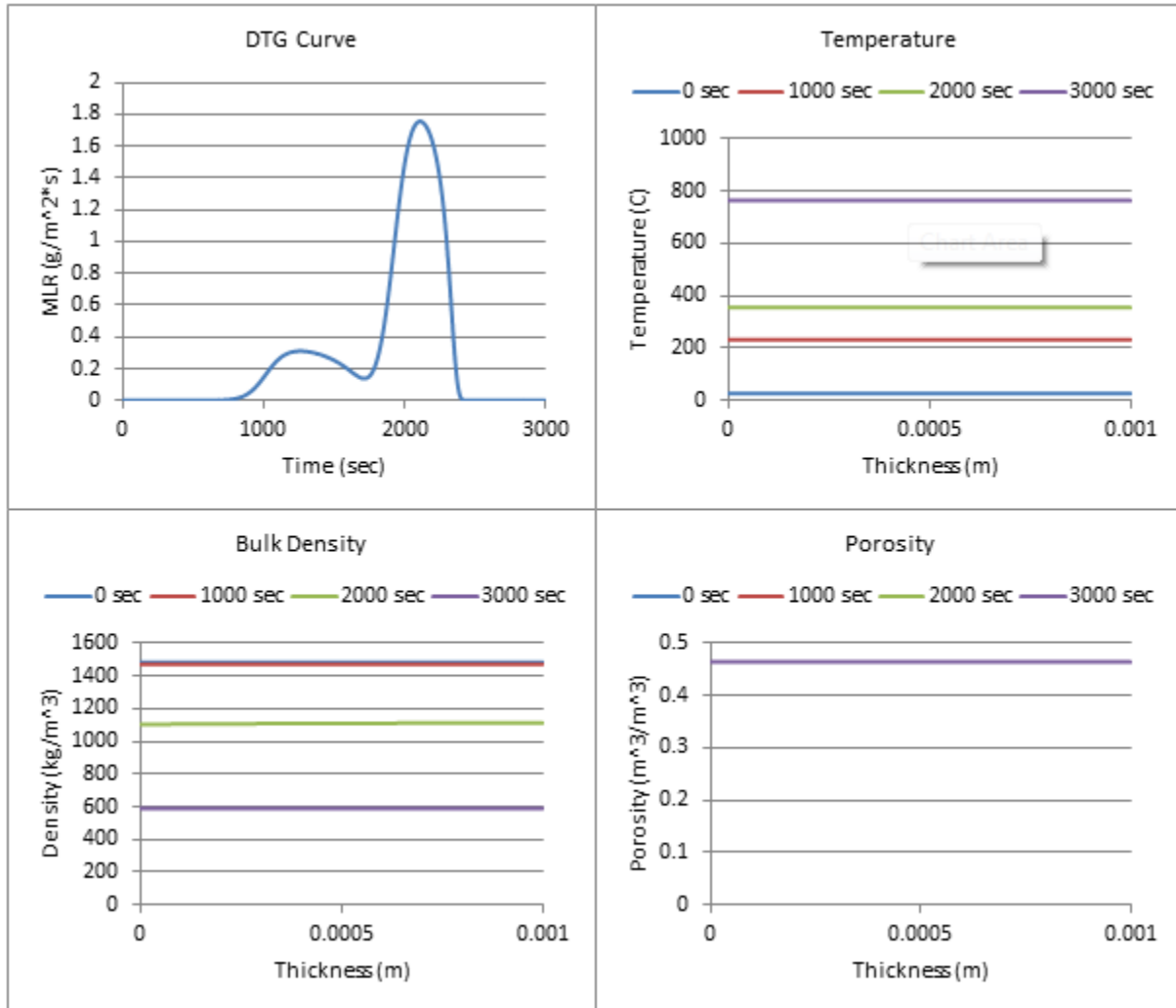
Figure 213: Profiles (500 W/m^2, 40% ATH)
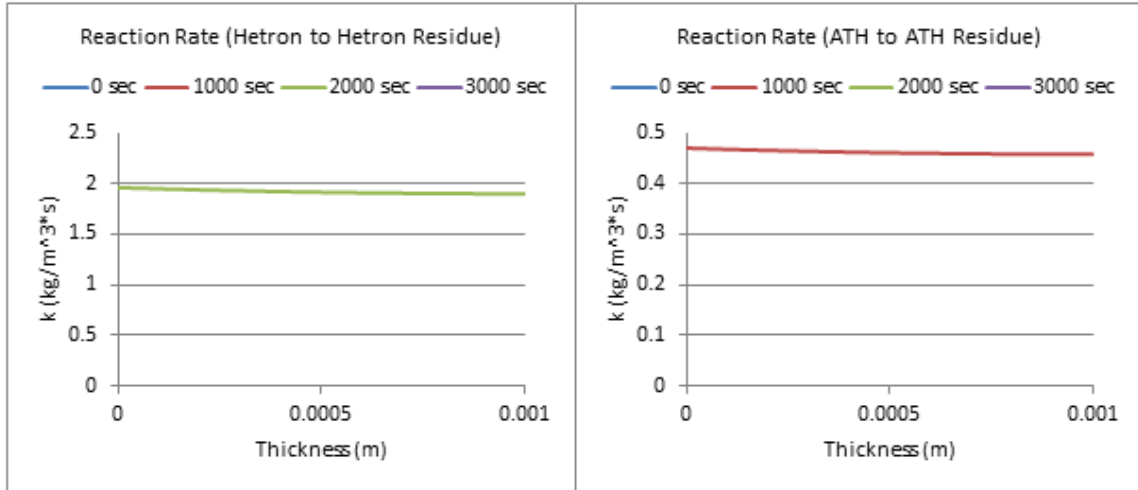
Figure 214: Reaction Rate Profiles (500 W/m^2, 40% ATH)
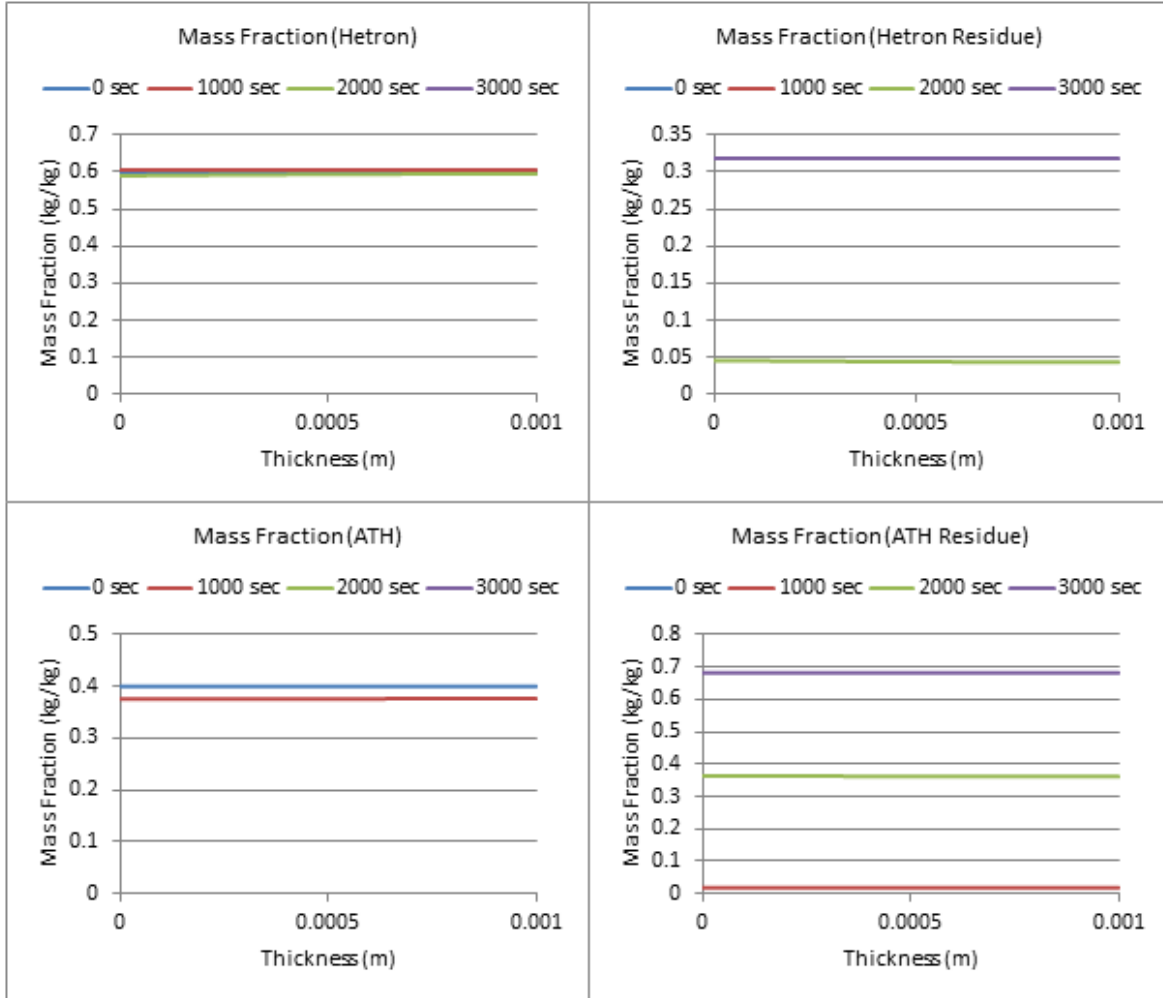
Figure 215: Mass Fraction Profiles (500 W/m^2, 40% ATH)

40% ATH, qe= 600 W/m^2
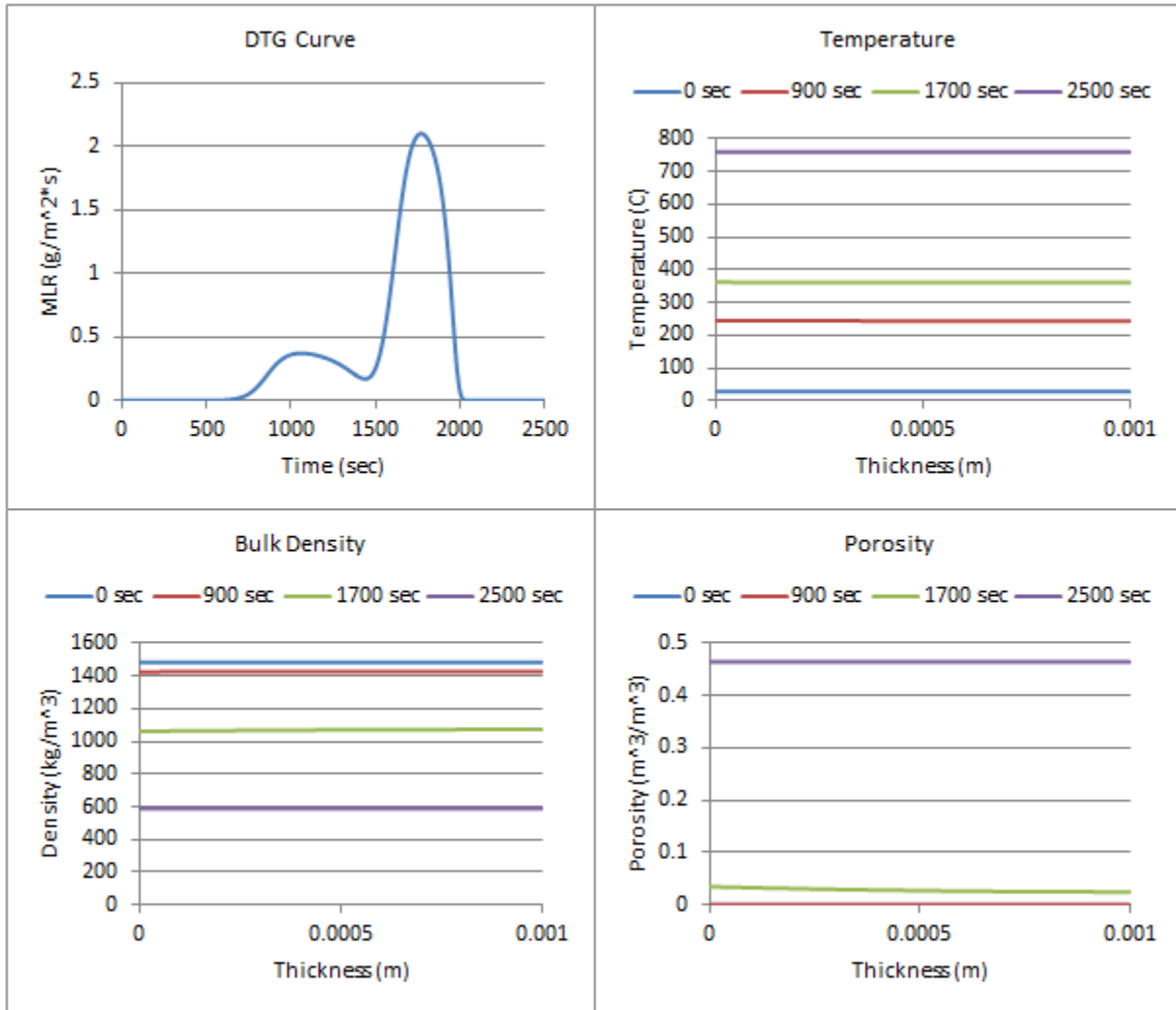
Figure 216: Profiles (600 W/m^2, 40% ATH)
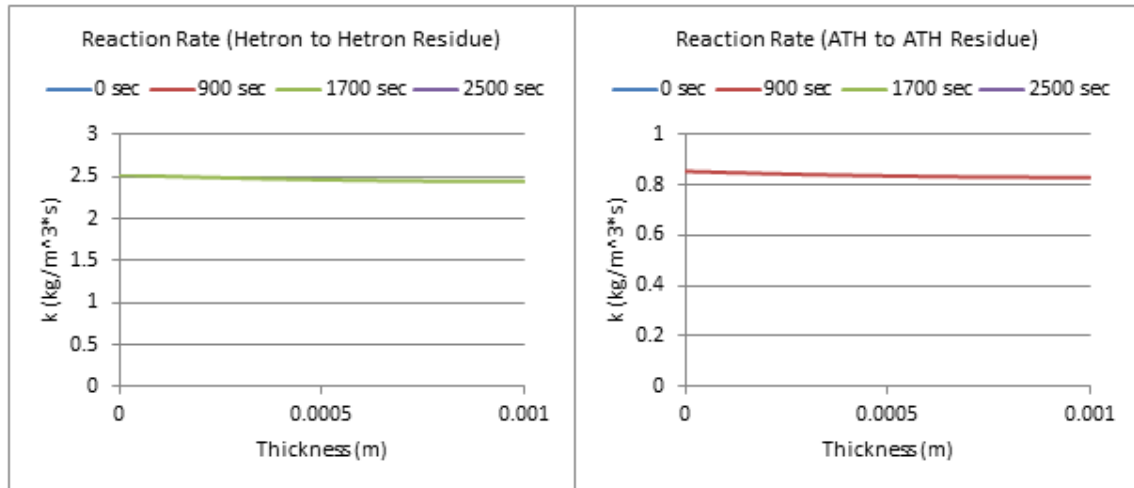
Figure 217: Reaction Rate Profiles (600 W/m^2, 40% ATH)
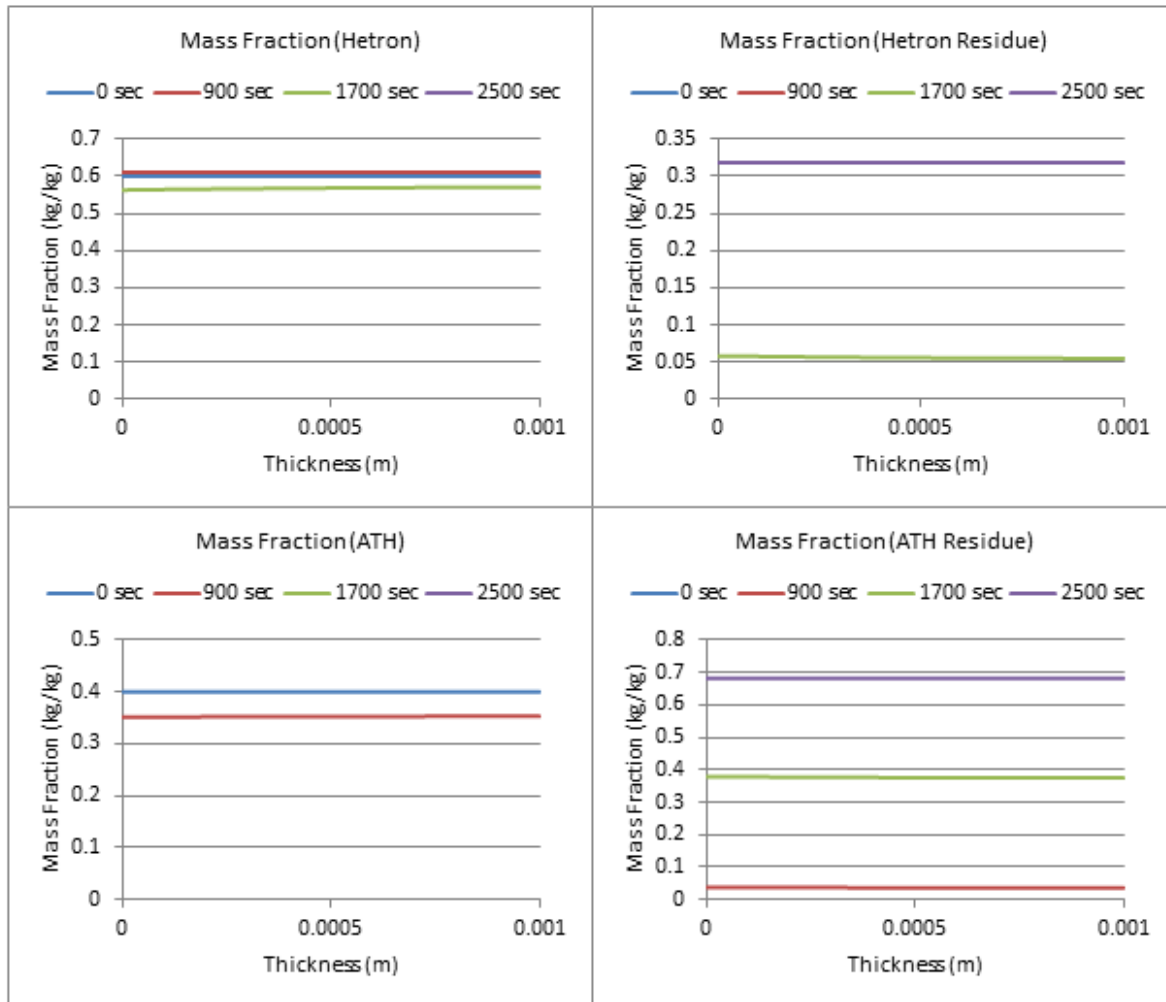
Figure 218: Mass Fraction Profiles (600 W/m^2, 40% ATH)

40% ATH, qe=700 W/m^2
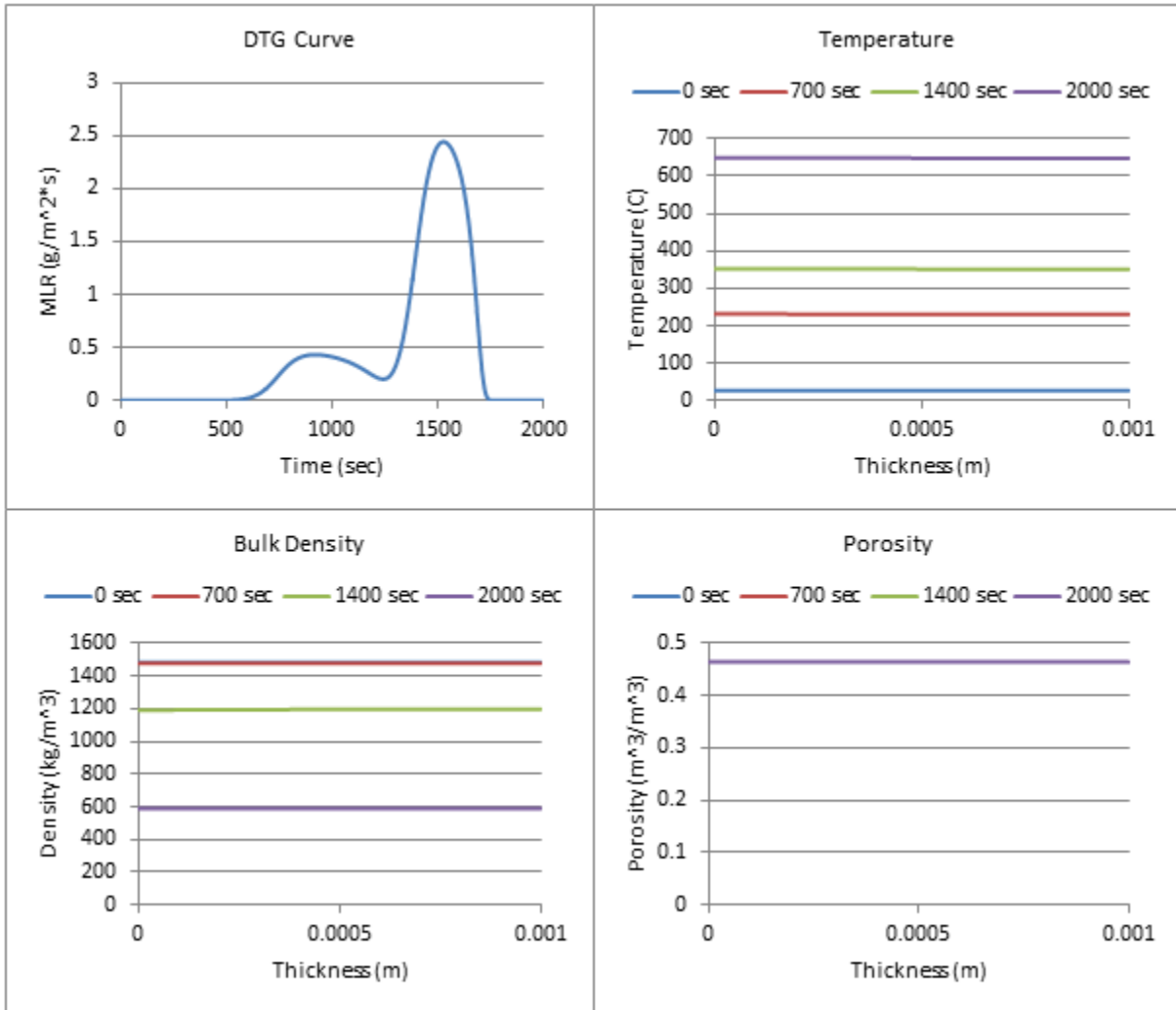
Figure 219: Profiles (700 W/m^2, 40% ATH)
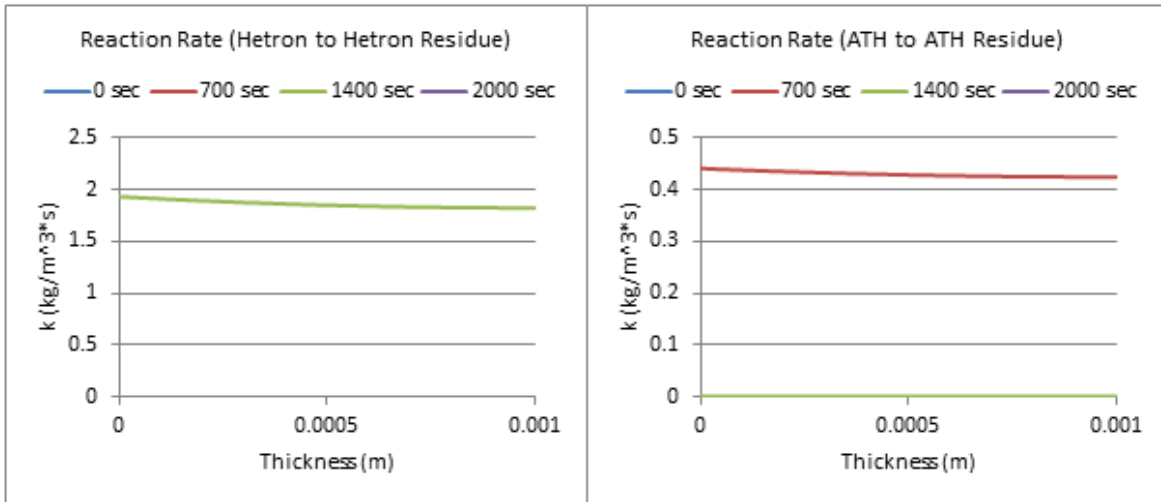
Figure 220: Reaction Rate Profiles (700 W/m^2, 40% ATH)
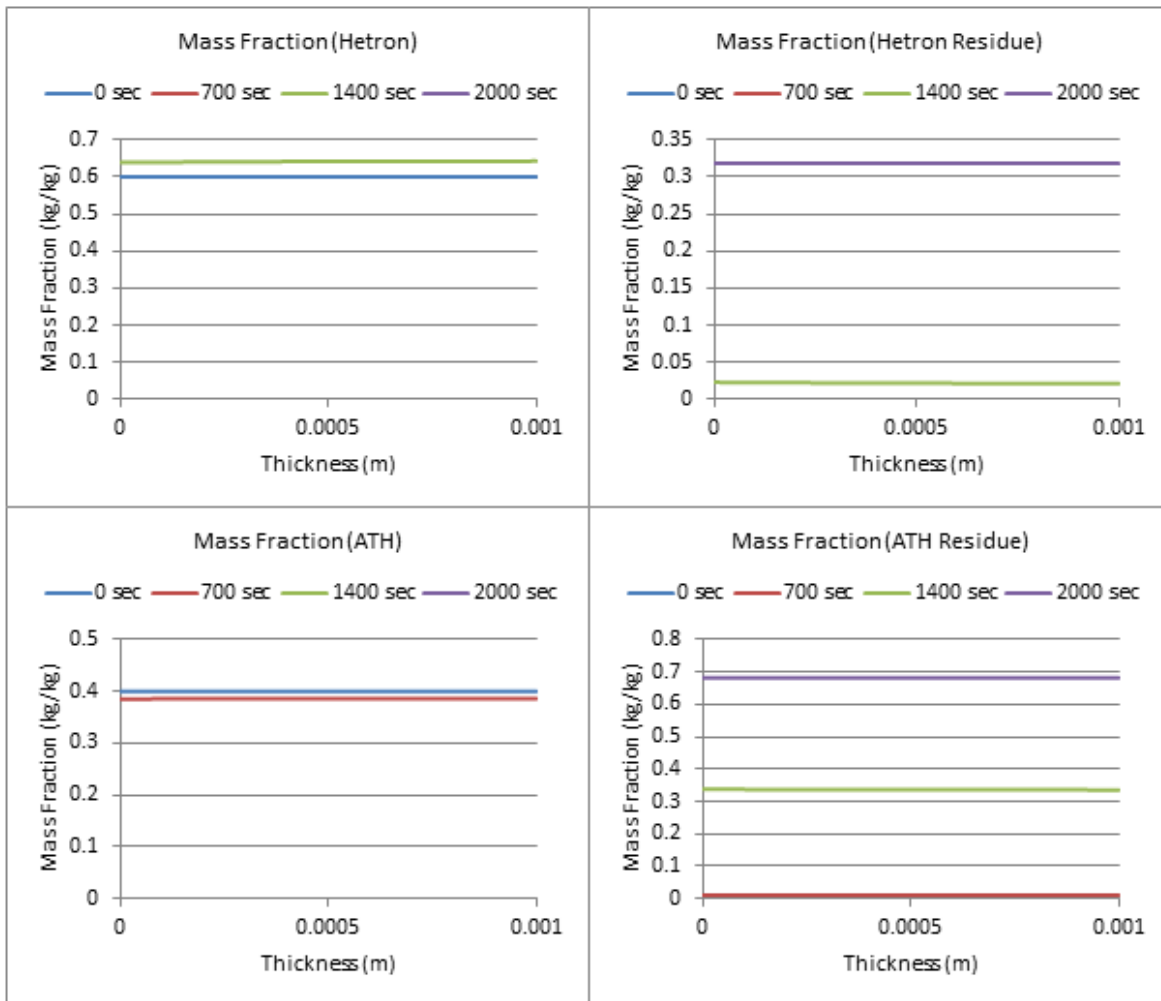
Figure 221: Mass Fraction Profiles (700 W/m^2, 40% ATH)

40% ATH, qe=800 W/m^2
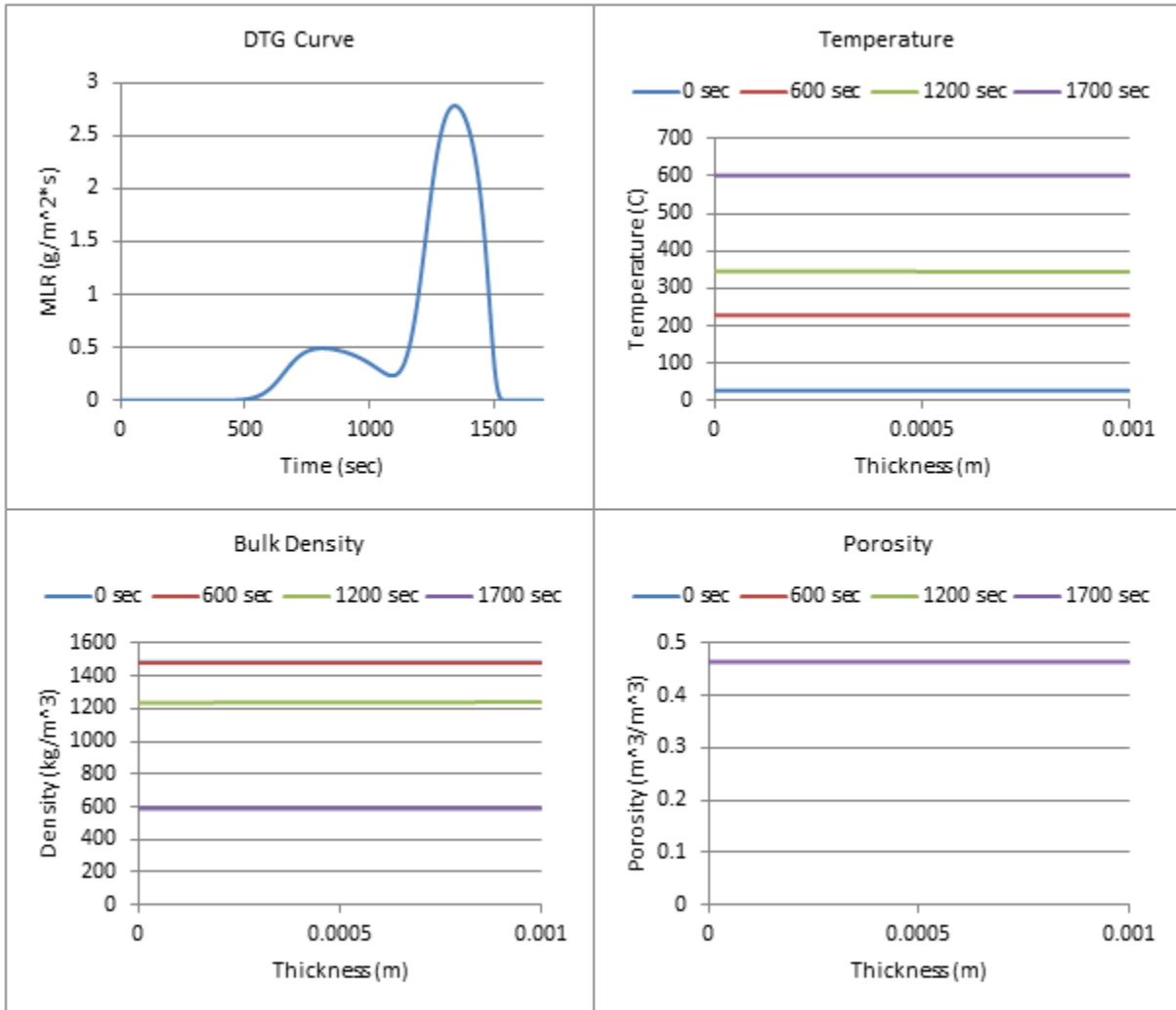
Figure 222: Profiles (800 W/m^2, 40% ATH)
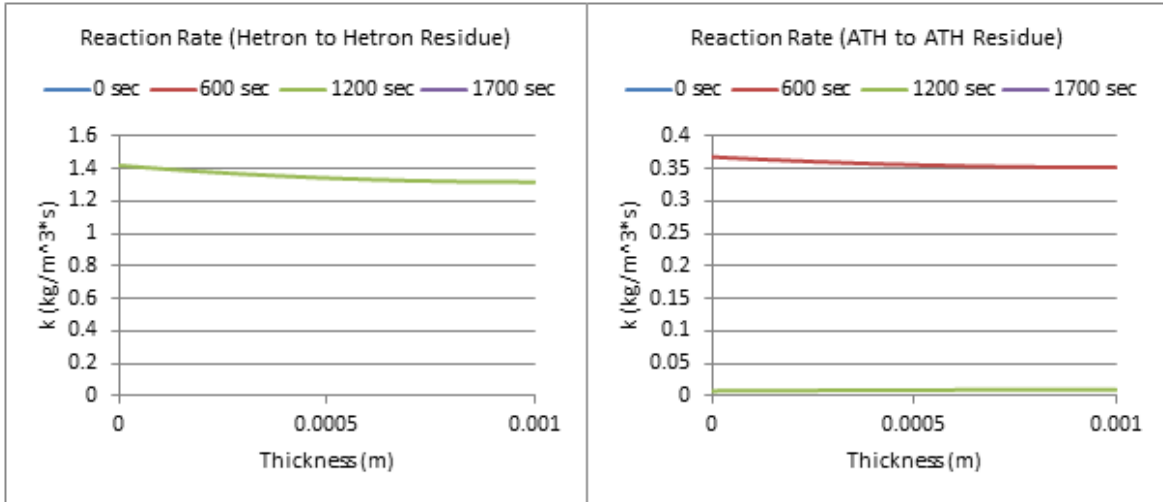
Figure 223: Reaction Rate Profiles (800 W/m^2, 40% ATH)
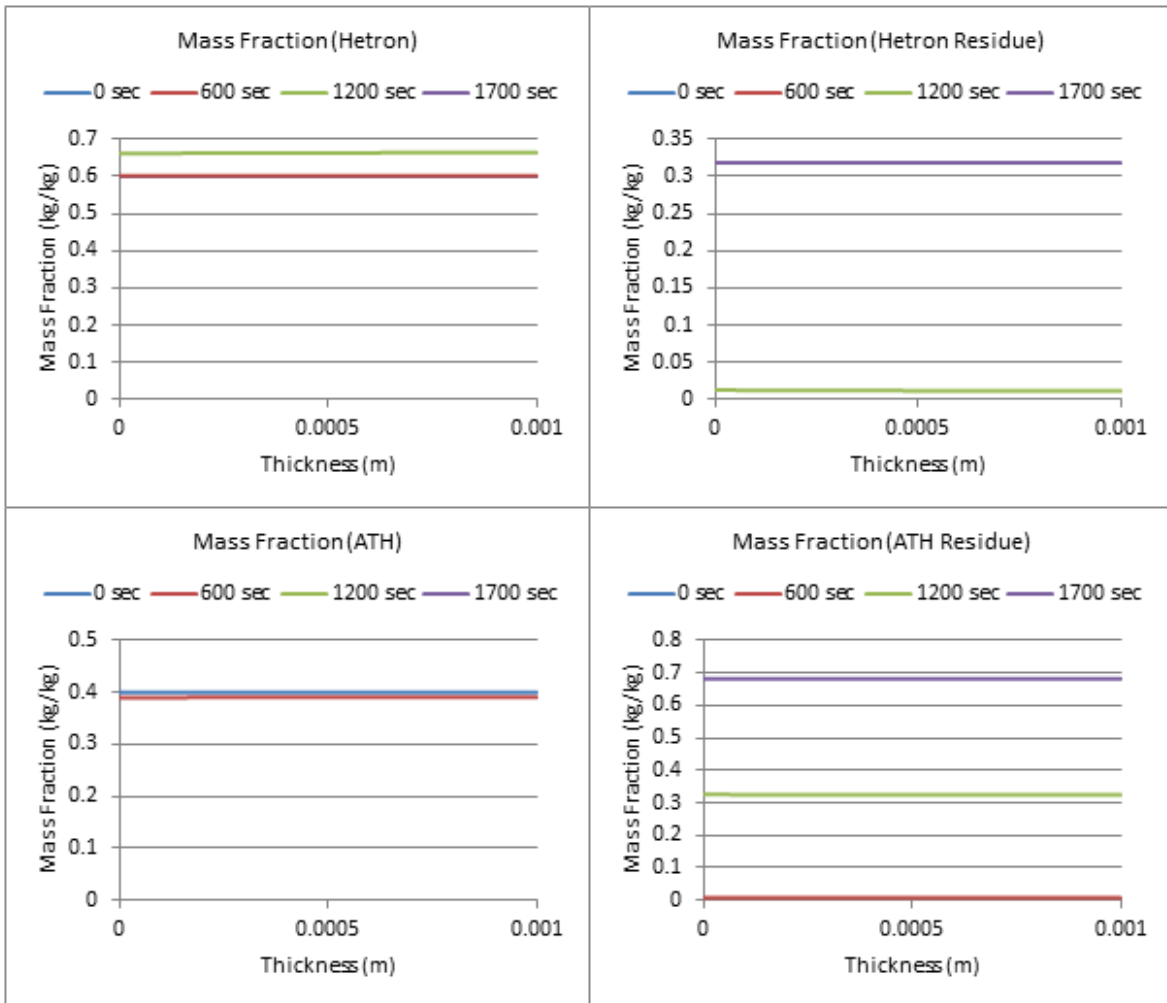
Figure 224: Mass Fraction Profiles (800 W/m^2, 40% ATH)

50% ATH, qe=100 W/m^2
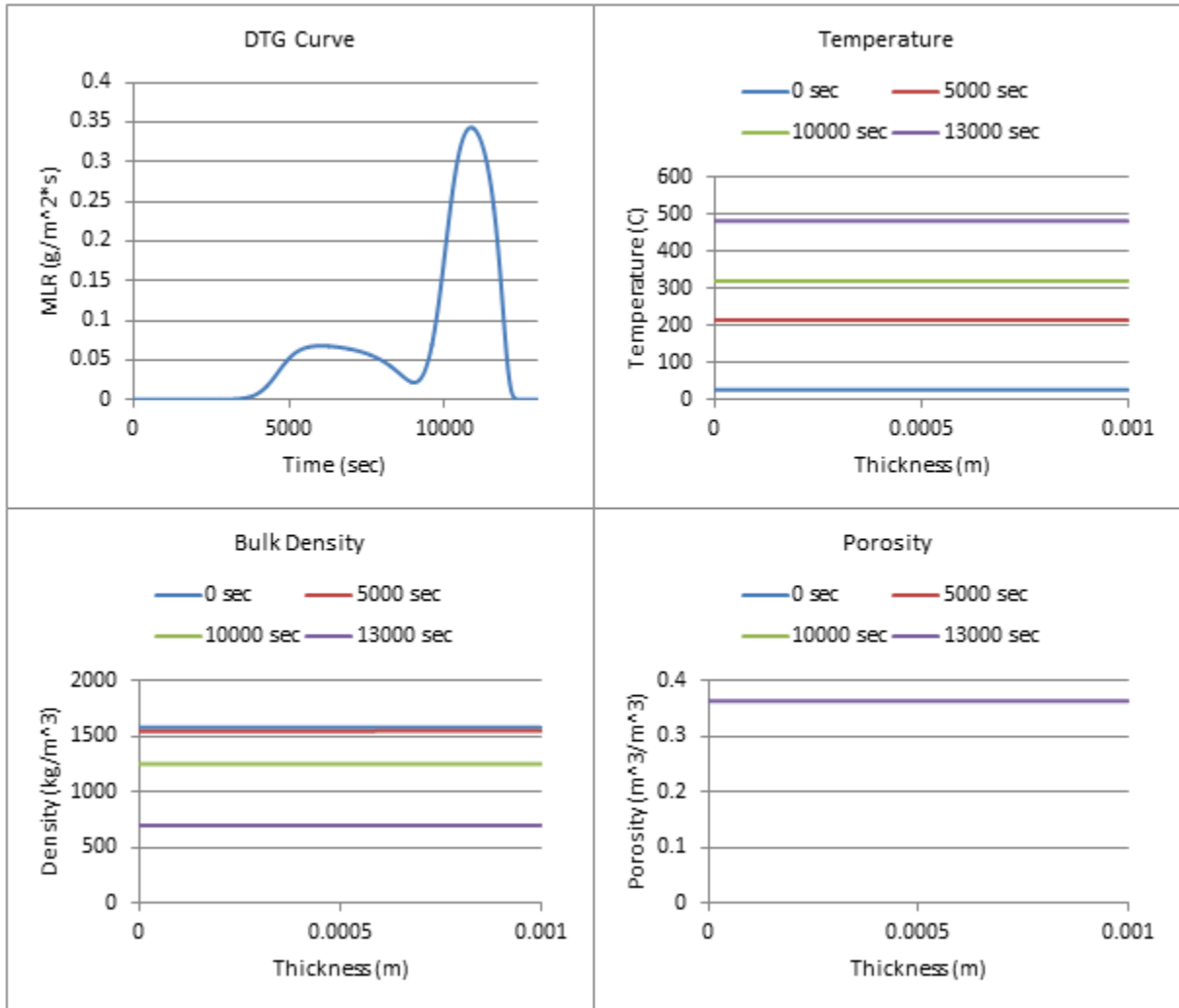
Figure 225: Profiles (100 W/m^2, 50% ATH)
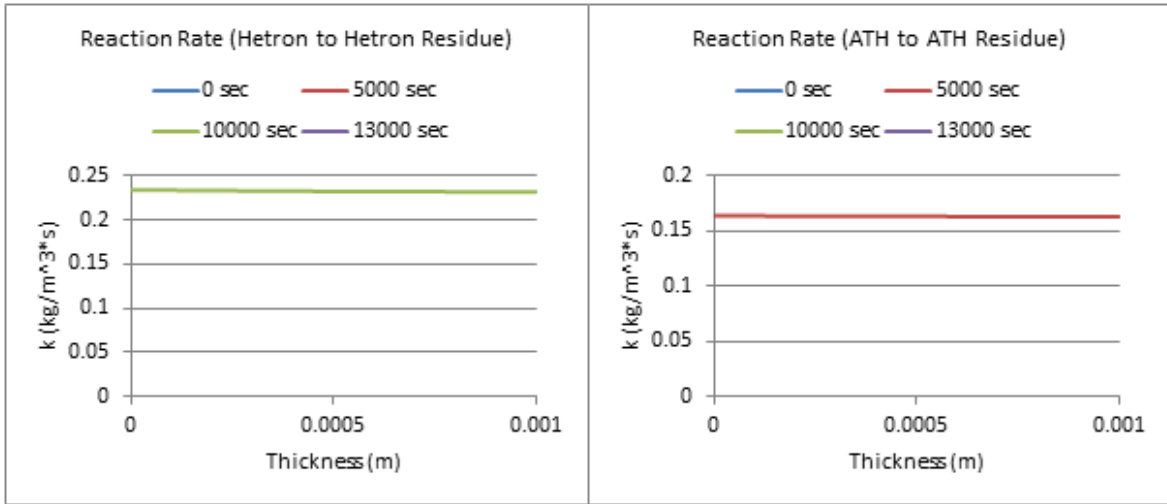
Figure 226: Reaction Rate Profiles (100 W/m^2, 50% ATH)
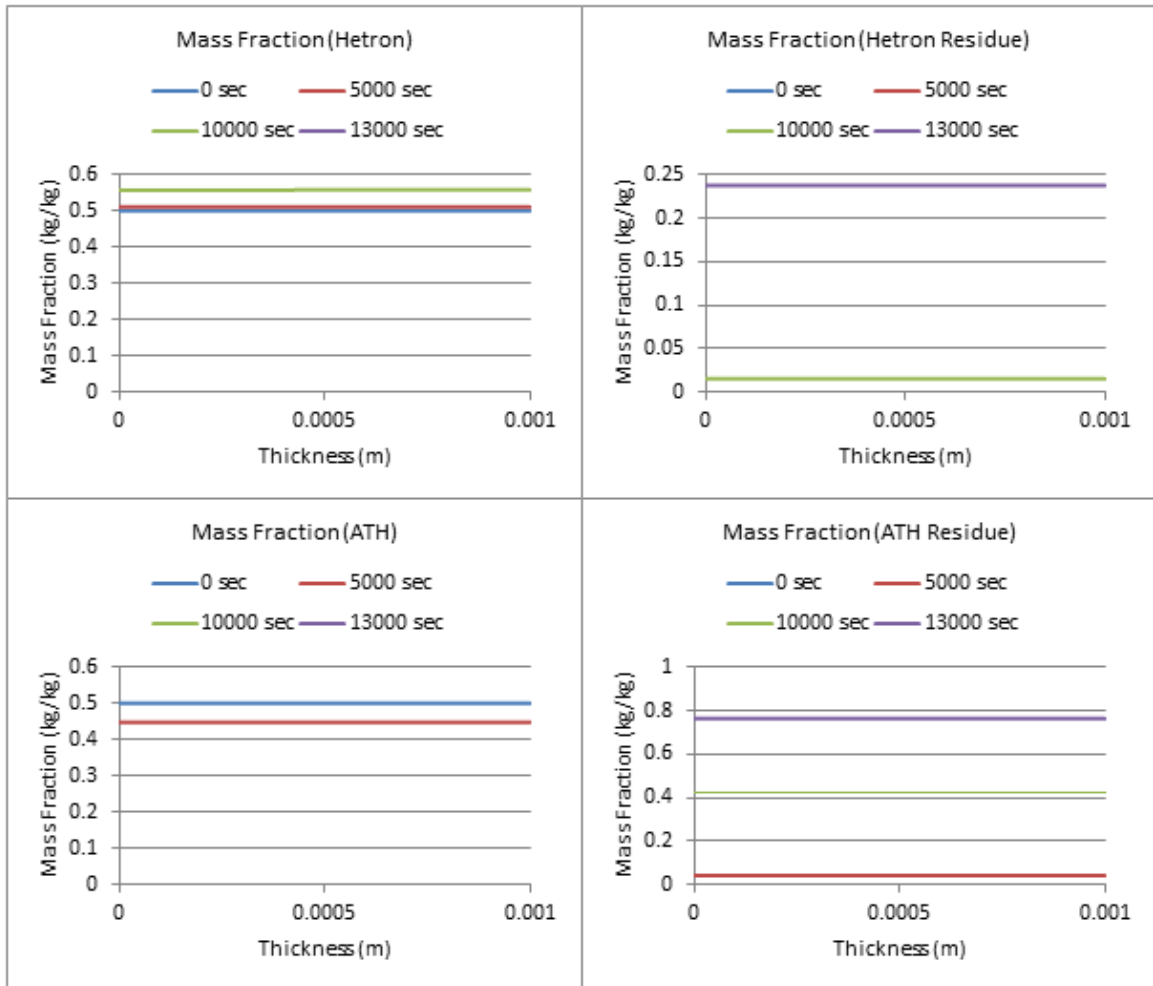
Figure 227: Mass Fraction Profiles (100 W/m^2, 50% ATH)

50% ATH, qe= 200 W/m^2
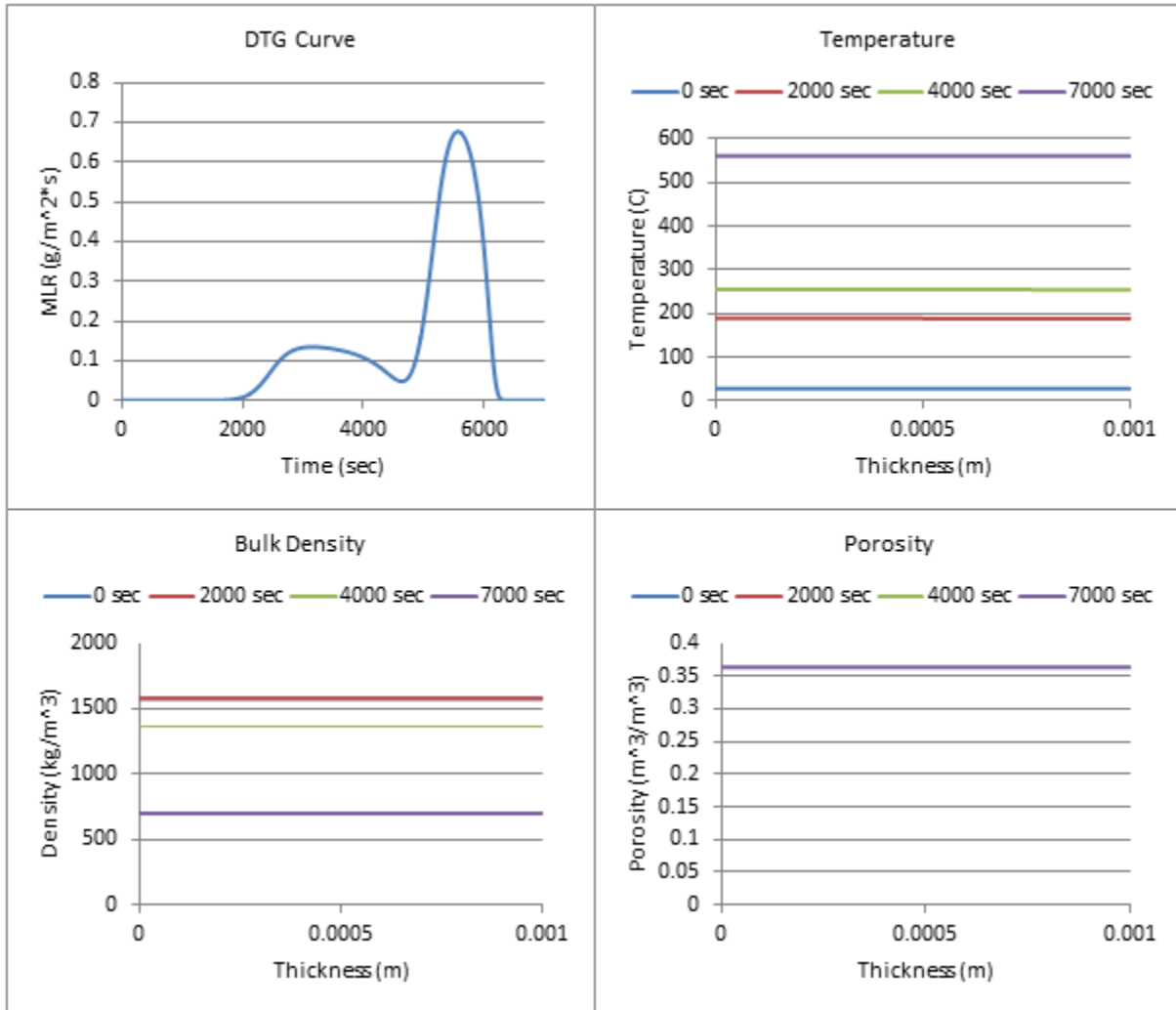
Figure 228: Profiles (200 W/m^2, 50% ATH)
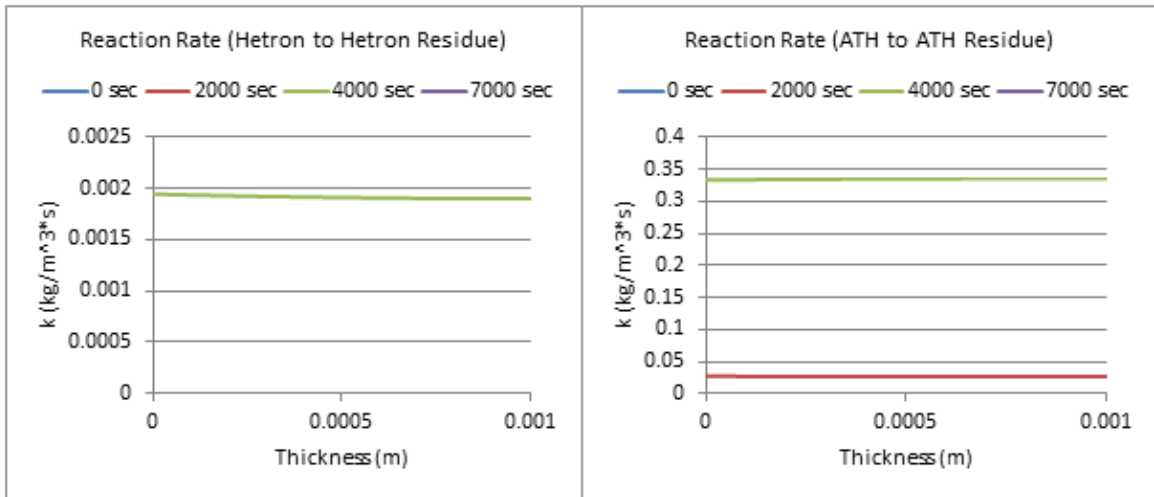
Figure 229: Reaction Rate Profiles (200 W/m^2, 50% ATH)
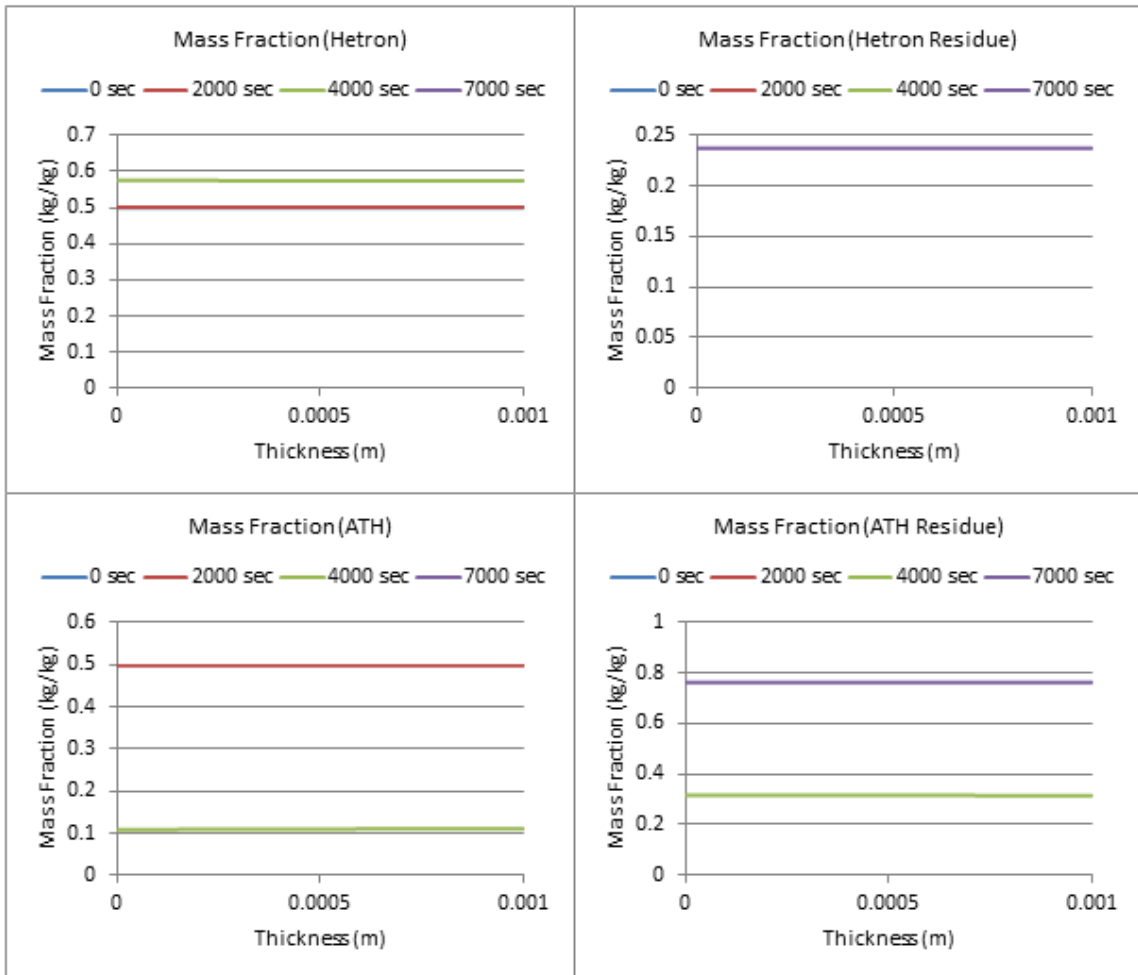
Figure 230: Mass Fraction Profiles (200 W/m^2, 50% ATH)

50% ATH, qe= 300 W/m^2
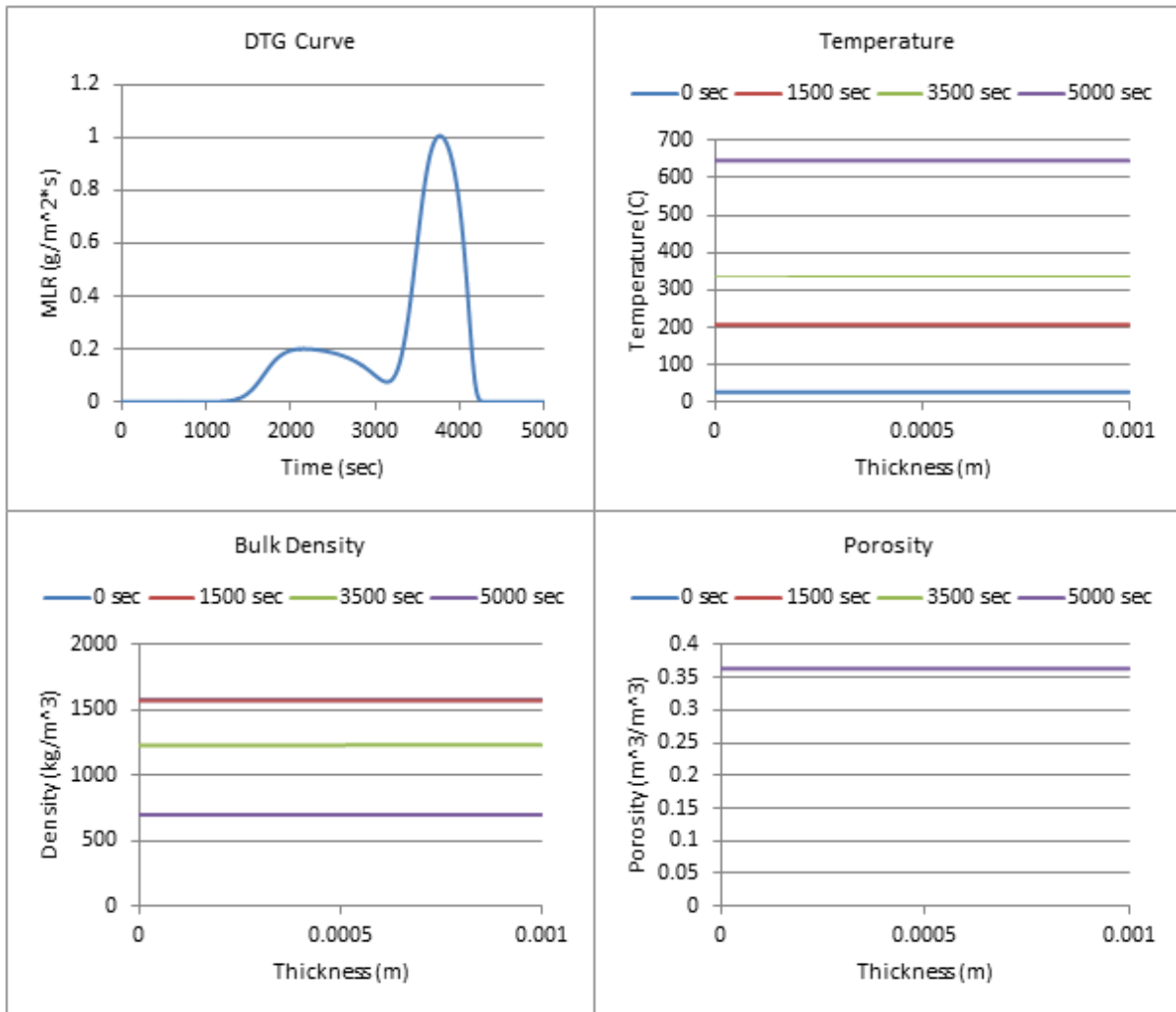
Figure 231: Profiles (300 W/m^2, 50% ATH)
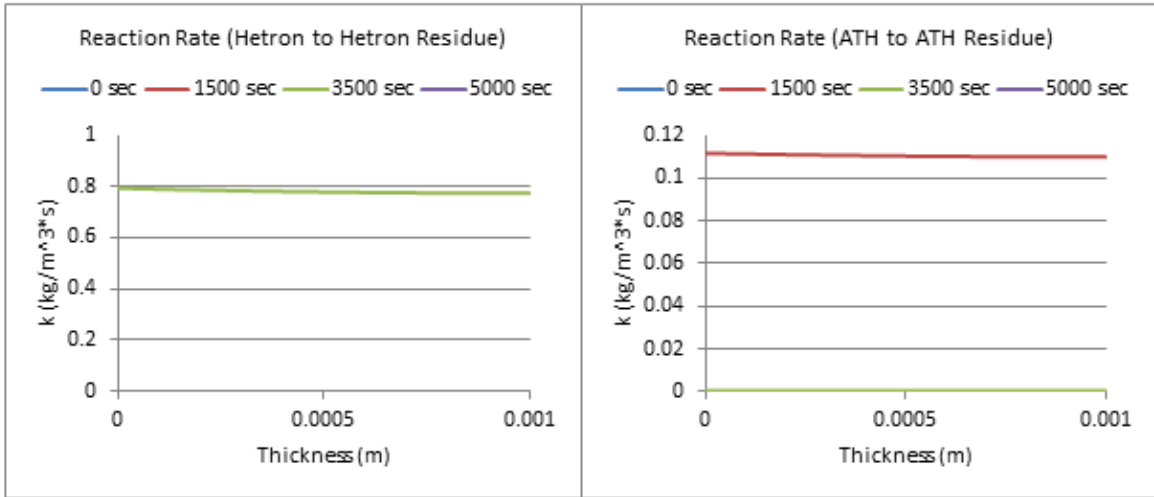
Figure 232: Reaction Rate Profiles (300 W/m^2, 50% ATH)
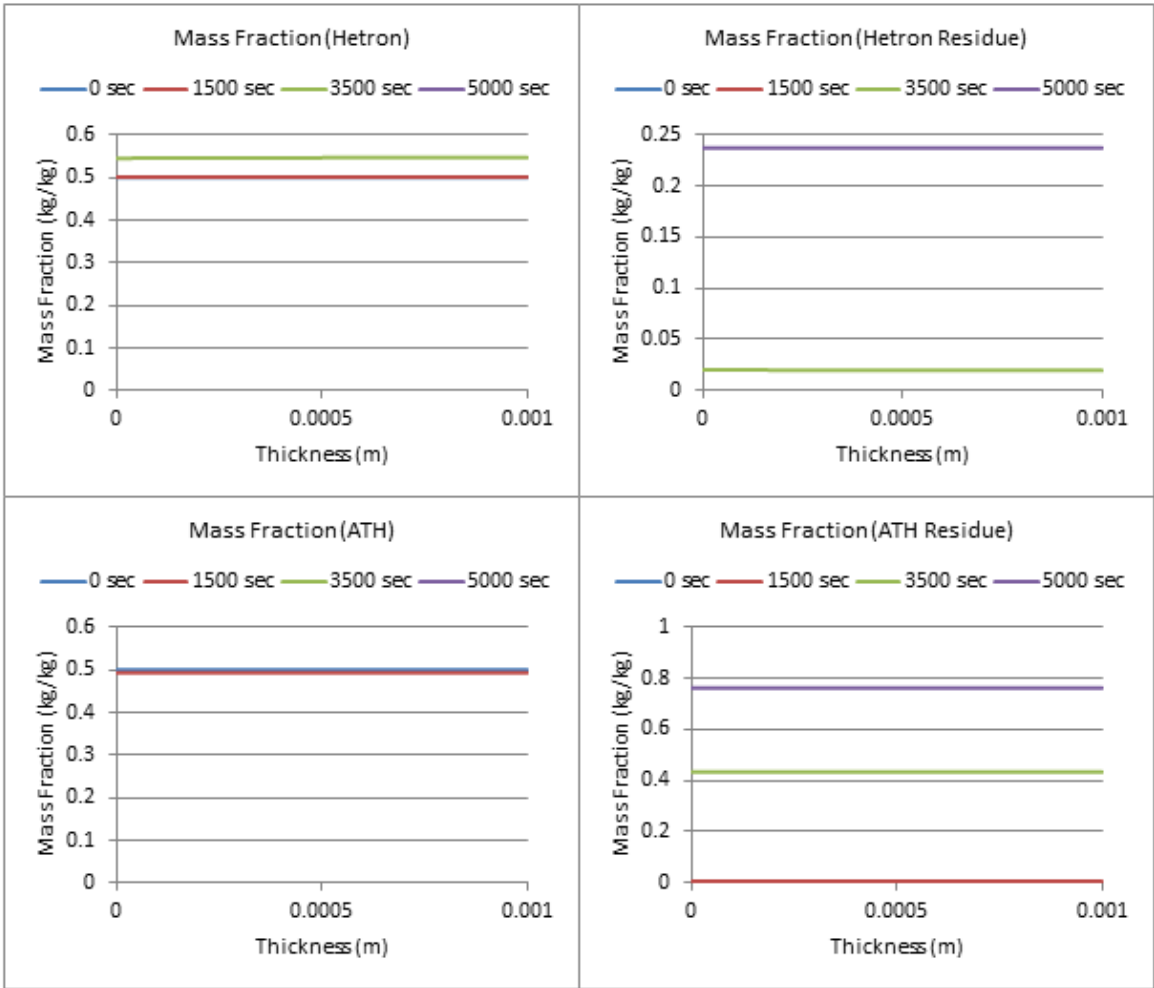
Figure 233: Mass Fraction Profiles (300 W/m^2, 50% ATH)

50% ATH, qe= 400 W/m^2
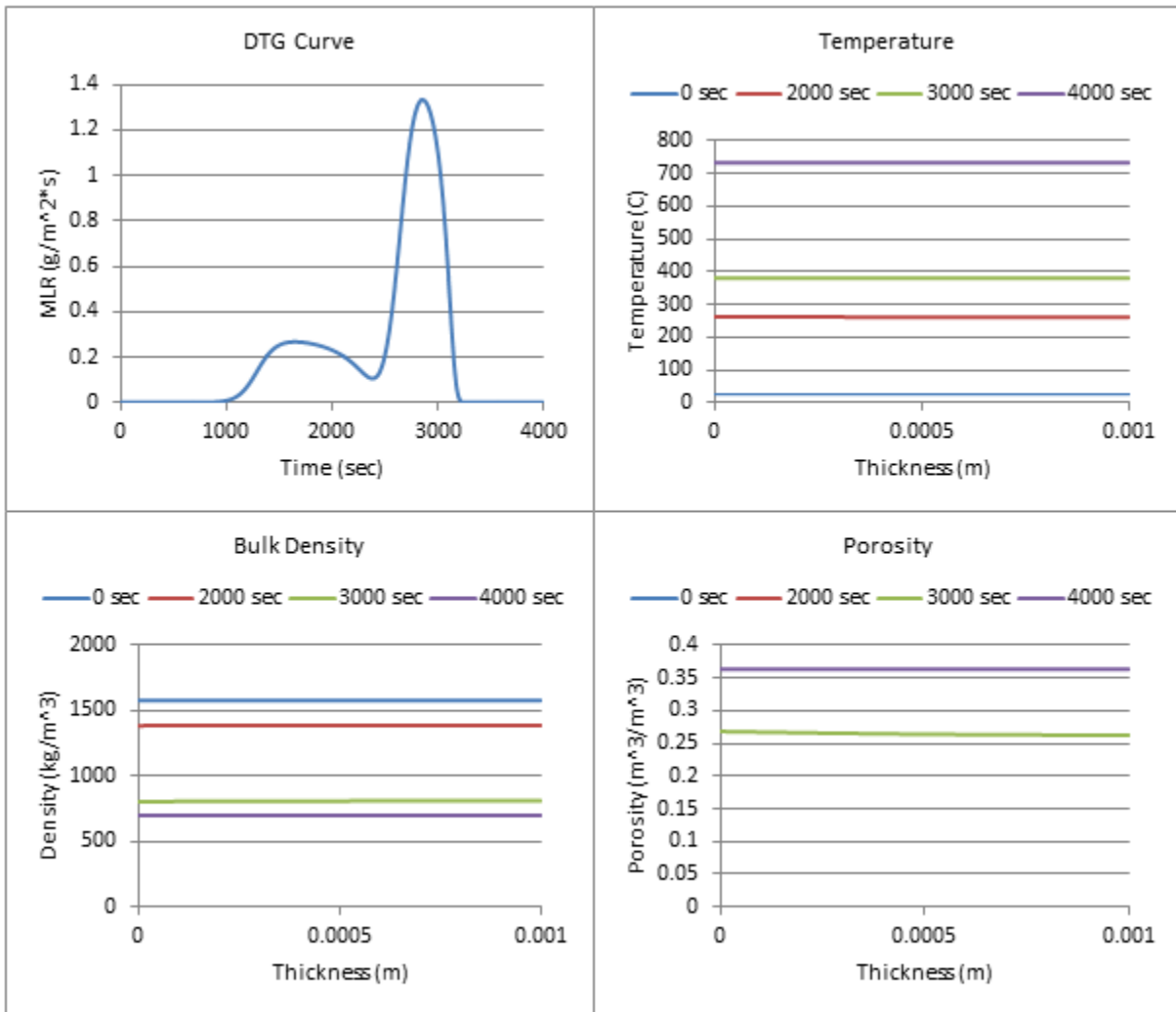
Figure 234: Profiles (400 W/m^2, 50% ATH)
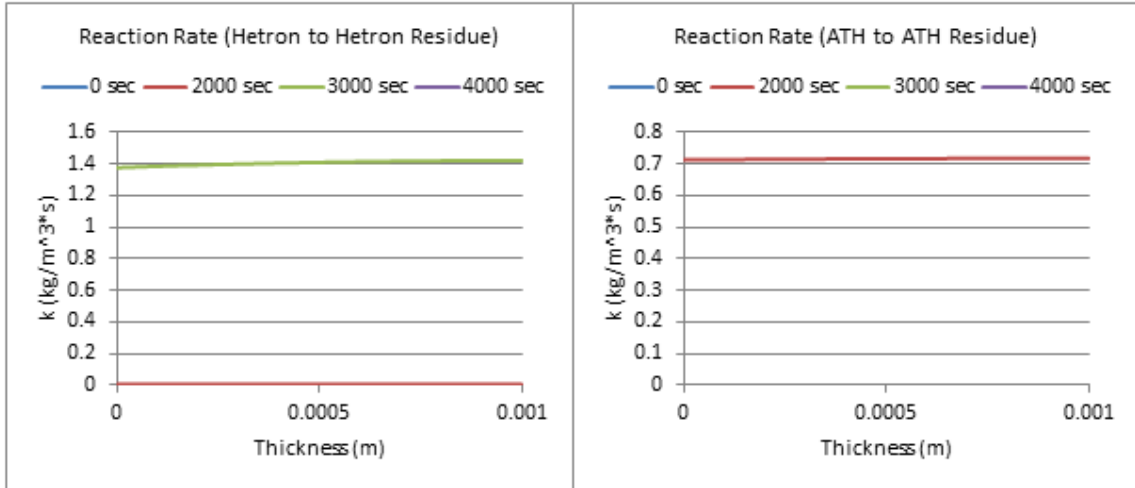
Figure 235: Reaction Rate Profiles (400 W/m^2, 50% ATH)
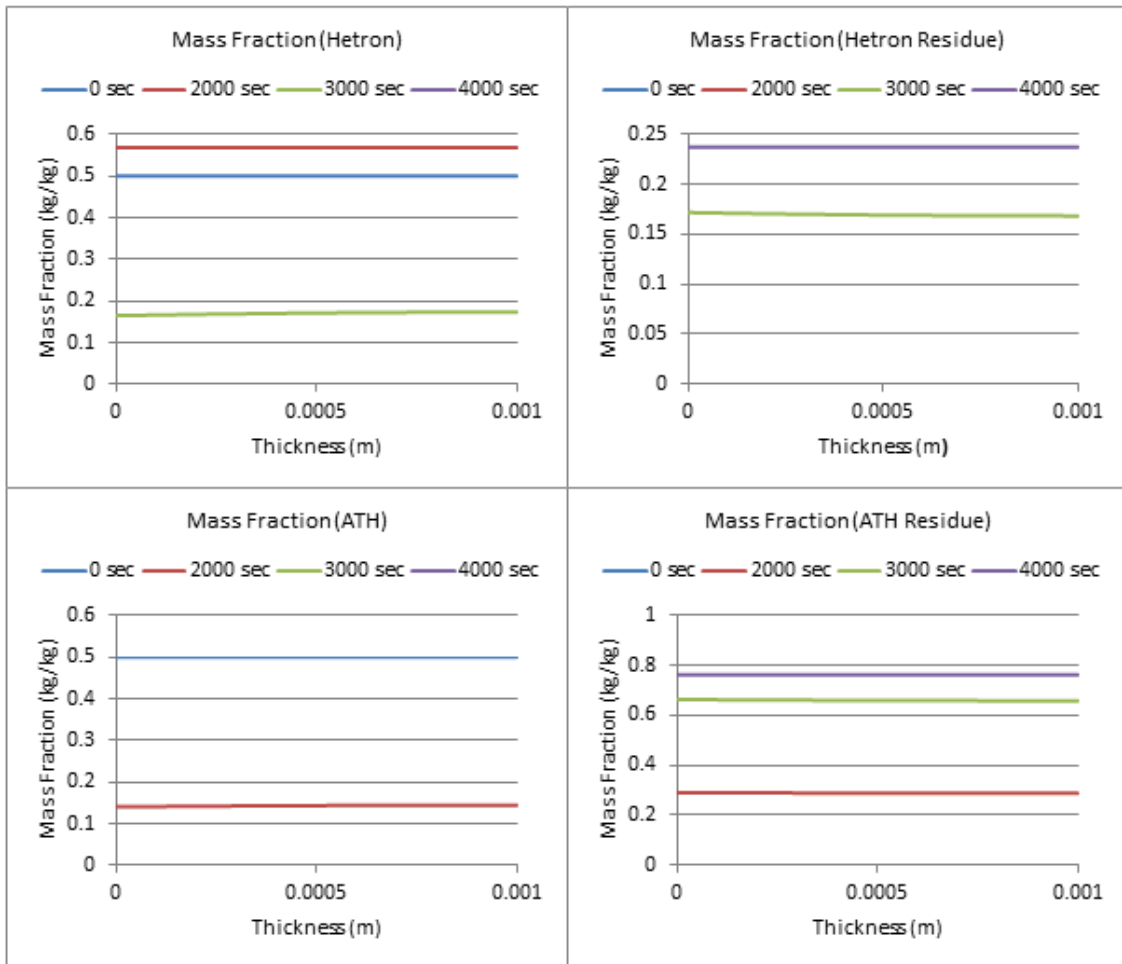
Figure 236: Mass Fraction Profiles (400 W/m^2, 50% ATH)

50% ATH, qe= 500 W/m^2
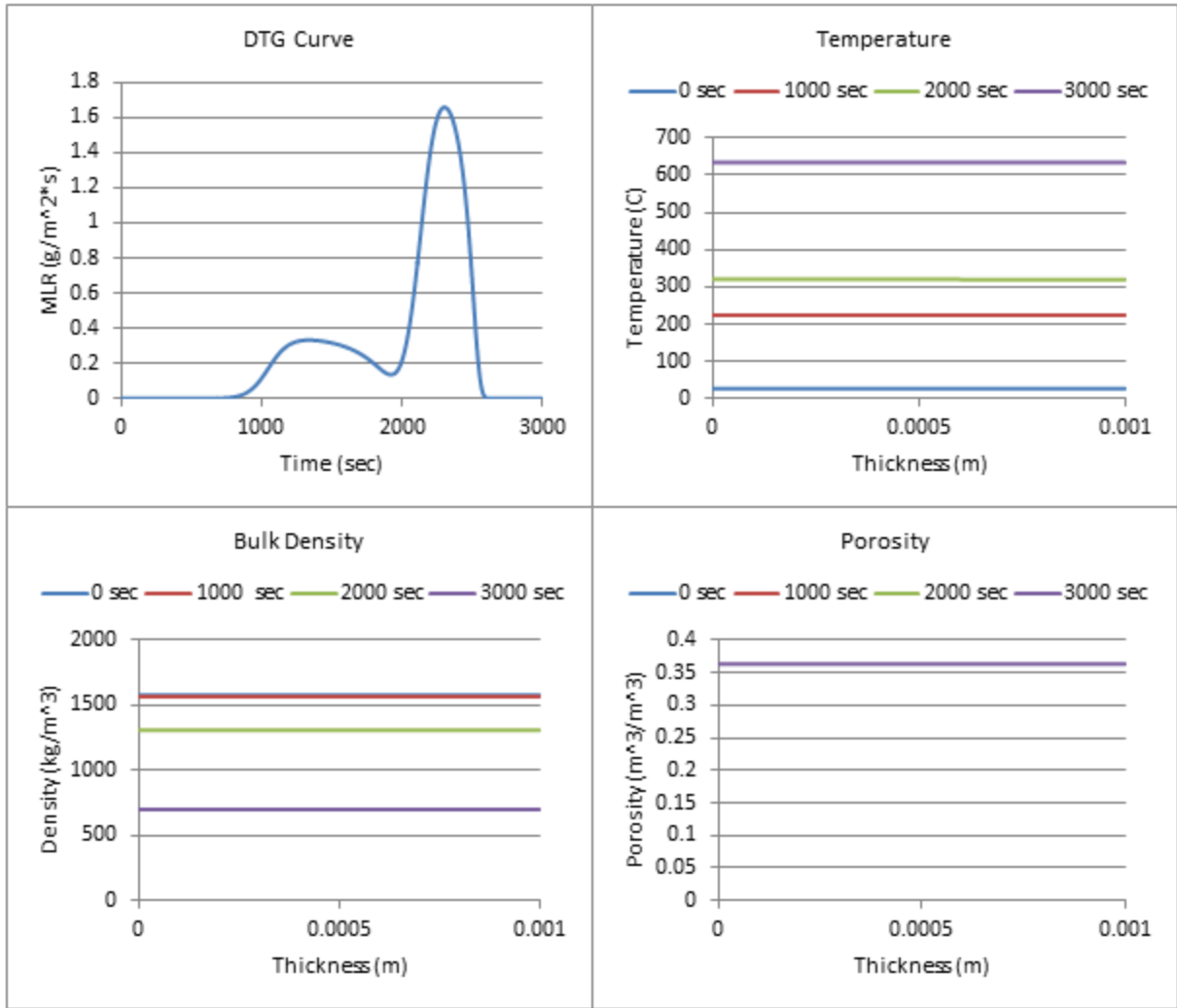
Figure 237: Profiles (500 W/m^2, 50% ATH)
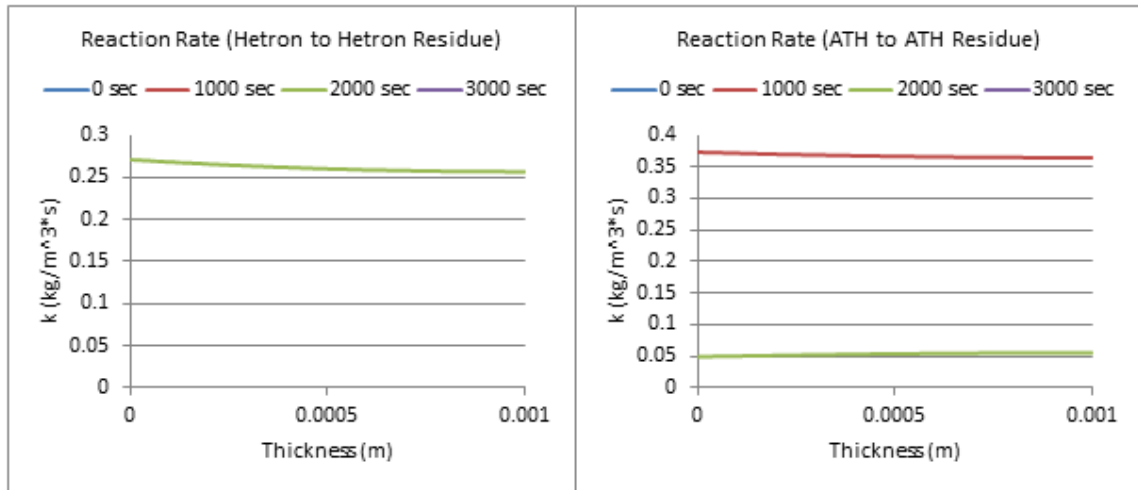
Figure 238: Reaction Rate Profiles (500 W/m^2, 50% ATH)
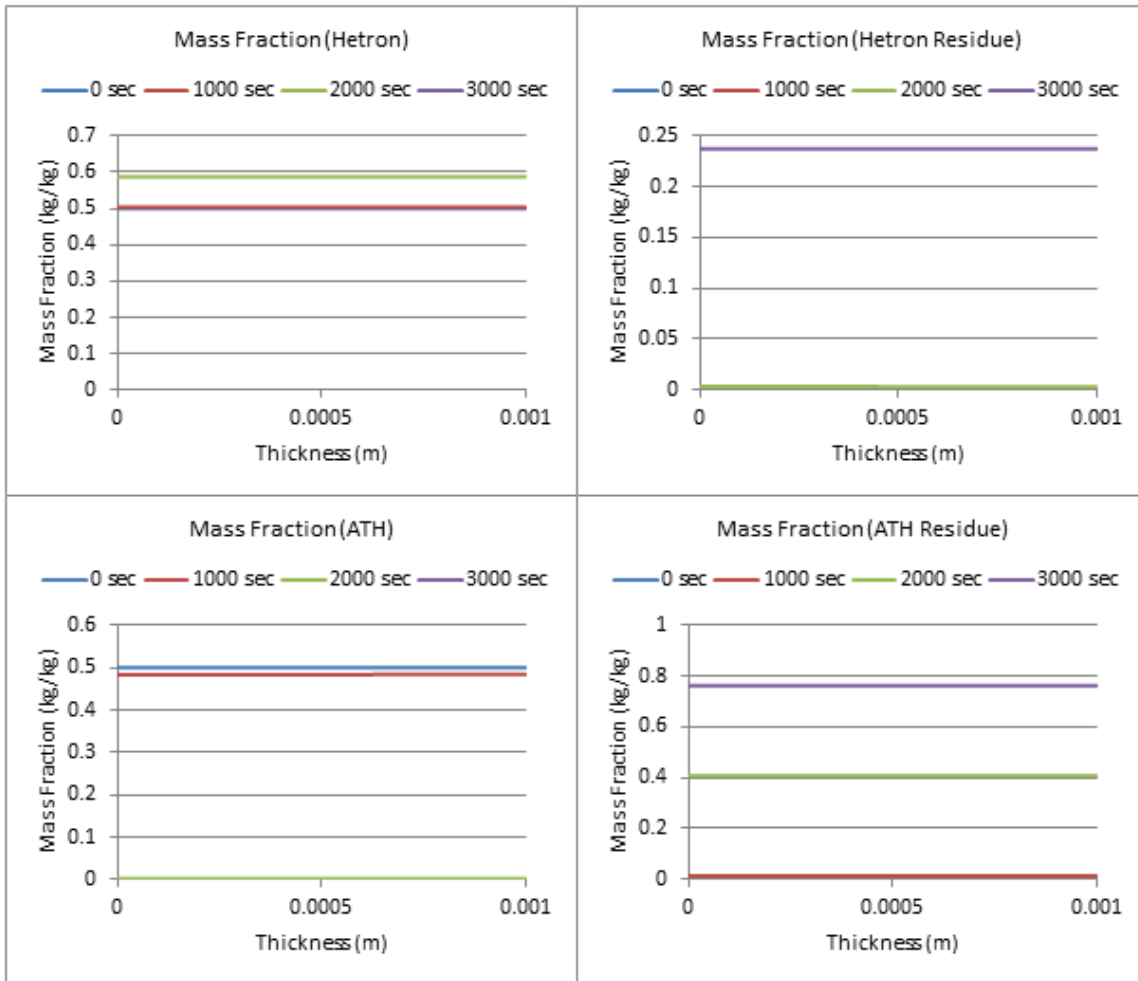
Figure 239: Mass Fraction Profiles (500 W/m^2, 50% ATH)

50% ATH, qe= 600 W/m^2
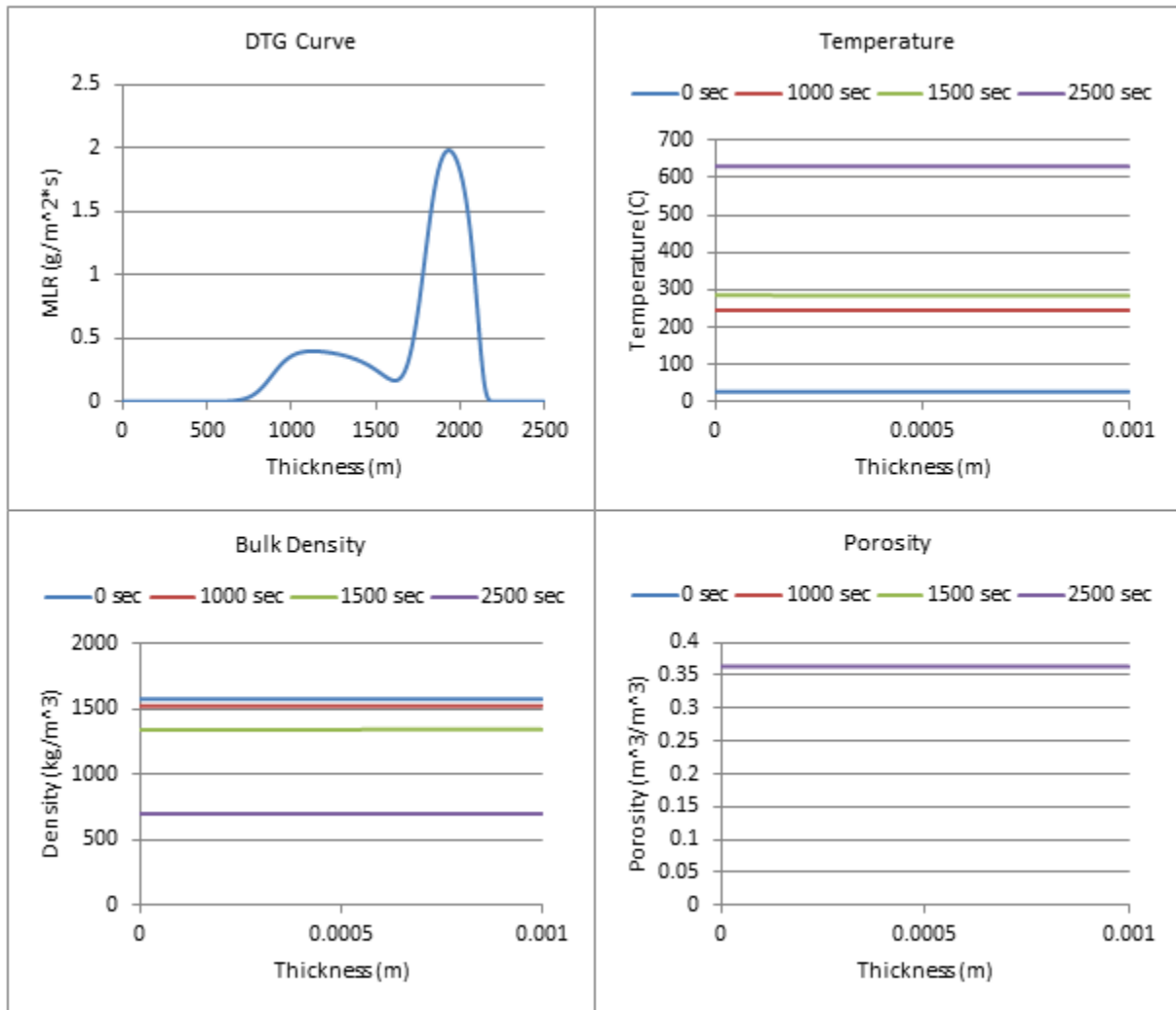
Figure 240: Profiles (600 W/m^2, 50% ATH)
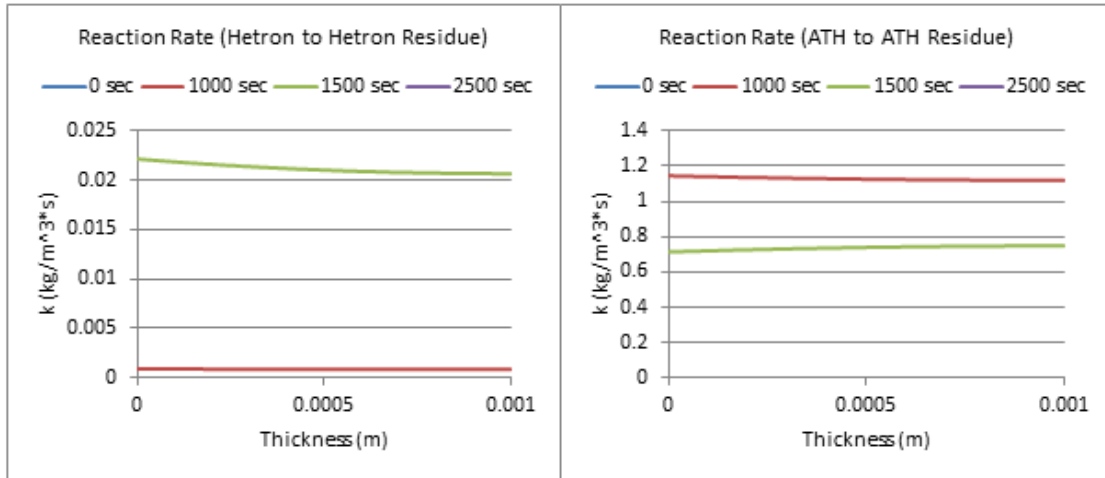
Figure 241: Reaction Rate Profiles (600 W/m^2, 50% ATH)
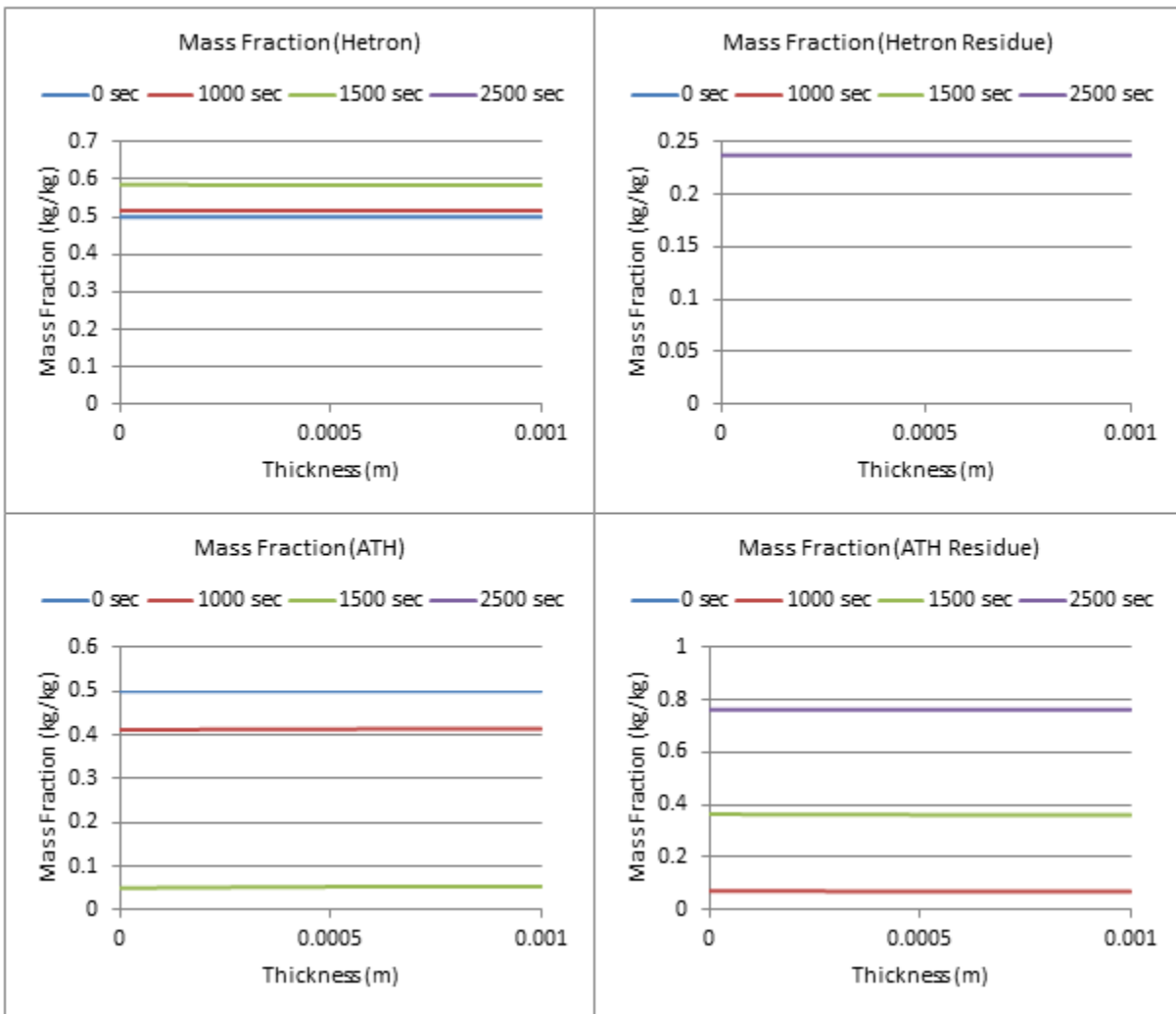
Figure 242: Mass Fraction Profiles (600 W/m^2, 50% ATH)

50% ATH, qe= 700 W/m^2
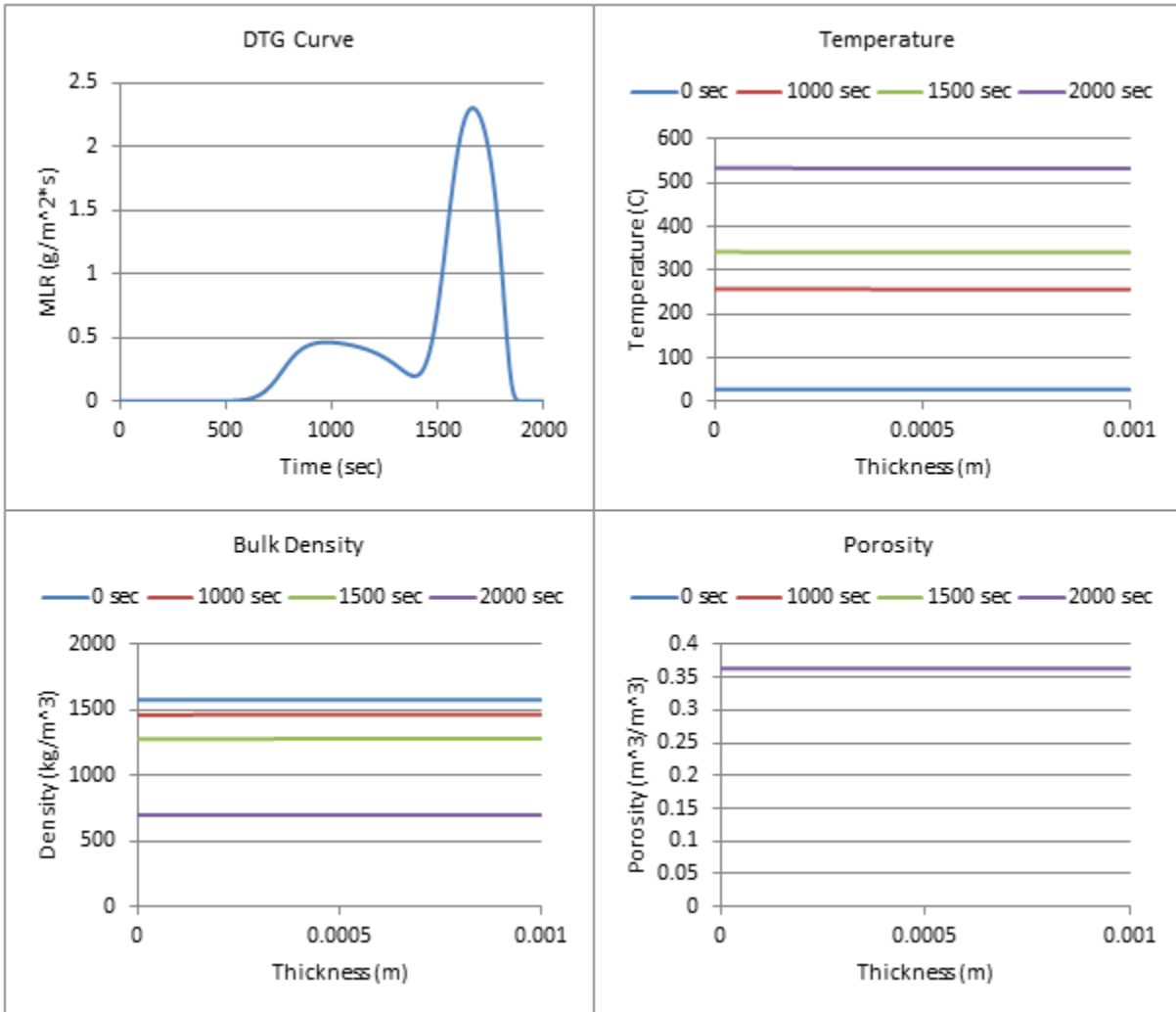
Figure 243: Profiles (700 W/m^2, 50% ATH)
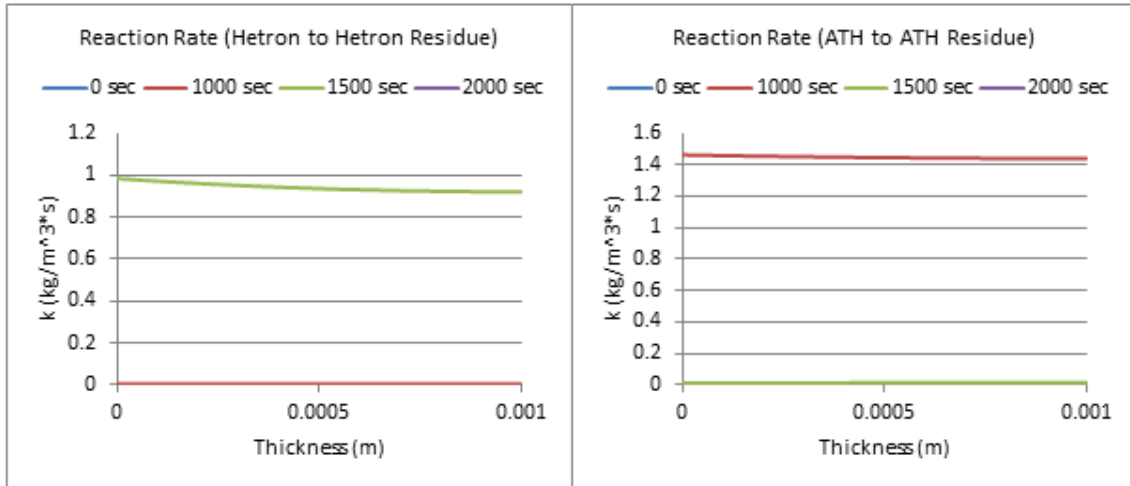
Figure 244: Reaction Rate Profiles (700 W/m^2, 50% ATH)
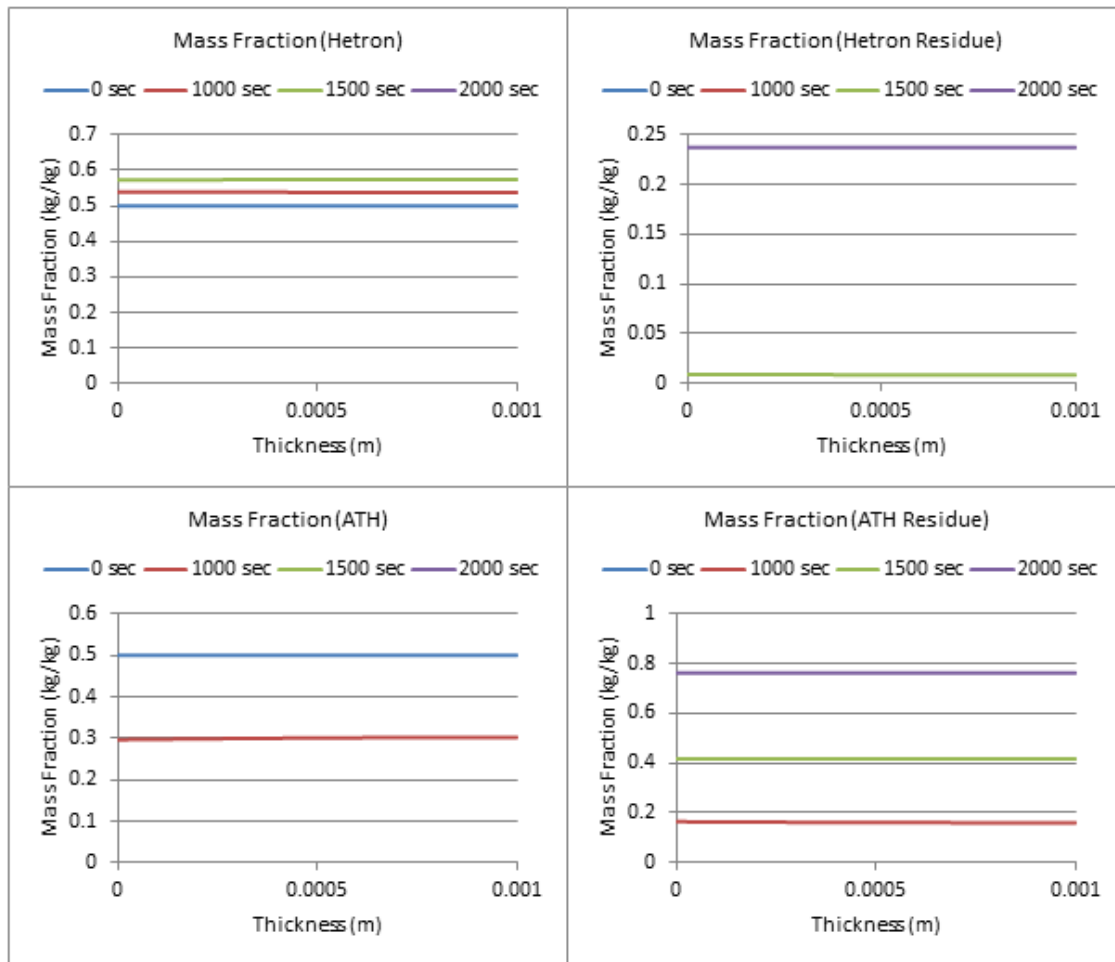
Figure 245: Mass Fraction Profiles (700 W/m^2, 50% ATH)

50% ATH, qe= 800 W/m^2
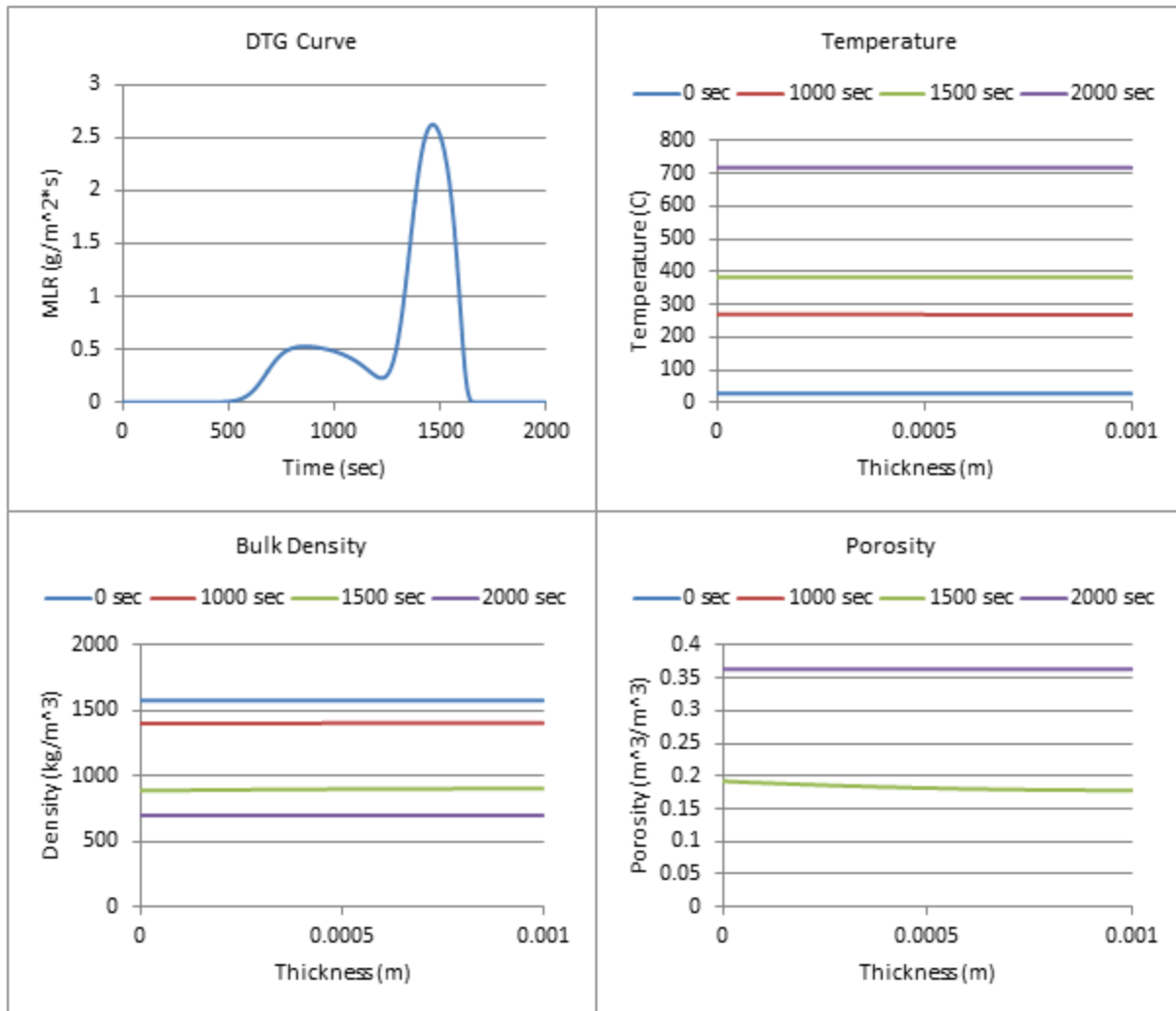
Figure 246: Profiles (800 W/m^2, 50% ATH)
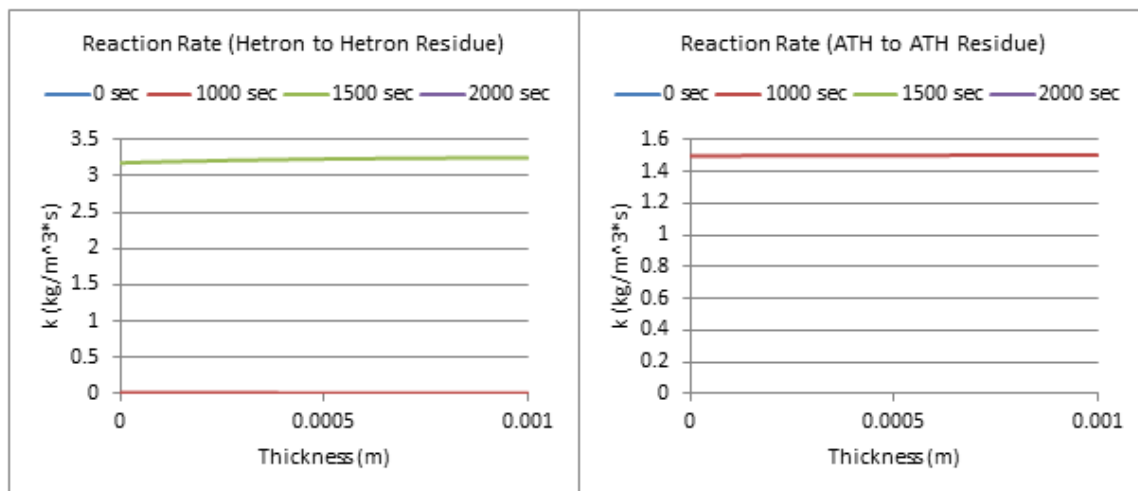
Figure 247: Reaction Rate Profiles (800 W/m^2, 50% ATH)

Page **223** of **324**
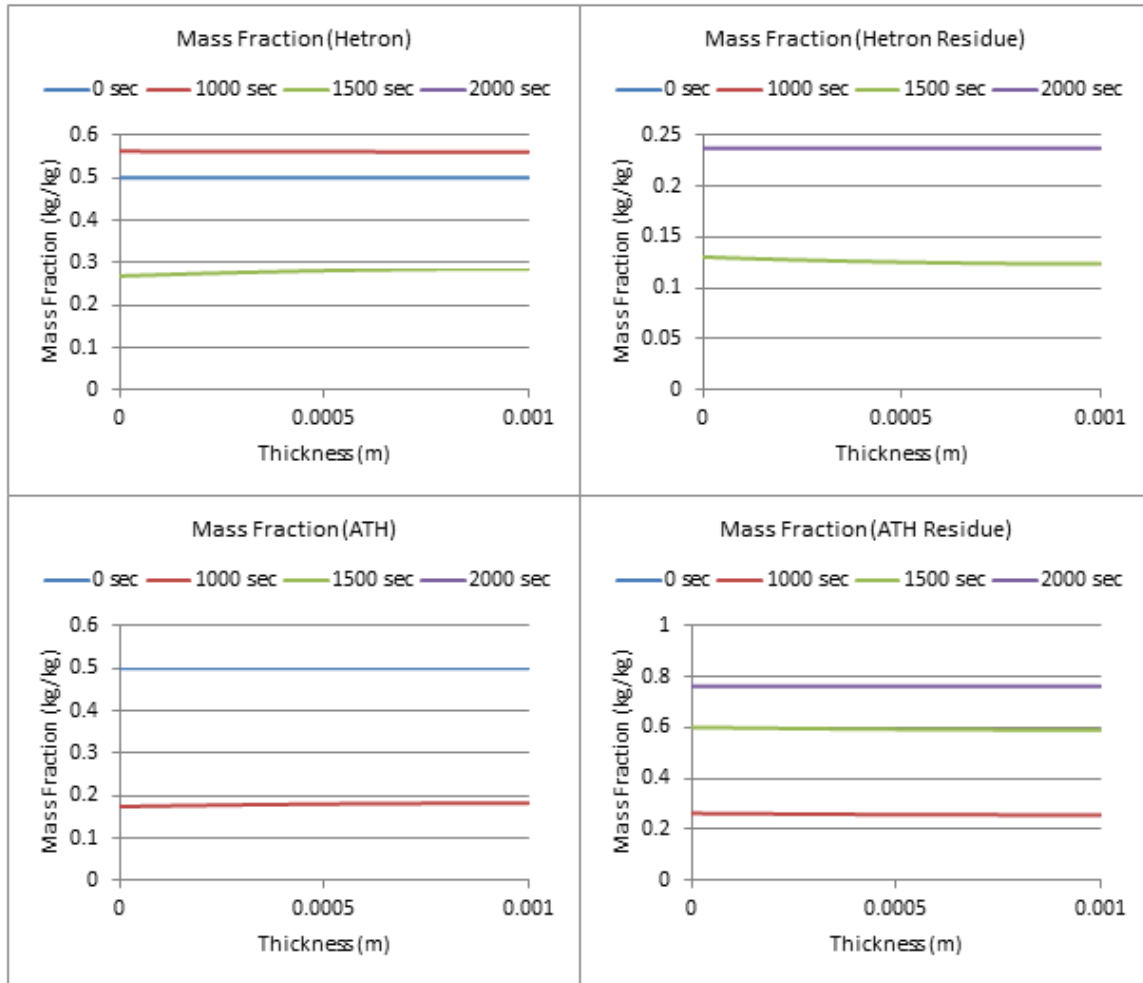
Figure 248: Mass Fraction Profiles (800 W/m^2, 50% ATH)

57% ATH, qe= 100 W/m^2
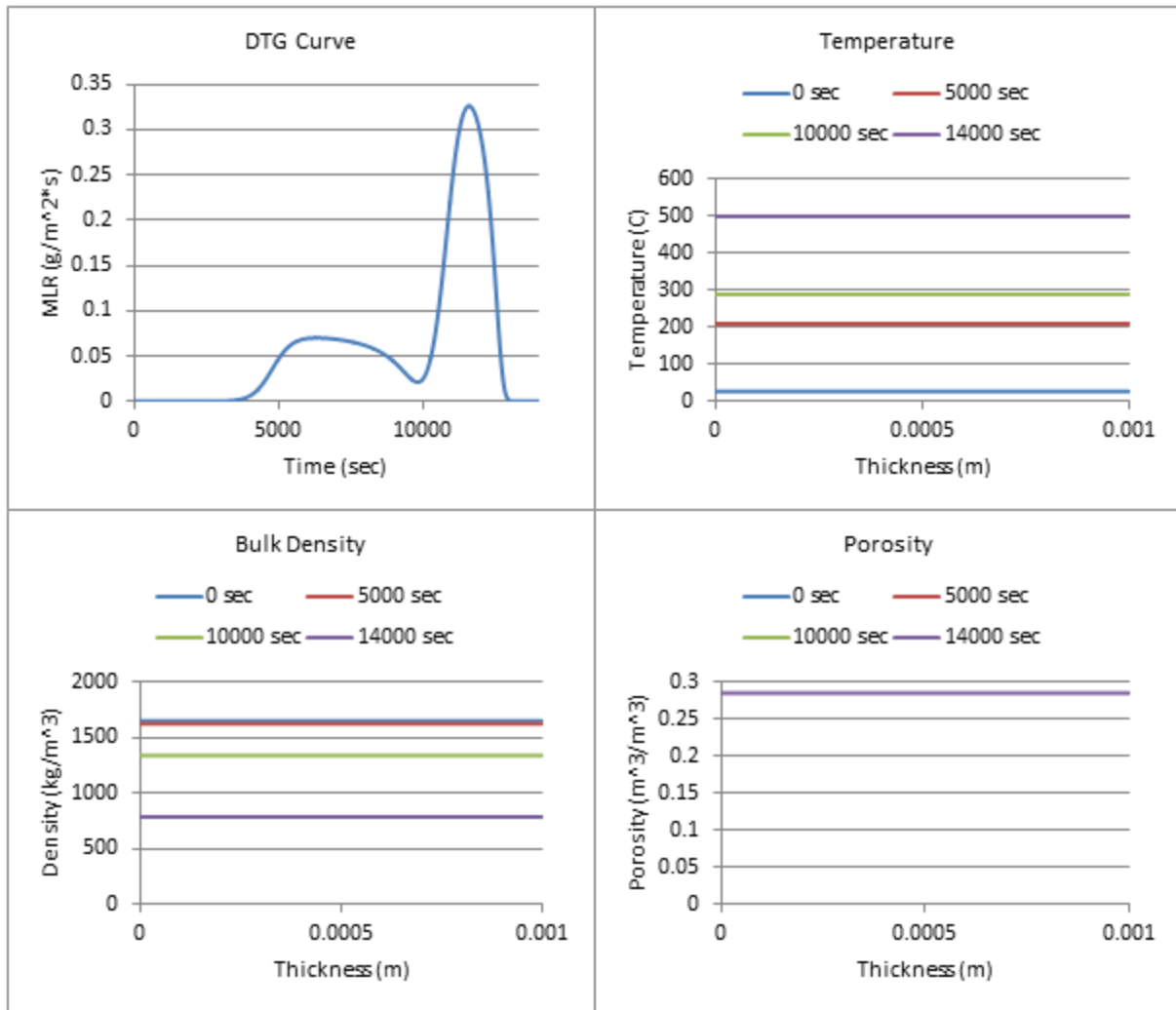
Figure 249: Profiles (100 W/m^2, 57% ATH)
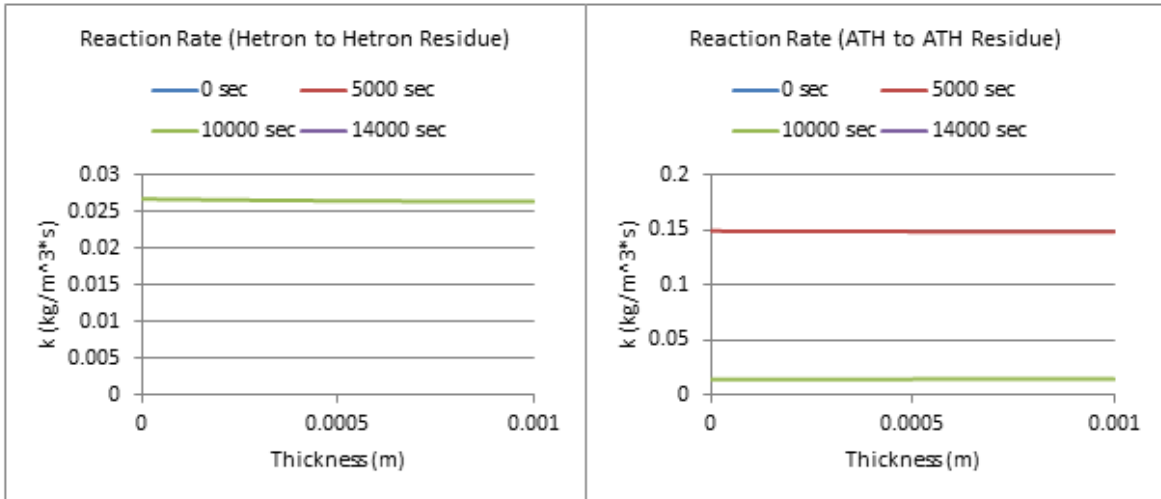
Figure 250: Reaction Rate Profiles (100 W/m^2, 57% ATH)
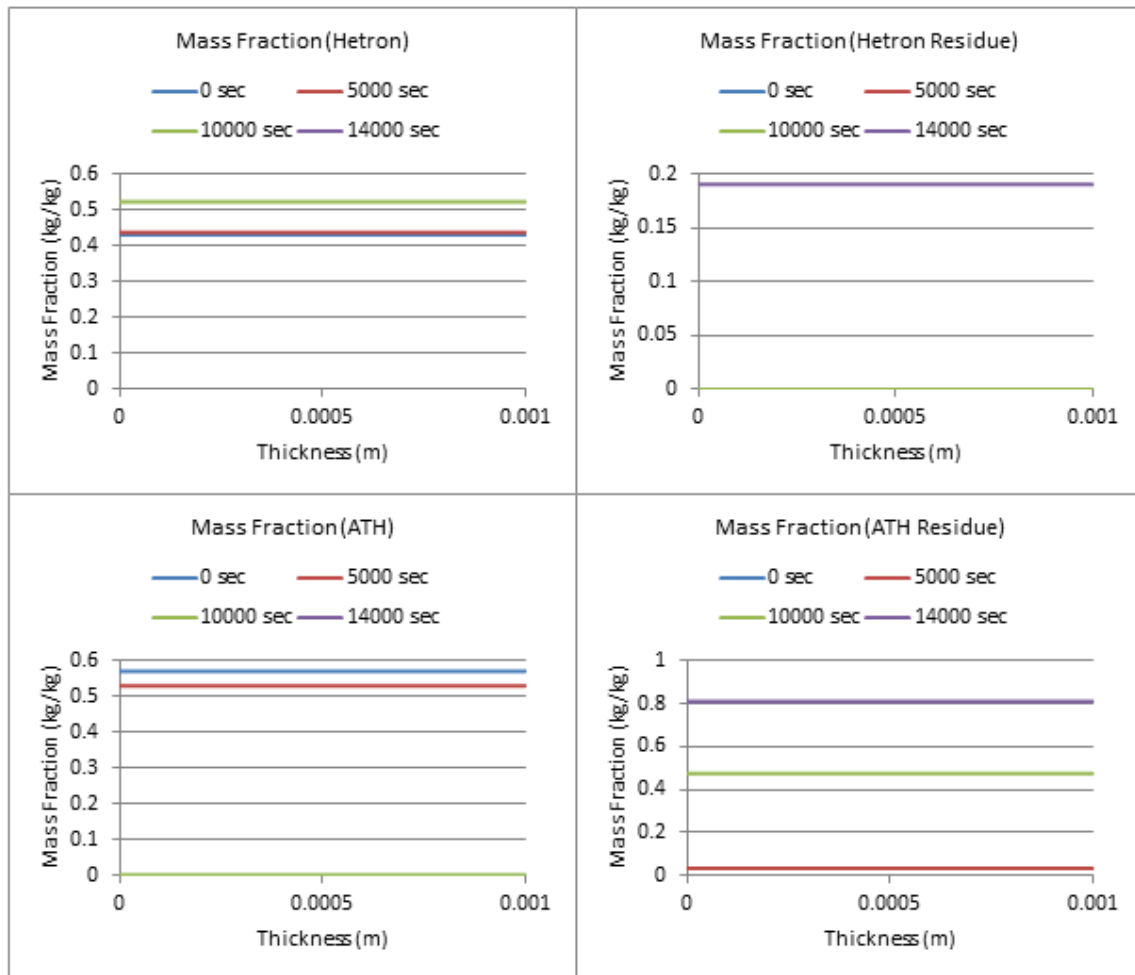
Figure 251: Mass Fraction Profiles (100 W/m^2, 57% ATH)

57% ATH, qe= 200 W/m^2
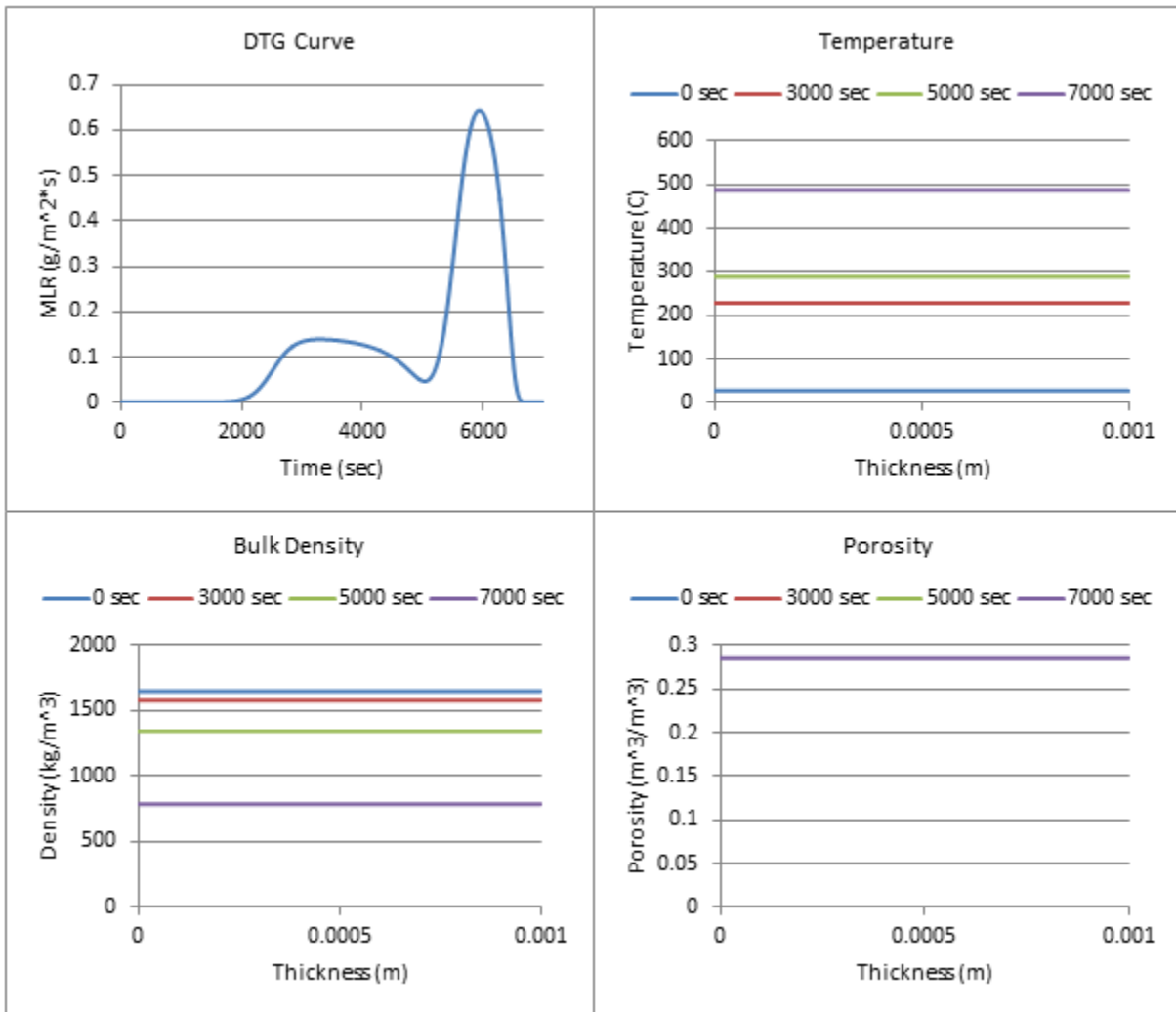
Figure 252: Profiles (200 W/m^2, 57% ATH)
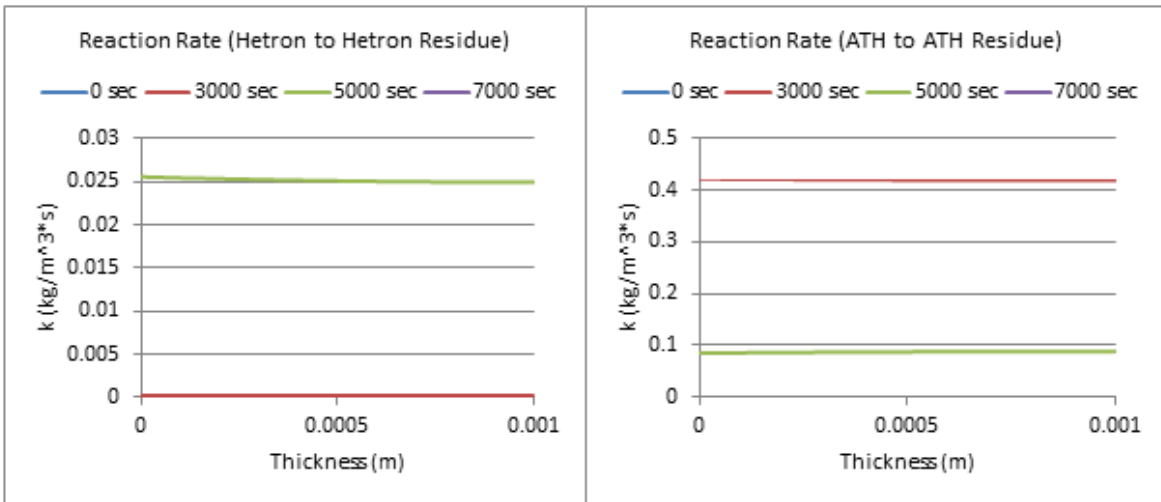
Figure 253: Reaction Rate Profiles (200 W/m^2, 57% ATH)
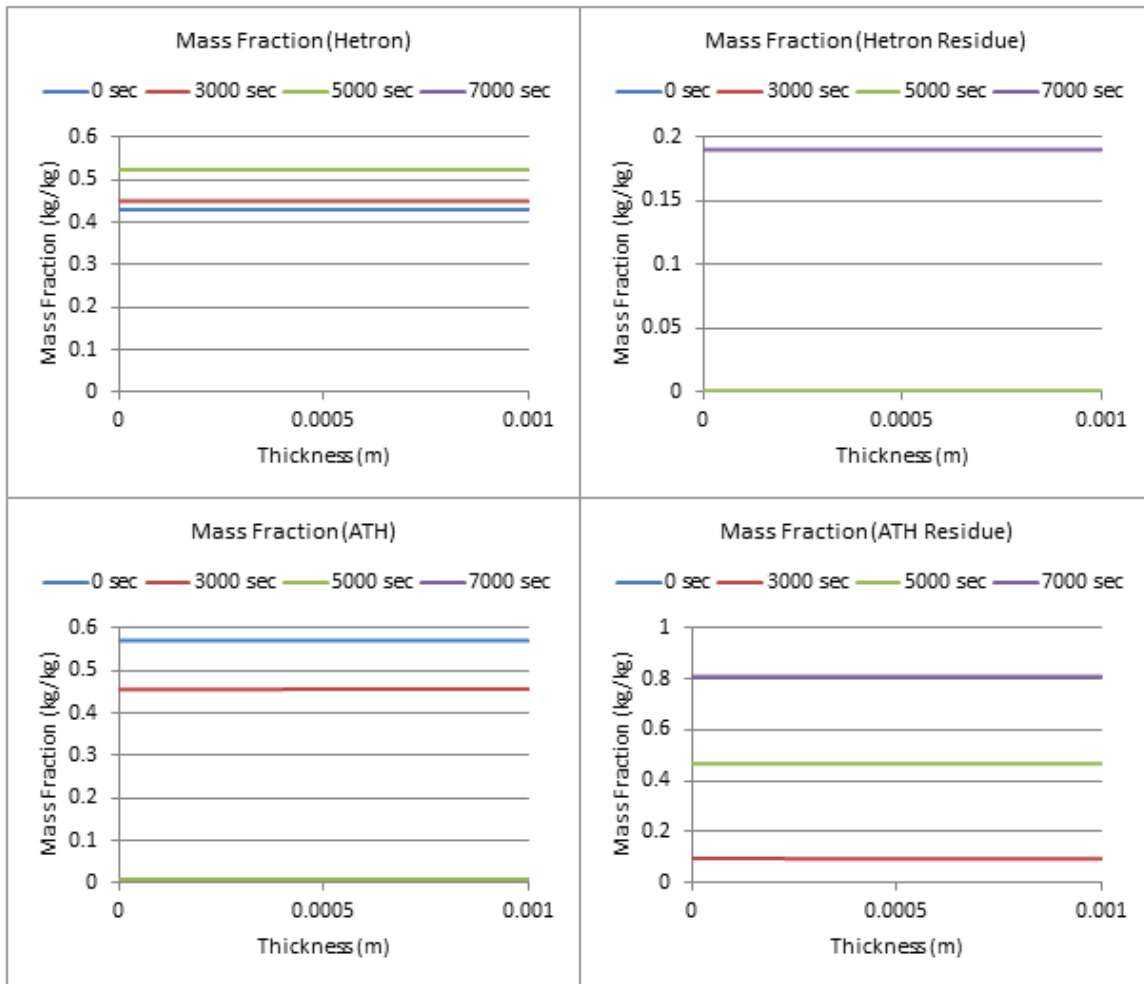
Figure 254: Mass Fraction Profiles (200 W/m^2, 57% ATH)

57% ATH, qe= 300 W/m^2
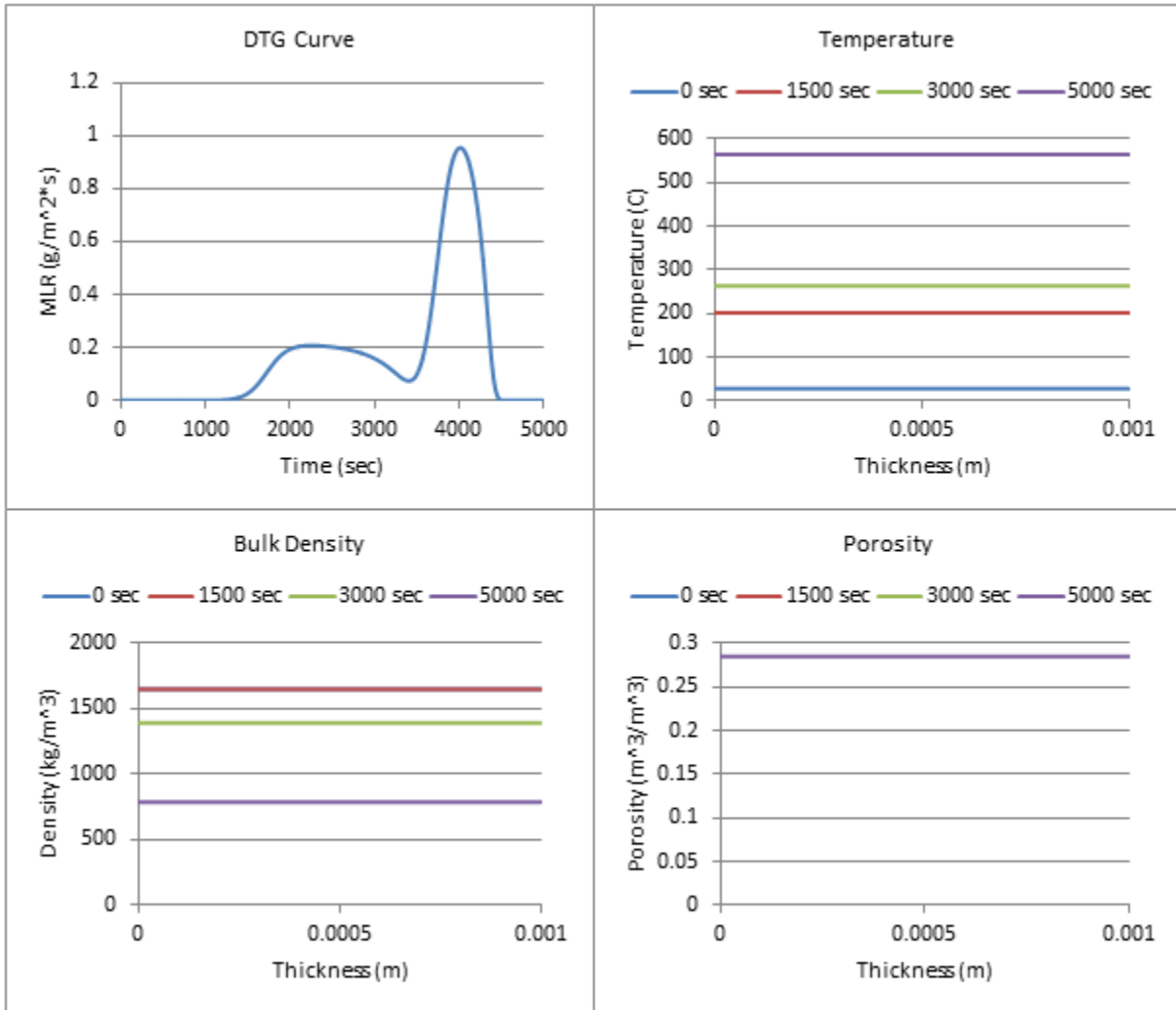
Figure 255: Profiles (300 W/m^2, 57% ATH)
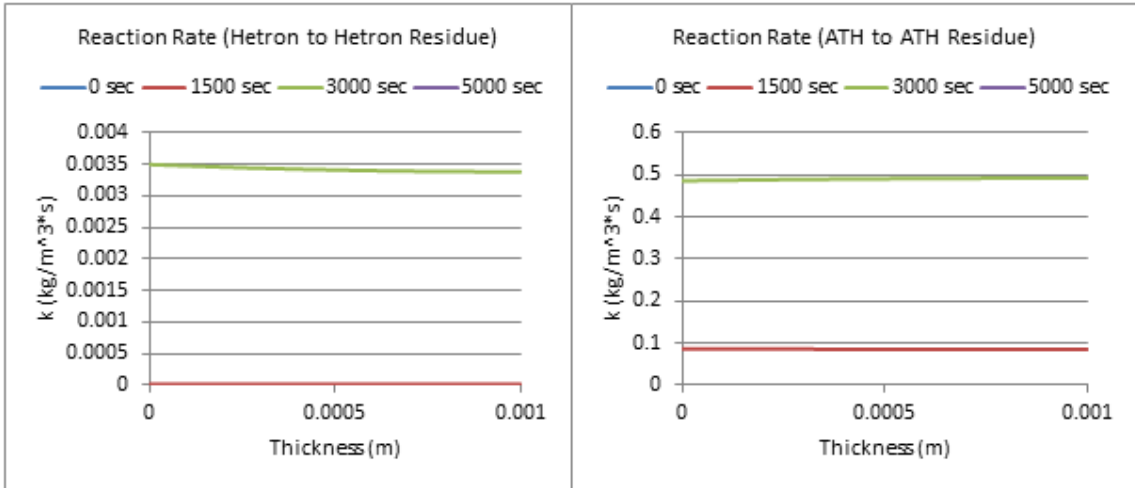
Figure 256: Reaction Rate Profiles (300 W/m^2, 57% ATH)
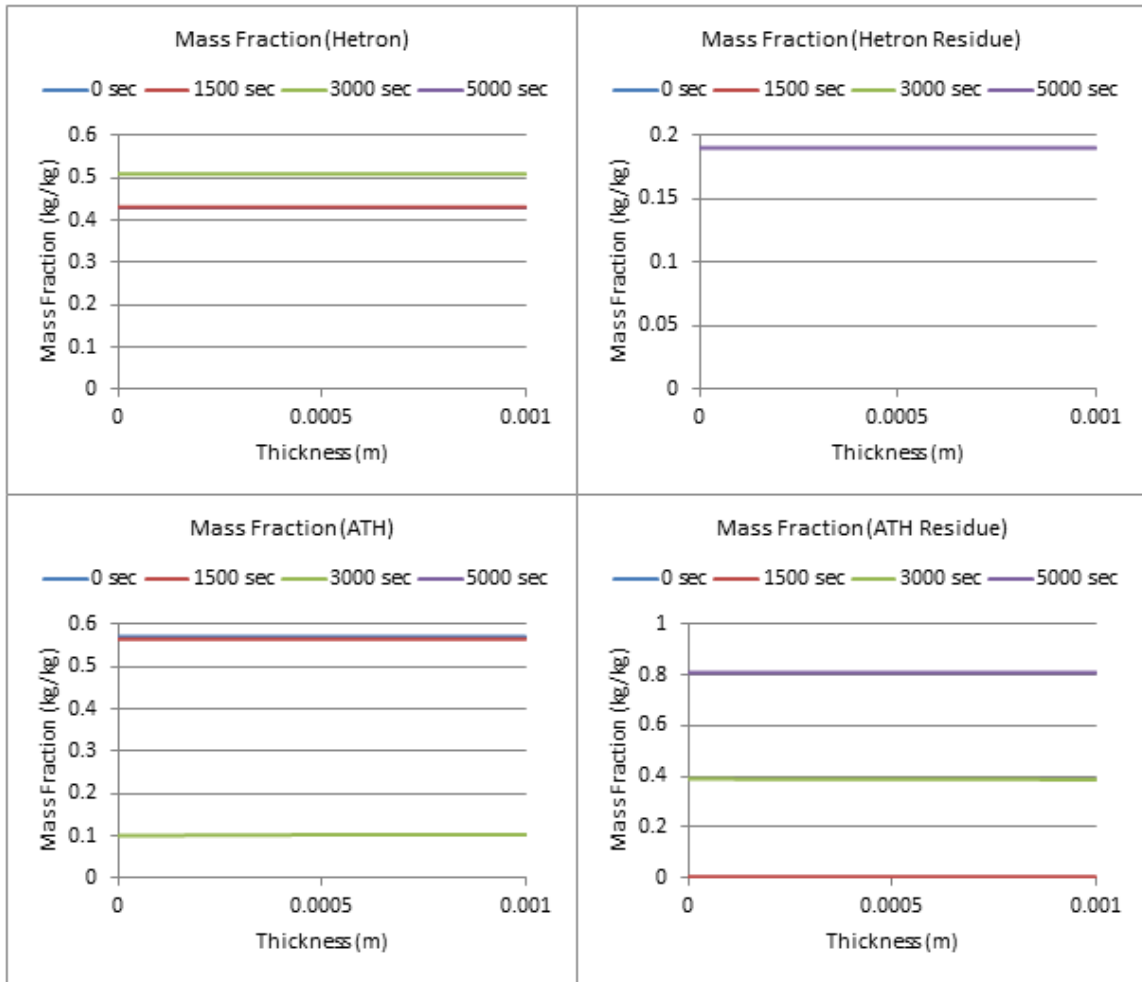
Figure 257: Mass Fraction Profiles (300 W/m^2, 57% ATH)

57% ATH, qe= 400 W/m^2
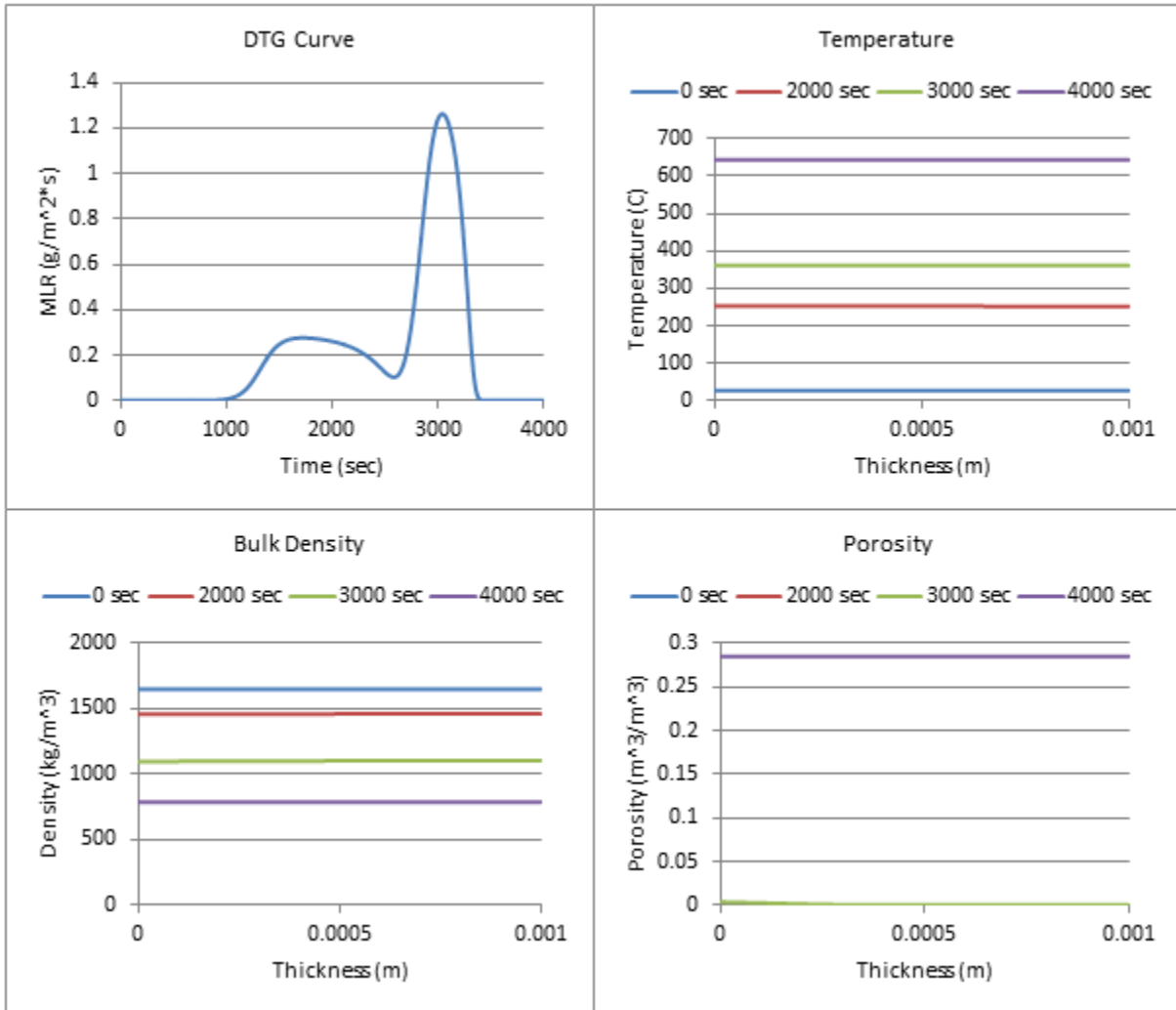
Figure 258: Profiles (400 W/m^2, 57% ATH)
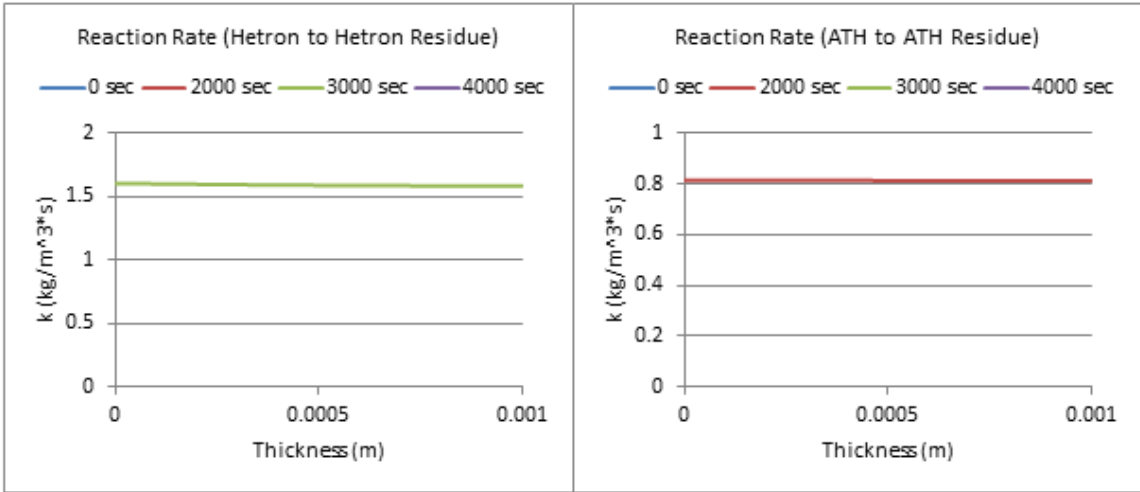
Figure 259: Reaction Rate Profiles (400 W/m^2, 57% ATH)
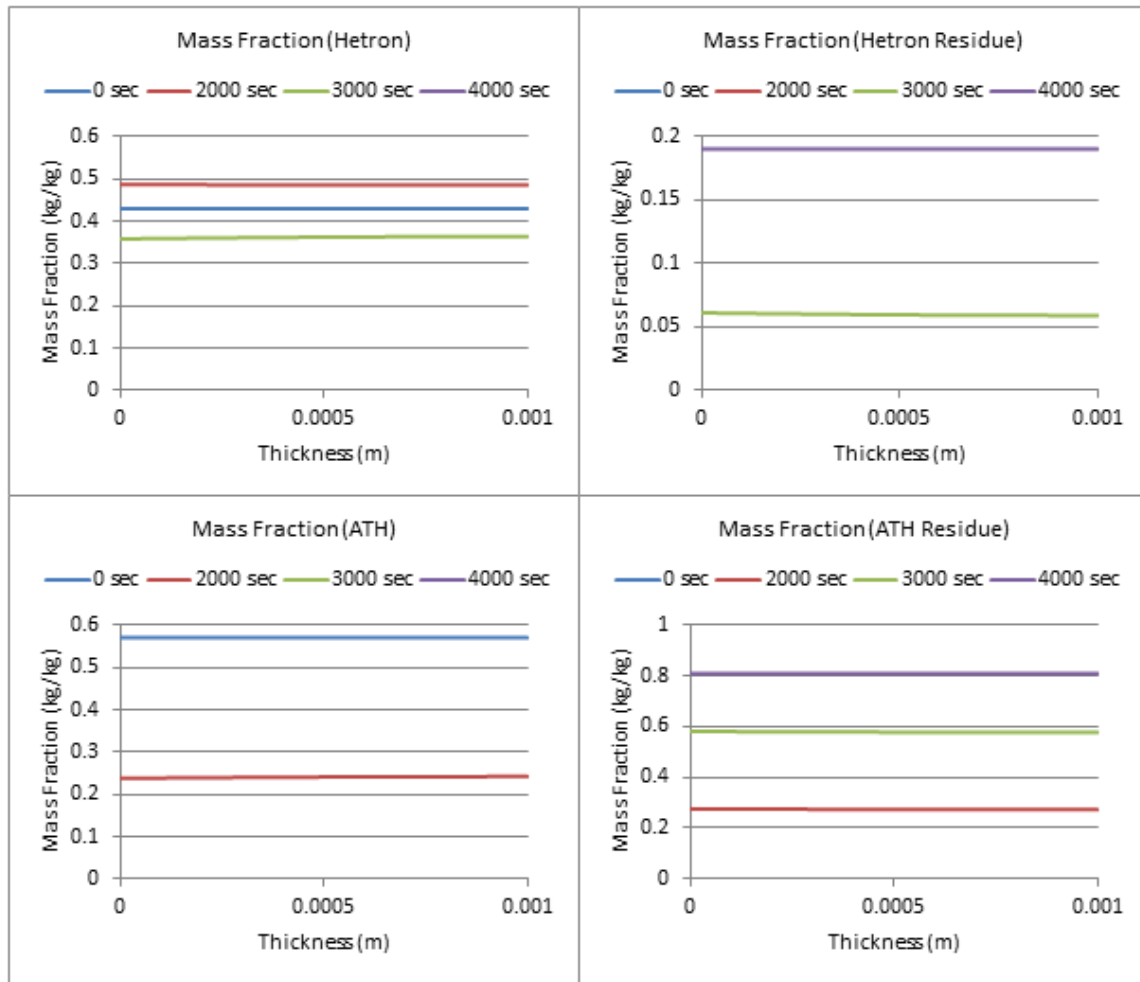
Figure 260: Mass Fraction Profiles (400 W/m^2, 57% ATH)

57% ATH, qe= 500 W/m^2
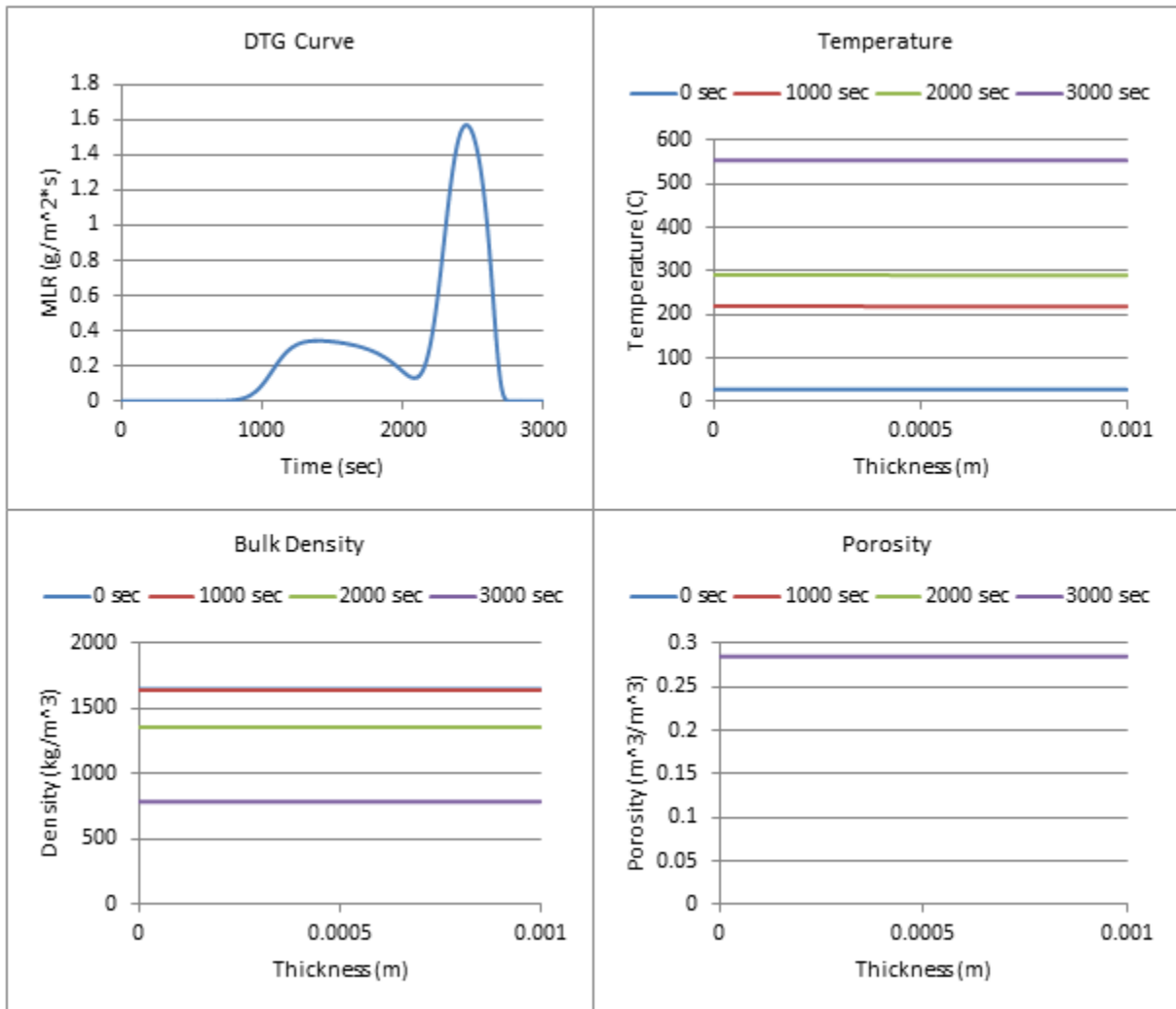
Figure 261: Profiles (500 W/m^2, 57% ATH)
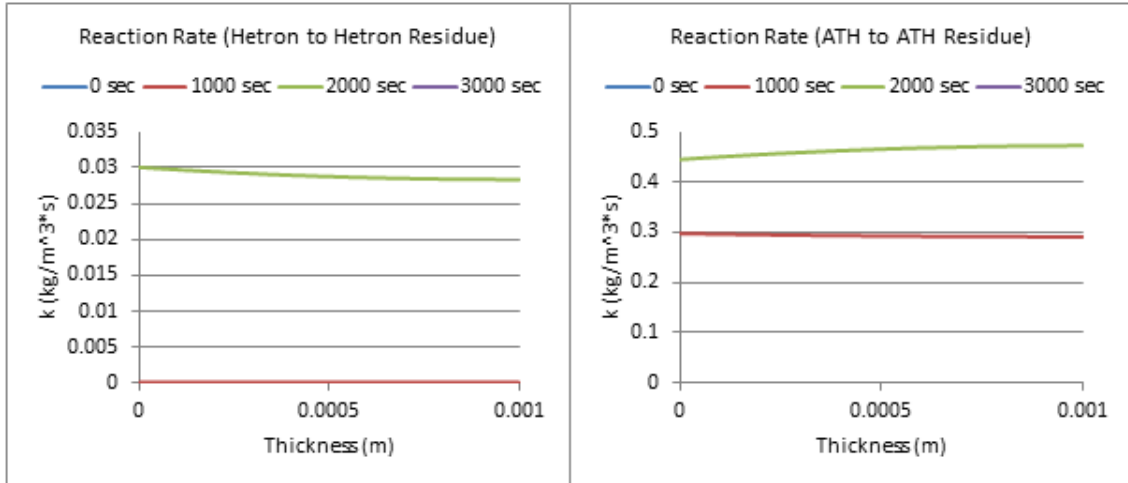
Figure 262: Reaction Rate Profiles (500 W/m^2, 57% ATH)
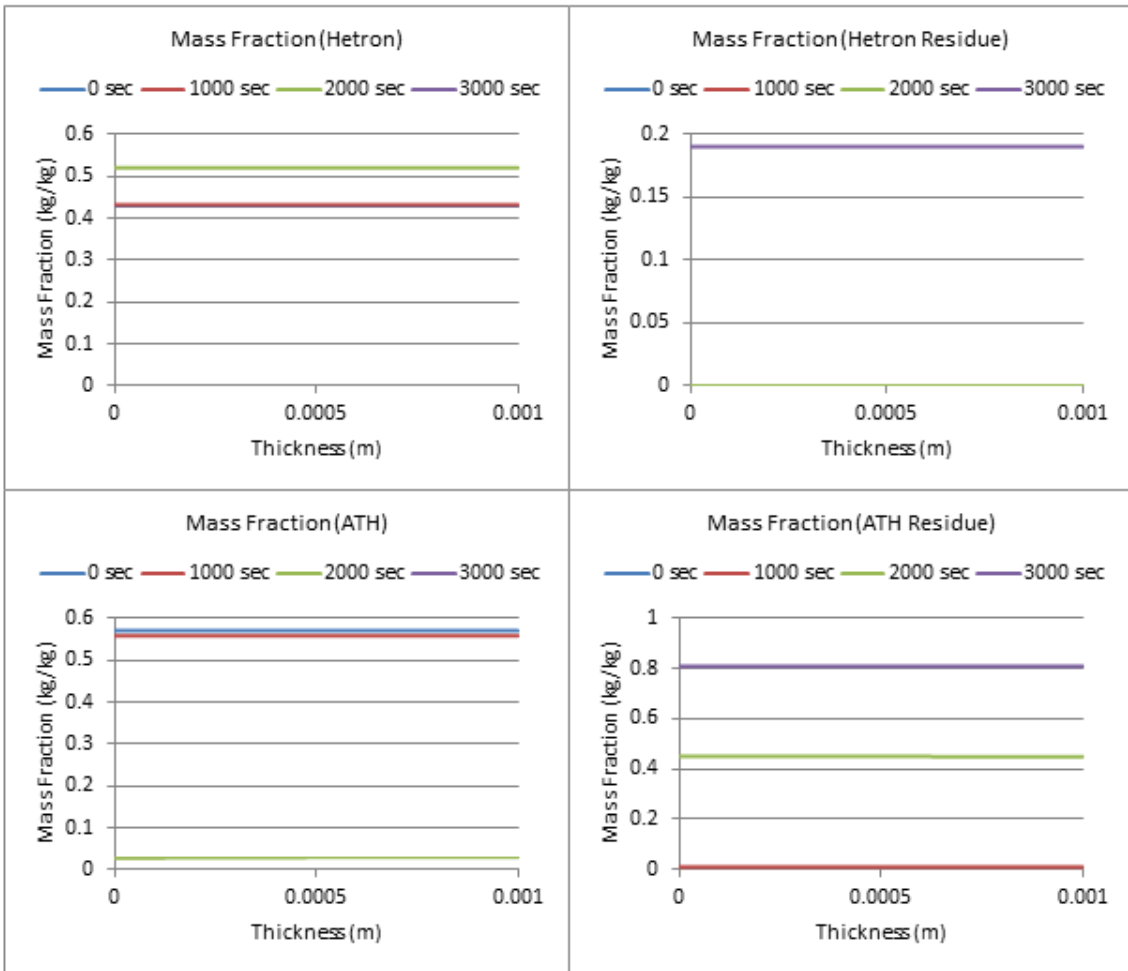
Figure 263: Mass Fraction Profiles (500 W/m^2, 57% ATH)

57% ATH, qe= 600 W/m^2
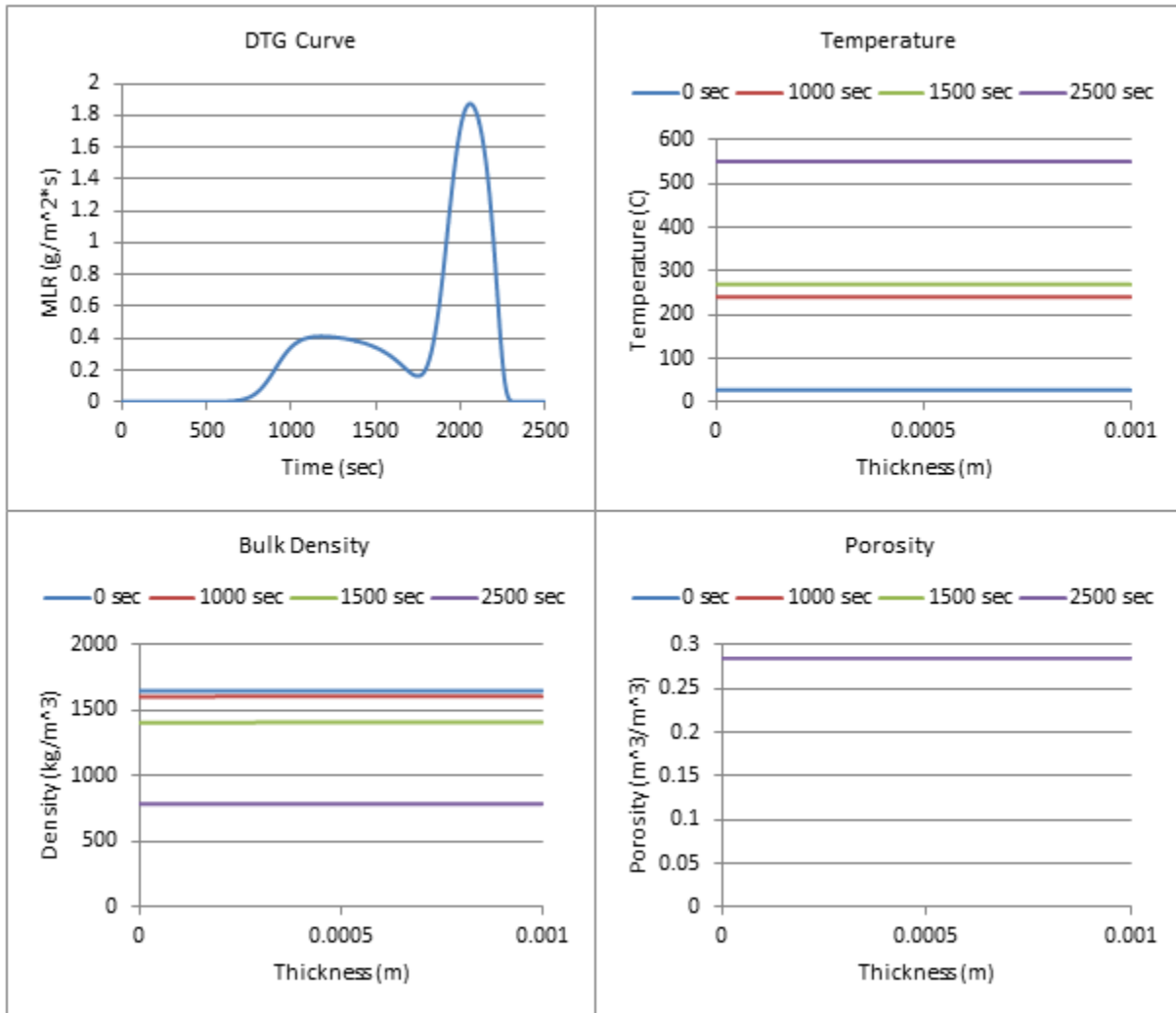
Figure 264: Profiles (600 W/m^2, 57% ATH)
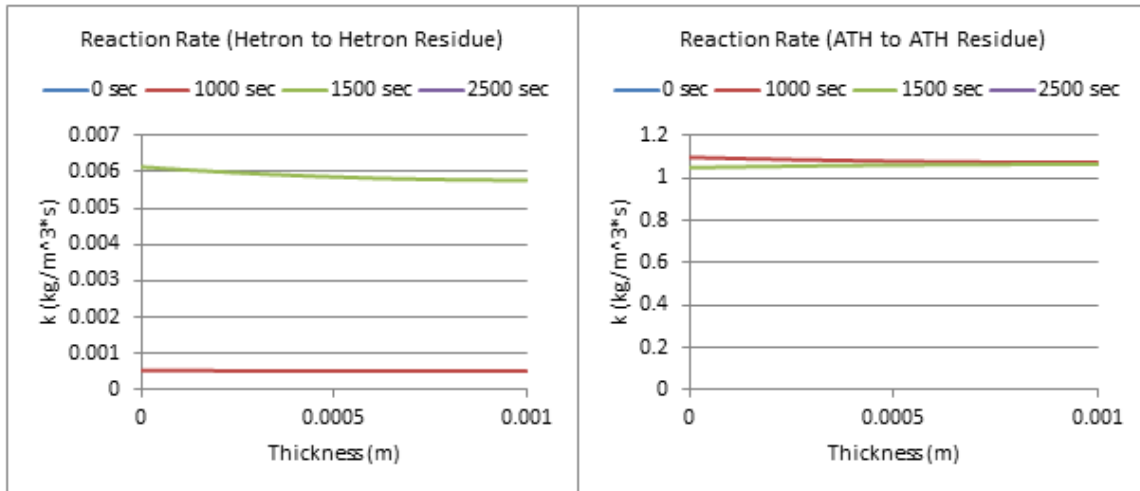
Figure 265: Reaction Rate Profiles (600 W/m^2, 57% ATH)
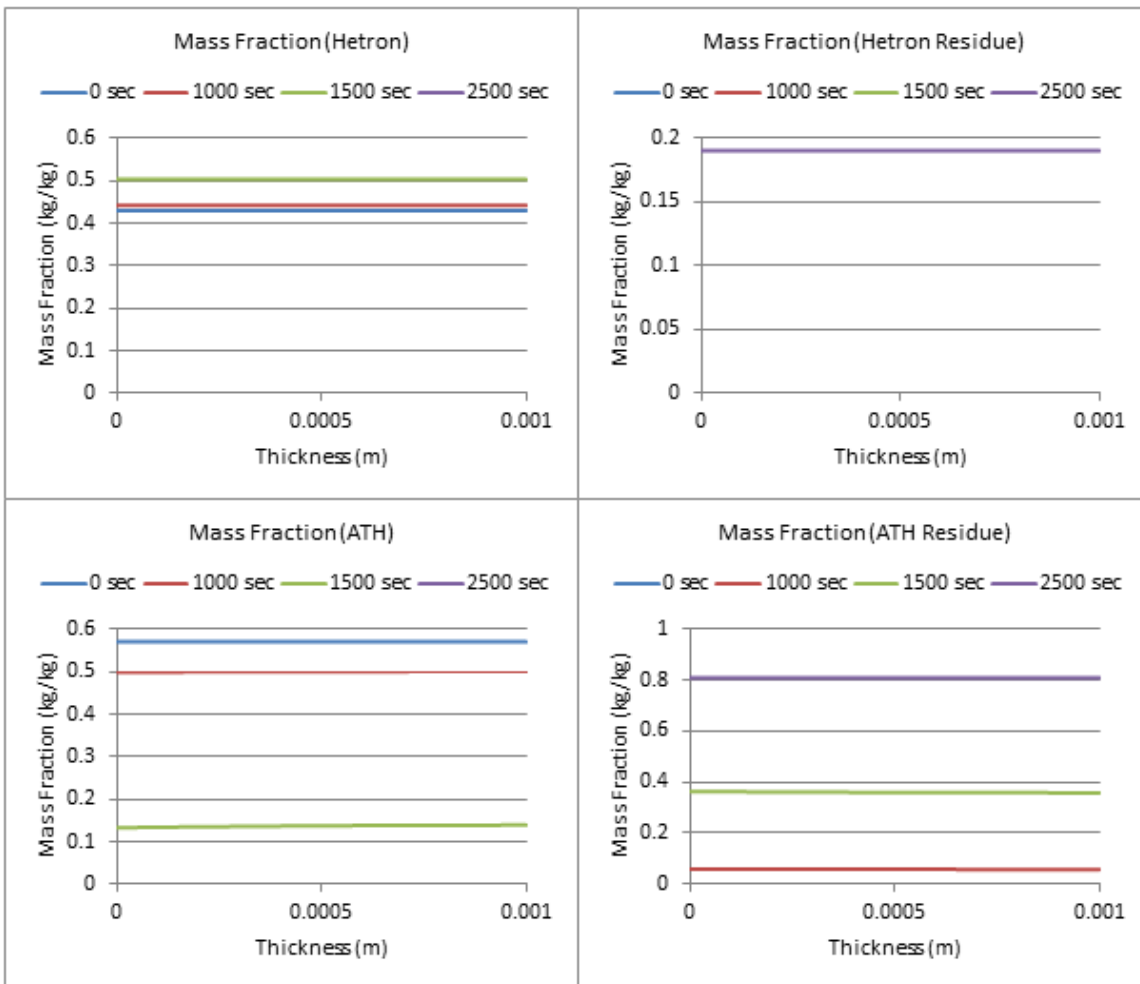
Figure 266: Mass Fraction Profiles (600 W/m^2, 57% ATH)

57% ATH, qe= 700 W/m^2
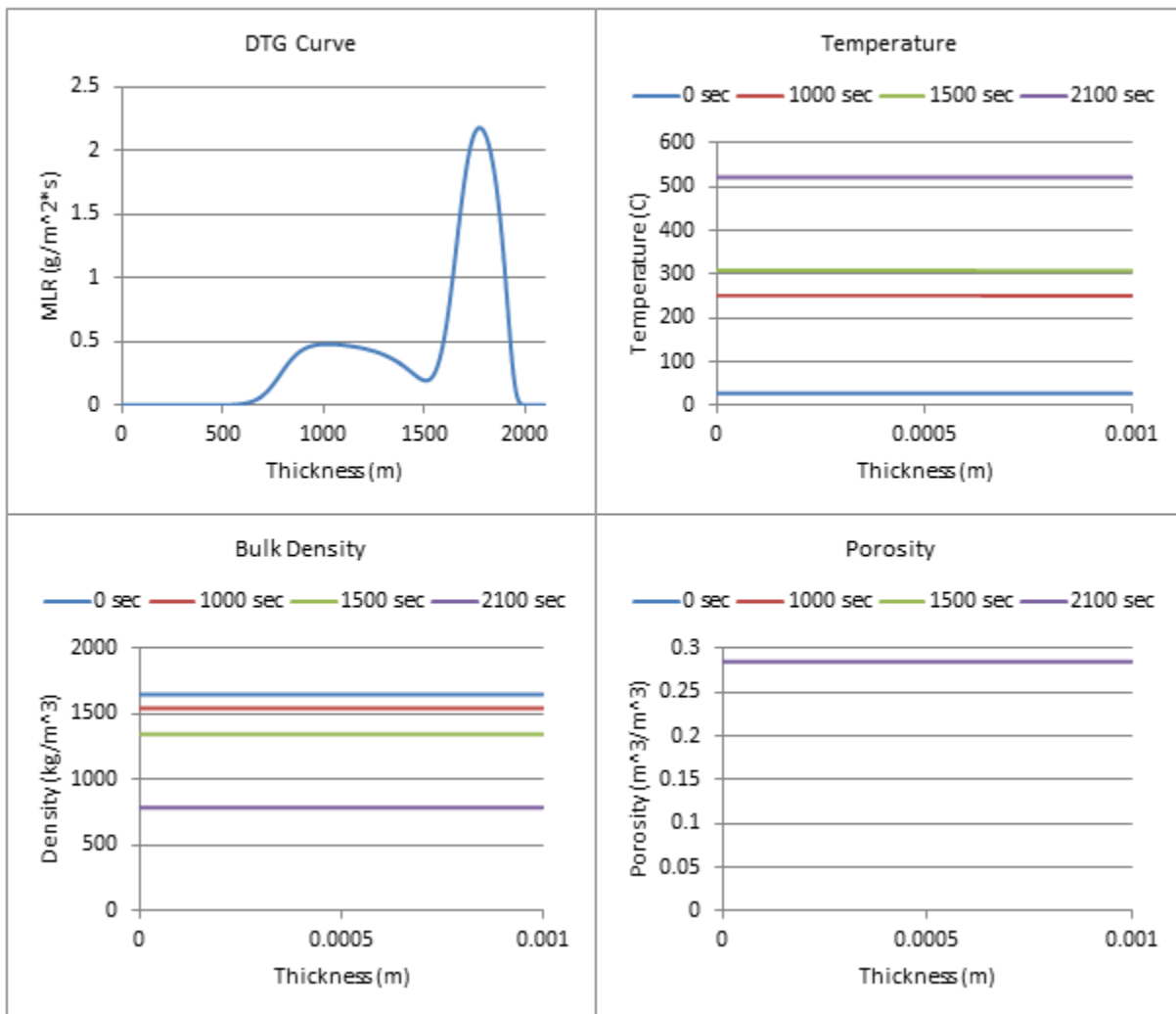
Figure 267: Profiles (700 W/m^2, 57% ATH)
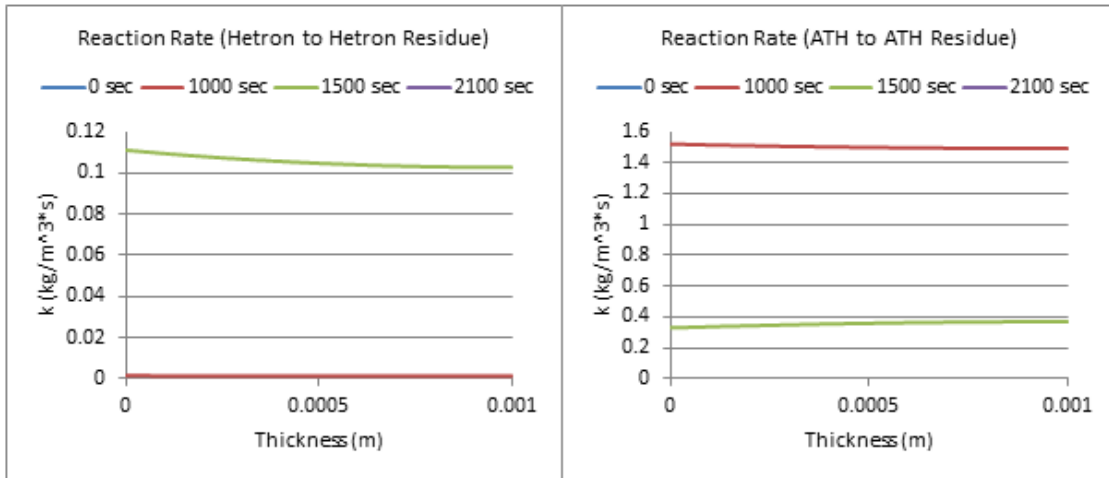
Figure 268: Reaction Rate Profiles (700 W/m^2, 57% ATH)
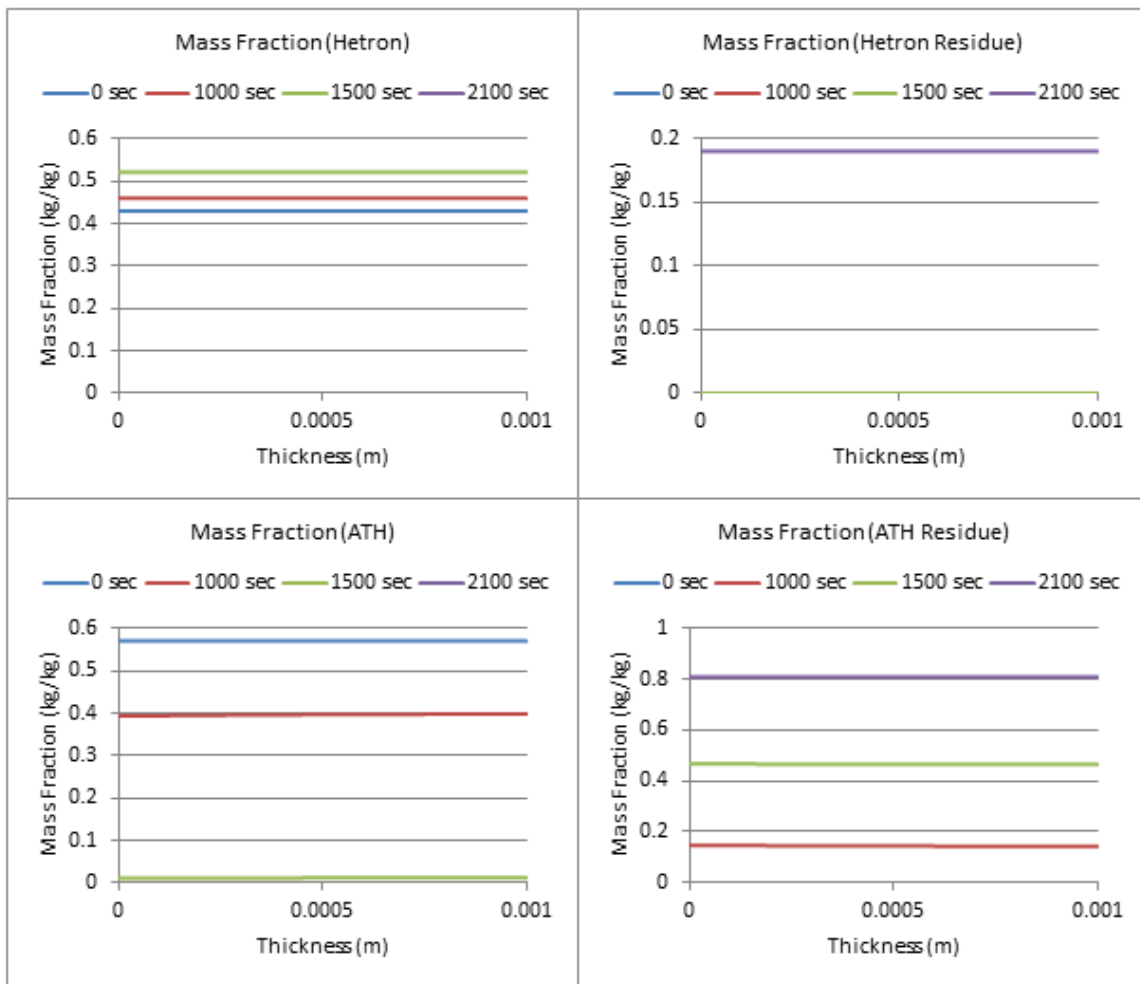
Figure 269: Mass Fraction Profiles (700 W/m^2, 57% ATH)

57% ATH, qe= 800 W/m^2
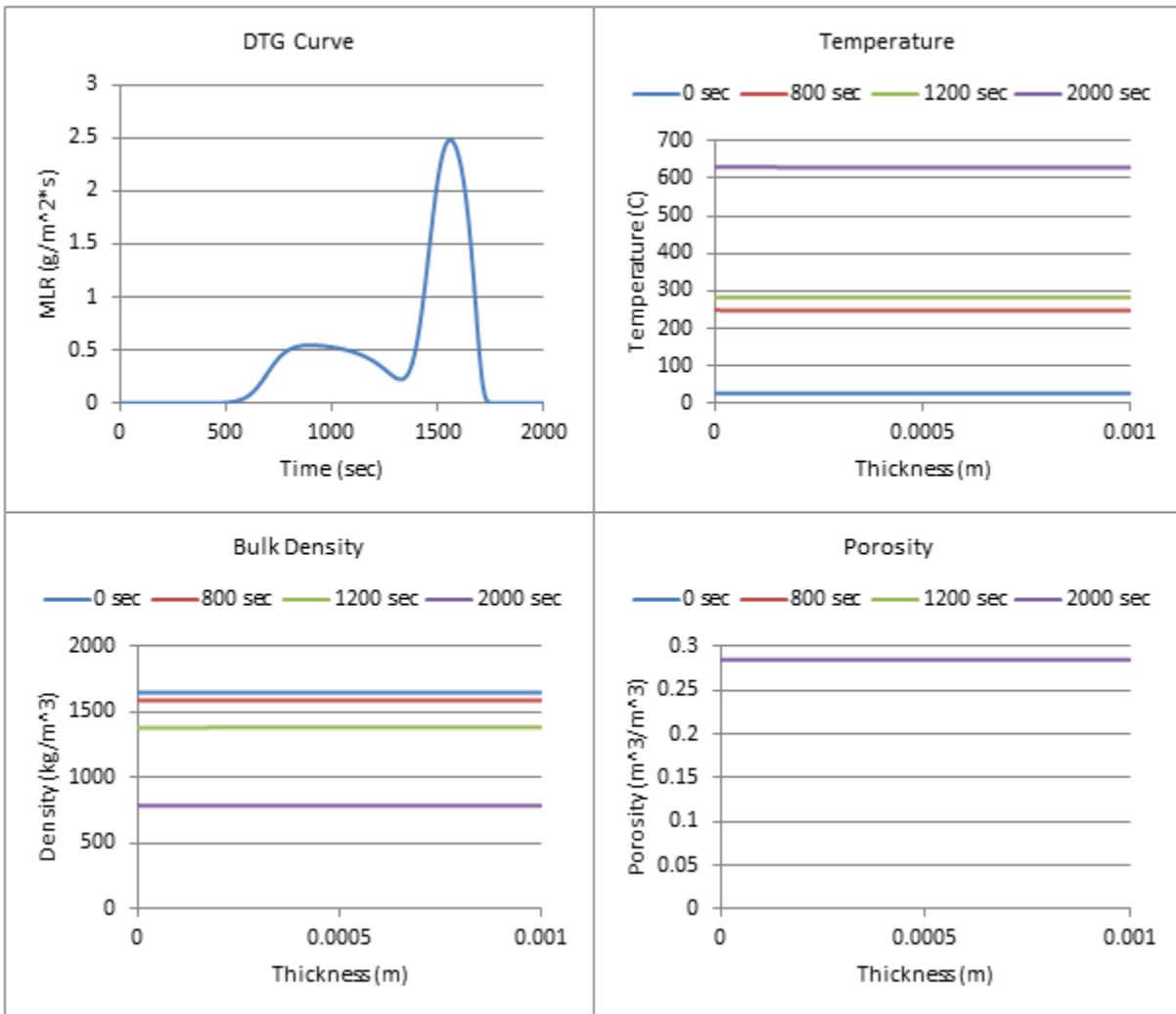
Figure 270: Profiles (800 W/m^2, 57% ATH)
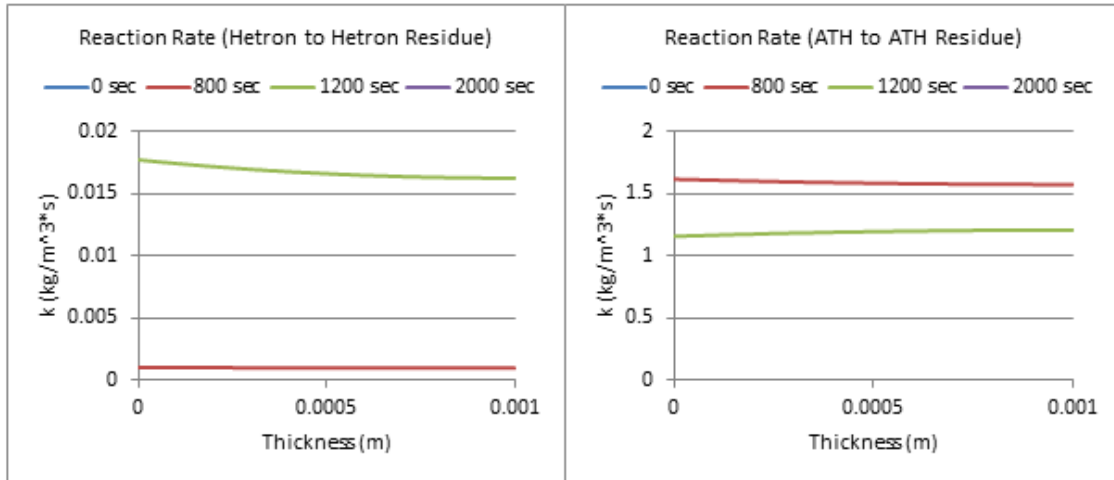
Figure 271: Reaction Rate Profiles (800 W/m^2, 57% ATH)
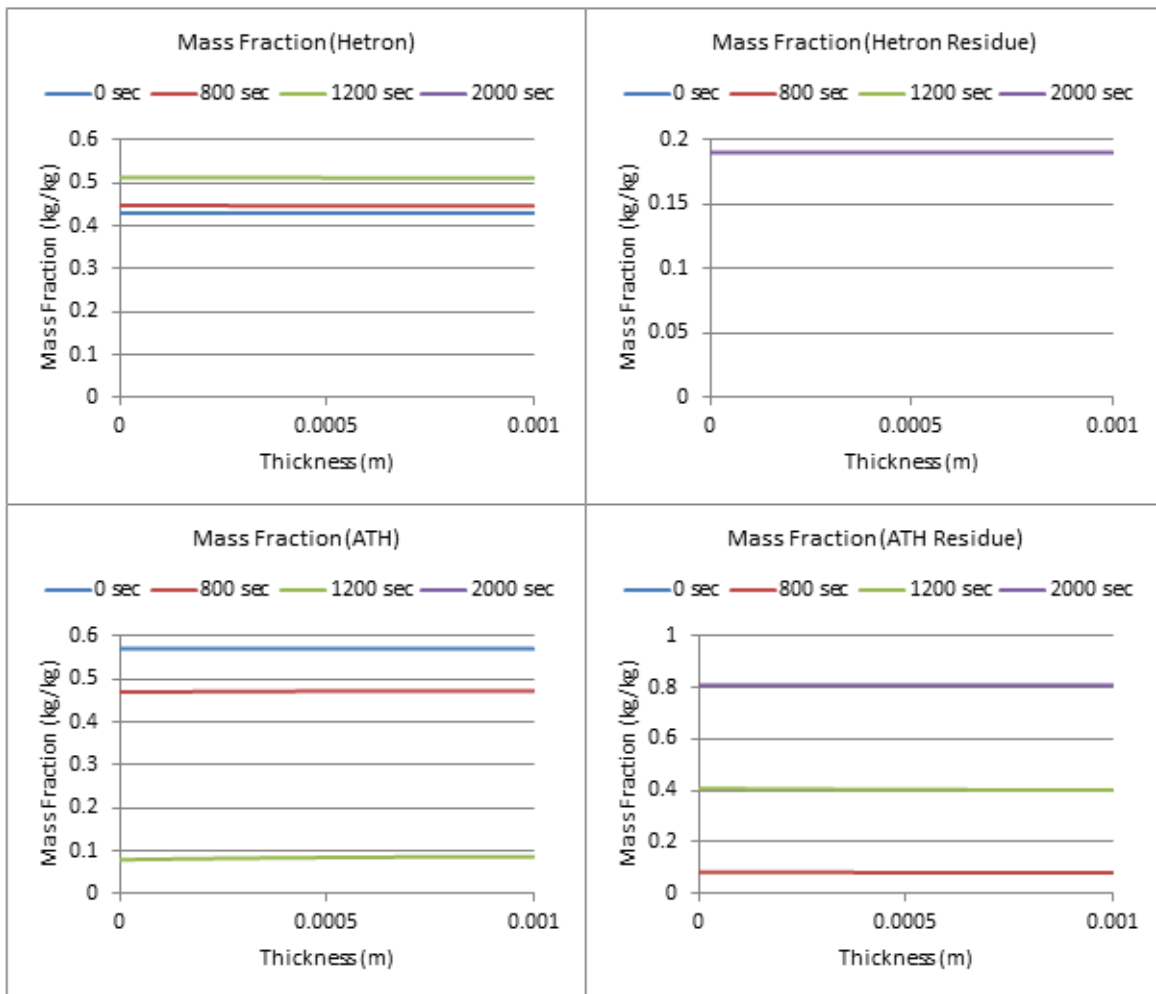
Figure 272: Mass Fraction Profiles (800 W/m^2, 57% ATH)

Appendix E.10: Heat Flux with Varying Levels of ATH

To better understand how the changes in heat flux change the MLR curve, the chosen range of heat flux values were all graphed together with varying levels of ATH. These can be seen in the graphs below.
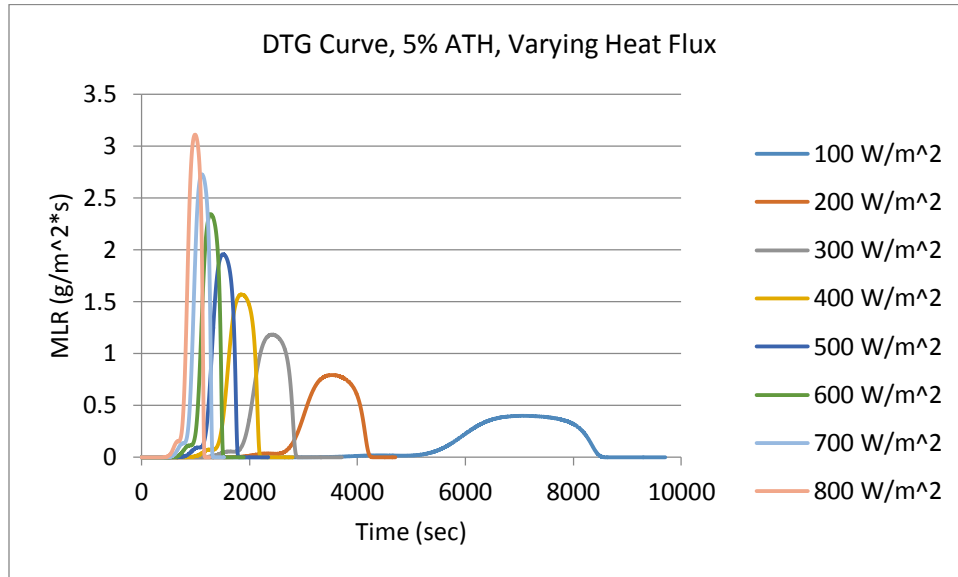
Figure 273: DTG Curve, 5% ATH, Varying Heat Flux
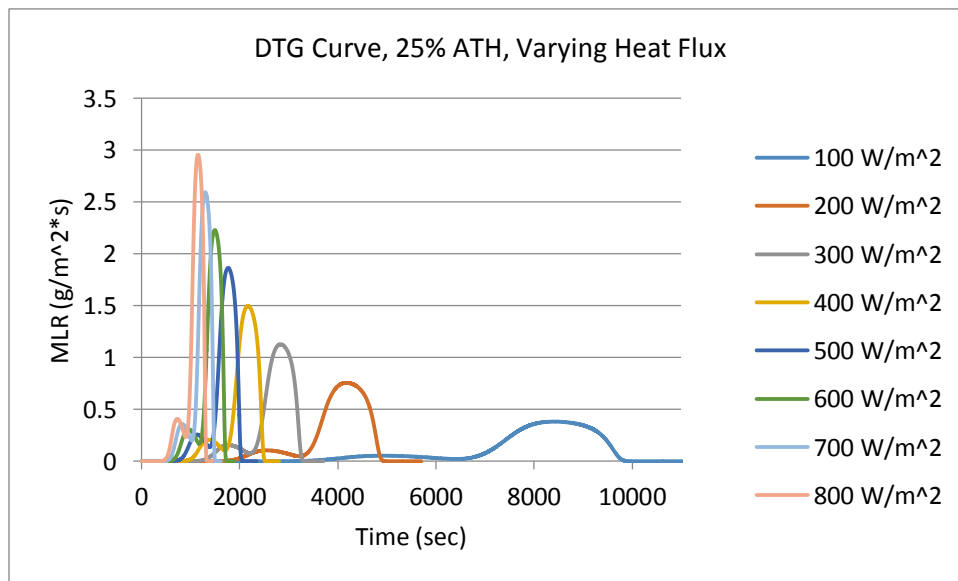
Figure 274: DTG Curve, 25% ATH, Varying Heat Flux
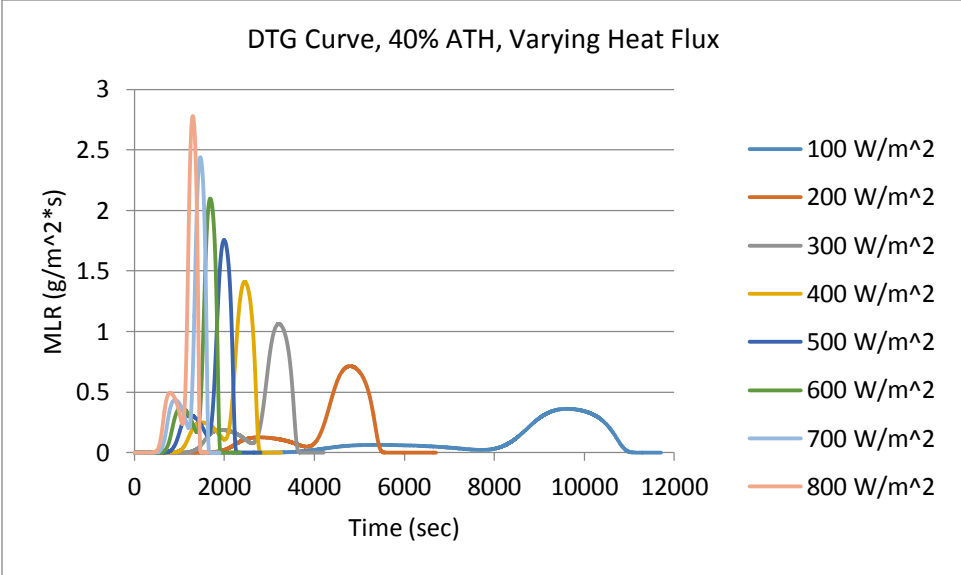
Figure 275: DTG Curve, 40% ATH, Varying Heat Flux
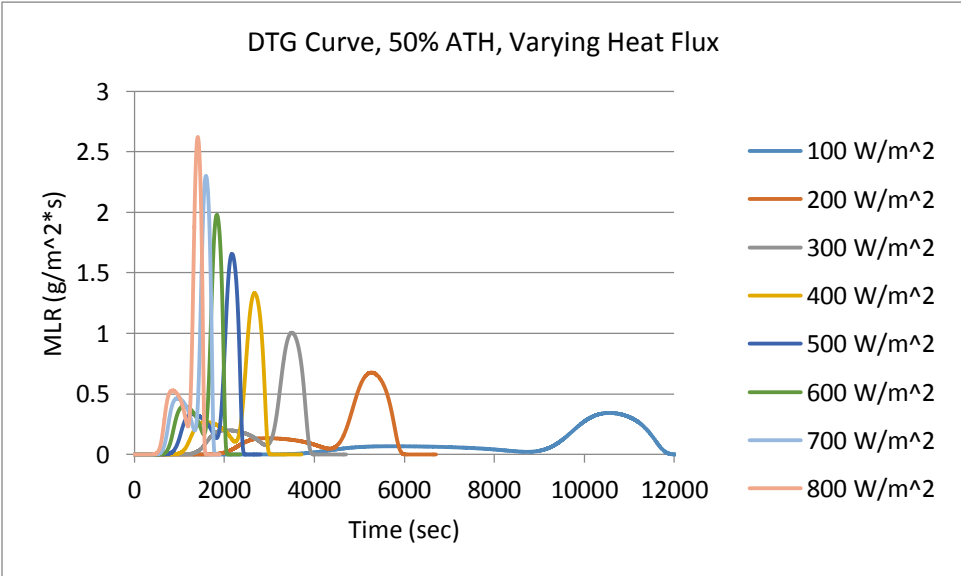
Figure 276: DTG Curve, 50% ATH, Varying Heat Flux
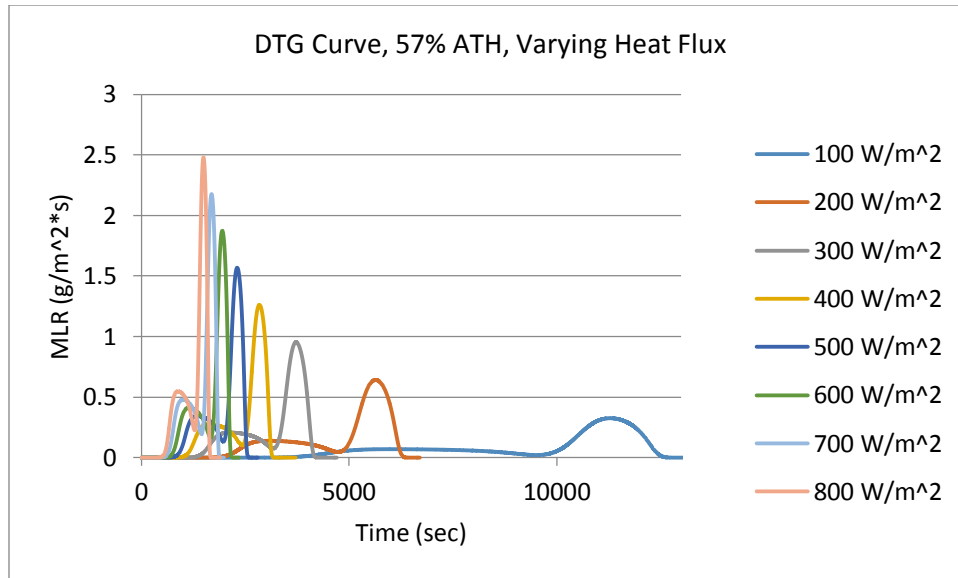
Figure 277: DTG Curve, 57% ATH, Varying Heat Flux

A graph was also created to a specific heat flux, with varying levels of ATH, to see how varying the ATH affected the results. This can be seen in the graph below.
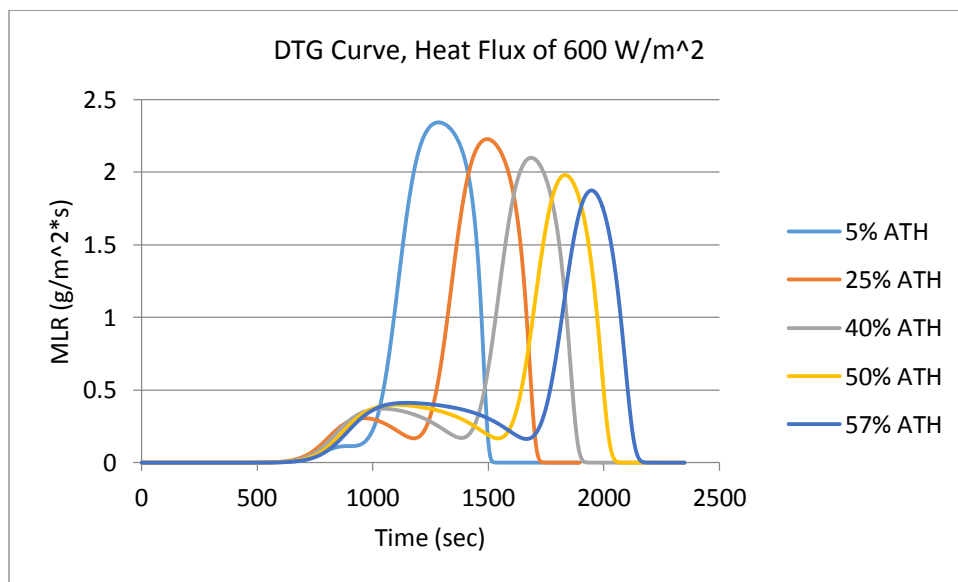
Figure 278: DTG Curve, Heat Flux of 600 W/m^2

Appendix E.11: 1mm vs 0.5mm Profile Comparison

Profiles were also created to compare a 1mm thick sample and a 0.5mm sample. A heat flux of 600 W/m^2 and 5% ATH was used for this simulation.
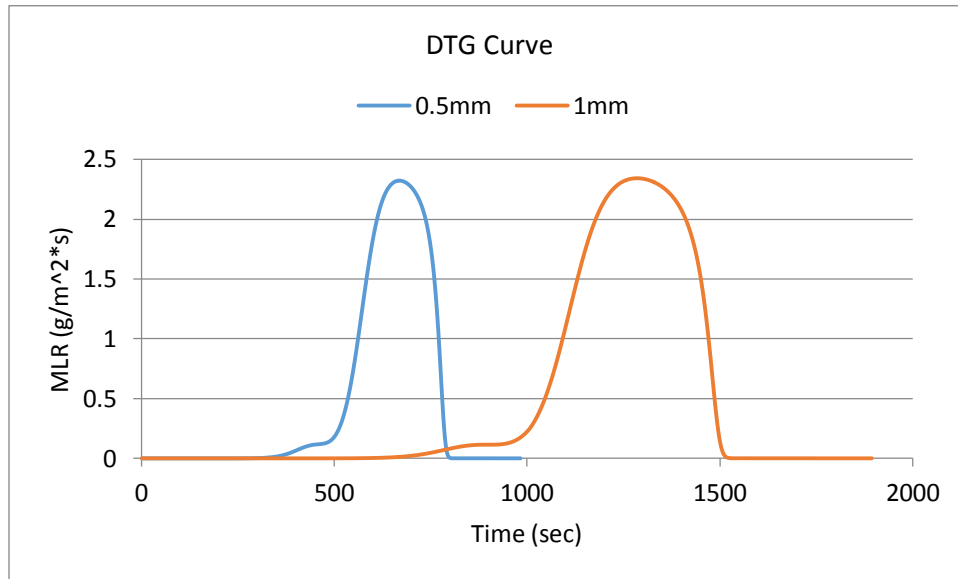
Figure 279: DTG Curves, 1mm vs 0.5mm
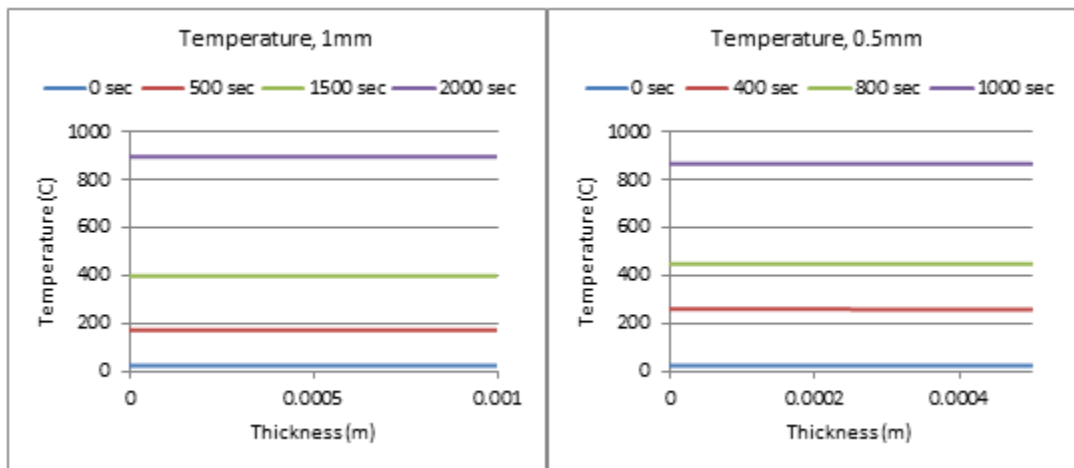
Figure 280: Temperature Profiles, 1mm vs 0.5mm
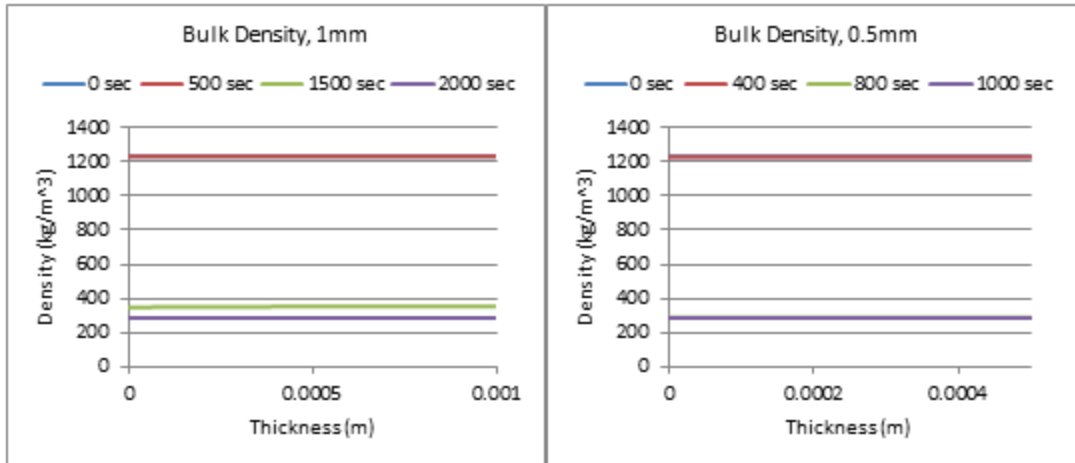
Figure 281: Bulk Density Profiles, 1mm vs 0.5mm
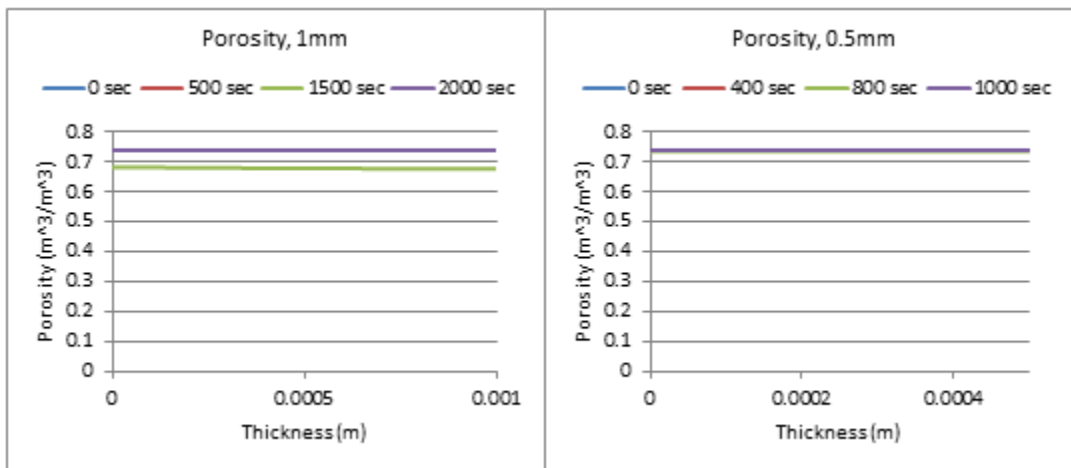
Figure 282: Porosity Profiles, 1mm vs 0.5mm
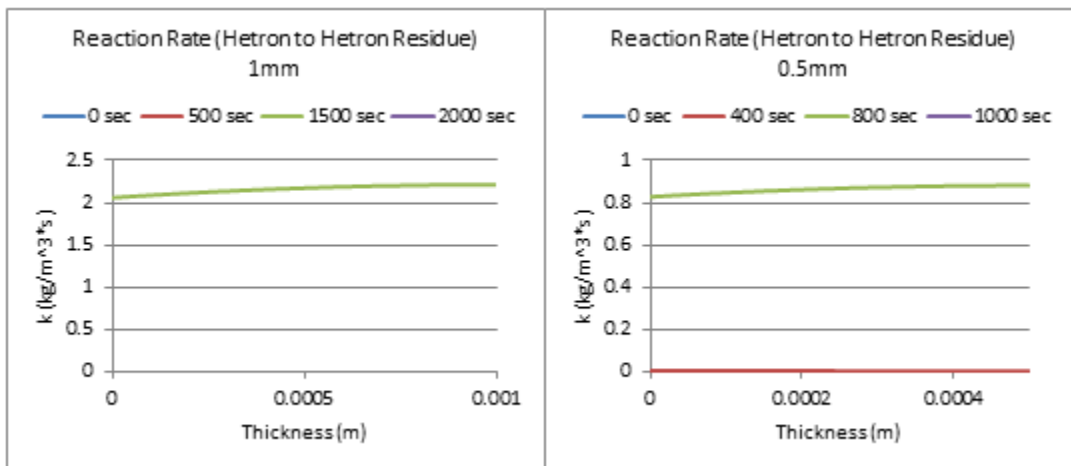
Figure 283: Reaction Rate (Hetron to Hetron Residue) 1mm vs 0.5mm
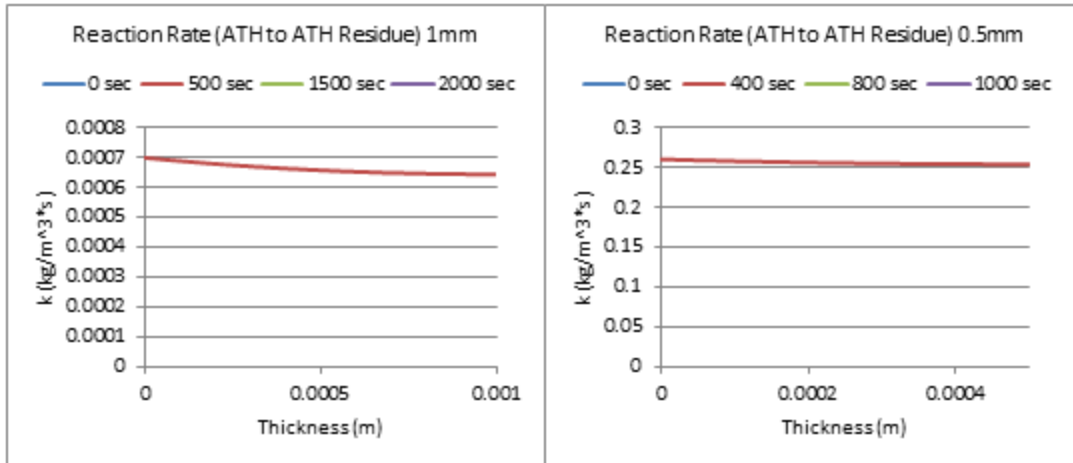
Figure 284: Reaction Rate (ATH to ATH Residue) 1mm vs 0.5mm
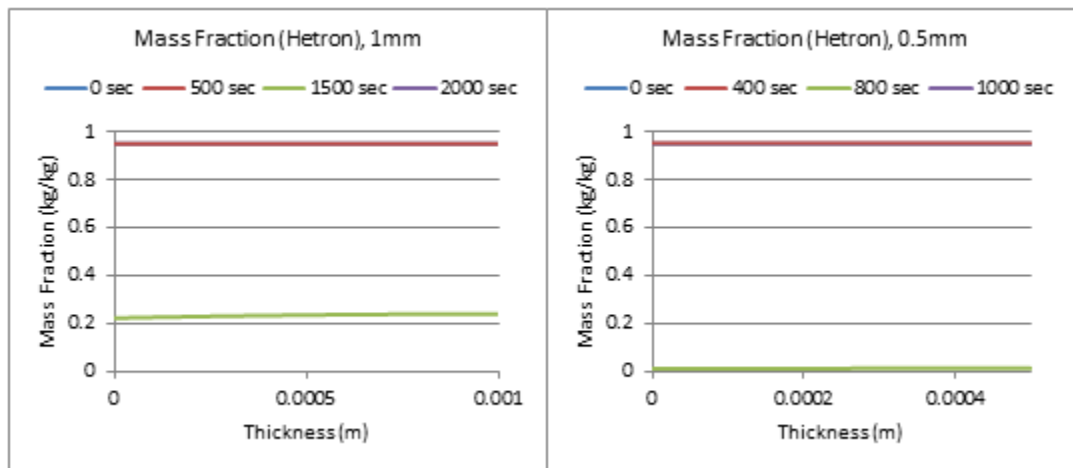
Figure 285: Mass Fraction (Hetron) 1mm vs 0.5mm
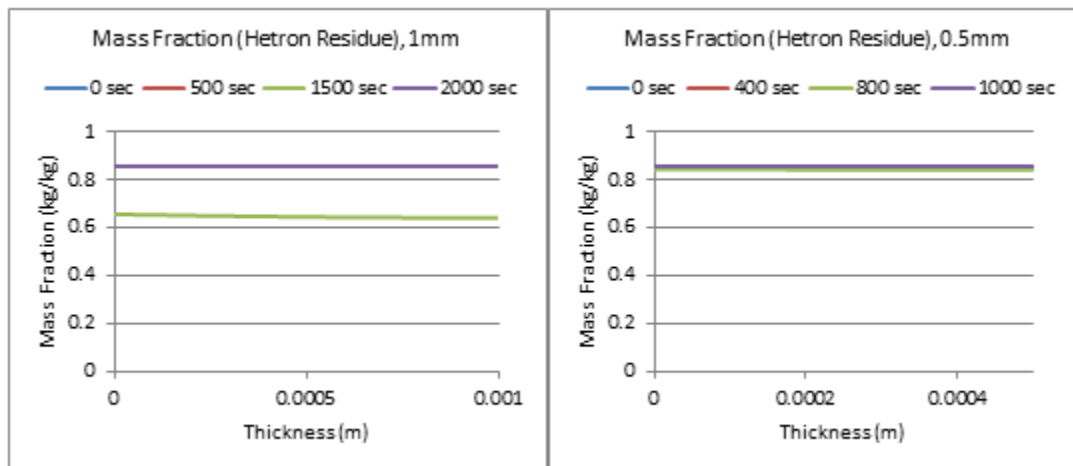
Figure 286: Mass Fraction (Hetron Residue) 1mm vs 0.5mm
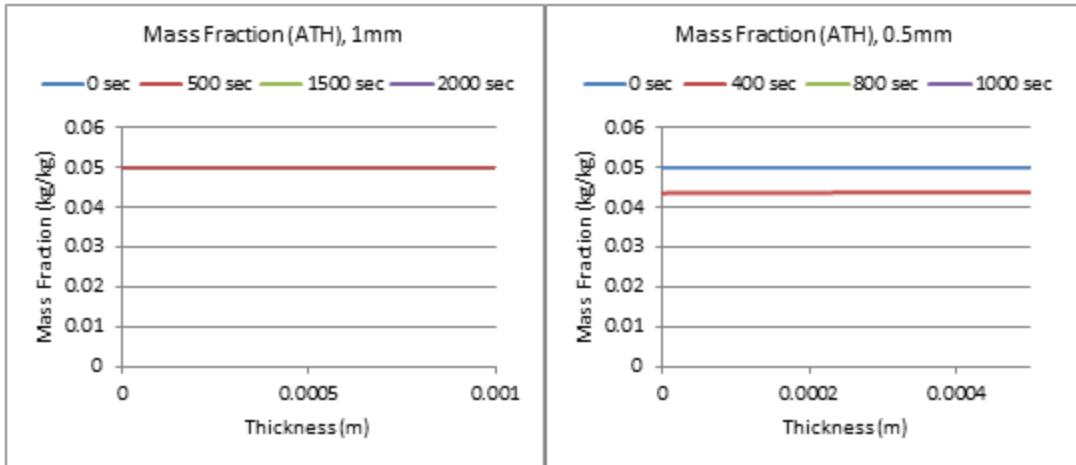
Figure 287: Mass Fraction (ATH) 1mm vs 0.5mm
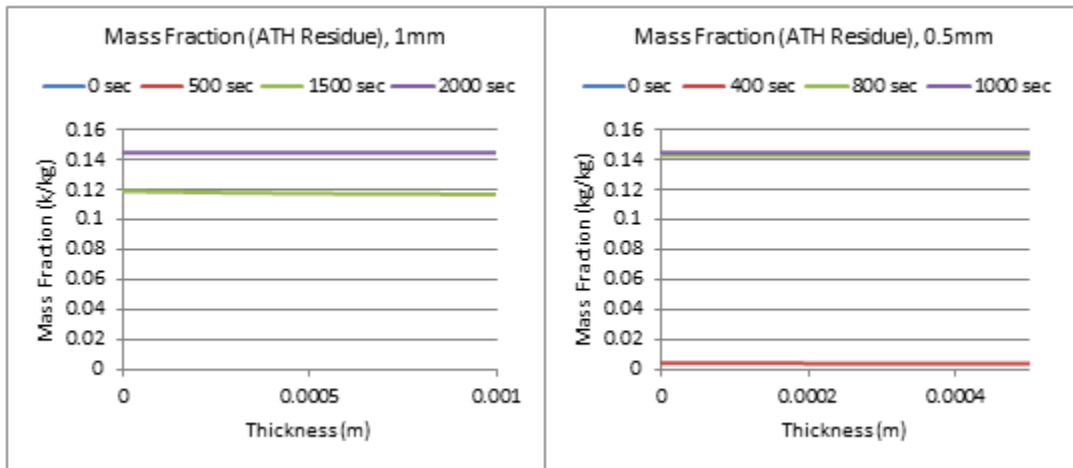
Figure 288: Mass Fraction (ATH Residue) 1mm vs 0.5mm

Appendix E.12: Gpyro Final Simulations, All Heating Rates, Ideal Mixing Model

The ideal mixing model comes from the isoconversional method, where Hetron and ATH are each modeled assuming to be single, separate reactions using an additive approach. All input parameters came from Gpyro. The ideal mixing model relies on the input of a temperature at each time step, which was also taken from a Gpyro simulation. The optimized parameters taken from Gpyro are shown in the Table below.

Table 22: Optimized Parameters for Ideal Mixing Model

Parameter	Hetron	ATH
E (Activation Energy)	195	140
Log(A) (Pre-exponential value)	13.7	11.4
n (Exponent)	1.125	1.25
f (Weight-loss Fraction)	0.13	0.56
Z (scaling constant)	0.707	0.084

Using the Gpyro values for parameters and Temperature is what allows the ideal mixing model to be run in terms of actual sample temperature.

In addition to the results found in the chapter on Gpyro, the same calculations were done for additional heating rates, which can be seen in the graphs below.
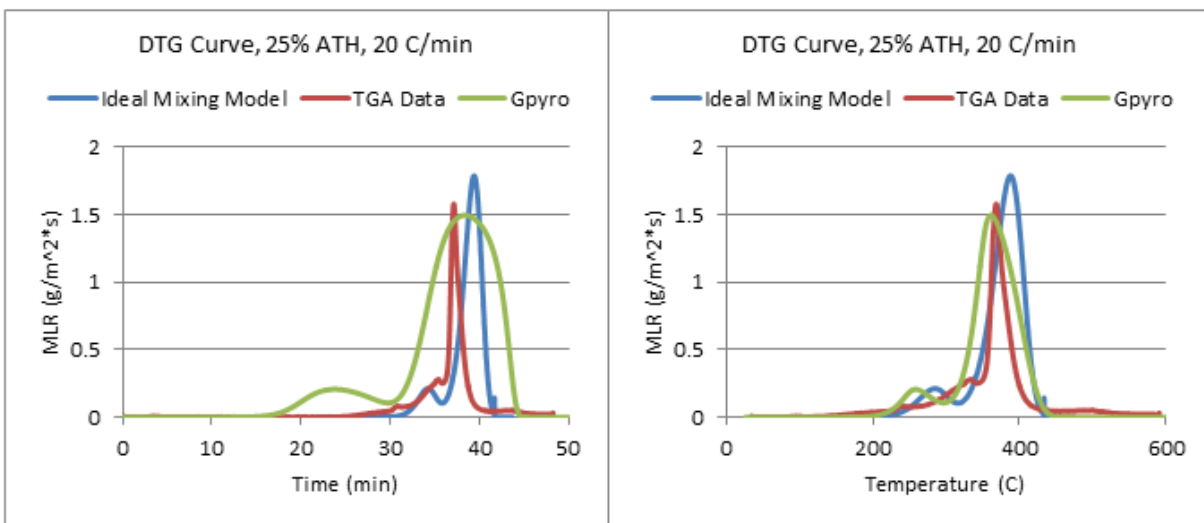
Figure 289: DTG Curve, Time vs Temperature Comparison, 20 C/min
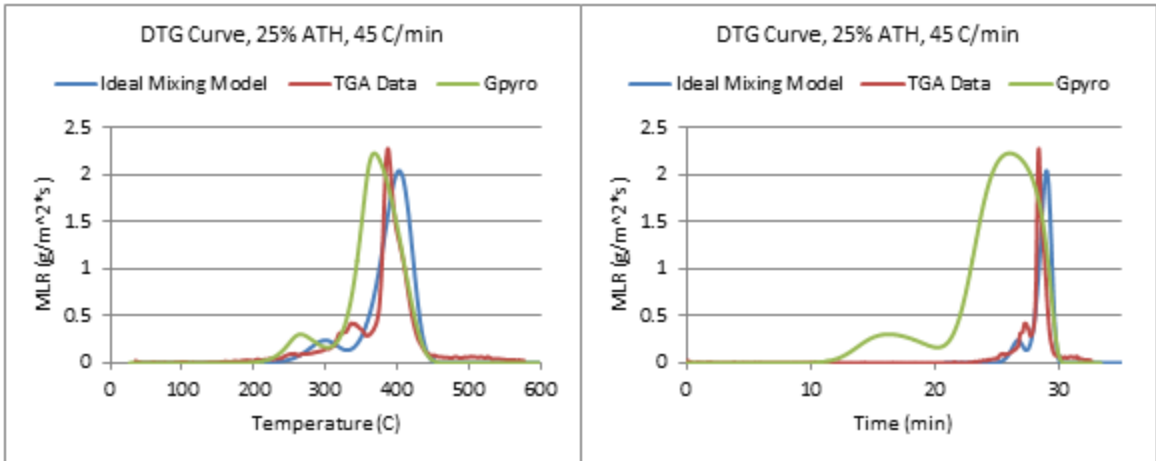
Figure 290: DTG Curve, Time vs Temperature Comparison, 45 C/min
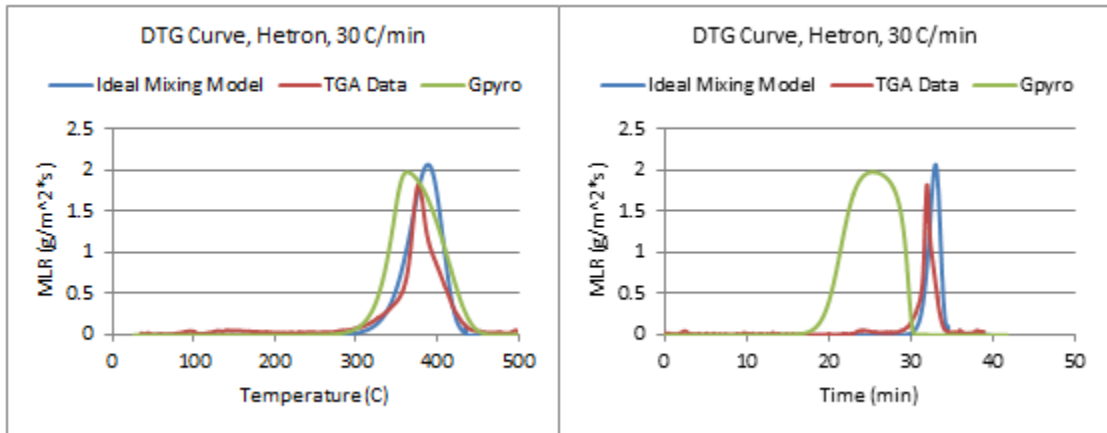
Figure 291: DTG Curve, Time vs Temperature Comparison, 30 C/min

Appendix F: Analysis Procedure

Appendix F.1: Isoconversional Method

Methods

As stated previously in Chapter 5, the isoconversional method is based off of the Arrhenius equation and the kinetic model as a function of α_1 which is defined as $\frac{m_o - m}{m_o - m_f}$. By rearranging the Arrhenius equation into a linear form, the following equation is formed:

$$\ln(\beta) = \ln\left(\frac{dT}{dt}\right) = \ln\left(\frac{Aexp\left(-\frac{E_a}{RT}\right)f(\alpha_1)}{\frac{d\alpha_1}{dt}}\right) = \ln\left(\frac{Af(\alpha_1)}{\frac{d\alpha_1}{dt}}\right) - \frac{E_a}{RT} \quad (6)$$

By plotting the natrual log of the heating rate β, $\ln(\beta)$, against $1/T$ for each conversion value from 0 to 1 a line of best fit can be found for each conversion value that is equal to $-E_a/R$. Once the slope is found it can be multiplied by $-R$ (-.008314) to find the activation energy at each conversion value. The temperatures are found from smoothed TGA data at four separate heating rates. In this analysis, heating rates of 10, 20, 30, and 45C/min were used. For more information on smoothing, see Appendix F.2: Runge Kutta Modeling. TGA data is converted to α_1 using the process outlined in Appendix F.2: Runge Kutta Modeling, and the temperature in Kelvin at conversion values ranging from 0.95 to 0.05 at incriments of 0.5 are recorded. This process is done for each heating rate at each conversion value. This in total equals four temperatures for each conversion value. A line of best fit is created using these four data points using the Microsoft Excel program LINEST. LINEST was used because it gives both lines of best fit and the associated error values.

Once the activation energy is calculated for each conversion value, the total activation energy can be found by taking an average over the decomposition range and the same can be done for the corresponding error values. For the Epoxy resin the decomposition range was found to be from $\alpha_1 = 0.5$ to 0.9. Results from the Epoxy resin mixture activation energy analysis can be found in Chapter 5 of this report.

PMMA Reference Material: Isoconversional

PMMA was tested in this way in order to compare the activation energies with those found in the literature. This was done prior to testing the Epoxy resin mixture to ensure we were conducting this analysis correctly before moving on to a material with unknown properties.

For each set of data from the TGA, one trial for each heating rate was chosen. For PMMA, the heating rates tested were 20, 30, 40, and 50C/min. The ln(β) vs 1/T graph below shows lines of best fits at each conversion degree.
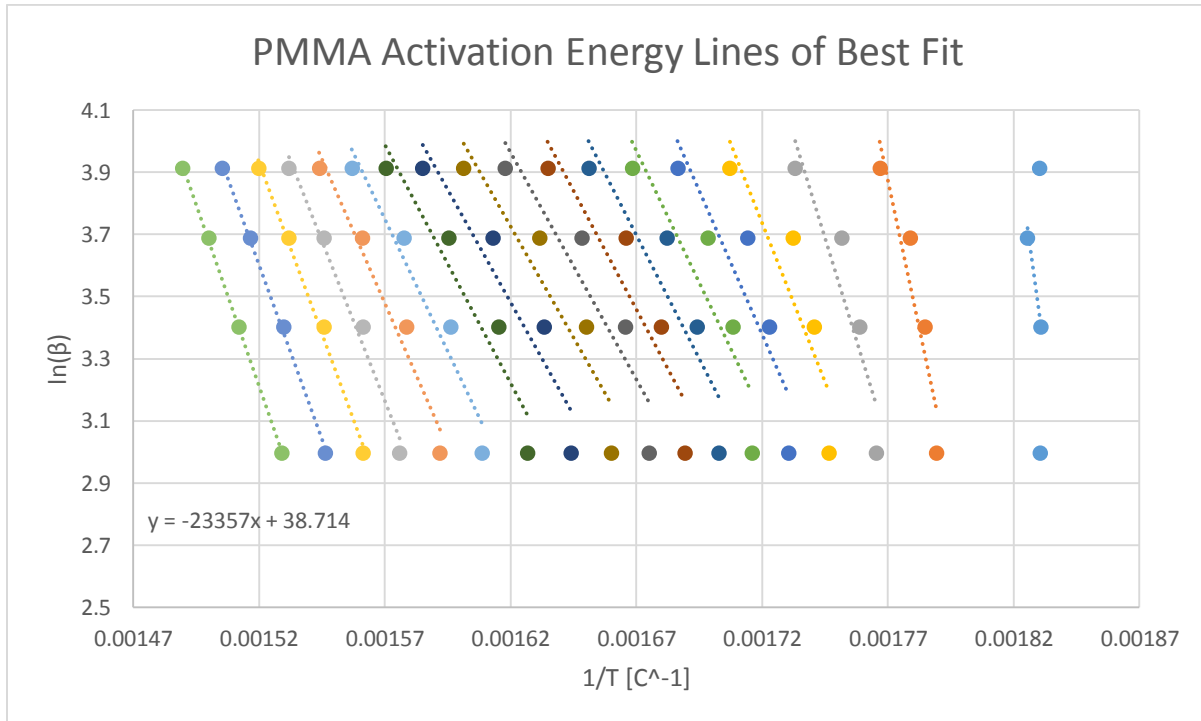
Figure 292: PMMA Lines of Best Fit

Although the lines of best fit are shown here, LINEST was used to get the actual slope and error values. These values were then plotted on a graph of Ea versus conversion degree, α_1.
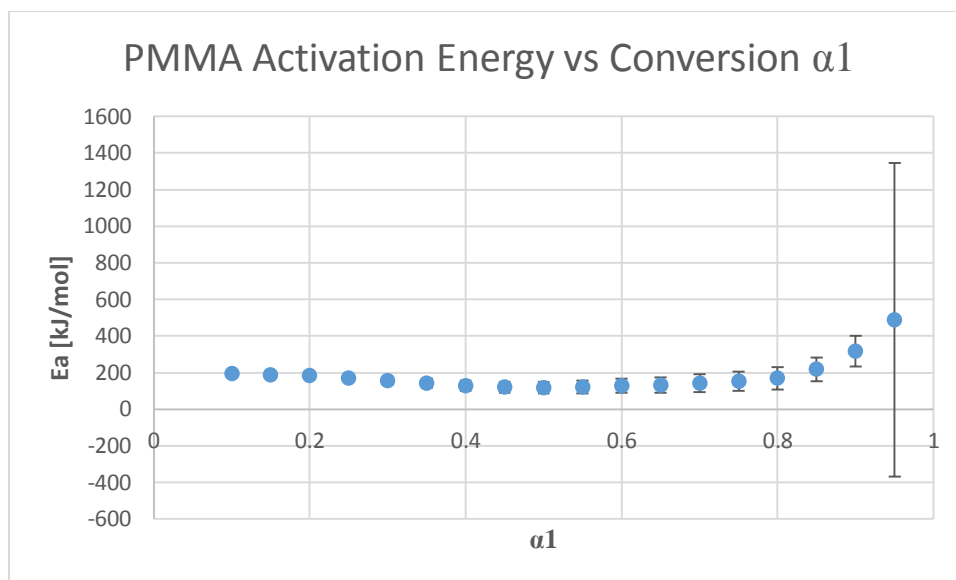
Figure 293: PMMA Activation Energy vs Conversion α1

The activation energies remain relatively constant until the higher conversion degrees where the activation energy increases. This increase in activation energy at higher conversion degrees could indicate that there are multiple reactions taking place [12]. The large error in the highest value of 0.95 makes sense because at higher α_1 values (lower conversion), the data from the TGA has yet to stabilize and often times reports the current mass as being larger than the initial mass which then reads an α_1 value of greater than 1. The range of decomposition for PMMA was determined to be from 0.9 to 0.1 conversion. The average activation energy calculated over this range was 160 with an error of 35 kJ/mol.

In a paper comparing results from PMMA with a high molecular weight to a low molecular weight, results were found that support the experimental activation energy [12]. In the analysis done in this experiment, they tested PMMA at 2, 5, 8, and 10 C/min, so we compared their data for 10 C/min to our data for 20 C/min to attempt to get as similar results as possible. The first plot below shows the experimental PMMA data at 20 C/min and the second plot shows the literature data for both the higher molecular weight and lower molecular weight PMMA samples.
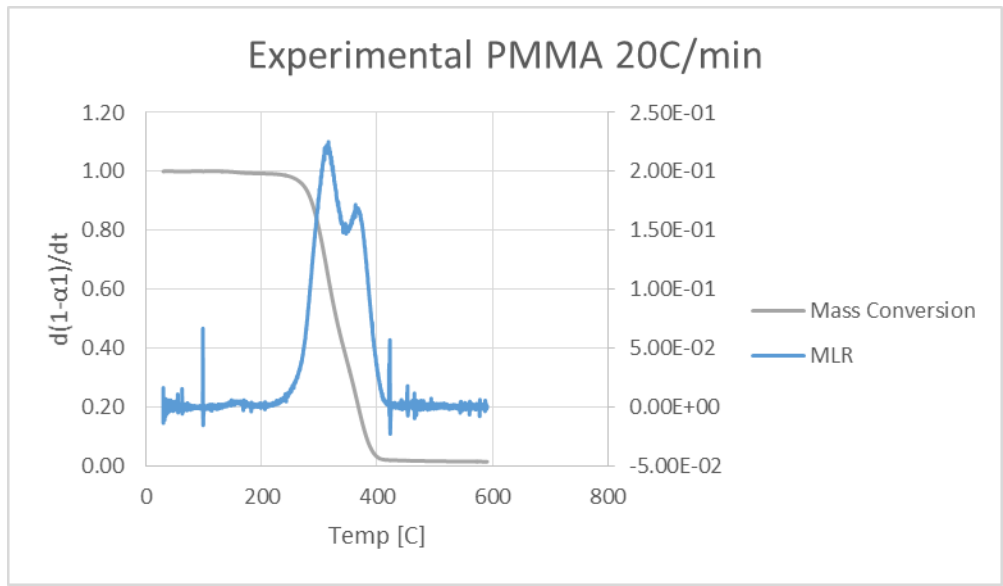
Figure 294: Experimental PMMA at 20C/min
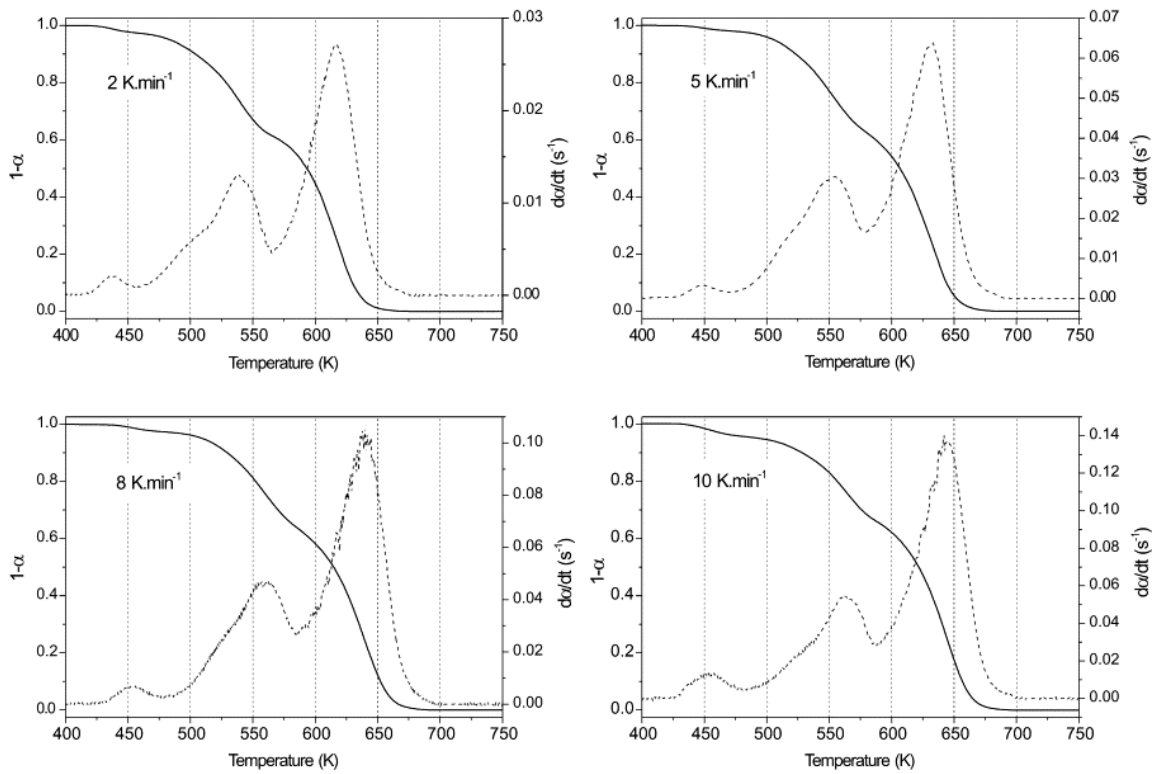
Figure 295: Literature results for 996,000 g/mol PMMA
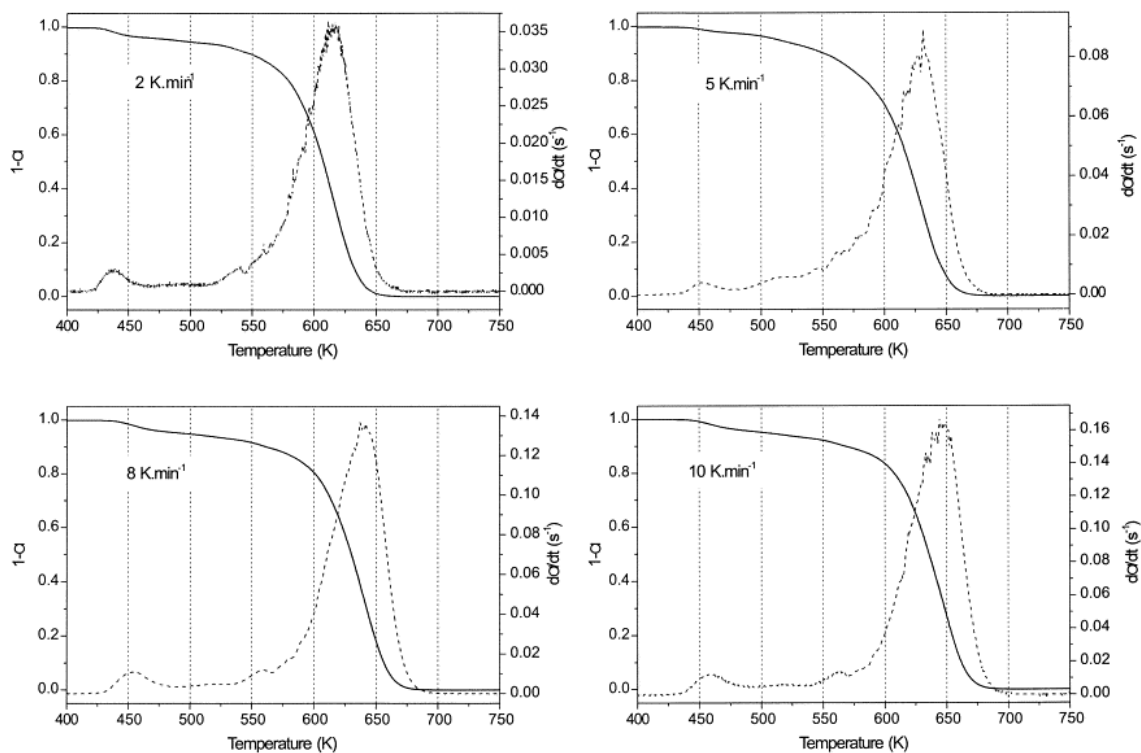
Figure 296: Literature results for 350,000 g/mol PMMA

Although the graphs for the experimental and literature data to not match for either molecular weight sample, the activation energies calculated for each show similar results. The literatures states that there are four potential reactions involved when testing PMMA but that only the first and fourth reactions hold any power over the reaction, thus the experimental data was compared to the first step in the literature based on numerical proximity [12].

Table 23: PMMA literature results

	350,000 g/mol Step 1	996,000 g/mol Step 1
2 C/min	183.3 +/- 3.4	190.8 +/- 1.2
5 C/min	186.6 +/- 3.5	189.0 +/- 1.2
8 C/min	178.5 +/- 3.3	188.9 +/- 1.2
10 C/min	181.6 +/- 3.4	191.1 +/- 1.2
Average	182.5 +/- 3.4	190.0 +/- 1.2

It is clear that despite the experimental data curve being more similar to the curve for the higher molecular weight PMMA, the experimental activation energy data fits well with the literature values for the 350,000 g/mol PMMA. Our value for the activation energy is 160 kJ/mol with an error of 35 kJ/mol, thus with the given error it is difficult to conclude an exact match. In addition it is not known whether the sample of PMMA tested in the lab matches the composition of that from the literature. Despite this, our data is reasonably accurate which suggests that we are both running the tests correctly and also are doing the isoconversional analysis correctly as well.

Appendix F.2: Runge Kutta Modeling

Methods

There are two main parts to consider when optimizing data from the TGA: experimental data and simulated data. The experimental data must be manipulated before the data can be modeled.

The TGA gives the Weight % in terms of αo equal to 100*(1-αo), and this can be converted to 1-αo. The TGA defines αo as $\alpha_o = \frac{m_o - m}{m_o} = 1 - \frac{m}{m_o}$

To account for the final mass, a separate form of the alpha term is used:

$$\alpha_1 = \frac{m_o - m}{m_o - m_f} = \frac{1 - \frac{m}{m_o}}{1 - \frac{m_f}{m_o}} \quad (7)$$

Writing α1 in terms of αo gives

$$\alpha_1 = \frac{m_o}{m_o - m_f} * \alpha_o = \frac{\alpha_o}{1 - \frac{m_f}{m_o}} \quad (8)$$

Differentiating this equation gives

$$\frac{d\alpha_1}{dt} = -\frac{1}{m_o - m_f} * \frac{dm}{dt} = \frac{\frac{d\alpha_o}{dt}}{1 - \frac{m_f}{m_o}} \quad (9)$$

$$\left(m_o - m_f\right)\frac{d\alpha_1}{dt} = -\frac{dm}{dt} \quad (10)$$

$$m_o \frac{d\alpha_o}{dt} = \left(m_o - m_f\right)\frac{d\alpha_1}{dt} \quad (11)$$

$$\frac{d\alpha_1}{dt} = \frac{m_o}{m_o - m_f}\frac{d\alpha_o}{dt} = \frac{\frac{d\alpha_o}{dt}}{1 - \frac{m_f}{m_o}} \quad (12)$$

For the experimental data, the $\frac{d\alpha_1}{dt}$ is calculated using the $\frac{d\alpha_o}{dt}$ given from the TGA as the derivative of the Weight %.

$\frac{d(1-\alpha_1)}{dt}$ was also calculated using

$$\frac{d(1-\alpha_1)}{dt} = \frac{-((1-\alpha_1)^{i-1} - (1-\alpha_1)^i)}{dt} \quad (13)$$

With i representing the time step. $\frac{d(1-\alpha_1)}{dt}$ can also be calculated using

$$\frac{d(1-\alpha_1)}{dt} = \frac{dm}{dt} * \frac{1}{m_o-m_f} \qquad (14)$$

according to the derivation of $1 - \alpha_1 = \frac{m-m_f}{m_o-m_f}$ from $\alpha_1 = \frac{m_o-m}{m_o-m_f}$.

$$\alpha_1 = \frac{m_o-m}{m_o-m_f} \quad (15)$$

$$1 - \alpha_1 = \frac{m_o-m_f-m_o+m}{m_o-m_f} = \frac{m-m_f}{m_o-m_f} \qquad (16)$$

After switching the experimental data from αo to α1, the data can be modeled Runge-Kutta 4th Order Modeling. The kinetic model has two equations: one for the rate of change of conversion and one for the heating rate as seen in Chapter 5: Kinetic Modeling. Because the model is being matched to experimental data in terms of α1, the model is produced in terms of α1.

Applying RK4 then looks like:

$$k1d(1-\alpha_1) = dt * \left[Aexp\left(-\frac{E_a}{R(T_o+\beta*t)}\right)\right](1-\alpha_1)^n \qquad (17)$$

$$k2d(1-\alpha_1) = dt * \left[Aexp\left(-\frac{E_a}{R(T_o+\beta*(t+0.5*dt))}\right)\right]((1-\alpha_1)+0.5*k1d(1-\alpha_1))^n \qquad (18)$$

$$k3d(1-\alpha_1) = dt * \left[Aexp\left(-\frac{E_a}{R(T_o+\beta*(t+0.5*dt))}\right)\right]((1-\alpha_1)+0.5*k2d(1-\alpha_1))^n \qquad (19)$$

$$k4d(1-\alpha_1) = dt * \left[Aexp\left(-\frac{E_a}{R(T_o+\beta*(t+dt))}\right)\right]((1-\alpha_1)+k3d(1-\alpha_1))^n \qquad (20)$$

$$(1-\alpha_1)_n = (1-\alpha_1)_{n-1} + \frac{1}{6}(k1d(1-\alpha_1) + 2(k2d(1-\alpha_1)+k3d(1-\alpha_1)) + k4d(1-\alpha_1)) \qquad (21)$$

The mass was found both for the experimental and simulated data by using the relationship of α1 to αo and solving for m.

$$1 - \alpha_o = 1 - \left(1 - \frac{m}{m_o}\right) = \frac{m}{m_o} \qquad (22)$$

To set up the experimental and simulated data, the experimental mass is found. (1- α1) is found and converted to -d(1- α1)/dt. Once the experimental data is set up, α1 is simulated using the

RK4 sequence from above, and the same procedure is followed to obtain graphs of (1- α1) and -d(1- α1)/dt.

Optimization of Parameters

Once the simulated and experimental data are ready to be optimized, the parameters A and n can be modified. The activation energy is a fixed value that was found via the OFW isoconversional method, and can be assumed constant throughout each heating rate. For more information on the isoconversional method see Appendix F.1: Isoconversional Method. The values for A and n are systematically changed to shift the simulated data to fit the experimental data. When optimizing the parameters, an error scheme was created in order to best fit the model. Three error values were created that encompasses the majority of the mass lost during the TGA experiment. One associated with the m/mo plot, one associated with the MLR plot, and one associated with the peak point of the MLR curve. The parameters of A and n were changed in order to minimize this error.

Error Scheme

The error scheme used to optimize the A and n parameters found in the Runge Kutta 4th Order modeling aimed to minimize the error over three main parts of the model. The first error is calculated by averaging the difference between the experimental and simulated curves from the -d(1- α1)/dt plot, the second from averaging the error from the 1- α1 curves, and the third from the difference between the peak points on the -d(1- α1)/dt curve. These three errors were weighted to create a total error.

$$E_T = 0.25E_1 + 0.25E_2 + 0.5E_3 \qquad (23)$$

The peak temperature error is weighted more heavily than the errors for the mass conversion plot and the derivative plot because we believe matching the peak point is more important in estimating the kinetic parameters than the other two errors because the derivative and mass conversion plots may shift themselves so that the peak is off, but in terms of each data point this is minimizing the error more so than if the peak heights matched.

Smoothing Curves

Ensuring that a decrease in peak temperature does not change by more than 5 degrees Celsius, these smoothing ranges have been chosen based on the approximate level of noise for each heating rate. The smoothing ranges were changed for each heating rate because on less noisy trials, if a high smoothing range is chosen, the peak temperature shifts dramatically, which is unnecessary due to the fact that less noisy graphs already have single peak temperature.

Table 24: Smoothing Curves

Heating Rate	Smoothing Range
10C/min	100 cells
20C/min	60 cells
30C/min	30 cells
45C/min	15 cells

Table 25: Unsmoothed vs Smoothed

Material/Heating Rate	Unsmoothed Peak Temp [C]	Smoothed Peak Temp [C]
Epoxy (Neat) 10C/min	327.4	324.1
Epoxy (Neat) 20C/min	334.6	329.5
Epoxy (Neat) 30C/min	341.0	337.2
Epoxy (Neat) 45C/min	347.4	344.7

Epoxy + 5% ATH 10C/min	313.8	307.8
Epoxy + 5% ATH 20C/min	335.3	330.2
Epoxy + 5% ATH 30C/min	340.0	335.9
Epoxy + 5% ATH 45C/min	348.9	345.8
Epoxy + 10% ATH 10C/min	315.1	318.6
Epoxy + 10% ATH 20C/min	331.1	334.0
Epoxy + 10% ATH 30C/min	333.8	336.9
Epoxy + 10% ATH 45C/min	341.8	344.9
Epoxy + 20% ATH 10C/min	322.0	329.3
Epoxy + 20% ATH 20C/min	331.3	334.7
Epoxy + 20% ATH 30C/min	340.2	343.8
Epoxy + 20% ATH 45C/min	366.0	369.4
Pure Hetron 10C/min	357.5	353.5
Pure Hetron 20C/min	372.7	369.2
Pure Hetron 30C/min	379.2	375.5
Pure Hetron 45C/min	386.0	383.0
Pure ATH 10C/min	277.4	272.2
Pure ATH 20C/min	290.7	283.8
Pure ATH 30C/min	299.3	294.5
Pure ATH 45C/min	301.0	297.6

Optimized Parameter Database

The following is a compilation of graphs showing how the simulated curves compare to the experimental curves for each material and heating rate. The analysis for ATH was done using testing data from previous years [17].

Epoxy (Neat):
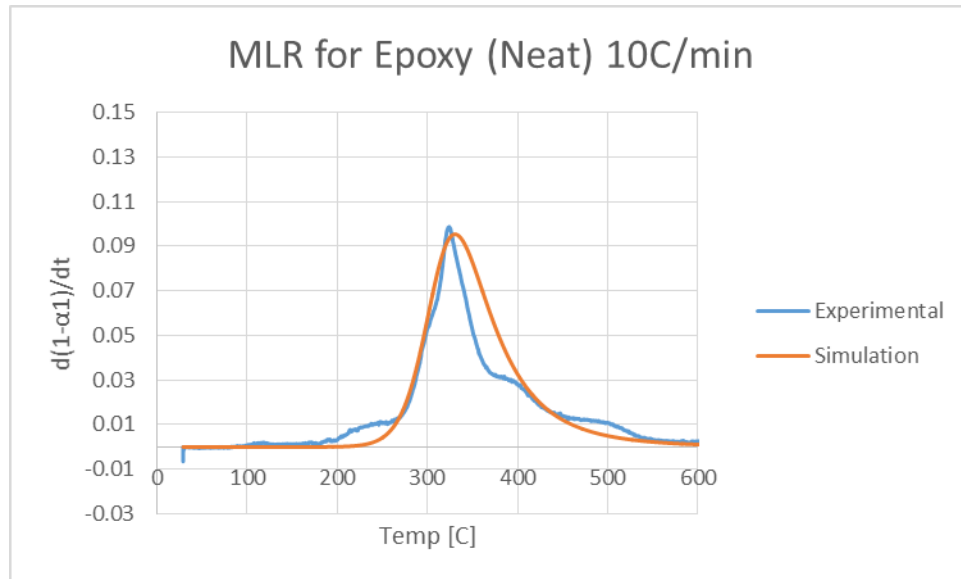
Figure 297: MLR for Epoxy (Neat) 10 C/min
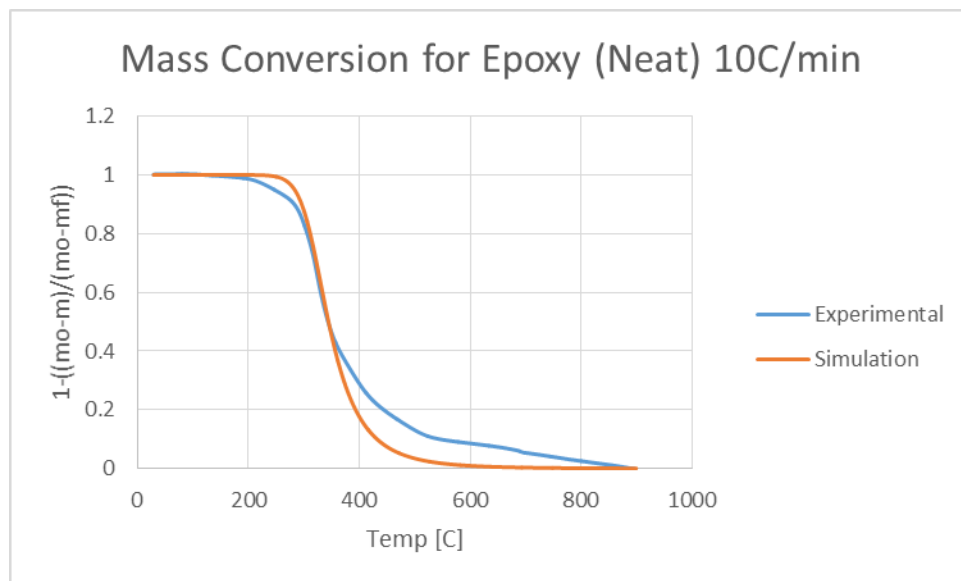
Figure 298: Mass Conversion for Epoxy (Neat) 10 C/min
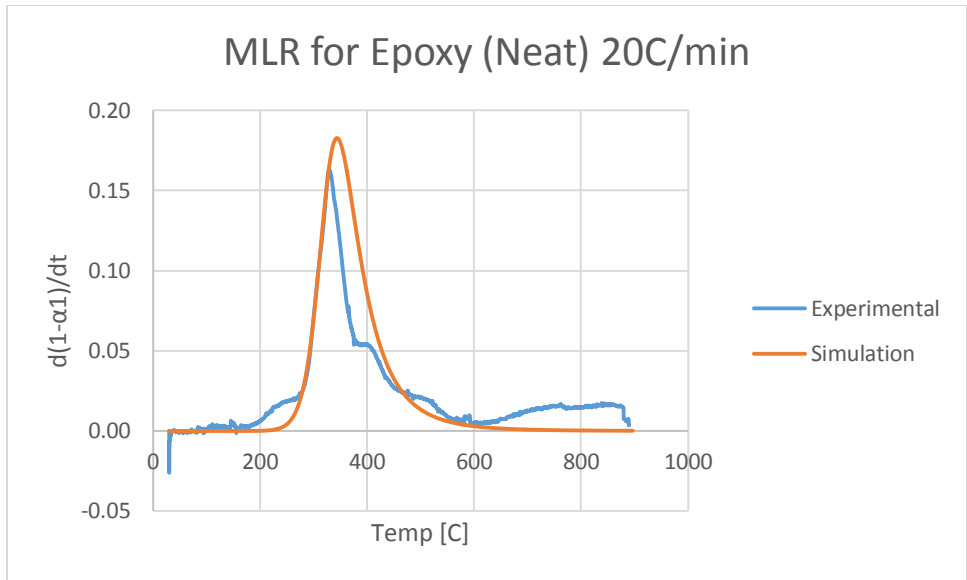
Figure 299: MLR for Epoxy (Neat) 20 C/min
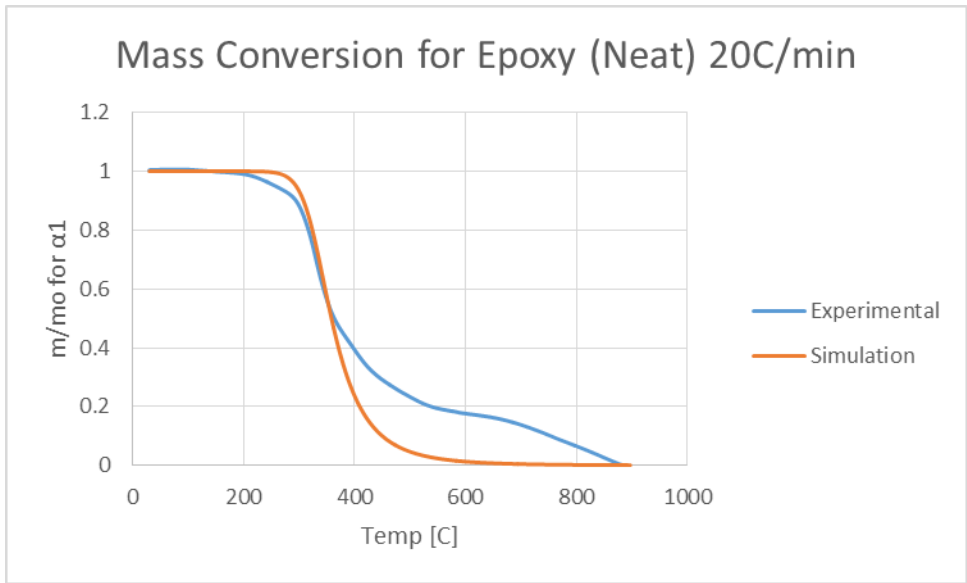
Figure 300: Mass Conversion for Epoxy (Neat) 20 C/min
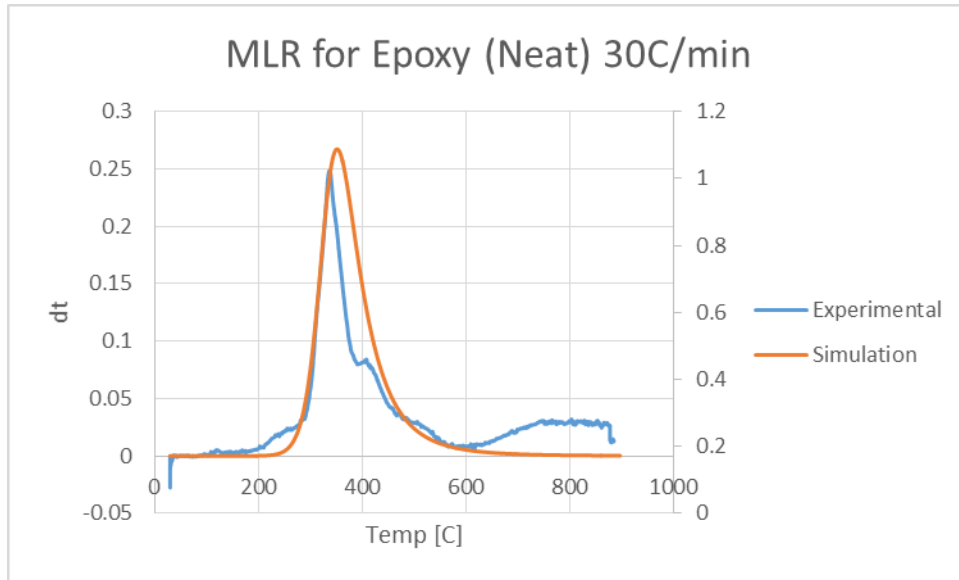
Figure 301: MLR for Epoxy (Neat) 30 C/min
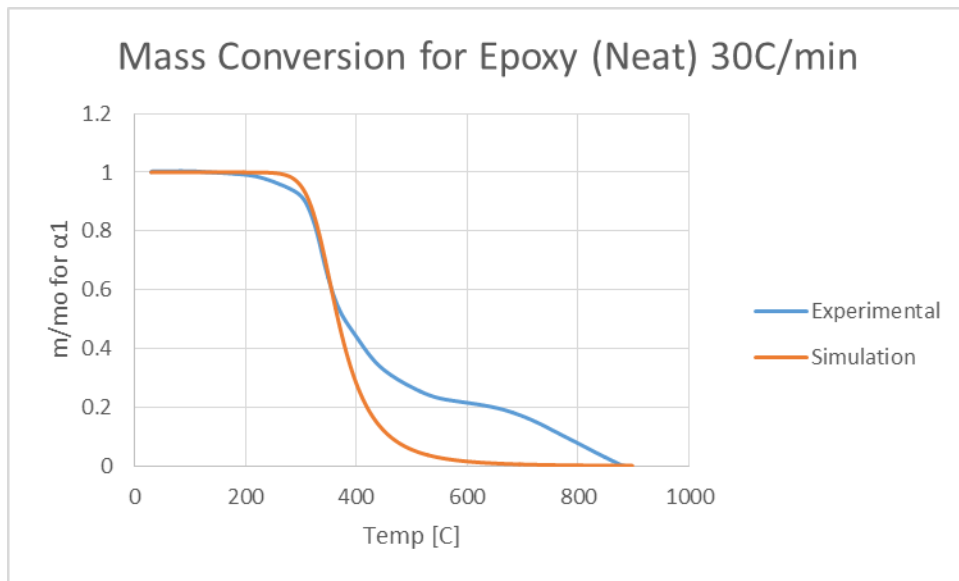
Figure 302: Mass Conversion for Epoxy (Neat) 30 C/min
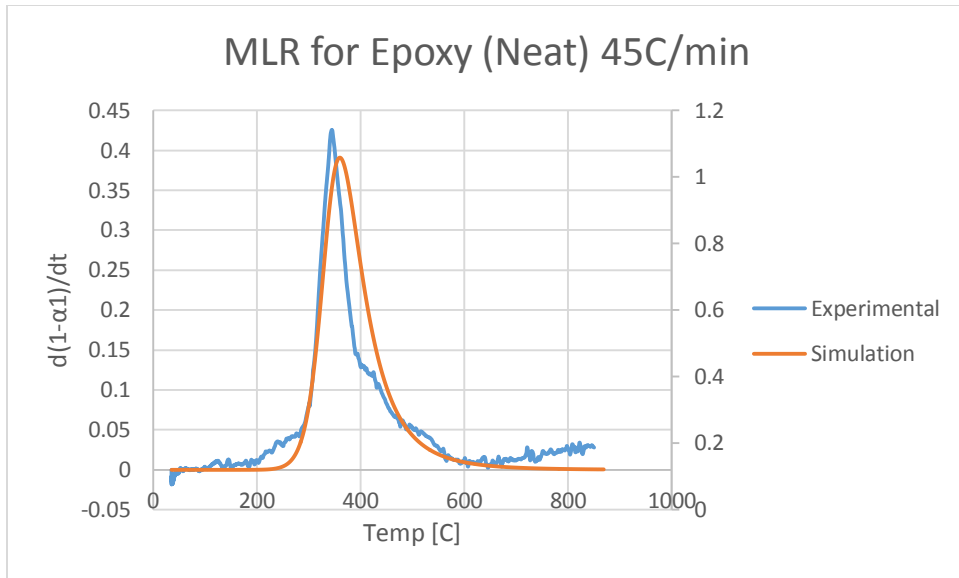
Figure 303: MLR for Epoxy (Neat) 45 C/min
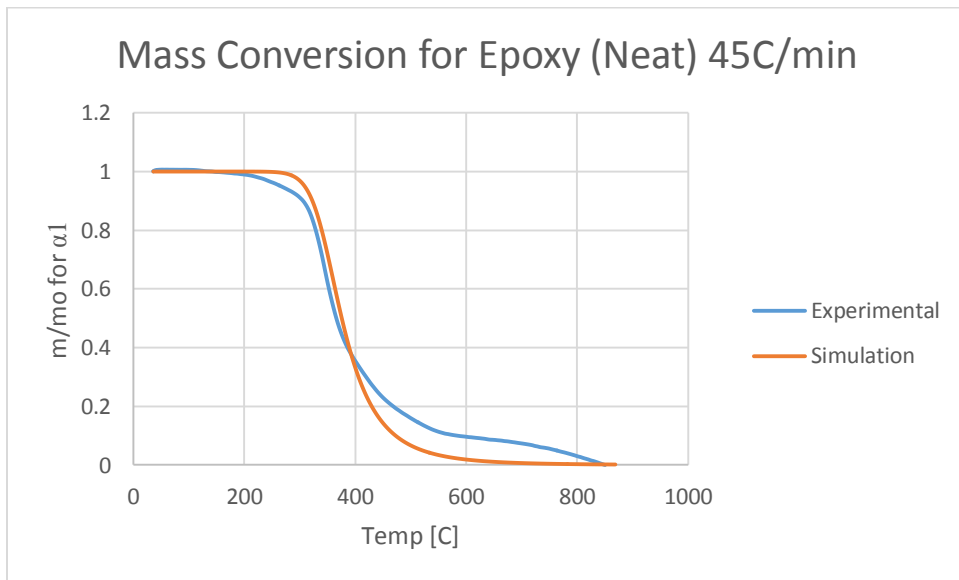
Figure 304: Mass Conversion for Epoxy (Neat) 45 C/min

Epoxy + 5% ATH:
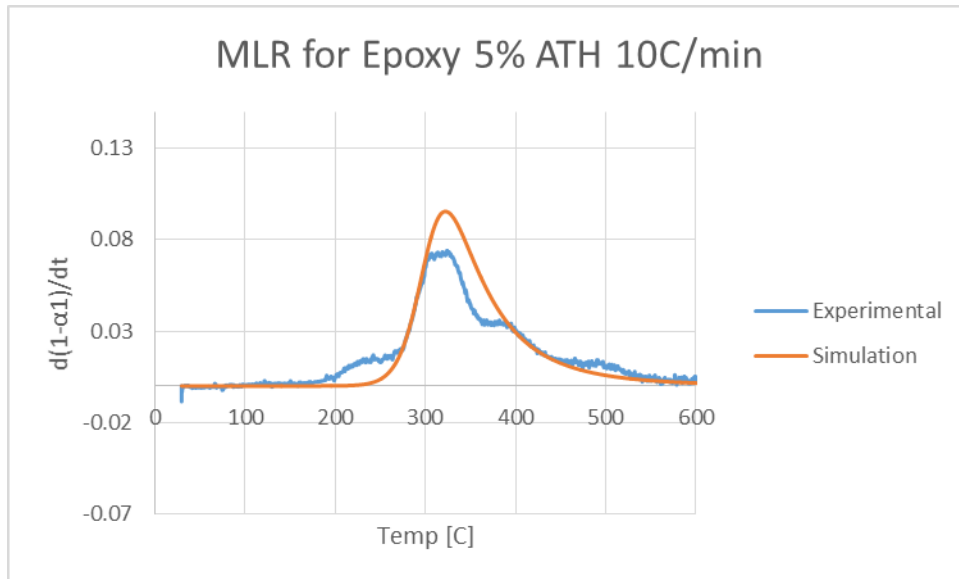
Figure 305: MLR for Epoxy 5% ATH 10 C/min
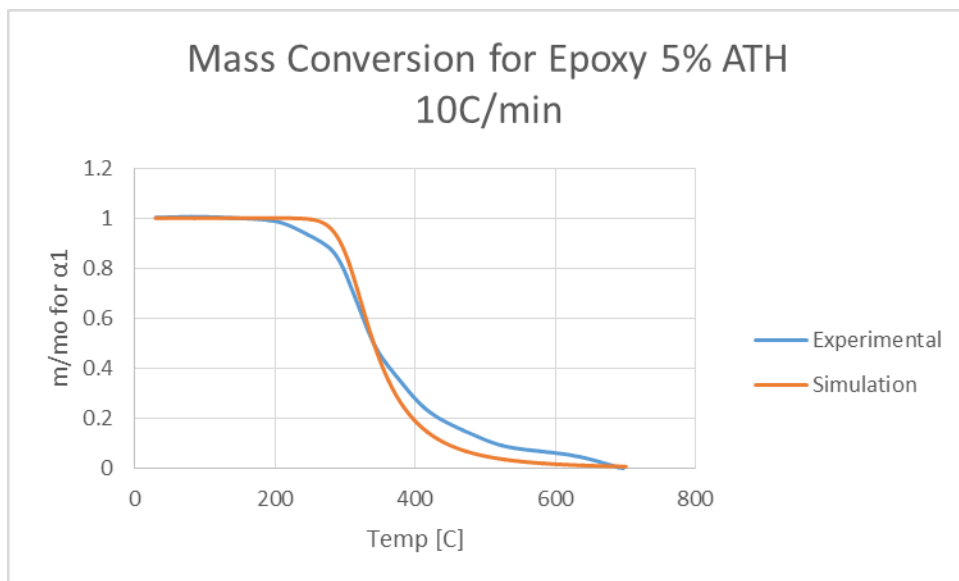
Figure 306: Mass Conversion for Epoxy 5% ATH 10 C/min
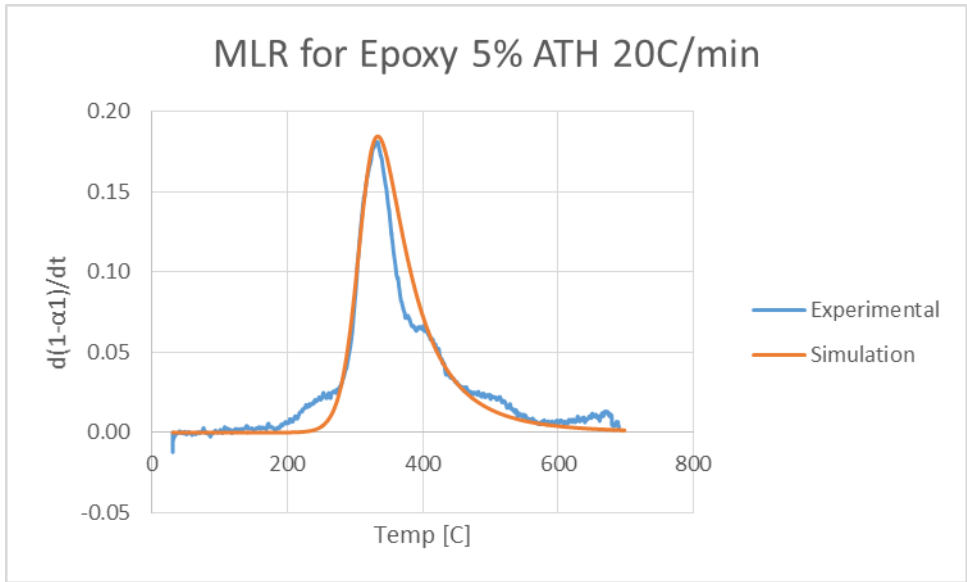
Figure 307: MLR for Epoxy 5% ATH 20 C/min
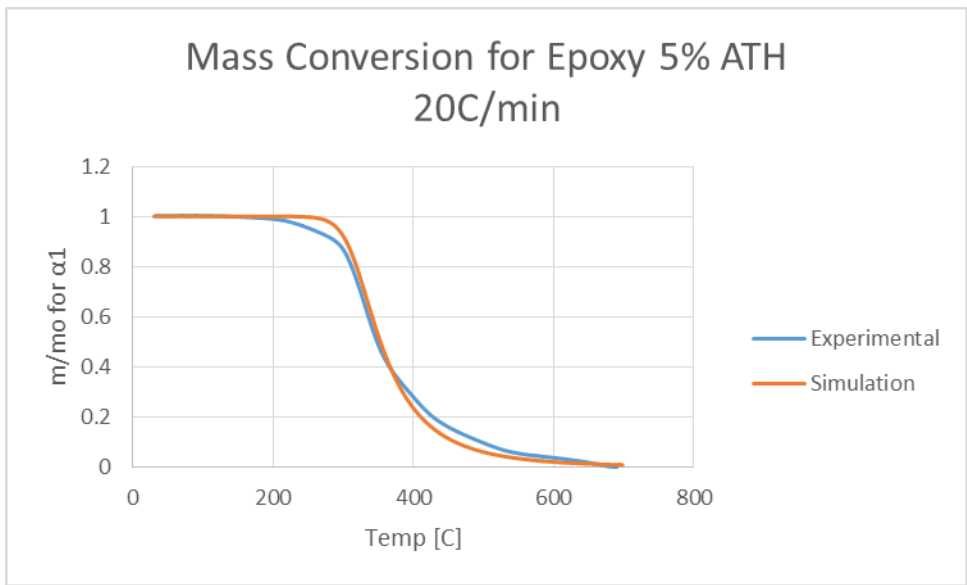
Figure 308: Mass Conversion for Epoxy 5% ATH 20 C/min
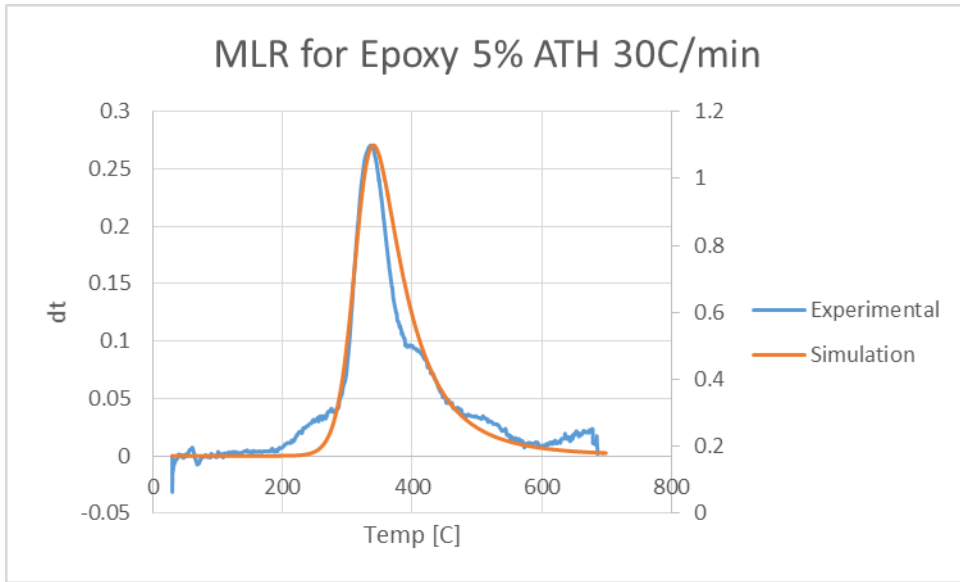
Figure 309: MLR for Epoxy 5% ATH 30 C/min
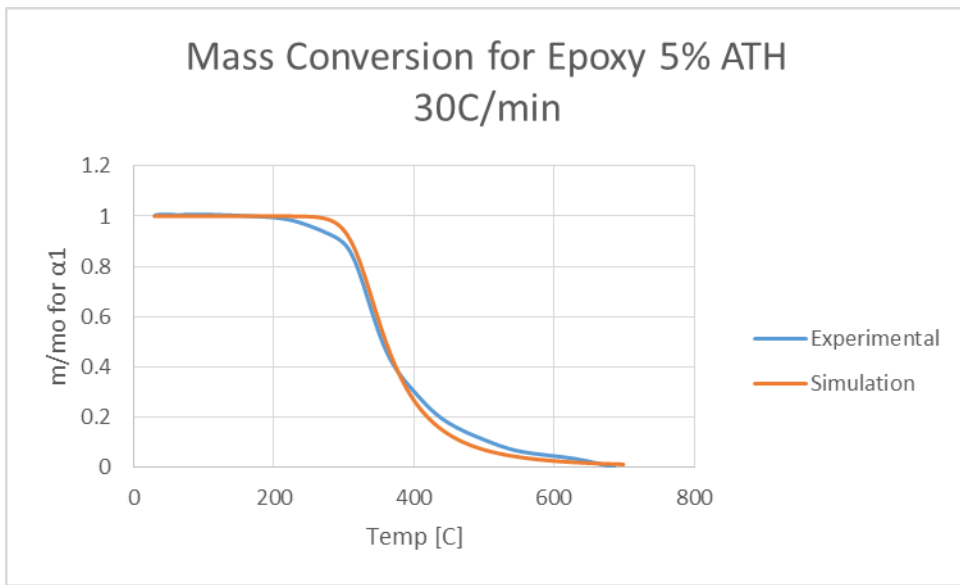
Figure 310: Mass Conversion for Epoxy 5% ATH 30 C/min
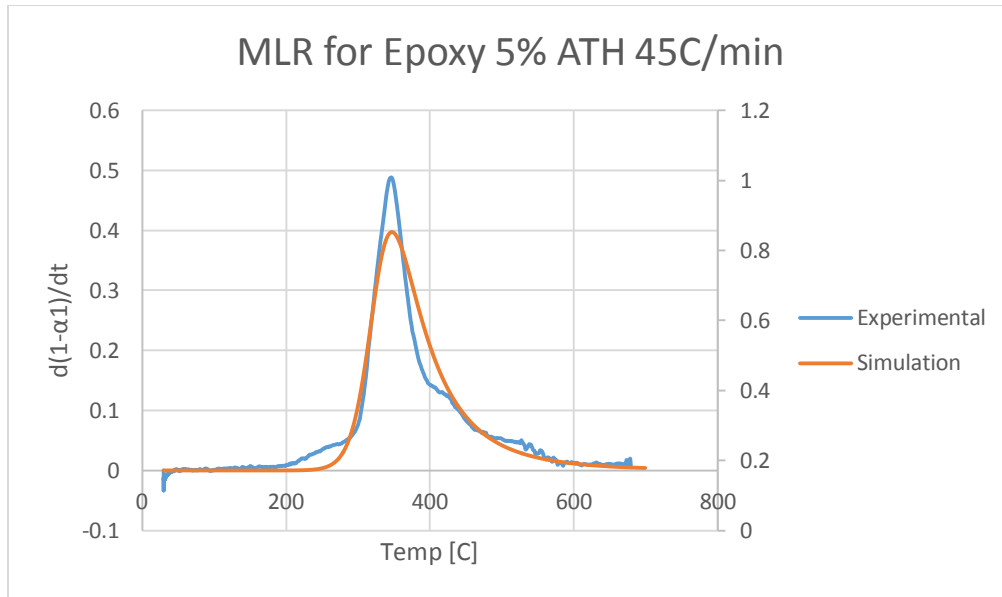
Figure 311: MLR for Epoxy 5% ATH 45 C/min
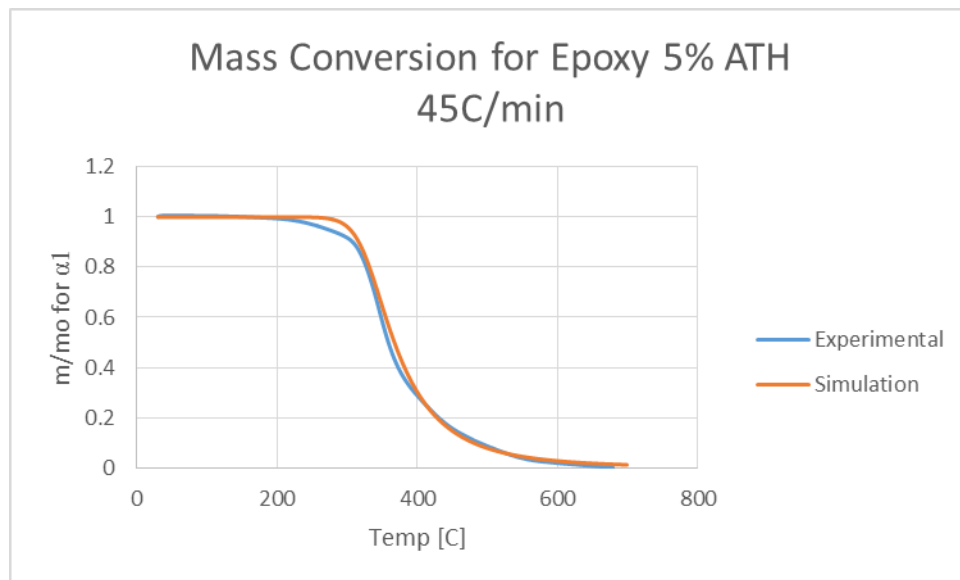
Figure 312: Mass Conversion for Epoxy 5% ATH 45 C/min

Epoxy + 10% ATH:
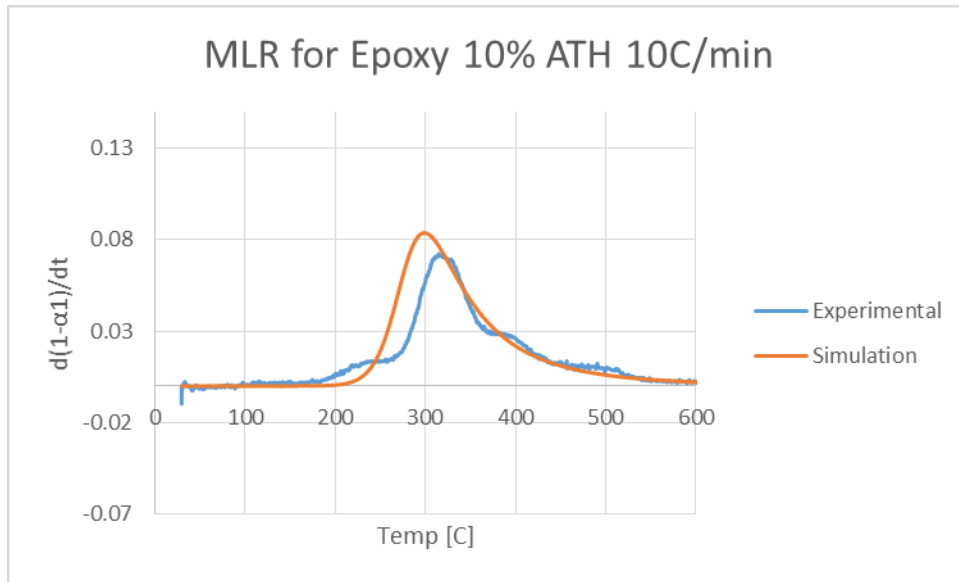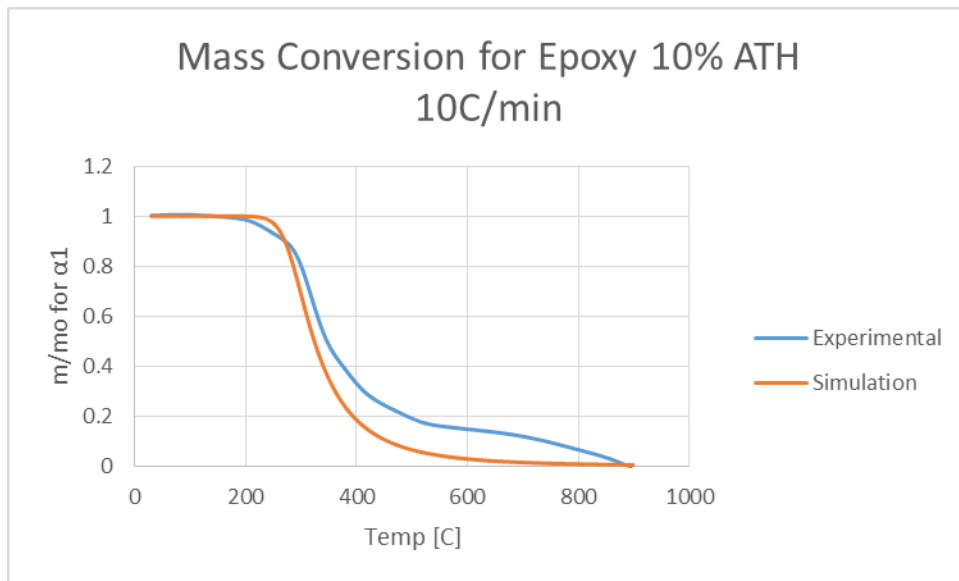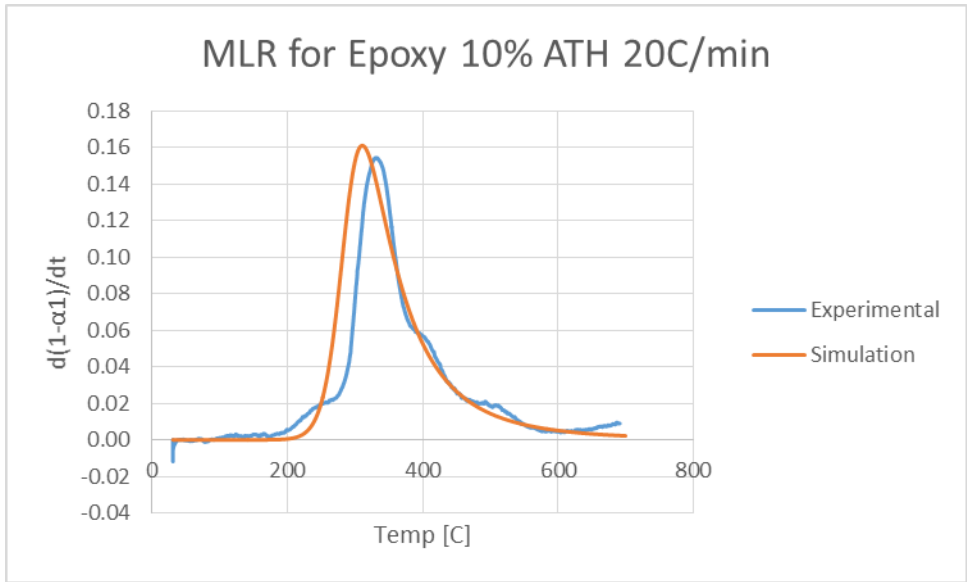
Figure 315: MLR for Epoxy 10% ATH 20 C/min
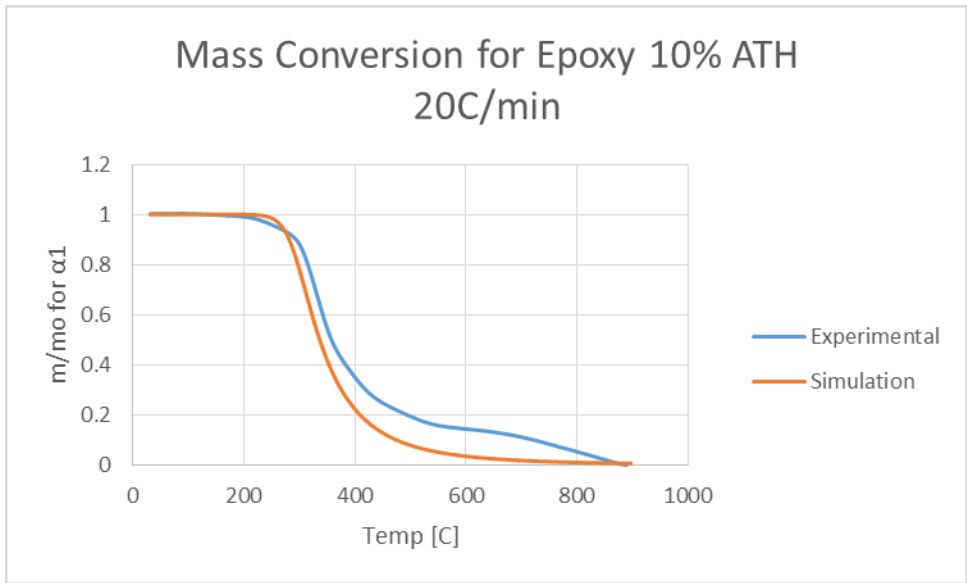
Figure 316: Mass Conversion for Epoxy 10% ATH 20 C/min
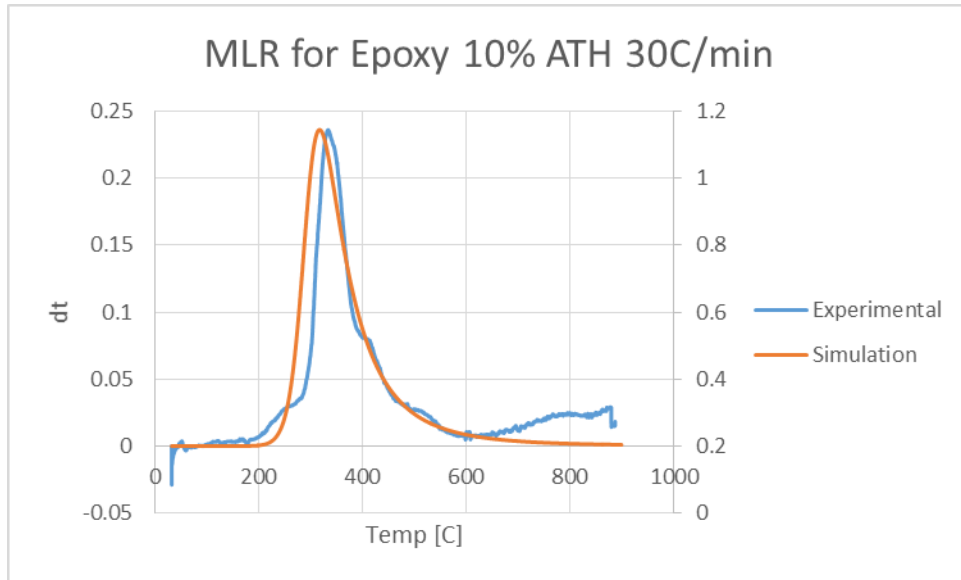
Figure 317: MLR for Epoxy 10% ATH 30 C/min
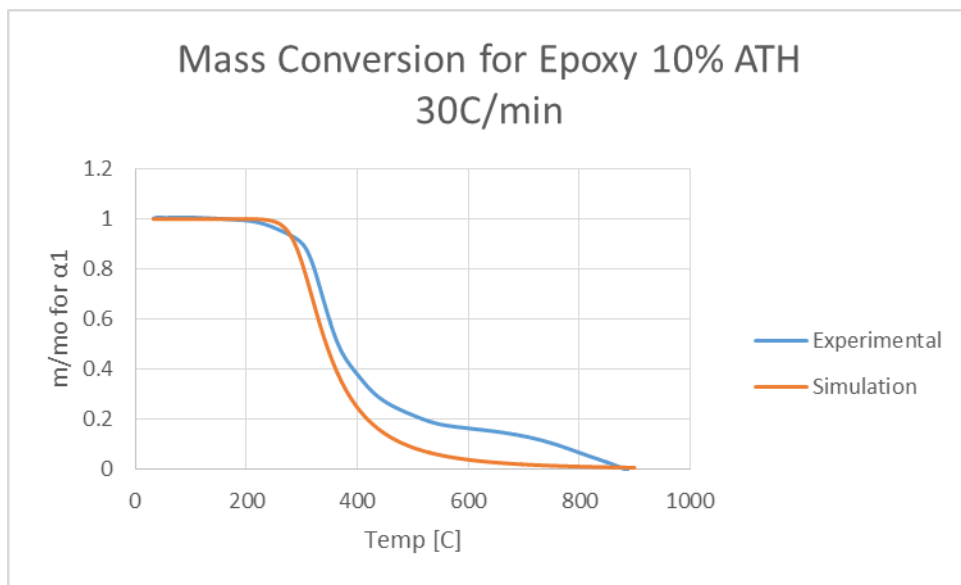
Figure 318: Mass Conversion for Epoxy 10% ATH 30 C/min
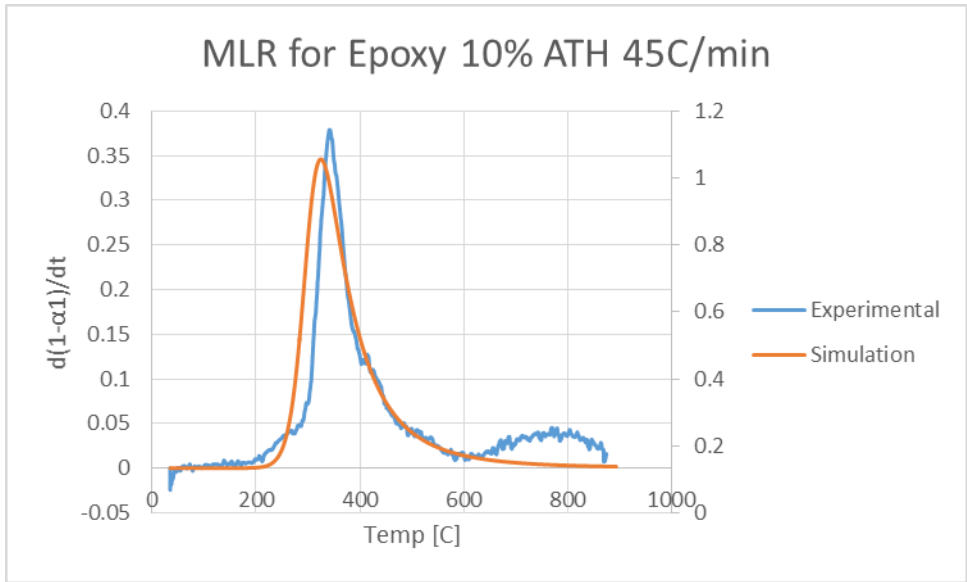
Figure 319: MLR for Epoxy 10% ATH 45 C/min
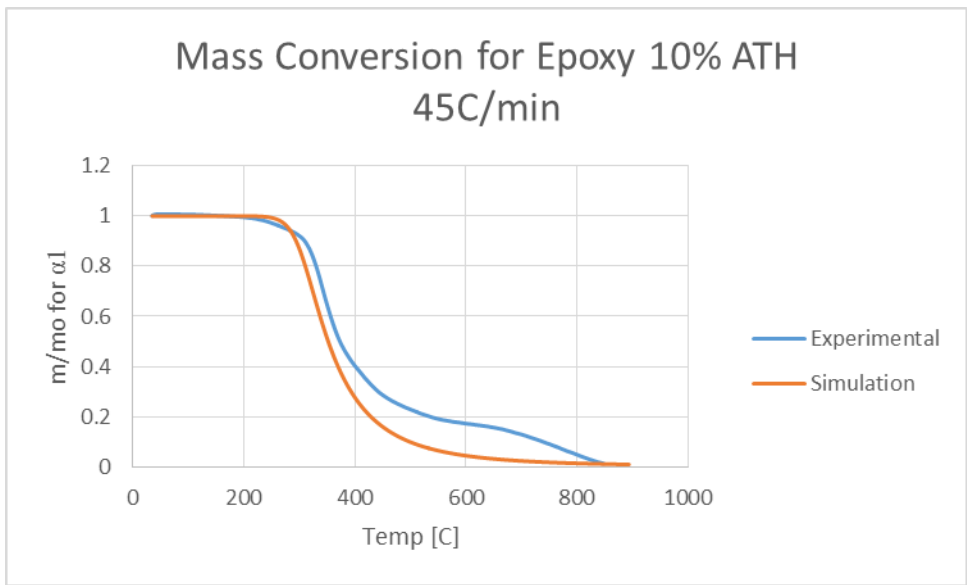
Figure 320: Mass Conversion for Epoxy 10% ATH 45 C/min

Epoxy + 20% ATH:
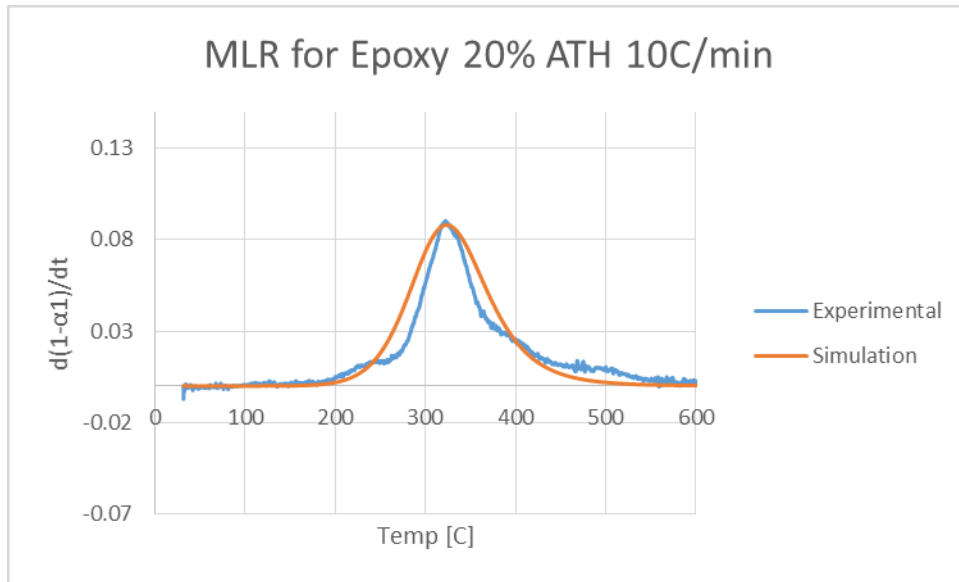
Figure 321: MLR for Epoxy 20% ATH 10 C/min
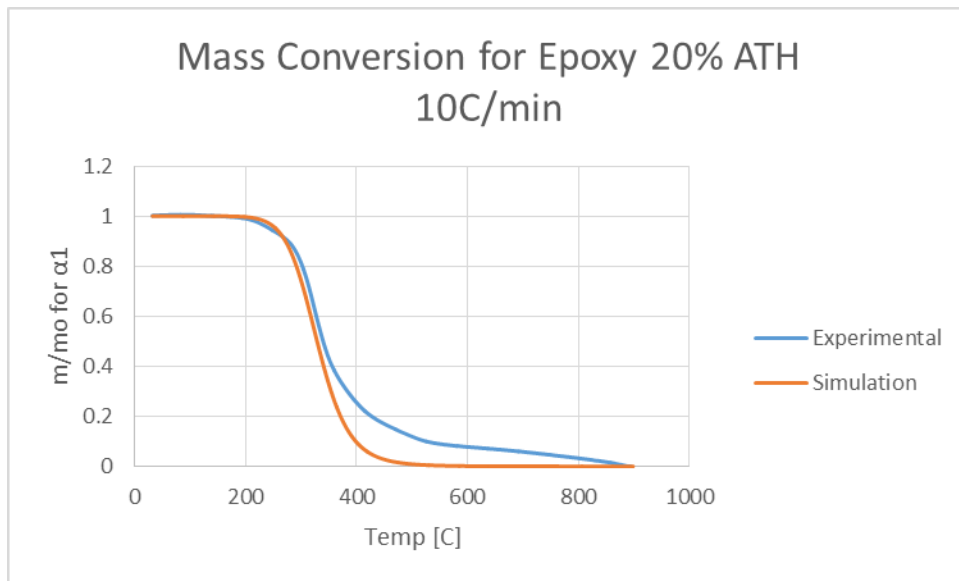
Figure 322: Mass Conversion for Epoxy 20% ATH 10 C/min
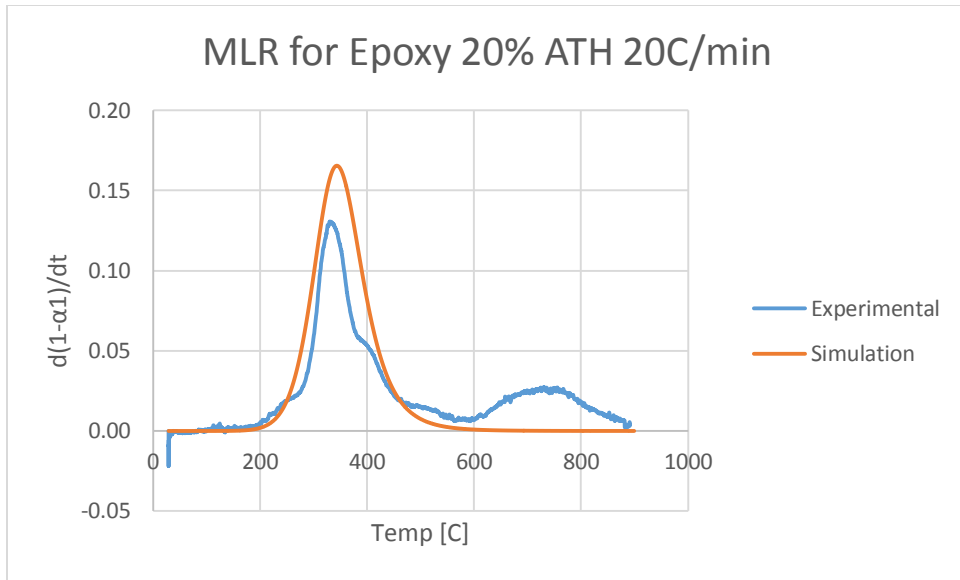
Figure 323: MLR for Epoxy 20% ATH 20 C/min
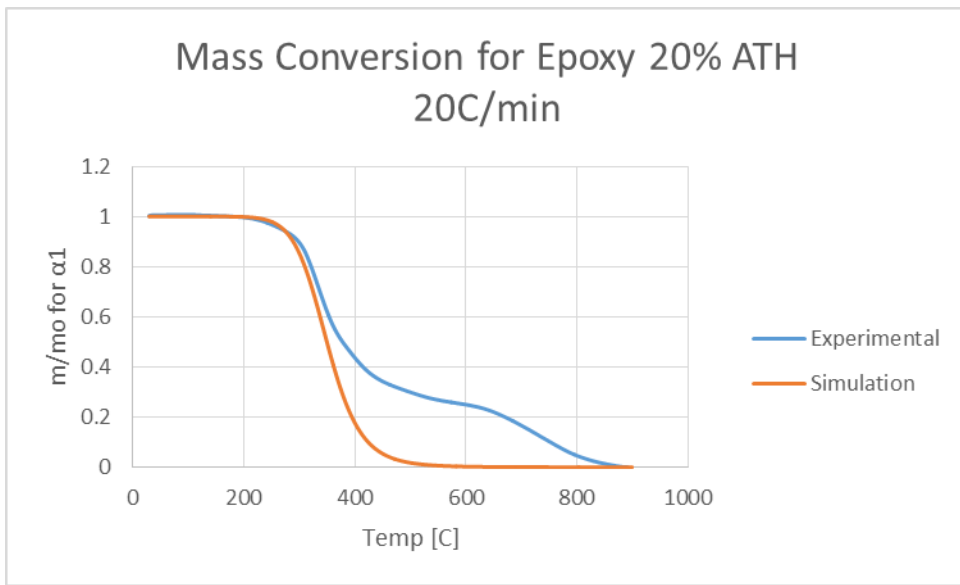
Figure 324: Mass Conversion for Epoxy 20% ATH 20 C/min
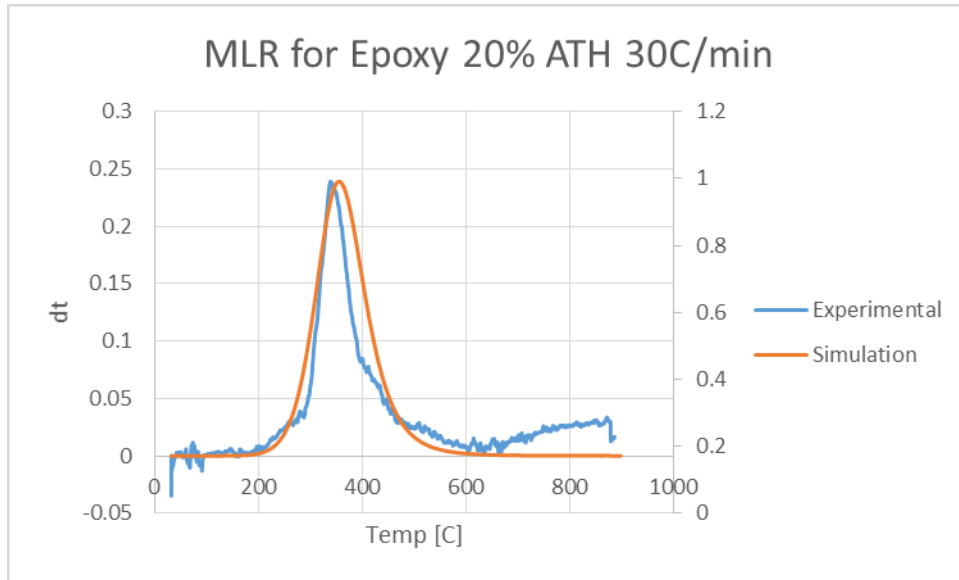
Figure 325: MLR for Epoxy 20% ATH 30 C/min
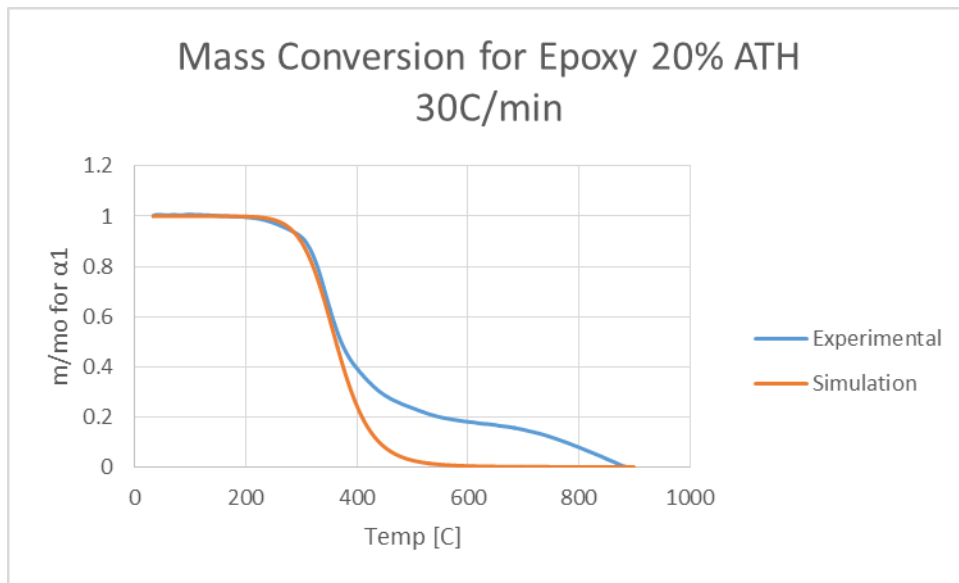
Figure 326: Mass Conversion for Epoxy 20% ATH 30 C/min
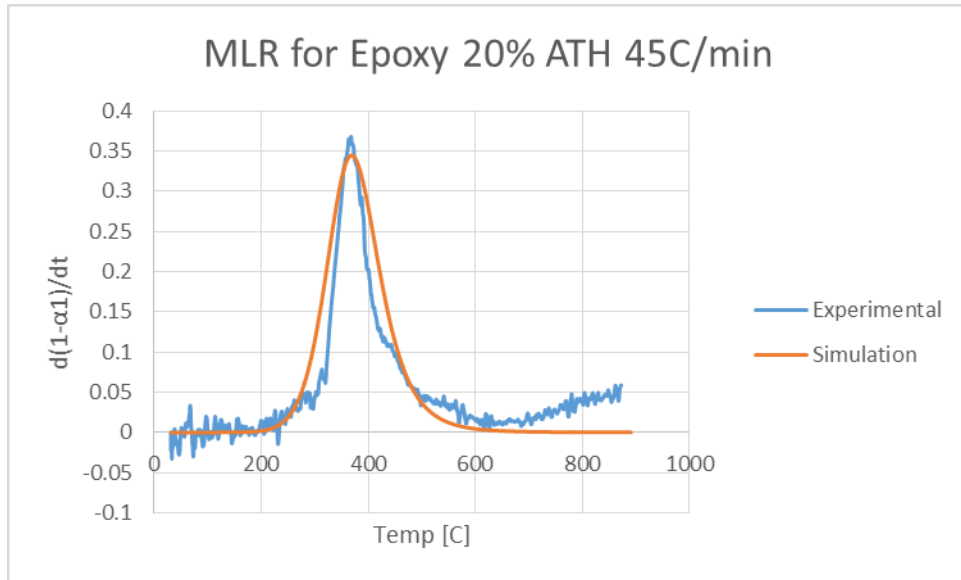
Figure 327: MLR for Epoxy 20% ATH 45 C/min
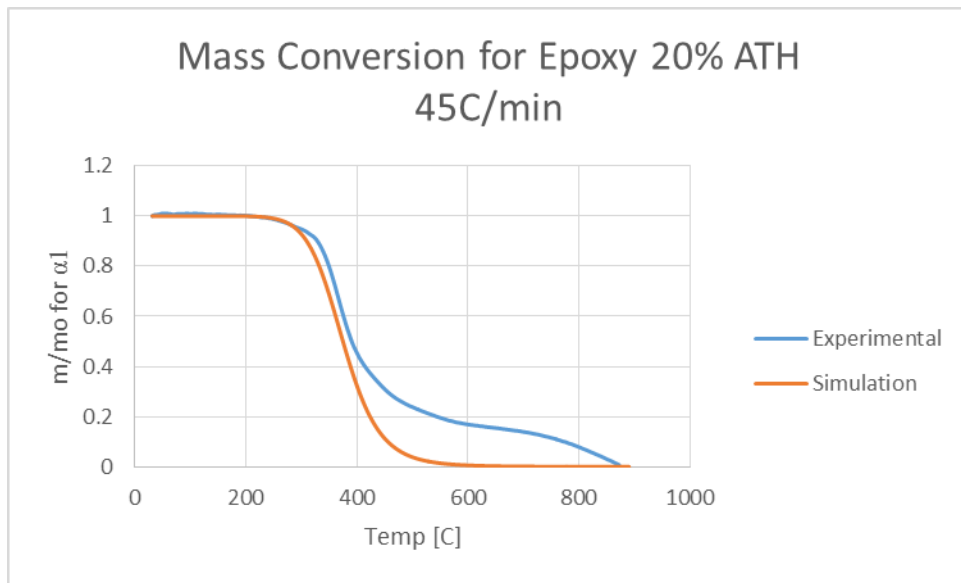
Figure 328: Mass Conversion for Epoxy 20% ATH 45 C/min

Pure ATH:
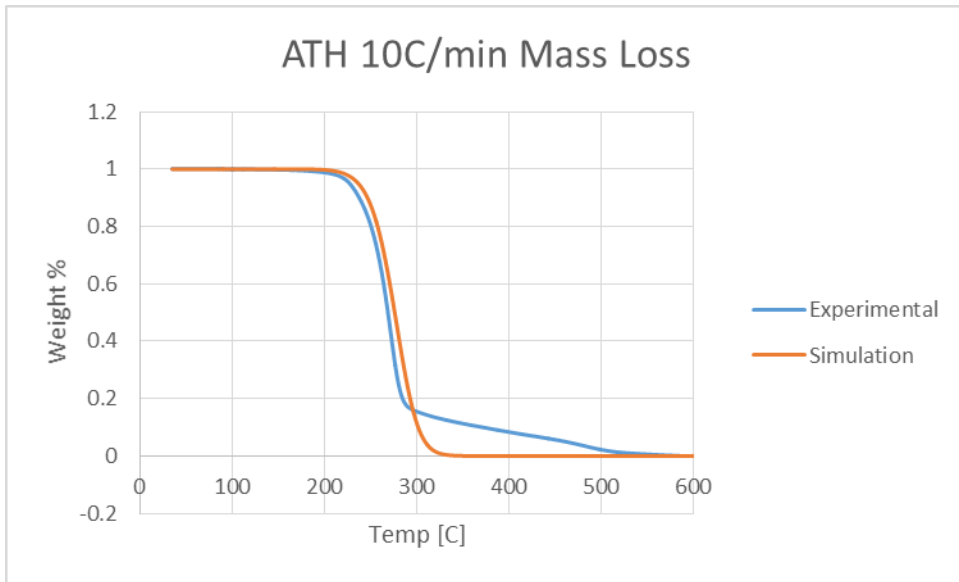
Figure 329: Pure ATH 10 C/min Mass Loss
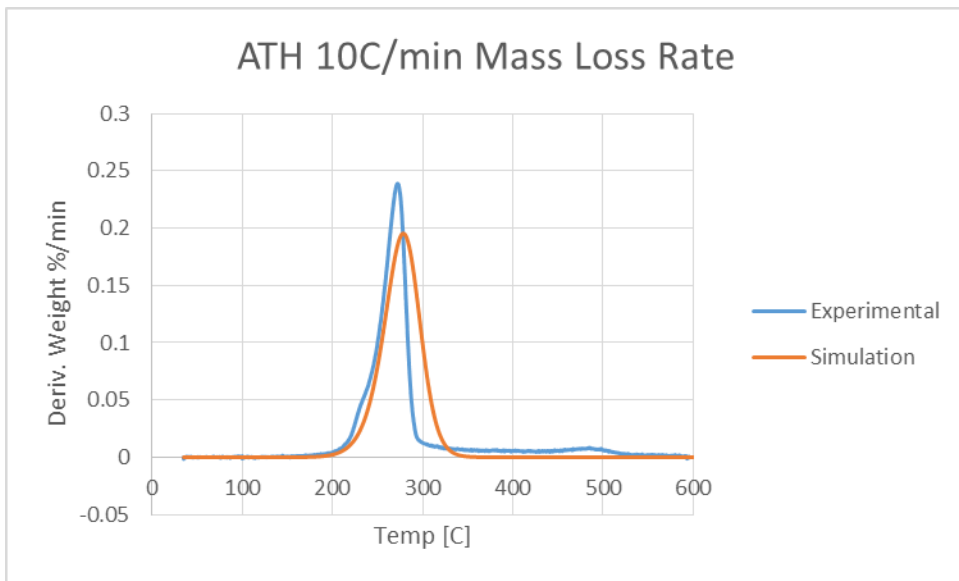
Figure 330: Pure ATH 10 C/min MLR
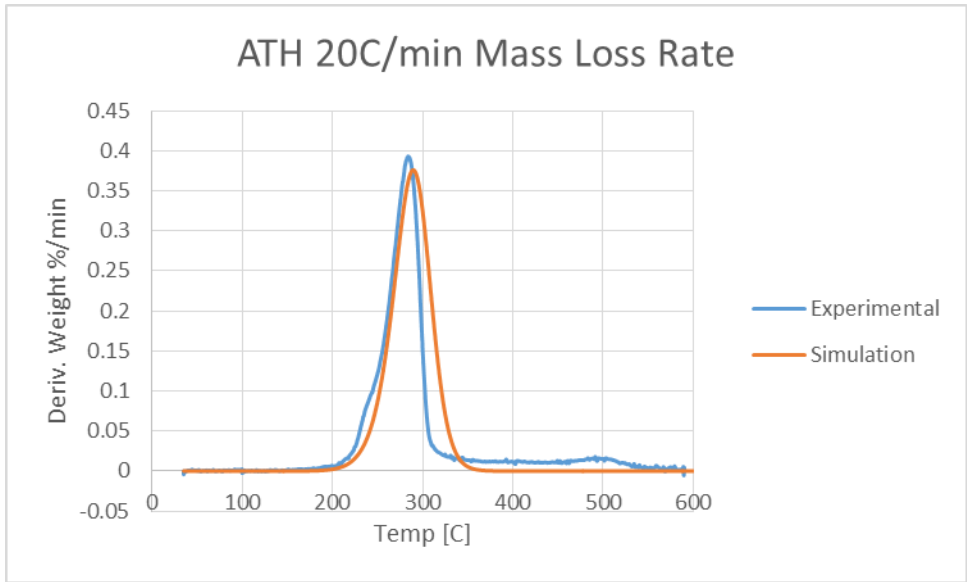
Figure 331: Pure ATH 20 C/min MLR
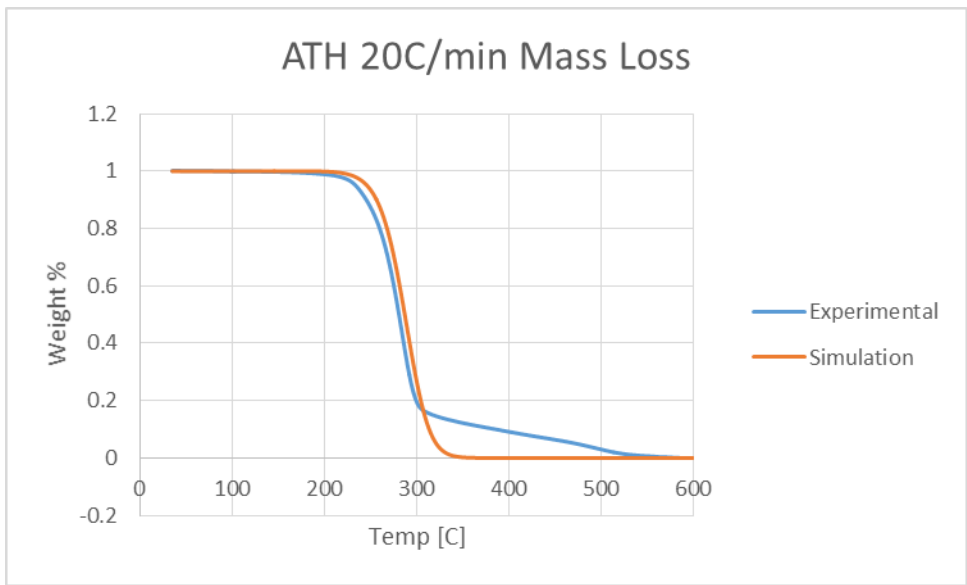
Figure 332: Pure ATH 20 C/min Mass Loss
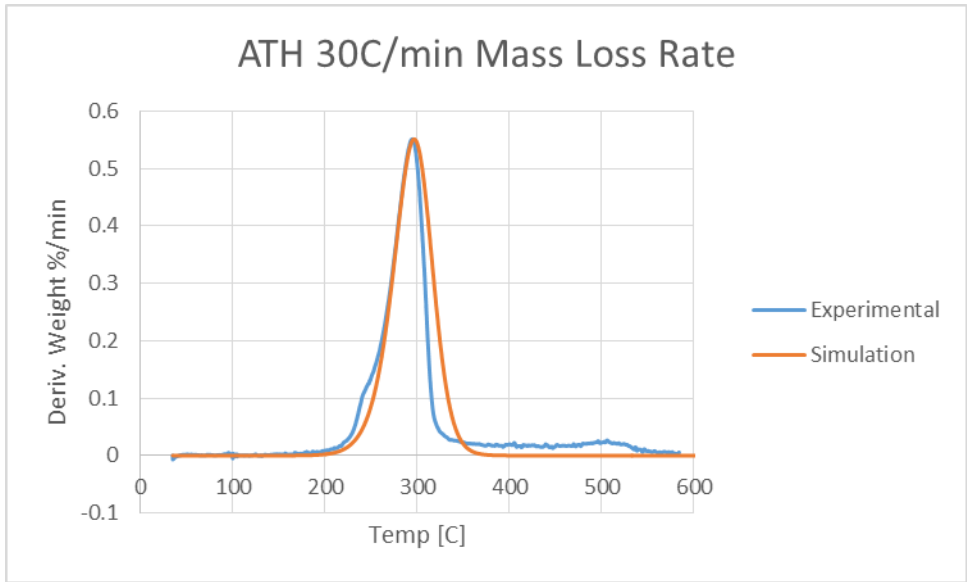
Figure 333: Pure ATH 30 C/min MLR
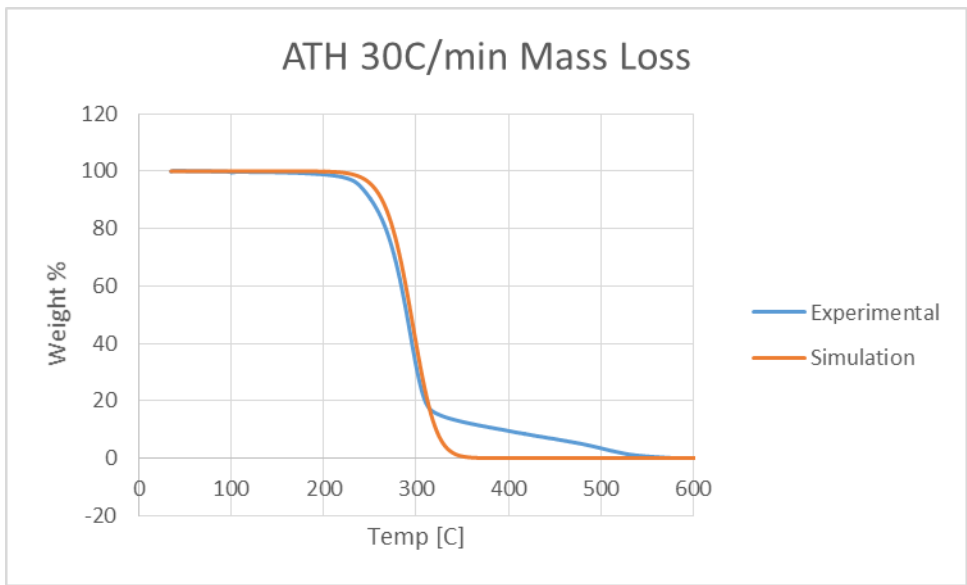
Figure 334: Pure ATH 30 C/min Mass Loss
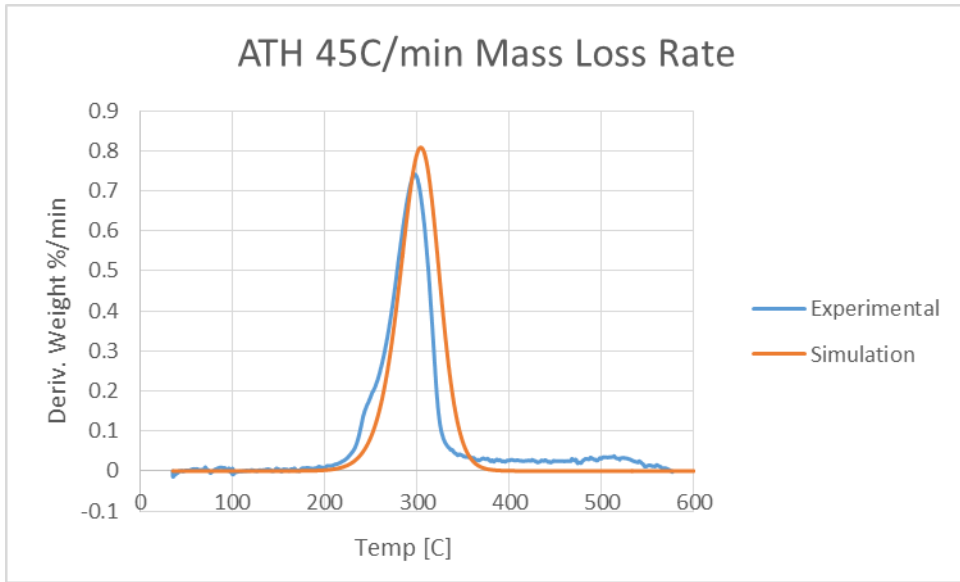
Figure 335: Pure ATH 45 C/min MLR
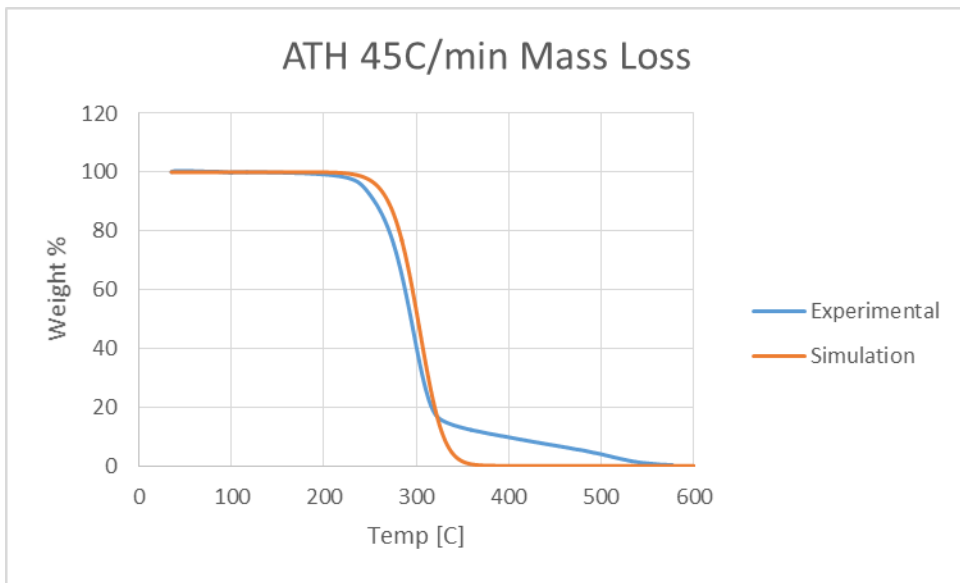
Figure 336: Pure ATH 45 C/min Mass Loss

PMMA Reference Material

As with the isoconversional method, PMMA was used to test the RK4 method. For PMMA, the heating rates tested were 20, 30, 40, and 50C/min. The figures below are the MLR and mass conversion graphs for PMMA at 20 C/min.
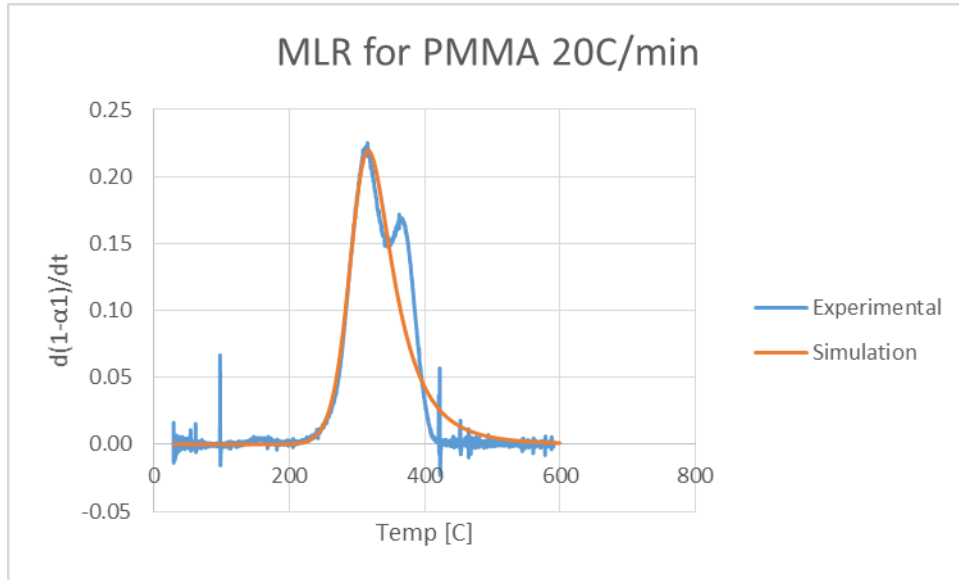
Figure 337: MLR PMMA Optimized Parameters
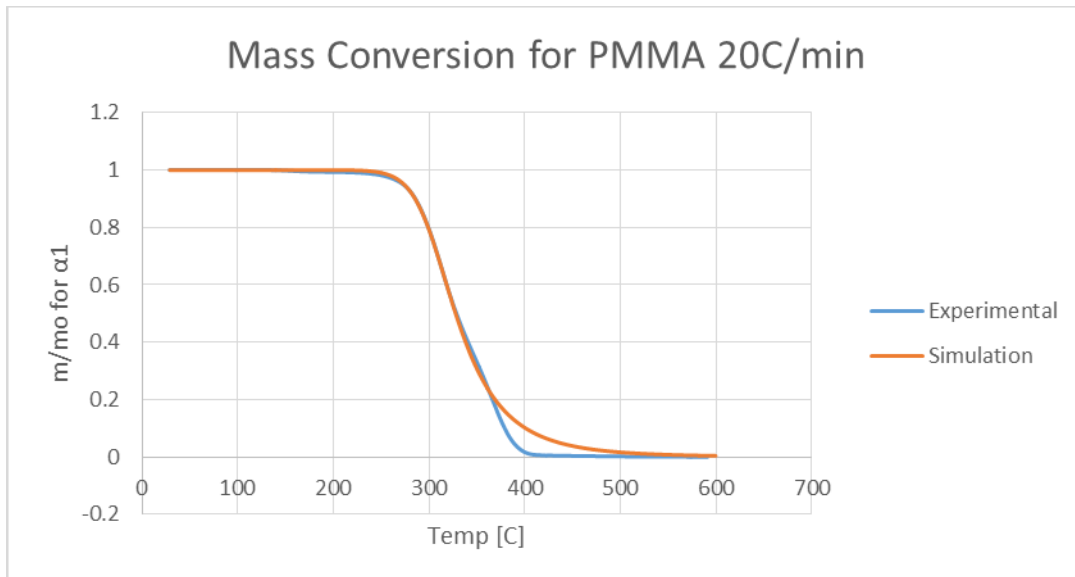
Figure 338: Mass Conversion PMMA Optimized Parameters

These graphs are produced experimentally by using a pre-exponential constant of 3e14 (logA=14.5) and an n value of 3.2. Although the top of the peaks on the MLR graph to not match up completely, the base of the peaks start and end at the same temperatures. This can be contributed to the fact that the isoconversional method assumes a single step reaction which would create a single peak, in addition to differences in the type of PMMA we tested to the type of PMMA tested in the literature. To test the accuracy of this method, the results for A and n were compared with literature values in Table 14 [12]. In the analysis done in this experiment, they tested PMMA at 2, 5, 8, and 10 C/min, so we compared their data for 10 C/min to our data for 20 C/min to attempt to get as similar results as possible.

Table 26: PMMA literature A and n values

	350,000 g/mol Step 1 log A	996,000 g/mol Step 1 log A	350,000 g/mol Step 1 n	996,000 g/mol Step 1 n
2 C/min	22.08 +/- 0.2	22.08 +/- 0.2	1.4 +/- 0.31	2.22 +/- 0.36
5 C/min	22.08 +/- 0.2	21.7 +/- 0.2	2.26 +/- 0.5	1.74 +/- 0.28
8 C/min	22.08 +/- 0.2	21.7 +/- 0.2	2.13 +/- 0.48	1.55 +/- 0.25
10 C/min	22.08 +/- 0.2	22.05 +/- 0.2	2.45 +/- 0.55	2.15 +/- 0.35
Average	22.08 +/- 0.2	21.8 +/- 0.2	2.06 +/- 0.46	1.9 +/- 0.31

Our experimental values are only slightly off from the literature values, thus we believe that we are running the tests accurately and correctly analyzing our data.

Appendix F.3: Heat of Decomposition

Below are the graphs for the heat of decomposition of the epoxy mixtures as well as the fireblock. The shaded area was the area that was integrated to determine the heat of decomposition.
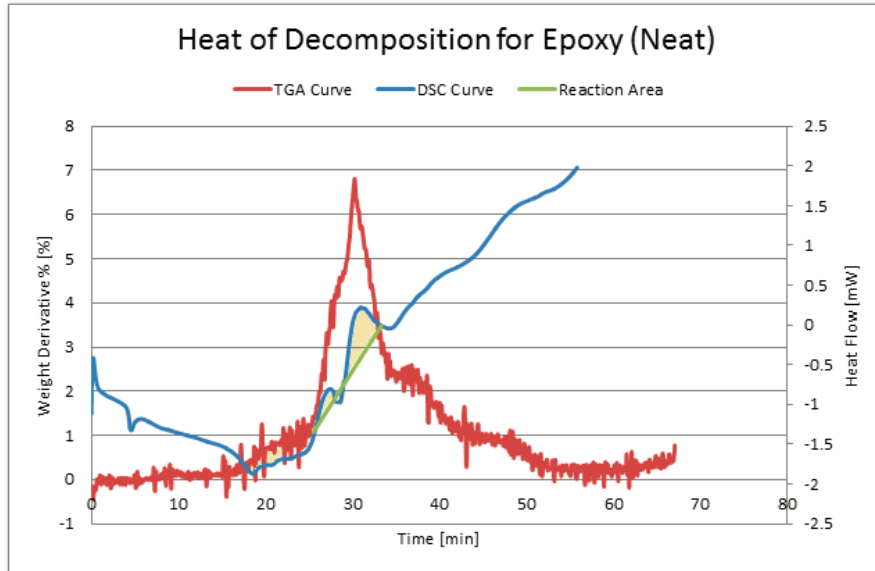
Figure 339: Heat of Decomposition for Epoxy (Neat)
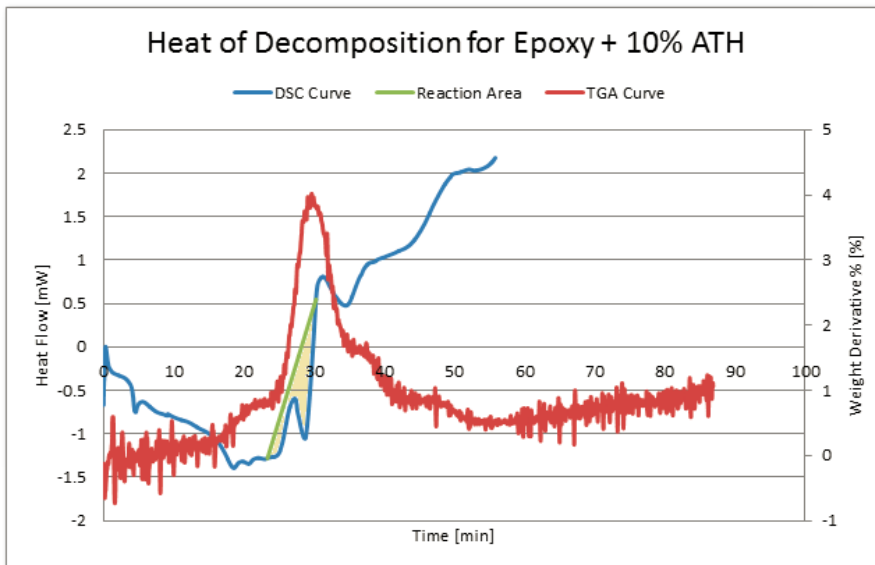
Figure 340: Heat of Decomposition for Epoxy + 10% ATH
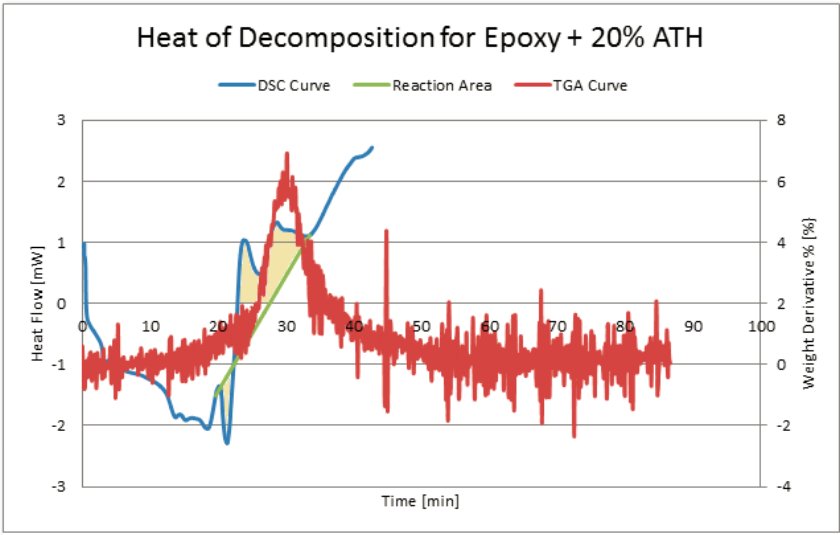
Figure 341: Heat of Decomposition for Epoxy + 20% ATH

Appendix G: TGA Database

The following is a compilation of our TGA data. This database includes overlays of the individual trials, overlays for each heating rate per material, and overlays of the change in ATH level

Appendix G.1: Data Trial Overlays

These graphs are the unsmoothed individual trials for each material.
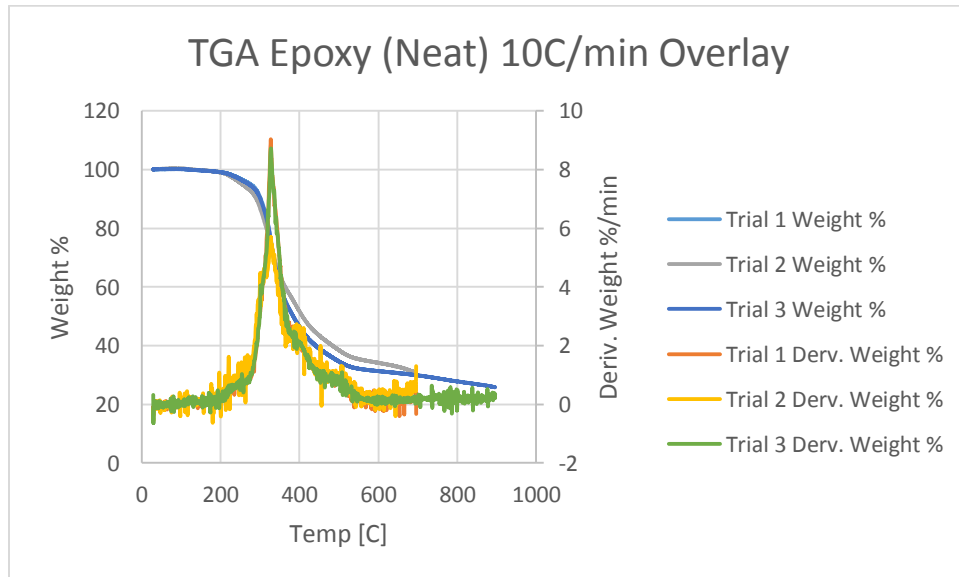
Epoxy (Neat):

Figure 342: TGA Epoxy (Neat) 10 C/min Overlay
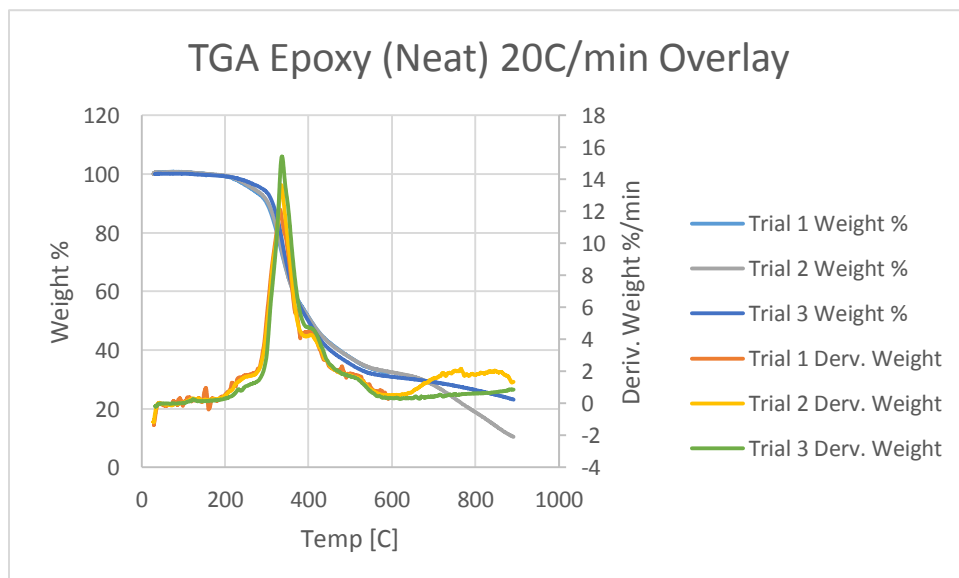
Figure 343: TGA Epoxy (Neat) 20 C/min Overlay
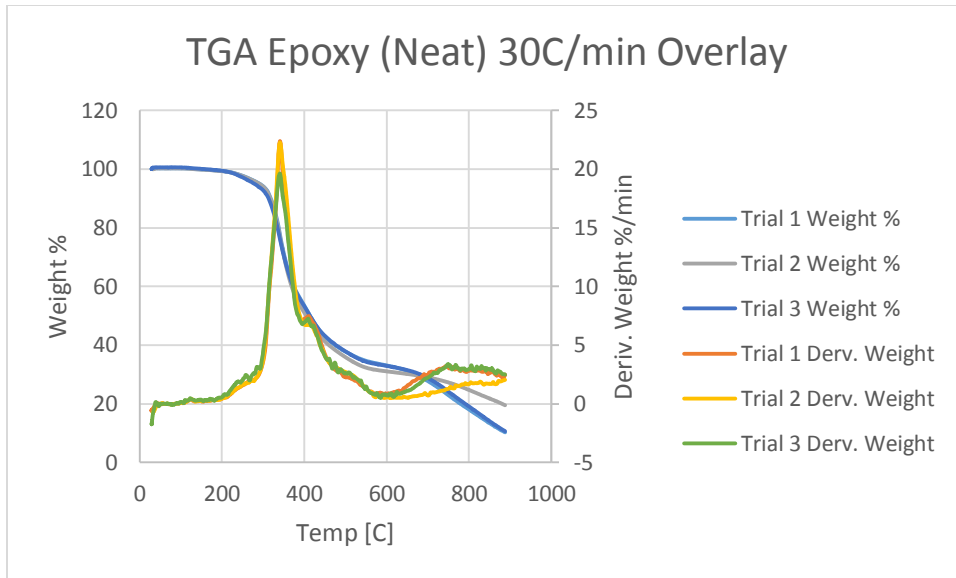
Figure 344: TGA Epoxy (Neat) 30 C/min Overlay
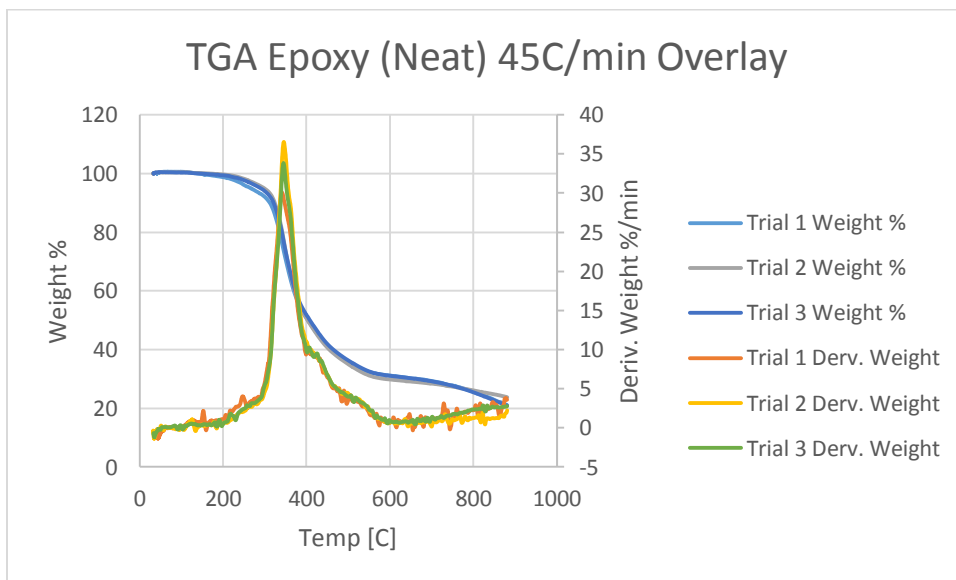
Figure 345: TGA Epoxy (Neat) 45 C/min Overlay

Epoxy plus 5% ATH:
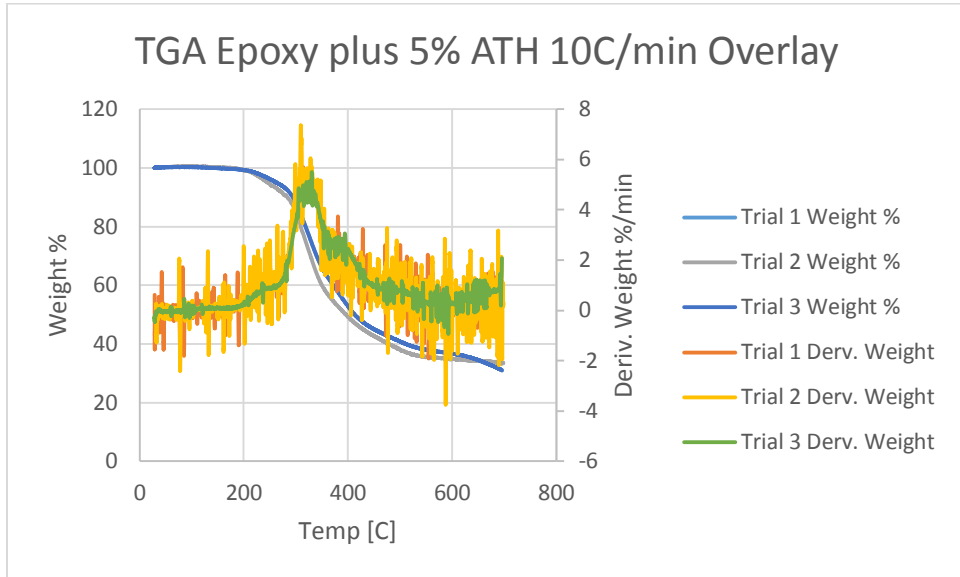
Figure 346: TGA Epoxy + 5% ATH 10 C/min Overlay
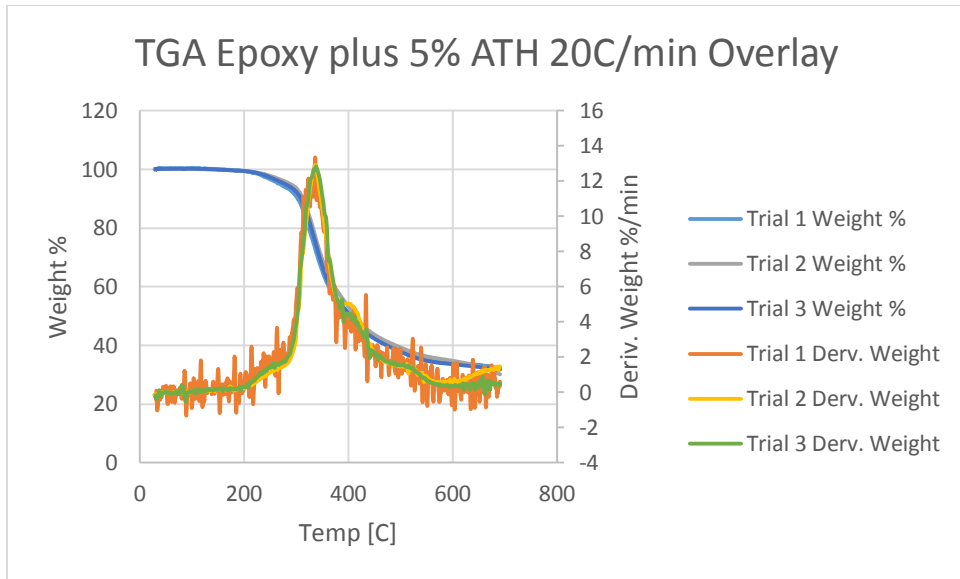
Figure 347: TGA Epoxy + 5% ATH 20 C/min Overlay
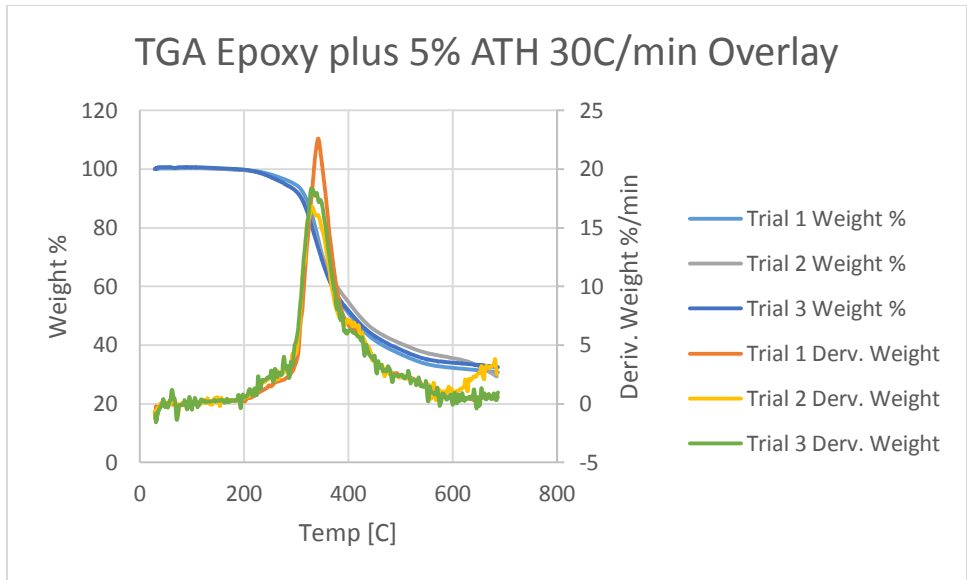
Figure 348: TGA Epoxy + ATH 30 C/min Overlay
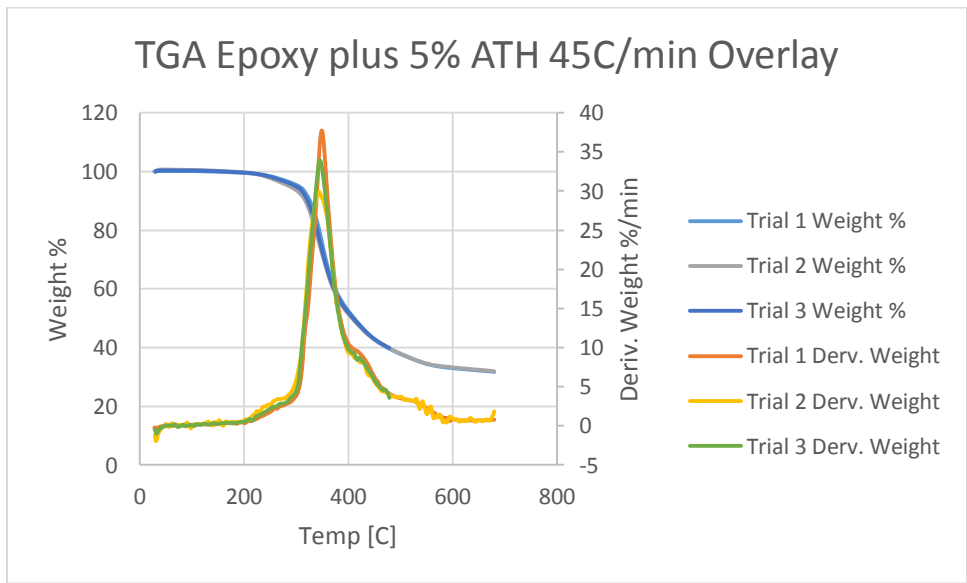
Figure 349: TGA Epoxy + 5% ATH 45 C/min Overlay

Epoxy plus 10% ATH:
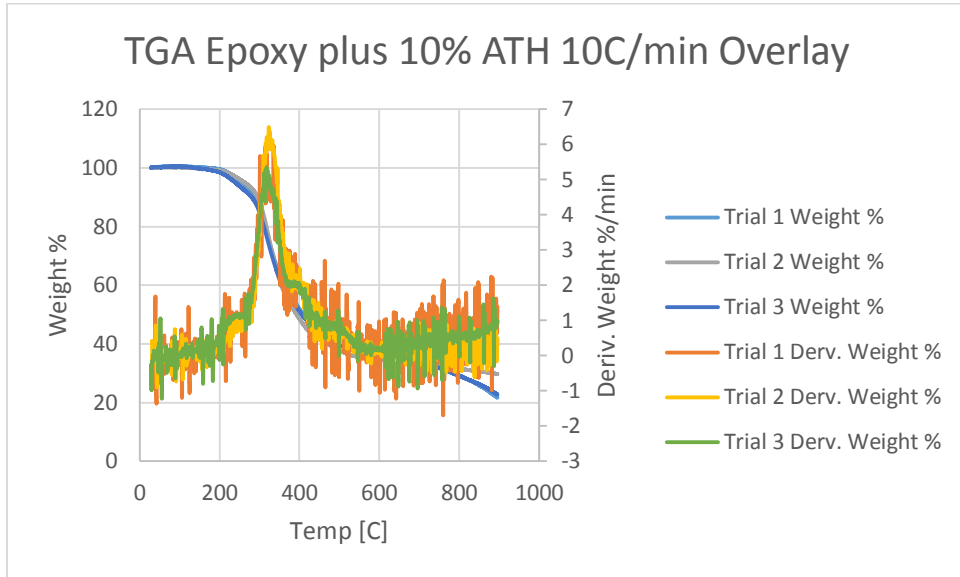
Figure 350: TGA Epoxy + 10% ATH 10 C/min Overlay
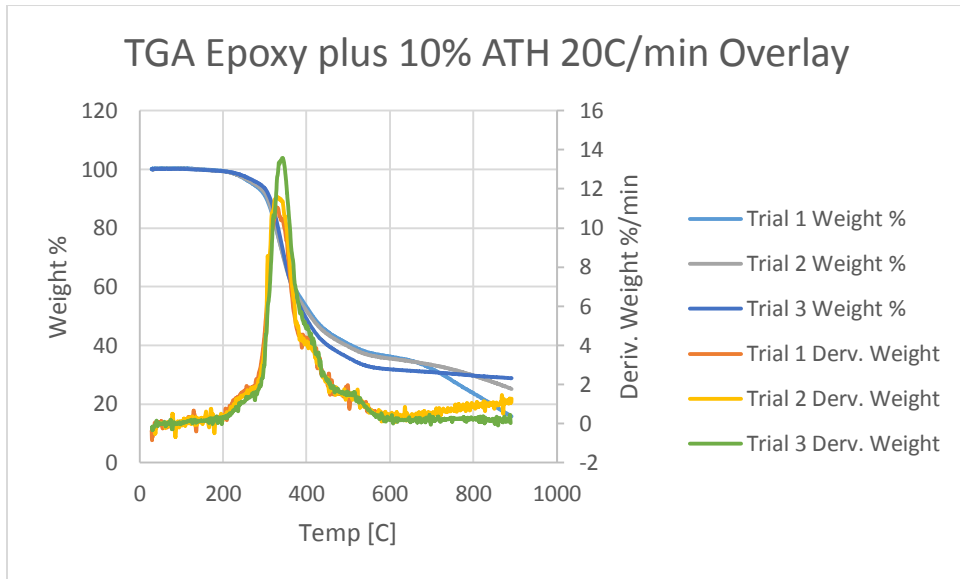
Figure 351: TGA Epoxy + 10% ATH 20 C/min Overlay
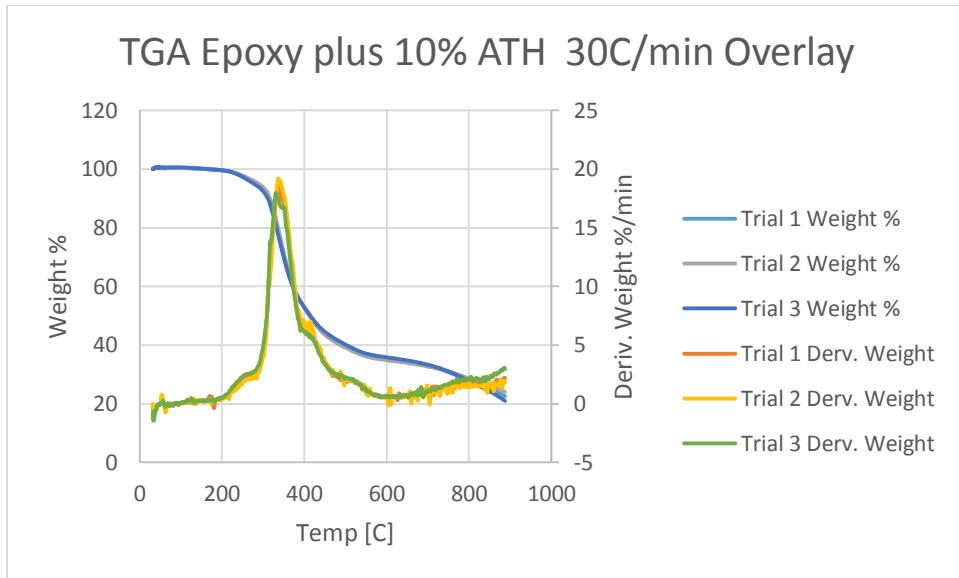
Figure 352: TGA Epoxy + 10% ATH 30 C/min Overlay
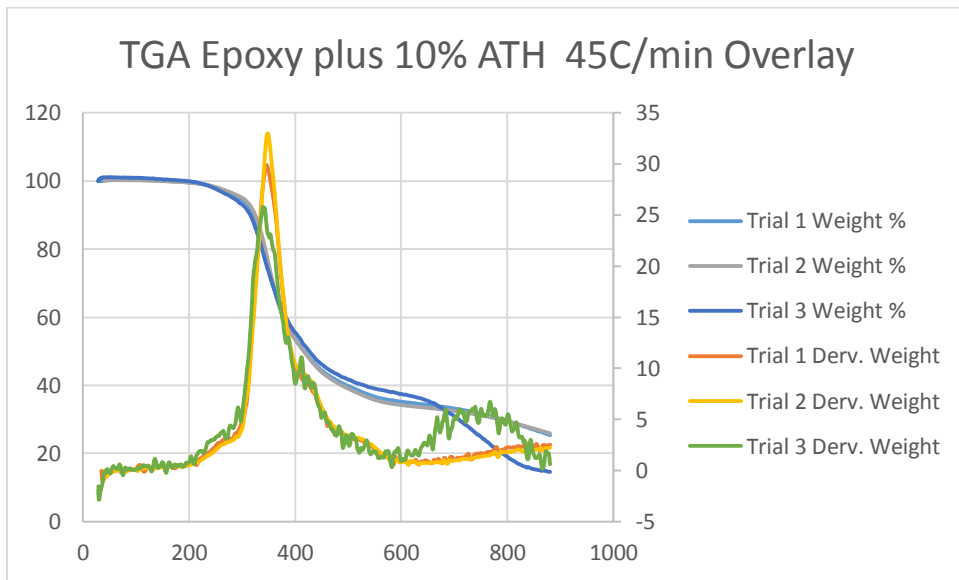
Figure 353: TGA Epoxy + 10% ATH 45 C/min

Epoxy plus 20% ATH:
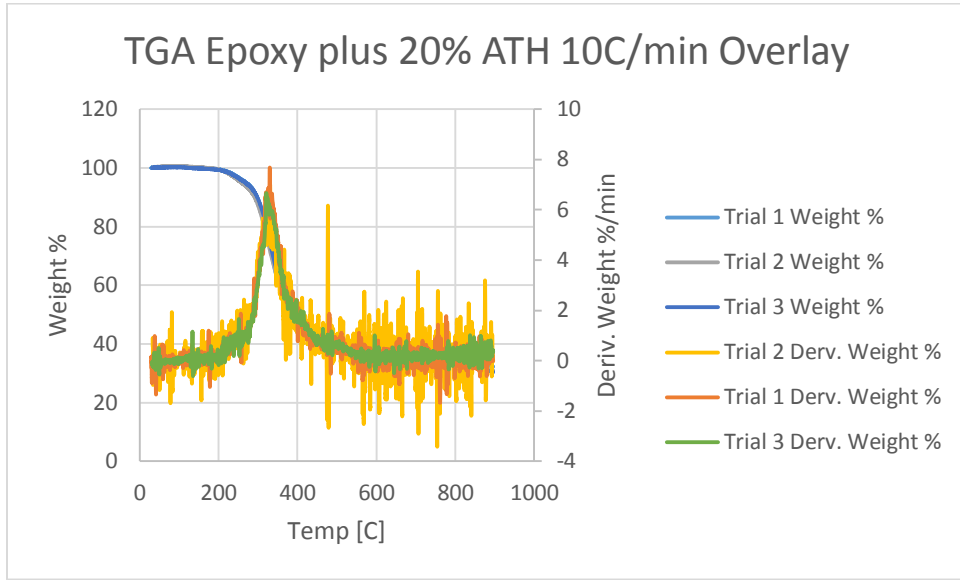
Figure 354: TGA Epoxy + 20% ATH 10 C/min Overlay
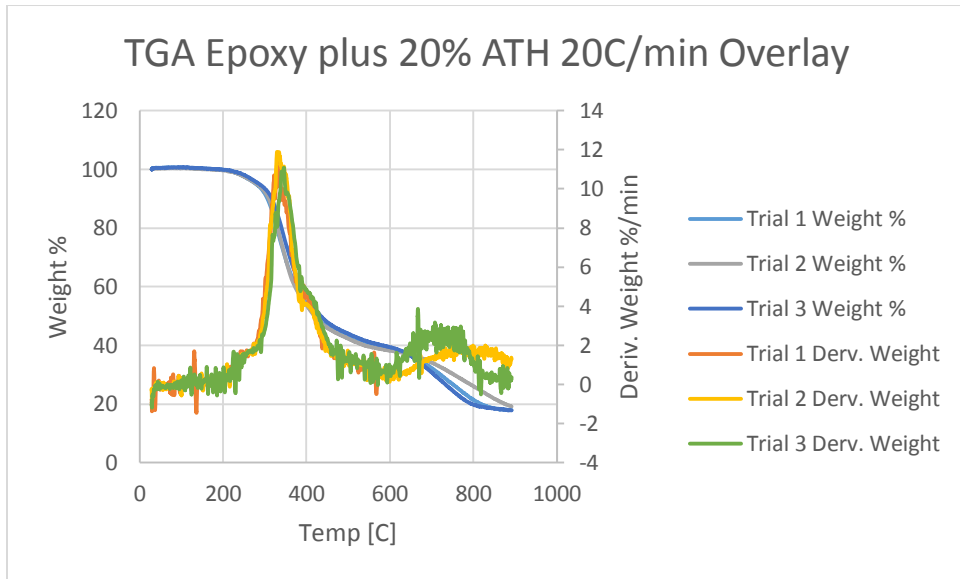
Figure 355: TGA Epoxy + 20% ATH 20 C/min Overlay
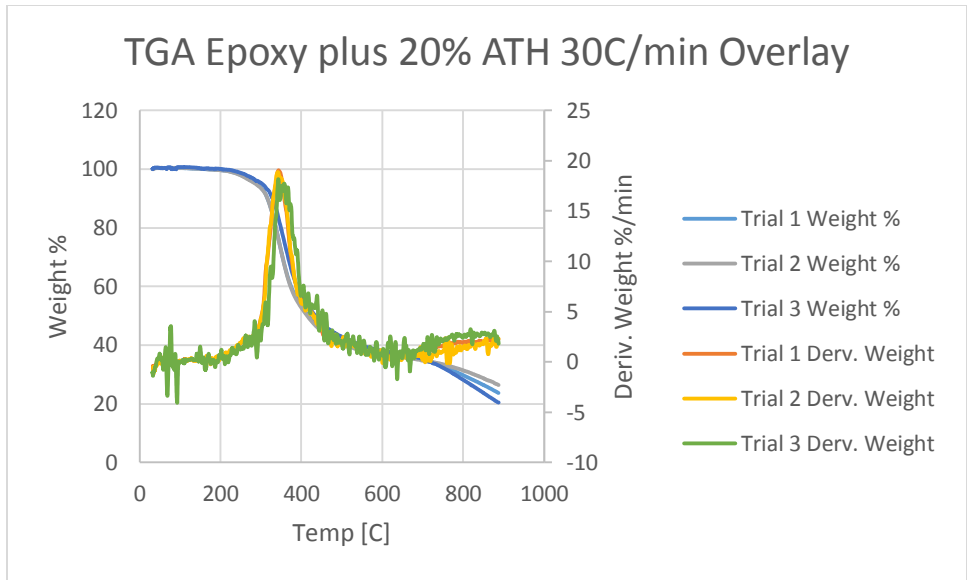
Figure 356: TGA Epoxy + 20% ATH 30 C/min
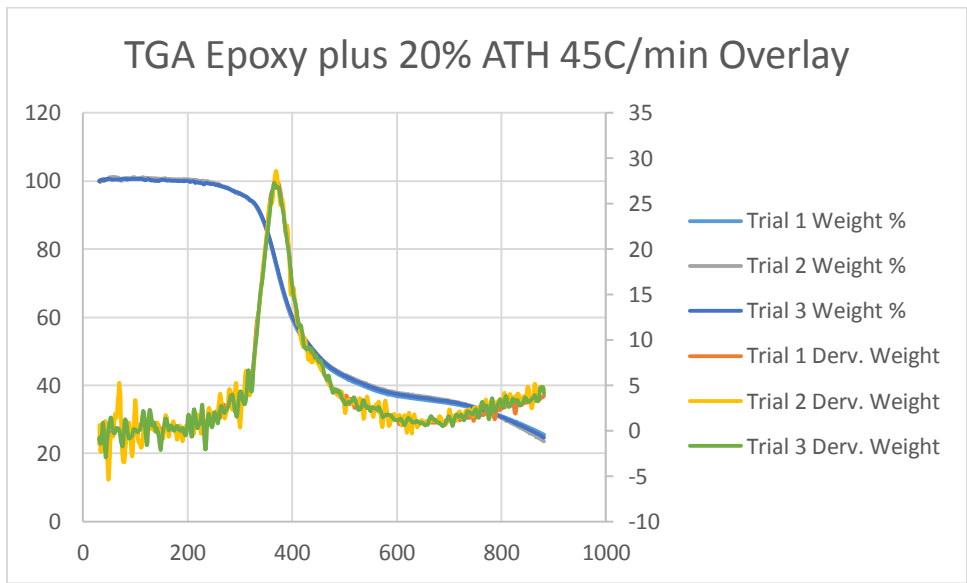
Figure 357: TGA Epoxy + 20% ATH 45 C/min

Fireblock:

Figure 359: TGA Fireblock 20 C/min Overlay
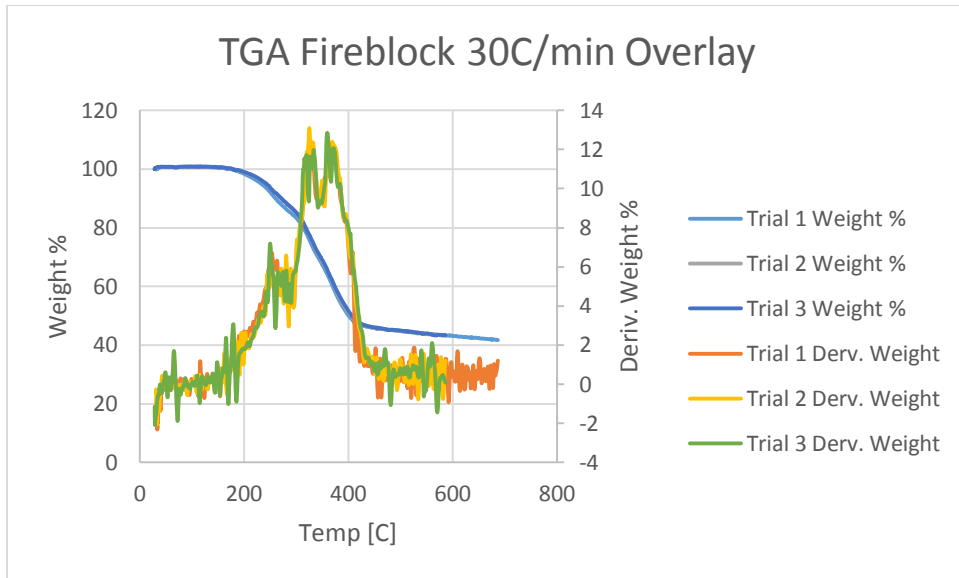
Figure 360: TGA Fireblock 30 C/min Overlay
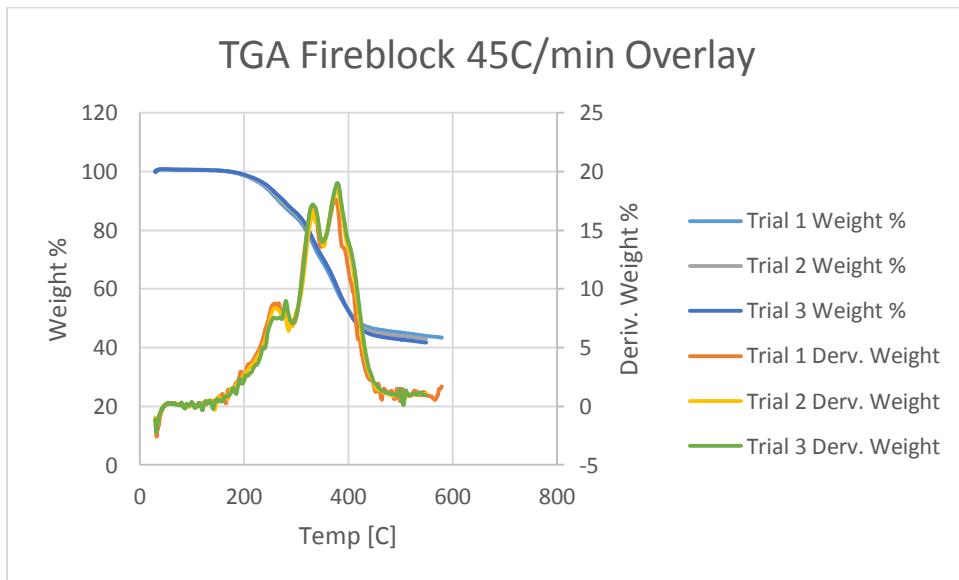
Figure 361: TGA Fireblock 45 C/min Overlay

Appendix G.2: Heating Rate Overlays

The following is a compilation of the average, smoothed trials for each heating rate overlaid for each material.
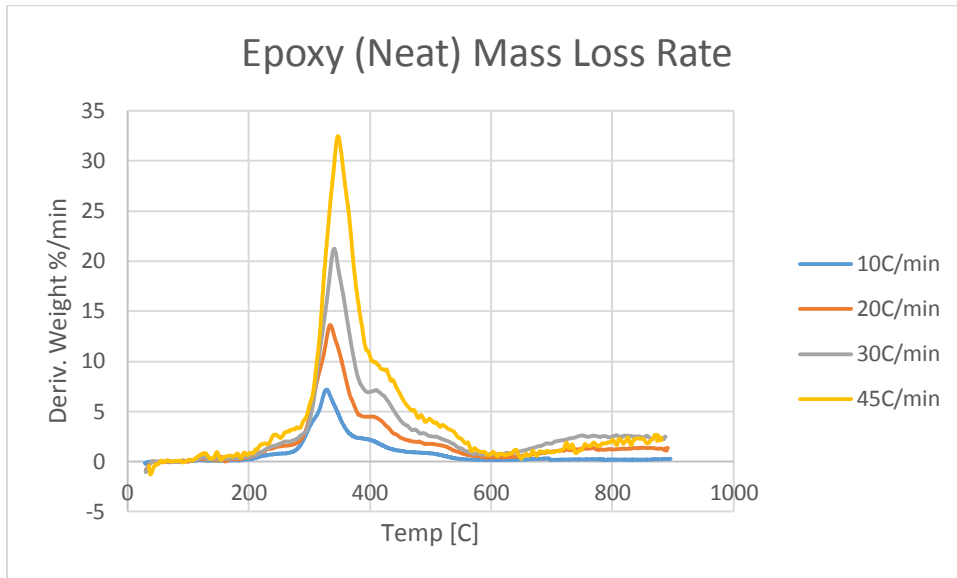
Epoxy (Neat):

Figure 362: Epoxy (Neat) MLR
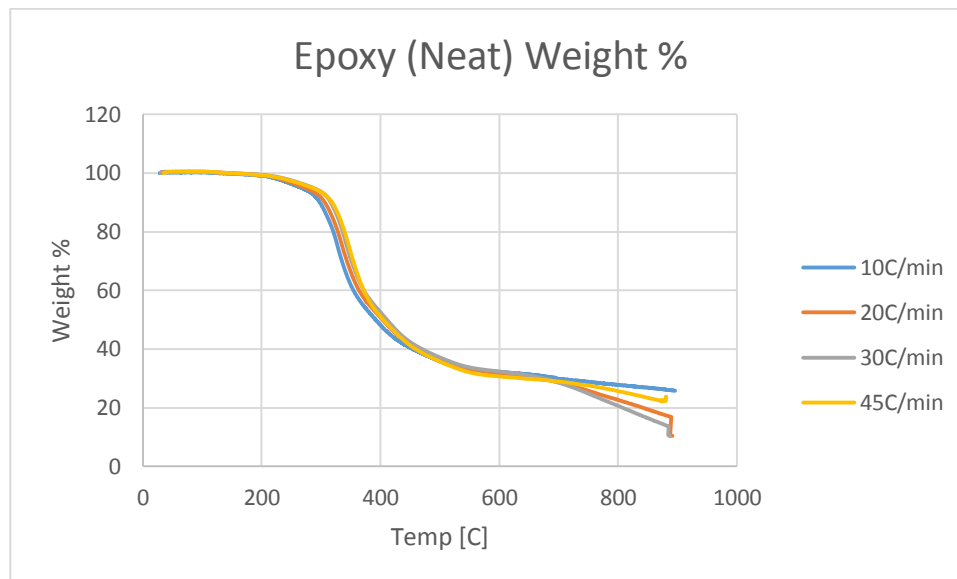
Figure 363: Epoxy (Neat) Weight %

Epoxy plus 5% ATH:
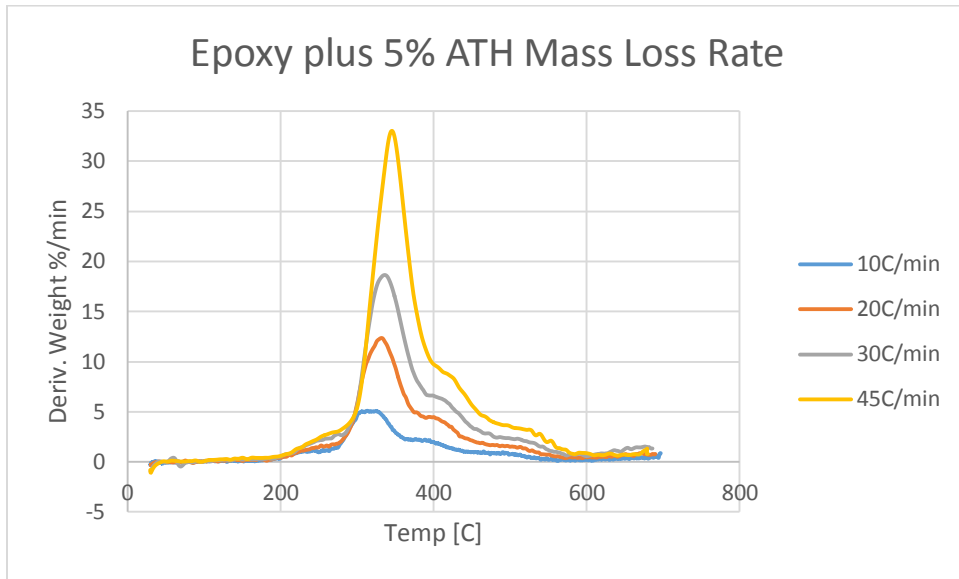
Figure 364: Epoxy + 5% ATH MLR
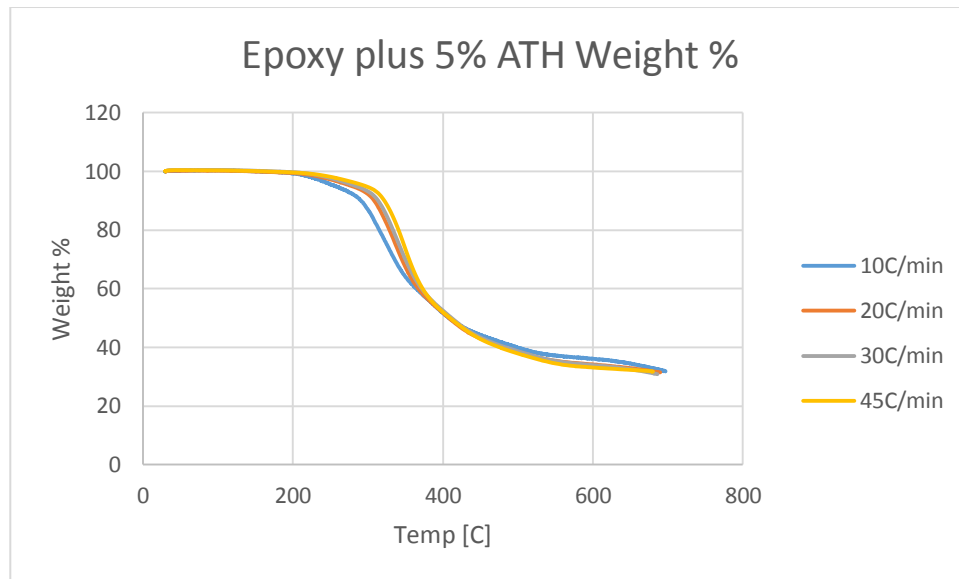
Figure 365: Epoxy + 5% ATH Weight %

Epoxy plus 10% ATH:
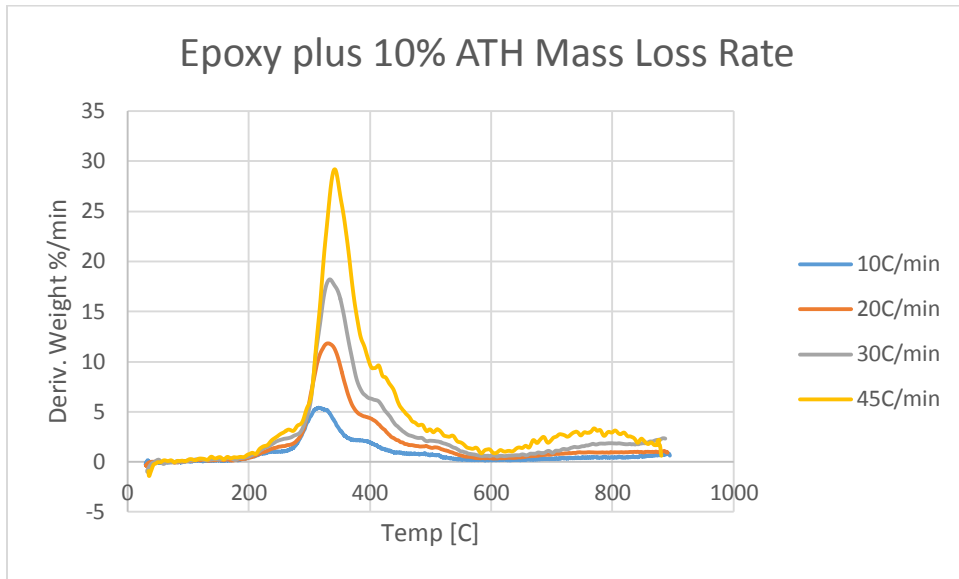
Figure 366: Epoxy + 10% ATH MLR
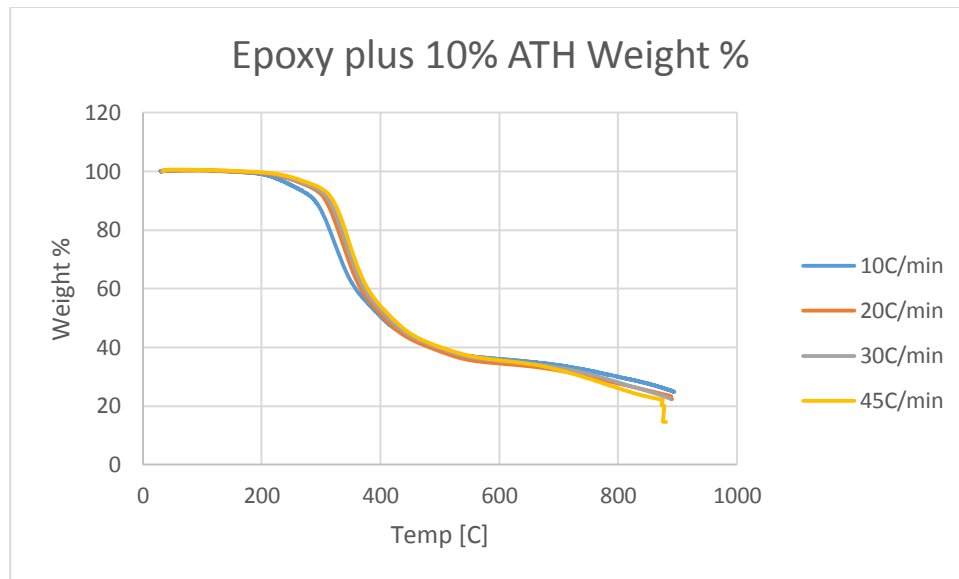
Figure 367: Epoxy + 10% ATH Weight %

Epoxy plus 20% ATH:
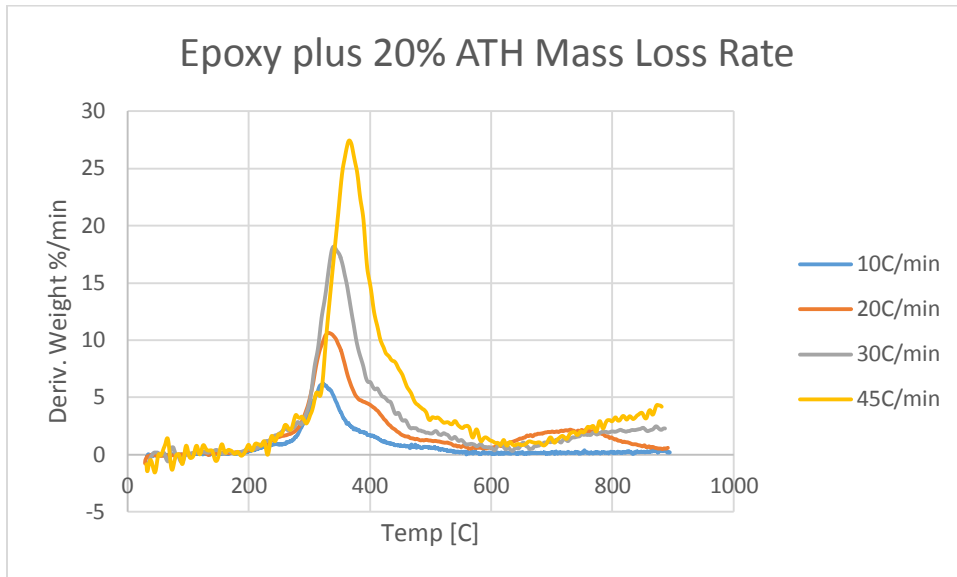
Figure 368: Epoxy + 20% ATH MLR
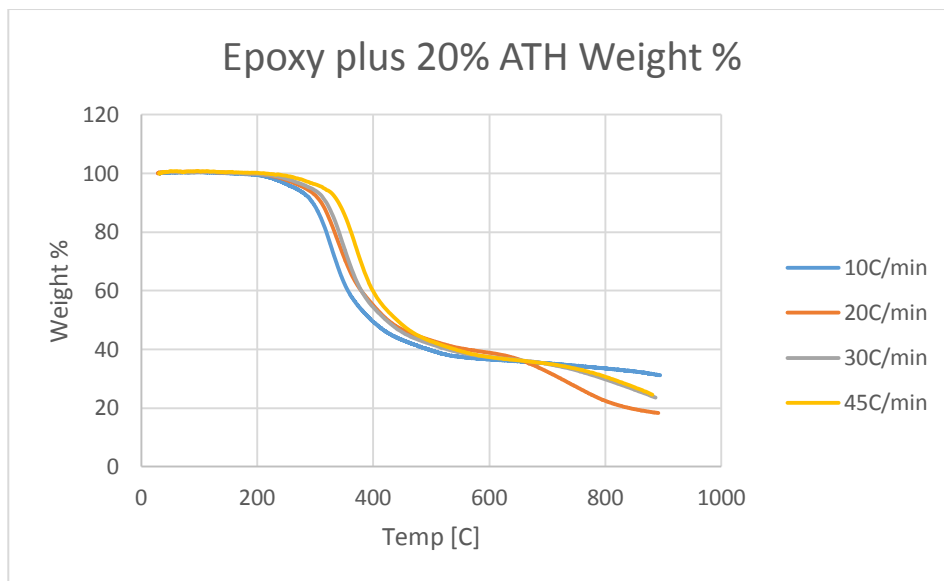
Figure 369: Epoxy + 20% ATH Weight %

Fireblock:

The graphs for Fireblock are unsmoothed, as they were not used in the analysis for our report.
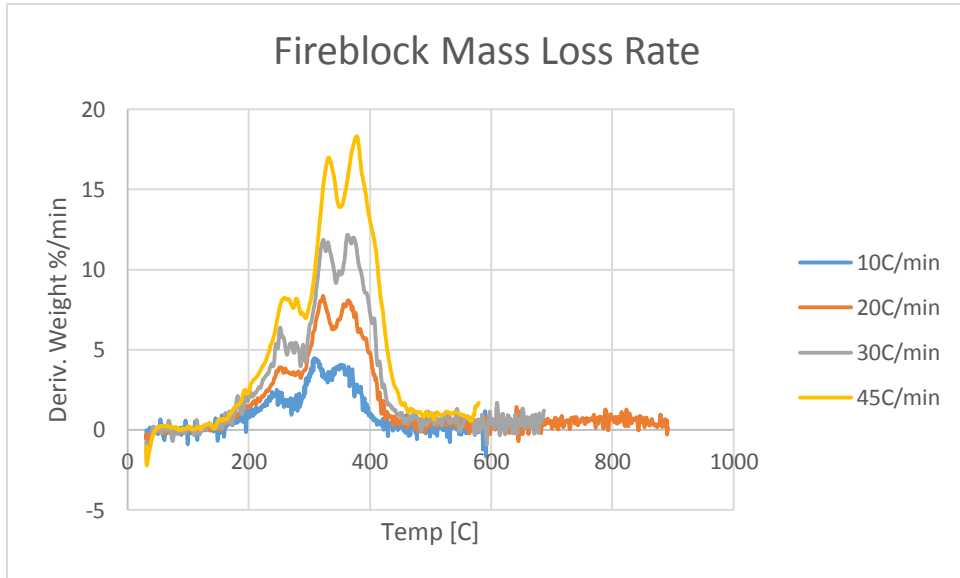
Figure 370: Fireblock MLR
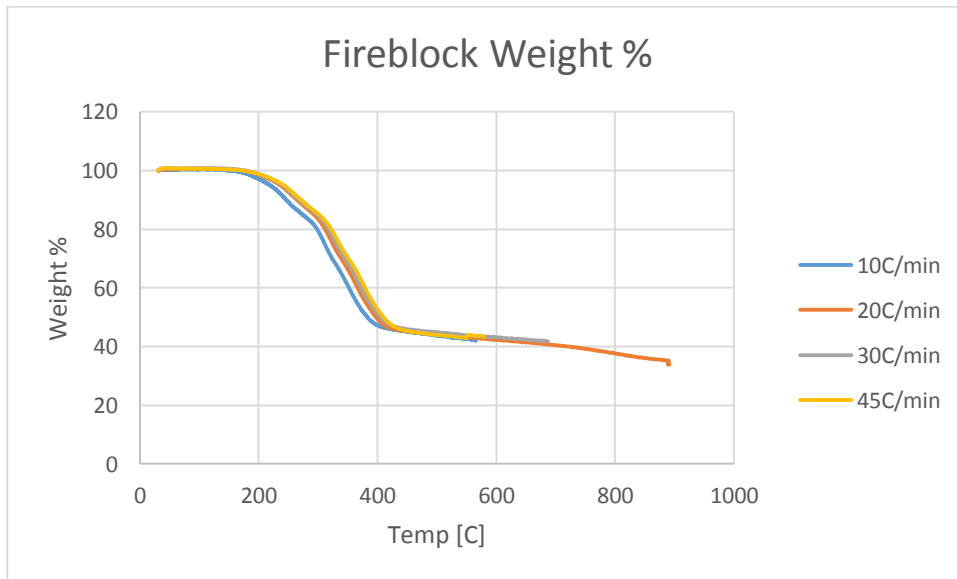
Figure 371: Fireblock Weight %

Appendix G.3: ATH Level Overlays

This data is a compilation of the average, smoothed trials for each material at each heating rate.

10 C/min:
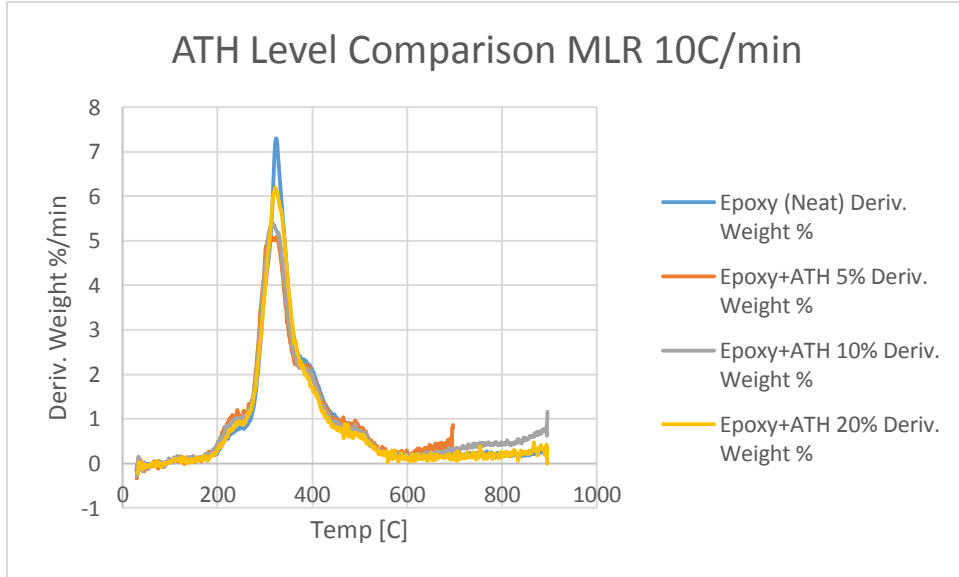
Figure 372: ATH Level Comparison MLR 10 C/min
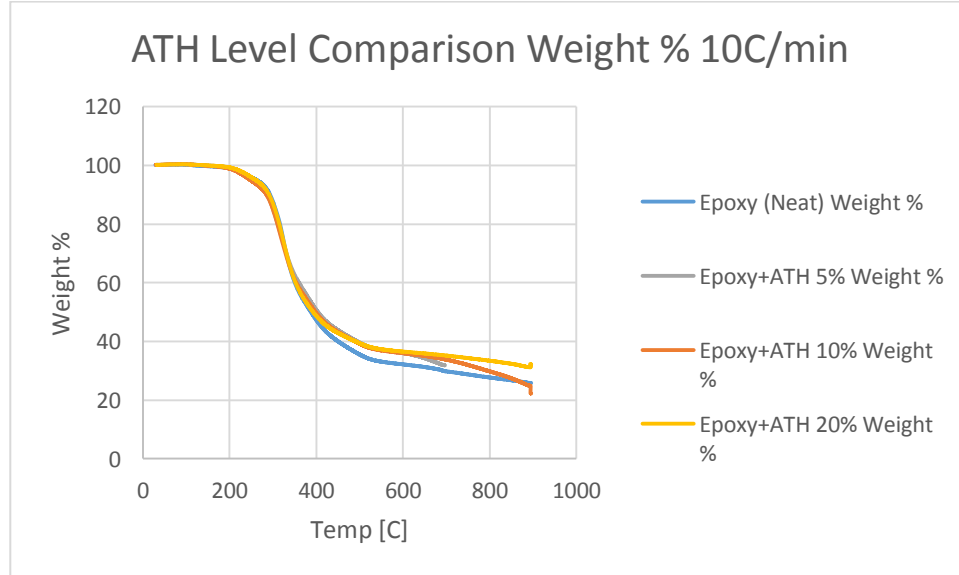
Figure 373: ATH Level Comparison Weight % 10 C/min

20 C/min:
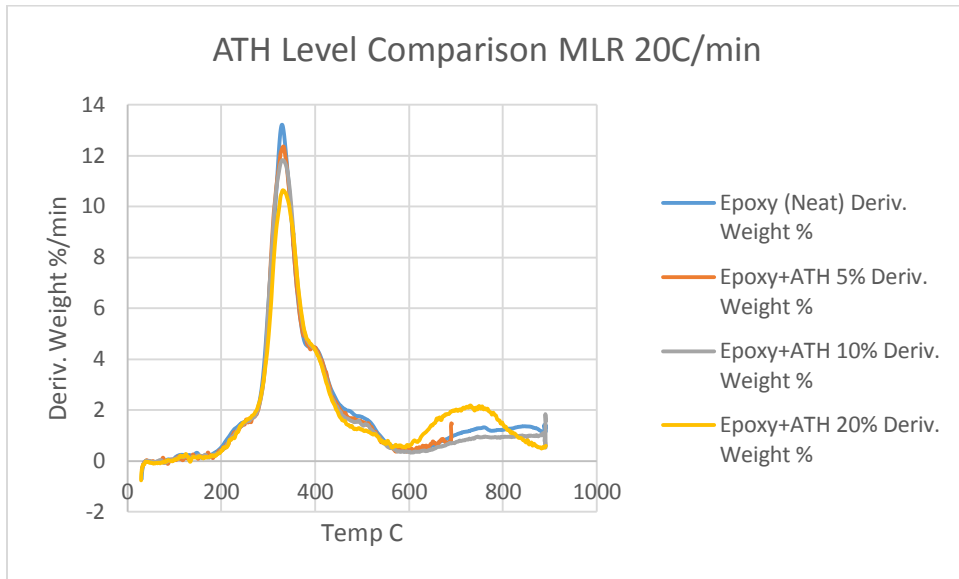
Figure 374: ATH Level Comparison MLR 20 C/min
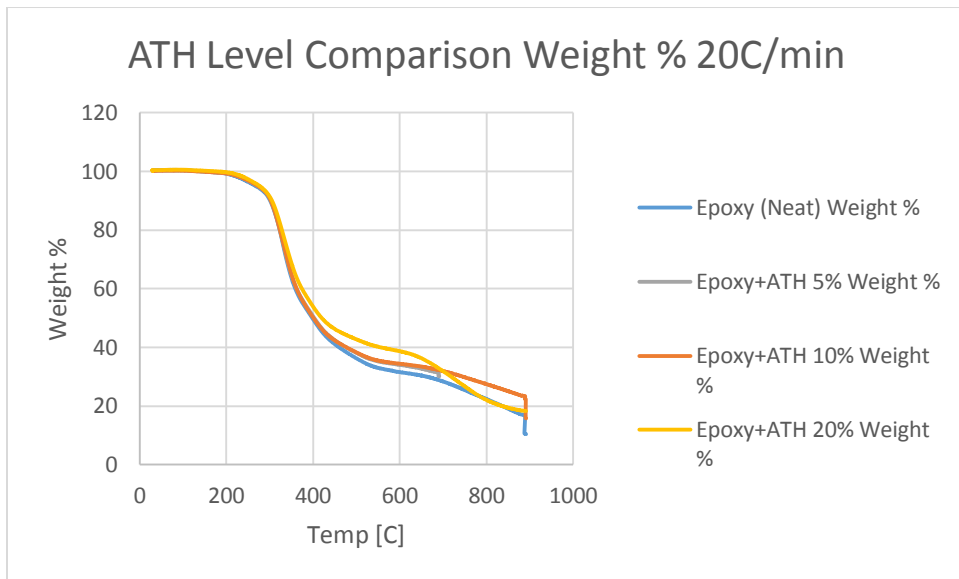
Figure 375: ATH Level Comparison Weight % 20 C/min

30 C/min:
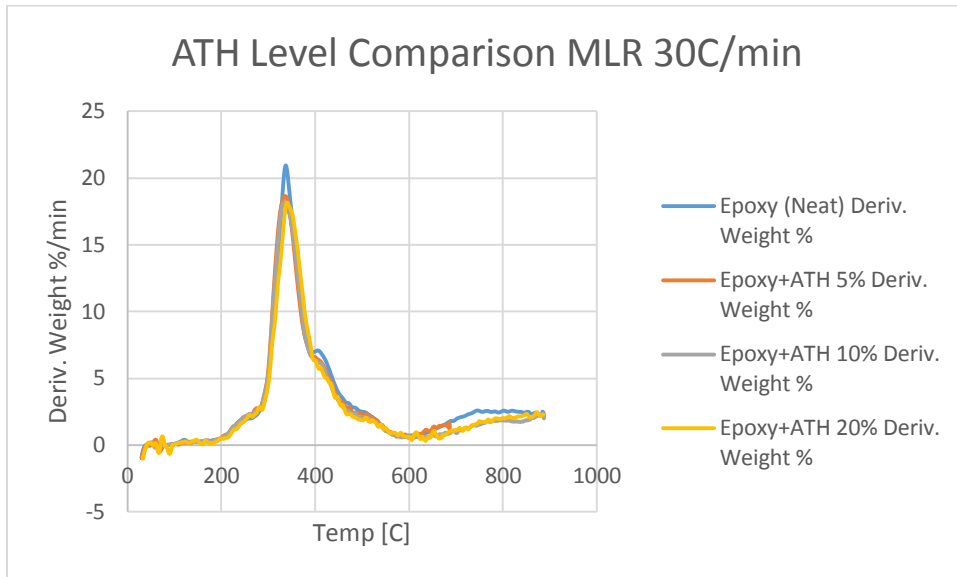
Figure 376: ATH Level Comparison MLR 30 C/min
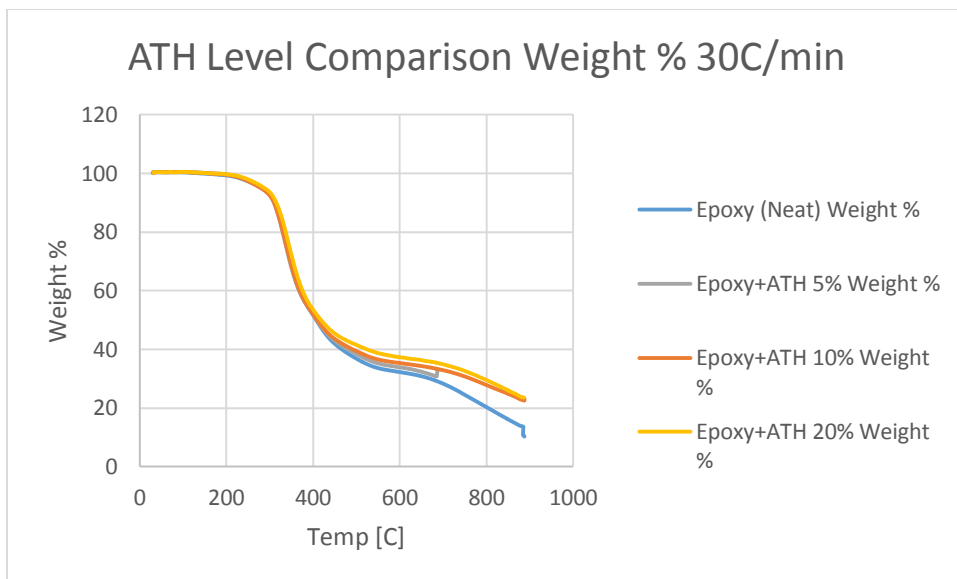
Figure 377: ATH Level Comparison Weight% 30 C/min

45 C/min:
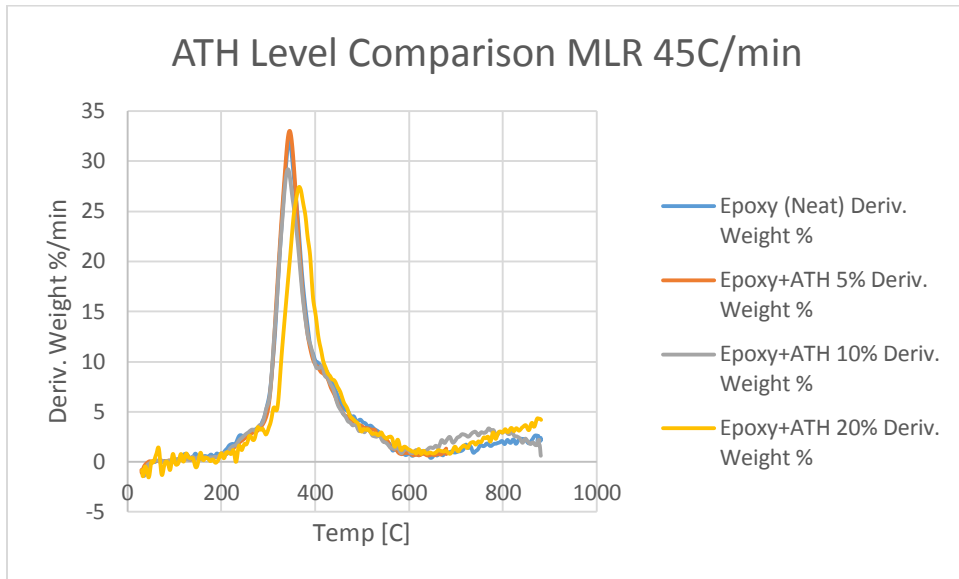
Figure 378: ATH Level Comparison MLR 45 C/min
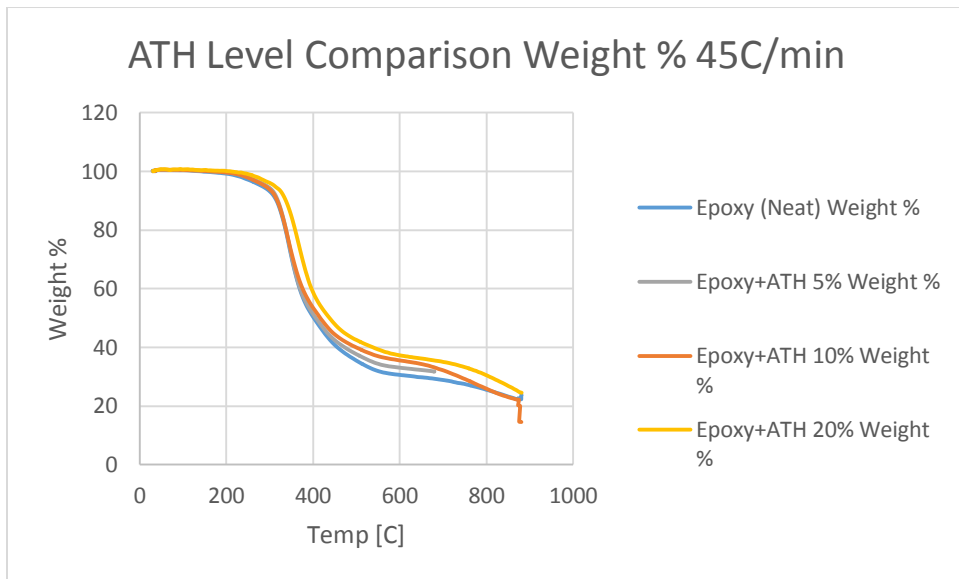
Figure 379: ATH Level Comparison Weight % 45 C/min

Appendix H: DSC Database
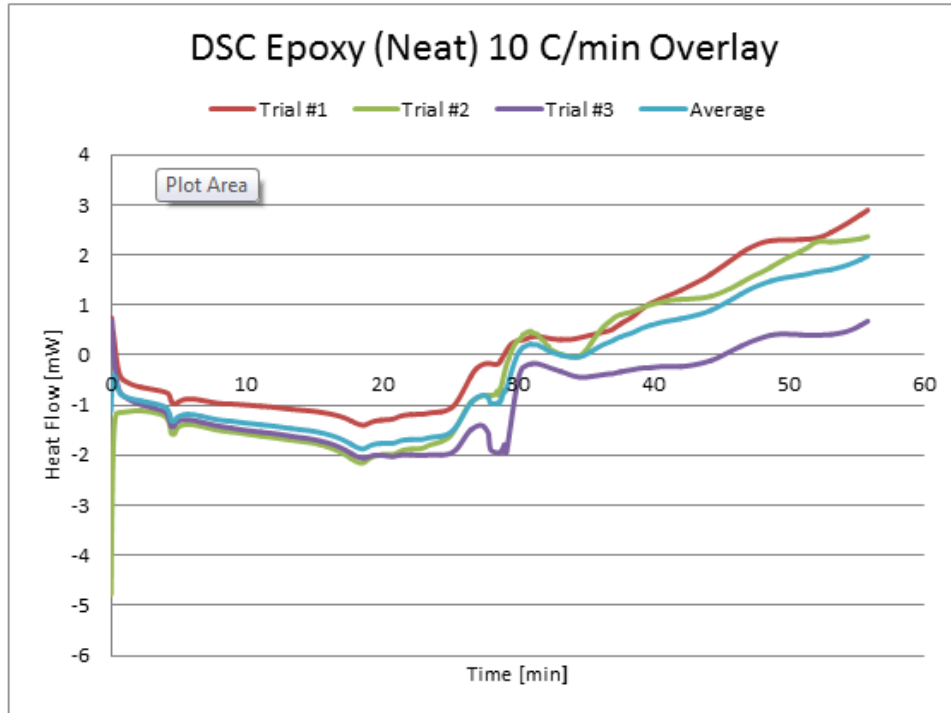
Figure 380: DSC Epoxy (Neat) 10 C/min Overlay
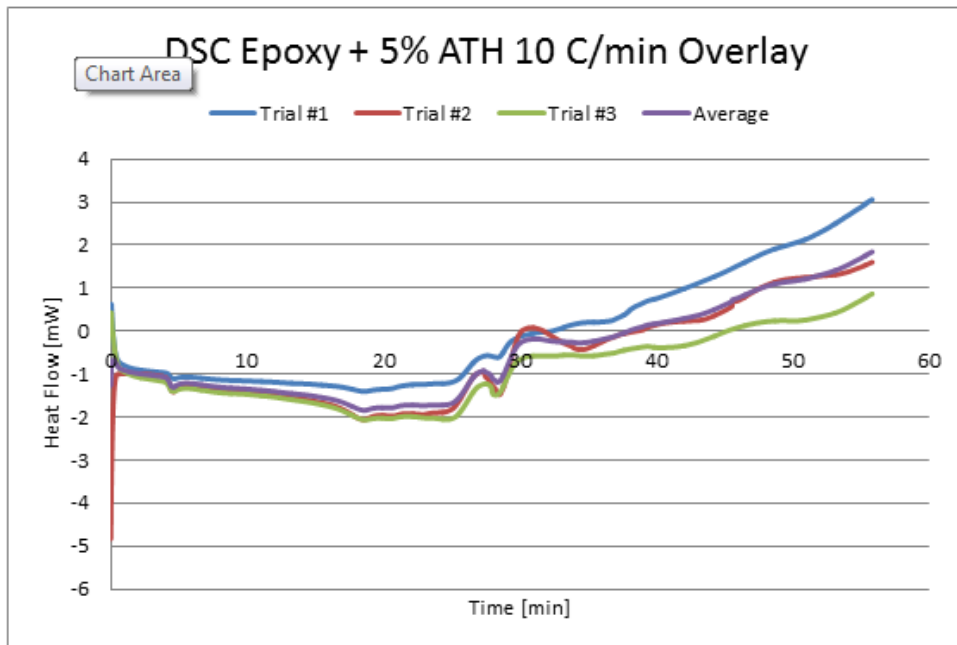
Figure 381: DSC Epoxy + 5% ATH 10 C/min Overlay
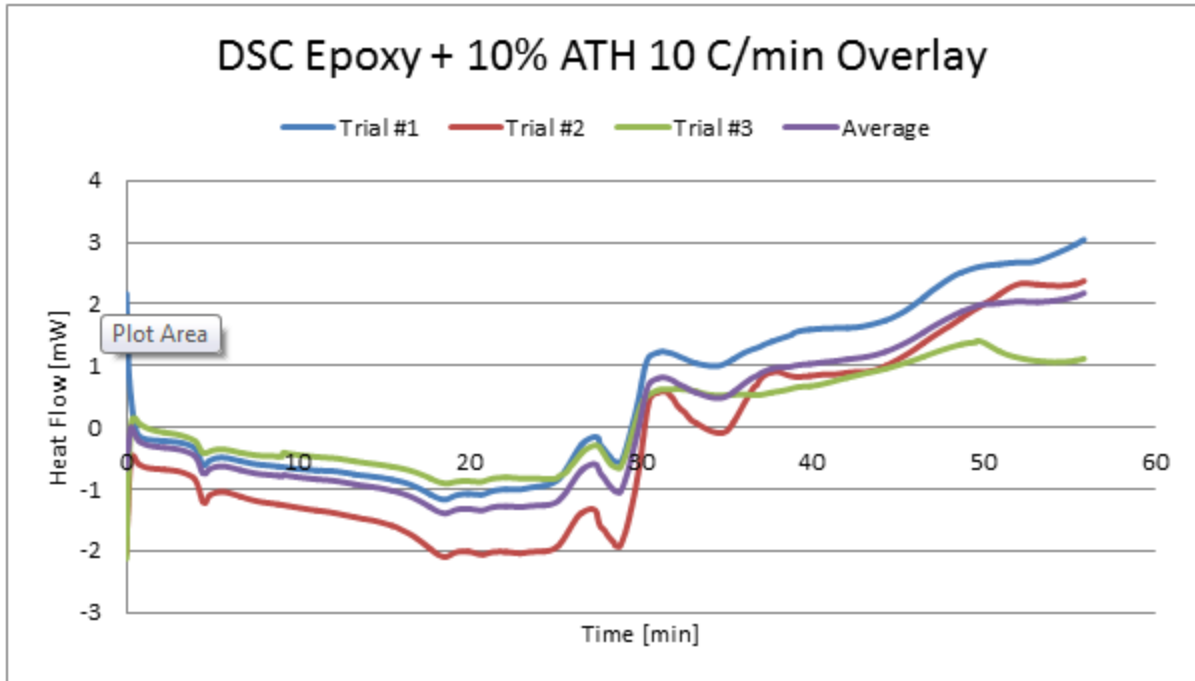
Figure 382: DSC Epoxy + 10% ATH 10 C/min Overlay
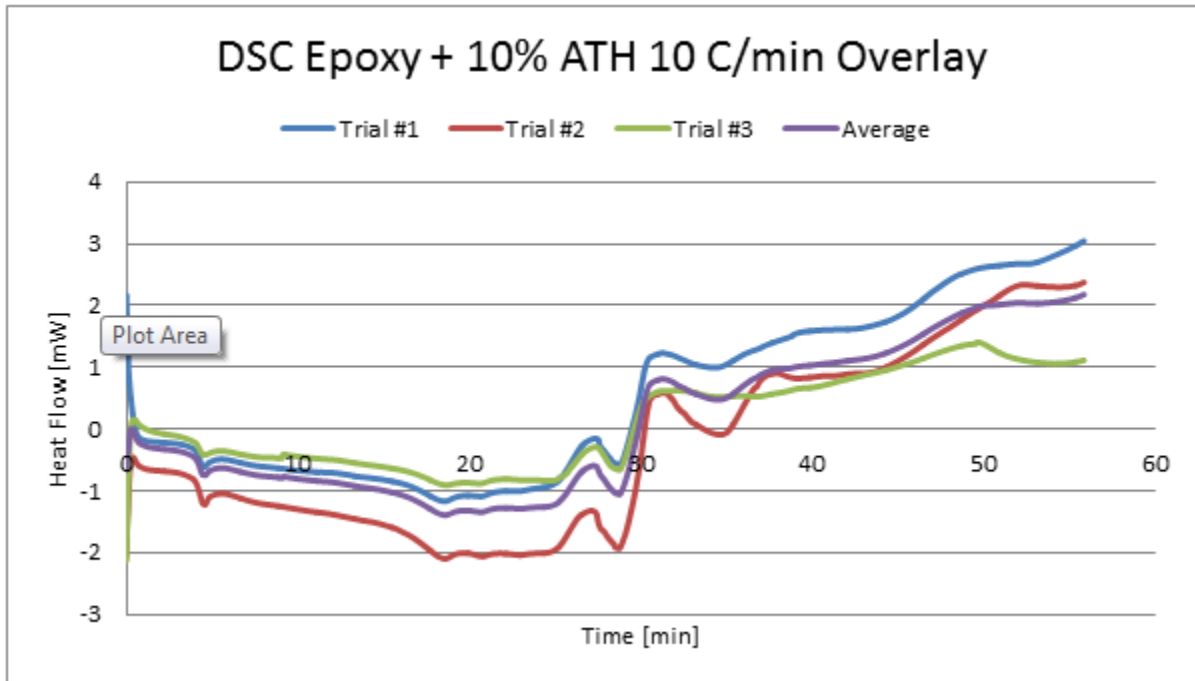
Figure 383: DSC Epoxy + 10% ATH 10 C/min Overlay
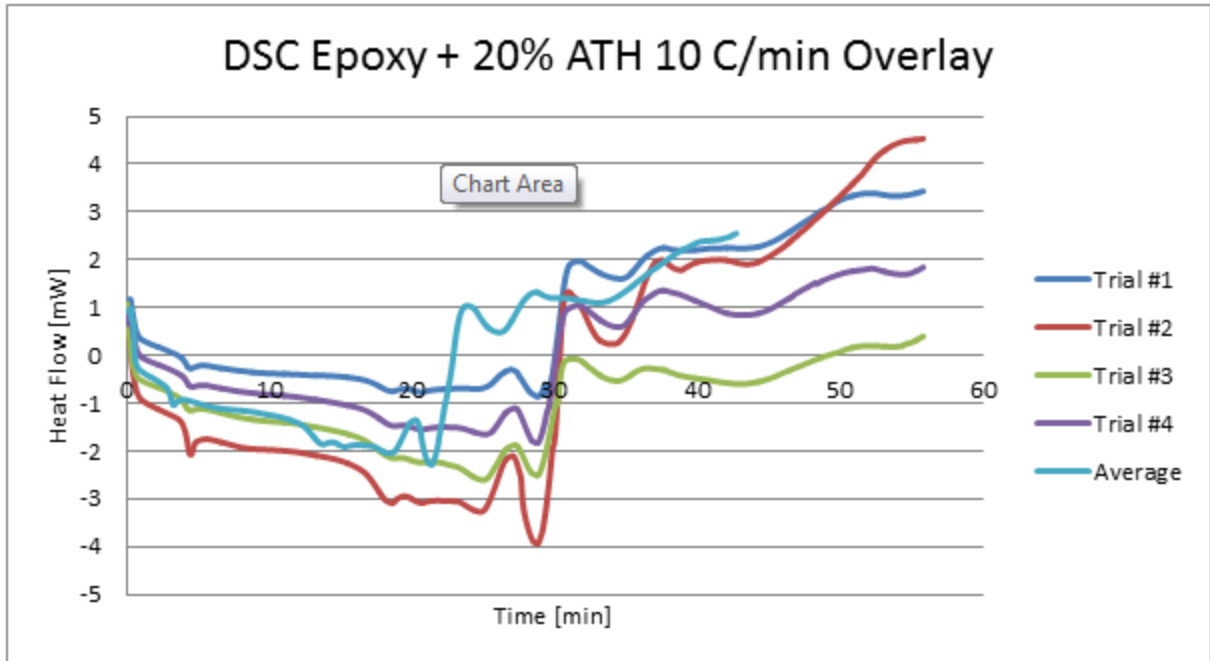
Figure 384: DSC Epoxy + 20% ATH 10 C/min Overlay
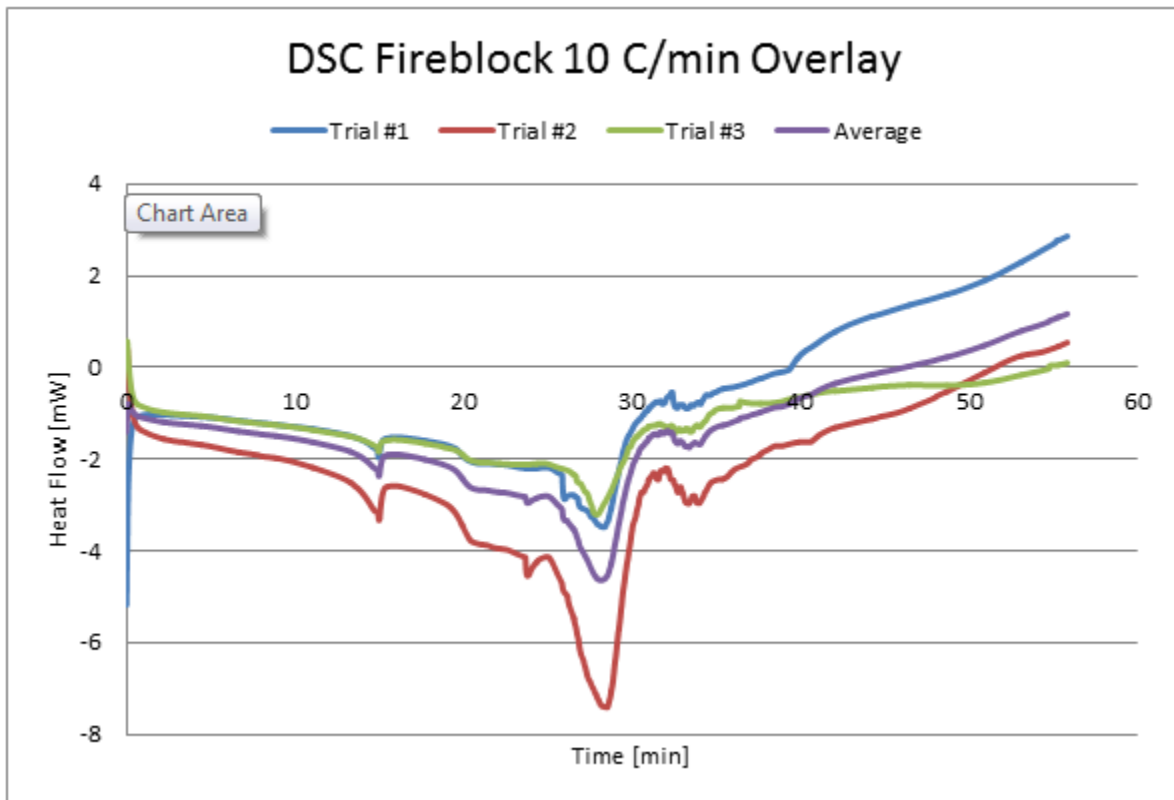
Figure 385: DSC Fireblock 10 C/min Overlay

Appendix I: TGA and DSC Overlay Database

This data is a compilation of the average, smoothed trials for each material at 10C/min.

Epoxy (Neat):
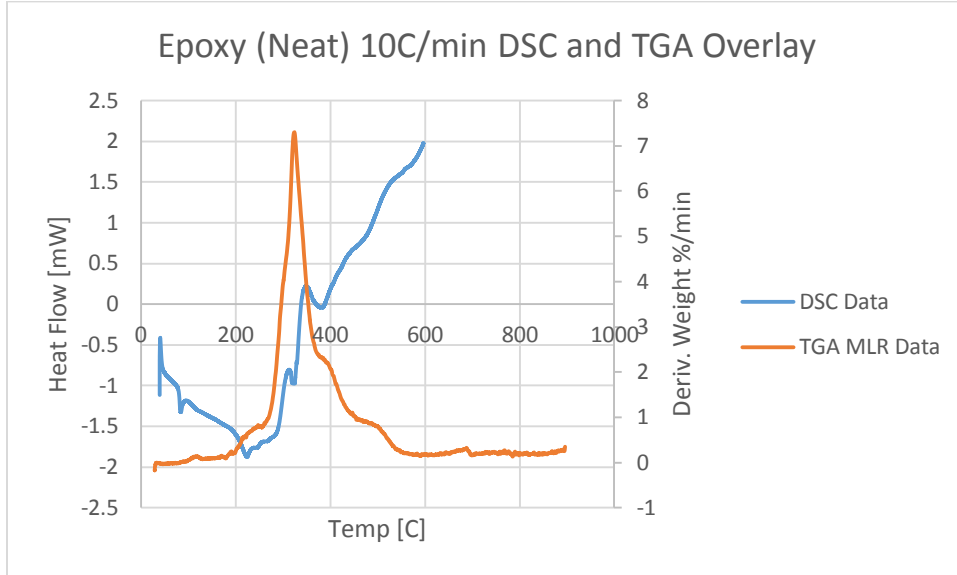
Figure 386: Epoxy (Neat) 10 C/min DSC and TGA Overlay
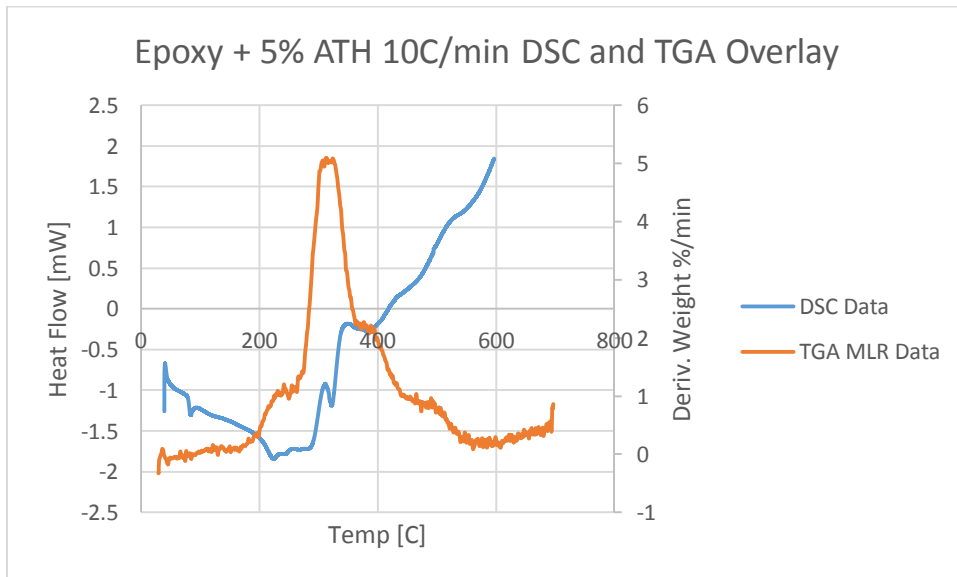
Epoxy plus 5% ATH:

Figure 387: Epoxy + 5% ATH 10 C/min DSC and TGA Overlay
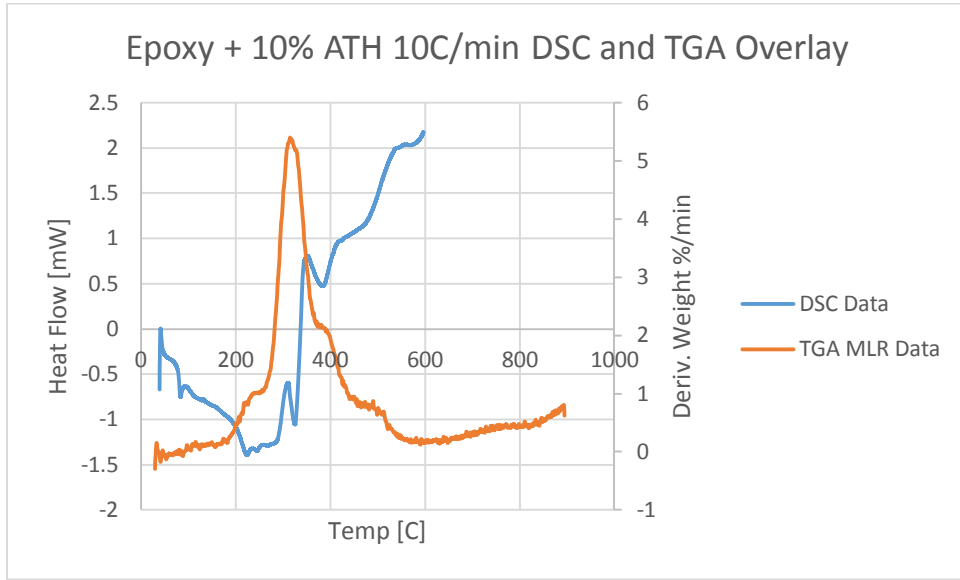
Epoxy plus 10% ATH:

Figure 388: Epoxy + 10% ATH 10 C/min DSC and TGA Overlay

Epoxy plus 20% ATH:
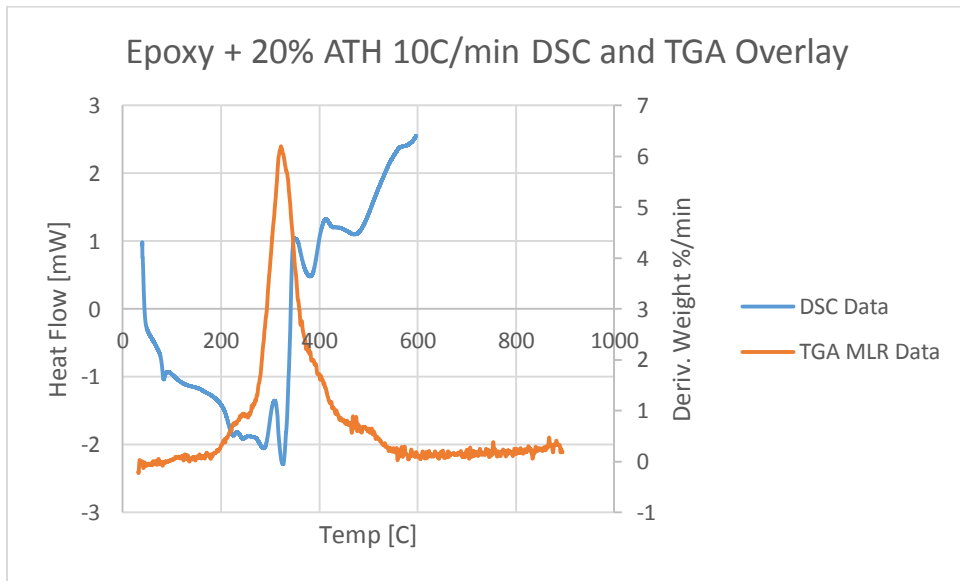
Figure 389: Epoxy + 20% ATH 10 C/min DSC and TGA Overlay

Appendix J: Thermal Lag

T∞= constant temperature

For the accuracy of the result, area (A) is replaced by a function of volume. The drop can be assumed as a thin cuboid. The volume can be express as:

$$V = 2 * L * A$$

The solution for each type of thermal lag is shown as below and plotted to study the thermal lag time.

$$\text{Machine thermal lag: } T_{Sample} = e^{\left[-\left(\frac{h}{2\rho Lc}\right)t\right]}(Ti - T_\infty) + T_\infty \quad (24)$$

$$\text{Diffusive thermal lag: } T_{Sample} = e^{\left[-\left(\frac{K}{2\rho L^2 c}\right)t\right]}(Ti - T_\infty) + T_\infty \quad (25)$$

$$\text{Combined thermal lag: } T_{Sample} = e^{\left[-\left(\frac{R_{total}}{\rho Vc}\right)t\right]}(Ti - T_\infty) + T_\infty \quad (26)$$

T infinity can be a constant temperature or becoming the heating rate as a function of time, which is $T_\infty = T_0 + \beta t$. Both cases are studied to see the relationship between the ambient temperature and actual sample temperature. In this case, the sample is assumed to put into a furnace with a constant ambient temperature. The lag time is around two times tc for each type of thermal lag. The table shows the relationship of the variable, characteristic time and the lag time for each case. tc and lag time is calculated and marked on the diagram.

Table 27: Diffusive Thermal Lag (T∞= constant)

L[mm]	tc [min]	Lag time	Lag time [min]
0.75	0.12	2.1*tc	0.25
1	0.24	2.0*tc	0.47
1.5	0.45	2.5*tc	1.14
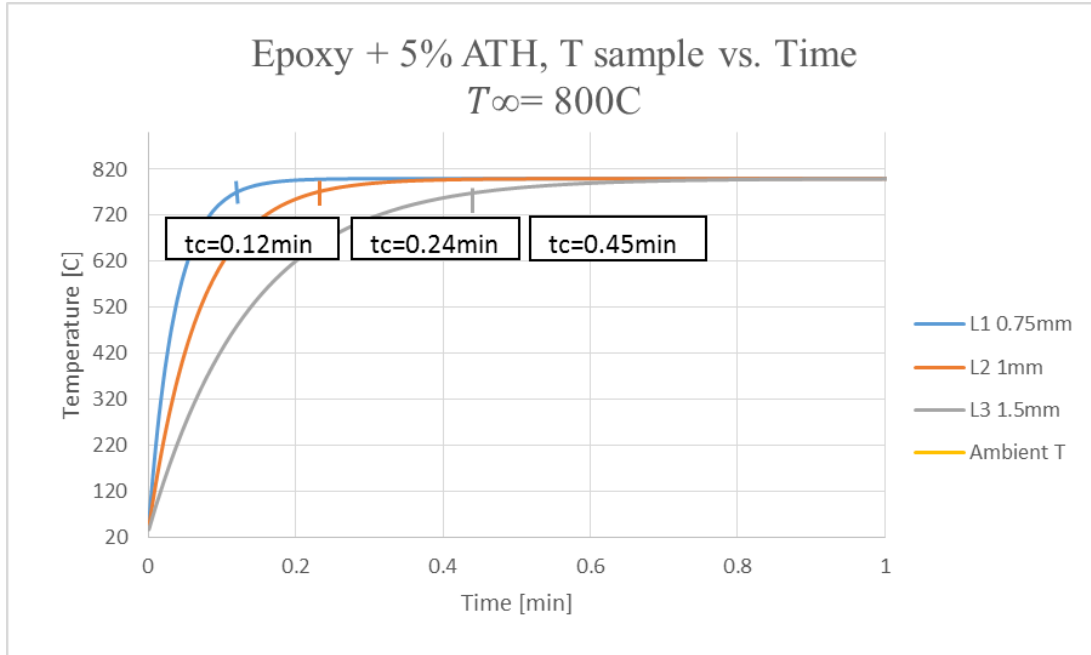
Figure 390: Characteristic time on diffusive thermal lag
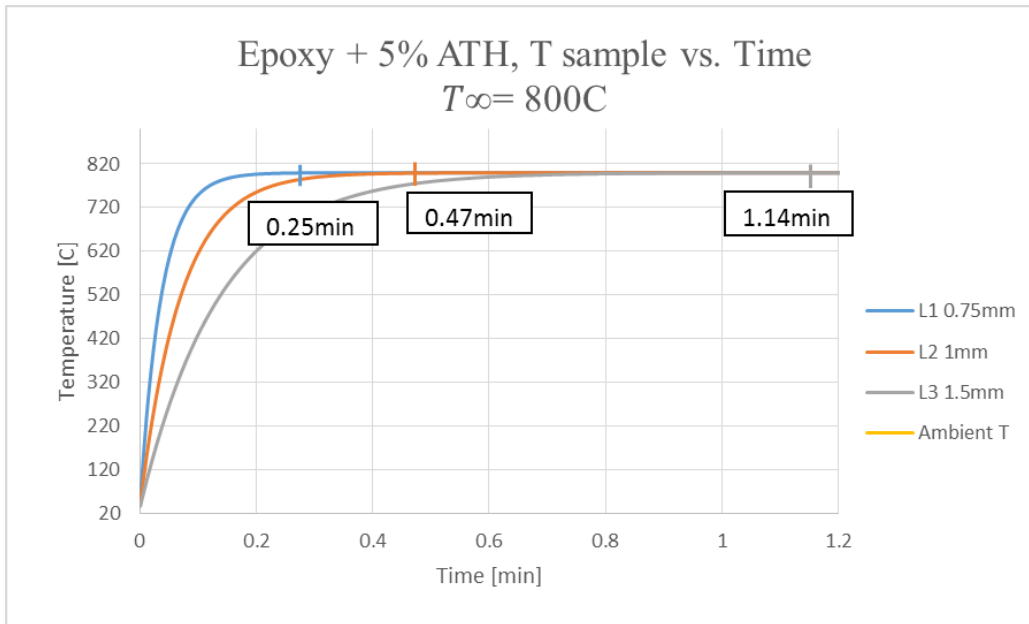
Figure 391: Lag time on diffusive thermal lag

h[W/m^2*K]	tc [min]	Lag time	Lag time [min]
10	0.84	2.7*tc	2.31
15	0.56	2.5*tc	1.39
20	0.42	2.9*tc	1.25
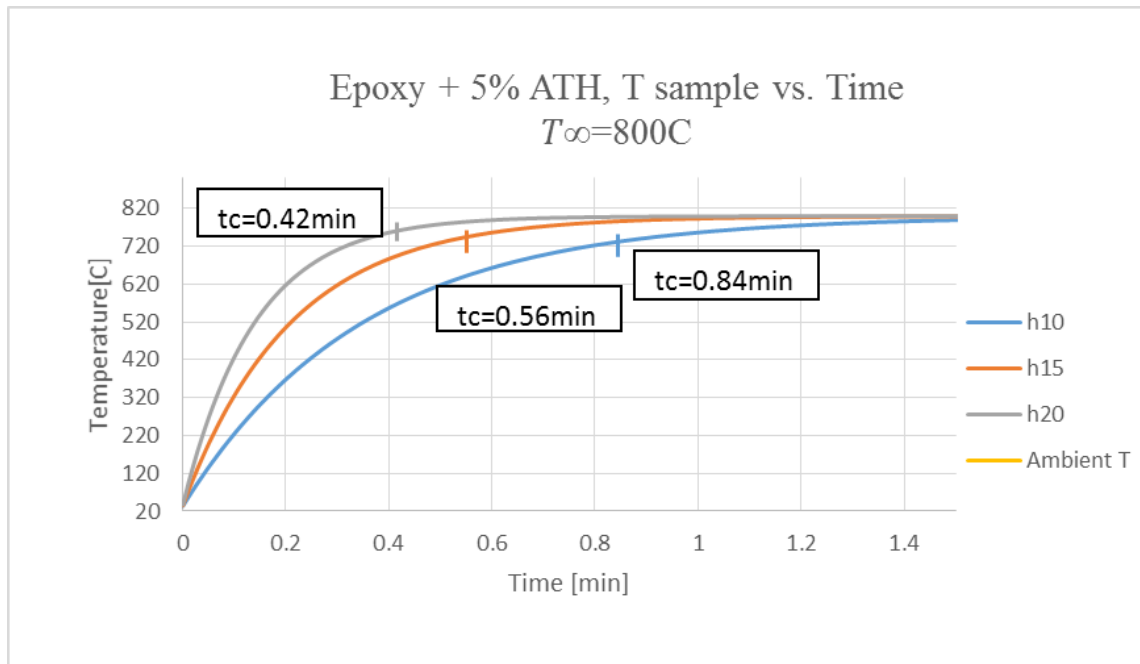
Figure 392: Characteristic time on machine thermal lag
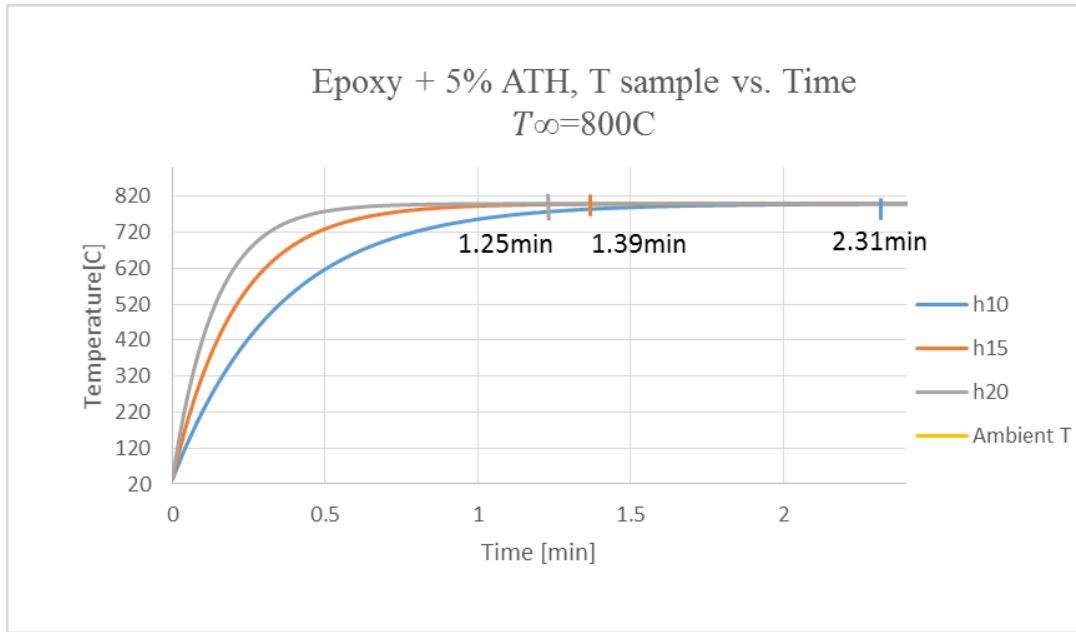
Figure 393: Lag time on machine thermal lag

Table 29: Combined Thermal Lag (T∞= constant)

L[mm]+h[W/m^2*K]	tc [min]	Lag time	Lag time [min]
0.75+20	1.15	1.7*tc	1.9
1+20	2.07	1.4*tc	3.0
1.5+20	9.13	1.4*tc	12.7
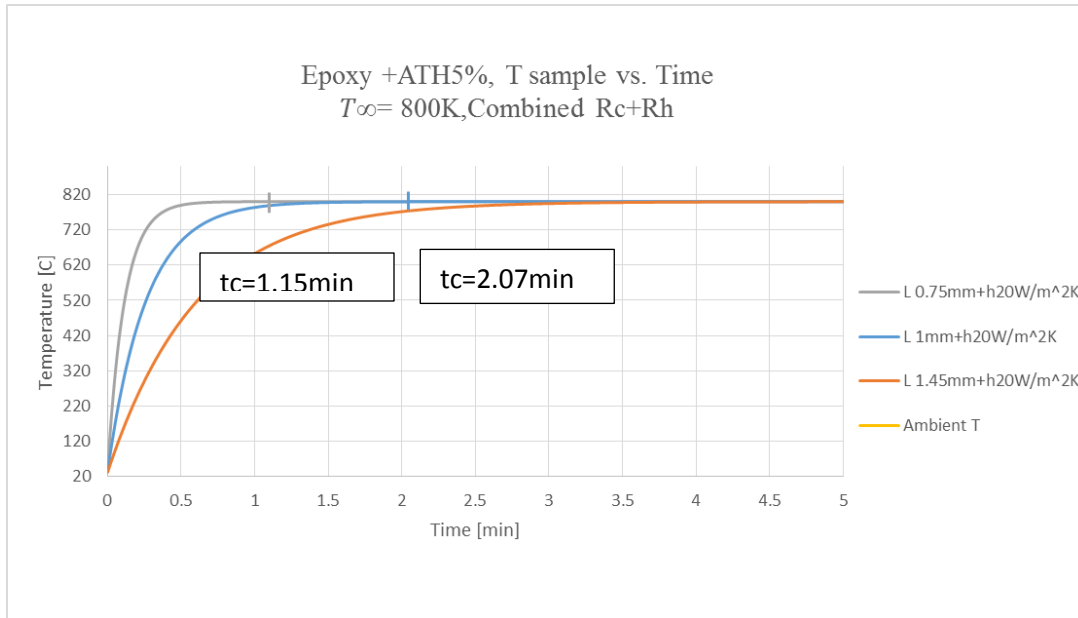
Figure 394: Characteristic time on combined thermal lag
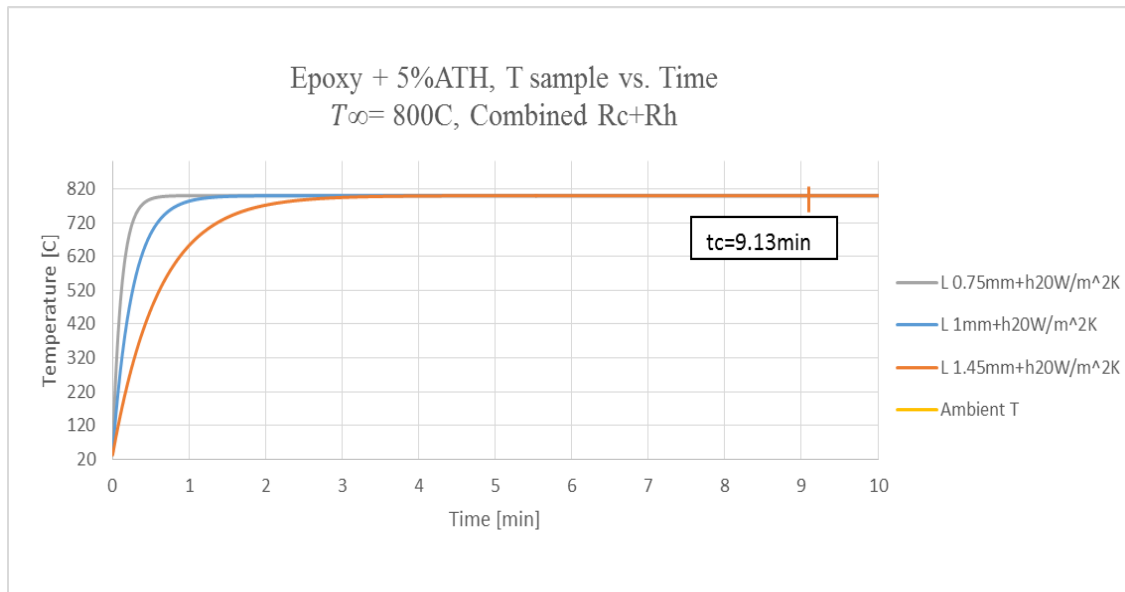
Figure 395: Characteristic time on combined thermal lag
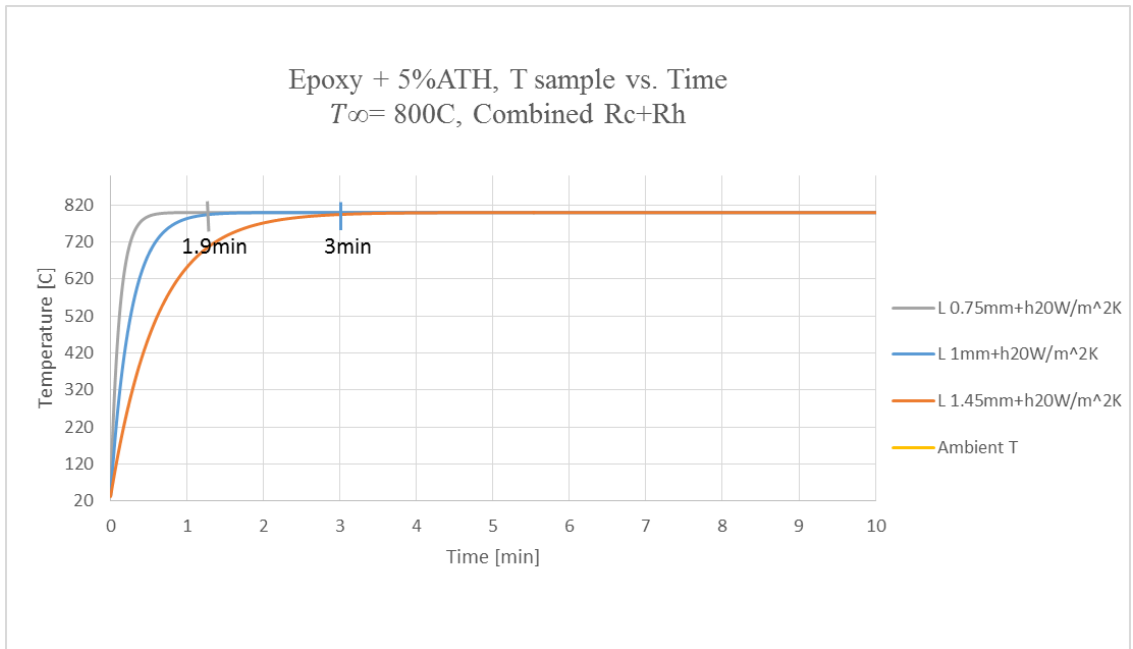
Figure 396: Lag time on combined thermal lag

Approximately Solution

The approximately solution use the same equations as $T_\infty = constant$ when plotting into Excel, but in a situation where there is a heating rate. The initial equation remains the same, but T infinity becomes the heating rate as a function of time, written as $T_\infty = T_0 + \beta t$. To observed the diagram, the sample temperature increases as ambient temperature increases. The temperature difference between the ambient temperature and sample temperature get bigger at the beginning. However, the temperature difference reaches to a highest number around one minutes and then starts to decrease for the rest of the test. The lag time is marked when the temperature difference is the biggest.

Table 30: Diffusive Thermal Lag (T∞= T0+βt)

L[mm]	tc[min]	Lag time	Lag time
0.75	0.12	2.6*tc	0.32
1	0.24	2.6*tc	0.63
1.45	0.45	2.1*tc	0.95
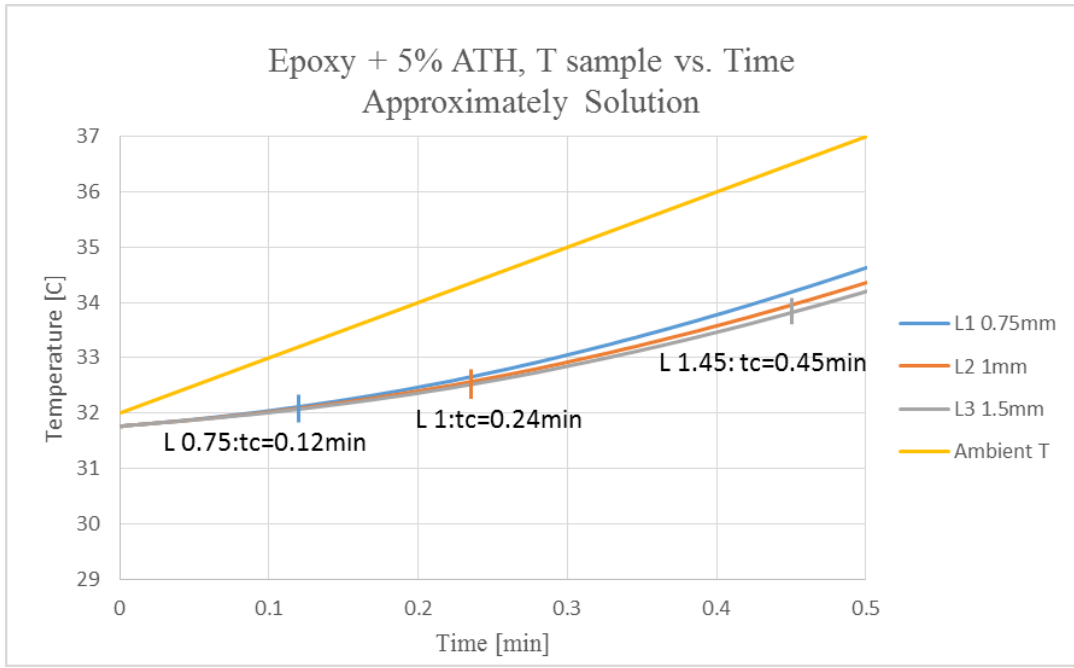
Figure 397: Characteristic time on diffusive thermal lag
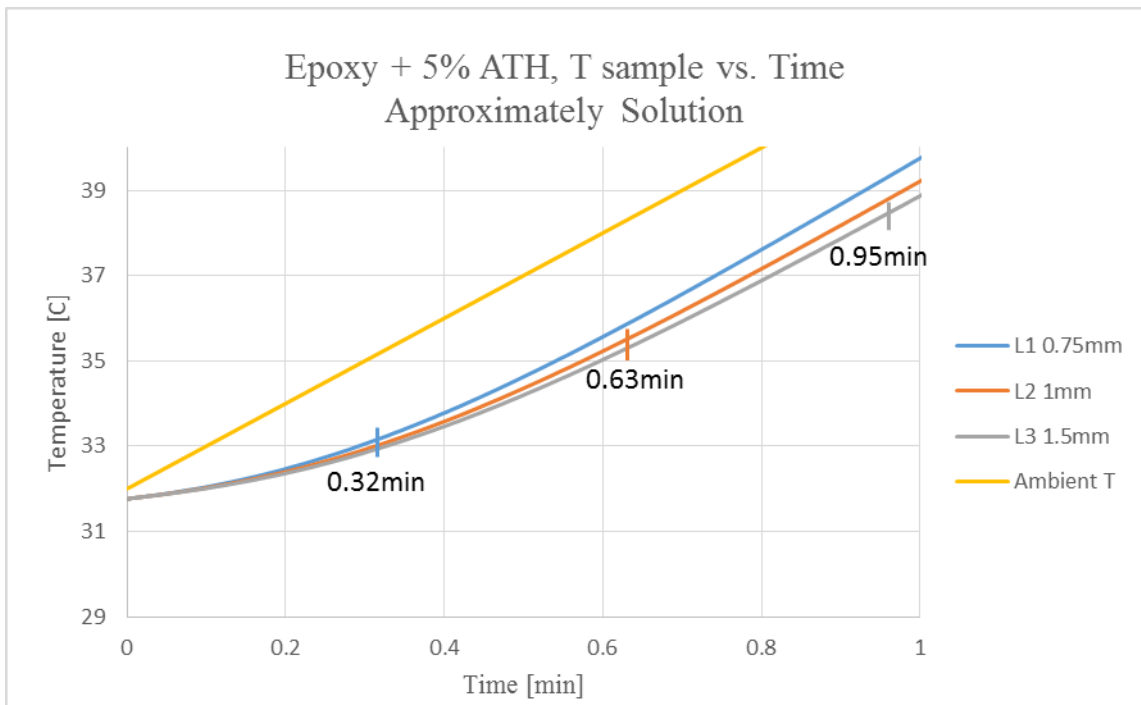
Figure 398: Lag time on diffusive thermal lag

Table 31: Machine Thermal Lag (T∞= T0+βt)

h[W/m^{2*}K]	tc[min]	Lag time	Lag time [min]

10	0.84	1.0*tc	0.85
15	0.56	1.4*tc	0.81
20	0.42	1.6*tc	0.70
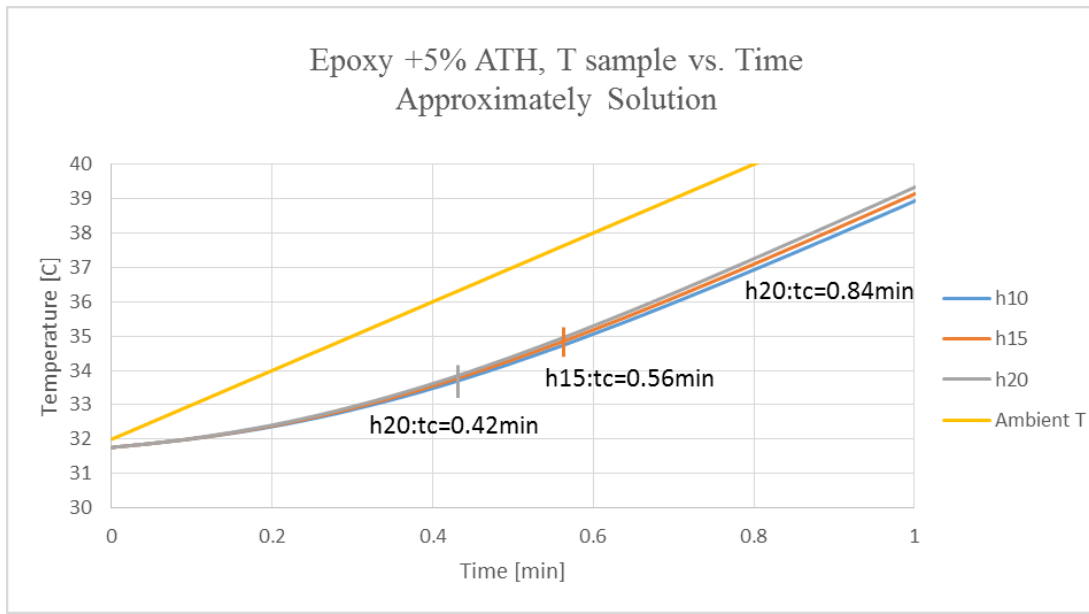
Figure 399: Characteristic time on machine thermal lag
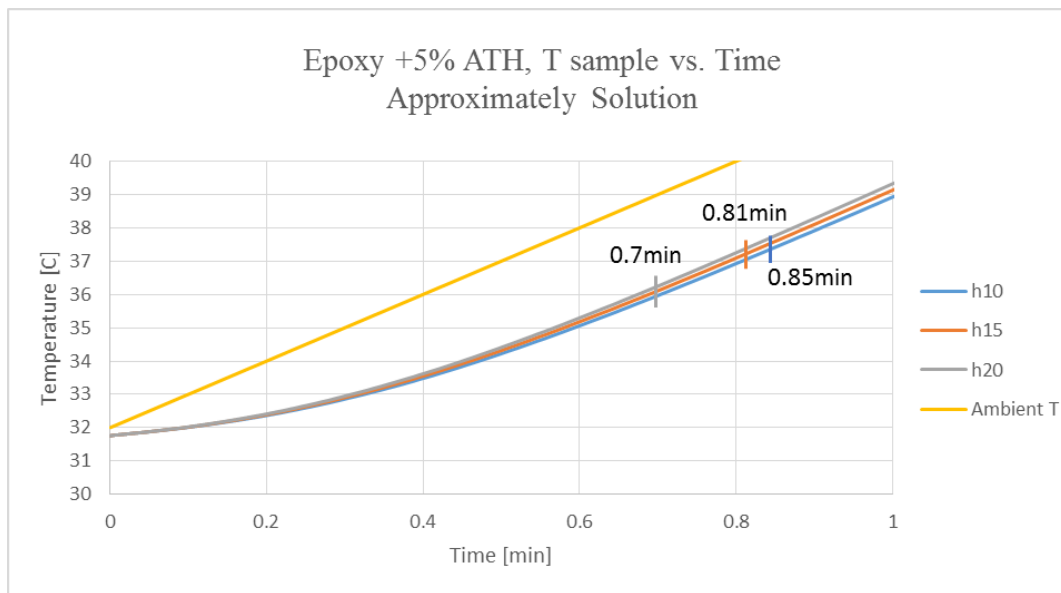
Figure 400: Lag time on machine thermal lag

L[mm]+h[W/m^2*K]	tc[min]	Lag time	Lag time [min]
0.75+10	0.83	3.4*tc	2.82
1+10	0.84	3.4*tc	2.85
1.45+10	0.85	3.4*tc	2.87
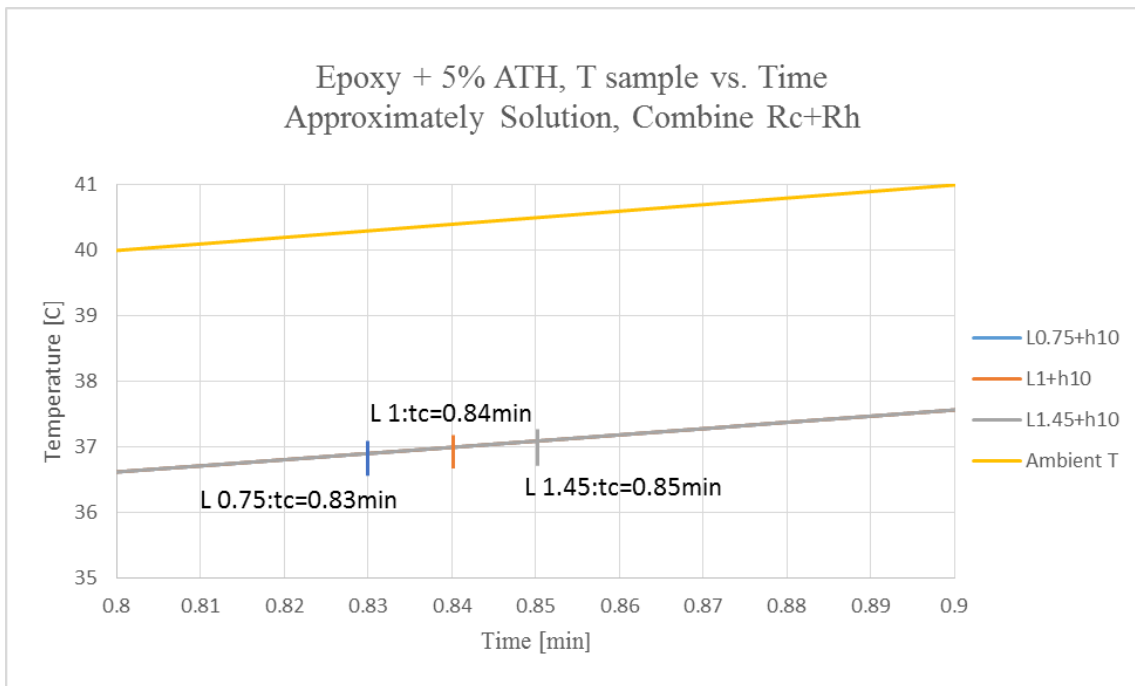
Figure 401: Characteristic time on combined thermal lag

Exact Solution

Exact solution was calculated by using first order ODE method. The lag time is longer comparing to the case of $T_\infty = constant$. In this case, the temperature of the furnace and the material are both changing in the diagram, so the relationship of both changing temperature becomes more complex. Characteristic time cannot represent 70% of the lag time. In this case, the lag time is around six times t_c.

Table 33: Machine Thermal Lag (Exact solution)

h[W/m^{2*}K]	tc[min]	Lag time	Lag time [min]
10	0.84	6.1*tc	5.2
15	0.56	6.1*tc	3.4
20	0.42	6.2*tc	2.6
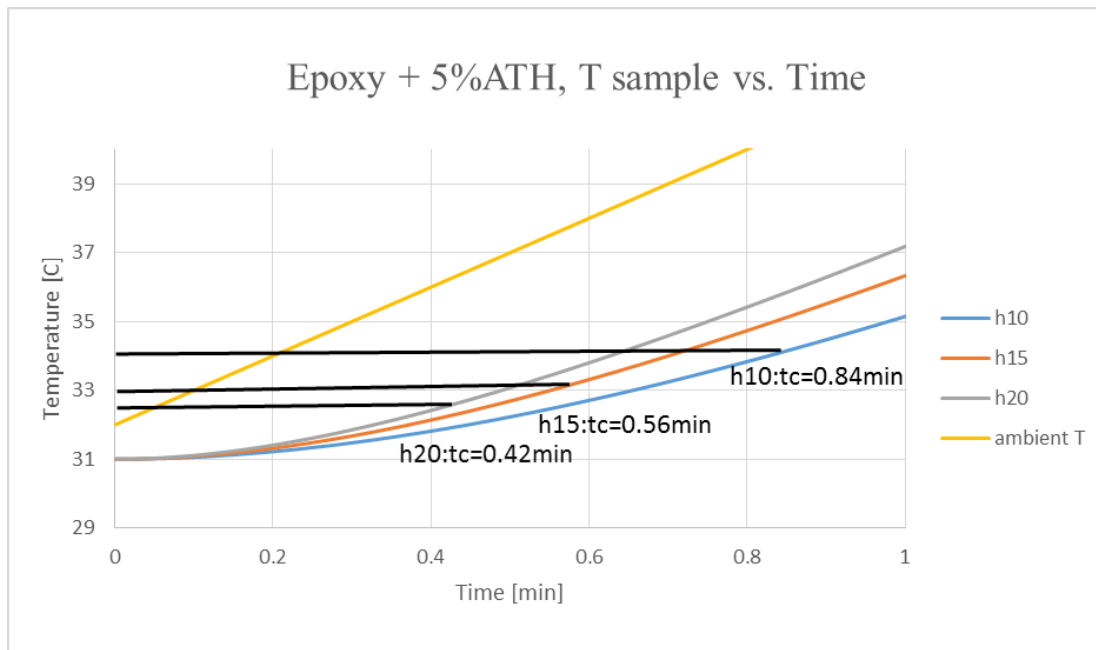
Figure 402: Characteristic time on machine thermal lag
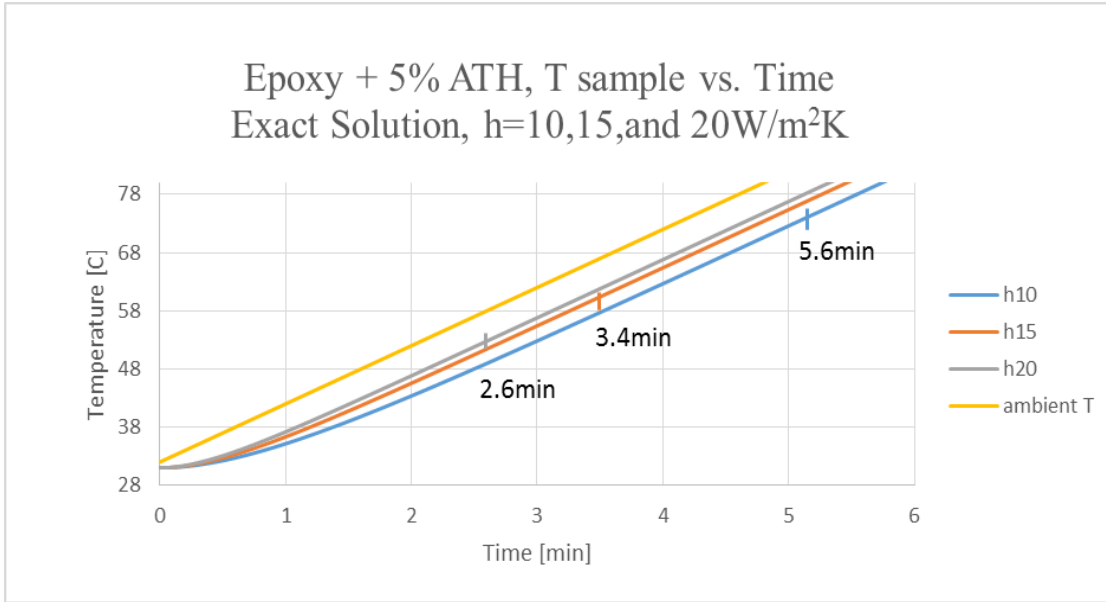
Figure 403: Lag time on machine thermal lag
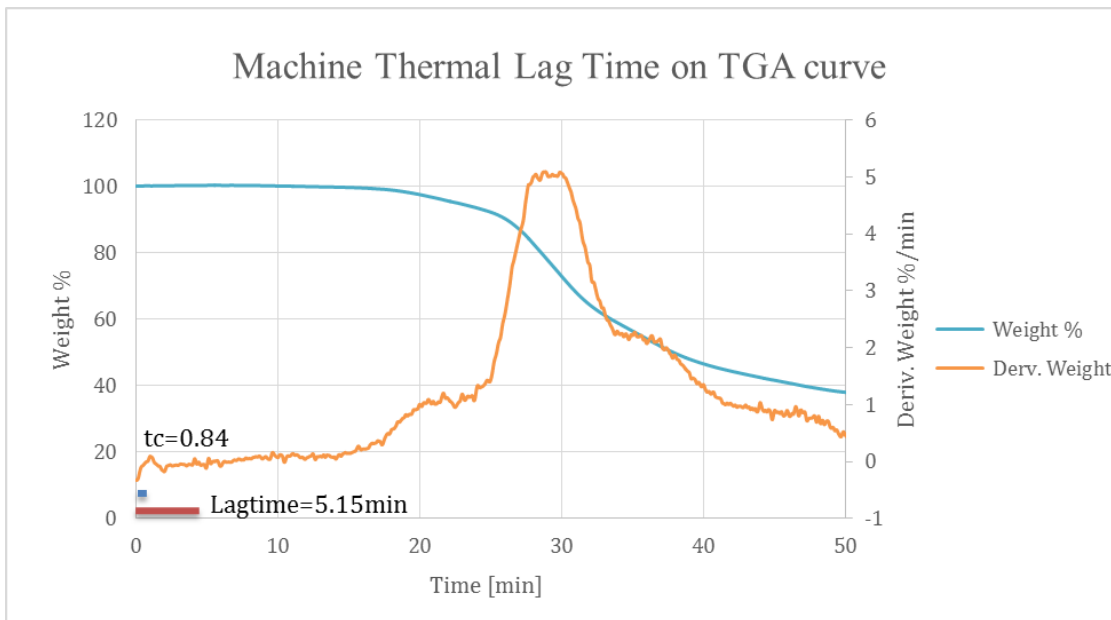
Figure 404: Machine thermal lag on TGA curve

Table 34: Combined Thermal Lag (Exact solution)

L[mm]+h[W/m²*K]	tc[min]	Lag time	Lag time [min]
0.75+20	0.83	6.8*tc	5.4
1+20	0.84	6.9*tc	5.8
1.45+20	0.85	6.9*tc	5.9
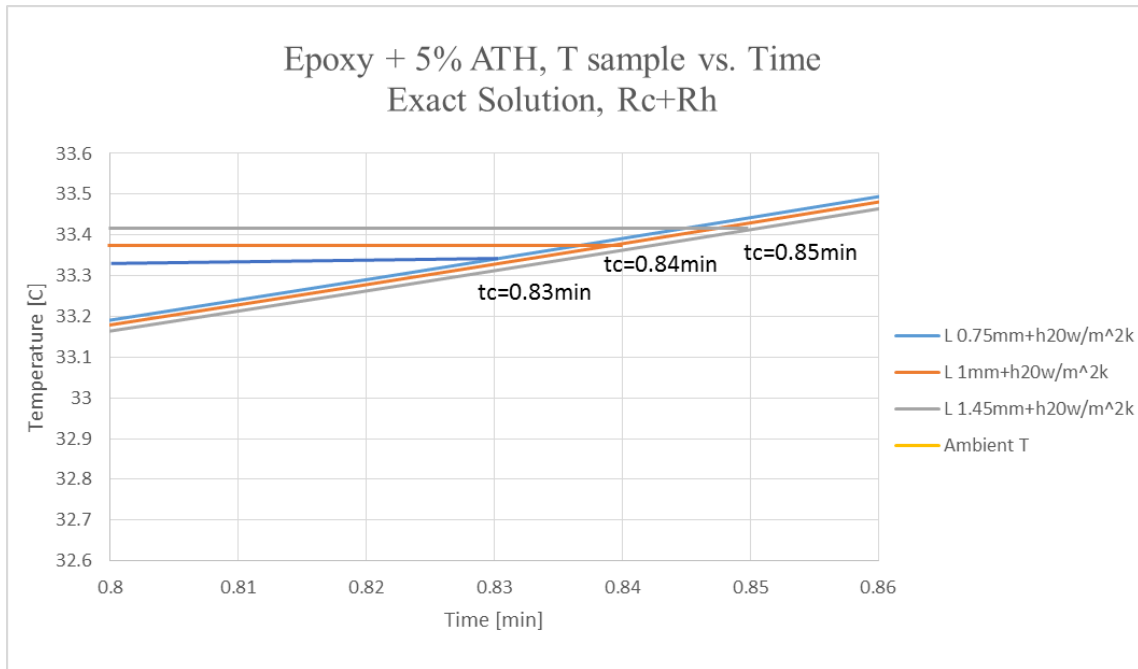
Figure 405: Characteristic time on combined thermal lag
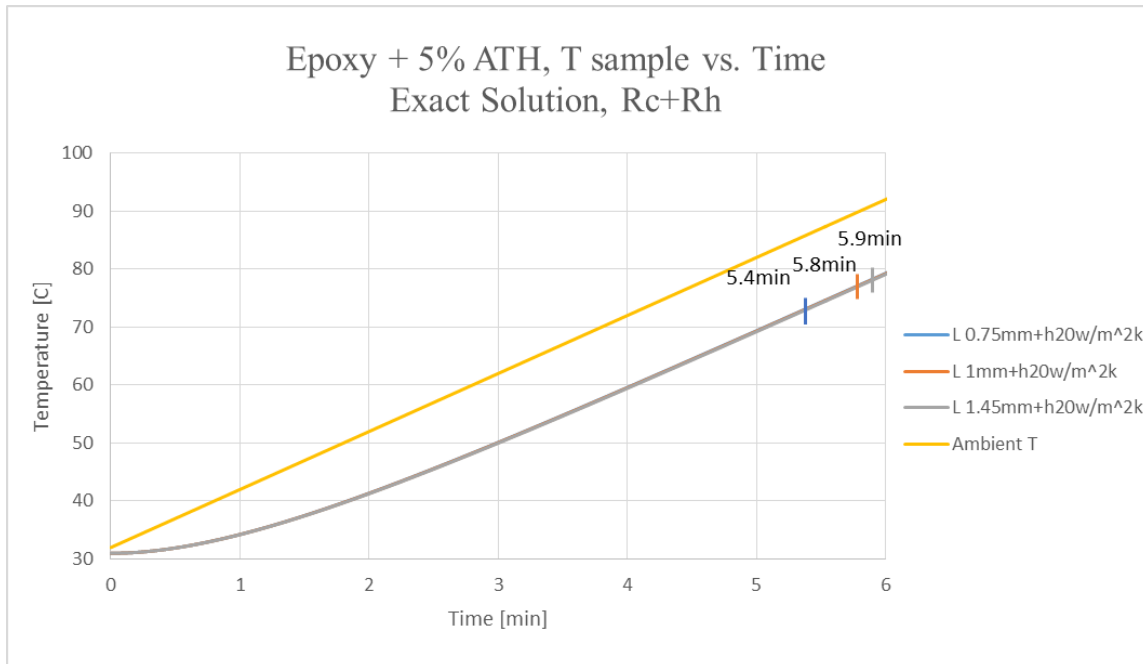
Figure 406: Lag time on combined thermal lag
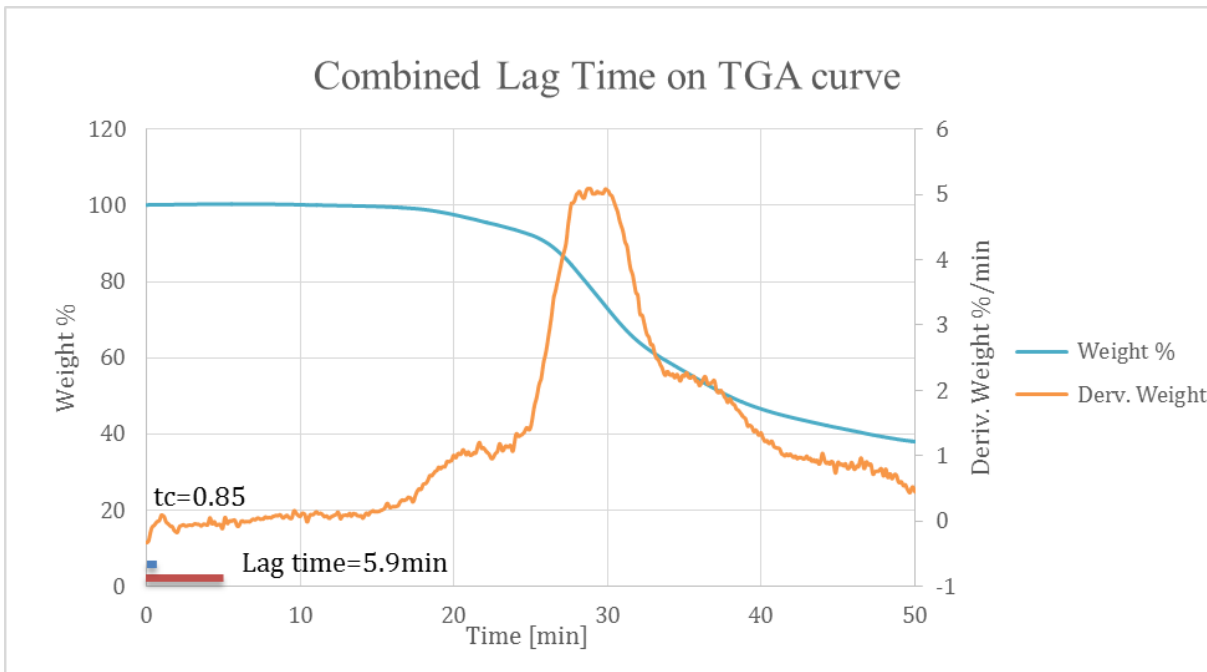
Figure 407: Combined thermal lag on TGA curve

References

[1] PerkinElmer. Characterization of Polymers Using TGA. Web. 13 Sept. 2014.

<http://depts.washington.edu/mseuser/Equipment/RefNotes/TGA_Notes.pdf>

[2] Bakis, C., Bank, L., Brown, V., Cosenza, E., Davalos, J., Lesko, J., Triantafillou, T. (n.d.). Fiber-Reinforced Polymer Composites for Construction—State-of-the-Art Review. *Journal of Composites for Construction*, 73-73.

[3] Kreysler & Associates. (n.d.). Retrieved September 10, 2014, from <http://kreysler.com/>

[4] Wilkie, C.A., Morgan, A.B., (2009). Fire Retardancy of Polymeric Materials, Second Edition. Taylor and Francis Group, LLC. Boca Raton, FL.

[5] Kandola, B.K., Biswas, B., Price, D., Horrocks, R. A., (2010). Studies on the effect of different levels of toughener and flame retardants on thermal stability of epoxy resin. *Polymer Degradation and Stability*. 95, 144-152.

[6] Salas, C. (n.d.). STANDARD OPERATING PROCEDURE (SOP) FOR TA Instruments TA Q500 Thermal Gravimetric Analysis.

[7] Ta Instruments Inc. - Diane Wylie. (2007). Differential Scanning Calorimeter. *DSC Q Series Getting Started Guide*.

[8] Paven, M. e. (2010). *Universal Standard Protocols for Temperature and Material Characerization Calibration with Pharmaceuticals by Thermal Analysis.* Cleavland: Department of Chemistry, University of Cleavland.

[9] University of Minnesota. (n.d.). *SOP (Standard Operating Procedure) for the Perkin-Elmer Pyris 1 DSC.* Minneapolis.

[10] TA Instruments. (2007, January). *DSC Differential Scanning Calorimeter.* Retrieved from TA Instruments:
<http://nmtprg.weebly.com/uploads/3/1/1/0/31101989/ta_mdsc_manual.pdf>

[11] Lautenberger, C. (2014). Gpyro-A Generalized Pyrolysis Model for Combustible Solids Technical Reference.

[12] Ferriol, M. Gentilhomme, A. Cochex M. Oget, N. & Mieloszynski, J.L. (2003). Thermal Degrdatation of poly(methyl methacrylate) (PMMA): modeling of DTG and TG Curves. Polymer Degradation and Stability, 79, 271-281.

[13] Lautenberger, C. (2014). Gpyro-A Generalized Pyrolysis Model for Combustible Solids Users' Guide.

[14] Lautenberger, C. (2007). A Generalized Pyrolysis Model for Combustible Solids. (Doctoral dissertation).

[15] Lautenberger, C. Kim, E. Dembsey, N. & Fernandez-Pello, C. (2008). The Role of Decomposition Kinetics in Pyrolysis Modeling-Application to a Fire Retardant Polyester Composite. *Fire Safety Science*, 9, 1201-1212.

[16] Kim, E., Dembsey, N. (2014). Parameter Estimation for Comprehensive Pyrolysis Modeling: Guidance and Critical Observations. *Fire Technology*, 5(2), 443-477.

[17] Gillespie, B., Long, M., McMillan, N. & Walde, C. (2014). *Determining Limitations of Kinetic Models for Pyrolysis Simulation of Fiber Reinforced Polymer Composites.* (Undergraduate Major Qualifying Project).